A KINETIC STUDY OF THE OLIGOMERIZATION OF PROPENE, BUTENE AND VARIOUS HEXENES OVER SOLID PHOSPHORIC ACID

BY

DEAGHLAN MARTIN McCLEAN

B. Sc. (Eng) (Cape Town)

Submitted to the University of Cape Town
in fulfilment of the requirements for the degree of

DOCTOR OF PHILOSOPHY

Department of Chemical Engineering
University of Cape Town
Rondebosch, Cape
South Africa

MAY 1987

ACKNOWLEDGEMENTS

I would like to express my sincerest thanks to my supervisors, Professor Cyril T O'Connor and to Dr Masami Kojima for their guidance and friendship during the course of this work.

I wish to thank Jack Fletcher, Marc Rautenbach, Werner Schumann, Gordon Reid and Antoinette Upton for their invaluable assistance and friendship over the years.

The following people and Institutions are also gratefully acknowledged:

SASOL, Caltex and the Council for Scientific and Industrial Research for financial and technical assistance. In particular Mr K Kriel and Dr M Dry of SASOL;

Professor Brian Paddon of the Department of Chemical Engineering for his perennial and enthusiastic assistance;

All on the technical staff particularly messrs A Barker and R Senekal of the Chemical Engineering Workshop without whose assistance this thesis would not have been possible;

The glassblower, Mr C Ledger, for his practical assistance and Miss B Williams for the mass spectroscopic analysis;

Mr T Classens for the use of his multi-parameter modelling program;

I would like to express special thanks to my wife, Helen, for her untiring and dedicated help with the typing of the thesis.

TO MY FATHER SEAMUS

SYNOPSIS

The oligomerization of propene, butenes and hexenes over solid phosphoric acid catalyst has been investigated using an internal recycle reactor, a pulse micro-catalytic reactor and a fixed bed reactor.

The relative reactivities of the propene, butenes and hexene feeds were examined in a pulse reactor. Mechanistic pathways, particularly for propene and butene oligomerization, have been proposed. In the pulse reactor at 1.65 MPa and 473 K the alkenes oligomerized according to the following order of decreasing reactivity: iso-butene, 2-methyl-1-pentene, 1-hexene and propene. In this reactor at 473 K and 1.63 MPa and at propene: 2-methyl-1-pentene and propene: C_9 molar ratios of 1.5:1 and 10:1 respectively, the C_{12} fraction was produced solely from the dimerization of C_6. At the higher propene (4.97×10^{-2} mol/l) and 2-methyl-1-pentene (0.86×10^{-2} mol/l) concentrations the fraction of C_{12} produced from dimerization of C_6 at C_3:C_6 and C_3:C_9 molar ratios of 6:1 and 15:1 respectively, was approximately 50%.

The internal gas recirculation reactor was characterized with respect to residence time and mass transfer characteristics. The reactor approached ideal CSTR performance at recycle ratios of approximately 15 to 20. A mass transfer coefficient of 8.5 $cm.s^{-1}$ was found for the napthalene-air system at impeller speeds of 2000rpm and atmospheric pressure. A superficial gas velocity of 140 $cm.s^{-1}$ was found for this system. Interphase and intraparticular mass transfer was negligible when propene was oligomerized at 1.5 MPa, 2000 rpm, 464 K, 101.5% H_3PO_4, and using a catalyst size fraction of 106-180 μm. At the extreme temperature and acid concentration conditions of 114% H_3PO_4, 503 K, 1.5 MPa, 2000 rpm and using the same catalyst size fraction, interphase mass transfer was insignificant and intraparticular diffusion was slow. The H_3PO_4 concentration was critical, affecting both catalyst activity and lifetime. Increases in conversion were accompanied by decreases in the average molecular weight of the liquid product fraction (C_{6+}) possibly due to the introduction of diffusional problems as the phase inside the reactor shifted towards the liquid phase.

While butene oligomerized to dimer, propene oligomerized predominantly to trimer and tetramer. This may be due to steric hindrance or heats of formation resulting in the preferential desorption of these molecules relative to the other oligomers of propene and butene.

The rate of propene oligomerization over the temperature range 443-473 K and over the H_3PO_4 concentration range of 102-107 % was related to its concentration by a near first order rate equation. The rate of 1-butene reaction was found to have a slightly higher order (1.23). Detailed rate equations for both cases are presented.

Five kinetic models have been tested for their ability to fit the rates of product formation and the rate of propene reaction as found in the internal recirculation reactor. Two of the models were empirical and two were based on the assumption that the oligomerization reactions are elementary. A fifth more fundamental model has been formulated according to the carbonium ion theory. The two empirical models gave the best fit to the data. Similar models were proposed for the 1-butene oligomerization. Of four possible models, only one of the empirical models gave the best fit.

The rate equation proposed for propene oligomerization was used to predict the performance of a fixed bed reactor with catalyst pellets using a one dimensional model. A number of simplifying assumptions were made and the predicted results were within 10% of the experimental data.

TABLE OF CONTENTS

	PAGE
ACKNOWLEDGEMENT	i
SYNOPSIS	iii
TABLE OF CONTENTS	iv
LIST OF FIGURES	xvii
LIST OF TABLES	xxviii
NOMENCLATURE	xxxviii
1. INTRODUCTION	1
1.1 Routes to the Production of Liquid Fuels	4
1.1.1 Low Temperature Fischer-Tropsch Processing	4
1.1.2 Oligomerization of Alkenes	5
1.1.3 Methanol Conversion, Coal Liquefaction and Natural Gas Conversion	5
1.2 The Oligomerization of Alkenes	5
1.3 Polymerization or Oligomerization Catalysts	6
1.4 Phosphoric Acids and Phosphates	9
1.4.1 Condensed Phosphoric Acids	10
1.5 Phosphoric Acid as a Catalyst	13
1.5.1 Phosphoric Acid as a Polymerization Catalyst	14
1.5.1.1 Solid Phosphoric Acid Catalyst (kieselguhr support)	16

1.6 Mechanism and Thermodynamics of Polymerization 17

1.6.1 Mechanism of Polymerization 17

1.6.1.1 Cationic Polymerization 17

1.6.1.2 Propene Oligomerization 19

1.6.1.3 Butene Oligomerization 22

1.6.2 Thermodynamics of Alkene Oligomerization 24

1.7 Reactors for Determining the Kinetics of Heterogeneous Catalytic Reactions 27

1.7.1 Background 27

1.7.2 Gradientless Reactors 29

1.7.2.1 Recycle Reactors 29

1.7.2.2 The Internal Recirculation Type Gradientless Reactor (Internal Recycle Reactor) 30

1.7.2.3 Examples of the Use of Gradientless Reactors to Obtain Kinetic Data 32

1.8 Objectives of the Present Study 33

2. MICRO-CATALYTIC PULSE REACTOR STUDIES 34

2.1 Introduction - Literature Review 34

2.1.1 Background 34

2.1.2 Pulse Reactor Types and Techniques 34

2.1.2.1 Elution with Reaction 35

2.1.2.2 Microcatalytic Technique 35

2.1.2.3 Deuterium Exchange 35

2.1.2.4 Reactor-Stop Technique 36

2.1.2.6 Sample Vacancy Technique 36

2.1.2.7 Heater Displacement Technique 36

2.1.3 Analysis of Pulse Reactor Data 36

2.1.3.1 Reactions of the Type $A \rightleftharpoons B$ 37

2.1.3.2 Reversible Reactions of the Type $A \rightleftharpoons B + C$ 37

2.1.3.3 Consecutive Reactions 37

2.1.4 Advantages and Disadvantages of the Pulse Technique 39

2.1.5 Applications of the Pulse Technique 40

2.2 Objectives of the Pulse Micro-Catalytic Studies 41

2.3 Experimental Apparatus and Procedure 42

2.3.1 The Pulse Technique Used in This Study 42

2.3.2 The Reactor System 42

2.3.3 Experimental Procedure and Analysis 45

2.3.3.1 Reaction Conditions 45

2.3.3.2 Typical Run Procedure 46

2.3.3.3 Phosphoric Acid Concentrations 47

2.3.3.4 Product Analyses 49

2.3.3.5 Reaction Data Workup 49

2.4 Reactor System Characterization 49

2.4.1 Gas Chromatograph Calibration 49

2.4.2 The Input and Output Pulse 52

2.4.3 Axial Pulse Dispersion 54

2.4.4 Single Slice Analysis 56

2.4.5 Mass Balance in Absence of Reaction 57

2.4.6 Reproducibility 57

2.4.7 Catalyst Activity and Lifetime 58

2.4.8 Differential Analysis 58

2.4.9 Equilibrium Conversions 58

2.4.9.1 Equilibrium Compositions of Straight Alkenes 60

2.4.9.2 Equilibrium Composition of C_4, C_5, C_6, C_7 and C_8 Alkene Groups 61

2.4.9.3 Equilibrium Compositions of a Combined C_4, C_5, C_6 and C_7 Alkene Group 61

2.4.9.4 Equilibrium Compositions of a Group of Alkanes 65

2.4.10 Determination of Phase Equilibria 66

2.5 Results and Discussion 68

2.5.1 Preliminary Results 68

2.5.1.1 Complete Analysis of Typical Pulse Experiment 68

2.5.2 Pure Propene results 72

2.5.2.1 Product Spectra 72

2.5.2.2 Reaction Pathways 73

2.5.2.3 Propene Rate-Concentration Data 77

2.5.3 Pure 2-Methyl-1-Pentene 78

2.5.3.1 Product Spectra 78

2.5.3.2 Reaction Mechanisms 79

2.5.3.3 2-Methyl-1-Pentene Rate-Concentration Data 83

2.5.4 Results for Various Other Hexene Isomers 83

2.5.5 Pure 1-Butene Results 84

2.5.5.1 Product Spectra 84

2.5.5.2 Reaction Mechanisms 85

2.5.5.3 Rate-Concentration Data for 1-Butene 88

2.5.6 Pure Iso-Butene Results 89

2.5.6.1 Product Spectra 89

2.5.6.2 Reaction Mechanisms 89

2.5.6.3 Rate-Concentration Data for Iso-Butene 92

2.5.7 Comparison of the Pure Feed Results 92

2.5.8 Propene + 2-Methyl-1-Pentene 93

2.5.8.1 Feed and Product Spectra 93

2.5.8.2 Reaction Mechanisms 95

2.5.9 Propene + 2-Methyl-2-Pentene 100

2.5.10 2-Methyl-1-Pentene + 1-Butene 100

2.5.10.1 Feed and Product Spectra 101

2.5.10.2 Reaction Mechanisms 102

2.5.11 2-Methyl-1-Pentene + Iso-Butene 104

2.5.11.1 Feed and Product Spectra 104

2.5.11.2 Reaction Mechanisms 105

2.5.12 Propene + 1-Butene 108

2.5.12.1 Feed and Product Spectra 108

2.5.12.2 Reaction Mechanisms 108

2.5.13 Propene + Iso-Butene 110

2.5.13.1 Feed and Product Spectra 111

2.5.13.2 Reaction Mechanisms 112

2.6 Conclusions 114

2.6.1 Oligomerization of Pure Olefins 114

2.6.2 Mixed Feeds Oligomerization 119

3. KINETIC STUDIES USING AN INTERNAL GAS RECIRCULATION REACTOR 120

3.1 Introduction 120

3.1.1 The Use of Gradientless Reactors to Obtain Intrinsic Kinetic Data 120

3.1.1.1 Residence Time Distribution Studies 121

3.1.1.2 Interphase Transport Effects 125

3.1.1.3 Intraparticular Diffusion Effects 127

3.1.1.4 Superficial Gas Velocities and the Recycle Ratio 130

3.1.2 The Modelling of Kinetic Data Obtained from Gradientless Reactors 132

3.1.2.1 Background to Kinetic Models 132

3.1.2.2 Building Kinetic Models 133

3.1.2.3 Solving and Analysing Kinetic Models 135

3.1.2.4 Tests for Model Accuracy 137

3.1.2.5 Use of Diagnostic Parameters 137

3.1.2.6 Empirical Modelling Techniques 138

3.1.2.7 Examples of Kinetic Studies and Modelling 138

3.1.3 Literature Review of Kinetic Studies on the Catalytic Polymerization Over Solid Phosphoric Acid 139

3.1.3.1 The Effect of Phosphoric Acid Concentration 142

3.1.3.2 The Effect of Space Velocity, Pressure and Olefin Concentrtion 143

3.1.3.3 The Effect of Temperature 143

3.1.3.4 The Effect of Feed Composition 143

3.1.3.5 The Effect of Process Variables on Product Yield and Quality 146

3.1.3.6 The Effect of Transport Resistances 147

3.2 Objectives of the Kinetic Studies 147

3.3 Experimental Apparatus and Procedure 148

3.3.1 The Reactor System 149

3.3.1.1 The Reactor System Used for the Residence Time Distribution Studies 149

3.3.1.2 The Reactor System Used for the Mass Transfer Studies (No Reaction) 150

3.3.1.3 The Reactor System Used for the Kinetic Studies 151

3.3.2 The Reactor 153

3.3.3 Experimental Procedure and Analysis 157

3.3.3.1 Residence Time Distribution Studies 157

3.3.3.2 Mass Transfer Studies 157

3.3.3.3 Kinetic Studies (and Mass Transfer with Reaction) 159

3.3.3.4 Product Analyses 162

3.3.3.5 Reaction Data Workup 162

3.4 Results 163

3.4.1 Reactor Characterization Without Reaction 163

3.4.1.1 Residence Time Distribution Studies 163

3.4.1.2 Interphase Mass Transfer Studies Using Napthalene 167

3.4.2 Reactor Characterization with Reaction 170

3.4.2.1 Detailed Analysis of a Typical Run 170

3.4.2.2 Mass Balance over the Reactor 175

3.4.2.3 Catalytic Activity of the Empty Reactor 176

3.4.2.4 Reproducibility and Steady State Behaviour of Experiments 176

3.4.2.5 Equilibrium Conversions and Phase Equilibria 179

3.4.2.6 Mass Transfer with Reaction 181

3.4.3 Preliminary Results 186

3.4.4 Propene Oligomerization Experiments 189

3.4.4.1 The Effect of Propene Concentration at 103% H_3PO_4 Concentration 190

3.4.4.2 The Effect of Propene Concentration at 114% H_3PO_4 Concentration 192

3.4.4.3 The Effect of Temperature at 111% H_3PO_4 Concentration 195

3.4.4.4 The Effect of Temperature at 102% H_3PO_4 198

3.4.4.5 The Effect of Ortho-Phosphoric Acid (H_3PO_4) Concentration Using a Pure Propene Feed 200

3.4.4.6 Low Conversion Experiments 202

3.4.5 1-Butene Oligomerization Experiments 202

3.4.5.1 The Effect of 1-Butene Concentration 204

3.4.5.2 The Effect of Temperature 205

3.4.5.3 The Effect of Acid Concentration 209

3.4.6 The Oligomerization of Iso-Butene 211

3.4.7 The Oligomerization of 1-Hexene 212

3.5 Discussion 214

3.5.1 The Residence Time Distribution Studies 214

3.5.2 Mass Transfer Studies 215

3.5.2.1 Mass Transfer Studies Using Napthalene 215

3.5.2.2 Intra-particular and Interphase Mass Transfer with Reaction 220

3.5.3 General Qualitative Findings 221

3.5.3.1 Propene Experiments 221

3.5.3.2 1-Butene and Iso-Butene Experiments 222

3.5.4 Simple Power Law Modeling of the Rate-Concentration Data 222

3.5.4.1 Modeling of the Propene Data 222

3.5.4.2 Modeling of the 1-Butene Data 230

3.5.5 Modeling of the Rate of Monomer Reaction and Rates of Product Formation 232

3.5.5.1 Modeling of the Propene Rate Data 232

3.5.5.2 Modeling of the 1-Butene Rate Data 254

3.6 Conclusions 266

4. ALKENE OLIGOMERIZATION REACTIONS OBER SOLID PHOSPHORIC ACID, USING A FIXED BED REACTOR 273

4.1 Introduction 273

4.1.1 Modelling the Behaviour of Fixed Bed Catalytic Reactors 275

4.2 Objectives of the Fixed Bed Reactor Studies 276

4.3 Experimental Apparatus and Procedure 277

4.3.1 The Reactor System 277

4.3.2 The Reactor 279

4.3.3 Experimental Procedure and Analysis 281

4.3.3.1 Run Procedure 281

4.3.3.2 Product Analyses 283

4.3.3.3 Reaction Data Workup 283

4.4 Results 284

4.4.1 Preliminary Results 284

4.4.1.1 Reproducibility of Experiments 284

4.4.1.2 Complete Analysis of a Typical Oligomerization Run 284

4.4.2 Propene Oligomerization 287

4.4.2.1 The Effect of H_3PO_4 Concentration 289

4.4.2.2 The Effect of Reaction Pressure 289

4.4.3 1-Butene Oligomerization 290

4.4.3.1 The Effect of H_3PO_4 Concentration 291

4.4.3.2 The Effect of Pressure 292

4.4.3.3 The Effect of Particle Size on Activity (Intra-particular Diffusion) and H_3PO_4 Concentration 293

4.4.4 Iso-Butene Oligomerization 293

4.5 Discussion 296

4.5.1 The Effects of Process Variables 296

4.5.2 Comparison of the Integral Reactor Results with those of the Internal Gas Recirculation Reactor 299

4.5.3 One Dimensional Analysis of the Integral Reactor 299

4.6 Conclusions 302

5. CONCLUDING REMARKS 305

REFERENCES 311

APPENDICES 328

Appendix A GC Method for Microcatalytic Pulse Analysis 329

Appendix B Equilibrium Conversion Data for Straight Chain Alkenes 330

Appendix C Equilibrium Conversion of C_5 and C_6 Alkenes 332

Appendix D Vapour Liquid Equilibria Determination 333

Appendix E GC Chromatogram of Typical Propene Oligomer Product 336

Appendix F Mass Spectrometer trace of Typical Oliomer Product 337

Appendix G Determination of Compressibility Factor, Z 338

Appendix H Product Spectra and Rate/Concentration data for Various Alkene Isomers 340

Appendix I GC Method for Gas Analysis 346

Appendix J One Dimensional Analysis of Fixed Bed Reactor 348

Appendix K Description of Procedures Followed By Mass Balance Program 352

Appendix L Optimised Solution of Kinetic Model 'A' of Section 3.4.5.1 360

Appendix M Experimental and Predicted Rates and Concentration Data for each of the Models of Section 3.5.5 364

LIST OF FIGURES

		PAGE
Figure 1.1	Flow Diagram of the SASOL Plants at Secunda	3
Figure 1.2	The H_3PO_4-H_2O System	11
Figure 1.3	Approximate Molecular Composition of Strong Phosphoric Acids in terms of the Number, n, of Phosphorus Atoms in the Molecule-ion.	12
Figure 1.4	Free Energy Change during Dimerization	24
Figure 1.5	Equilibrium Conversion for Propene Dimerization to 1-Hexene and trans-3-Methyl-2-Pentene	25
Figure 1.6	Free Energy Changes for the Polymerization of Propene	26
Figure 1.7	Standard Berty type Internal Recycle Reactor (Fixed Basket)	31
Figure 2.1	Schematic of Pulse Reactor System	43
Figure 2.2	Gas Sampling Valve used for the Pulse Experiments	45
Figure 2.3	H_3PO_4 Concentration as a Function of Water Vapour Pressure over the range 97% to 104% H_3PO_4	48
Figure 2.4	H_3PO_4 Concentration as a Function of Water Vapour Pressure over the range 100% to 108% H_3PO_4	48
Figure 2.5	Pulse: GC Calibration: Propene & Butenes	50
Figure 2.6	Pulse: GC Calibration: Hexenes	50
Figure 2.7	The Input & Output Pulses using a 2-Methyl-1-Pentene Feed	53
Figure 2.8	Output Pulse and Bed Residence Time using a 2-Methyl-1-Pentene Feed	53

Figure 2.9	Pulse: Output Curve (Propene Feed)	55
Figure 2.10	Pulse: Dispersion Test 2 (Propene Feed)	56
Figure 2.11	Equilibrium Data for Straight Alkenes at 433K	62
Figure 2.12	Equilibrium Data for Straight Alkenes at 458K	62
Figure 2.13	Equilibrium Data for Straight Alkenes at 483K	63
Figure 2.14	Equilibrium Data for Pentenes over the Temperature Range: 443K to 483K	63
Figure 2.15	Equilibrium Data for Hexenes over the Temperature Range of 433 to 493 K	64
Figure 2.16	Equilibrium Data for C_4, C_5, C_6 and C_7 Alkenes at 473K and between 0.1 and 100 bar	64
Figure 2.17	Phase Diagram for Feed and Product Mixture of Run No. 4 of Section 2.5.13	68
Figure 2.18	Pulse: Propene Product Spectra at 473 K and 1.54 MPa	73
Figure 2.19	Pulse: 2-Methyl-1-Pentene Product Spectrum at 473 K and 1.54 MPa	80
Figure 2.20	Pulse: Rate-Concentration Data - Hexenes	84
Figure 2.21	Pulse: 1-Butene Product Spectra at 473 K and 1.55 MPa	86
Figure 2.22	Pulse: Iso-Butene Product Spectra at 473 K and 1.53 MPa	90
Figure 2.23	Pulse: Rate-Concentration Data for Pure Feeds	93
Figure 2.24	Pulse: 2M1P + C_3: Product Spectra at 473 K and 1.55 MPa	96

Figure 2.25	Pulse: C_{12} (Product) vs 2M1P Concentration Taken from the Data of Table 2.12.	99
Figure 2.26	Pulse: 2M1P + 1-Butene: Product Spectra at 473 K and 1.53 MPa	102
Figure 2.27	Pulse: Iso-Butene + 2M1P: Product Spectra at 473 K and 1.54 MPa	105
Figure 2.28	Pulse: 1-Butene + Propene: Product Spectra at 473 K and 1.53 MPa	109
Figure 2.29	Pulse: Iso-Butene + Propene: Product Spectra at 473 K and 1.55 MPa	112
Figure 3.1	Schematic Diagram of the Tanks-in-Series Model	123
Figure 3.2	The Effectiveness Factor as a Function of the Parameter ML for Various Catalyst Shapes and for Volume Change during Reaction	128
Figure 3.3	Different Rate Controlling Regimes for Strongly Exothermic Reactions in Porous Catalysts	129
Figure 3.4	Different Rate Controlling Regimes for Strongly Exothermic Reactions in Porous Catalysts	129
Figure 3.5	Flow Device for Measuring Pressure Drop Versus Flowrate through the Bed in an Internal Recycle Reactor	131
Figure 3.6	Comparison of the Rate Constants of both Langlois & Walkey and Bethea & Karchmer at Equivalent Acid Concentrations	141
Figure 3.7	Bethea & Karchmer's Rate Constant as a Function of the Ortho-Phosphoric Acid Concentration	142
Figure 3.8	Arrhenius Plots of both Bethea & Karchmer and Langlois & Walkey	144

Figure 3.9	Rate Constant Correction Factor of McMahon et al.	145
Figure 3.10	A Comparison of the Observed and Predicted Rate Constants produced by McMahon et al.	146
Figure 3.11	Reactor System used for Residence Time Studies	149
Figure 3.12	The Reactor system used for the Mass Transfer Studies	150
Figure 3.13	Schematic of Internal Gas Recirculation Reactor System	152
Figure 3.14	The Internal Recycle Reactor Assembly	154
Figure 3.15	Detailed Diagram of Magnedrive Assembly	155
Figure 3.16	Calculation of Mass Transfer Coefficients	159
Figure 3.17	Mass Transfer Coefficients for Napthalene in Hydrogen: Basket Empty	168
Figure 3.18	Mass Transfer Coefficients for Napthalene in Hydrogen: Basket Full	169
Figure 3.19	Mass Transfer Coefficient as a Function of Pressure: Non-diffusing Component - Air	169
Figure 3.20	Typical Oligomerization Experiment Conversion and WHSV versus Time	172
Figure 3.21	Typical Oligomerization Experiment Reactor Temperature and Conversion as functions of time	172
Figure 3.22	Typical Oligomerization Experiment Liquid Product Concentration and Propene Conversion versus Time	173
Figure 3.23	Typical Oligomerization Experiment Rate of Propene Reaction and Conversion versus Time	174

Figure 3.24	Typical Oligomerization Experiment Water Dew Point in Feed versus Time on Stream	175
Figure 3.25	Steady State Behaviour of the Internal Recycle Reactor: The Effect of Controlling Acid Concentration	177
Figure 3.26	Internal Recycle Reactor Induction Period	180
Figure 3.27	Internal Recycle Reactor: Reproducibility	180
Figure 3.28	Internal Recycle Reactor: Reaction Rate versus Impeller Speed at 101.5% H_3PO_4 and 464 K	183
Figure 3.29	Internal Recycle Reactor: Reaction rate versus Impeller Speed at 114% H_3PO_4 and 478 K	183
Figure 3.30	Internal Recycle Reactor: Reaction Rate versus Particle Size at 464 K	184
Figure 3.31	Internal Recycle Reactor: Reaction Rate versus Particle Size at 114% H_3PO_4 and 503 K	184
Figure 3.32	The Effect of Hydration on Reaction Rates	188
Figure 3.33	The Effect of Hydration on Product Spectra	188
Figure 3.34	Rate of Propene Reaction as a Function of Propene Reactor Concentration at 103% H_3PO_4	192
Figure 3.35	Product Concentrations as Functions of the Propene Reactor Concentration at 103% H_3PO_4	193
Figure 3.36	Rate of Propene Reaction as a Function of the Propene Reactor Concentration at 114% H_3PO_4	194
Figure 3.37	Product Concentrations as Functions of the Propene Reactor Concentration at 114% H_3PO_4	194
Figure 3.38	Rate of Propene Reaction as a Function of Temperature at 111% H_3PO_4	197

Figure 3.39	Product Concentrations as functions of the Reactor Temperature at 111% H_3PO_4	197
Figure 3.40	Rate of Propene Reaction as a Function of Temperature at 102% H_3PO_4	199
Figure 3.41	Propene Product Concentrations as Functions of Reactor Temperature at 102% H_3PO_4	199
Figure 3.42	Rate of Propene Reaction as a Function of H_3PO_4 Concentration for a Pure Propene Feed	201
Figure 3.43	Propene Product Concentrations as Functions of H_3PO_4 Concentration for a Pure Propene Feed	201
Figure 3.44	The Effect of Conversion on Product Distribution for a Pure Propene Feed	203
Figure 3.45	Rate of 1-Butene Reaction as a Function of the 1-Butene Reactor Concentration	206
Figure 3.46	Product Concentrations as Functions of the 1-Butene Reactor Concentration	206
Figure 3.47	Rate of 1-Butene Reaction as a Function of Temperature at 103% H_3PO_4	208
Figure 3.48	Product Concentrations as Functions of the Reactor Temperature	208
Figure 3.49	Rate of 1-Butene Reaction as a Function of H_3PO_4 Concentration at 446.5 K	210
Figure 3.50	Product Concentrations as Functions of the H_3PO_4 Concentration	210
Figure 3.51	Typical Product Spectra from Iso-Butene Oligomerization Over Solid Phosphoric Acid	212
Figure 3.52	Typical Product Spectra from 1-Hexene Oligomerization Over Solid Phosphoric Acid	213

Figure 3.53 Simple Power Law Fit to Propene Rate/Concentration Data Obtained at 464 K and 103% H_3PO_4 223

Figure 3.54 Power Law Fit to Rate Constant vs H_3PO_4 concentration Data at 464 K for Propene Oligomerization 225

Figure 3.55 Arrhenius Type Plot of Rate Constant as a Function of Temperature for Propene Oligomerization at 102% H_3PO_4 225

Figure 3.56 Predicted and Experimental Propene Reaction Rates as Functions of Propene Concentration at 464 K and 114% H_3PO_4 227

Figure 3.57 Percentage Error Analysis as Determined from Predicted and Experimental Propene Reaction Rates as Functions of Propene Concentration at 464 K and 114% H_3PO_4 227

Figure 3.58 Predicted and Experimental Propene Reaction Rates as Functions of Reactor Temperature at 111% H_3PO_4 228

Figure 3.59 Percentage Error Analysis as Determined from Predicted and Experimental Propene Reaction Rates as Functions of Reactor Temperature at 111% H_3PO_4 229

Figure 3.60 Simple Power Law Fit to 1-Butene Rate/Concentration Data at 464 K and 103% H_3PO_4 231

Figure 3.61 Power Law Fit to Rate Constant vs H_3PO_4 Concentration for 1-Butene Oligomerization at 446.5 K 231

Figure 3.62 Arrhenius Type Plot of Rate Constant versus Reaction Temperature at 103% H_3PO_4 for 1-Butene Oligomerization 232

Figure 3.63 Model P1: Predicted and Experimental Product Concentrations as Functions of Propene Concentrations at 103% H_3PO_4 and 464 K 235

Figure 3.64 Model P1: Predicted and Experimental Reaction Rates as Functions of Propene Concentrations at 103% H_3PO_4 and 464 K 235

Figure 3.65 Model P2: Predicted and Experimental Product Concentrations as Functions of Propene Concentrations at 103% H_3PO_4 and 464 k 238

Figure 3.66 Model P2: Predicted and Experimental Reaction Rates as Functions of Propene Concentrations at 103% H_3PO_4 and 464 K

Figure 3.67 Model P3: Predicted and Experimental Product Concentrations as Functions of Propene Concentrations at 103% H_3PO_4 and 464 K 239

Figure 3.68 Model P3: Predicted and Experimental Reaction Rates as Functions of Propene Concentrations at 103% H_3PO_4 and 464 K 239

Figure 3.69 Model P4: Predicted and Experimental Product Concentrations as Functions of Propene Concentrations at 103% H_3PO_4 and 464 K 241

Figure 3.70 Model P4: Predicted and Experimental Reaction Rates as Functions of Propene Concentrations at 103% H_3PO_4 and 464 K 241

Figure 3.71 Percentage Error Analysis , as determined from the Predicted and Experimental Dimer Concentration, as functions of Propene Concentration at 464 K and 103% H_3PO_4 for Models P1, P2, P3 and P4 242

Figure 3.72 Percentage Error Analysis, as determined from the Predicted and Experimental Trimer Concentration, as Functions of Propene Concentration at 464 K and 103% H_3PO_4 for Models P1, P2, P3 and P4 243

Figure 3.73 Percentage Error Analysis, as determined from the Predicted and Experimental Tetramer Concentration, as functions of Propene Concentration at 464 K and 103% H_3PO_4 for Models P1, P2, P3 and P4 243

Figure 3.74 Percentage Error Analysis, as determined from the Predicted and Experimental Propene Rate, as functions of Propene Concentration at 464 K and 103% H_3PO_4 for Models P1, P2, P3 and P4 244

Figure 3.75 Percentage Error Analysis, as determined from the Predicted and Experimental Dimer Rate, as functions of Propene Concentration at 464 K and 103% H_3PO_4 for Models P1, P2, P3 and P4 244

Figure 3.76 Percentage Error Analysis , as determined from the Predicted and Experimental Trimer Rate, as functions of Propene Concentration at 464 K and 103% H_3PO_4 for Models P1, P2, P3 and P4 245

Figure 3.77 Percentage Error Analysis, as determined from the Predicted and Experimental Tetramer Rate, as functions of Propene Concentration at 464 K and 103% H_3PO_4 for Models P1, P2, P3 and P4 245

Figure 3.78 Predicted and Experimental Product Concentrations as functions of Propene Concentration at 464 K and 114% H_3PO_4 using Model P3 255

Figure 3.79 Predicted and Experimental Rates as functions of Propene Concentration at 464 K and 114% H_3PO_4 using Model P3 255

Figure 3.80 Predicted and Experimental Product Concentrations as functions of Propene Concentration at 464 K and 114% H_3PO_4 using Model P4 256

Figure 3.81 Predicted and Experimental Rates as Functions of Propene Concentration at 464 K and 114% H_3PO_4 using Model P4 256

Figure 3.82 Predicted and Experimental Product Concentrations as Functions of Reactor Temperature at 111% H_3PO_4 using Model P3 257

Figure 3.83 Predicted and Experimental Rates as functions of Reactor Temperature at 111% H_3PO_4 using Model P3 257

Figure 3.84	Predicted and Experimental Product Concentrations as functions of Reactor Temperature at 111% H_3PO_4 using Model P4	258
Figure 3.85	Predicted and Experimental Rates as functions of Reactor Temperature at 111% H_3PO_4 using Model P4	258
Figure 3.86	Model B4: Predicted and Experimental Product Concentrations as Functions of 1-Butene Concentration at 103% H_3PO_4 and 464 K	263
Figure 3.87	Model B4: Predicted and Experimental Reaction Rates as Functions of 1-Butene Concentrations at 103% H_3PO_4 and 464 K	263
Figure 3.88	Percentage Error Analysis, as determined from the Predicted and Experimental Concentration at 464 K and 103% H_3PO_4 for Model B4	264
Figure 4.1	Schematic of Fixed Bed Reactor System	278
Figure 4.2	Micro-reactor Developed by Snel	280
Figure 4.3	Schematic Layout of the Packed Small Reactor Volume	282
Figure 4.4	Integral Reactor Reproducibility Runs: 1-Butene Conversion as a Function of Time on Stream	285
Figure 4.5	Integral Reactor Reproducibility Runs: Catalyst Bed Temperature During the Run as a Function of Catalyst Bed Depth	285
Figure 4.6	1-Butene Conversionn and WHSV as Functions of Time on Stream	287
Figure 4.7	Product Spectra as a Function of Time on Stream for a Typical Oligomerization Experiment using a 1-Butene feed	288
Figure 4.8	Integral Reactor: Propene Oligomerization Product Spectrum Versus Time on Stream for Different Acid Concentrations	290

Figure 4.9	Integral reactor: Propene Oligomerization Product Spectrum Versus Time on Stream at Different Reactor Pressures	291
Figure 4.10	Integral reactor Runs: Iso-Butene Conversion as a Function of Time on Stream	295
Figure 4.11	Integral Reactor Runs: Iso-Butene Run C1 Accumulative Product Mass Versus Time on Stream	295
Figure 4.12	Integral Reactor Runs: Iso-Butene Run Nos. C1-C4 Mole Fractions of Dimer, Trimer and Tetramer	296
Figure E.1	GC Chromatogram of Typical Propene Oligomer Product	336
Figure F.1	Mass Spectrometer Trace of Typical Oligomer Product	337

LIST OF TABLES

		PAGE
Table 1.1	Product Selectivities of the SASOL Fixed Bed and Synthol Reactors	3
Table 1.2	Selected Properties of Liquid and Solid Products from SASOL Reactors	4
Table 1.3	The Relationship between the Cationic and Anionic Oxides in Phosphates	9
Table 1.4	Standard Free Energy Change (kcal) of Polymerization per Monomer Unit Added	26
Table 1.5	Summary of Laboratory Reactor Ratings	28
Table 2.1	Relative Response Factors of Hydrocarbons	51
Table 2.2	Product Spectra for analysis Points in Figure 2.9	54
Table 2.3	Product Spectra for Analysis Points in Figure 2.10	55
Table 2.4	Concentrations for Propene Reproducibility Tests	57
Table 2.5	Alkanes Used in the Equilibrium Calculation of Section 2.4.9.4	65
Table 2.6	Area Counts and Concentrations for a Typical Pulse	69
Table 2.7	Concentrations in the Reactor Exit	71
Table 2.8	Product Spectra for Pure Propene at 473 K and 1.54 MPa	72
Table 2.9	Averaged Reactor Concentrations of the Feed	73
Table 2.10	Pure Oligomer Fractions Prior to Cracking	77
Table 2.11	Rate Concentration Data for Pure propene	77

Table 2.12	Product Spectra for 2-Methyl-1-Pentene at 473 K and 1.54 MPa	79
Table 2.13	Averaged 2-Methyl-1-Pentene Concentration	79
Table 2.14	Estimated Molar Ratios of C_{12} to Cracked Products in Table 2.8 Based on the Results of Both Tables 2.8 and 2.12	81
Table 2.15	Rate Concentration Data for 2-Methyl-1-Pentene	83
Table 2.16	Reaction Orders for C_6 Isomer Polymerization	84
Table 2.17	Product Spectra for 1-Butene at 473 K and 1.55 MPa	85
Table 2.18	Average Reactor Concentrations of the Feed	85
Table 2.19	Rate-Concentration Data for 1-Butene	89
Table 2.20	Product Spectra for Iso-Butene at 473 K and 1.53 MPa	90
Table 2.21	Averaged Reactor Concentrations of the Feed	91
Table 2.22	Rate-Concentration Data for Iso-Butene	92
Table 2.23	Reactant Feed Concentrations at the Reactor Inlet at 473 K and 1.55 MPa	94
Table 2.24	Product Spectra at Reactor Exit	94
Table 2.25	Reactant's Reactor Concentrations and Conversion Levels	95
Table 2.26	Fraction of C_{12} Produced from $C_6 + C_6$ and $C_9 + C_3$	100
Table 2.27	Reactor Concentrations at the Reactor Inlet at 473 K and 1.53 MPa	101
Table 2.28	Product Spectra at the Reactor Exit	101

Table 2.29	Reactant Concentrations and Conversion Levels of Reactants	102
Table 2.30	Reactor Concentrations at the Reactor Inlet at 473 K and 1.54 MPa	105
Table 2.31	Product Spectra at the Reactor Exit	106
Table 2.32	Averaged Reactor Concentrations of the Reactants	106
Table 2.33	Reactant Concentrations at the Reactor Inlet at 473 K and 1.53 MPa	108
Table 2.34	Product Spectra at the Reactor Exit	109
Table 2.35	Averaged Reactor Concentrations of the Reactants	110
Table 2.36	Reactant concentrations at the Reactor Inlet at 473 K and 1.55 MPa	111
Table 2.37	Product Spectra at the Reactor Exit	111
Table 2.38	Averaged Reactor Concentrations and the Conversions of the Reactants	112
Table 3.1	Equivalent N (number of Tanks) for Various Mixing Speeds (One Parameter Model)	163
Table 3.2	Five Parameter Model Analysis for Varying Impeller speeds: Basket Empty	164
Table 3.3	Five Parameter Model Analysis for Varying Impeller Speeds: Basket Full	164
Table 3.4	N, the Number of Tanks in Series, for Various Flowrates (One Parameter Model)	166
Table 3.5	Five Parameter Model Analysis for Varying Flowrates: Basket Full	166
Table 3.6	Five Parameter Model Analysis of Varying Flowrates: Basket Empty	166

Table 3.7 N, Number of Tanks in Series, for Various Temperatures: Basket Empty 167

Table 3.8 Experimental Conditions for Typical Oligomerization Run of Section 3.4.2.1 171

Table 3.9 Water Balance Over the Internal Recirculation Reactor 178

Table 3.10 Experimental Conditions for Bulk Gas Phase Mass Transfer Experiments 182

Table 3.11 Experimental Conditions used for Intra-particular Diffusion Experiments 185

Table 3.12 Experimental Conditions Used to Examine the Effect of Catalyst Hydration on Reactor Behaviour 187

Table 3.13 Experimental Conditions Used to Determine the Effect of Varying Propene Concentration 190

Table 3.14 Internal Recycle Reactor: Product Reactor Concentrations and Rate of Propene Reaction as Functions of Propene reactor Concentrations at 103% H_3PO_4 191

Table 3.15 Internal Recycle Reactor: Product Reactor Concentrations and Rate of Propene Reaction as Functions of the Propene Reactor Concentration at 114% H_3PO_4 195

Table 3.16 Internal Recycle Reactor: Product Reactor Concentrations and Rate of Propene Reaction as Functions of Reaction Temperature at 111% H_3PO_4 196

Table 3.17 Internal Recycle Reactor: Product Reactor Concentration and Rate of Propene Disappearance as Functions of Reactor Temperature at 102% H_3PO_4 198

Table 3.18 Internal Recycle Reactor: Product Concentrations, Propene Concentrations and Reaction Rate as Functions of H_3PO_4 Concentration for a pure Propene Feed 200

Table 3.19 Product Spectra, Reaction Rate and Propene Concentration as Functions of Propene Conversion 202

Table 3.20 Conditions Used for the Oligomerization of 1-Butene 204

Table 3.21 Internal Recycle Reactor: Product Reactor Concentrations and Rate of 1-Butene Reaction as Functions of 1-Butene Concentrations 205

Table 3.22 Internal Recycle Reactor: Product Reactor Concentrations, 1-Butene Reactor Concentrations and Reaction Rates as Functions of Reactor Temperature 207

Table 3.23 Internal Recycle Reactor: Product Concentrations, Reaction Rates and 1-Butene Concentrations as Functions of H_3PO_4 Concentration 209

Table 3.24 Internal Recycle Reactor: Iso-Butene Product Spectra 212

Table 3.25 Internal recycle Reactor: 1-Hexene Product Spectra and Reaction Rate 213

Table 3.26 Conditions used to Obtain Superficial Gas Velocities for the Napthalene-air System 217

Table 3.27 Superficial Velocities Estimated from Various Pressure Drop Equations 219

Table 3.28 Superficial Gas Velocities Estimated from Mass Transfer Coefficients 219

Table 3.29 Predicted and Experimental Rates of Propene Reaction at 464 K and 114% H_3PO_4 226

Table 3.30 Predicted and Experimental Rates of Propene Reaction at 111% H_3PO_4 229

Table 3.31 The Average Percentage Deviation Lines for the error Analysis Plots of Both the Oligomer Concentrations and Rates of Reaction/Production for the Models P1 to P4 246

Table 3.32 The Calculated Rate Constants k_1, k_3, k_5 and k_9 of Model P3 at Various Temperatures Calculated from the Data of Table 3.17 249

Table 3.33 The Calculated Rate Constants k_1, k_3, k_5 and k_9 of Model P3 at Various H_3PO_4 Concentrations Calculated from the Data of Table 3.18 250

Table 3.34 The Calculated Rate Constants k_1, k_3, k_5 and k_9 of Model P4 at Various Temperatures Calculated from the Data of Table 3.17 251

Table 3.35 The Calculated Rate Constants k_1, k_3, k_7 and k_9 of Model P3 at Various H_3PO_4 Concentrations Calculated from the Data of Table 3.18 252

Table 3.36 Experimental and Predicted Concentration Data for 1-Butene Models B2 and B4 261

Table 3.37 Experimental and Predicted Rate Data for 1-Butene Models P2 and P4 262

Table 3.38 The Average Percentage Deviations for the Residual Analysis Plots for the Rates and Concentrations of Model B4 262

Table 3.39 The Calculated Rate Constants k_1, k_3 and k_5 of Model B4 as Calculated at the Conditions of the Experiments in Table 3.22 265

Table 3.40 The Rate Constants k_1, k_3, and k_5 of Model B4 at Various H_3PO_4 Concentrations calculated from the Data of Table 3.23 265

Table 4.1	Experimental Conditions for Typical Oligomerization Run of Section 4.4.1.2	286
Table 4.2	Experimental Conditions Used for Propene Oligomerization Experiments	288
Table 4.3	Propene Conversion and Liquid Product Oligomer Concentrations of Runs 1,3 and 4 of Section 4.4.2	289
Table 4.4	Propene Conversion and Liquid Product Oligomer Compositions of Runs P1, P2 and P4 of Section 4.4.2	290
Table 4.5	Experimental Conditions Used for 1-Butene Oligomerization Experiments	292
Table 4.6	1-Butene Conversion and Liquid Product Oligomer Concentrations of Runs B1 and B2 of Section 4.4.3	292
Table 4.7	1-Butene Conversion and Liquid Product Oligomer Concentrations of Runs B1 and B5 of Section 4.4.3	293
Table 4.8	1-Butene Conversion and Liquid Oligomer Concentrations of Runs B6 and B7 of Section 4.4.3	293
Table 4.9	Experimental Conditions Used for Iso-Butene Oligomerization Experiments	294
Table 4.10	Results of the One Dimensional Model Analysis for Propene Oligomerization at the Conditions Described for Run 1 in Table 4.2	301
Table B.1	Equilibrium Conversion Data for Straight Alkenes at 433 K	330
Table B.2	Equilibrium Conversion Data for Straight Alkenes at 458 K	330
Table B.3	Equilibrium Conversion Data for Straight Alkenes at 483 K	331
Table C.1	Equilibrium Conversion of a Group of C_5 Alkenes	332

Table C.2	Equilibrium Conversion of a Group of C_6 Alkenes	332
Table G.1	Second Virial Coefficients and Compressibility Factor for Propene-Nitrogen Mixture	339
Table H.1	Product Spectra for 2-Methyl-2-Pentene	340
Table H.2	2-Methyl-2-Pentene Rate/Concentration Data	340
Table H.3	Product Spectra for 3-Methyl-1-Pentene	341
Table H.4	3-Methyl-1-Pentene Rate/Concentration Data	341
Table H.5	Product Spectra for 3-Methyl-2-Pentene	342
Table H.6	3-Methyl-2-Pentene Rate/Concentration Data	342
Table H.7	Product Spectra for 4-Methyl-1-Pentene	343
Table H.8	4-Methyl-1-Pentene Rate/Concentration Data	343
Table H.9	Product Spectra for Cis-4-Methyl-2-Pentene	344
Table H.10	Cis-4-Methyl-2-Pentene Rate/Concentration Data	344
Table H.11	Product Spectra for 1-Hexene	345
Table H.12	1-Hexene Rate/Concentration Data	345
Table M.1	Experimental and Predicted Concentration Data for Propene Model P1	364
Table M.2	Experimental and Predicted Rate Data for Propene Model P1	365
Table M.3	Experimental and Predicted Concentration Data for Propene Model P2	365
Table M.4	Experimental and Predicted Rate Data for Propene Model P2	366

Table M.5 Experimental and Predicted Concentration Data for Propene Model P3 366

Table M.6 Experimental and Predicted Rate Data for Propene Model P3 367

Table M.7 Experimental and Predicted Concentration Data for Propene Model P4

Table M.8 Experimental and Predicted Rate Data for Propene Model P4 368

Table M.9 Experimental and Predicted Concentration Data for Propene Model B1 368

Table M.10 Experimental and Predicted Rate Data for Propene Model B1 369

Table M.11 Experimental and Predicted Concentration Data for Propene Model B2 369

Table M.12 Experimental and Predicted Rate Data for Propene Model B2 370

Table M.13 Experimental and Predicted Concentration Data at 464 K and 114% H_3PO_4 for Model P3 and the Data of Table 3.15 370

Table M.14 Experimental and Predicted Rate Data at 464 K and 114% H_3PO_4 for Model P3 and the Data of Table 3.15 371

Table M.15 Experimental and Predicted Concentration Data at 464 K and 114% H_3PO_4 for Model P4 and the Data of Table 3.15 371

Table M.16 Experimental and Predicted Rate Data at 464 K and 114% H_3PO_4 for Model P4 and the Data of Table 3.15 372

Table M.17 Experimental and Predicted Concentration Data at 111% H_3PO_4 for Model P3 and the Data of Table 3.16 372

Table M.18 Experimental and Predicted Rate Data at 111% H_3PO_4 for Model P3 and the Data of Table 3.16 373

Table M.19 Experimental and Predicted Concentration Data at 111% H_3PO_4 for Model P4 and the Data of Table 3.16. 373

Table M.20 Experimental and Predicted Rate Data at 111% H_3PO_4 for Model P4 and the Data of Table 3.16 374

NOMENCLATURE

CSTR - Continuous Stirred Tank Reactor

FID - Flame Ionisation Detector

GC - Gas Chromatograph

GSV - Gas Sampling Valve

Kc - Mass Transfer Coefficient

MTG - Methanol to Gasoline

MOGD - Mobil Olefins to Gasoline and Distillate

R - Recycle Ratio

RON - Research Octane Number

RRF - Relative Response Factor

SMM - Synthetic Mica-Montmorillonite

WHSV - Weight Hourly Space Velocity

1. INTRODUCTION

Large scale industrial use of catalysts originated in the mid-18th century with the introduction of the lead chamber process for the manufacture of sulphuric acid. While the need for a catalyst was recognized, the scientific basis for its chemical and kinetic action only came much later and this is a trend that persists to this day (Heinemann, 1981).

The potential of a catalyst to tailor, to some extent, the product spectrum of a reaction, has led to the large research effort in catalytic science this century. The reaction pathway, for example, may differ for catalyzed and non-catalyzed reactions (e.g., catalytic vs thermal cracking (Ryland et al., 1958)).

It was estimated that by 1981 over twenty percent of all industrial products had underlying catalytic steps in their manufacture (Heinemann, 1981). The great majority of catalytic processes are based on heterogeneous catalysis. Amongst these it is the heterogeneously catalyzed organic reactions that have come to dominate due to their wide application in the petroleum industry and, of these, catalytic cracking is by far the most important. After a major breakthrough in 1936, the first commercial cracking plant opened in 1937 and, over three decades later, half the total U.S. crude oil capacity was being cracked catalytically (Lloyd, 1972).

In the last few decades there has been more emphasis on novel catalysts that produce better products and product yields, and which can be used in existing or slightly modified equipment. The major reason for this trend lies in the escalating construction costs of industrial plants, with the concomitant increase in the financial risk of failure.

In 1902 it was found that methane was formed by passing mixtures of hydrogen and carbon monoxide over nickel and cobalt catalysts. In 1923, Franz Fischer and Hans Tropsch reported the conversion of carbon monoxide and hydrogen to hydrocarbon products using an alkylized iron catalyst (Dry, 1981). Thirteen years later the first four Fischer-Tropsch production plants were in operation, producing 200 000 tonnes of hydrocarbons per annum, but after World War II, production was severely cut back (Frohning et al., 1982).

It was the discovery of vast natural gas and crude oil reserves in the Middle East in the 1950's that caused a discontinuation of Fischer-

Tropsch processes (Jager, 1978). Several articles on the Fischer-Tropsch Synthesis process have been published (Frohning et al., 1982; Jager, 1978; Dry, 1981; Anderson 1956).

After South Africa's acquisition of the American and German Fischer-Tropsch process rights, the South African Coal, Oil and Gas Corporation Limited (SASOL) was formed in 1950. The first Sasol plant, SASOL 1, was commissioned in 1955. Since 1955 many changes have been made to the process which have stimulated the growth of the chemical process industries in this country (Hoogendoorn, 1982). The OPEC oil crisis in 1973 led to the design and building of two, much larger plants. These plants, called SASOL 2 and 3, were to concentrate primarily on the production of gasoline (Public Relations Department, SASOL, 1980).

Several reviews on the history of the SASOL process have been published (Hoogendoorn, 1982; Public Relations Department, SASOL, 1980). Some salient features of the SASOL process are discussed below.

Figure 1.1 is a simplified block flow diagram of the Secunda plants (Dry, 1981). The primary products are ethene, gasoline and diesel fuel (Dry, 1982b). A large amount of flexibility is allowed for in the product work-up. The overall gasoline to diesel ratio can be varied from about 10:1 to 1:1 (Dry, 1981). The Synthol reactors (Tables 1.1 and 1.2) produce high percentages of alkenes, and less than 50% of the Synthol reactor products fall into the gasoline and diesel fuel range. The remaining products are converted by methane reforming, wax cracking and the oligomerization of C_3 and C_4 alkenes. About one third of the total liquid fuel output is produced by alkene oligomerization over solid phosphoric acid in the CATPOLY process.

The gasoline from the Synthol reactors needs upgrading. This is done by isomerizing the C_5 and C_6 alkenes and platforming of the C_7 - C_{11} fraction. To obtain a leaded product with RON 93 (Brink & Swart, 1982) the primary product, gasoline, is blended with that from the products of oligomerization of the C_3 and C_4 alkenes. The viscosity of the diesel from oligomerization is too low and the fuel is too branched. After hydrogenation it yields a cetane number of 33-35. After blending with the Synthol diesel, this is marketed with a cetane number of 46 (Brink & Swart, 1982).

This diesel fuel has poorer density and viscosity characteristics than desired (Brink & Swart, 1982); nonetheless it conforms to the South

African standards. The low cetane value of this diesel fuel and, even more so, the poor density and viscosity characteristics, are of concern to SASOL.

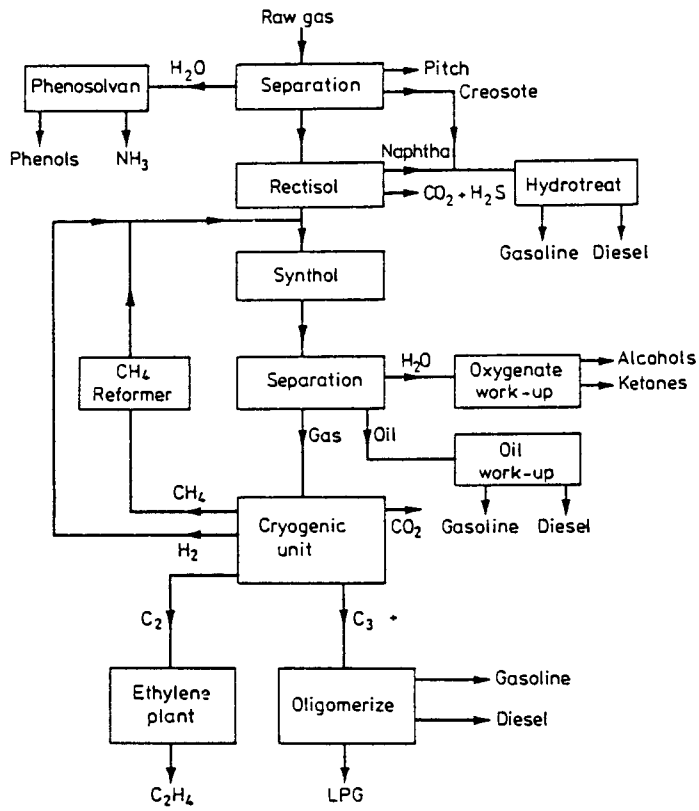

Figure 1.1 Flow diagram of the SASOL Plants at Secunda (Dry, 1981)

Table 1.1 Product selectivities of the SASOL fixed bed and Synthol reactors (Dry, 1981).

Product	Composition/% carbon atom	
	Fixed bed at 493 K	Synthol at 598 K
CH_4	2.0	10
C_2H_4	0.1	4
C_2H_6	1.8	4
C_3H_6	2.7	12
C_3H_8	1.7	2
C_4H_8	3.1	9
C_4H_{10}	1.9	2
C_5 to C_{11} (gasoline)	18	40
C_{12} to C_{18} (diesel)	14	7
C_{19} to C_{23}	7	
C_{24} to C_{35} (Medium Wax)	20	4
$>C_{35}$ (Hard Wax)	25	
Water soluble non-acid chemicals	3.0	5
Water soluble acids	0.2	1

Table 1.2 Selected properties of liquid and solid products from SASOL reactors (Dry, 1981).

Product Cut	Property	Fixed Bed[a]	Synthol[a]
Gasoline C_5—C_{11}	Olefins	32%	65%
	Paraffins	60%	14%
	Aromatics	0%	7%
	Alcohols	7%	6%
	Ketones	0.6%	6%
	Acids	0.4%	2%
	n-Paraffins	95%[b]	55%[b]
	RON (Pb free)	~35	88
Diesel C_{12}—C_{18}	Olefins	25%	73%
	Paraffins	65%	10%
	Aromatics	0%	10%
	Alcohols	6%	4%
	Ketones	<1%	2%
	Acids	0.05%	1%
	% n-Paraffins	93%[b]	60%[b]
	Cetane No	75	55
Medium Wax C_{24}—C_{35}	Olefins	10%	—

[a] wt. % of cut except for RON and cetane No
[b] % of the paraffins which are straight chained

1.1 ROUTES TO THE PRODUCTION OF LIQUID FUELS

As mentioned above the Sasol fuel has poor density and viscosity characteristics. The diesel to gasoline ratio does not satisfy the South African demand. It has however been shown, both theoretically and practically, that the diesel selectivity from a Fischer-Tropsch synthesis is limited by the Shultz-Flory distribution to less than about 25 % (Jager et al., 1982).

There are several routes to the production of liquid fuels. Some of these will be discussed very briefly.

1.1.1 Low Temperature Fischer-Tropsch Processing

This process would involve using the fixed or slurry bed Fischer-Tropsch reactors. The fixed bed Arge reactors can produce large quantities of good quality diesel (Tables 1.1 and 1.2). Diesel to gasoline volume ratios of between 3:1 and 6:1 with cetane numbers of approximately 65 are possible. The technology for this process is proven. SASOL, with experience from their SASOL 1 plant, have been considering this alternative (Dry, 1982a; Dry, 1982b; Jager et al., 1982).

Several catalysts have been proposed for changing the process selectively, but most indicate an ability to produce very low chain

length alkenes in the range C_2 to C_4 (Falbe et al., 1982; Hammer et al., 1982; Ballivet-Tkatchenko et al., 1982). Few of these catalysts produce good diesel selectivity (Gaube, 1983).

1.1.2 Oligomerization of Alkenes

This route is followed extensively by oligomerizing the alkenes (C_3 and C_4) over solid phosphoric acid in the CATPOLY process. The fuel quality (in the South African context) suffers from the drawbacks already mentioned above. A large research effort is at present being dedicated primarily to the use of alternative catalysts and also to a better understanding of the existing process. The development of ZSM-5 for Mobil's MOGD (Mobil olefins to gasoline and distillate fuels) process (Tabak, 1984a, b) is an example of the search for alternative catalysts.

1.1.3 Methanol Conversion, Coal Liquefaction and Natural Gas Conversion

Coal can be readily converted to methanol. Methanol can be converted to gasoline via the Mobil MTG (methanol to gasoline) process, (Kohll & Leonard, 1982; Garkisch & Gaensslen, 1982; Penick et al., 1978).

Although direct coal liquefaction is becoming an important alternative. ~~to gasification routes,~~ the liquid products contain large amounts of aromatics (Manudhane at al., 1982).

Natural gas deposits are largely methane and it is likely, in the foreseeable future, that methane will be converted to liquid fuels via the methanol route (MTG process) as is done in New Zealand.

1.2 THE OLIGOMERIZATION OF ALKENES

In the SASOL process potentially high value materials are converted into low value fuel products. The polymer products such as polyethylene, polypropylene, synthetic rubber, detergents, etc., are economically more valuable than liquid fuels. Internationally, alkenes are converted into a wide spectrum of chemical products, such as those mentioned above (Kirk & Othmer, 1951; Maddams, 1963). The SASOL process is, however, more important in the South African context. Use of the present feedstocks, natural gas and natural gas liquids, for alkene production might become increasingly expensive and limited (Quang et al., 1981). It is predicted that the heavy liquid fraction from crude oil cracking will become an important feedstock for alkene production (Klein, 1980) and hence the use of coal as a raw material is being investigated

(Janardanarao, 1980). The use of Fischer-Tropsch synthesis to produce low chain length alkenes is therefore of great importance. Many catalysts are being studied for this purpose (Falbe et al., 1982; Hammer et al., 1982; Ballivet-Tkatchenko et al., 1982; Murchison, 1981; Fraenkel & Gates, 1980).

There are other routes for alkene production. The Dow Chemical Corporation has developed a process (Stowe & Murchison, 1982) for converting aqueous phase Fischer-Tropsch products to LCA (low chain length alkenes) and another process produces alkenes from coal via methanol with very good selectivities (Inui & Yakegami, 1982; Inui et al., 1982).

The production of gasoline from alkenes began in 1931 (Oblad et al., 1958). These were non-catalytic thermal processes and were soon replaced by catalytic processes (McMahon et al., 1963). It was the rapid development of catalytic cracking, with its high yield of low molecular weight olefins, and the outbreak of World War II with its demands for high quality gasoline, that accelerated the pace of production of gasoline from alkenes (McMahon et al., 1963).

Ipatieff's work (Ipatieff et al., 1935) on the polymerization of olefins with liquid phosphoric acid led to the development of several commercial processes and catalysts. Phosphoric acid catalysts are by far the most prominent, solid phosphoric acid being the most important. The commercial catalysts include phosphoric acid on kieselguhr, copper pyrophosphate-charcoal and phosphoric acid-coated quartz chips (McMahon et al., 1963).
Ipatieff and other researchers carried out almost all of the early research on the polymerization of olefins and introduced several patents and possible mechanisms (Ipatieff, 1935a, b and c; Ipatieff & Corson, 1935; Ipatieff & Komarewsky, 1937; Whitmore, 1934a, b; Ipatieff et al., 1935; Ipatieff & Pines, 1935; Ipatieff & Pines, 1936; Ipatieff & Corson, 1936; Ipatieff & Schaad, 1938; Ipatieff & Corson, 1938; Ipatieff & Schaad, 1948; Ipatieff, 1934).

Some other catalysts used for oligomerizing alkenes include Friedel-Crafts type catalysts - aluminium chloride, boron hydrofluoride (Lachance & Eastham, 1976) as well as silica-aluminas, clays and zeolites (Pines, 1981). Organometallic catalysts are very active for the polymerization of ethene and propene (Doi et al., 1982) to high molecular weight compounds although the use of Ziegler type catalysts in conjunction with a cracking catalyst (i.e., supported on zeolites) could

conceivably yield products in the liquid fuels range. The products from these catalyst systems are of little use in the fuels industry. Alkene metathesis reactions (Banks, 1979) represent another route to possible formation of linear alkenes in the C_{12}-C_{16} range from propene and butene.

Of all these routes, acid catalyzed alkene oligomerization to liquid fuels is one of the most promising. This is evidenced by the large volumes of literature published in recent years. Active research has been carried out on the pentasil group zeolites (Naccache & Taarit, 1980) in order to impose shape selectivity by zeolites on reactions (Weisz, 1980; Weisz, 1973). Alkene reactions over many zeolites have been described (Norton, 1964; Lapidus et al., 1973; Fasol, 1983; Wolthuizen et al., 1980; Anderson et al., 1980; Fajula & Gault, 1981; Gati & Knözinger, 1972; Myers, 1970; Stul et al., 1983; Heinemann et al., 1983; Bercik et al., 1978; Swift & Black, 1974; Hattori et al., 1973; Haag, 1967).

ZSM-5, Ni-SMM and boralite, amongst others, have shown promise (Bercik et al., 1978; Occelli et al., 1985). ZSM-5 has been the focus of Mobil's research effort for several decades. This has resulted in their recent MOGD (Mobil Olefins to Gasoline and Distillate fuels) process which produces high quality diesel from propene and butene (Tabak, 1984a, b; Marsh et al., 1984; Tabak et al., 1985). The process can be operated in either the gasoline or "distillate" mode. This allows for a wide range of product flexibility. Gasoline to "distillate" ratios from 0.012 to greater than 100 are possible. The "distillate" after hydrotreating, has a cetane value of approximately 52.

Ni-SMM (a synthetic clay material) has been shown to oligomerize propene to products in the C_9 - C_{18} range. Due to its potential to produce high performance jet fuels and low pour hydraulic and transformer oils, research has been recently renewed into examining its potential in the production of diesel fuels (Jacobs, 1987; Bercik et al., 1978; Bercik, 1978; 1979).

1.3 POLYMERIZATION OR OLIGOMERIZATION CATALYSTS

Commercial alkene oligomerization to produce liquid fuels (gasoline) began in 1931 (Oblad et al., 1958). The first plants employed thermal oligomerization, but catalytic processes were introduced in 1935 (Ipatieff et al., 1935). The formation of low chain-length polymers from propene and butenes was commercialised to convert low chain-length

olefins, formed as a by-product of oil cracking operations to gasoline range hydrocarbons (Egloff & Heinert, 1951). These processes for producing polymer gasoline used acidic catalysts and gave complex mixtures of products, generally with a low selectivity to dimers. The reactions follow the carbonium ion mechanism, the acid catalyst transferring a proton to the olefin (Habeshaw, 1973). This mechanism (Whitmore, 1934a, b) can explain the products obtained but has difficulty predicting the final product composition, because the carbonium ions readily rearrange and undergo further reaction (Langlois, 1953). Progress in this field was accelerated by increasing availability of gaseous alkenes from catalytic cracking and during World War II hydrogenated oligomer gasoline was used in aviation fuel.

Catalysts used in polymerization are predominantly acid catalysts, solid phosphoric acid being commercially the most prominent. It is preferred to liquid phosphoric acid since it is less corrosive. Most of the early work on these catalysts was carried out by V. N. Ipatieff and co-workers (Ipatieff et al., 1935; Ipatieff, 1935a, b and c, Ipatieff & Corson, 1935; Ipatieff & Schaad, 1938; Ipatieff & Komarewsky, 1937; Ipatieff & Pines, 1935; Ipatieff & Pines, 1936; Ipatieff & Corson, 1936; Ipatieff & Corson, 1938; Ipatieff & Schaad, 1948; Ipatieff, 1934).

Catalytic polymerization can be classified as being either free radical or ionic in nature and ionic polymerization can be further subdivided into cationic or anionic (Oblad et al., 1958). Peroxides and other sources of free radicals are catalysts for free radical polymerization. Anionic polymerization catalysts are basic materials such as metallic sodium. Cationic catalysts include acids such as sulphuric acid, solid oxides such as alumina-silica and Friedel-Crafts catalysts such as aluminium chloride. It is their ability to act as strong acids that gives rise to their catalytic activity for polymerization. In the theory of cationic polymerization the catalyst is regarded as a strong acid of the Brönsted type, i.e., a proton containing acid.

Commercially the most common acid catalysts are sulphuric acid and phosphoric acids and phosphates (Oblad et al., 1958). Friedel-Crafts type catalysts such as aluminium chloride and boron trifluoride (Lachance & Eastham, 1976) with HCl or H_2O as promoters, zinc chloride, titanium chloride, synthetic silica aluminas (Oblad et al., 1958) and zeolites (Pines, 1981) are sometimes used.

Metals and metal containing catalysts are sometimes used particularly in the polymerization of acetylenes, diolefins and ethylene. Organometallic

catalysts such as $TiCl_4$-$Al(C_2H_5)_3$ are very active for the polymerization of ethene and propene (Doi et al., 1982) to high molecular weight compounds.

One of the most actively studied polymerization catalyst groups in recent years is the zeolites, in particular those of the pentasil group (Naccache & Taarit, 1980). Gaseous alkene reactions (isomerization and oligomerization) have been described over zeolites A and X (Norton, 1964; Lapidus et al., 1973), zeolite Y (Lapidus et al., 1973; Fasol, 1983), ZSM-5 (Holthuizen et al., 1980; Anderson et al., 1980), mordenite (Fajula & Gault, 1981; Rautenbach, 1986), alumina (Gati & Knözinger, 1972; Myers 1970), montmorillonite (Stul et al., 1983), synthetic clays (Heinemann et al, 1983; Bercik et al., 1978; Swift & Black, 1974; Hattori et al., 1973; Fletcher, 1984) and cationic exchange resins (Haag, 1967; Schumann, 1983).

1.4 PHOSPHORIC ACIDS AND PHOSPHATES

All phosphates can be represented stoichiometrically as combinations of oxides. The ratio of cationic oxides (R) to anionic oxides (P_2O_5) determines the type of phosphate. If the mole ratio of the cationic to anionic oxide is three, the substance is an orthophosphate. If it lies between one and two, the substance is a polyphosphate and in a pyrophosphate the ratio is exactly two. A ratio of exactly unity gives a metaphosphate. If the ratio lies between zero and unity, the substance is an ultraphosphate (Van Wazer, 1953). This relationship is tabulated in Table 1.3 (which is arranged in order of increasing R) along with the

Table 1.3 The relationship between the cationic and anionic oxides in phosphates.

Oxide ratio, R[a]	Name	General formula of normal sodium salt	Structures
Condensed			
0	Phosphorus pentoxide	$(P_2O_5)_n$	P_4O_{10} molecules or continuous structures
Between 0 and 1	Ultraphosphates	$(xNa_2O)P_2O_5$ for $0 < x < 1$	Interconnected chains and/or rings
1	Metaphosphates	$Na_n(PO_3)_n$ $n = 3, 4, \ldots$	Rings (or extremely long chains)
Between 1 and 2	Polyphosphates	$Na_{n+2}P_nO_{3n+1}$ $n = 2, 3, 4, 5, \ldots$	Chains
2	Pyrophosphate	$Na_4P_2O_7$	Two phosphorus atoms
Between 2 and 3	Mixtures of pyro- and orthophosphates	—	—
Simple Structures			
3	Orthophosphate	Na_3PO_4	One phosphorus atom
> 3	Orthophosphate + metal oxide (including double salts and solid solutions)	—	—

[a] $(Na_2O + H_2O_{compn.} + CaO + \ldots)/P_2O_5$.

general chemical formulas of the various phosphates of normal sodium salt. Metaphosphoric acid referred to in the early literature is no longer recognized as a definite compound (McMahon et al., 1963).

Orthophosphoric acid, H_3PO_4, is a tribasic acid, strong as regards the first dissociation, moderately weak as regards the second and very weak as regards the third (Van Wazer, 1953). The ionization constants at 298 K are $K_1=.75x10^{-2}$, $K_2=0.6x10^{-7}$ and $K_3=3x10^{-13}$. Pure 100% orthophosphoric acid is a white crystalline solid (monodinic) that melts at 315.4 K to a syrupy liquid which has a tendency to supercool. Physical measurements indicate considerable hydrogen-bond formation in orthophosphoric acid (Simon & Schultz, 1939). There is also a crystalline semihydrate of orthophosphoric acid, $H_3PO_4 \cdot \frac{1}{2}H_2O$, which melts at 302.3 K. The phase diagram of the system H_3PO_4-H_2O up to 100% H_3PO_4 is given in Figure 1.2. Because of supercooling, phosphoric acid solutions will often remain liquid at much lower temperatures than those shown in Figure 1.2. The density, heat capacity, boiling point, electrical conductivity and refractive index of orthophosphoric acid solutions of various concentrations are given by Monsanto Chemical Company (1946) and Van Wazer (1953). Vapour pressure and viscosity data of phosphoric acid solutions are also given as functions of temperature.

Phosphoric acid is chemically quite inactive at room temperature (Van Wazer, 1953). For this reason it is sometimes used as a substitute for sulphuric acid when the oxidizing properties of the latter are not wanted. The reduction of phosphoric acid by strong reducing agents such as hydrogen or carbon does not occur at a measurable rate at temperatures below 523-673 K. At higher temperatures phosphoric acid is fairly reactive towards most metals and their oxides. A list of many forms of sodium and calcium orthophosphates is given by Van Wazer (1953).

1.4.1 Condensed Phosphoric Acids

A series of acids having a H_2O: P_2O_5 mole ratio of less than three can be prepared by heating mixtures of phosphorus pentoxide with orthophosphoric acid and/or water. By boiling orthophosphoric acid, water can be evaporated until an azeotropic mixture is formed. The azeotrope varies from 91.1 to 92.1% P_2O_5 (pure H_3PO_4 contains 72.4% P_2O_5) as the system pressure increases from 101 to 753 mm Hg (Tarbutton & Deming, 1950). The corresponding boiling points range from 967 to 1142 K. The vapour pressures corresponding to the various compositions of phosphoric acids are given by the following equation:

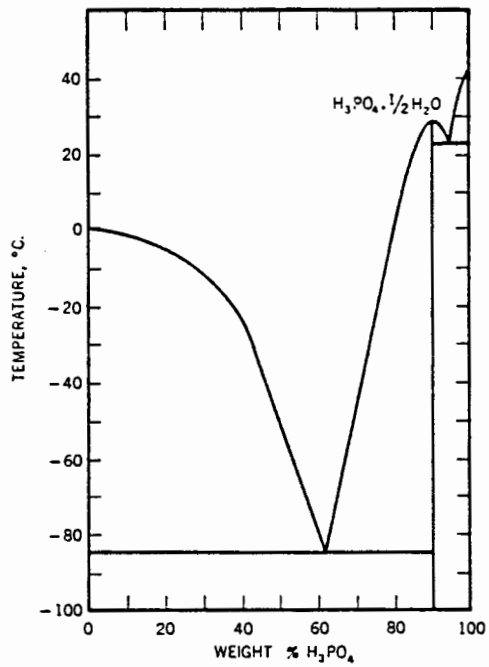

Figure 1.2 H_3PO_4-H_2O system

$$\text{Log}_{10}\ P_{mm} = 8.61 - \frac{(\%P_2O_5 - 60)^2/0.268 + 2450}{T}$$

where $\%P_2O_5$ lies between 60 and 95. The boiling point and composition of vapour over the boiling acid are given by Van Wazer (1953) as functions of the acid composition. Variation of the heat vapourization with composition of the acid is also given by Van Wazer.

The best known of these condensed acids is pyrophosphoric acid, $H_4P_2O_7$ which has a melting point of 334 K. Once melted pyrophosphoric acid is very difficult to recrystalize and can take up to several months to solidify at room temperature. This is due to the decomposition of the pyrophosphoric acid upon melting (Bell, 1948; Durgin et al., 1937; Van Wazer, 1953). Upon melting, pyrophosphoric acid dissociates into a mixture which contains orthophosphoric acid and some polyphosphoric acids. According to Van Wazer (1953) this is probably attributable to the close similarity between the hydrogen-oxygen and phosphorus-oxygen bonds.

The acids obtained by boiling orthophosphoric acid or adding phosphorus pentoxide to it, or by melting crystalline phosphoric acid, all belong to a continuous group of amorphous condensed phosphoric acid mixtures, which extend from pure phosphorus pentoxide to orthophosphoric acid. Figure 1.3 shows how the orthophosphoric acid fraction decreases as the total composition is removed from that equivalent to H_3PO_4 (between the ortho and pyro compositions).

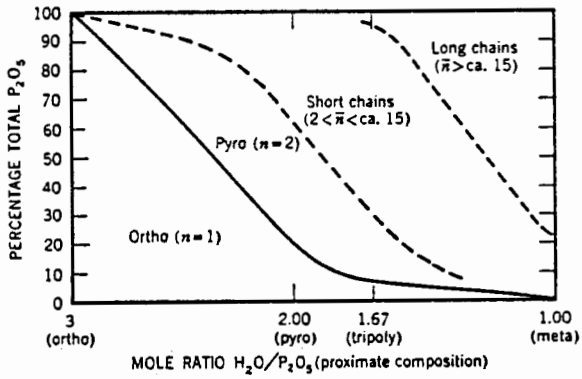

Figure 1.3 Approximate molecular composition of strong phosphoric acids in terms of the number, n, of phosphorus atoms in the molecule-ion.

There appears to be an equilibrium composition mixture of chain phosphoric acids corresponding to every given ratio of H_2O and P_2O_5 in these amorphous compositions. In the range from 72 to 82% P_2O_5 the acids have an oily appearance; in the range from 82 to 89% P_2O_5 they progress through tar and taffy like stages; and above 90% P_2O_5 they are brittle glasses.

When any of the condensed phosphoric acids are dissolved in water, hydrolysis to orthophosphoric acid takes place. The rate of hydrolysis is externally dependent upon temperature. At 298 K the half-life for the formation of orthophosphoric acid from the condensed form is a matter of days, whereas at 373 K the half-life is measured in minutes. Because of the reasonably long life at room temperature, the condensed phosphoric acids can be studied in aqueous solution at room temperature.

In the manufacture of phosphoric acid from elemental phosphorus three steps are involved:

1. Burning of the phosphorus
2. Hydration of the resulting phosphorus pentoxide
3. Collection of the mists formed

In most plants the elemental phosphorus is burned as a liquid. Corrosion is a serious problem in all installations. Details and operating data from a phosphoric acid plant are given by Striplin (1948).

The oldest and most economical method for making crude phosphoric acid is to treat phosphate rock with sulphuric acid, thereby precipitating calcium sulphate and releasing phosphoric acid. (This is known as the wet process.) The phosphoric acid obtained in this way must be purified.

Van Wazer (1953) has described a method for determining the total P_2O_5 in any phosphate. Another method is that of the AOAC (1950).

1.5 PHOSPHORIC ACID AS A CATALYST

Catalytically, phosphoric acid has been used principally for the polymerization of C_3 and C_4 olefins (Langlois, 1953). In this regard the great majority of all commercial polymerization units in the petroleum industry utilize phosphoric acid as a catalyst (Oblad et al., 1958; McMahon et al., 1963). The most widely used form is the extruded form of the calcined phosphoric acid and kieselguhr composite developed by Universal Oil Products Company. Several examples of its use have been described (Deeter, 1950; Egloff & Weinert, 1951; Ipatieff & Corson, 1936, 1938; Ipatieff et al, 1935).

Phosphoric acid, in several forms, can be employed catalytically in a large number of reactions other than the polymerization of olefins. There are many patents covering the use of various phosphates as catalysts in the vapour phase hydration of olefins, with steam, to the corresponding alcohols. A list of such patent numbers is given by Dunstan & Howes (1936).

One field of organic chemistry in which phosphoric acid, as a catalyst, finds application is the alkylation of aromatic hydrocarbons by olefinic hydrocarbons to produce compounds of a mixed alkyl-aryl character (Ipatieff, 1935 b). One such reaction involves the formation of isopropyl benzol by the treatment of benzol with propene according to the following reaction:

$$C_6H_6 + C_3H_6 \rightleftharpoons C_6H_5 \cdot C_3H_7$$

Phosphoric acid can also be used to cause condensation reactions between either ethers or alcohols and aromatic hydrocarbons in which water is primarily split off to yield olefins. Phosphoric acid may also be used with olefins in the alkylation of ring compounds containing substituent groups, notably phenols and amines. Phosphoric acid catalysts in essentially solid form can also be used in isomerization reactions. Various phenolic ethers, for example, can be isomerized to the corresponding alkylated phenols. Another application is the manufacture of acid esters from olefins and aliphatic carboxyllic acids according to the following reaction type:

$$CH_3COOH + C_4H_8 \rightleftharpoons CH_3COOC_4H_9$$

Other examples include miscellaneous types of dehydration reactions upon aliphatic hydroxy compounds.

An important application involves the treatment of cracked gasoline vapours (Ipatieff, 1935b). By using properly prepared and sized phosphoric acid-absorbent granules as filler in treating towers, and temperatures and pressures common to the fractionaters of cracking plants (366 K to 473 K and .71 MPa to 2.03 MPa), the olefinic constituents of these gas mixtures may be selectively polymerized, either in one, or several stages. The gum-forming olefins, which would otherwise appear in the gasoline from the plant, are converted to high boiling materials which are left behind as bottom reflux in the final fractionating step. A certain proportion of the normally gaseous mono-olefins present is polymerized to form gasoline boiling range liquids of superior anti-knock value. In this way, both yield and quality of the gasoline from the cracking process is improved (Ipatieff, 1935b).

The examples given above are only some of the many possible catalytic uses of phosphoric acid.

1.5.1 Phosphoric Acid as a Polymerization Catalyst

As already mentioned, catalytically, phosphoric acid has been used principally as a polymerization catalyst in the polymerization of C_3 and C_4 olefins (Langlois, 1953). It has been employed commercially in three different forms (Langlois, 1953).

1. A catalyst consisting of a thin film of phosphoric acid supported on fine quartz sand.
2. A calcined composite of phosphoric acid and kieselguhr.
3. A copper pyrophosphate composition which apparently owes its activity to a partial conversion to free phosphoric acid.

The calcined composite of phosphoric acid and kieselguhr is the most active of the catalysts used in polymerization and has the greatest active surface area (Jones, 1956). This process has been described in detail by Egloff & Weinert (1951).

Although there may still be some units using the copper pyrophosphate catalyst, its lower activity for the conversion of propene and 2-butene, which are made in greater quantities by catalytic-cracking units than by thermal crackers, has caused many of these units to be converted to the solid phosphoric acid catalyst (Jones, 1956). This process is described

by Steffens et al. (1949). The process was patented by Polymerization Process Corporation. Its use was almost exclusively for non-selective polymerization (Sherwood, 1957). Steffens et al. (1949) studied the effect of process variables on performance over copper pyrophosphate catalyst.

Since the start of commercial polymerization, liquid phosphoric acid on various supports has been tried, but none has been as successful as the solid phosphoric type (kieselguhr) (Jones, 1956). In 1937 a commercial sized unit using liquid phosphoric acid on quartz was built (Langlois & Walkey, 1951). The advantages of this catalyst are low cost, widespread commercial availability, simplicity of regeneration, high mechanical strength and ready adaptability to a variety of feedstocks and types of service (Langlois & Walkey, 1951). In this process the catalyst is made inside the reaction zone by placing the support (quartz) in the reactor, filling the reactor with liquid phosphoric acid and then draining off the excess acid, prior to the introduction of the feed. The catalyst is replaced by washing off the acid layer and recoating the retained quartz particles in situ (Sherwood, 1957). The catalyst can be used over a wide range of pressure, temperature and water content of the feedstock. Accidental overhydration does no permanent damage to the catalyst (Langlois & Walkey, 1951), but ammonia and amines are poisons. Due to the small surface area of the catalyst support employed, relatively large reactor sections are required for a given polymer product (Jones, 1956).

Ipatieff (1935a) used 100% liquid phosphoric acid to polymerize both propene and butene (Ipatieff & Corson, 1935a) at a temperatures of up to 477 K and pressures up to 5.06 MPa. Ipatieff & Pines (1936) polymerized propene at 605 K to 644 K in the presence of 90% phosphoric acid and with an initial reactor pressure of 82 atm. Investigators at the Massacuesetts Institute of Technology examined polymerization using liquid phosphoric acid (10 to 30%) (Monroe & Gilliland, 1938). They found that the percentage of higher boiling products increased with increasing conversion. Investigators at I.G. Farbersindustrie (I.G. Farbensindustrie Report) examined the polymerization of propene using concentrated liquid phosphoric acid at 4.05 MPa and 473 K. In agreement with Ipatieff, they found that the molecular weight of the polymer could be varied by varying the acid strength and adding certain metallic salts to the phosphoric acid. Bethea and Karchmer (1956) examined the polymerization of propene using liquid phosphoric acid over a wide range of temperatures, pressures and acid concentrations. Dunstan and Howes

(1936) investigated the polymerization action of phosphoric acid and some of its salts.

1.5.1.1 Solid phosphoric acid catalyst (kieselguhr support)

These catalysts are produced by a series of relatively simple steps comprising (Ipatieff, patent, 1935b): mixing a liquid phosphoric acid and adsorbent material (kieselguhr) in selected proportions, heating at temperatures of about 453 K to 493 K, followed by grinding and sizing to produce particles of the desired size. The temperatures employed in the mixing step can range from 393 K to 453 K. In this range the acid is fluid enough to enable rapid mixing by mechanical devices. The calcination temperatures can range from 453 K to 573 K without damaging the structure, strength or catalytic efficiency of the particles produced. The calcination step renders the catalyst solid. Depending on the calcination temperatures, the calcining period can last from 20 hours up to 60 hours (Ipatieff, 1935b). The catalyst consists of white or grey cylindrical-shaped pellets. It is hard when dry, but is extremely hygroscopic.

These catalysts are poisoned by alkaline materials in the reactor feed. The most commonly encountered poisons of this type are ammonia and combined organic nitrogen compounds of a basic nature. Neither oxygen nor butadiene are classified as catalyst poisons, but their presence in the feed has a deleterious effect on the catalyst life. The presence of oxygen results in the formation of long-chained polymers, boiling much above the gasoline-distillation range. This heavy polymer, or tar, remains on the catalyst, coating the surfaces and plugging the catalyst voids. Butadiene over-polymerizes to tar (Jones, 1956). Most dienes and acetylenes produce a similar result. Sulphur is a temporary poison (United Catalysts Inc., operating instructions).

Operating variables of importance include catalyst acid strength, reaction temperature, pressure, contact time and feedstock composition. These variables control both the extent of conversion and the quality and composition of the polymer and are discussed in more detail in Section 3.1.3. The kinetics of olefin oligomerization and polymerization have been studied by Bethea & Karchmer (1956) using liquid phosphoric acid, Langlois & Walkey (1951) using liquid phosphoric acid on quartz, and Friedman & Pinder (1971) using solid phosphoric acid. The kinetics are described in detail in Section 3.1.5.

Descriptions of the industrial process have been given by McMahon et al. (1963), Egloff & Weinert (1951), Sachanen (1940), Jones (1956) and Oblad et al.(1958).

1.6 MECHANISM AND THERMODYNAMICS OF POLYMERIZATION

1.6.1 Mechanism of Polymerization

Catalytic polymerization reactions are classified as either free radical or ionic mechanisms. Ionic mechanisms are further subdivided into cationic or anionic polymerization.

Examples of free radical catalysts are peroxides. Anionic catalysts are basic substances such as metallic sodium. These catalysts readily dimerize propene to a mixture of double bond isomers of 2-methyl-pentene at 423-473 K and 7-35 MPa (Germain, 1969). In this reaction the carbanium dimer is unstable and in an alkene environment the reaction is highly selective for dimers.

1.6.1.1 Cationic polymerization

Examples of various catalysts in this group are:

TYPE	EXAMPLE	CHEMICAL
Acids	Phosphoric acid	H_3PO_4
Solid oxides	Silica-alumina	SiO_2 - Al_2O_3
Friedel Crafts	Aluminium chloride	$AlCl_3$

All these catalysts are acidic in the Brönsted sense. The nature of the Brönsted acid is dependent on the so called co-catalyst in the case of Friedel-Crafts and solid oxide catalysts.

Catalyst:	$AlCl_3$	SiO_2 - Al_2O_3
Co-catalyst:	HCl	H_2O
Idealized Brönsted acid:	$(H^+)(AlCl_4^-)$	$(H^+)(Al(-O-Si)_4^-)$

It was shown by Ipatieff and Grosse (1936) that in the polymerization of ethene over $AlCl_3$, H_2O or HCl is essential for polymerization activity. Similarly, with other catalysts, the Brönsted acid forming co-catalyst is essential for catalyst activity. These catalysts can all generate carbonium ions in alkenes by adding the proton from the acid to the extra electron pair in the double bond (pi electrons). From calculations of proton affinities of C-atoms in the double bond, Evans and Polanyi

(1947) have shown that the proton will add to the end carbon atom, thus obeying Markownikoff's rule in the formation of the carbonium ion.

Thus: $H^+ + C{=}C{-}C \longrightarrow C{-}C^+{-}C$

The carbonium ion so generated may add to another alkene, forming a higher molecular weight carbonium ion. This, in turn, can either add to further alkenes, or yield its corresponding alkenic polymer by elimination (usually of a proton). According to McMahon et al., (1963) five basic carbonium ion reactions summarize polymerization reactions.

1. The carbonium ion may add to an olefin to form a carbonium ion of higher molecular weight, or the carbonium ion may decompose to form a smaller carbonium ion and an olefin.
2. The carbonium ion may isomerize by migration of a proton. Tertiary carbonium ions are more stable than secondary ions which, in turn, are more stable than primary ions.
3. The carbonium ion may isomerize by migration of a methyl group.
4. A hydride ion may be abstracted from another molecule or from another carbonium ion.
5. The carbonium ion may eliminate a proton, forming an olefin.

In addition to polymerization, carbonium ions can also -

- Lose a proton either (i) to the catalyst, so regenerating the acid, or (ii) by transfer to another alkene generating a new carbonium ion.
- Add a hydride ion by transfer from a hydrocarbon.
- Cause a hydrocarbon to crack.
- Cause a hydrocarbon to isomerize.
- Lose a hydride ion to become a 'double carbonium ion'. This may cause further reactions such as cyclization to occur.
- After cyclization, the hydrogen thus generated may be used in saturating other alkenes.

Thus the products of 'polymerization' reactions will be complex mixtures which may include alkanes, alkenes, aromatics and other cyclic compounds. In addition to these products the catalyst becomes covered in a layer of coke (a black, amorphous, organic substance of low hydrogen content). Due to the extremely complex nature of the products, the term polymerization must be used with some qualification. Schmerling & Ipatieff (1950) proposed the following definitions:

True polymerization - yields products which consist of alkenes with molecular weights which are integral multiples of the monomer alkene.

Conjunct polymerization - yields a complex mixture of alkanes, alkenes, alkadienes, cyclo-alkanes and alkenes, and aromatics with the number of carbon atoms not corresponding to integral multiples of the monomer.

Copolymerization - inter- or cross polymerization of two or more different alkenes.

With regard to the above definitions, the term oligomerization will be used in this work to encompass the overall process occurring during a reaction of the type involved when propene reacts over solid phosphoric acid catalyst. This is largely true polymerization with some conjunct polymerization. Also intended by oligomerization is that the polymers (oligomers) so formed consist of only several monomer units (Germain, 1969).

1.6.1.2 Propene oligomerization

Proton addition to the olefin proceeds in a manner which gives the more stable (secondary) rather than the less stable (primary) carbonium ions (Hart, 1964; McMahon et al., 1963).

An isopropyl carbonium ion can react with a molecule of propene to give a dimeric ion which can loose a proton, in either of two ways, to form simple propene dimer (McMahon et al., 1963).

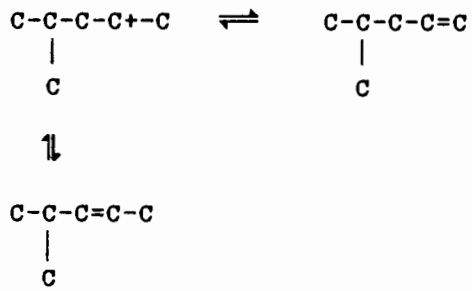

McMahon et al. (1963) have noted that the dimeric ion may rearrange before elimination of a proton according to the following:

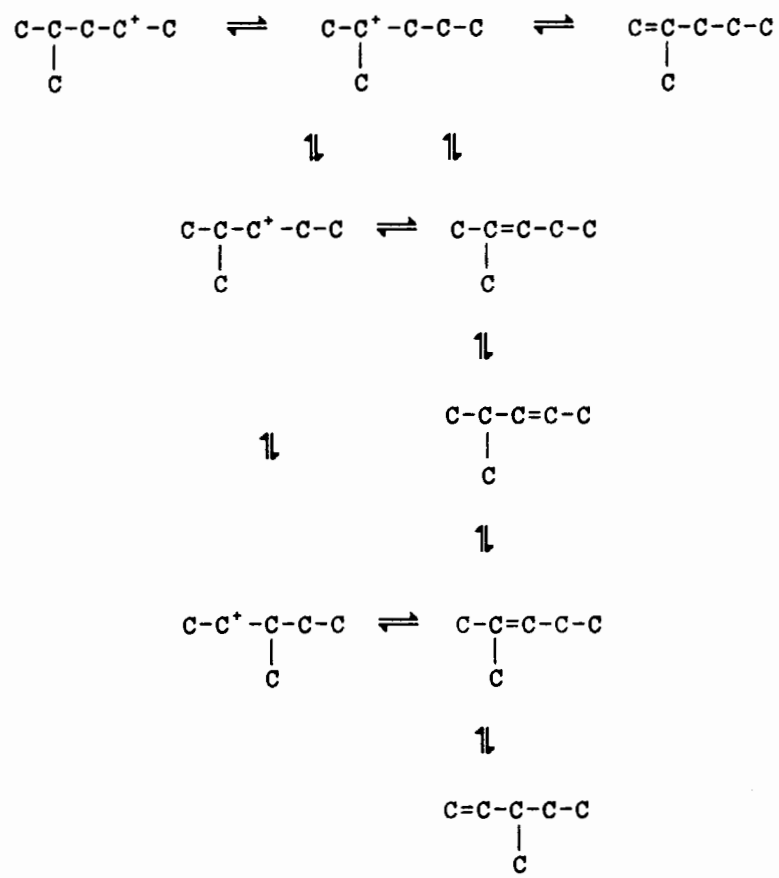

Under conditions where propene undergoes oligomerization, trimers are formed more readily than dimers. With solid phosphoric acid catalyst at 433 K and 1 MPa, the products of propene oligomerization consist of approximately 50% nonenes, 25% dodecenes and less than 5% hexenes (Schmerling & Ipatieff, 1950). This low yield of hexene can be explained in terms of the relative stability of the propene dimer and monomer carbonium ions. The dimer can generate a tertiary carbonium ion which is more stable than the secondary carbonium ion of the monomer, and will therefore exist for a longer time before expelling a proton. There is, therefore, a greater chance for the dimer to further add another monomer, than there is for monomer dimerization.

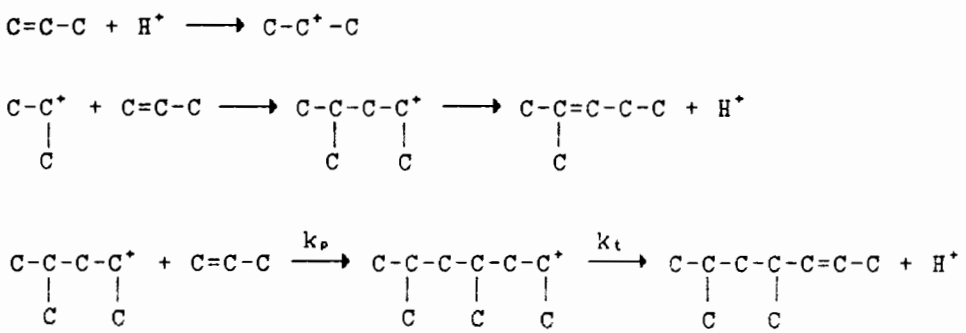

The degree of polymerization is related to the ratio (kp/kt) of addition (propogation) and proton loss (rupture).

kp = rate of further alkene addition (polymerization)

kt = rate of proton expulsion to form an alkene (termination)

The last reaction represents either the return of H^+ to the catalyst or the transfer of H^+ to an olefin molecule (Germain, 1969).

Due to isomerization and hydrogen transfer, the polymeric structures do not correspond to the simple reaction scheme presented above. According to Germain (1969), the dimer, trimer and tetramers of propene, for example, should have the following structures (with double bond isomers):

Dimer

```
C-C-C=C-C
  |
  C
```

Trimer

```
C-C-C-C-C=C-C
  |   |
  C   C
```

Tetramer

```
C-C-C-C-C-C-C=C-C
  |   |   |
  C   C   C
```

and double bond isomers

Skeletal isomers will, however, be present under most reaction conditions (Schmerling & Ipatieff, 1950) and thus, for the propene dimer (ignoring double bond position), according to Germain (1969), the following possibilities exist:

```
C-C-C-C-C     C-C-C-C-C     C-C-C-C     C
  |               |           | |       |
  C               C         C C     C-C-C-C
                                      |
                                      C
```

Trimers and tetramers are very complex mixtures. Trimerization occurs by addition of propene to dimeric ions. The C_9 carbonium ion can rearrange, resulting in many product structures. The propene trimer may crack to form non-multiple units of monomer.

Conjunct polymerization, producing saturated and unsaturated products, can occur by hydrogen transfer when a carbonium ion abstracts hydrogen from an olefin to produce an olefinic carbonium ion plus a paraffin (Ipatieff & Pines, 1936). The olefinic carbonium ions produce polyolefinic material that fouls polymerization catalysts (McMahon et al., 1963). There is a transition from true polymerization at 366 K to conjunct polymerization at 561 K with phosphoric acid (McMahon et al., 1963). High acid concentrations also favour conjunct polymerization.

The above carbonium ion mechanism proposed by Whitmore (1934) is the most widely accepted for alkene polymerization in heterogeneous

catalysis (Schmerling & Ipatieff, 1950; Flory, 1969; Langlois, 1953; McMahon et al., 1963).

The existence of a free alkyl carbonium ion in the same sense as an ion in solution (Langlois, 1953) has been seriously questioned. Many investigators prefer a carbonium ion which is never separated significantly from the anion of the catalyst, but where the two exist as an ion pair. There are those who prefer to consider an even lesser degree of charge separation, perceiving the intermediate in terms of a polarized molecule. For the purpose of explaining the structure of products formed, the degree of charge separation is insignificant.

This mechanism is different from that postulated by Ipatieff (1935a) for homogeneous polymerization using phosphoric acid, which involves intermediate ester formation.

1.6.1.3 Butene oligomerization

It has been shown (McCubbin & Adkins, 1930; Whitmore & Church, 1932), in the polymerization of iso-butene, that the two octenes, namely 2,4,4-trimethyl-1-pentene and 2,4,4-trimethyl-2-pentene, are produced in the ratio of about 4:1 in the presence of dilute sulphuric acid. This is representative of several acid catalysts (Schmerling & Ipatieff, 1950). The sequence is illustrated by the following equations:

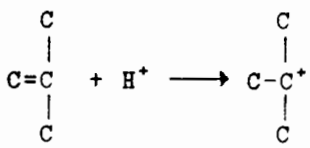

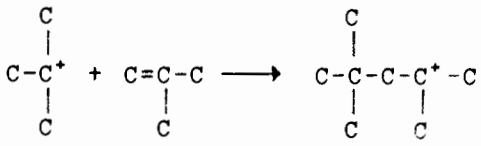

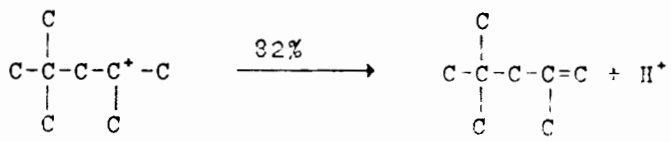

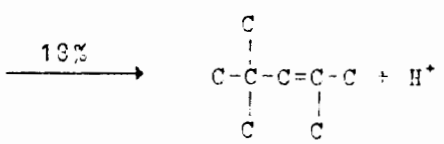

2,4,4-trimethyl-1-pentene is formed in larger amounts since the elimination of a proton from the methyl group adjacent to the electron deficient carbon atom, occurs more readily than from the neopentyl system (Schmerling & Ipatieff, 1950). The structure of these two isomers was proved by ozonation by McCubbin & Adkins (1930).

In addition, whereas there are only two protons in the methalene group of the neopentyl system, there are six hydrogens attached to the methyl carbons. The eliminated proton can add to the reaction chain. The relative difficulty of removing a proton from the neopentyl group has been illustrated (Whitmore et al., 1942). Trimers are formed mostly by reaction of the t-butyl carbonium ion with the dimers, and partly by the reaction of the iso-octyl carbonium ion with the monomer (Whitmore & Church, 1932; Whitmore et al., 1941).

The carbonium ion formation is directly related to the proton affinity of the olefin (Germain, 1969), hence the higher reactivity of iso-butene when compared to that of the n-butenes, propene or ethylene. The isomers present in the trimerized isobutene product have been examined by Whitmore et al. (1941) and McCubbin (1931). A summary of their findings is given by Schmerling & Ipatieff (1950) and Oblad et al. (1958).

In addition to polymerization, phosphoric acid causes considerable isomerization with the butenes. Hence in many instances the material which was actually polymerized might have been a mixture of the isomeric butenes, the relative amounts of which would depend upon the experimental conditions.

Little work has been carried out on the polymerization of 1-butene and 2-butene (the chemistry of petroleum derivatives). Schmerling & Ipatieff (1950) have listed the dimerized products obtained when sec-butyl alcohol is treated with sulphuric acid at 353 K under pressure. The dimerized and trimerized products obtained when 2-butene is polymerized in the presence of activated floridin have also been described (Schmerling & Ipatieff, 1950). The trimerized products were explained using the carbonium ion mechanism.

Schmerling & Ipatieff (1950) have reviewed possible mechanisms and the products obtained from the polymerization of several methyl butenes (pentenes), dimethylbutenes and the polymerization of mixed olefins (e.g., C_3 and C_4). The products and mechanisms will not be discussed.

1.6.2 Thermodynamics of Alkene Oligomerization

Oblad et al. (1958) have examined the thermodynamics of oligomerization of gaseous mono-alkenes to gaseous alkene products. Phase changes and deviations from ideality were ignored.

Figure 1.4 (taken from Oblad et al.) shows the free energy change during dimerization of C_2 through C_6 mono-olefins as a function of temperature. (The lines for C_4 and C_5 which are not shown are almost superimposable on the C_6 line). Note that the free energy change for the dimerization of propene to trans 3-methyl-2-pentene is greater than that for the dimerization to the terminal olefins (Figure 1.5).

The former (isomers of the corresponding higher olefins) are always the structures of ~~highest~~ lowest energy. The equilibrium conversion, therefore, of an alpha olefin to a high alpha olefin, will always be less than the corresponding conversion of an alpha olefin to an iso-olefin.

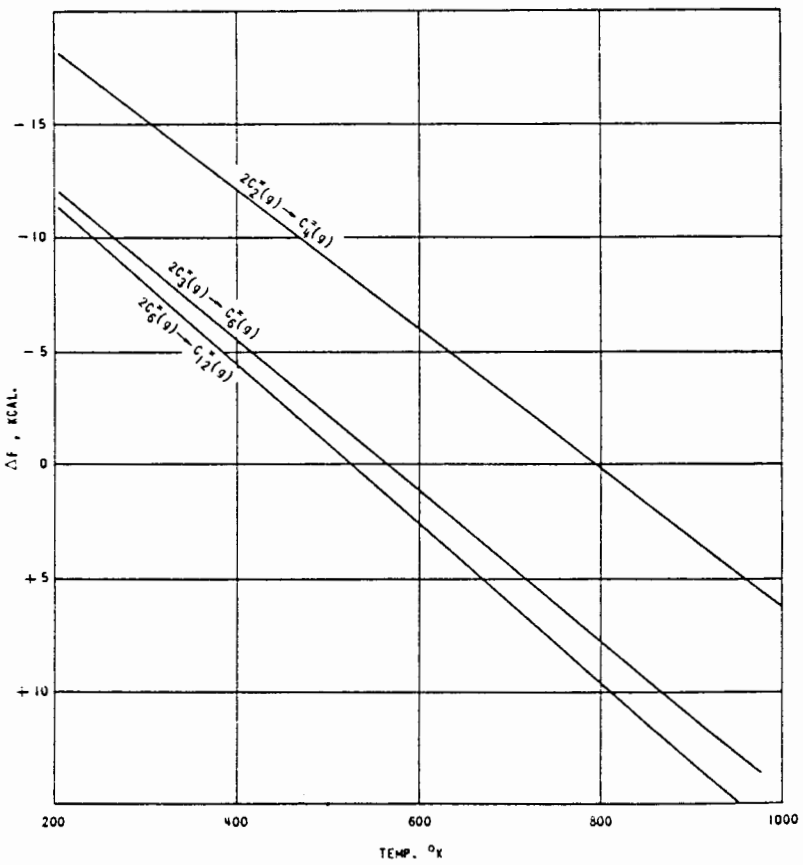

Figure 1.4 Free energy change during dimerization

For comparative purposes, the equilibrium conversion as a function of temperature and pressure is shown in Figure 1.5 for the following dimerization reactions:

$$2C_3\ (g) \longrightarrow \text{1-hexene}\ (g)$$

$$2C_3\ (g) \longrightarrow \text{trans-3-methyl-2-pentene}\ (g)$$

These gas phase reactions provide only limited information on 2-phase heterogeneous reactions. Dimerization of beta olefins or iso-olefins to the corresponding higher olefins will be similar to the alpha olefin - alpha dimer relationship. The dimerization of beta olefins or iso-olefins to alpha olefins is always favoured.

In the production of polymers greater than dimer from alpha olefins, the free energy versus temperature curves fan out from a constant point (Oblad et al., 1958) at a temperature between 500 and 600 K. This is

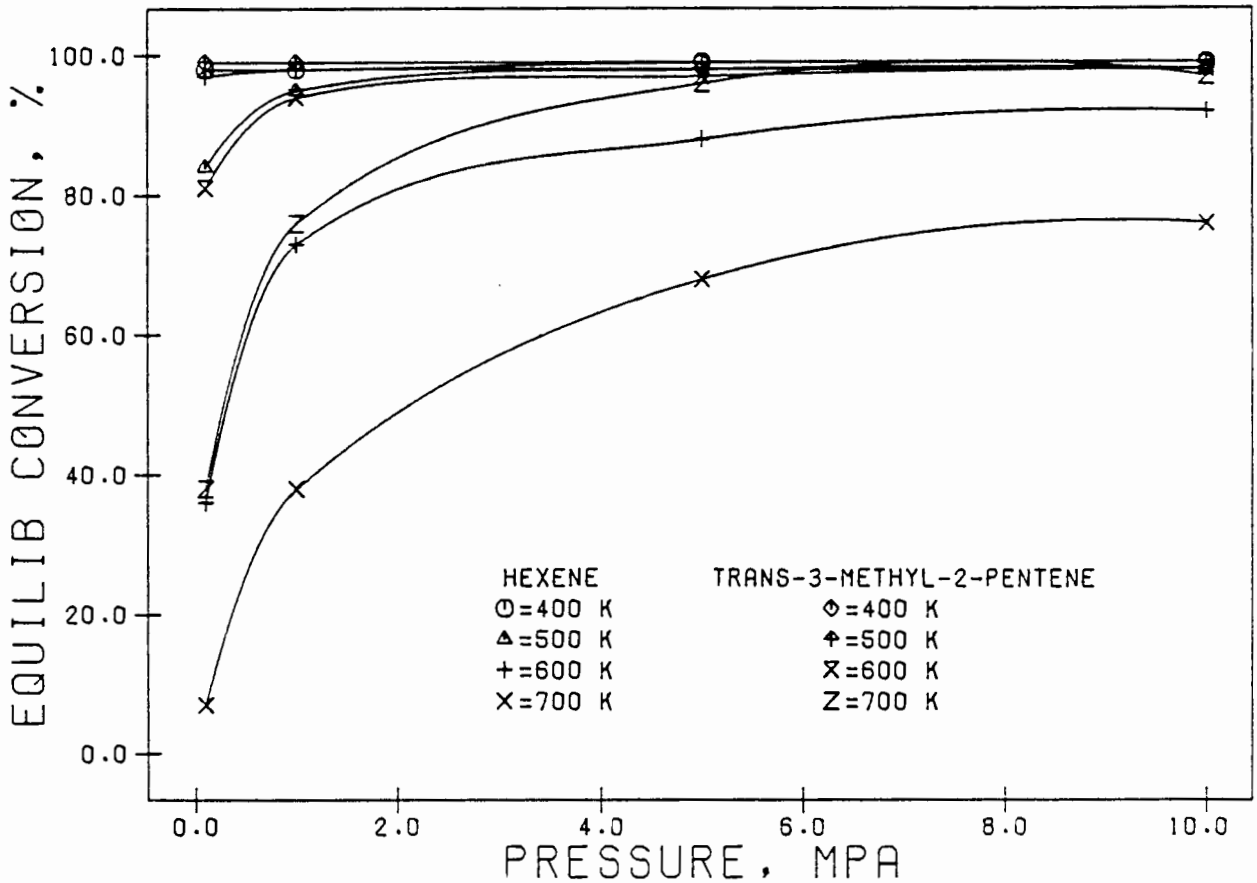

FIG 1.5 EQUILIBRIUM CONVERSION FOR PROPENE DIMERIZATION TO 1-HEXENE AND TRANS-3-METHYL-2-PENTENE

illustrated for propene in Figure 1.6 for the polymerization to higher terminal olefins.

With respect to the free energy changes in the polymerization of propene and 1-butene, the free energy change of adding a monomer to a growing

chain seems to remain constant after the dimer has formed (Oblad et al., 1958). This is illustrated in Table 1.4.

Table 1.4 Standard free energy change (kcal) of polymerization per monomer unit added.

	C_3				C_4		
Temp K	Dimer	Trimer	Pentamer	Hexamer	Dimer	Tetramer	Pentamer
298.1	-9.18	-9.01	-8.93	-8.92	-9.5	-9.22	-9.17
600	1.2	1.5	1.65	1.69	1.2	1.63	1.71
900	10.9	11.45	11.7	11.76	11.5	12.1	12.15

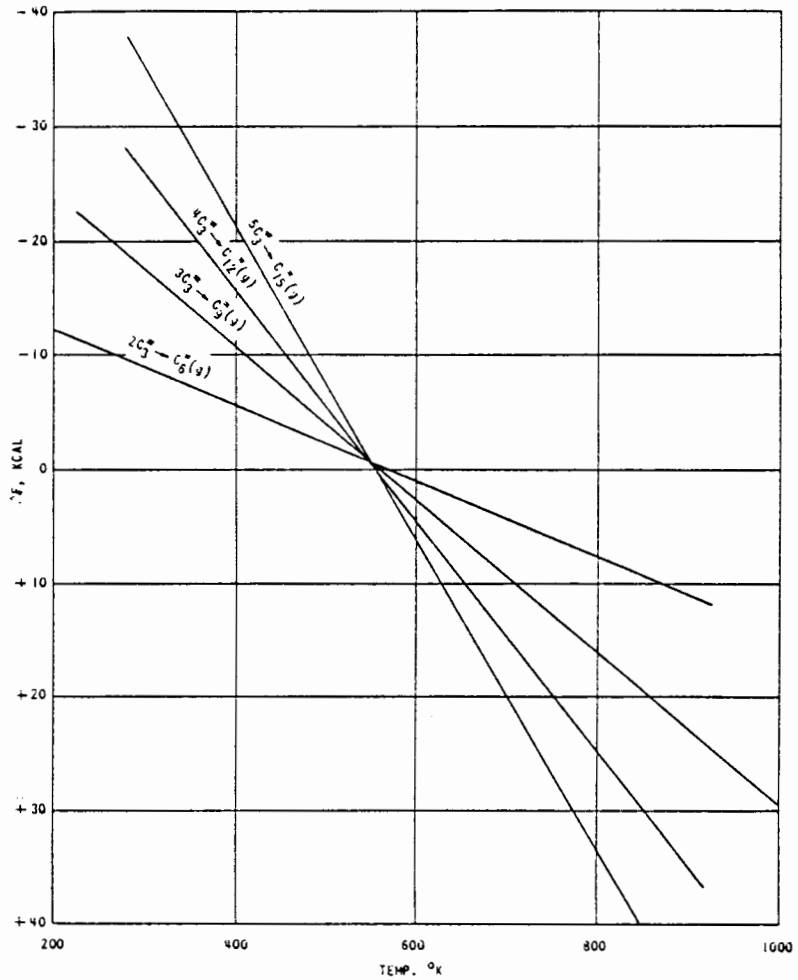

Figure 1.6 Free energy changes for the polymerization of propene

Taking a single olefin species, such as propene, the free energy change for the formation of the higher polymers can be estimated theoretically from the corresponding energy of dimerization (Oblad et al., 1958). The free energy change per mole of monomer for the higher polymers should approach twice the change for the dimer formation (provided heat and entropy effects are constant) and hence the higher oligomers are

favoured over the dimer. Oblad et al. (1958) note that, up to the formation of C_6 hexamer, the heat of reaction follows the theoretical relationship more closely than the free energy change, indicating that the entropy change is not constant up to the hexamer formation. They suspect, however, that the free energy change would approach the theoretical value for polymers higher than n=6.

1.7 REACTORS FOR DETERMINING THE KINETICS OF HETEROGENEOUS CATALYTIC REACTIONS

1.7.1 Background

The choice of a suitable reactor for carrying out experiments under conditions where meaningful kinetic rate expressions can be obtained, is of great importance, and depends on the objectives of the research (Cooke, 1979). This is particularly true of catalytic reactions in which external and pore diffusion resistances are important. Radial and axial transport effects in the reactor must be accounted for. The choice of a laboratory catalytic reactor must therefore be made on the basis of several considerations (Doraiswamy & Tajbl, 1974; Weekman, 1974).

The central problem in obtaining kinetic data from any reactor is to be certain that one is evaluating the rate of the intrinsic chemical reaction on the catalyst surface (Cooke, 1979). The measurement of the rate of chemical reaction occurring on the surface of a catalyst is made in terms of bulk concentrations and temperatures. For these bulk concentrations to reflect the chemical kinetics accurately, there must be an absence of concentration gradients between the bulk gas phase and the catalyst surface. Reactions which are affected by gas-film resistances show very marked deviations from their true rates because of the poor heat transfer across the stagnant gas film and the exponential dependence of the rate on temperature (Cooke, 1979).

Concentration gradients can also occur inside the pores of a catalyst particle. This is called pore-diffusion resistance. Similar to gas-film resistance, the absence of concentration and temperature gradients inside the catalyst pores is essential for the intrinsic kinetics to be measured.

There are many laboratory reactor types. A list of the more common types is given below:

- differential reactor
- fixed bed reactor
- stirred batch reactor
- stirred-contained solids reactor
- continuous stirred tank reactor
- straight through transport reactor
- recirculating transport reactor
- pulse reactor

A summary of the ratings of the reactors for sampling and analysis, isothermality, residence contact time, selectivity disguise-decay and construction problems is given in Table 1.5 (Heekman, 1974). The ratings are specific to a three-phase system with a powdered decaying catalyst. The interpretation of the ratings for other systems is straightforward.

Advantages and disadvantages of many laboratory catalytic reactors have been widely reported (Doraiswamy & Tajbl, 1974; Christoffel, 1982; Heekman, 1974).

Table 1.5 Summary of laboratory reactor ratings.

Reactor type	Sampling and analysis	Isothermality	Residence contact time	Selectivity disguise-decay	Construction problems
a. Differential	P-F	F-G	F	P	G
b. Fixed bed	G	P-F	F	P	G
c. Stirred batch	F	G	G	P	G
d. Stirred cont. solids	G	G	F-G	P	F-G
e. C. S. T. R.	F	G	F-G	G	P-F
f. Straight through transport	F-G	P-F	F-G	G	F-G
g. Recirculating	F-G	G	G	G	P-F
h. Pulse	G	F-G	P	F-G	G

P = Poor F = Fair G = Good

1.7.2 Gradientless Reactors

Gradientless reactors are those reactors that are capable of performing at, or close to, gradientless conditions, where there are no external catalyst heat or mass transfer limitations (Kuchanski & Squires, 1976). There are many versions of this reactor type. Two well known examples are those of Carberry (1964) and Berty (Berty et al.,1969; Berty, 1974). In the famous Carberry reactor the catalyst is mounted on the agitator (inside the reactor) and the high rotational speeds provide good catalyst-fluid contact. In the Berty type the catalyst is held stationary and the fluids are internally recycled through the catalyst bed by means of an internal blower. Sampling and analysis of the product composition of these reactors present no problems. Good mixing is possible and isothermality should be achieved. Residence times can be measured accurately. These reactors are difficult to construct. There are many examples of these reactor types (Carberry, 1964; Tajbl et al., 1966, 1967; Tajbl, 1969 a, b; Garanin et al., 1967; Brown & Bennett, 1970; Berty et al., 1969; Berty, 1974; Livbjerg & Villadsen, 1971; Mahoney, 1974; Choudhary & Doraiswamy, 1972; Perkins & Rase, 1958; Satterfield & Roberts, 1968; Butt et al., 1962; Leinroth & Sherwood, 1964; Ford & Perlmutter, 1964; Relyea & Perlmutter, 1968; Brisk et al., 1968; Barcicki et al., 1981; Caldwell, 1983; Ke-Chang & Nobile, 1986). A good review of these reactors has been given by Bennett et al. (1972).

Many of these reactors have some outstanding features for a particular application, but only those with centrifugal internal blowers can assure steady state operation (Berty, 1984). Of these, very few permit the close estimations of internal flow, and hence, of the heat and mass transfer conditions at the catalyst (Berty, 1974).

1.7.2.1 Recycle reactors

Reactors that are simple in construction, such as fixed bed and adiabatic reactors, approach their ideal conditions in commercial size rather than on a lab scale. On a small scale they are handicapped by significant temperature and concentration gradients that are not even well defined. In contrast, recycle reactors and CSTR's (continuous stirred tank reactors) in general come much closer to their ideal state in small sizes (Berty, 1984).

All recycle reactors and CSTR's may be regarded as differential reactors (Jankowski et al, 1978; Berty, 1984). The purpose of a recycle reactor can be deduced from a differential reactor if one considers that, close

to the ideally small conversion, the feed has almost the same concentration as the discharge. (Remember that in all CSTR's and recycle reactors, the reaction takes place at the discharge conditions, or very close to them.) Just enough fresh reactants can be added to make up for the chemical change and for the reactants lost in the exit stream. This eliminates the analytical problems with the once through differential reactors (Berty, 1984). There are many published examples of the more common laboratory recycle reactors (Carberry, 1964; Brisk et al., 1968; Tajbl et al., 1966; Bennett et al., 1972; Mahoney, 1974; Berty, 1974; Berty, 1977; Robinson & Mahoney, 1977; Mahoney et al., 1978; Myers & Robinson, 1978; Berty, 1979; Barcicki et al., 1981; Gangwal, 1982; Ke-Chang & Nobile, 1986; Caldwell, 1983).

Internal recycle systems, which approximate CSTR behaviour, are probably the most useful reactors for obtaining catalytic kinetic data, since external circulation is plagued by mechanical pumps and the need to cool and reheat the recycle stream, resulting in poor operation (Mahoney et al., 1978). CSTR behavior can be achieved in a recycle reactor only if the recycle ratio is greater than 25 (Carberry, 1964). An overview of recycle reactors has been given by Berty (1984).

1.7.2.2 The internal recirculation type gradientless reactor (internal recycle reactor)

The internal recycle reactor (fixed basket) was developed by Berty at Union Carbide in the early 1960's. At that time little interest was shown in the new reactor type. Some years later interest had developed and by the late 1970's the use of recycle reactors was commonplace (Berty, 1984). A review of many internal recycle reactors is given by Jankowski et al.(1978). An example of a standard Berty type gradientless (fixed basket, internal recycle) reactor is shown in Figure 1.7.

The most significant advantage of this reactor type, as previously mentioned, is the removal, to a large extent, of mass and heat transfer gradients. Since the reactor permits reaction studies at isothermal conditions with uniform concentrations, it eliminates the need for the solution of partial-differential equations. Each steady state experiment yields a reaction rate that is calculated from the ordinary mass balance equations for a CSTR (Mahoney et al., 1978):

$$\frac{W}{F} = \frac{X_o - X_i}{r_p}$$

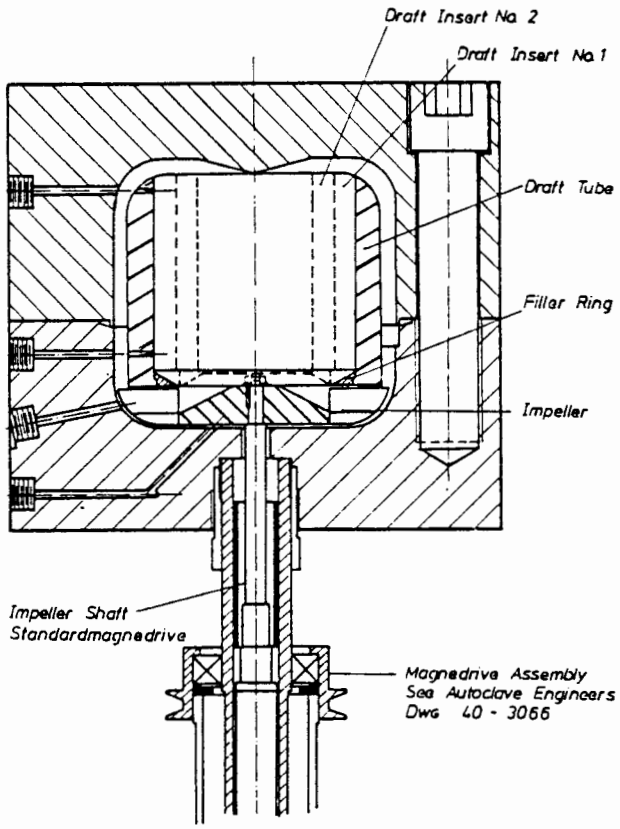

Figure 1.7 Standard Berty type internal recycle reactor (fixed basket) (Berty, 1974).

where W = mass of catalyst

F = molar feed rate of catalyst

X_i = inlet concentration of reactant

X_o = outlet concentration of reactant

r_p = global rate of reaction per unit mass of catalyst

These reactors can be problematic in studies where the reaction products are qualified by some practical tests (Berty, 1984). Examples include:

1. The production of polymer olefins for subsequent conversion to plasticiser alcohols, where the product quality is tested after one or more reactions, and no exact relationship for quality can be expressed.
2. The conversion of a complex natural product into a partially modified material that is used for an empirically defined purpose, such as a thickener.
3. When there is a possibility of homogeneous reactions in the empty spaces of the reactor.
4. When reactions on the walls of the reactor are a possibility.

In summary, internal recirculation reactors are highly suitable for catalyst testing and kinetic studies (Berty, 1984).

1.7.2.3 Examples of the use of gradientless reactors to obtain kinetic data

There are many examples of the use of these reactors to obtain intrinsic kinetic data. Tajbl et al. (1966) demonstrated the operability of the 'Carberry reactor' by examining the palladium-catalyzed oxidation of CO with O_2. Mahoney (1974) used a Berty type (fixed bed) reactor to determine the kinetics of ultraforming. Ultraforming, which is a high-severity catalytic naptha reforming process, operates at high conversions, and the catalyst deactivates rapidly between regenerations. Mahoney concentrated on the reactions of n-heptane catalyzed by a commercial platinum-on-alumina catalyst which had been activated by a halide promoter. Berty (1974) used his now famous internal recycle reactor to study the kinetics of ethylene hydrogenation on Harshaw 3210-T catalyst. He also examined the oxidation of propene to acrolein and found that a catalyst which had previously been discarded (based on fixed bed laboratory reactor studies) was dramatically more active than the catalyst which had been chosen as the most active.

Robinson & Mahoney (1977) designed an internal recycle reactor to study the multiphase coal hydroliquefaction process. They successfully tested various catalysts for short term ageing behaviour, in the absence of transport limitations. Myers & Robinson (1978) used a similar reactor to study the kinetics of the three phase dibenzothiophene desulphurization. Their results compared favourably with those performed in a trickle bed reactor by Frye and Mosby (1967). Caldwell (1983) studied the kinetics of the dehydration of ethanol in his modified version of Berty's internal recycle reactor. Carberry et al. (1985) recently developed an internal recycle (Carberry type) reactor that permits the accurate determination of intrinsic kinetics for three-phase systems. Their reactor is based on a gas-liquid reactor (Manor & Schmitz, 1984), in which a multiblade rotor creates a thin film of liquid on the cylindrical wall. Ke-Chang & Nobile (1986) studied the intrinsic kinetics of SO_2 oxidation on a commercial vanadium catalyst. Their study concentrated on the construction of a Berty type reactor and an extensive characterization of the reactor. Berty (1979) has given some very useful hints and methods that can be used in the testing of commercial atalysts in recycle reactors. Santacesaria & Carra (1983) studied the kinetics of steam reforming methanol, catalyzed by a

commercial Cu-Zn catalyst, in a Berty type reactor. They modelled the kinetic data according to a Langmuir-Hinshelwood model.

1.8 OBJECTIVES OF THE PRESENT STUDY

The objectives of this work are to study, inter alia, the kinetics of the oligomerization of C_3 and C_4 alkenes over phosphoric acid on kieselguhr using an internal gas recirculation reactor, to obtain satisfactory rate equations and to test these equations on the performance of an integral reactor. In addition to the characterization of the reactor system (with respect to transport effects) and the kinetic study, the oligomerization of C_3, C_4, C_6 and mixtures of these alkenes is studied using pulse reactor techniques.

The reactor system is characterized with respect to both mass and heat transport and residence time characteristics.

Rate equations are developed for the oligomerization of the C_3 and C_4 alkenes and proposals made regarding the mechanism of the oligomerization of C_3, C_4 and C_6 alkenes over phosphoric acid on kiesulguhr.

The rate equations are used to predict the results from an integral reactor and these results are compared to the actual results obtained.

2. MICRO-CATALYTIC PULSE REACTOR STUDIES

2.1 INTRODUCTION - LITERATURE REVIEW

2.1.1 Background

The pulse microcatalytic technique has established itself in the field of heterogeneous catalysis as an important analytical tool (Verma & Kaliaguine, 1973). Pulse reactors have become almost standard equipment for rapid catalyst screening in the petroleum industry and have found extensive application for fundamental reaction mechanism studies in both industrial and academic catalytic laboratories (Galeski & Hightower, 1970). The technique has found very useful applications in situations where either the reactants or the catalysts are in short supply, or are too expensive to be used in a steady state flow reactor (Verma & Kaliaguine, 1973).

2.1.2 Pulse Reactor Types and Techniques

There are at least two types of pulsed catalytic reactors (Galeski & Hightower, 1970). They are:

1. Chromatographic column reactors.
2. Pulse systems in which the reactor bed and chromatographic column are independent.

In the chromatographic column reactor, the catalyst also serves as a partitioning column to separate the products and the reactants (Langer et al., 1969). In most pulsed catalytic reactors, some degree of elution will occur.

There are many systems in which the reactor bed and chromatographic column are independent. The simplest form of microcatalytic pulse reactor is a gas chromatograph with a small, tubular fixed-bed catalytic reactor placed in the carrier gas stream between the sampling valve and the partitioning column. The reactant slugs are introduced via the sampling port, mixed with the carrier gas and carried through the catalyst bed. On their exit, the reactants and products are separated immediately in the partitioning column and detected by an appropriate detector (flame ionization or thermal conductivity).

This system has severe limitations. The reaction pressure and the contact time with the catalyst are limited. To avoid this, the carrier gas can be split into two streams - one stream operating under chromatographic conditions and the other under variable conditions. Generally in these systems the reactants and products are separated from the carrier gas by freezing in traps. Effective trapping is sometimes very difficult. Igarashi & Ogino (1982) and Steingaszner & Pines (1966) have developed useful high pressure catalytic pulse reactors.

A common gas pulse injection is by means of a hypodermic syringe into a T connection, in the carrier gas stream. Small amounts of air accompany such injections (Galeski & Hightower, 1970). By-pass dosing systems avoid this problem. For a fixed doser volume, a known amount of reactant can be injected by adjusting the doser pressure at a fixed temperature. Liquids are often pulsed by saturating them in a separate carrier gas stream, a portion of which is trapped and sent into the reactor.

The most common reactor is a tube containing a centered thermocouple. The bed length is generally greater than the diameter to avoid channelling, and all contacting lines have as small diameters as possible to minimize dispersion. Several pulse techniques (Scott & Phillips, 1980) are described below.

2.1.2.1 Elution with reaction

In this technique a small sample is injected into a gas stream at the beginning of the column. Using the catalyst as column material results in a chromatogram with information about the reaction occurring on the column. Information about the adsorption of the sample molecules on the catalyst surface can be obtained from the shape and retention time of the eluted peak of unreacted sample.

2.1.2.2 Microcatalytic technique

This classical technique has been described by Kokes et al. (1955). The system would consist of a reactor containing a small amount of catalyst through which a pulse of reactant in a stream of carrier gas is passed. The analysis is usually performed on a gas chromatograph.

2.1.2.3 Deuterium exchange

With this technique, which is an application of 2.1.2.1 or 2.1.2.2, a small sample of deuterium is injected into a hydrogen carrier gas stream

passing through the catalyst and its emergence is followed by a katharometer. The retention of the deuterium measures the exchange of the deuterium with adsorbed hydrogen, water and hydrocarbons.

2.1.2.4 Reactor-stop technique

This system is similar to (3) above but here the reactant is stopped on a longer reactor for varying periods of time and then swept off with the products to the GC column.

2.1.2.5 Stopped-flow technique

This is a variation of (1) above in which the gas flow through the reactor column is stopped from time to time so that the chromatographic process is switched off, while the reaction is allowed to continue. With each restart of the gas flow, sharp chromatographic peaks are generated on top of the normal "reaction" chromatogram, each peak corresponding to one volatile product of the reaction formed during the stop period.

2.1.2.6 Sample vacancy technique

Reactant is carried continuously through a reactor and GC column. Periodically, feed samples are switched into the gas flow between the reactor and GC columns, generating a differential chromatogram, in which the positive peaks measure the amount of reactant which has reacted, the negative peaks the amounts of the various volatile products and the difference the amount of involatile product.

2.1.2.7 Heater displacement technique

Samples, here, are driven through the catalyst by means of a carrier gas and an external moving heater.

2.1.3 Analysis of Pulse Reactor Data

The theory of chemical processes in micro-catalytic pulse reactors can be classified into two main groups (Yanovskii & Berman, 1972). The first involves the rapid attainment of adsorption equilibrium, and the second takes into consideration the rate of attaining equilibrium between gases and solids. Most research has been concerned with linear adsorption isotherms, but some research showing non-linear isotherms has been reported (Hattori & Murakami, 1968).

The nature of adsorption equilibria and the kinetics of adsorption have a different effect on the degree of conversion, depending on the reaction order and its specific mechanism (Yanovskii & Berman, 1972). The simultaneous treatment of adsorption kinetics and the longitudinal and internal diffusion involves considerable mathematical difficulties.

Hattori & Murakami (1974) have emphasized that the pulse reaction kinetics, coupled with an irreversibly adsorbed reactant, may be significantly different from that with the reversible adsorption.

When investigating reversible reactions in a micro-catalytical reactor, some of the features responsible for the rate of a heterogeneous reaction must be taken into account (Yanovski & Berman, 1972). Probably the most important factor is the possibility of separating reactants and products on the catalyst layer during the reaction.

2.1.3.1 Reactions of the type $A \rightleftharpoons B$

The difference in the adsorption coefficients of A and B will cause the rate of the reverse reaction to decrease. The same effect is possible as a result of diffusion when the adsorption coefficients of A and B are equal (Berman et al., 1970).

2.1.3.2 Reversible reactions of the type $A \rightleftharpoons B + C$

For reactions of this type, spatial separation of B and C will induce a change in the degree of conversion of A as a result of partial or full inhibition of the reverse reaction (Roginskii et al., 1961).

2.1.3.3 Consecutive reactions

For those of the type $A + B \rightleftharpoons R$

$R + B \rightleftharpoons S$

the separation of B and R will result in a decrease in the yield of S and in an accumulation of the intermediate product R (Hattori & Murakami, 1968; Murakami et al., 1968). This effect depends on the pulse width at the inlet, as its decrease intensifies separation (Yanovskii & Berman, 1972). In the case of a reaction of the type $A \rightleftharpoons R$ and $2R \rightleftharpoons S$, such an effect can arise from the difference in the adsorption coefficients of reactant A and the intermediate product R.

When the rate at which adsorption equilibrium is reached is slow, the difference between the results obtained by pulse and flow methods will

be even greater because of the different degrees of catalyst surface coverage.

Most catalysts require an induction period before exhibiting a constant level of activity. Hall and Emmett (1959) have found, in the hydrogenation of ethylene, that the activity on their copper-nickel alloy catalyst increased strongly with increasing slug number, when the catalyst was treated in flowing helium for 30 minutes at 300°C.

Sometimes the results obtained with the pulse technique are significantly different from those obtained with the continuous flow technique. Hattori & Murakami (1974) found that the main difference between the two techniques was primarily due to the separation between the components in the catalyst bed and from the lowering of the concentration due to the broadening of the pulse. They found that the effect of those factors was dependent on the pulse width. They also noted that the results in the pulse technique approached those in the continuous flow technique with an increase in the pulse width (the continuous flow technique corresponds to the pulse technique with an infinite pulse width). Another way to reduce the difference between the two techniques is to reduce the contact time (Hattori & Murakami, 1973; Toyota & Echigoya, 1968). Hattori & Murakami (1973) noted, however, that the above cannot be applied to all reactions.

Basset and Habgood (1960) showed for first order reactions that quantitative analysis was possible. However, they used a relatively simple reaction where the rate of adsorption had to be fast relative to the rate of the surface reaction. The adsorption isotherm was assumed to be linear. Their analysis was made possible by the fact that, although the reactant partial pressure varied from point to point through the reactant pulse, for first order reactions the fractional conversion of reactants to products was independent of pressure.

Gaziev et al. (1963) extended the work of Basset and Habgood to non-first order kinetic equations, using square and triangular input pulses having no axial dispersion. The equations used were confirmed experimentally by Schwab & Watson (1965). Bett & Hall (1968), however, found a difference between the results obtained from the micro-catalytic technique and the flow technique for a zero order reaction. Blanton et al. (1968) and Makar & Merrill (1972) extended the pulse technique to more general cases of non-first order kinetics. They neglected the pulse dispersion by introducing a dispersion column upstream of the catalyst bed. The Gaussian-shaped pulse was made broad enough so that it could be

assumed that axial dispersion in the bed had a negligible effect on the width of the peak. Verma & Kaliaguine (1973) continued this approach with a further simplification in their study of the oxidation of ethylene over a silver catalyst. They reduced the ratio of catalyst bed length to total pulse length so that the reactant concentration could be considered to be constant over the entire length of the bed. They ensured that conversion over the bed was differential. Their results, which agreed partially with those of their flow experiments, showed that one of the major drawbacks of the pulse technique as a quantitative kinetic tool was the need for an instantaneous attainment of adsorption equilibrium. Sica et al. (1978) found reasonable agreement between kinetic parameters, based on power-law and Langmuir-Hinshelwood rate models, obtained from pulsed and steady state flow experiments for the hydrogenation of benzene on a nickel catalyst.

2.1.4 Advantages and Disadvantages of the Pulse Technique

Micropulse reactors are useful tools with which to investigate heterogeneously catalyzed gas-phase reactions. These devices can be complex or surprisingly simple depending on the results desired and the resources available (Reichle, 1981). The insight obtained from these reactors should supplement, not replace, that obtained from steady state kinetics (Bett & Hall, 1968). There are many advantages and disadvantages associated with the use of micro-catalytic pulse reactors. The most important are listed below.

Advantages

1. Activity and selectivity data can be obtained rapidly (Reichle, 1981; Hall & Emmett, 1959).
2. Unlike steady state flow reactors, hot-spots do not occur (Reichle, 1981; Hall & Emmett, 1959).
3. Extremely small amounts of both catalyst and feed can be used (Verma & Kaliaguine, 1973).
4. Qualitative analysis for linear processes is rapid and relatively simple (Hall & Emmett, 1959).
5. It is a simple technique to use for catalyst life experiments (Reichle, 1981).

Disadvantages

1. For quantitative analysis of results, knowledge of the adsorption characteristics are essential (Hattori & Murakami, 1974).
2. The catalyst is generally in an unstable condition (Reichle, 1981; Hall et al., 1960).

3. Steady state is generally not obtained with respect to adsorption of the gases (Hall et al., 1960).
4. Due to the unsteady state conditions that generally prevail, quantitative analysis is extremely difficult (Verma & Kaliaguine, 1973).
5. Results obtained very often differ from those in continuous systems. This is especially so for non-linear systems (Reichle, 1981; Murakami et al., 1968).

2.1.5 Applications of the Pulse Technique

The pulse micro-catalytic reactor has had extensive use in the field of heterogeneous catalysis since its introduction. Up until 1960 this technique was used only as a qualitative tool (Keulemans & Vogue, 1959; Hall & Emmett, 1959; Hall et al., 1960).

Bassett and Habgood (1960) were the first to quantitatively analyse the results from a pulse system in their study of the catalytic isomerization of cyclopropane. Steingaszner and Pines (1966) designed a novel high-pressure pulse micro-reactor that could withstand pressures of up to 70 atmospheres.

Blanton et al. (1968) used the pulse micro-catalytic reactor to quantitatively solve non-linear rate equations in their study of the hydrogenation of ethylene over alumina. Since then many researchers have quantitatively analysed their pulse reactor data (Bett & Hall, 1968; Murakami et al., 1968; Suzuki & Smith, 1971; Yanovskii & Berman, 1972; Verma & Kaliaguine, 1973; Sica et al., 1978)

In an effort to extend the quantitative application of the pulse micro-catalytic reactor to as many linear and non-linear systems as possible, several authors have rigorously analysed the chemical and physical processes encountered (Masamune & Smith, 1964; Roginski & Rozental, 1964; Kubin, 1965; Kucera, 1965; Kocirik, 1967; Denisova & Rozental, 1967; Padberg & Smith, 1968; Murakami et al., 1968; Schneider & Smith, 1968; Adrian & Smith, 1970; Suzuki & Smith, 1971; Hattori & Murakami, 1973; Hattori & Murakami, 1974; Furusawa et al., 1976; Igarashi & Ogino, 1982).

Despite the simplicity and speed of operation of pulsed micro-catalytic reactor systems, the complexities encountered in the quantitative

analysis of results remain a severe drawback. Their versatility lies in their use as a qualitative tool.

2.2 OBJECTIVES OF THE PULSE MICRO-CATALYTIC STUDIES

The primary objective of the pulse micro-catalytic studies is to examine the relative reactivities of various hexene isomers over solid phosphoric acid. Due to the extremely high cost and limited availability, the hexene isomers can not be polymerized using a continuous flow or batch reactor. The only convenient reactor which can handle extremely small quantities of reactants is the pulse micro-catalytic reactor.

The second objective is to compare the reactivities of the hexene isomers with those of propene, 1-butene and iso-butene and to examine the effect on the reactivities and selectivities of mixing these reactants. It is also hoped to obtain a better understanding of the basic reaction pathways followed in the polymerization of the above feedstocks.

The objectives of this study may therefore be listed as follows:

1. To investigate the relative reactivities of the following hexene isomers:

   1-hexene
   2-methyl-1-pentene
   2-methyl-2-pentene
   3-methyl-1-pentene
   3-methyl-2-pentene
   4-methyl-1-pentene
   Cis-4-methyl-2-pentene

2. To compare the reactivities of the above-mentioned hexene isomers with those of propene, 1-butene and iso-butene.

3. To investigate the effect of mixed feedstocks on the reactivities and selectivities of the individual reactants.

4. To obtain a better understanding of the major reaction pathways followed in the polymerization of the propene, butene and hexene feedstocks.

5. To determine, if possible, which of the following reaction sequences is the most dominant in the production of the C_{12} oligomer:

$$C_3 + C_9 \longrightarrow C_{12}$$
$$C_6 + C_6 \longrightarrow C_{12}$$

2.3 EXPERIMENTAL APPARATUS AND PROCEDURE

2.3.1 The Pulse Technique Used in this Study

The micro-catalytic pulse technique used in this study was based largely on that used by Igarashi & Ogino (1982). The high pressure requirement of this work did not permit the use of a chromatographic column reactor, due to the maximum permissible pressure of the gas chromatograph's carrier gas. Similar to the system used by the above-mentioned workers, the high pressure was maintained by an independent, inert carrier gas. Unlike their system, the reaction products, with the inert carrier gas, were passed through a gas sampling valve, enabling the analysis of discrete sample slices. The most serious disadvantage was that, with the analysis of discrete sample slices, the possibility existed of not being able to obtain a representative analysis of the entire exit pulse. It will be shown that this problem was overcome.

2.3.2 The Reactor System

The reactor system used for the micro-catalytic pulse experiment is shown schematically in Figure 2.1.

Nitrogen, which was used as the inert carrier gas, was fed to the system from a high pressure cylinder. The inlet pressure was controlled by means of a regulator on the nitrogen cylinder. The nitrogen was bubbled through a temperature controlled water bath. The temperature of the water bath determined the partial pressure of the water in the nitrogen stream and, therefore, the acid concentration (% H_3PO_4) on the catalyst, at a given pressure and nitrogen flowrate. The water vapour content of the nitrogen stream was accurately determined by passing a bleed from the inlet nitrogen stream over an aluminium oxide sensor. The sensor signal was converted to a dew point reading by a Panametrics model 700 hygrometer. The bleed stream then passed through a gas flowmeter and was vented.

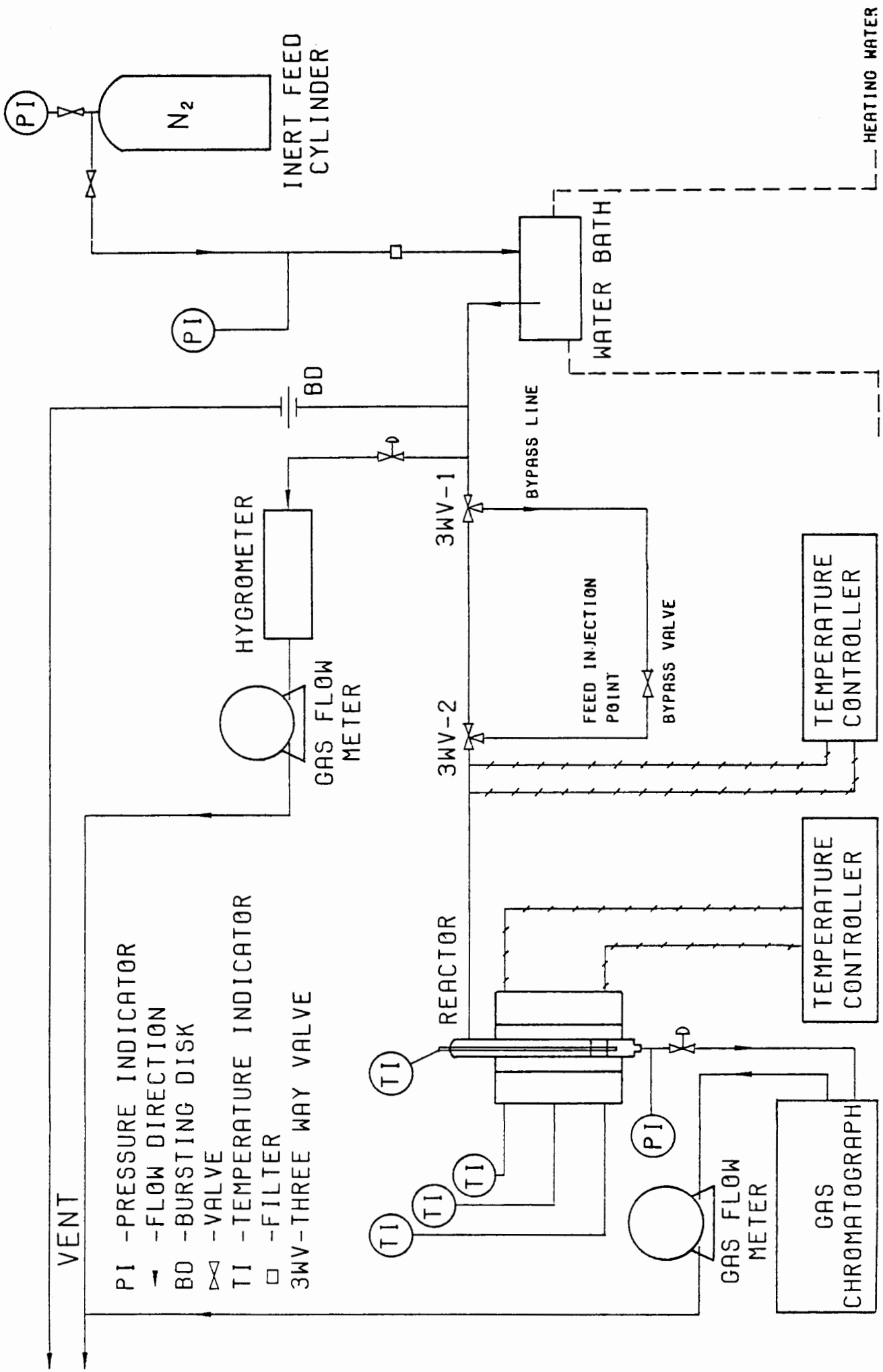

FIG 2.1 SCHEMATIC OF PULSE REACTOR SYSTEM

At any stage the nitrogen carrier could be diverted through the bypass line to pick up the reactant slug. This was done by switching the two three-way valves situated at the inlet and outlet of the bypass section. The pulse was then carried directly to the reactor where it reacted over the solid phosphoric acid catalyst. The temperature of the inlet line, from the water bath to the reactor, was heated to reactor temperature

using heating tapes (Isotape ITH150). The reactor was also heated using similar heating tapes which were independent of those on the inlet line. From the reactor the pulse passed through a fine metering valve, which was used to control the flowrate, and was then carried to a gas sampling valve on a gas chromatograph (VARIAN model 3700). The outlet section from the reactor exit to the gas sampling valve was heated to 10 K above the reactor temperature. On leaving the gas sampling port the effluent gas flow was measured with a gas flow meter and was finally vented. The temperatures of all heated sections were controlled using Eurotherm temperature controller systems (Model 101).

The reactor used was a cylindrical stainless steel tube 4.3mm in diameter and 90mm long. A 3.2mm thermowell ran down the length of the bed, enabling the measurement of the entire bed temperature. The inlet and outlet lines were connected to the reactor by means of standard SWAGELOK fittings. The heating of the reactor was critical. Ensuring uniform wall temperatures was difficult and could only be achieved by even winding of the heating tape and adequate insulation, using ½" asbestos rope. Two layers of insulation were necessary, giving a total insulated thickness of one inch. The catalyst was held in the reactor by glass wool. There were two pressure gauges on the reactor system. The first was situated upstream of the water bath and the second, immediately after the reactor. No significant pressure drop was observed.

The gas sampling valve (VARIAN GSV model 3180) used, is shown in Figure 2.2. This was a six port valve with a 0.25cm^3 sample loop. In the open position, the effluent from the reactor flowed into the sample port, through the sample loop and out to vent. The GC carrier gas, in this position, flowed into the carrier port and directly out through the column port to the separating column and the detector. In the closed position, the GC carrier gas flowed into the carrier port, through the sample loop and out of the column port to the separating column. The reactor effluent, in this position, flowed in through the sample port and directly out through the vent port. By switching the valve from the

open to the closed position, a sample from the reactor effluent could be captured and analysed on the GC.

The gas chromatographic separation was performed on a 5.6m long, 6mm O.D. glass column packed with 3% silicone OV-101 on Chromosorb W-HP, 100/120 mesh. The gas chromatograph was a VARIAN 3700.

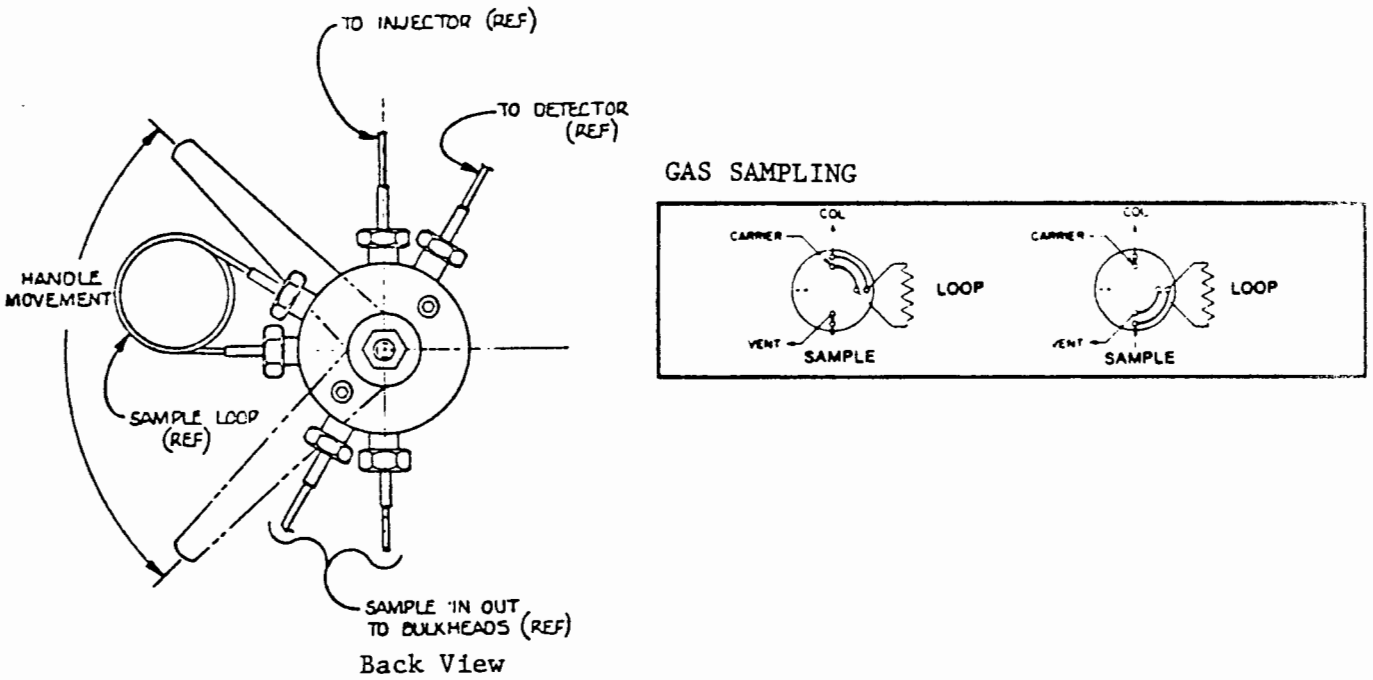

Figure 2.2 Gas sampling valve used for the pulse experiments

2.3.3 Experimental Procedure and Analysis

2.3.3.1 Reaction conditions

All of the experiments were carried out under the same set of conditions. There were two variables, namely, the reactant type and the quantity of reactants. The conditions used are listed below.

Catalyst:

Type	:	Phosphoric acid on kieselguhr
Size fraction	:	106-180 microns
Mass	:	0.707g
Age	:	0-14 days
H_3PO_4 conc	:	104%

Carrier gas:

Type	:	N_2

Flowrate : 0.98-1.02 l/hr

Dewpoint(1 bar) : 255 K

Temperatures:

Water bath : 293 K

Pre-heat section: 473 K

Reactor : 473 K

Exit line : 483 K

Pressures:

Inlet N_2 : 16.3-16.5 bar (abs)

Reactor exit : 16.3-16.5 bar (abs)

2.3.3.2 Typical run procedure

For the first experiment, the entire reactor system was set to the above conditions. Once the conditions had been obtained, the system was allowed to stabilize for 12 hours. This was done to allow the set H_3PO_4 concentration to be obtained. Initially the stainless steel lines had large amounts of water adsorbed on them and required long periods to reach their steady state. The system was completely stabilised after 12 hours.

The method of injecting the reactants depended on whether the reactant was a gas, a liquid or a mixture of the two. The gases were loaded by filling a section between the second three-way valve and the bypass valve. This was done by disconnecting the inlet line (SWAGELOK fittings) to the bypass valve, connecting the valve to a line from the cylinder containing the required gas (CADAC cylinder No.7), filling the line up to the desired pressure, closing the bypass valve, and then removing the line from the cylinder and replacing it with the bypass line. The hexenes were loaded in a similar manner but they were injected as liquids through the open bypass valve into the sample line. Once injected, the bypass valve was closed and the bypass line was reconnected to the valve. To load a mixture of a gas and hexene, the hexene was first injected and then the sample line was filled with the C_3 or the C_4 gas. To load a mixture of gases, the gas with the lower vapour pressure had to be loaded first, followed by the one with the higher vapour pressure. Any given feed did not vary significantly in composition.

Once the sample line was filled, the bypass valve was opened and the two three-way valves were switched simultaneously. The nitrogen carrier, which was redirected through the bypass section, picked up the reactant pulse and carried it to the reactor.

After a given time, a slice of the exit pulse could be captured and sent through the GC separating column by turning the gas sampling valve to the closed position. Only one slice could be taken per experiment due to the long GC analysis time (30 minutes). Once the slice had been captured, the three-way valves were switched to their initial positions.

Several blank runs were performed, in the absence of catalyst, to determine the activity of the empty reactor and pipes. No activity was measured with any of the feeds.

2.3.3.3 Phosphoric acid concentrations

Phosphoric acids of all strengths have a small, but measureable, partial pressure of water in equilibrium with the liquid (McMahon et al., 1963). If water is not introduced with the reactor feed, the catalyst would dehydrate.

The commercial supplier of a solid phosphoric acid on kieselguhr has supplied a set of curves relating H_3PO_4 concentration to water vapour pressure, over a range of reactor temperatures (Figure 2.3). Knowledge of the dewpoint of the water in the reactor feed, enables the determination of the water vapour pressure. Using the water vapour pressure inside the reactor, with the reactor temperature, enables the direct determination of the H_3PO_4 concentration from Figure 2.3.

A comparison between Figure 2.3 and Figure 2.4 shows good agreement. The data in Figure 2.4 were determined by Brown & Whitt (1952). Figure 2.4 is used to estimate H_3PO_4 concentrations greater than 104%. H_3PO_4 concentrations are defined as follows:

$$\% H_3PO_4 = \frac{\text{weight of phosphoric acid in sample if all phosphorous were present as } H_3PO_4}{\text{actual weight of sample}} \times 100$$

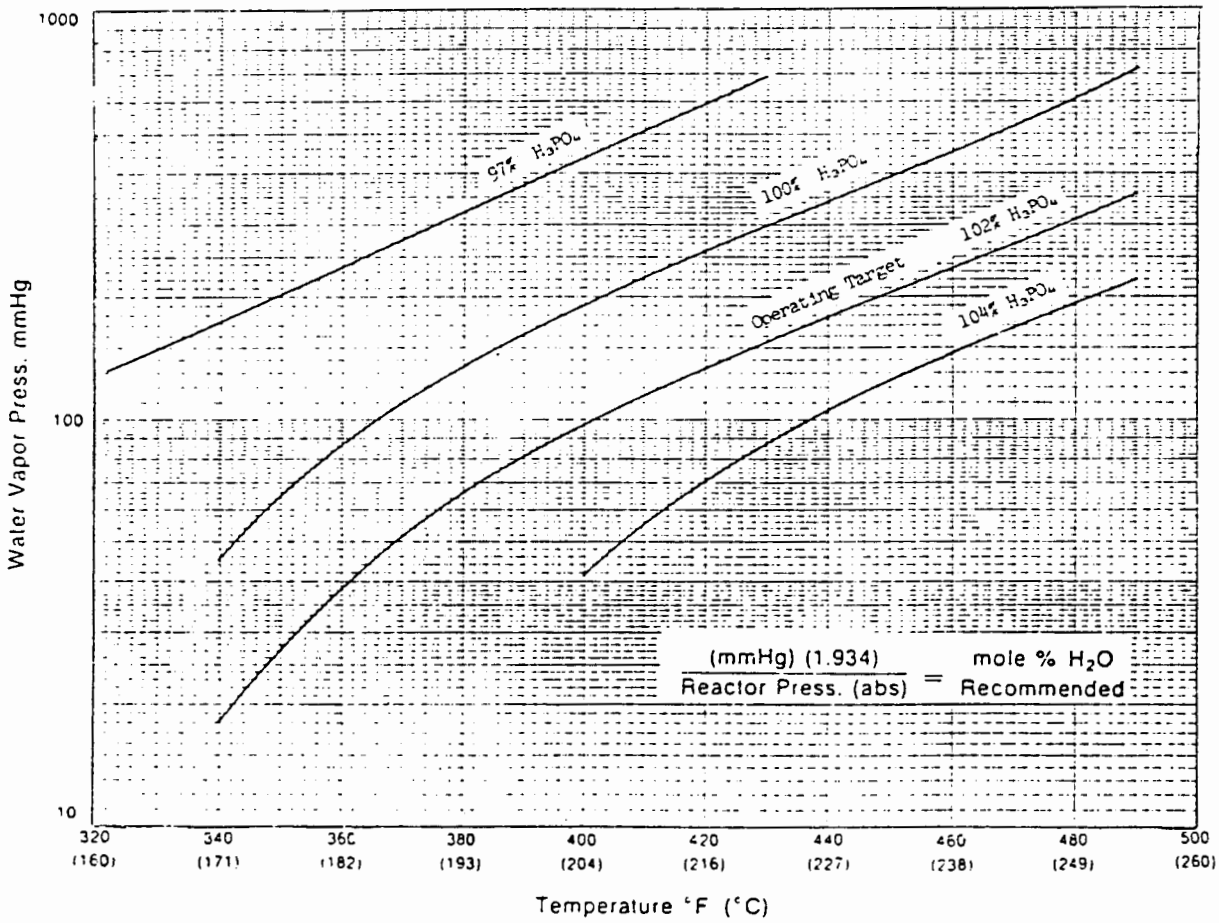

Figure 2.3 H_3PO_4 concentration as a function of water vapour pressure over the range 97% to 104% H_3PO_4 (United catalysts Inc., operating instructions)

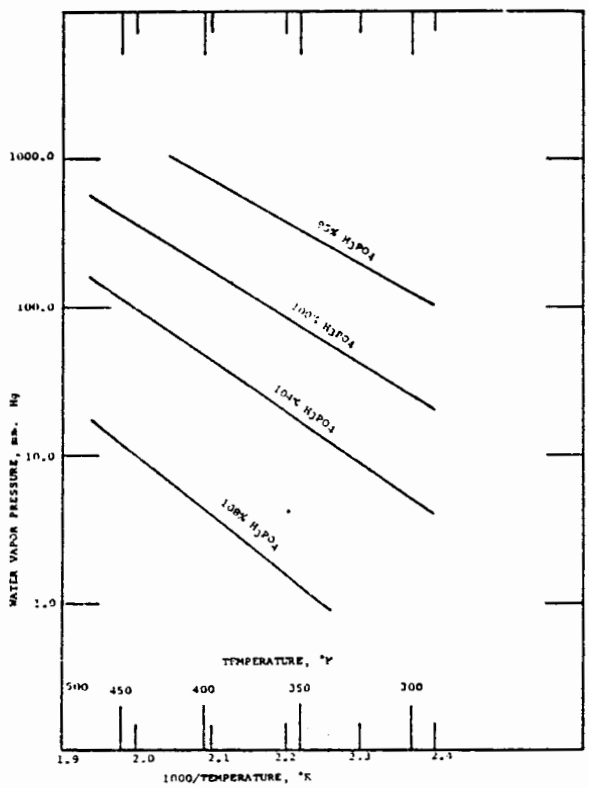

Figure 2.4 H_3PO_4 concentration as a function of water vapour pressure over the range 100 to 108 % H_3PO_4 (Brown & Whitt, 1952)

2.3.3.4 Product analyses

The products were analysed on a VARIAN 3700 GC. The GC operating conditions are listed in Appendix A. Identification of the chromatographic peaks was achieved by mass spectroscopy. Relative response factors were not all equal. Calibration curves for propene, 1-butene, iso-butene, the hexene isomers and the n-alkanes are shown in Section 2.4.1. Due to the complexity of the product spectra and overlapping of some eluted peaks, the peaks were grouped according to chain length.

2.3.3.5 Reaction data workup

The chromatographic results appear as area counts. By the use of calibration curves (Section 2.4.1) these could be converted to masses. Knowing the conditions in the sampling loop, these masses could be converted to molar concentrations. Based on the total area count for each gas sample valve injection, the amount of reactant fed could be calculated, and hence its degree of conversion (see 2.5.1.1).

Provided conversions are low (less than 10%) the pulse reactor can be assumed to be differential. Knowing the catalyst mass, the molar flowrate and the conversion of the feed, the rate of disappearance of a given reactant at a given reactor concentration can be determined. From the corresponding rate-concentration data sets, it was possible to estimate an order of reaction. It must be remembered that the micro-catalytic pulse reactor was in an unstable condition (Reichle, 1981; Hall et al., 1960), with the accompanying unsteady state conditions prevailing (Hall et al., 1960; Verma & Kaliaguine, 1973). The calculated rate-concentration data must therefore be interpreted with extreme caution.

2.4 REACTOR SYSTEM CHARACTERIZATION

2.4.1 Gas Chromatograph Calibration

A flame ionization detector was used for the analysis of the hydrocarbons in these experiments. As a first approximation for hydrocarbons, the chromatographic area count obtained was considered to be approximately proportional to mass, irrespective of the component. It is well known that deviations occur especially for gaseous compounds. As a result, it was necessary to obtain calibration curves (Figure 2.5 and Figure 2.6), relating GC area counts to mass, for each of the reactants used in these experiments.

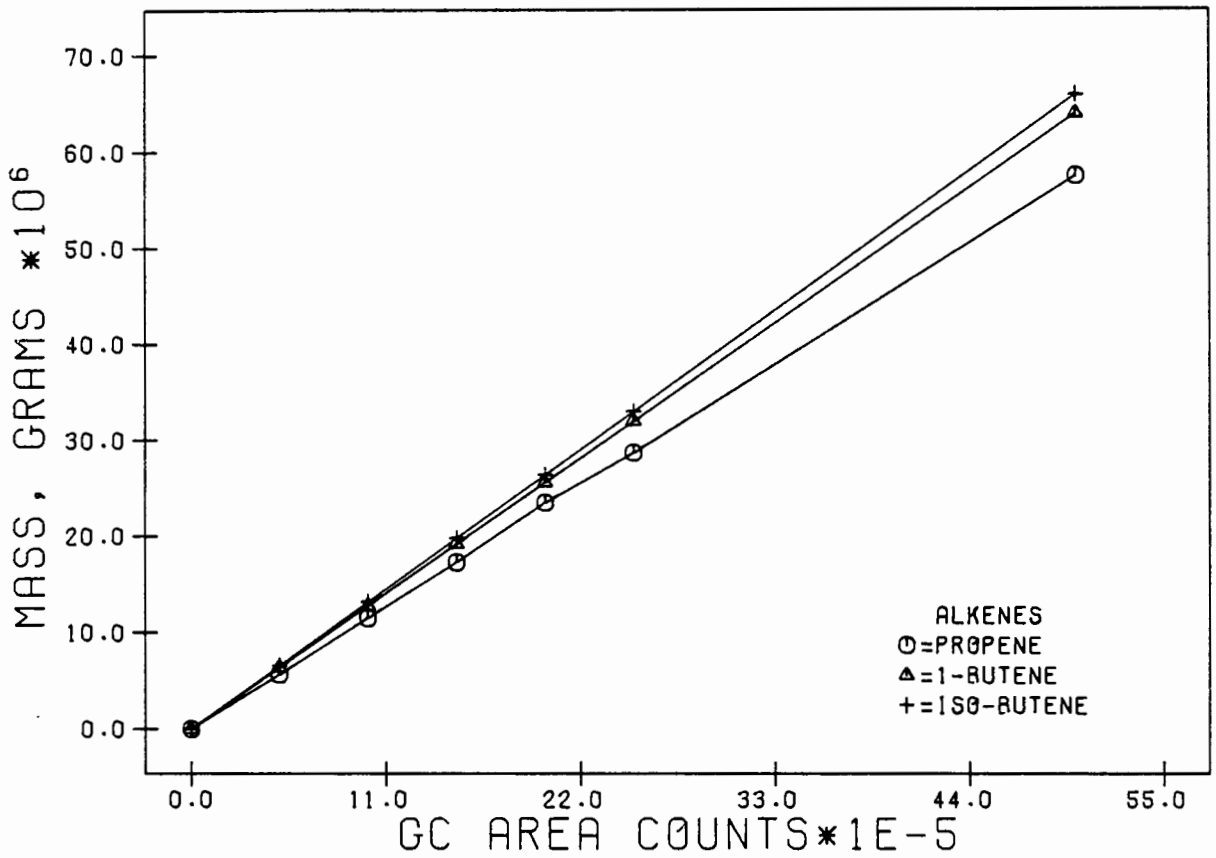

FIG 2.5 PULSE: GC CALIBRATION: PROPENE & BUTENES

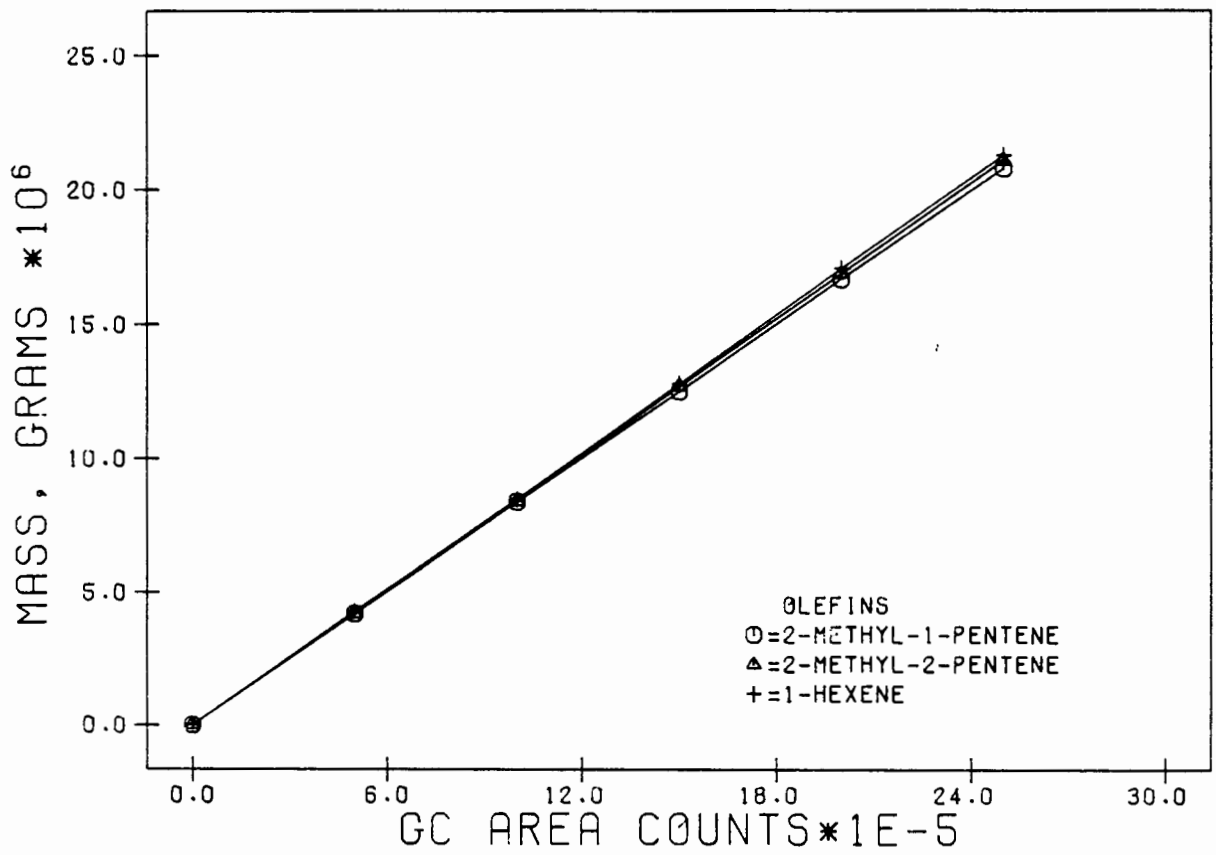

FIG 2.6 PULSE: GC CALIBRATION: HEXENES

For alkanes and alkenes of longer chain length than the pentanes or pentenes, sample mass was considered to be approximately proportional to GC area count within the linear range of the GC detector although deviations could occur. A common method of determining deviations from the above linear relationship is to calculate relative response factors (RRF). Once response factors were determined, area counts could be readily converted to mass%. For normalization, the factors were made relative to one standard component in the sample. The basic formula is:

$$RRF_i = \frac{\text{Amount}_i}{\text{Area}_i} \times \frac{\text{Area std peak}}{\text{Amt std peak}}$$

It is clear from the above formula that the relative response factor of the standard must be equal to unity. The closer the relative response factor is to unity, the smaller is the change in detector response from the standard molecule to that molecule. Using octane as the standard, relative response factors for the alkanes, from pentane to nonodecane, were calculated. The results are shown in Table 2.1 below.

Table 2.1 Relative response factors of hydrocarbons

Sample name	Relative response factor	Sample name	Relative response factor
pentane	1.04	hexane	1.02
heptane	1.02	octane	1.00
nonane	0.99	decane	0.98
undecane	0.99	dodecane	0.97
tridecane	0.99	tetradecane	1.00
pentadecane	1.01	hexadecane	1.00
heptadecane	1.01	octadecane	0.99
nonodecane	1.00		

The relative response factors of the alkanes deviated by less than 4% from unity. Based on these results the response factors for hydrocarbons of chain length greater than or equal to pentene were considered to be equal to unity, despite the degree of branching and unstauration in these products. The direct relationship between GC area counts and sample mass for propene, 1-butene, iso-butene and the various hexene isomers, has been indicated in Figures 2.5 and 2.6.

2.4.2 The Input and Output Pulse

Hattori & Murakami (1974) noted that, as the pulse width increased, the results in the pulse technique approached those in the continuous flow technique. They found that the main difference in results obtained, using these two techniques, was primarily due to the separation between the components in the catalyst bed and from the lowering of the concentration, due to the broadening of the pulse. The effect of these factors was dependent on the pulse width.

Input and output concentration-time curves were obtained for 2-methyl-1-pentene by taking discrete sample slices at several points on each curve. The input pulse was measured at the entrance to the reactor (by diverting the gas flow at this point directly to the gas sampling valve on the GC). The output pulse was measured at the normal outlet of the reactor. The concentration-time curves were obtained under normal operating conditions (see Section 2.3.3.1). The output curve was generated using catalyst in the reactor and hence some degree of 2-methyl-1-pentene conversion was obtained. The maximum conversion obtained (at the crest of the output pulse curve in Figure 2.7) was 9%, with an average of about 5% for the entire pulse and therefore the concentrations of 2-methyl-1-pentene in the output pulse would be somewhat lower than those in the input pulse, in the region of the crest (due to the higher conversions there), despite any dispersion that takes place. The shapes of these input and output pulses are shown in Figure 2.7.

A similar result was found for propene. Note that the pulse broadens. Axial dispersion was an additional reason for the lowering of the maximum 2-methyl-1-pentene concentration at the pulse crest relative to the maximum of the input pulse. The difference in the concentrations of the input and output curves, in the vicinity of the crests, was approximately 10%-13%. It appears, therefore, that the drop in the feed concentration, as it moved through the bed, was largely governed by the degree of conversion (at 9% conversion) rather than the dispersion at these conversion levels.

The larger the pulse width, the closer the continuous flow technique is approached. The pulse width, relative to the catalyst bed length, is given in Figure 2.8. Note that the bed length in Figure 2.8 is given as a time equivalent.

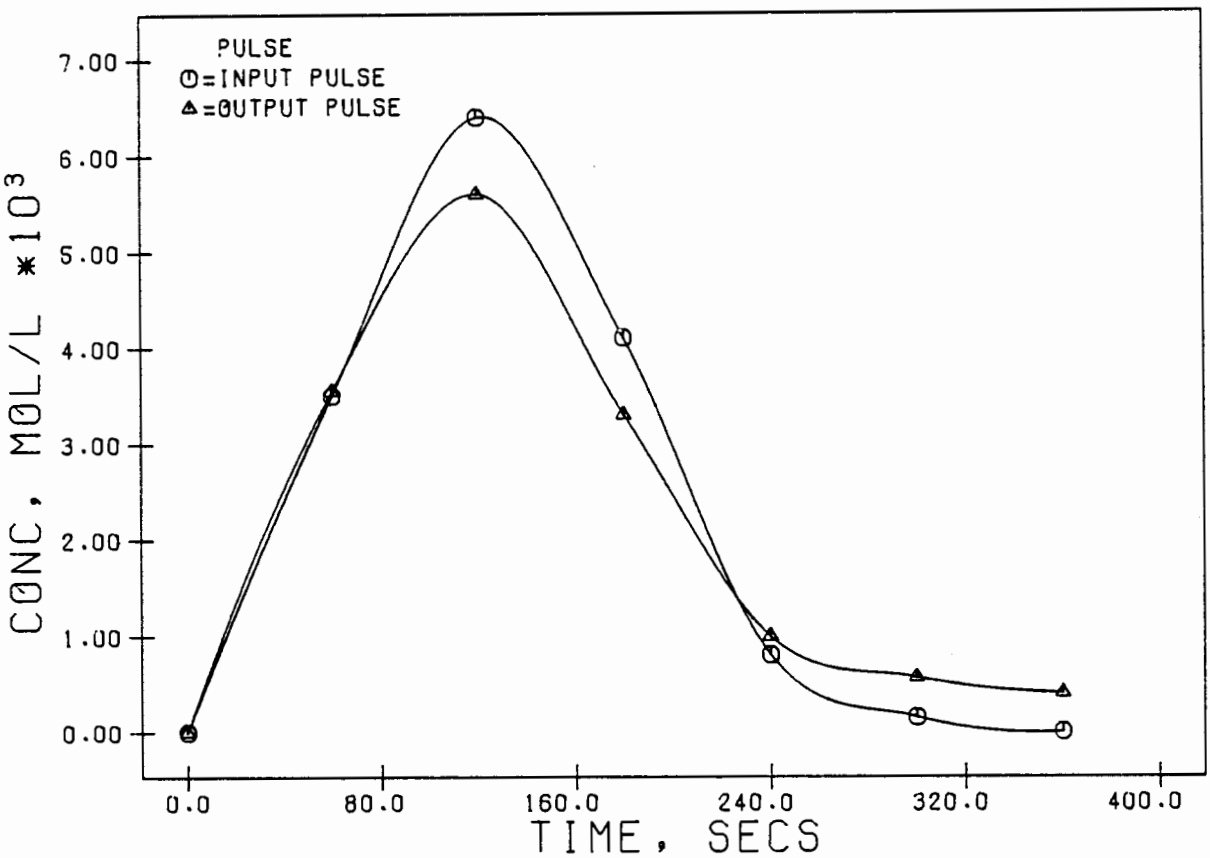

FIG 2.7 THE INPUT AND OUTPUT PULSES USING A 2-METHYL-1-PENTENE FEED

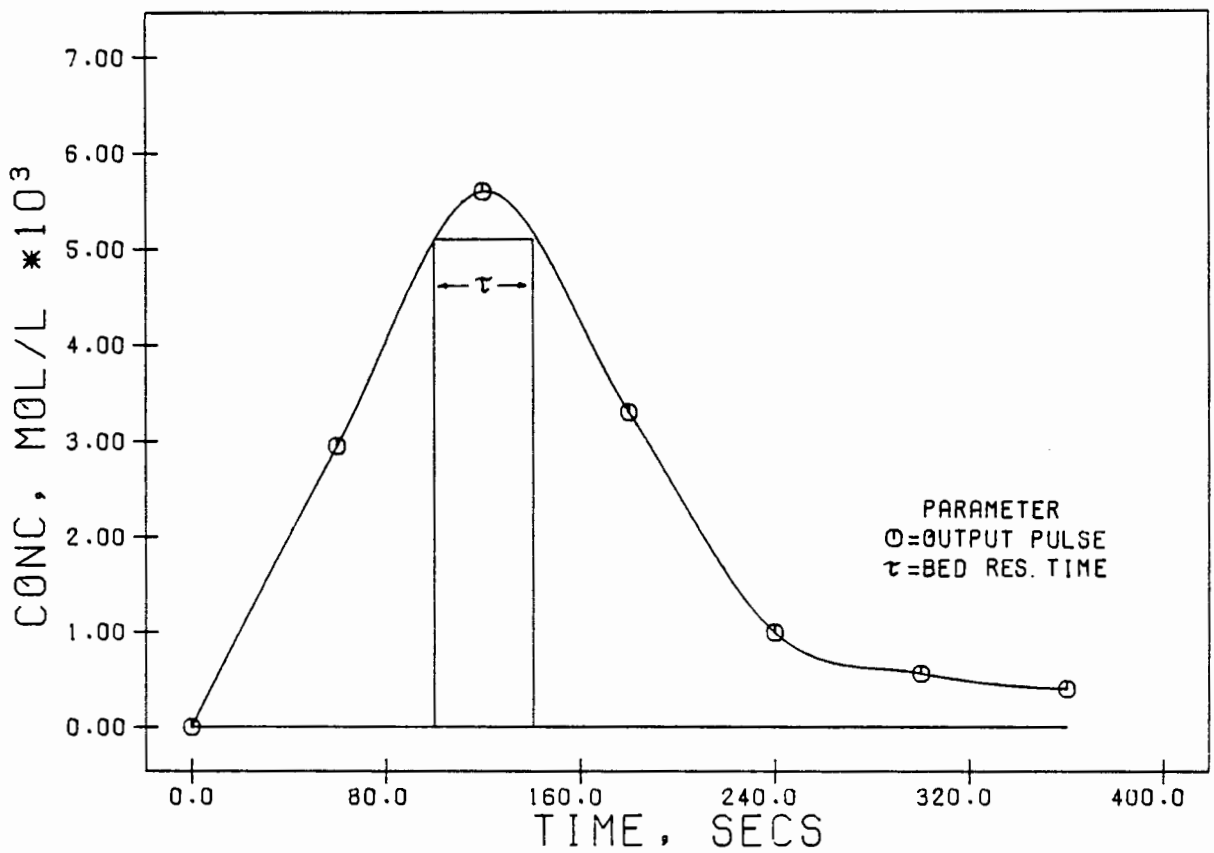

FIG 2.8 OUTPUT PULSE AND BED RESIDENCE TIME USING A 2-METHYL-1-PENTENE FEED

The relative pulse width was large. Between the times of 100 and 140 seconds, the concentration of the pulse (Figure 2.8) in the vicinity of the crest, at any one time, varied by a maximum of 7% as it moved through the bed (Figure 2.8 represents the case with the largest variation in feed concentration), in the absence of reaction. However, the effect of the feed concentration drop, as the pulse moved through the reactor bed, was difficult to quantify, not only due to the concentration change, but also because the system was in an unstable state (due to the changing conditions as the pulse moved through the bed).

2.4.3 Axial Pulse Dispersion

Axial dispersion results in a degree of separation of the longer chain-length compounds from the shorter. Any build up of long chain compounds in the pulse tail was considered to be an indication of axial dispersion.

Several propene pulses were injected. Each pulse was analysed at a different time slice, resulting in the analysis as indicated in Figure 2.9. From each analysis, the propene conversion and product spectra were calculated. These results are shown in Table 2.2. The procedure for calculating the concentrations is shown in 2.5.1.1.

Table 2.2 Product spectra for analysis points in Figure 2.9

Sample No.	Feed X_A%*	Time secs	Feed conc. mol·l^{-1}	Concentrations in sample loop [mol·l^{-1}] C_6	C_9	C_{12}
1	2.0	25	1.0×10^{-2}	0.6×10^{-4}	0.1×10^{-4}	0
2	3.0	45	2.5×10^{-2}	1.5×10^{-4}	0.6×10^{-4}	0.057×10^{-4}
3	4.8	101	6.4×10^{-2}	5.5×10^{-4}	3.0×10^{-4}	0.510×10^{-4}
4	3.1	210	2.7×10^{-2}	1.6×10^{-4}	0.7×10^{-4}	0.060×10^{-4}
5	2.1	255	1.0×10^{-2}	0.7×10^{-4}	0.1×10^{-4}	0

* X_A% = percentage conversion

Without dispersion, the results at sample points 2 & 4 and 1 & 5 would be equal. The result at sample 4 had a higher percentage of longer chain length products, indicating some degree of dispersion, but the increase was minimal and fell within the limits of experimental error.

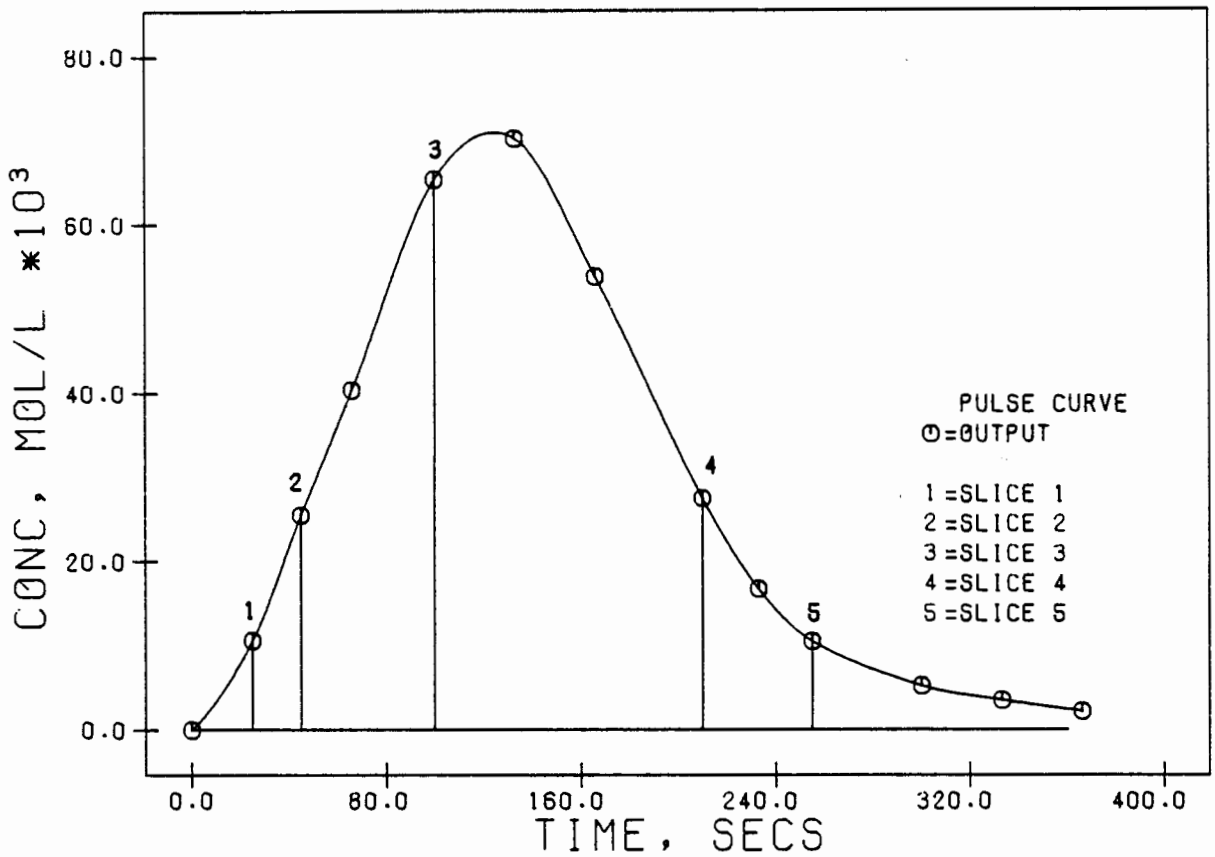

FIG 2.9 PULSE: OUTPUT CURVE(PROPENE FEED)

A further indication of the degree of axial dispersion was ascertained by comparing the product spectra at each of the samples in Figure 2.10. Sample slice 2 here is equivalent to sample slice 4 in Figure 2.9. Sample 1 was obtained by injecting less sample. The feed concentrations for samples 1 and 2 were essentially equal. If similar product spectra were obtained then this would provide further evidence of the negligible effect of axial dispersion. This experiment was carried out and the results are shown in Table 2.3. The product spectra were shown to be quite similar and hence axial dispersion was neglected.

Table 2.3 Product spectra for analysis points in Figure 2.10

Sample No.	Feed X_A%	Feed conc. $mol \cdot l^{-1}$	Concentrations in sample loop [$mol \cdot l^{-1}$] C_6	C_9	C_{12}
1	2.9%	2.8×10^{-2}	1.5×10^{-4}	0.7×10^{-4}	0.065×10^{-4}
2	3.1%	2.7×10^{-2}	1.6×10^{-4}	0.7×10^{-4}	0.060×10^{-4}

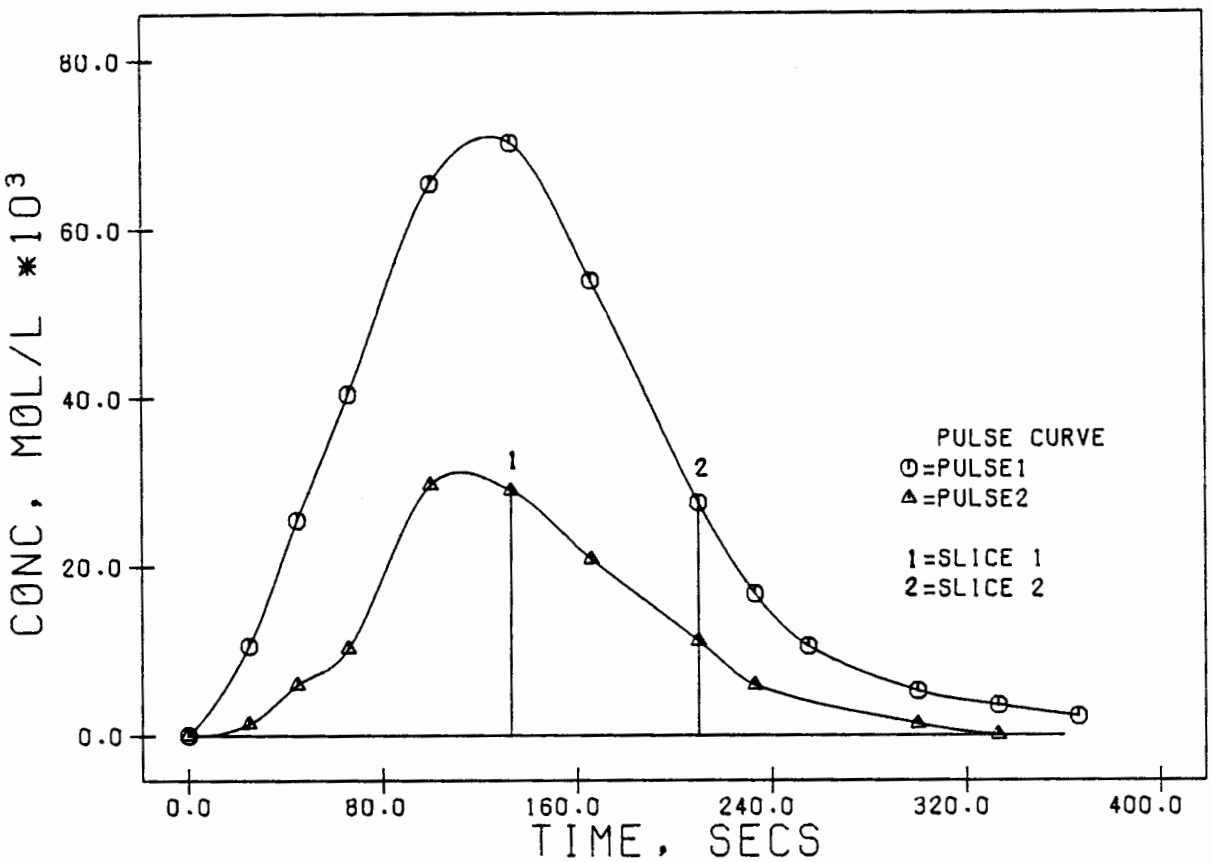

FIG 2.10 PULSE: DISPERSION TEST 2(PROPENE FEED)

2.4.4 Single Slice Analysis

It has been shown that axial dispersion was negligible, despite broadening of the pulse as it traveled through the reactor. The gas sampling valve which captured 0.25cm^3 per sample represented less than 1% of the total pulse width. It would have required many of these slices to have obtained a representative analysis of the entire pulse. Analysis of the entire pulse became more complicated by the changing concentration as the pulse moved through the catalyst bed. The comparison between different sized pulses became even more complicated. The analysis, however, focuses on the region of the injection pulse where the feed concentration was maintained constant to within 5% (this is the region in the vicinity of the crest, i.e., the analysis between t=100 and t=140 seconds in Figure 2.9). For each experiment a single slice was taken from this region (0.25cm^3 in the gas sampling valve). From the output slice, the concentration of the input slice was back calculated by using the simplification of a constant pulse concentration. Some degree of error was incurred here since it was shown in 2.4.2 that some pulse broadening occured, which was accompanied by a drop in the pulse concentration. It should be noted that the effects of dispersion have been shown to be negligible.

This procedure had the advantage of allowing good qualitative comparisons between many different reactants, both simply and quickly.

2.4.5 Mass Balance in Absence of Reaction

Three micro-litres, or 2.01×10^{-3} g, of 2-methyl-pentene were pulsed into the reactor several times. Each time, a slice was analysed at a different sample on the exit pulse, each slice representing a concentration of the 2-methyl-1-pentene (no conversion) at the sample loop conditions (1.44 bar and 423 K). Each of these concentrations was converted to a concentration at STP conditions (298 K and 1.01 bar). The result was a concentration-time curve for the exit pulse similar to that shown in Figure 2.8. Since the flowrate at STP conditions was known (1 litre/hr) the X axis in Figure 2.8 could be converted to volume. Integrating this curve gave the total mass of 2-methyl-1-pentene in the exit pulse. The total integrated mass obtained was 2.00×10^{-3}g. This yielded a mass loss of 0.5% which was acceptable.

2.4.6 Reproducibility

A reproducibility test was performed by injecting three identical amounts of propene and analysing the equivalent sample slice from each exit pulse. (Since the operating conditions did not change, equivalent slices eluted from the reactor system at the same time.) The analyses of the feed's reactor concentration and the exit concentrations of the three major oligomers are shown in Table 2.4. Note that the reactor concentrations of propene were all approximately equal (within 4%). This signifies that equivalent slices were indeed obtained.

Table 2.4 Concentrations for propene reproducibility tests

		Reactor Concentrations		
C_3 Conversion X_A %	propene mol/l	Dimer mol/l	Trimer mol/l	Tetramer mol/l
3.1 %	2.70×10^{-2}	1.60×10^{-4}	0.70×10^{-4}	0.06×10^{-5}
3.0 %	2.61×10^{-2}	1.57×10^{-4}	0.65×10^{-4}	0.06×10^{-5}
3.0 %	2.72×10^{-2}	1.55×10^{-4}	0.71×10^{-4}	0.06×10^{-5}

The reproducibility obtained was adequate, with the largest variation occurring in the tetramer (approximately 6% span).

2.4.7 Catalyst Activity and Lifetime

It was found that, under the conditions used in these experiments, no drop in catalyst activity was observed after fifteen days of continual use, despite the rather high temperature, high acid concentration and low pressure used.

2.4.8 Differential Analysis

A reactor can be considered to be operating differentially when the reaction rate can be considered to be constant at all points within the reactor (Levenspiel, 1972). In the case of fixed bed reactors, this assumption is generally reasonable only for small conversions or for shallow small reactors. The average reaction rate for each run in a differential reactor is given by the following equation:

$$(-r_A)_{ave} = \frac{F_{A0}(X_{A,out} - X_{A,in})}{W}$$

where F_{A0} = molar feed rate of component A to the reactor

$X_{A,in}$ = fractional conversion of reactant A entering the reactor

$X_{A,out}$ = fractional conversion of reactant A leaving the reactor

W = mass of catalyst

In many of the pulse experiments performed in this work, the conversions were small enough (X_A less than 10%) to permit the assumption of a differential reactor. There were, however, experiments (those using the butenes and mixed feeds) whose conversions were too high to allow for this assumption. Such an assumption, in these cases, would result in significant error.

2.4.9 Equilibrium Conversions

The procedure used here to determine the equilibrium composition of a system has been discussed in detail by Smith & Van Ness (1975). The method is based on the fact that, at equilibrium, the total Gibbs free energy of a system has its minimum value. The problem is to find the composition which minimizes G^t (Gibbs free energy) for specified temperatures and pressures, subject to the constraints of material balances.

The following is a summary of the procedure used for gas phase reactions.

1. The constraining equations are formulated, i.e., the material balances. A material balance on each element k can be written as follows.

$$\sum_i n_i a_{ik} = A_k$$

where n_i = the number of moles of species i

a_{ik} = the number of atoms of the kth element present in each molecule of chemical species i

A_k = the total number of atomic weights of the kth element present in the system, as determined by the initial constitution of the system.

2. The Lagrange multipliers, λ_k, are introduced next, one for each element, by multiplying each element balance by its λ_k. The equations are summed over k giving

$$\sum_k \lambda_k \left(\sum_i n_i a_{ik} - A_k \right) = 0$$

3. A new function F is formed by addition of this sum to G^t. The new function is identical to G^t because the summation term is zero. The partial derivatives of F and G^t with respect to n_i will be different because the function F incorporates the constraints of the material balances.

4. The minimum value of F and G^t occurs when the partial derivatives of F with respect to n_i are zero. The expression for these derivatives may therefore be set to zero giving.

$$\left(\frac{\partial F}{\partial n_i} \right)_{T,P,n_i} = \left(\frac{\partial G^t}{\partial n_i} \right)_{T,P,n_i} + \sum_k \lambda_k a_{ik} = 0$$

The first term on the right is the definition of chemical potential and so this equation becomes:

$$\mu_i + \sum_k \lambda_k a_{ik} = 0$$

The chemical potential is given by $\mu i = G^{\circ} + RT \ln \hat{a}_i$. For gas phase reactions and standard states as the pure ideal gases at 1 bar, this becomes:

$\mu_i = G^\circ_i + RT\ln\hat{f}_i$ where $\hat{f}_i$ is the fugacity of species i

G°_i can be set equal to zero for all elements in their standard states giving, for compounds $G^\circ_i = \Delta G^\circ_{fi}$ (the standard Gibbs free energy change of formation for species i). The fugacity can be eliminated in favour of the fugacity coefficient i.e., $\hat{f}_i = y_i \hat{\phi}_i P$.

The resulting equation is

$$\Delta G^\circ_i + RT\ln(y_i \hat{\phi}_i P) + \sum_k \lambda_k a_{ik} = 0$$

Equilibrium compositions were estimated using the Simulation Sciences computer package, PROCESS (Simulation Sciences, 1983). The Redlich-Kwong equation of state was used to account for non-ideality. The assumption of gas phase was made throughout the calculations, although at the higher pressures used, mixed phases were present. A severe limitation of the thermodynamic study was the limited amount of both heats of formation and free energies of formation for many alkenes especially those of chain length greater than C_6. The following were examined:

1. Equilibrium compositions of straight chain alkenes over a temperature range of 433 to 483 K and a pressure range of 0.001 bar to 15 bar.
2. Equilibrium compositions of all alkenes i.e., as many as there was data for, from carbon chain length C_4 to C_8. Each carbon chain length group was examined separate to the rest. The calculations were performed over the temperature range of 433 to 493 K.
3. The equilibrium compositions of a combined group of C_4, C_5, C_6 and C_7 alkenes, again using as many alkenes as possible (data permitting). The calculations were performed at 473 K and over 0.001 and 1 bar.
4. The equilibrium compositions of a group of 50 alkanes (straight and branched) from the butanes up to the nonanes. The calculations were carried out at 473 K and between the pressures of 0.001 and 15 bar.

2.4.9.1 Equilibrium compositions of straight alkenes

Due to the scarcity of heat of formation and free energy data for many branched alkenes of carbon chain length greater than C_6, it was not possible to determine accurately how closely equilibrium was approached. To obtain an indication of the compositions that might prevail, the equilibrium compositions of various straight chain alkenes were determined over a temperature range of 433 K to 483 K and a pressure range of 0.001 to 15 bar. The data are listed in Appendix B. The data are also shown graphically, at three temperatures, in Figures 2.11, 2.12

and 2.13. Mole fractions are plotted as functions of total system pressure. The equilibrium fractions of the C_6, C_7, C_8, C_9 and C_{10} alkenes are not shown due to the small amount obtained. It is quite clear from Figures 2.11, 2.12 and 2.13 that higher pressures favour, as is expected, the longer chain length alkenes.

2.4.9.2 Equilibrium composition of C_4, C_5, C_6, C_7 and C_8 alkene groups

The equilibrium compositions of C_4, C_5, C_6, C_7 and C_8 alkene groups (straight and branched alkenes) were determined at various temperatures. Due to the limited thermodynamic data, only three alkene isomers in each of the C_7 and C_8 groups were examined. Data were obtained over a temperature range of 433 K to 493 K. The analysis was carried out over the pressure range of 1 to 100 kPa, although the results were independent of pressure in this range. The results quoted are therefore applicable over the pressure range of 1 to 100 kPa. The results of the C_4, C_7 and C_8 alkene groups (over the entire temperature range) were as follows, in order of decreasing stability:

C_4 alkenes iso-butene > trans-2-butene > cis-2-butene > 1-butene

C_7 alkenes 2-heptene > 4-methyl-1-hexene > 1-heptene

C_8 alkenes trans-2-octene > 2-ethyl-1-hexene > 1-octene

The results for the C_5 and C_6 alkene groups are shown graphically in Figures 2.14 and 2.15. Six C_5 isomers and sixteen C_6 isomers were used in the calculations. The isomers used and the data for the C_5 and C_6 isomer groups are listed in Appendix C. Mole fractions are plotted as functions of temperature for all of the C_5 isomers (Figure 2.14) and the six most abundant C_6 isomers (Figure 2.15).

2.4.9.3 Equilibrium compositions of a combined C_4, C_5, C_6 and C_7 alkene group

Similar calculations to those in Section 2.4.9.2 above were carried out using a combined C_4, C_5, C_6 and C_7 alkene group in order to provide an indication of the most stable isomers in this alkene category. These were the same alkenes as those used in Sections 2.4.9.1, and 2.4.9.2. The calculations were carried out at various temperatures and pressures. It was found that in the 453 K to 473 K temperature range that there was relatively little change in the mole fraction sof the isomers. For this reason the results will be shown for the 473 K calculations at various pressures. The ten most stable isomers are shown (mole fractions) as functions of pressure in Figure 2.16.

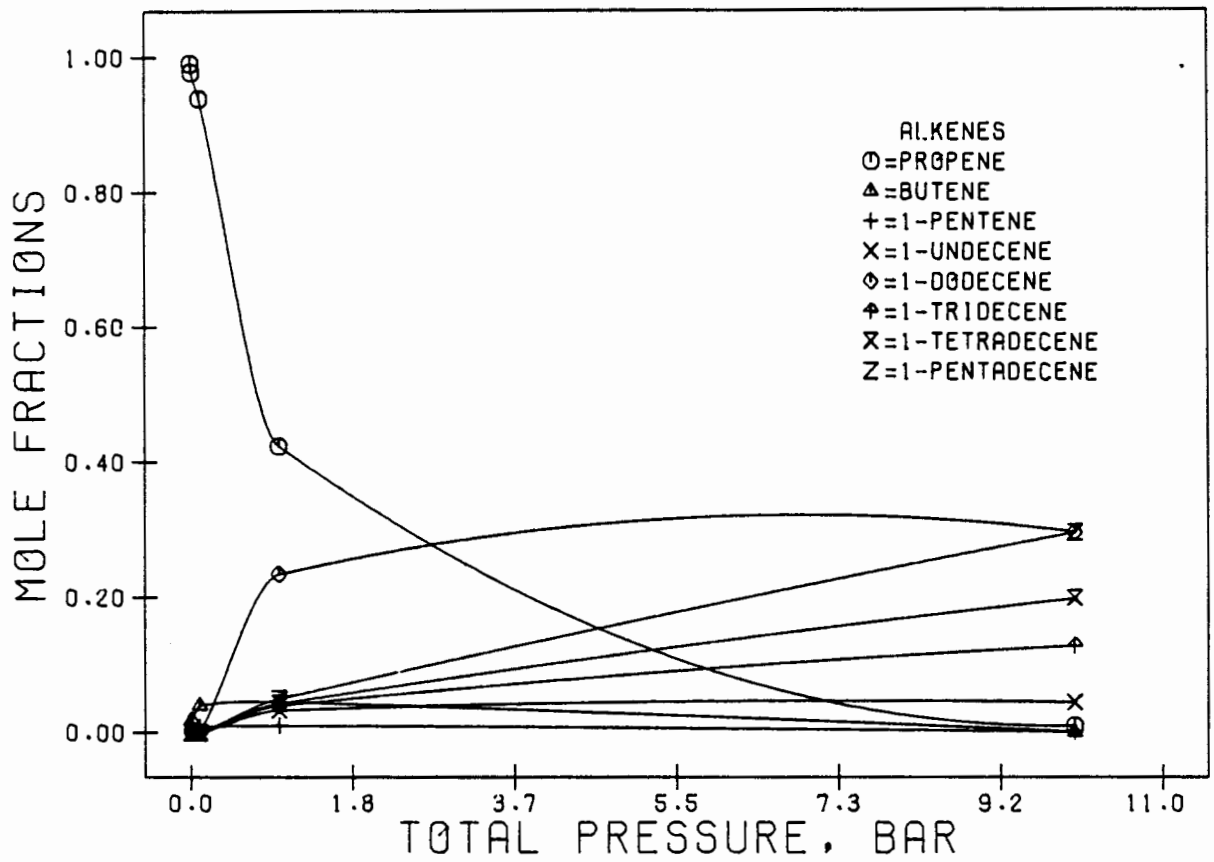

FIG 2.11 EQUILIBRIUM DATA FOR STRAIGHT ALKENES AT 433 K

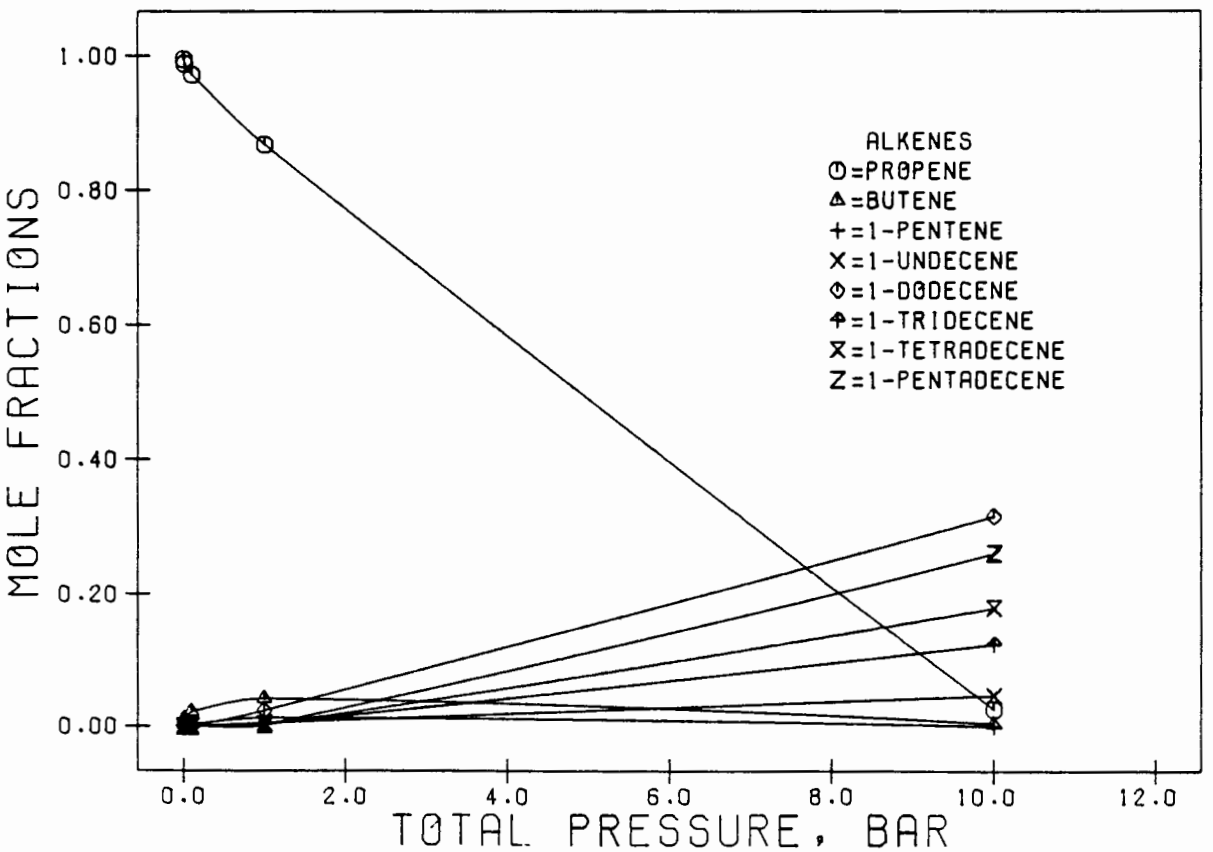

FIG 2.12 EQUILIBRIUM DATA FOR STRAIGHT ALKENES AT 458 K

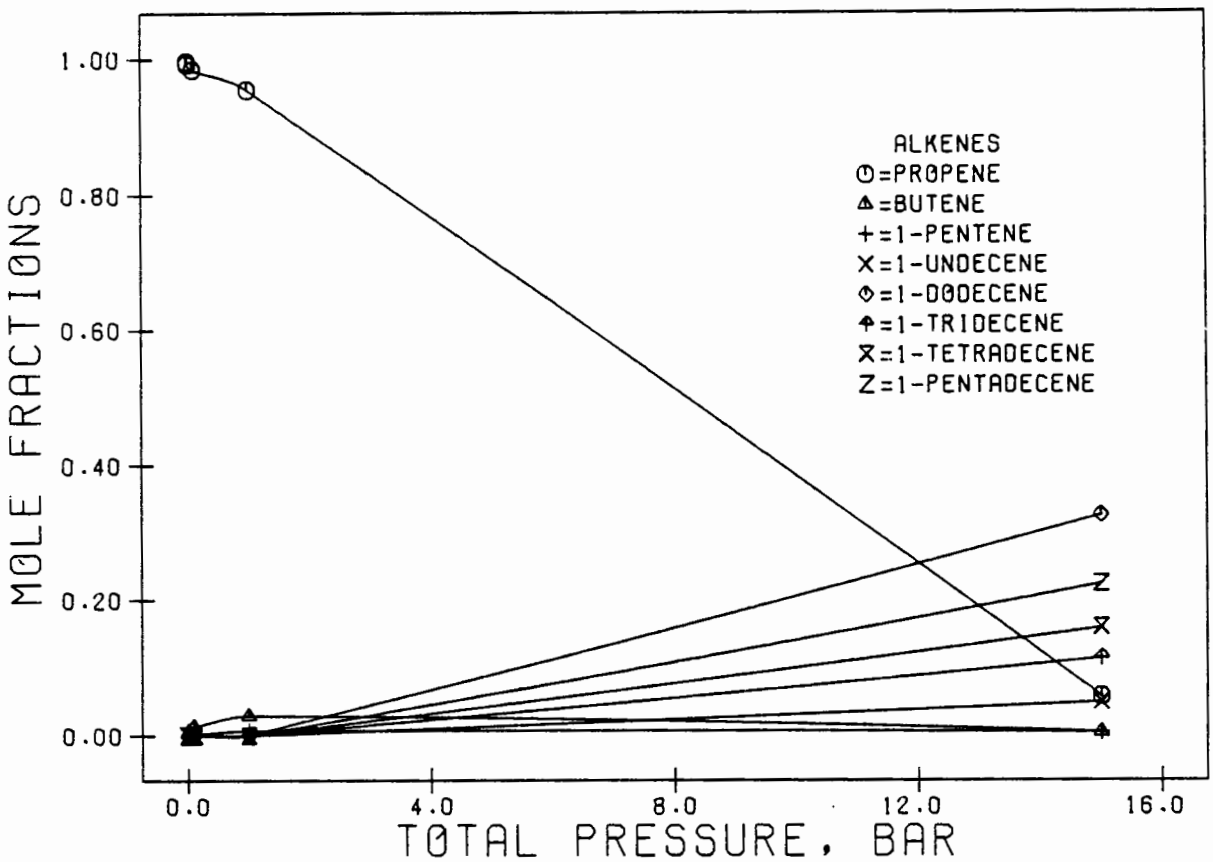

FIG 2.13 EQUILIBRIUM DATA FOR STRAIGHT ALKENES AT 483 K

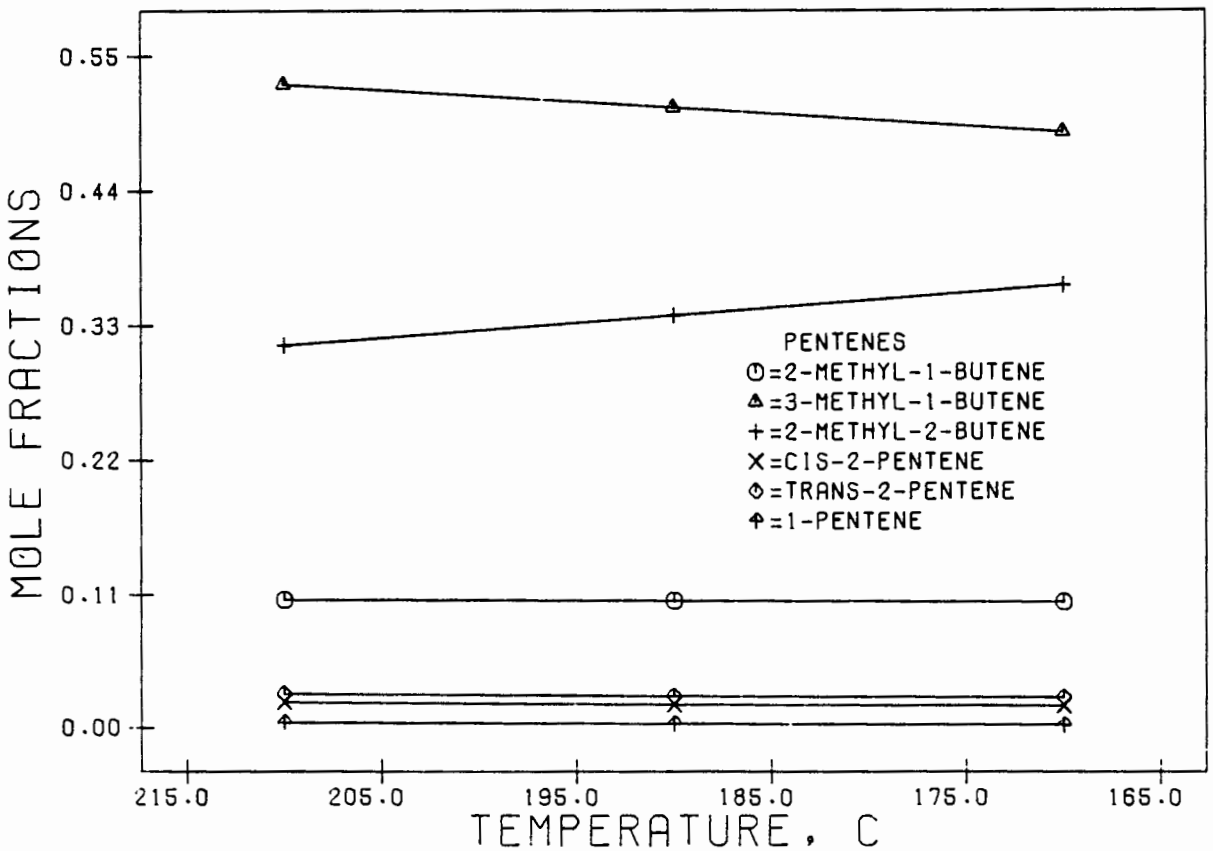

FIG 2.14 EQUILIBRIUM DATA FOR PENTENES OVER THE TEMPERATURE RANGE: 443 K TO 483 K

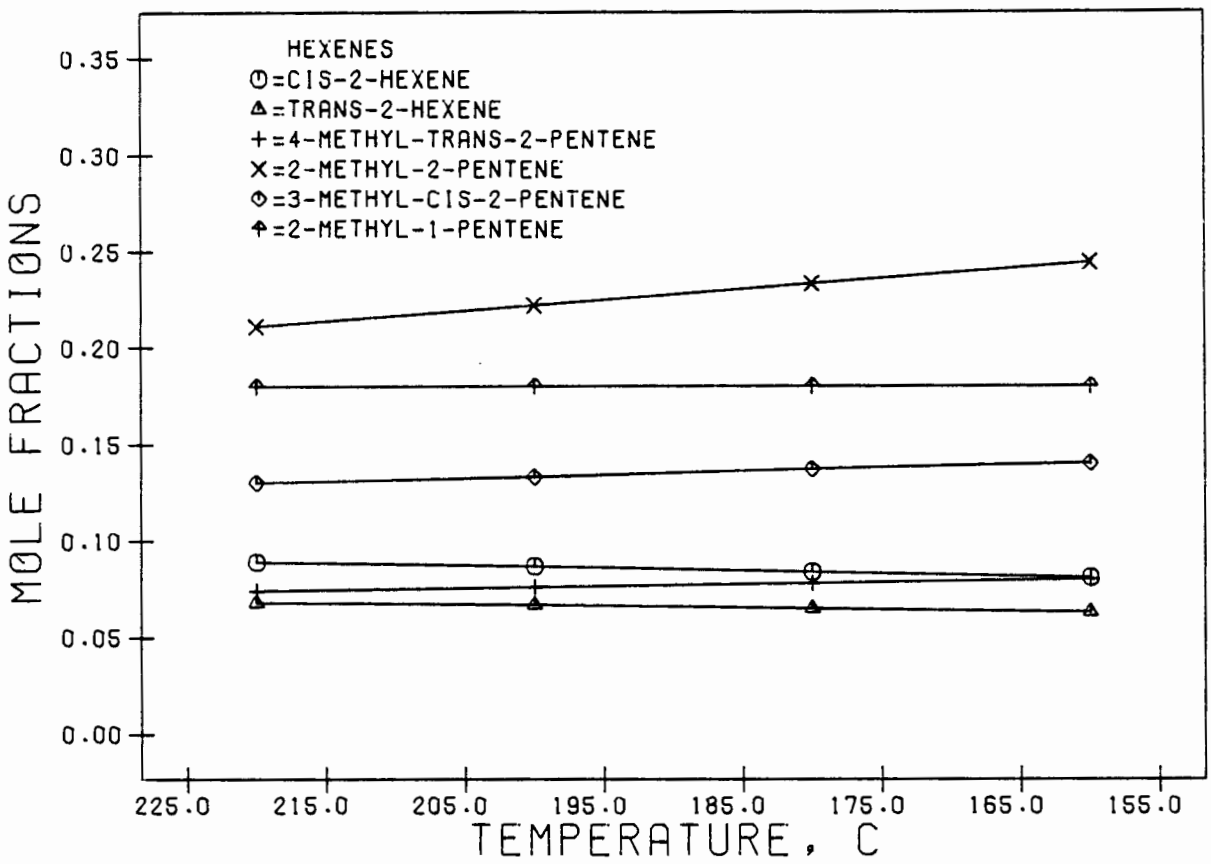

FIG 2.15 EQUILIBRIUM DATA FOR HEXENES OVER THE TEMPERATURE RANGE OF 433 TO 493 K

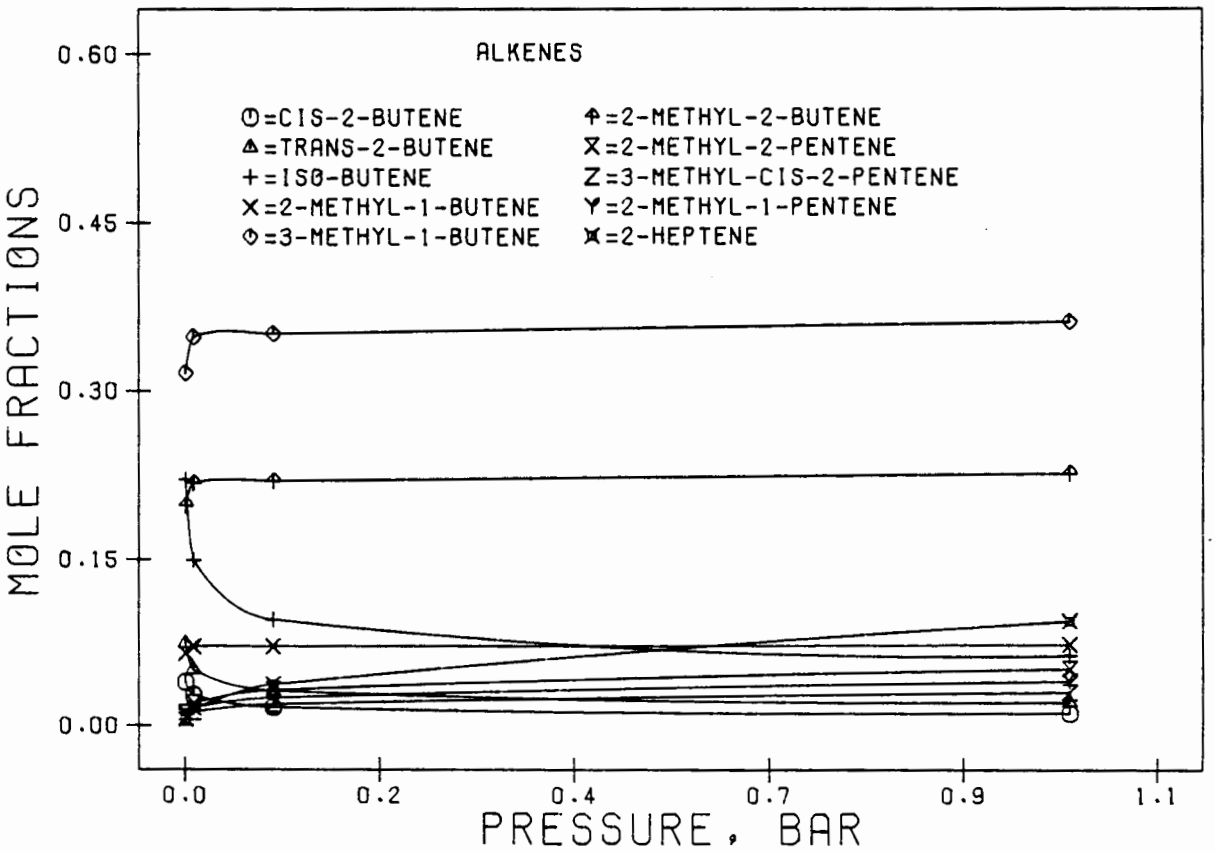

FIG 2.16 EQUILIBRIUM DATA FOR C4, C5, C6 AND C7 ALKENES AT 473 K AND BETWEEN 0.1 AND 100 KPA

2.4.9.4 Equilibrium compositions of a group of alkanes

Equilibrium compositions were determined for a group of 50 alkanes ranging from C_3 to C_9. It was found that there was relatively little change in the equilibrium compositions with temperature in the desired temperature range of 453 K to 473 K. The alkanes used are listed in Table 2.5. Hydrogen was included as a component in order to satisfy the mass balance. Although in this work little or no alkanes were produced, the calculations with the alkanes were carried out with the hope of providing an indication of the trends followed by the alkenes.

The equilibrium compositions at the highest pressure used (15 bar) which should shift the equilibrium composition towards the higher alkanes comprised only propane, butane and iso-butane, the mole fraction of all other alkanes being equal to zero. It is quite clear therefore that there is no correlation between the alkanes and the alkenes in this regard.

Table 2.5 Alkanes used in the equilibrium calculation of Section 2.4.9.4.

1. Propane	26. 4-methyl-heptane
2. Butane	27. Octane
3. Iso-butane	28. 2,2,3,3-tetramethyl-butane
4. Iso-pentane	29. 2,2,3-trimethyl-pentane
5. 2,2-dimethyl-propane	30. 2,2,4-trimethyl-pentane
6. Pentane	31. 2,3,3-trimethyl-pentane
7. 2,2-dimethyl-butane	32. 2,3,4-trimethyl-pentane
8. 2-methyl-pentane	33. 3,3-diethyl-pentane
9. 2,3-dimethyl-pentane	34. 2,2-dimethyl-3-ethyl-pentane
10. 3,3-dimethyl-pentane	35. 2,4-dimethyl-3-ethyl-pentane
11. 3-ethyl-pentane	36. 2,2-dimethyl-heptane
12. 2,2,3-trimethyl-butane	37. 3-ethyl-heptane
13. Heptane	38. 2-methyl-octane
14. 3-methyl-hexane	39. 3-methyl-octane
15. 2,2-dimethyl-hexane	40. 4-methyl-octane
16. 2,3-dimethyl-hexane	41. Nonane
17. 2,4-dimethyl-hexane	42. 2,2,3,3-tetramethyl-pentane
18. 2,5-dimethyl-hexane	43. 2,2,3,4-tetramethyl-pentane
19. 3,3-dimethyl-hexane	44. 2,2,4,4-tetramethyl-pentane
20. 3,4-dimethyl-hexane	45. 2,3,3,4-tetramethyl-pentane
21. 3-ethyl-hexane	46. 2,3,4-trimethyl-hexane
22. 2-methyl-3-ethyl-pentane	47. 2,2,5-trimethyl-hexane
23. 3-methyl-3-ethyl-pentane	48. 2,3,3-trimethyl-hexane
24. 2-methyl-heptane	49. 2,3,5-trimethyl-hexane
25. 3-methyl-heptane	50. Hydrogen

2.4.10 Determination of Phase Equilibria

The fundamental problem of vapour-liquid equilibria deals with a multicomponent system of N non-reacting chemical species for which the phase rule variables are temperature, pressure, N-1 liquid mole fractions and N-1 vapour mole fractions. Thus there are 2N variables (Smith & Van Ness, 1975). Application of the phase rule yields F=N and this means that, for an equilibrium state, only N of the 2N variables are independent. Once N phase rule variables are specified, the remaining N variables can be determined by simultaneous solution of the N equilibrium relations of the form $\hat{f}_i^V = \hat{f}_i^L$

where $\hat{f}$ = fugacity

^{V} = vapour phase

^{L} = liquid phase

For a component in a vapour mixture $\hat{f}_i^V = y_i \hat{\Phi}_i^V P_t$ and for a component in a liquid solution $\hat{f}_i^L = x_i \gamma_i^L f_i^{oL}$

where $\hat{\Phi}_i$ = fugacity coefficient

P_t = total pressure

γ_i = liquid phase activity coefficient

x_i, y_i = mole fractions in liquid and gas phases

To satisfy the criterion for equilibrium, $y_i \hat{\Phi}_i^V P_t = x_i \gamma_i^L f_i^{oL}$. At low pressures, when the critical region is not approached, the assumption can be made that the liquid phase properties γ_i and f_i^o are independent of pressure. For phase equilibrium at high pressure, or where the critical region is approached, the thermodynamic functions for the liquid phase cannot be assumed to be independent of pressure. The simple two term virial equation is no longer satisfactory (at high pressures) for the calculation of vapour-phase properties.

The first realistic general method, based on thermodynamics, was proposed for this calculation by Chao & Seader (1961). Several refinements have been proposed since then (Robinson & Chao, 1971; Lee et al., 1973). The basic equation is given below.

$$K = \frac{\gamma_i^L f_i^{oL}}{\hat{\Phi}_i^L P_t} \quad \text{where } K = y_i/x_i$$

The fugacity coefficient is defined as $\Phi_i = \hat{\Phi}_i / P_t$. Substituting for the fugacity gives

$$K_i = \frac{\gamma_i \hat{\Phi}_i^L}{\hat{\Phi}_i}$$

This implies that here the standard state fugacity is the fugacity of pure liquid i at the temperature and pressure of the system. In order to determine the phase equilibria γ_i, ϕ_i^L and $\hat{\phi}_i$ need to be determined at the desired temperatures and pressures. The procedures used to determine these parameters are given in Appendix D.

There are three classes of vapour-liquid equilibria problems. These are the bubble point, dewpoint and flash calculations.

For the bubble point calculations, from a known liquid composition and pressure, the temperature and vapour phase (equilibrium) composition can be found using the equations discussed above. This can be done at many pressures. In the dewpoint calculations, the temperature and liquid phase compositions are found from given gas phase compositions at each pressure. A phase diagram can therefore be drawn up.

In the flash calculations, from a mixture with a known composition and at a given temperature and pressure, the mole fractions of each component in the vapour and liquid are determined.

In order to determine whether there was any liquid phase present in any of the experiments in this study, a phase diagram was plotted for the experiment most likely to have any liquid phase present. The experiment used was Run 4 of Section 2.5.13.1 where a mixed propene/iso-butene feed was used. The phase diagram is shown in Figure 2.17. Nitrogen is not included in the phase calculation. The partial pressure of the hydrocarbon mixture is less than 1.37 bar. (determined simply, from the mole fractions listed in Section 2.5.13.1 and the total pressure used). The dew point of this hydrocarbon mixture at 1.37 bar is approximately 345 K (see Figure 2.17) and hence it can be concluded that no liquid phase was present in any of the pulse experiments, since the operating temperature was 473 K throughout.

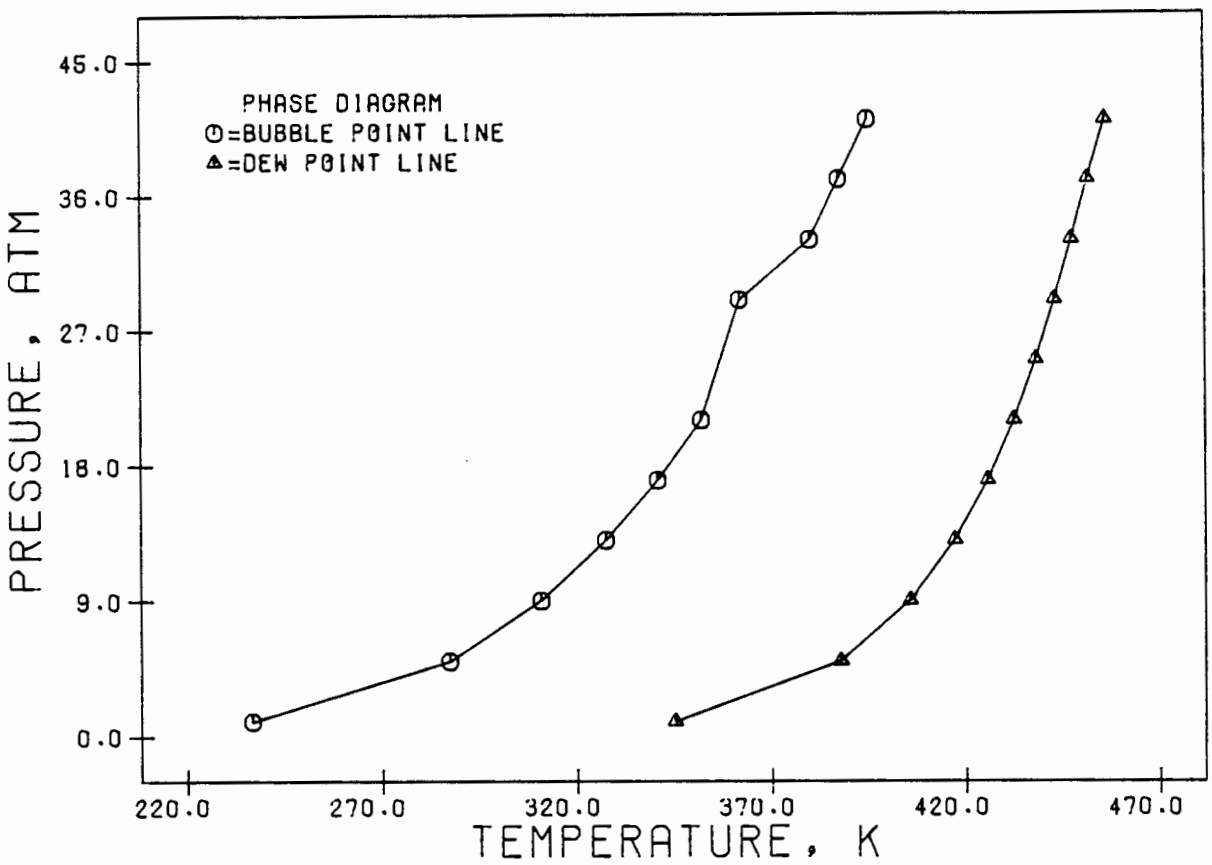

FIG 2.17 PHASE DIAGRAM FOR FEED AND PRODUCT MIXTURE OF RUN NO.4 OF SECTION 2.5.13

2.5 RESULTS AND DISCUSSION

2.5.1 Preliminary Results

2.5.1.1 Complete analysis of typical pulse experiment

A detailed analysis of a typical micro-catalytic pulse experiment is given in order to indicate features common to all the experiments. Not only does this analysis provide an indication of the stability of various parameters in all the runs (e.g., the reproducibility of the gas chromatographic separation), but it also indicates several features inherent in the reaction (e.g., aspects of the reaction mechanism).

The experiment to be considered is that where the sample line is filled up to a pressure of 500 kPa gauge with pure propene. The experimental conditions are listed in Section 2.3.3.1.

Component identification and separation

A sample slice is captured on the gas sampling valve 660 seconds after the pulse was introduced into the nitrogen stream. The chromatographic conditions are listed in Appendix A. A typical chromatograph is shown in Appendix E. Component identification is carried out using mass spectroscopy. The mass spectrograph corresponding to the chromatograph in Appendix E is shown in Appendix F. Note the overlap in some of the peaks. As explained in Section 2.3.3.3, the separation is done according to carbon chain length. The chromatographic area count for each group can be converted to mass using the calibration curves in Figures 2.5 and 2.6. These masses are converted to moles and molar concentrations (G.C. sample loop size = $0.25cm^3$). The area counts and concentrations are listed in Table 2.6.

Before the above concentrations (at sample loop conditions) can be converted to their equivalent concentrations at the reactor exit (at reactor conditions), the compressibility factor, Z, of the gases inside the reactor must be calculated.

Table 2.6 Area counts and concentrations of a typical pulse.

	Area counts	Concentration in the loop C [mole/l]
propene	5954000	$7.67x10^{-3}$
C_4	0	0
C_5	27410	$1.3x10^{-5}$
C_6	194600	$7.7x10^{-5}$
C_7	61050	$2.1x10^{-5}$
C_8	40470	$1.2x10^{-5}$
C_9	228200	$6.1x10^{-5}$
C_{10}	24210	$0.6x10^{-5}$
C_{11}	5333	$0.1x10^{-5}$
C_{12}	53960	$1.1x10^{-5}$
		$\Sigma C = 7.87x10^{-3}$

Assuming that the ideal gas law applies to the sample gas in the sample loop, the total number of moles in a litre at loop conditions is given by:

$$N_T = \frac{PV}{RT} = \frac{146\ kPa \times 1000\ cm^3}{8319 \times 423K}$$

$$= 4.15 \times 10^{-2}\ \text{mole/l at sample loop conditions}$$

where $R = 8319\ kPa \cdot cm^3 \cdot mole^{-1} \cdot K^{-1}$

P = loop pressure, kPa

V = 1 litre

T = temperature in loop, K

The total number of moles of propene and products in one litre at the same conditions (in the sample slice) is given by:

$N_P = \Sigma C$ (Table 2.6)

$= 7.87 \times 10^{-3}$ mole/l

N_T = total number of moles per liter at sample loop conditions

N_P = total number of moles of propene + products at sample loop conditions

The ratio of N_P to N_T is equivalent to a mole fraction of 0.19, the balance being nitrogen. This particular example, by choice, represents the largest hydrocarbon: nitrogen ratio encountered in these experiments and therefore will represent the largest deviation from ideality. In the majority of cases the mole fraction of hydrocarbons will be less than 10%. For the purposes of calculating the lowest possible compressibility factor, this example will be used. A detailed calculation of the compressibility factor for a 4:1 (mole ratio) nitrogen: propene mixture at the conditions listed in Section 2.3.3.1, is given in Appendix G. Note that the procedure used can be extended to three or more component systems.

The value of Z obtained is 0.999. Z can therefore be assumed to be equal to unity throughout these experiments (both in the loop and in the reactor).

The total molar concentration of nitrogen + hydrocarbons inside the reactor is equal to 0.4225 mole/l at 1.66 MPa and 473K. The concentrations of the gases, given at sample loop conditions in Table 2.6, can now be converted to concentrations at reactor conditions. The results, together with mole fractions of each component, are shown in Table 2.7. Note that these concentrations are at the reactor exit.

Traces of hydrocarbons greater than C_{12} were detected, but are not shown, since they are smaller than the experimental error.

The amount of propene fed to produce the product spectrum shown in Table 2.7, can easily be back-calculated (remembering that dispersion is considered to be negligible). The only source of the reaction products is propene. The amount of propene fed is therefore equal to 3.50 g/l (ΣC_2). The mass of propene in the sample slice is equal to 3.28 g/l (see Table 2.7). It is assumed that there is no density change in the reactor due to both the large amount of inert and the low conversions. The fractional conversion of propene is given by:

$$X_A = \frac{3.50 - 3.28}{3.50} \times 100 = 6.3\%$$

Table 2.7 Concentrations in the reactor exit.

	Reactor concentrations		
	[mole/l] C_1	[g/l] C_2	mole% of products
propene	7.8×10^{-2}	3.28	——
C_4	0.0	0.0	0.0
C_5	1.3×10^{-4}	9×10^{-3}	6.5
C_6	7.9×10^{-4}	6.6×10^{-2}	38
C_7	2.1×10^{-4}	2.1×10^{-2}	10
C_8	1.2×10^{-4}	1.3×10^{-2}	6.0
C_9	6.2×10^{-4}	7.8×10^{-2}	30
C_{10}	5.9×10^{-5}	8×10^{-3}	2.9
C_{11}	1.2×10^{-5}	2×10^{-3}	0.6
C_{12}	1.1×10^{-4}	1.9×10^{-2}	5.3
	$\Sigma C_1 = 8.0\times10^{-2}$	$\Sigma C_2 = 3.496$	

It will be assumed that the reactor behaves differentially. The rate of disappearance of propene, as the sample slice moves through the reactor bed, is equal to :

$$(-rC_3)_{ave} = \frac{X_a \; v \; C_{A0}}{W}$$

$$= \frac{0.063 \times 0.098 \times 8.3\times10^{-2}}{0.707}$$

$$= 7.2\times10^{-4} \text{ mole.hr}^{-1}.g_{cat}^{-1}$$

where X_a = fractional conversion of propene = 0.063

v = volumetric flowrate of gas in the reactor

= 0.098 l/hr

C_{ao} = concentration of feed at reactor conditions

= 8.3×10^{-2} mole/l

W = mass of catalyst = 0.707g

The average concentration of propene in the reactor (which is determined by taking the arithmetic mean of the inlet and outlet concentration) is equal to 8.1×10^{-2} mole/l. Several rate-concentration data points would enable the estimation of the reaction order from a simple power law fit, remembering that the pulse reactor is in an unsteady state and that the reaction order could quite conceivably differ from that obtained using a continuous steady state technique.

2.5.2 Pure Propene Results

2.5.2.1 Product spectra

Product reactor concentrations from four experiments are shown in Table 2.8. The averaged reactor concentrations of the feed are shown in Table 2.9.

Table 2.8 Product spectra for pure propene at 473 K and 1.54 MPa.

	Exit concentrations [mole/l]$\times10^4$				mole% in exit			
	Run 1	Run 2	Run 3	Run 4	Run 1	Run 2	Run 3	Run 4
C_5	0.4	0.6	1.0	1.3	11.9	10.3	7.9	6.5
C_6	1.6	2.7	5.1	7.9	43.4	42.8	40.6	38.4
C_7	0.7	0.9	1.6	2.1	17.8	14.0	12.6	10.3
C_8	0.2	0.3	0.9	1.2	5.4	5.0	7.0	6.0
C_9	0.6	1.3	3.2	6.2	17.5	21.5	25.1	30.0
C_{10}	0.1	0.1	0.3	0.6	1.9	2.4	2.4	2.9
C_{11}	0.0	0.0	0.0	0.1	0.3	0.3	0.3	0.6
C_{12}	0.1	0.2	0.5	1.1	1.9	3.7	4.0	5.3

Table 2.9 Averaged reactor concentrations of the feed.

Propene conversion	3.1%	3.8%	4.8%	6.2%
C_3 [mole/l]x10^2	2.7	3.9	6.4	8.3

The different propene conversions listed in Tables 2.8 and 2.9 are obtained by injecting different sized pulses (separate experiments). Figure 2.18 shows the product concentrations in the reactor exit as a function of propene concentration in the reactor.

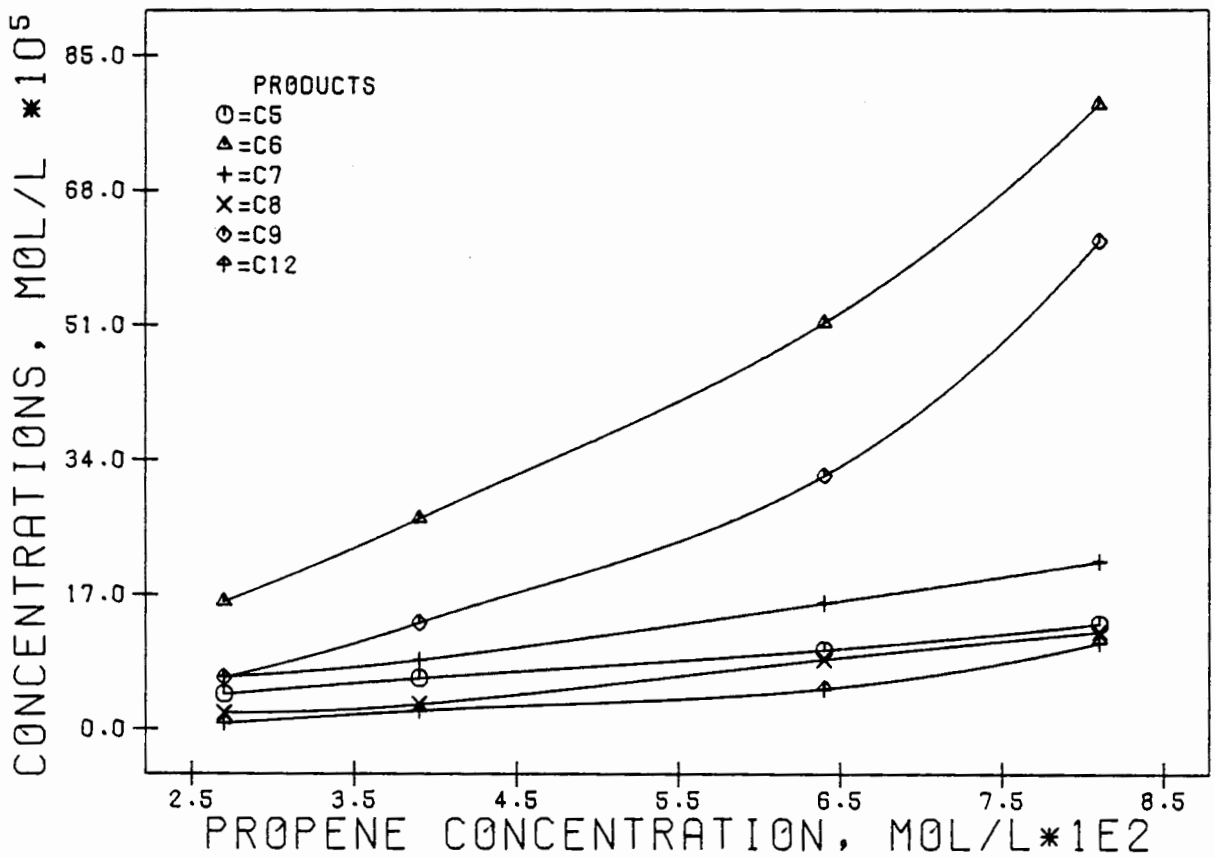

FIG 2.18 PULSE: PROPENE PRODUCT SPECTRA AT 473 K AND 1.54 MPA

2.5.2.2 Reaction pathways

Consider the reaction pathway network shown overleaf. The purpose of the network is to indicate those routes that are believed to be possible. The reference to carbon numbers, e.g., C_4 implies the entire fraction (all isomers) of that carbon chain length.

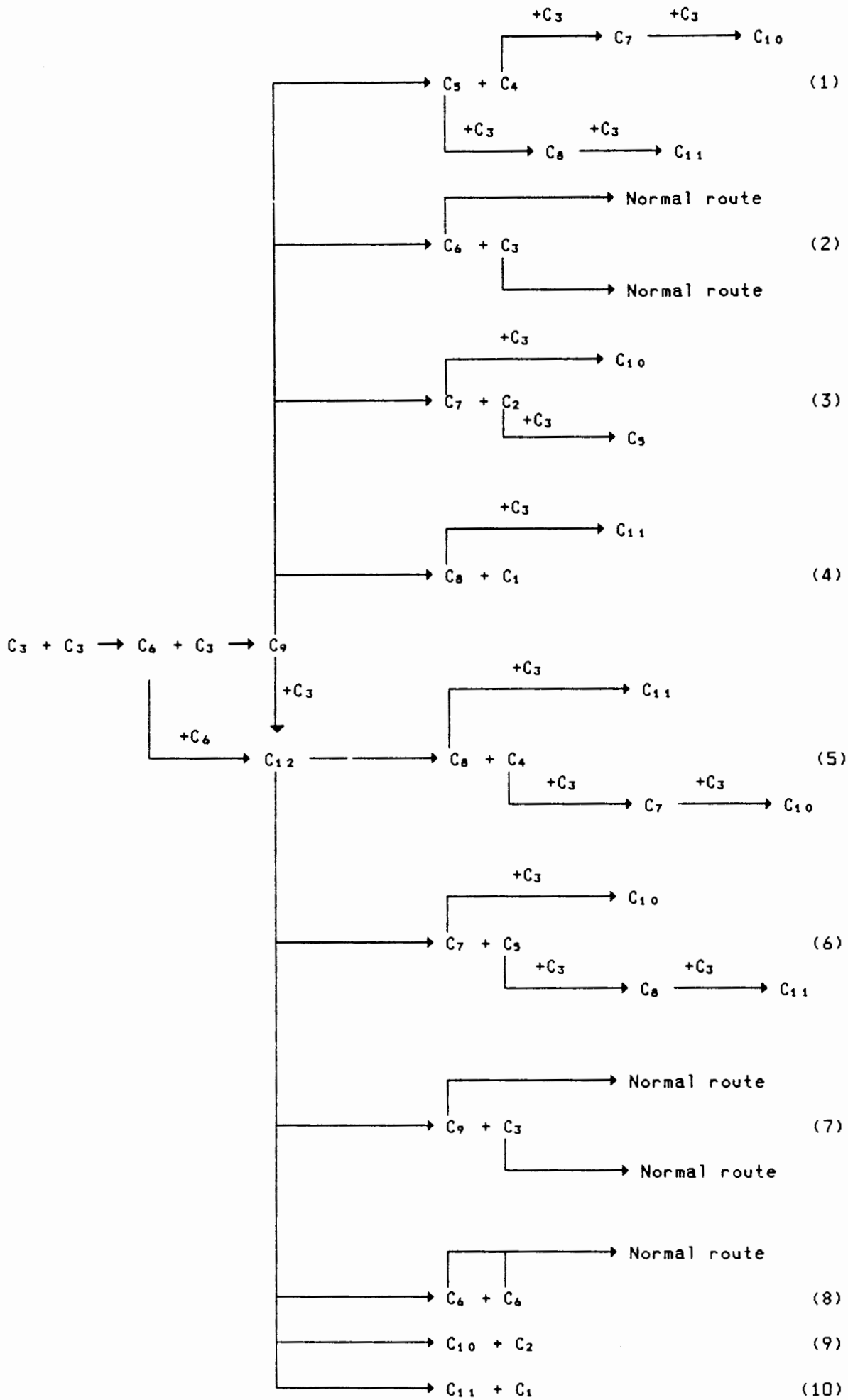
Route
+C3
+C3
C7
C10
C5 + C4
(1)
+C3
+C3
C8
C11
Normal route
C6 + C3
(2)
Normal route
+C3
C10
C7 + C2
(3)
+C3
C5
+C3
C11
C8 + C1
(4)
C3 + C3 → C6 + C3 → C9
+C3
+C3
C11
+C6
C12
C8 + C4
(5)
+C3
+C3
C7
C10
+C3
C10
C7 + C5
(6)
+C3
+C3
C8
C11
Normal route
C9 + C3
(7)
Normal route
Normal route
C6 + C6
(8)
C10 + C2
(9)
C11 + C1
(10)

1. Cracking of the C_9 fraction.

The C_9 fraction could crack according to the routes shown above. From examination of the product spectrum it seems unlikely that the C_9 would crack to $C_7 + C_2$ or $C_8 + C_1$ since neither C_1 nor C_2 were observed in the product spectra. Although it is possible for C_2 to react to completion with any C_3, this is not thermodynamically favoured at these conditions, particularly in view of the fact that the concentrations of C_2 and C_8 would be extremely low.

The alkene isomers of C_9 that are actually produced are not known and neither are the isomers of the C_7 and C_8 fractions; it is therefore not possible to determine thermodynamically which of the routes above are most favoured under these conditions. Considering Route (1), the cracked product, C_5, can combine with propene to produce C_8 and likewise, the C_4 to produce C_7. No C_4 was observed in the product, although it is quite possible that it would be undetectable due to overlapping by the C_3 peak. It is also possible that the C_4 could react to completion with the C_3. Due to the high concentration of propene, it is quite possible that the C_{10} and C_{11} fractions are formed by the following reactions as indicated in the reaction network:

$$C_7 + C_3 \longrightarrow C_{10}$$
$$C_8 + C_3 \longrightarrow C_{11}$$

At first glance, the occurrence of five consecutive reactions, e.g.,

$$(1)\quad C_3 + C_3 \longrightarrow C_6$$
$$(2)\quad C_6 + C_3 \longrightarrow C_9$$
$$(3)\quad C_9 \longrightarrow C_5 + C_4$$
$$(4)\quad C_5 + C_3 \longrightarrow C_8$$
$$(5)\quad C_8 + C_3 \longrightarrow C_{11}$$

may seem unlikely. Table 2.8 shows however that extensive cracking was occurring. Although not shown above, it must be pointed out that C_{10} and C_{11} fractions could conceivably be produced from the following routes:

$$C_6 + C_4 \longrightarrow C_{10}$$
$$C_5 + C_6 \longrightarrow C_{11}$$

The concentrations of both the C_6 and the C_4 and C_5 fractions were extremely low relative to the concentrations of propene and on this basis it is unlikely that the these reactions would proceed to any significant extent.

This mechanism requires that the total number of moles of $C_5 + C_8 + C_{11}$ is equal to the number of moles of $C_4 + C_7 + C_{10}$. Examination of the results in Table 2.8 shows that this condition is satisfied in all four cases, with a maximum error of 10% in Run 1 where experimental error was significant, due to the small concentrations. It is assumed that the C_4 fraction reacts to completion. Path (3) also requires that this condition be met, yet for reasons previously mentioned path (3) is considered to be unlikely at these conditions.

2. Cracking of the C_{12} fraction.

The C_{12} fraction can crack according to the routes given above. For reasons previously mentioned it is unlikely that the C_{12} cracked according to routes (9) and (10) although thermodynamically this could not be shown here. The cracking of the C_{12} fraction according to routes (7) and (8) will not be discussed in detail since these routes are simply the reverse of the normal oligomerization routes and their extent can not be determined here. With regard to routes (5) and (6) the cracked products could combine with propene to produce longer chain products. For route (6), where the C_{12} cracks to C_5 and C_7, the following condition (mole balance) must be satisfied.

$$C_5 + C_8 + C_{11} = C_7 + C_{10}$$

This is essentially the same condition as for C_9 cracking. It has been shown that this is satisfied.

For route (5), where the C_{12} cracks to C_8 and C_4, the C_8 could crack further to $C_5 + C_3$ and then react with the C_3 (propene) to produce C_{11}. The C_4 could react with the C_3 to produce C_7 and hence C_{10}. The following mole balance must be satisfied:

$$C_8 + C_5 + C_{11} = C_7 + C_4 + C_{10}$$

This is the same condition as that of C_{12} cracking to $C_5 + C_7$ and C_9 cracking to $C_5 + C_4$.

It is clear from the above discussion that either route (5) of the C_9 cracking pathway, route (5) of the C_{12} cracking pathway or route (6) of the C_{12} cracking pathway, or any combination of all three, could be occurring. Based on these mechanisms, the equivalent oligomer concentrations prior to cracking are listed in Table 2.10. Two sets of

oligomer fractions are shown. The first is for exclusive cracking of C_9 and the second for C_{12} cracking. (Either of the two C_{12} cracking mechanisms will yield the results shown in Table 2.10)

Table 2.10 Pure Oligomer fractions prior to cracking.

	C_9 cracking [mole/l]x10^4				C_{12} cracking [mole/l]x10^4			
	Run 1	Run 2	Run 3	Run 4	Run 1	Run 2	Run 3	Run 4
C_6	1.6	2.7	5.1	7.9	1.6	2.6	5.1	7.9
C_9	1.3	2.4	5.1	8.9	0.6	1.3	3.2	6.2
C_{12}	0.1	0.2	0.5	1.1	0.8	1.2	2.4	3.8

3. Production of the C_{12} fraction:

From the results no clear indication can be obtained of the relative rates of reaction of $C_9 + C_3 \longrightarrow C_{12}$ and

$$C_6 + C_6 \longrightarrow C_{12}.$$

2.5.2.3 Propene rate-concentration data

The rates of disappearance of propene and the respective averaged reactor concentrations are listed in Table 2.11. (See Section 2.5.1.1 for analysis).

Table 2.11 Rate-concentration data for propene.

X_A %	rate [mole$\cdot$hr$^{-1}\cdot g_{cat}^{-1}$]	C_3 concentration [mole$\cdot l^{-1}$]
3.1	1.2×10^{-4}	2.7×10^{-2}
3.8	2.1×10^{-4}	3.9×10^{-2}
4.8	4.3×10^{-4}	6.4×10^{-2}
6.2	7.2×10^{-4}	8.1×10^{-2}

This data is fitted to a power-law function of the following type:

$$(-rC_3)_{ave} = kC_3^n$$

Note that the H_3PO_4 concentration in all of these experiments was maintained constant. The calculated value of n is equal to 1.7,

indicating near second order dependence on propene concentration. It will be shown later that, for the continuous flow technique (which operates under high propene concentrations), the rate of propene disappearance has first order dependence on its concentration in the reactor. This may be explained by the Langmuir-Rideal adsorption mechanism (Haag, 1967).

Reaction between an adsorbed molecule and one that is not adsorbed (Langmuir-Rideal mechanism) is very rare in gas phase kinetics (see phase equilibria calculations in Section 2.4.10). If the dimerization reaction is the rate limiting reaction, the mechanism would yield:

$$A + * \overset{K_A}{\rightleftharpoons} A^*$$

$$A^* + A \xrightarrow{k_2} B$$

$$B^* \overset{K_B}{\rightleftharpoons} B + *$$

where A = monomer,
B = dimer.

The rate of formation of B is then $r = k_2 A A^* = \dfrac{k_2' K_A A^2}{1 + K_A A + K_B B}$

$$\approx \frac{k_2' K_A A^2}{1 + K_A A}$$

Omitting $K_B B$ from the denominator is justified at low conversions (A>>B). The limiting cases are:

high surface coverage: $r = k_2' A$

low surface coverage: $r = k_2' K_A A^2 = k_2'' A^2$

The observed first and second order kinetics at high and low concentrations respectively, are consistent with a Langmuir-Rideal mechanism.

2.5.3 Pure 2-Methyl-1-Pentene

2.5.3.1 Product spectra

The product reactor concentrations for each experiment are shown in Table 2.12, while the averaged concentrations of 2-methyl-1-pentene in the reactor are listed in Table 2.13.

Table 2.12 Product spectra for 2-methyl-1-pentene at 473 K and 1.54 MPa.

	Exit concentrations [mole/l]x10^5			mole% in exit		
	Run 1	Run 2	Run 3	Run 1	Run 2	Run 3
C_3	0.6	1.1	1.6	11.2	3.0	1.0
C_4	2.3	9.8	21.0	46.3	27.0	24.4
C_5	1.0	7.9	22.5	19.4	21.7	26.2
C_7	0.0	8.5	22.6	0.0	23.3	26.3
C_8	0.3	2.4	5.0	6.2	6.6	5.8
C_9	0.0	0.0	0.3	0.0	0.0	0.3
C_{10}	0.0	0.2	0.5	0.0	0.7	0.6
C_{11}	0.0	0.1	0.1	0.0	0.2	0.1
C_{12}	0.8	6.4	12.4	17.0	17.6	14.4

Table 2.13 Averaged 2-methyl-1-pentene concentration.

	Run 1	Run 2	Run 3
2M1P Concentration [mole/l]x10^3	1.2	4.4	7.7

Figure 2.19 shows the product concentration in the reactor exit as a function of the average 2-methyl-1-pentene concentration in the reactor.

2.5.3.2 Reaction mechanisms

The following can be noted from the results in Tables 2.8 and 2.12. It should be noted that the comparison of the 2-methyl-1-pentene results to the dimer of the C_3 polymerization is valid only if the active dimer is the 2-methyl-1-pentene, or if it is as active and selective as the other C_6 isomers. It will be shown later that the reactivities of the other hexenes are not largely different from that of 2-methyl-1-pentene (Section 2.5.4). It has also been shown previously (Section 2.4.9.2)

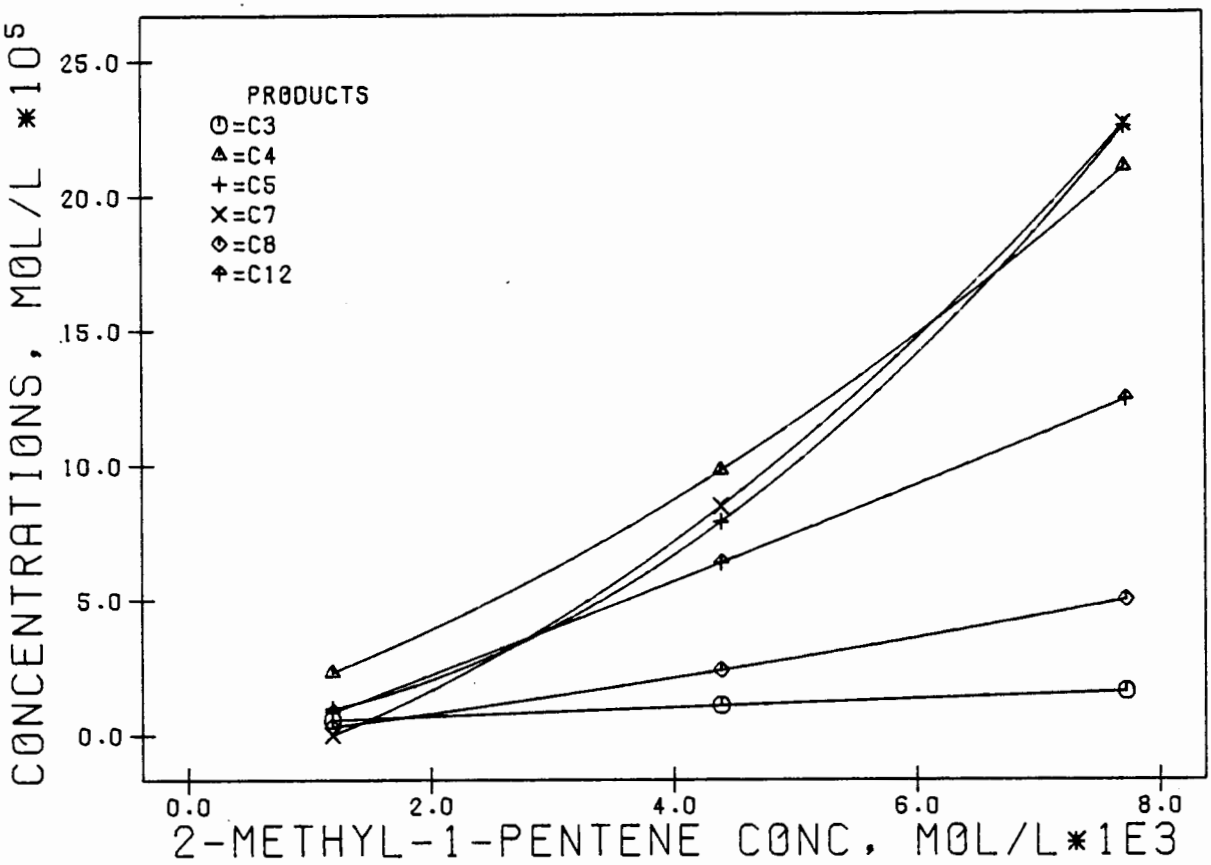

FIG 2.19 PULSE: 2-METHYL-1-PENTENE PRODUCT SPECTRUM AT 473 K AND 1.54 MPA

that the four most stable hexene isomers under these conditions are 4-methyl-trans-2-pentene, 2-methyl-2-pentene, 2-methyl-1-pentene and 3-methyl-cis-2-pentene. It will be shown in Section 2.5.4 that these isomers of C_6 all have similar rates of oligomerization over solid phosphoric acid under these conditions. It is therefore quite reasonable to expect the 2-methyl-1-pentene results to be fairly representative of the C_6 fraction.

From the use of hexene standards the C_6 isomers, which are the result of isomerization, were identified, not only in the 2-methyl-1-pentene feed experiments but also the propene feed experiments. In both cases not only were the same isomers identified but it was found that approximately the same percentage of each isomer (with respect to the total C_6 fraction) was present. There were essentially six isomers that were identified, accounting for over 95% of the C_6 fraction. Only one isomer was not identifiable. The isomers identified and their respective percentages of the total C_6 fraction are given below.

4-methyl-1-pentene and 3-methyl-1-pentene	1%
cis-4-methyl-2-pentene	10%
2-methyl-1-pentene	10%

2-methyl-2-pentene	50%
3-methyl-2-pentene	25%
unknown	4%

Thermodynamically, 4-methyl-2-pentene, 2-methyl-1-pentene, 2-methyl-2-pentene and 3-methyl-2-pentene are the four most stable of the C_6 alkenes.

Consider the reaction pathways for the cracking of the C_{12} fraction shown in Section 2.5.2.2 in conjunction with the data of Table 2.12.

1. The extent of C_{12} cracking was large (see Table 2.12).

2. The ratio of C_{12} to cracked products in Tables 2.8 and 2.12 was approximately the same at the higher concentrations of C_{12} (12×10^{-5} mole/l). In the pure 2-methyl-1-pentene experiments the ratio appeared to remain approximately constant. The ratio however decreased as the C_{12} concentration decreased in Table 2.8 (pure propene experiments) indicating that as the C_{12} concentration decreased the cracking from another source (possibly C_9) is became more predominant (see Table 2.14 below).

   Comparing the concentrations in Table 2.8 with those of Table 2.12 an estimate can be obtained of the expected fraction of cracked products in Table 2.8 (pure propene experiments) that are due to C_{12} cracking. The estimates which are only approximate are shown in Table 2.14.

Table 2.14 Estimated molar ratios of C_{12} to cracked products in Table 2.8 based on the results of both Tables 2.8 and 2.12.

	Data From Table 2.8				Data From Table 2.12		
C_{12} concentration [mole/l]$\times 10^5$	1.0	2.0	5.0	11.0	0.8	6.4	12.4
[Ratio]$\times 10^2$	7.1	10.5	13.1	20.7	19.0	21.0	16.8
Cracked products due to C_{12} cracking (mole%)	35	55	65	100			

3. The product spectra in Table 2.12 suggest that the production of C_{10} and C_{11} in the pure propene case was not due to $C_6 + C_4$ and $C_6 + C_5$, respectively.

4. In Table 2.12 the concentration of C_{12} is approximately related to that of C_6 by the following relationship:

$$[C_{12}] = 0.19 \cdot [C_6]^{1.5}$$

Using this relationship to obtain the expected amount of C_{12} formed from 2-methyl-1-pentene, at a concentration of 3.9×10^{-4} mole/l (this is regarded as the average C_6 concentration in the reactor for the pure propene Run 4 of Table 2.8) the amount of C_{12} expected is 0.15×10^{-5} mole/l. This is approximately 1.4% of the amount of C_{12} formed in the pure propene Run 4. This implies that, if the 2-methyl-1-pentene (or some other isomer with similar reactivity) were the active isomer and it reacted to the same extent in both the pure propene and pure 2M1P cases, the production of C_{12} in the pure propene case would be mainly due to $C_9 + C_3$ under these conditions.

5. Consider again the reaction pathways discussed in Section 2.5.2.2 in conjunction with the results of Table 2.12. The results in Table 2.12 support the postulate that there was little or no cracking of C_{12} to either C_{10}, C_{11} or C_9 as was predicted in Section 2.5.2. The results also indicate that the C_{12} fraction did crack to both $C_7 + C_5$ and $C_8 + C_4$.

6. The most likely mechanisms for the cracking of the C_{12} fraction are as follows (routes (1) and (2) of Section 2.5.2.2 for C_{12} cracking):

$$C_{12} \longrightarrow C_7 + C_5$$
$$C_{12} \longrightarrow C_8 + C_4$$

A brief examination of the mole ratios in Table 2.12 indicates that the C_8 fraction is possibly cracking further as follows:

$$C_8 \longrightarrow 2C_4$$

The production of the C_3 could be from either of the following:

$$C_8 \longrightarrow C_5 + C_3$$
$$C_7 \longrightarrow C_4 + C_3$$

7. It is also possible that the 2-methyl-1-pentene cracked to some extent.

It should be noted that the product concentrations in Run 1 were extremely small. The accuracy of the G.C. detection at this level is poor and unreliable.

2.5.3.3 2-methyl-1-pentene rate concentration data

The rate concentration data for the 2-methyl-1-pentene experiments are shown in Table 2.15

Table 2.15 Rate concentration data for 2-methyl-1-pentene.

X_A%	Reaction Rate [mole·hr^{-1}·g$_{cat}^{-1}$]	2M1P concentration [mole/l]
3.4	6.3×10^{-6}	1.2×10^{-3}
8.6	5.6×10^{-5}	4.4×10^{-3}
10.8	1.3×10^{-4}	7.7×10^{-3}

From a simple power-law fit of the type $(-rC_6)_{ave} = kC_6^n$, the value of n obtained was n = 1.6 (linear regression coefficient, r^2 = 1.00).

2.5.4 Results for Various Other Hexenes Isomers

The following C_6 feeds were also investigated:

- 2-methyl-2-pentene
- 3-methyl-1-pentene
- 3-methyl-2-pentene
- 4-methyl-1-pentene
- cis-4-methyl-2-pentene
- 1-hexene

The product spectra and rate/concentartion data o· the above hexenes are shown in Appendix H. All except 1-hexene showed similar results to those of 2-methyl-1-pentene. Product spectra were all similar and therefore will not be presented here. The mechanistic discussions pertaining to 2-methyl-1-pentene are equally applicable to all of these hexene isomers, including 1-hexene.

The relative rates of reactivity were all similar, except those of 1-hexene. Figure 2.20 is a plot of reaction rate, as a function of concentration, for each of the C_6 isomers. Notice that Figure 2.20 is a log-log plot. The slope of each line gives the value of n in the following simple power-law function:

$$(-rC_6)_{ave} = kC_6^n$$

The values of n for each of the isomers are listed in Table 2.16. It is clear that there is no significant difference in the orders of these

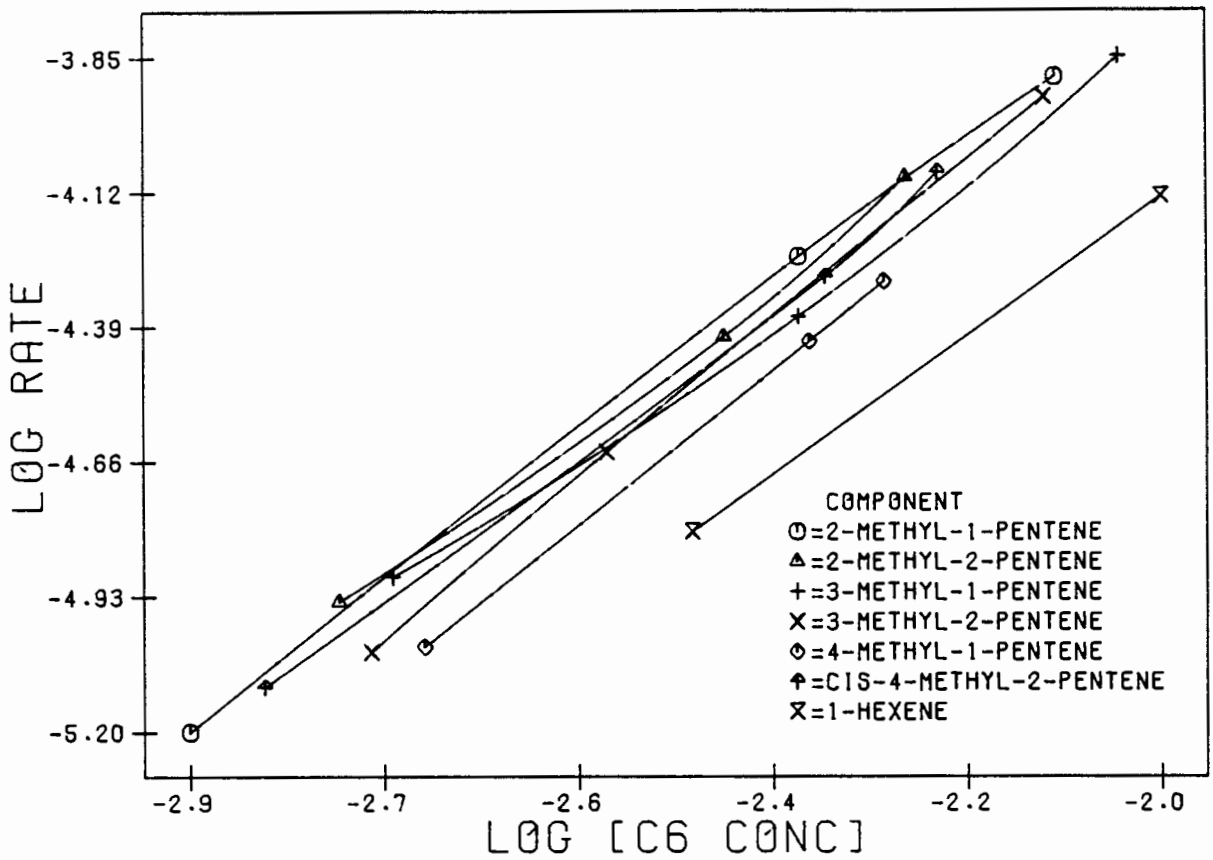

FIG 2.20 PULSE: RATE-CONCENTRATION DATA - HEXENES

reactions. It is also clear from Figure 2.20 that 1-hexene is far less reactive than the other C_6 isomers.

Table 2.16 Reaction orders for C_6 isomer polymerization.

C_6 Isomer	Reaction order, n	C_6 Isomer	Reac order, n
2-methyl-1-pentene	1.60	4-methyl-1-pentene	1.75
2-methyl-2-pentene	1.60	cis-4-methyl-2-pentene	1.60
3-methyl-1-pentene	1.50	1-hexene	1.50
3-methyl-2-pentene	1.75		

2.5.5 Pure 1-Butene Results

2.5.5.1 Product spectra

Product concentrations in the reactor exit are shown in Table 2.17. Averaged reactor concentrations of the feed are shown in Table 2.18.

Table 2.17 Product spectra for 1-butene at 473 K and 1.55 MPa.

	Exit concentrations [mole/l]x10^{+5}			moles in exit [mole%]		
	Run 1	Run 2	Run 3	Run 1	Run 2	Run 3
C_3	3.2	8.5	12.0	15.1	2.7	4.0
C_5	4.3	11.5	31.9	20.4	19.6	10.7
C_6	1.9	5.1	20.2	9.0	8.1	6.8
C_7	0.6	3.8	25.0	2.8	6.1	8.4
C_8	10.6	37.5	190	50.2	59.9	63.6
C_9	0.4	1.4	7.8	1.9	2.2	2.6
C_{10}	0.0	0.2	2.0	0.0	0.3	0.7
C_{11}	0.0	0.0	1.5	0.0	0.0	0.5
C_{12}	0.1	0.6	8.4	0.5	1.0	2.8

Table 2.18 Average reactor concentrations of the feed.

	Run 1	Run 2	Run 3
1-butene concentration [mole$\cdot$l^{-1}]x10^3	4.8	9.4	25.0

The averaged concentration of the feed in the reactor, given in Table 2.18, is simply the arithmetic mean of the inlet and outlet concentrations. Figure 2.21 shows the product concentrations at the reactor exit as a function of the averaged 1-butene concentration in the reactor.

Due to the reactivity of the 1-butene, the conversions were high. At the expense of operating under non-differential conditions it was decided (for comparative purposes) to perform these experiments under identical conditions to those of the other feeds.

2.5.5.2 Reaction mechanisms

Consider the reaction pathway network, shown overleaf, in conjunction with the product spectra in Table 2.17.

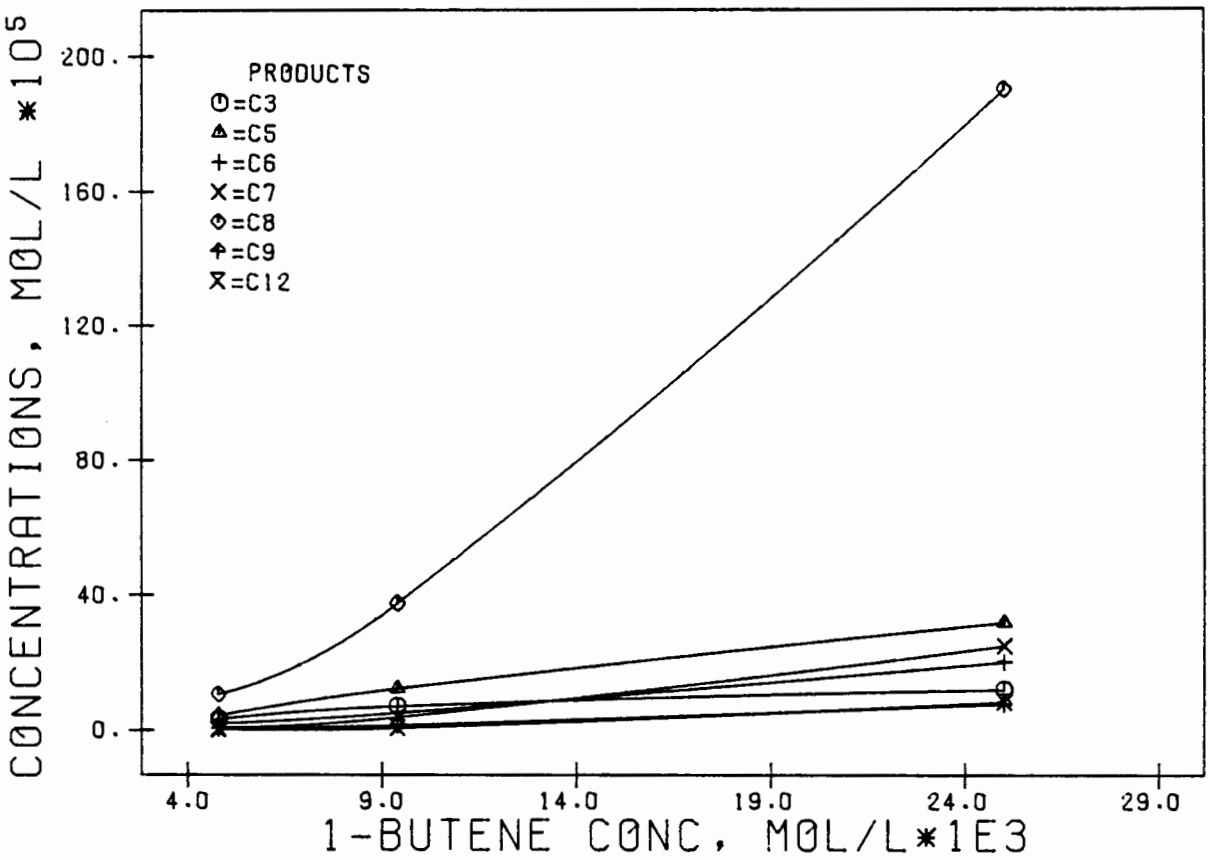

FIG 2.21 PULSE: 1-BUTENE PRODUCT SPECTRA AT 473 K AND 1.55 MPA

1. The dimerization reaction of 1-butene was very much faster than the trimerization reaction.

2. Similar to previous feeds, cracking was extensive.

3. Based on previous discussion there appears to be two major sources of the cracked products. They could be the products of C_8 cracking (route (2)), or C_{12} cracking (route (3)), or both.

4. The cracking mechanism for C_8 would be as follows:

$$C_8 \longrightarrow C_5 + C_3$$
$$C_3 + C_4 \longrightarrow C_7$$
$$C_7 + C_4 \longrightarrow C_{11}$$
$$C_5 + C_4 \longrightarrow C_9$$

This mechanism requires that $C_5 + C_9 = C_3 + C_7 + C_{11}$ (mole balance). This requirement is satisfied in all three experiments.

5. The cracking mechanism for C_{12} could be as follows:

$$C_{12} \longrightarrow C_7 + C_5 \quad \text{and/or} \quad C_{12} \longrightarrow C_8 + C_4$$
$$C_7 + C_4 \longrightarrow C_{11}$$
$$C_5 + C_4 \longrightarrow C_9$$

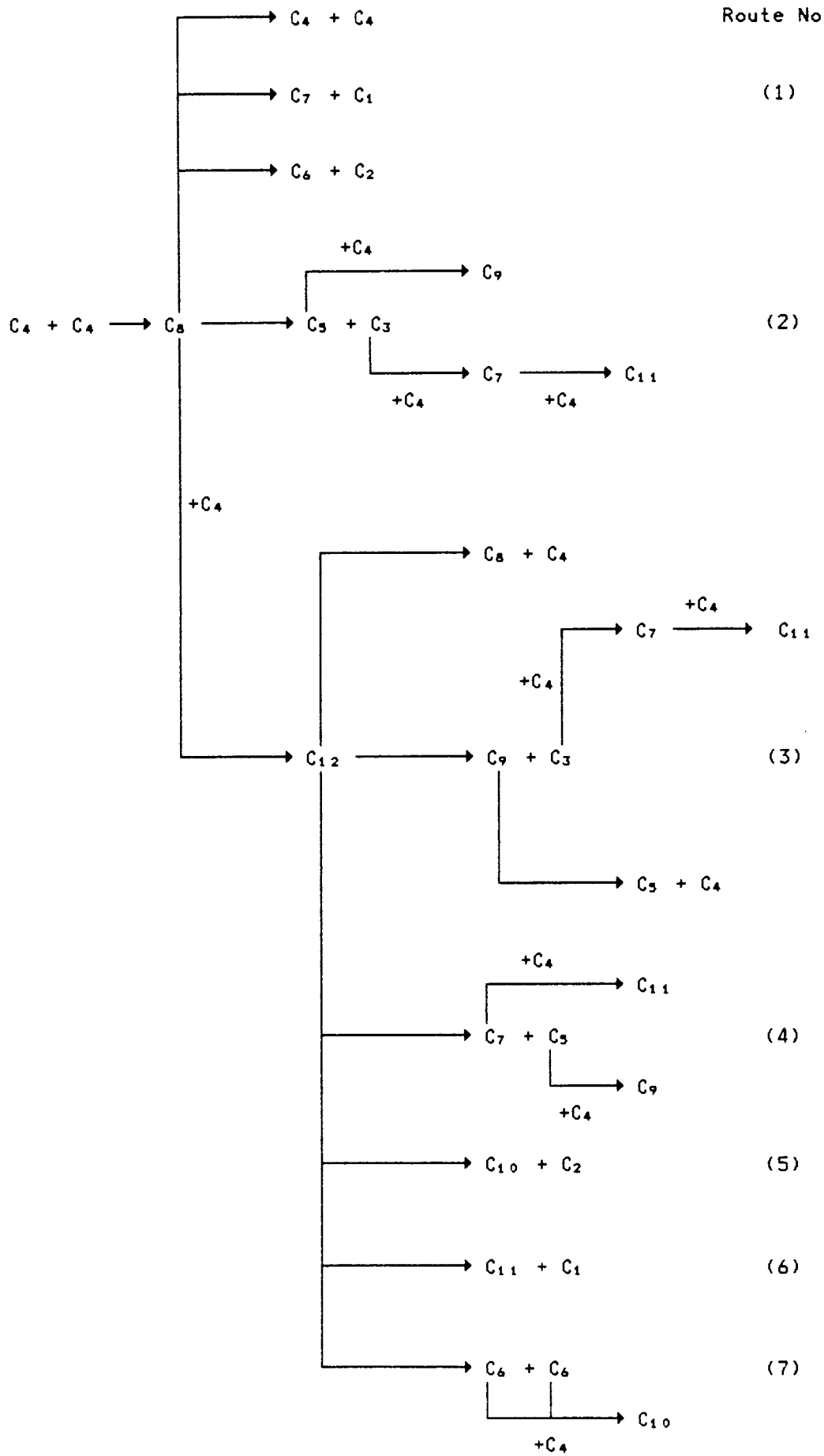

The cracking of C_{12} to C_8 and C_4 can neither be proved nor disproved due to the cracked products being oligomers of the original 1-butene feed. For the cracking of the C_{12} to C_7 and C_5 The mechanism would require that $C_5 + C_9 = C_7 + C_{11}$ (mole balance). This requirement is

not satisfied and hence this route could not be the sole contributor of the cracked products.

The results of the pure C_6 experiments suggest strongly that there is a significant amount of C_8 cracking (note the C_{12} concentrations in relation to the concentration of C_3 and C_5) to C_5 and C_3. The large amount of C_5 and C_3 here (relative to those in the pure C_6 experiments) is indicative of the fact that C_8 cracking must be substantial.

No indication of C_{12} cracking according to the following reaction can be obtained since the reaction is simply the reverse of the original forward reaction but the reaction is expected to occur, based on the pure 2-methyl-1-pentene experiments:

$$C_{12} \longrightarrow C_8 + C_4$$

The cracking of the C_{12} fraction according to the following can neither be proved nor disproved:

$$C_{12} \longrightarrow C_9 + C_3$$

It was indicated in Section 2.5.3.2 that the cracking of C_{12} to C_8 and C_4 was quite likely. It was also indicated that C_{12} did not crack to C_9 + C_3. This is quite likely here, since if C_{12} were to crack to C_9 + C_3, the required mole balances for the mechanisms in (4) and (5) would not be satisfied.

6. The C_6 presence is likely to be due to cracking of the C_{12} fraction.

7. As indicated in Section 2.5.3.2, the cracking of C_{12} to C_{10} + C_2 and C_{11} + C_1 did not occur to any appreciable extent.

8. Based on the pure 2-methyl-1-pentene experiments it is unlikely that there was any significant cracking of C_6 to C_3.

2.5.5.3 Rate-concentration data for 1-butene

The rate concentration data are shown in Table 2.19. 1-butene conversions were very high and hence no power-law fit was performed due to the errors incurred in using an averaged reactor concentration of the feed. Under these circumstances the reactor was probably no longer

Table 2.19 Rate concentration data for 1-butene.

X_A%	Reaction rate $[mole \cdot hr^{-1} \cdot g_{cat}^{-1}] x10^3$	$[C_4]_{ave}$ $[mole/l] x10^3$
7.0	4.9	4.8
12.8	17.8	9.4
20.0	77.6	25.0

behaving as a differential reactor. It was not possible to determine the extent to which the conversions were removed from equilibrium since the exact alkene isomers were not known. Despite the large errors incorporated by calculating the reaction rates using the assumption of a differential reactor, the rates were still shown here, simply as a rough estimate for comparative purposes.

It is quite clear from the data that the 1-butene polymerized at a significantly faster rate than the C_3 and C_6's under these conditions.

2.5.6 Pure Iso-Butene Results

2.5.6.1 Product spectra

The accurate G.C. analysis of some of the smaller compounds was difficult here due to the large extent of overlapping of the C_3, C_4 and C_5 peaks. As a result, there may be some error in the quantification of these peaks. The product concentrations at the reactor exit are shown in Table 2.20. Averaged reactor concentrations (arithmetic mean of the inlet and outlet reactor concentrations) of the feed are listed in Table 2.21.

The calculated averaged feed concentrations in the reactor are the arithmetic means of the inlet and outlet concentrations. Figure 2.22 shows the product concentrations at the reactor exit as a function of the average iso-butene concentration in the reactor.

2.5.6.2 Reaction mechanisms

Consider the reaction pathway shown in Section 2.5.5.2 in conjunction with the results in Table 2.20. The following can be noted:

Table 2.20 Product spectra for iso-butene at 473 K and 1.53 MPa.

	Exit concentrations [mole/l]x10^5			Moles in exit [mole%]		
	Run 1	Run 2	Run 3	Run 1	Run 2	Run 3
C_3	8.5	19.0	34.1	11.2	8.6	7.1
C_5	8.7	26.7	57.7	11.6	12.0	11.9
C_6	1.3	4.0	8.7	1.8	1.8	1.8
C_7	3.7	12.7	30.9	5.0	5.7	6.4
C_8	51.1	150	325	67.9	67.8	67.3
C_9	1.0	4.0	11.6	1.4	1.8	2.4
C_{10}	0.2	1.0	2.6	0.3	0.4	0.5
C_{11}	0.0	0.7	2.3	0.0	0.3	0.5
C_{12}	0.5	3.3	9.8	0.7	1.5	2.0

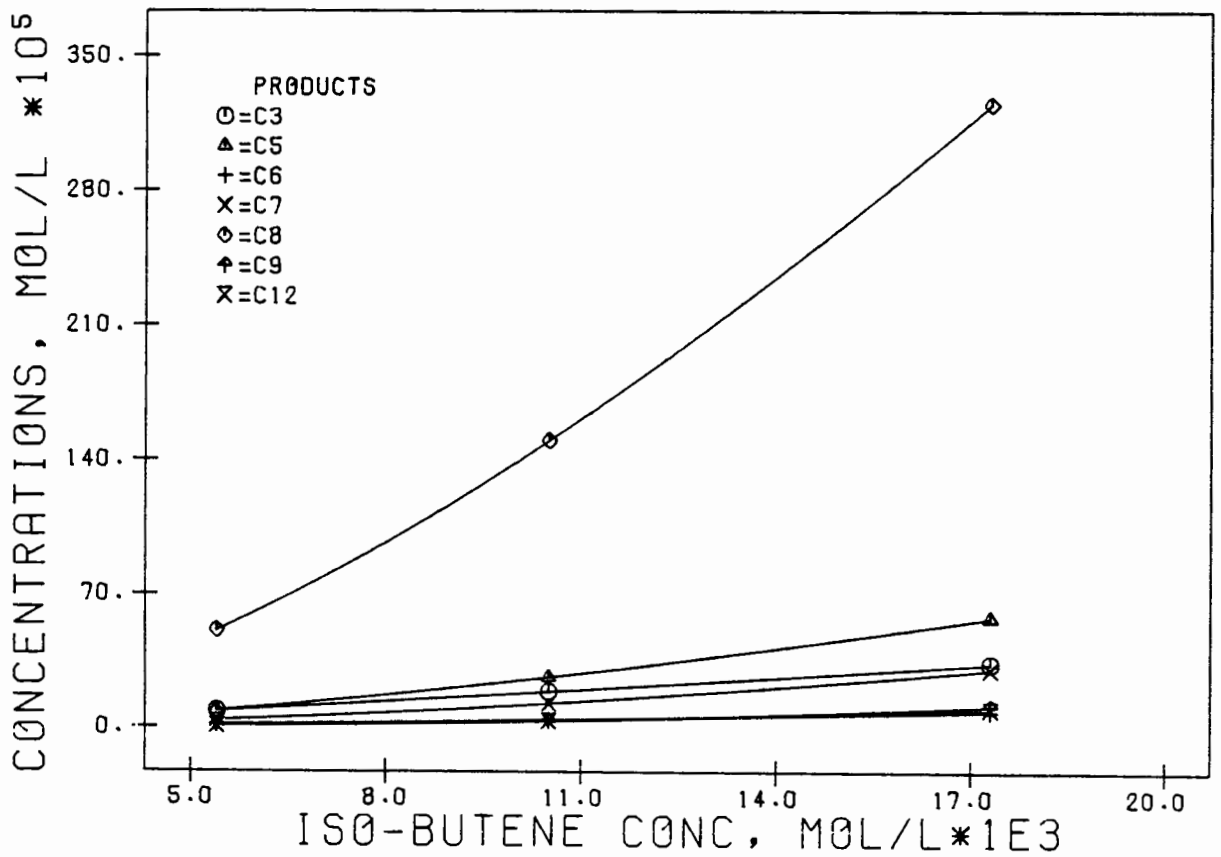

FIG 2.22 PULSE: ISO-BUTENE PRODUCT SPECTRA AT 473 K AND 1.53 MPA

Table 2.21 Averaged reactor concentrations of the feed.

	Run 1	Run 2	Run 3
Iso-butene concentration [mole/l]x10^3	5.4	10.5	17.3

1. The dimerization reaction of iso-butene was much faster than the trimerization reaction.

2. Cracking was extensive.

3. The large amounts of C_3 present indicate that C_8 was most probably cracking to C_5 + C_3. It is extremely unlikely, as was found in the pure C_6 experiments, that the C_3 would be a product of C_{12} cracking to C_9 + C_3, as indicated by the concentrations of C_9 and C_3.

4. The cracking of C_8 suggests that, despite the different products obtained, there may well have been cracking of the C_8 fraction in the 1-butene experiments.

5. The following two mechanisms could explain the cracked products:

$$C_8 \longrightarrow C_5 + C_3$$
$$C_5 + C_4 \longrightarrow C_9$$
$$C_3 + C_4 \longrightarrow C_7$$
$$C_7 + C_4 \longrightarrow C_{11}$$

$$C_{12} \longrightarrow C_7 + C_5$$
$$C_8 \longrightarrow C_5 + C_3$$
$$C_5 + C_4 \longrightarrow C_9$$
$$C_7 + C_4 \longrightarrow C_{11}$$
$$C_3 + C_4 \longrightarrow C_7$$

Both of these mechanisms can be satisfied by the product spectra. Once again it is not possible to predict from thermodynamics which is the more likely reaction due to the lack of information about which isomers were present and the lack of thermodynamic data on alkenes of chain length greater than C_6. There is therfore no evidence to suggest which of these two mechanisms was more likely, but based on the pure C_6 experiments it appears that most of the cracked products were due to C_8 cracking.

6. The C_6 could be due to the cracking of the C_{12} fraction.

7. As in the 1-butene experiments, the following mechanism can neither be proved nor disproved

$$C_{12} \longrightarrow C_8 + C_4$$

8. The cracking of C_{12} to $C_{11} + C_1$ and $C_{10} + C_2$ is unlikely to occur as mentioned in previous discussion. The GC results showed no traces of C_1 or C_2.

2.5.6.3 Rate-concentration data for iso-butene

The rate concentration data are shown in Table 2.22

Table 2.22 Rate-concentration data for iso-butene.

X_A%	Reaction Rate [mole$\cdot hr^{-1} \cdot g_{cat}^{-1}$]	$[C_4]_{ave}$ [mole/l]x10^3
21.7	1.8×10^{-4}	5.4
31.9	5.6×10^{-4}	10.5
40.7	12.3×10^{-4}	17.3

Similar to the 1-butene experiments, the conversions were very high and, therefore, the reactor did not behave as a differential reactor. Again the reaction rates were used only as rough estimates for comparative purposes.

Comparison of the iso-butene rate-concentration data with that of 1-butene indicates that iso-butene was significantly more reactive.

2.5.7 Comparison of the Pure Feed Results

Figure 2.23 is a plot of reaction rate, as a function of concentration, for the following oligomerization reactions:

propene
1-butene
iso-butene
2-methyl-1-pentene
1-hexene

The order of reactivities at these conditions is: iso-butene, 1-butene, 2-methyl-1-pentene, 1-hexene, propene. Although the reactor may have been operating non-differentially, in some cases, Figure 2.23 serves simply to indicate the relative reactivities of the various olefins under these conditions. The log-log plot is used to provide a simpler comparison.

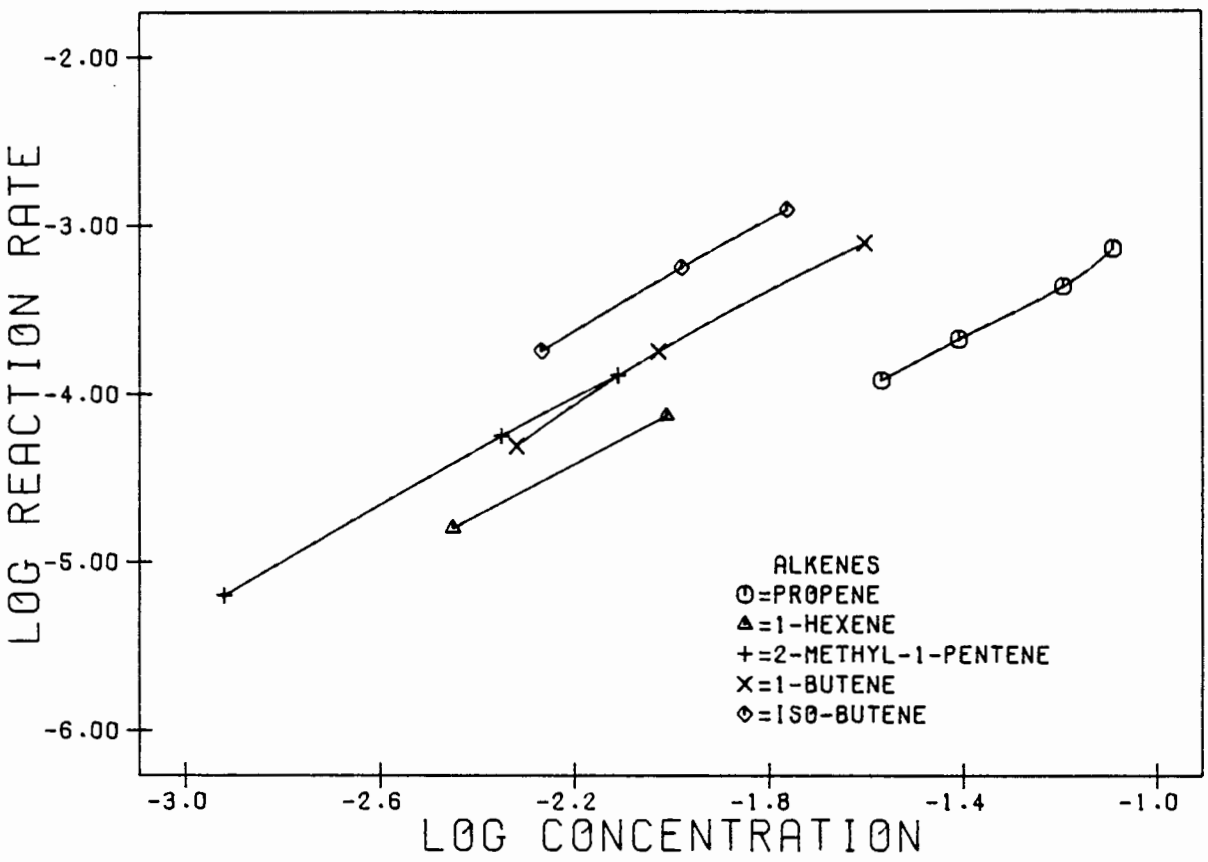

FIG 2.23 PULSE: RATE CONCENTRATION DATA FOR PURE FEEDS

2.5.8 Propene + 2-Methyl-1-Pentene

Several experiments were carried out by keeping the 2-methyl-1-pentene concentration constant and varying the propene concentration. The relatively high propene concentrations resulted in a large overlap between the propene and C_4 peaks. Some error may therefore be incurred in the estimation of the C_4 concentration in the reactor.

2.5.8.1 Feed and product spectra

The feed concentrations (inlet to the reactor) are listed in Table 2.23. Concentrations of the products at the reactor exit are shown in Table 2.24. It should be noted, from Table 2.23, that the 2-methyl-1-pentene

inlet concentrations did vary, although it was attempted to keep the concentrations constant. This should be borne in mind when comparing the four runs.

Table 2.23 Reactant feed concentrations at the reactor inlet at 473 K and 1.55 MPa.

	propene [mol•l^{-1}]	2M1P [mol•l^{-1}]
Run 1	0	1.1×10^{-2}
Run 2	1.3×10^{-2}	9.4×10^{-3}
Run 3	3.0×10^{-2}	8.9×10^{-3}
Run 4	5.2x10-2	1.1×10^{-2}

See Sections 2.5.2.2 and 2.5.3.2 for detailed discussions on the respective pure propene and pure 2-methyl-1-pentene oligomerizations.

Table 2.24 Product spectra at reactor exit.

	Exit concentrations [mol•l^{-1}] x10^5				Moles in exit [%]			
	Run no.				Run no.			
	1	2	3	4	1	2	3	4
C_3	3.3	—	—	—	2.7	—	—	—
C_4	30.1	19.4	22.2	27.7	25.0	8.9	6.7	5.6
C_5	31.7	21.1	18.6	20.5	26.3	9.7	5.6	4.1
C_7	30.2	30.2	33.7	40.9	25.1	13.9	10.2	8.3
C_8	5.7	13.6	21.6	32.3	4.7	6.3	6.5	6.5
C_9	0.7	117	213	334	0.6	54.1	64.4	67.6
C_{10}	0.9	2.2	4.5	7.8	0.7	1.0	1.4	1.6
C_{11}	0.3	0.4	0.9	1.6	0.2	0.2	0.3	0.3
C_{12}	17.4	12.7	16.3	29.5	14.5	5.8	4.9	6.0

Table 2.25 shows the averaged reactor concentrations of both the propene and 2-methyl-1-pentene. As indicated previously, these averages are the arithmetic means of the inlet and outlet reactor concentrations. The conversions of each reactant are shown in Table 2.25. For these calculations the initial concentrations of each feed had to be known.

Feed concentrations at the entrance to the reactor were not determined directly but indirectly. One method of determining the concentrations was by injecting the pure feeds individually and measuring the area counts corresponding to known injection sizes. The other complimentary approach was to inject combined feeds but instead of using two alkenes (as is done in this work) only one alkene and one alkane were injected, e.g., hexane and 1-butene or propane and 2-methyl-1-pentene. The purpose of this was to reduce, as far as possible, any doubt as to which hydrocarbons corresponded to which feed, since the alkane was inert. Once the feed concentartions had been calculated the conversions of each feed in the mixture could easily be determined as described in Section 2.5.11. Conversions were high, especially those of 2-methyl-1-pentene and as a result, the reactor might well not be operating differentially. It is not known how close the reactor was operating to equilibrium. Figure 2.24 shows the exit reactor concentrations of the products as a function of changing propene concentration. (Note that the inlet 2-methyl-2-pentene concentration was essentially constant.)

Table 2.25 Reactant's reactor concentrations and conversion levels.

	Propene		2-Methyl-1-Pentene	
	Concentration $[mol \cdot l^{-1}] \times 10^2$	Conversion X_A	Concentration $[mol \cdot l^{-1}] \times 10^2$	Conversion X_A
Run 1	0.00	0	1.04	11
Run 2	1.23	10.9	0.83	23
Run 3	2.86	9.0	0.73	36
Run 4	4.97	9.1	0.86	43

2.5.8.2 Reaction mechanisms

The following can be noted from Tables 2.24 and 2.25, remembering that Run 1 contained only pure 2-methyl-1-pentene as a feed. Consider, also, the reaction pathway network in Section 2.5.2.2.

1. Cracking: Similar to previous experiments, cracking was extensive.

2. Rate of reaction of propene with 2-methyl-1-pentene: Comparing Run 1 in Table 2.9 (3.1% propene conversion) and Run 1 in Table 2.25 with Run 3 in Table 2.25 and their respective product spectra, it is very

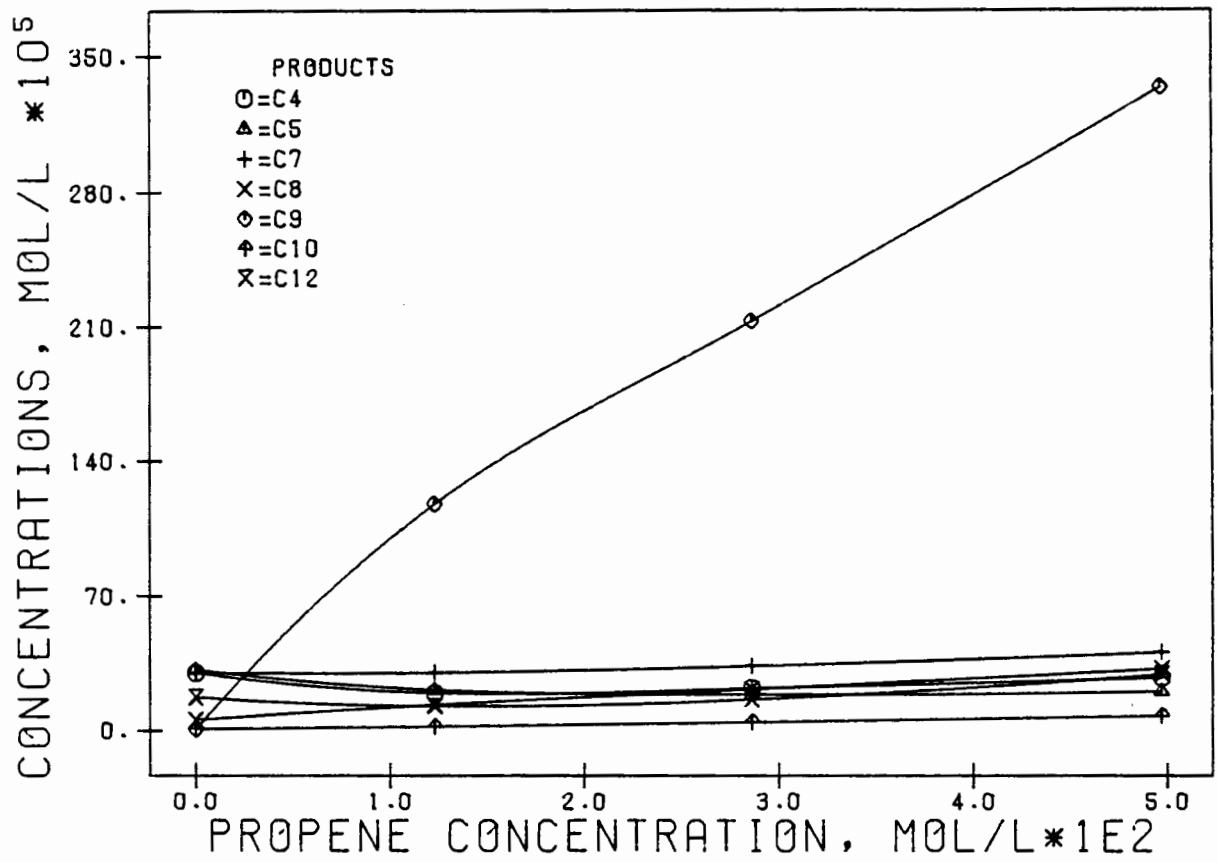

FIG 2.24 PULSE: 2M1P+C3: PRODUCT SPECTRA AT 473 K AND 1.55 MPA

clear that the rate of reaction of propene with 2-methyl-1-pentene was very much greater (3 to 4 times in this case) than either of the dimerization reactions (see Figure 2.24).

3. Conversion of propene: From Runs 2, 3 and 4 in Table 2.25 it can be seen that the conversion of propene decreased very slightly as the propene concentration increased. This is not surprising due to the high concentrations of propene used (relative to 2-methyl-1-pentene). In Run 2, the concentration of propene was about 1.5 times higher than that of 2-methyl-1-pentene. All else being equal, each propene molecule would have nearly as much chance of encountering a 2-methyl-1-pentene molecule as a propene molecule. In Run 4, the propene concentration was significantly higher than that of 2-methyl-1-pentene. The driving force had therefore shifted to the oligomerization of propene. Since the dimerization of propene is much slower than the reaction of propene with 2-methyl-1-pentene, the propene conversion fell as its concentration increased.

4. Cracking of C_9 and C_{12}: The possibilities of the C9 and C12 fraction cracking will now be examined.

(a) C_9 cracking: It has been shown that the C9 fraction is quite likely to crack according to the following mechanism:

$$C_9 \longrightarrow C_5 + C_4$$
$$C_5 + C_3 \longrightarrow C_8$$
$$C_8 + C_3 \longrightarrow C_{11}$$
$$C_3 + C_4 \longrightarrow C_7$$
$$C_7 + C_3 \longrightarrow C_{10}$$

The cracking of C_9 to C_6 and C_3 will not be examined in any detail since this is simply the reverse of the main forward oligomerization reaction.

Examination of Run 1 indicates, as shown previously, that the formation of C_{10} and C_{11} is not very significant (compare the product distribution of Run 3 in Table 2.12 with that of Run 2 in Table 2.24). A mole balance for the cracking of C_9 would give:

$$C_5 + C_8 + C_{11} = C_4 + C_7 + C_{10}$$

This mole balance is not satisfied. Cracking of the C_9 only is therefore not likely.

(b) C_{12} and C_9 cracking only: A comparison between Run 3 of Table 2.12 and Run 2 of Table 2.24 indicates similar concentrations of C_{12} in the product. Assuming that the extent of C_{12} cracking was similar in both cases (based on similar C_{12} concentrations in the reactor exit), the amount of C_9 that cracked to C_5 and C_4 can be estimated. The resultant ratio of C_{12} cracked to C_9 cracked would be 4.5:1. A comparison of the C_4, C_5, C_7 and C_8 fractions in the above two Runs indicates that the following reactions did occur:

$$C_4 + C_3 \longrightarrow C_7$$
$$C_5 + C_3 \longrightarrow C_8$$

It is clear from Run 1 that the following reactions occurred:

$$C_8 \rightleftharpoons 2C_4$$
$$C_8 \rightleftharpoons C_5 + C_3$$

In the presence of relatively large concentrations of C_3, however, it is likely that the forward reaction, $C_3 + C_5 \longrightarrow C_8$, will predominate over the reverse.

It has been shown in Section 2.5.3.2 that C_{12} cracked primarily according to the following mechanism:

$$C_{12} \longrightarrow C_7 + C_5$$
$$C_{12} \longrightarrow C_8 + C_4$$

A brief examination of the results in Table 2.24 shows that the two reactions can easily produce the observed product spectra, but there are also many combinations of these two reactions that will produce the observed results. It is therefore not possible to determine the extent to which C_{12} cracked to C_5 and C_7 as opposed to C_8 and C_4.

5. Production of C_{12}: It is uncertain as to which of the following two reactions is responsible for the production of C_{12}.

$$C_6 + C_6 \longrightarrow C_{12}$$
$$C_3 + C_9 \longrightarrow C_{12}$$

Examination of Runs 2 and 3 in Tables 2.23-2.25 shows that:

a. The concentration of 2-methyl-1-pentene in the feed remains roughly constant.

b. The concentration of 2-methyl-1-pentene in the reactor was lower in Run 2 than in Run 3.

c. The C_{12} concentration increased with increasing C_3 concentration. This increase in C_{12} production can result from only one source (note from Table 2.25 that the reactor concentration of C_6 remained approximately constant): i.e., $C_9 + C_3 \longrightarrow C_{12}$ (provided that the presence of C_3 does not increase the rate of C_6 dimerization or that the C_3 did not produce C_6 isomers which dimerize much faster than 2-methyl-1-pentene). A similar trend occured in Runs 2 and 4. Based on the reactor concentration of the 2-methyl-1-pentene in Run 2 and the pure C_6 and C_3 data, it seems that the C_{12} fraction in Run 2 was entirely due to the dimerization of C_6. Using the same basis, about 50% of the C_{12} fraction in Run 4 is formed from $C_9 + C_3$ and about 50% from $C_6 + C_6$. This will be discussed in more detail later.

Close examination of Run 4 in Table 2.8 and Run 1 in Table 2.12 shows that the maximum expected amount of C_{12}, produced by dimerization of the C_6 fraction in Run 4 of Table 2.8, is less than 0.05×10^{-4} mol/l (provided the C_3 presence does not enhance the dimerization of the C_6 and does not produce C6 dimers that dimerize much faster than 2-methyl-1-pentene). If this is so then the C_{12} produced in Run 4 of Table 2.8 was due primarily to $C_3 + C_9$ (>95%).

The following method will be used to estimate how much C_{12} was produced from C_6 + C_6 and C_9 + C_3. At the conditions used in these experiments it is known, from the pure feed experiments, how much C_{12} was produced from a feed of pure 2-methyl-1-pentene (by extrapolating the pure feed results). It will be assumed that this was not affected by the presence of propene, provided that the average reactor concentration was constant. From the mixed feed results, the balance of the C_{12} was produced from C_9 + C_3. The amounts produced by each reaction can therefore be estimated.

Figure 2.25 shows the product concentration of C_{12} as a function of the 2-methyl-1-pentene concentration in the reactor (arithmetic mean of the inlet and outlet concentration).

Table 2.26 shows, for each mixed feed run, the concentration of C_{12} due to C_6 + C_6 (Figure 2.25), the total C_{12} concentration and hence the concentration of C_{12} due to C_9 + C_3 (by mole balance). The percentage contribution of C_9 + C_3 to the total amount of C_{12} produced, for each run, is also shown.

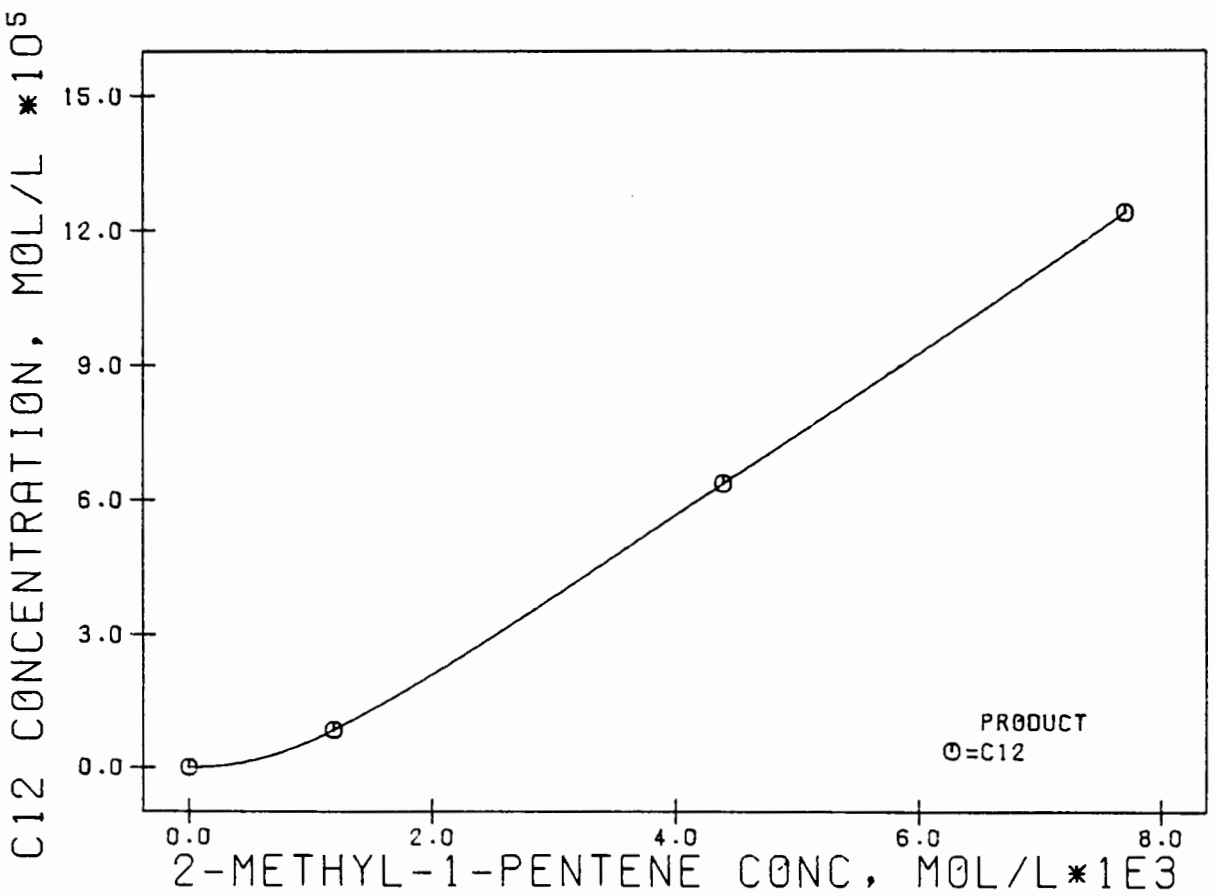

FIG 2.25 PULSE: C12 (PRODUCT) VS 2MIP CONCENTRATION TAKEN FROM THE DATA OF TABLE 2.12

Table 2.26 Fraction of C_{12} produced from C_6 + C_6 and C_9 + C_3.

	C_{12} from C_6+C_6 [mol•l^{-1}]	Total C_{12} [mol•l^{-1}]	C_{12} from C_9+C_3 [mol•l^{-1}]	[%]
Run 2	1.4×10^{-4}	1.3×10^{-4}	———	—
Run 3	1.3×10^{-4}	1.6×10^{-4}	0.3×10^{-4}	21
Run 4	1.3×10^{-4}	2.9×10^{-4}	1.6×10^{-4}	54

The total amount of C_{12} produced in Run 2 (Table 2.26) was less than that produced by a pure C_6 feed at an equivalent concentration (reactor concentration). This could imply that, in the presence of propene the reactivity of 2-methyl-1-pentene is higher than that without the presence of propene. The difference may also be due to experimental error.

The above calculations were repeated using the assumption that only the C_{12} cracked (the case above is equivalent to the case where only the C_9 cracked) and the amount of C_{12} was taken as the total amount produced prior to cracking (i.e., if there was no cracking at all). These calculations produced similar results to those in Table 2.26, with a slightly smaller fraction of the C_{12} being formed from C_9 + C_3.

Moving from Run 2 to Run 4 the ratio C_3/C_9 increased from about 10.5 to 15 and the ratio C_3/C_6 increased from about 1.5 to 6.

2.5.9 Propene + 2-Methyl-2-Pentene

Similar experiments to the co-oligomerization of propene and 2-methyl-1-pentene were carried out using 2-methyl-2-pentene. The results were found to be very similar and will not be discussed.

2.5.10 2-Methyl-1-Pentene + 1-Butene

Mixtures of 1-butene and 2-methyl-1-pentene were pulsed into the reactor. The concentrations of 1-butene (feed concentrations) were kept constant to within 30%, while the 2-methyl-1-pentene concentrations were varied.

2.5.10.1 Feed and product spectra

The feed concentrations at the inlet to the reactor are listed in Table 2.27. Concentrations of the products at the reactor exit are listed in Table 2.28.

Table 2.27 Reactant concentrations at the reactor inlet at 473 K and 1.53 MPa.

	2-methyl-1-pentene [mol·l^{-1}]	1-butene [mol·l^{-1}]
Run 1	0	1.22×10^{-2}
Run 2	1.6×10^{-3}	1.71×10^{-2}
Run 3	4.0×10^{-2}	1.40×10^{-2}
Run 4	10.0×10^{-2}	1.42×10^{-2}

Table 2.28 Product spectra at the reactor exit.

	Exit concentrations [mol·l^{-1}x10^{5}]				Mols in exit [mol%]			
	Run 1	Run 2	Run 3	Run 4	Run 1	Run 2	Run 3	Run 4
C_3	8.8	5.1	5.9	6.7	20.5	5.9	7.7	4.2
C_5	11.7	37.7	23.7	59.7	27.3	36.3	30.9	37.2
C_6	1.5	—	—	—	3.5	—	—	—
C_7	0.5	10.1	6.0	24.8	1.2	11.5	7.8	15.5
C_8	19.1	21.6	31.2	22.1	44.5	24.8	40.6	13.8
C_9	0.7	3.7	3.1	6.1	1.6	4.2	4.1	3.8
C_{10}	0.1	12.2	5.6	27.3	0.2	14.0	7.3	17.0
C_{11}	0.0	0.5	0.3	2.0	0.0	0.5	0.4	1.3
C_{12}	0.5	2.4	1.0	11.5	1.2	2.8	1.3	7.2

Table 2.29 lists the averaged reactor concentrations of both the 1-butene and the 2-methyl-1-pentene at each conversion level. Conversions are too high to be regarded as differential. Figure 2.26 shows the exit reactor concentrations of the products as a function of changing 2-methyl-1-pentene concentration (the 1-butene concentration remained approximately constant).

Table 2.29 Reactor concentrations and conversion levels of reactants.

	1-butene		2-methyl-1-pentene	
	[mol•l^{-1}]x10^{3}	X_A%	[mol•l^{-1}]x10^{3}	X_A%
Run 1	11.9	5.1	0.0	0
Run 2	16.6	6.0	1.41	24
Run 3	13.7	3.9	3.74	13
Run 4	13.6	8.0	9.40	12

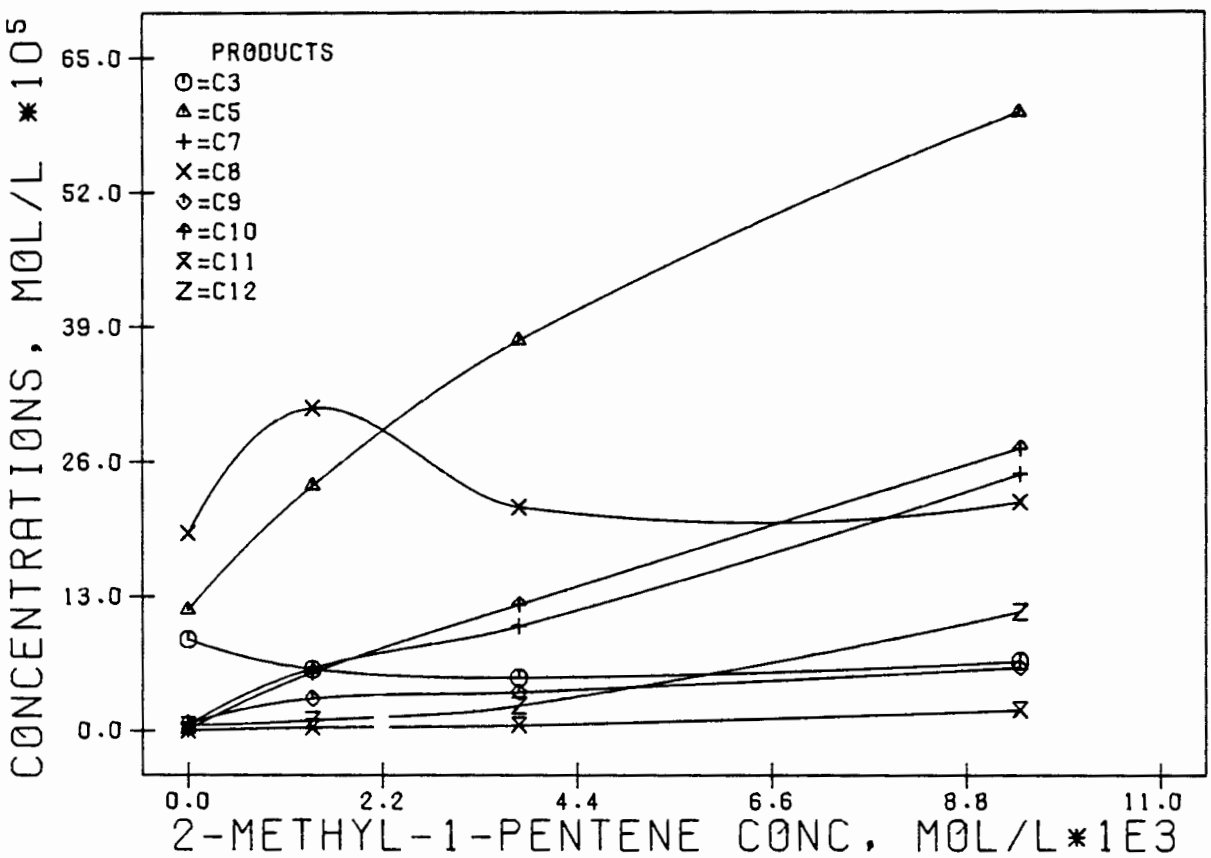

FIG 2.26 PULSE: 2M1P+1-BUTENE: PRODUCT SPECTRA AT 473 K AND 1.53 MPA

2.5.10.2 Reaction mechanisms

The following can be noted from the data in Tables 2.27 and 2.28 (see also Figure 2.26).

1. Cracking: There was a large degree of cracking.

2. C_{10} production: From the pure feed experiments it was found that the rate of 1-butene oligomerization was higher than the rate of 2-methyl-1-pentene oligomerization. Not knowing the true mechanisms or

rate equations of the reaction of 1-butene with 2-methyl-1-pentene, it is difficult to compare the rate of C_{10} produced from the reaction of 1-butene with 2-methyl-1-pentene to the rates of oligomerization of the individual feedstocks. The presence of cracked products further complicates any comparisons.

By comparing Run 2 of Table 2.24 with Run 4 of Table 2.28 it can be seen that the rate of reaction of $C_3 + C_6$ was higher than the rate of $C_6 + C_4$ (despite the larger extent of C_{10} cracking in the latter), while noting that the average reactor concentrations of the feeds were higher in the $C_6 + C_4$ experiments.

3. Conversions: the results in Table 2.29 indicate that:

   a. The conversion of 2-methyl-1-pentene decreased significantly with an increase in its reactor concentration (in the presence of 1-butene). It was still significantly higher than when it reacted alone.

   b. Comparing Runs 3 and 4 (Table 2.29), it appears that the 1-butene conversion decreased as the 2-methyl-1-pentene concentration was decreased (1-butene concentration remained approximately constant). Examination of the pure 1-butene run indicates a relatively higher conversion of 1-butene when compared with the conversions of Runs 3 and 4 (where 2-methyl-1-pentene was present). Although it may seem that Run 1 contradicts the results of Runs 3 and 4 this may not necessarilly so. It is quite possible that the presence of the 2-methyl-1-pentene (or possibly the $C_6 + C_4$ reaction) inhibits the rate of 1-butene dimerization or simply that the rate of 1-butene dimerization is not only faster than the rate of 2-methyl-1-pentene dimerization (which it is) but also faster than the rate of 1-butene + 2-methyl-1-pentene. This could then explain why the conversion of the 1-butene would drop in the presence of the 2-methyl-1-pentene. Whether the inhibition be true or not it is still resonable to expect that the conversion of 1-butene could increase with an increase in the concentration of 2-methyl-1-pentene (while the concentration of 1-butene is being held constant) since the increase shifts the driving force of the reaction ($C_6 + C_4 \longrightarrow C_{10}$) to the right. Run 2 is not compared due to the higher concentration of 1-butene and, hence, the higher conversion of 1-butene.

4. Cracking of C_{12}: The cracking of C_{12} has previously been discussed in detail (Sections 2.5.3.2 and 2.5.8.2). No further discussion of C_{12} cracking will be given here.

5. C_5 production: The large presence of C_5 indicates that there was some degree of C_{10} cracking. The simultaneous cracking of the C_{12}, C_{10} and C_8 makes it impossible to determine the extent of each reaction under these experimental conditions.

6. Production of C_{11}: It is probable that the C_{11} fraction was produced from $C_4 + C_7$. It has been shown previously that rate of $C_5 + C_6$ was small (relative to the amount of C_{11} produced). The concentrations of C_8 and C_3 were small and not likely to contribute to the C_{11} production.

7. Production of C_{12}: The C_{12} can be produced either by $C_6 + C_6$ or $C_8 + C_4$. Judging from the pure feed experiments it appears that the majority of the C_{12} was produced by dimerization of the 2-methyl-1-pentene.

2.5.11 2-Methyl-1-Pentene + Iso-butene

The experiments in this section were carried out by maintaining a constant iso-butene concentration (at the entrance to the reactor) and varying the 2-methyl-1-pentene concentration. Some degree of overlap was found on the following chromatographic peaks which, in some cases, made integration and identification difficult:

1. C_6 and C_7
2. C_7 and C_8
3. C_{10} and C_{11}
4. C_{11} and C_{12}

2.5.11.1 Feed and product spectra

The feed concentrations at the inlet to the reactor are listed in Table 2.30. Concentrations of the products at the reactor exit are shown in Table 2.31.

Table 2.32 lists the averaged reactor concentrations of both the iso-butene and 2-methyl-1-pentene, and the corresponding conversions of each. Figure 2.27 shows the exit reactor concentrations of the products as a function of changing 2-methyl-1-pentene concentration.

Table 2.30 Reactant concentrations at the reactor inlet at 473 K and 1.54 MPa.

	2-methyl-1-pentene [mol•l^{-1}]	iso-butene [mol•l^{-1}]
Run 1	—	1.25×10^{-2}
Run 2	1.8×10^{-3}	1.4×10^{-2}
Run 3	3.6×10^{-3}	1.1×10^{-2}
Run 4	9.2×10^{-3}	1.0×10^{-2}

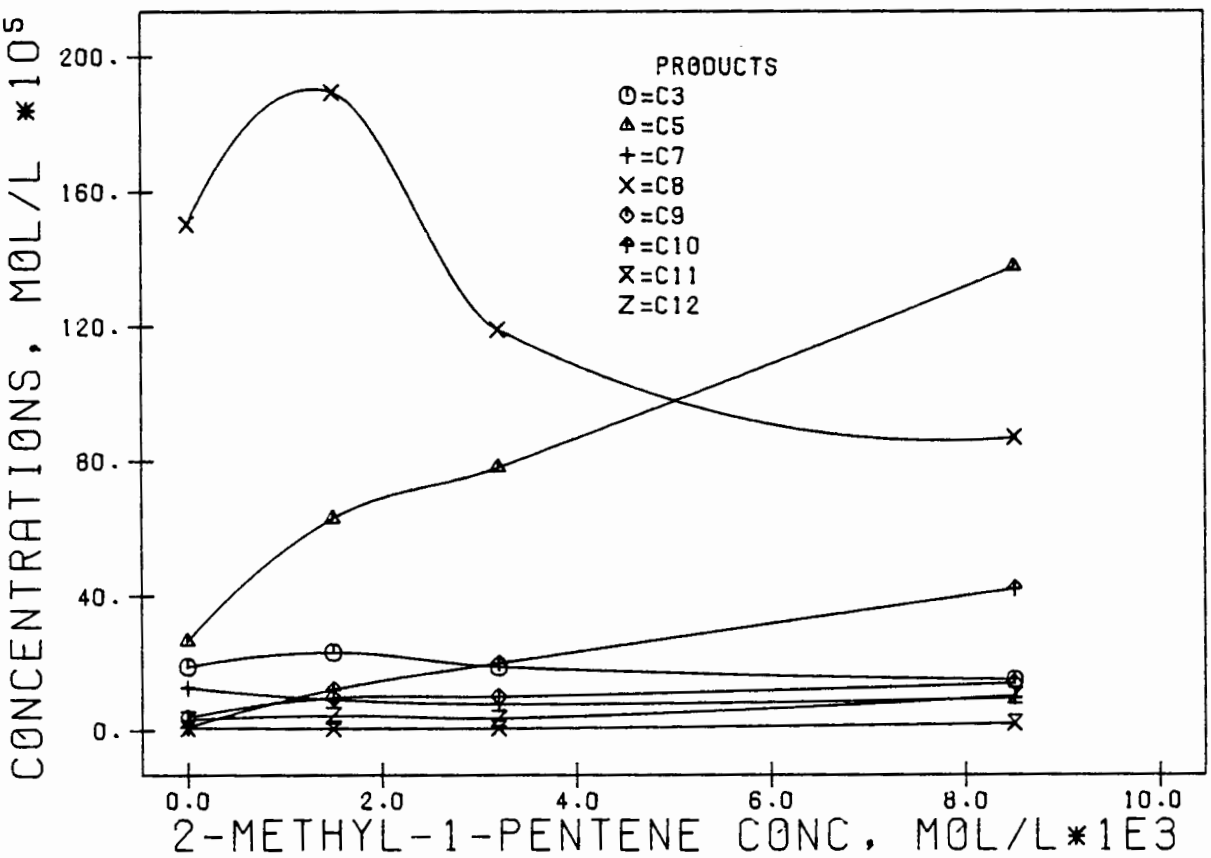

FIG 2.27 PULSE: ISO-BUTENE+2M1P: PRODUCT SPECTRA AT 473 K AND 1.54 MPA

2.5.11.2 Reaction mechanisms

The following can be noted from Tables 2.31, 2.32 and Figure 2.27.

1. Cracking: Similar to all other pulse experiments performed, cracking was extensive.

Table 2.31 Product spectra at the reactor exit.

	Exit concentrations [mol•l^{-1}x10^5]				Mols in exit [mol%]			
	Run 1	Run 2	Run 3	Run 4	Run 1	Run 2	Run 3	Run 4
C_3	19.0	23.3	18.9	15.0	8.6	7.5	7.3	4.7
C_5	26.7	63.1	78.1	138	12.0	20.2	30.2	43.3
C_6	3.9	—	—	—	1.8	—	—	—
C_7	12.7	9.1	7.8	9.6	5 7	2.9	3.0	3.0
C_8	150	189	119	87	67.8	60.7	46.1	27.3
C_9	4.0	9.8	10.1	14.0	1.8	3.1	3.9	4.4
C_{10}	1.0	12.3	20.1	42.1	0.4	3.9	7.8	13.3
C_{11}	0.7	0.5	0.6	2.0	0.3	0.1	0.2	0.6
C_{12}	3.3	4.5	3.6	10.3	1.5	1.4	1.4	3.2

Table 2.32 Averaged reactor concentrations of the reactants.

	2-methyl-1-pentene		Iso-butene	
	[mol•l^{-1}]	X_A%	[mol•l^{-1}]	[X_A%]
Run 1	—	—	10.5x10^{-3}	32
Run 2	1.5x10^{-3}	32	12x10^{-3}	34
Run 3	3.2x10^{-3}	21	9.3x10^{-3}	31
Run 4	8.5x10^{-3}	16	8.4x10^{-3}	32

2. Cracking of C_{12}: The cracking of C_{12} will not be discussed (see Sections 2.5.3.2 or 2.5.8.2 for detailed discussion).

3. C_3 production: Examination of the pure feed experiments indicates that the extremely high concentrations of C_5, in Run 2, are largely a result of $C_{10} \longrightarrow 2C_5$. An estimate, based on the pure feed results, of the source of C_5 in Runs 2 and 4 would be:

Run 2 C_5 from $C_{12} \longrightarrow C_7 + C_5$ 20%

C_5 from $C_8 \longrightarrow C_5 + C_3$ 10%

C_5 from $C_{10} \longrightarrow 2C_5$ 70%

Run 4	C_5 from C_{12}	$\longrightarrow C_7 + C_5$	50%
	C_5 from C_8	$\longrightarrow C_5 + C_3$	10%
	C_5 from C_{10}	$\longrightarrow 2C_5$	40%

4. Rate of C_{10} production: The results of Run 2 in Table 2.32 indicate that the iso-butene and 2-methyl-1-pentene had similar averaged reactor concentrations. The concentration of the iso-butene was slightly higher. The reactant concentrations at the reactor inlet indicate that the iso-butene concentration in Run 2, was about 25% higher than that of 2-methyl-1-pentene. The concentration of C_8 in the product spectra, for the same run, was about 8 or more times higher than that of C_{12}, indicating that $C_4 + C_4$ was much faster than $C_6 + C_6$ (see Figure 2.27).

   Examination of the C_{10} concentration indicates that it was approximately half that of C_8. Taking cracking into account, it would appear that the C_8 and C_{10} concentrations (pre-cracking) were similar. Therefore there is no clear indication as to which of the two reactions was faster.

   A comparison between the rate of production of C_{10} and C_{12} cannot be made, since the respective rate equations are unknown. Although four times as much C_{10} was produced as C_{12}, the combined initial concentration of $C_4 + C_6$ was more than double that of C_6 and, not knowing the concentration dependence of these two reactions, no comparison can be made. For a general comparison regarding the rates of reactions, knowledge of the rate equations is essential.

5. Conversions: In a similar manner to the other mixed feed results, the conversion of 2-methyl-1-pentene increased as its concentration decreased (while the iso-butene concentration remained approximately constant). The iso-butene conversion, however, remained constant (see Table 2.32).

6. C_{10} cracking: It is likely that some of the C_{10} cracked to $C_7 + C_3$. It is difficult to estimate due to the simultaneous cracking of C_{12} and the repolymerization of C_3.

7. Production of C_9: It is not clear from the data in Table 2.31 whether the C_9 fraction was produced by $C_5 + C_4$, $C_6 + C_3$ or both.

8. Production of C_{12}: Based on the pure feed analysis, the production of C_{12} is likely to be due to both $C_8 + C_4$ and $C_6 + C_6$. In Run 2, the bulk of the C_{12} was produced by $C_6 + C_6$.

2.5.12 Propene + 1-Butene

Four experiments were carried out by maintaining a constant (or as constant as possible) 1-butene concentration and varying the propene concentration. Chromatographic overlap was observed between the following peaks:

1. C_3 and C_4 fractions
2. C_7 and C_8 fractions
3. C_8 and C_9 fractions
4. C_9 and C_{10} fractions
5. C_{10} and C_{11} fractions
6. C_{11} and C_{12} fractions

2.5.12.1 Feed and product spectra

Feed concentrations at the inlet to the reactor are listed in Table 2.33. Product concentrations at the reactor exit are listed in Table 2.34. Due to the high feed concentrations, the C_3 and C_4 produced are not detected.

Table 2.33 Reactant concentrations at the reactor inlet at 473 K and 1.53 MPa.

	propene [mol•l^{-1}]	1-butene [mol•l^{-1}]
Run 1	———	1.16×10^{-2}
Run 2	0.61×10^{-2}	1.50×10^{-2}
Run 3	1.27×10^{-2}	1.46×10^{-2}
Run 4	2.48×10^{-2}	1.17×10^{-2}

Table 2.35 lists the averaged reactor concentrations of both the 1-butene and the propene and the corresponding conversions of each. Figure 2.28 shows the exit reactor concentrations of the products as a function of the propene concentration.

2.5.12.2 Reaction Mechanisms

The following points can be noted from the results in Tables 2.33, 2.34 and 2.35 and Figure 2.28.

Table 2.34 Product spectra at the reactor exit.

	Exit concentrations [mol·l^{-1}x10^5]				mols in exit [mol%]			
	Run 1	Run 2	Run 3	Run 4	Run 1	Run 2	Run 3	Run 4
C_3	8.8	—	—	—	20.5	—	—	—
C_5	11.7	12.4	12.5	10.8	27.3	22.8	20.6	15.9
C_6	1.5	9.0	12.2	20.2	3.5	16.7	20.2	29.8
C_7	0.5	9.4	10.7	10.0	1.2	17.3	17.7	14.9
C_8	19.1	17.9	17.1	14.2	44.5	32.8	28.3	21.0
C_9	0.7	3.3	3.9	7.1	1.6	6.0	6.5	10.5
C_{10}	0.1	1.3	2.4	4.0	0.2	2.3	4.0	5.9
C_{11}	0.0	0.6	0.8	0.5	0.0	1.1	1.3	0.8
C_{12}	0.5	0.5	0.5	0.8	1.2	0.8	0.9	1.1

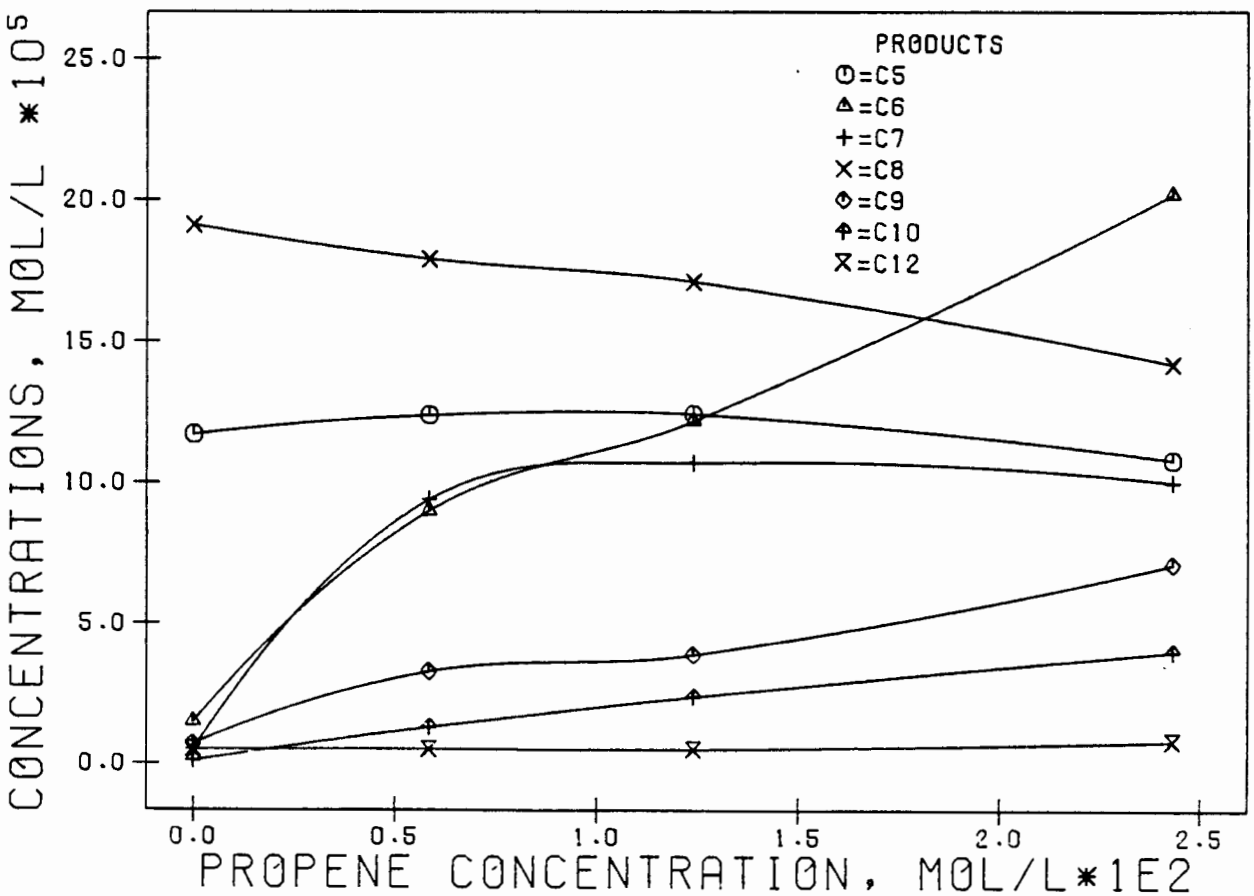

FIG 2.28 PULSE: 1-BUTENE+PROPENE: PRODUCT SPECTRA AT 473 K AND 1.53 MPA

Table 2.35 Averaged reactor concentrations of the reactants.

	propene		1-butene	
	[mol•l^{-1}]	X_A%	[mol•l^{-1}]	X_A%
Run 1	—	—	1.13×10^{-2}	5.5
Run 2	0.59×10^{-2}	5.0	1.52×10^{-2}	5.1
Run 3	1.24×10^{-2}	3.9	1.43×10^{-2}	4.7
Run 4	2.43×10^{-2}	4.1	1.15×10^{-2}	3.7

1. Previous results: The following have been discussed in several other sections and thus will not receive attention here:
   - cracking in general
   - C_{12} cracking and the production of C_{12}
   - C_8 cracking to C_5 + C_3
   - the production of C_5, C_9, C_{10} and C_{11}

2. Conversions: The concentration-conversion data in Table 2.35 show similar trends to the data for other mixed feeds.

3. Rates of C_3 + C_3, C_4 + C_4 and C_3 + C_4: The pure feed analysis has shown that the rate of C_3 + C_3 was significantly lower than the rate of 1-butene dimerization. Examination of the C_8 and C_6 fractions in Run 3 (similar initial C_3 and C_4 concentrations) supports this finding (remembering that a large fraction of the C_8 cracks to C_5 + C_3). It would appear from Run 3 that the rate of C_3 + C_4 was significantly lower than the rate of 1-butene dimerization. (This run is used here because the initial concentrations of C_3 and C_4 were similar.) However, it would appear from this run that the rate of C_3 + C_4 was similar to the rate of propene dimerization. Using the parallel of a truly heterogeneous catalyst with the corresponding acid sites, this could represent the rate limiting adsorption of the propene onto the acid sites.

2.5.13 Propene + Iso-butene

Four experiments were carried out, maintaining a constant iso-butene concentration and varying the propene concentration. Overlap on the following chromatographic peaks was observed:

(a) propene and the C_4 fraction
(b) C_8 and C_9 fractions
(c) C_6 and C_7 fractions
(d) C_7 and C_8 fractions

2.5.13.1 Feed and product spectra

Table 2.36 lists the propene and iso-butene concentrations at the inlet to the reactor. Product concentrations at the reactor exit are listed in Table 2.37

Table 2.36 Reactant concentrations at the reactor inlet at 473 and 1.55 MPa.

	propene concentration [mol•l^{-1}]	iso-butene concentration [mol•l^{-1}]
Run 1	—	1.21×10^{-2}
Run 2	0.80×10^{-2}	1.17×10^{-2}
Run 3	1.31×10^{-2}	1.29×10^{-2}
Run 4	2.50×10^{-2}	1.31×10^{-2}

Table 2.37 Product spectra at the reactor exit.

	Exit concentrations (mol•l-1x10^{5})				Mols in exit (mol%)			
	Run 1	Run 2	Run 3	Run 4	Run 1	Run 2	Run 3	Run 4
C_3	19.0	—	—	—	8.6	—	—	—
C_5	26.7	37.3	38.6	32.9	12.0	11.2	9.1	6.7
C_6	3.9	37.3	49.0	59.0	1.8	11.2	11.6	12.0
C_7	12.7	85.3	134.0	179	5.7	25.6	31.7	36.6
C_8	150	152	171	172	67.8	45.7	40.6	35.1
C_9	4.0	5.7	6.7	8.5	1.8	1.7	1.6	1.7
C_{10}	1.0	8.4	14.7	28.2	0.4	2.5	3.5	5.8
C_{11}	0.7	1.6	2.5	3.3	0.3	0.5	0.6	0.7
C_{12}	3.3	5.0	5.7	6.7	1.5	1.5	1.3	1.4

The averaged reactor concentrations of the iso-butene and propene, and the corresponding conversions of each, are listed in Table 2.28. Figure 2.29 shows the exit reactor concentrations of the products as a function of the propene concentration.

Table 2.38 Averaged reactor concentrations and the conversions of the reactants.

	propene		iso-butene	
	$mol \cdot l^{-1}$	X_A %	$mol \cdot l^{-1}$	X_A %
Run 1	—	—	1.02×10^{-2}	32
Run 2	0.66×10^{-2}	34	0.96×10^{-2}	36
Run 3	1.18×10^{-2}	19	1.01×10^{-2}	44
Run 4	2.26×10^{-2}	19	1.04×10^{-2}	41

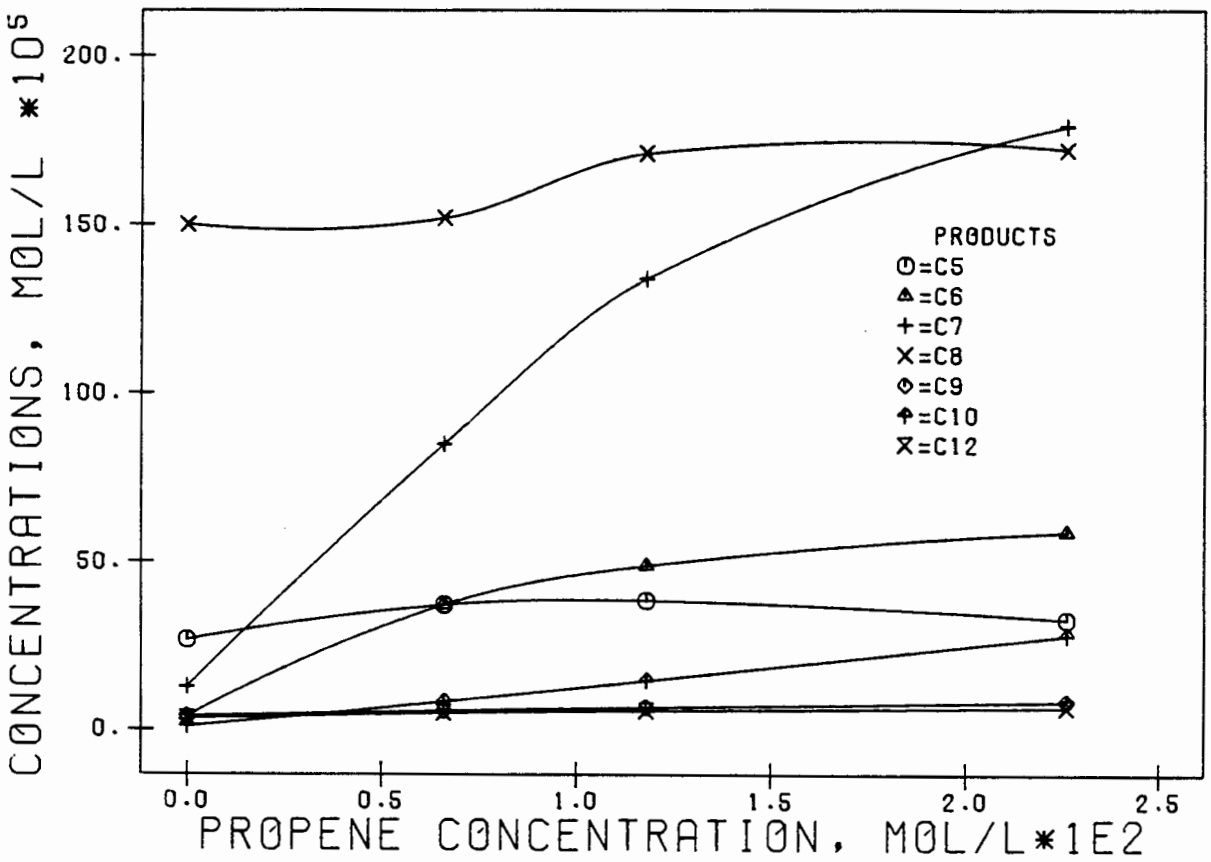

FIG 2.29 PULSE: ISO-BUTENE+PROPENE: PRODUCT SPECTRA AT 473 K AND 1.55 MPA

2.5.13.2 Reaction mechanisms

The following discussion is based on the results in Tables 2.36, 2.37 and 2.38 and Figure 2.29

1. General: Cracking in general, C_{12} cracking, the production of C_{12}, C_8 cracking and the production of C_5, C_9, C_{10} and C_{11} will not be discussed as they have already been discussed in detail.

2. Conversions: The results of Table 2.38 show similar trends to those of previous mixed feeds. As the propene concentration decreased, its conversion rose as expected (since it was reacting mostly with the more active iso-butene, and the dimerization of propene was slower than the reaction of propene with iso-butene). The iso-butene conversions showed a different trend to those of other mixed feeds. The conversion in Run 1 (pure iso-butene) was lower than in the other three runs (unlike previous mixed feeds). This lower conversion is to be expected if the propene did not inhibit the iso-butene conversion in any way. The C_3 then provides an additional reaction pathway, leading to higher total iso-butene conversions. The conversion of iso-butene to C_8 was constant in all four runs (noting that the initial iso-butene concentration in Runs 2 and 3 was higher than that in Runs 1 and 4). These findings are not general, but are limited to the specific cases mentioned here.

3. Rate of $C_3 + C_3$, $C_4 + C_4$ and $C_3 + C_4$: Examining the product spectra in Table 2.37, it is quite clear, as was shown for the pure feed experiments, that the rate of dimerization of iso-butene was much faster than the rate of propene dimerization. It can also be seen that the rate of iso-butene dimerization was faster than the rate of production of C_7 from propene + iso-butene. The rate of production of C_7 from propene + iso-butene was in turn much faster than the rate of propene dimerization. Although these results are specific to these experimental conditions, it is quite likely that they would hold under most conditions.

4. Propene activity in the presence of iso-butene: Comparing the data of Run 2 in Tables 2.36 and 2.37 with the data of Run 1 (3.1% conversion run) in Tables 2.8 and 2.9, it can be seen that the concentration of propene in the former case was lower than in the latter. However, the production of C_6 in the mixed feed run (propene + iso-butene) was significantly higher than in that of the pure feed. The production of C_9 was slightly higher and the production of C_{12} was dramatically higher (clearly due to the increased C_6 concentration). Examination of the pure iso-butene Run 2 (36.9% conversion level) in Table 2.19 shows that its effect on the production of C_6 is minimal. Its effect was not minimal with respect to the production of C_9 and C_{12}. It is clear, therefore, that the propene was very much more active in the presence of iso-butene than when it was alone.

2.6 CONCLUSIONS

Extrapolation of the pulse experimental results to other operating regions of interest, such as regions of higher alkene partial pressures, lower weight hourly space velocities and typical steady state operating conditions as would be found in industrial fixed bed reactors (with their accompanying mass and heat transfer limitations) could possibly lead to significant errors. For example, as one moves from a system of low alkene partial pressure to a system of high partial pressure it would not be unreasonable to experience a shift in the order of a particular reaction. This could quite conceivably result in a particular alkene being more reactive than another at low pressures but less reactive at high pressures. Although this could not be checked for many of the alkene isomers, such as the hexenes (due to the extremely small quantities available), examination of the results in Chapter 3 indicates that the same order of increasing reactivities found there, at the higher partial pressures, for propene and the butenes is maintained here in the pulse experiments.

It has been shown thermodynamically that at the conditions used in the pulse experiments (very low partial pressures of alkenes) extensive cracking is favoured. The large extents of cracking that were observed in the pulse experiments were therefore expected. Due to the lack of thermodynamic data (particularly heats of formation) for many branched alkenes of carbon chain length greater than 6, the determination of the thermodynamically most stable isomers and hence the most likely cracking reaction pathways followed could not be adequately substantiated in this way and are therefore based mainly on the particular product spectra obtained.

In the examination of cracking reactions attention was mainly focussed on the cracking of the hydrocarbons to non-oligomeric products, i.e., reverse reactions were not examined in detail due to the difficulty in determining the extent of such reactions, although it was quite clear from many of the experiments that reverse reactions were not insignificant.

2.6.1 Oligomerization of pure olefins

It was found from the pure propene and pure 2-methyl-1-pentene experiments that the amount of cracked products which depended on the concentrations of the C_9 and C_{12} fractions (particularly the C_{12} fraction) were due mainly to C_{12} cracking at C_{12} concentrations above

$1x10^{-4}$ mole/l, despite a constant C_{12}/C_9 mole ratio. This implies that, under these conditions, the relative fractions of cracked products were insensitive to the ratio of C_{12}/C_9 in the reactor. It can also be concluded that, at these conditions, the rate of C_{12} cracking was far more concentration sensitive than was C_9, viz., the C_{12} cracking rate equation had a higher order than that of C_9.

From the pure propene, 1-butene, iso-butene and 2-methyl-1-pentene results, it has been found that the following cracking reactions for C_{12} were the most likely:

$$C_{12} \longrightarrow C_7 + C_5,$$

$$C_{12} \longrightarrow C_8 + C_4.$$

It has also been shown, for the feed consisting of pure propene, that the C_7 and C_8 fractions did recombine to some extent with the propene to form C_{10} and C_{11}.

With respect to the cracking of C_9 the most likely route is as follows:

$$C_9 \longrightarrow C_5 + C_4.$$

Isomerization of the C_6 alkenes was rapid and, irrespective of the starting isomer, the final hexene fraction (after reaction) consisted of approximately the same fractions of each isomer, hence the similar results obtained with each of the isomers. The four most abundant isomers produced were, in order of decreasing mole fraction; 2-methyl-2-pentene, 3-methyl-2-pentene, 2-methyl-1-pentene and cis-4-methyl-2-pentene. Thermodynamically this has been shown to be reasonable.

An interesting feature of the reverse reactions was that from the 2-methyl-1-pentene and the butene experiments it was found that the rate of the reaction: $C_{12} \longrightarrow C_9 + C_3$ was very small relative to other cracking reactions, despite the large amounts of C_{12} cracking that did occur. This result suggests that under normal operating conditions, where cracking is far less likely to occur, this reaction can be ignored.

With regard to the oligomerization of 1-butene and iso-butene it was found in both cases that, unlike propene, the dimerization reactions were extremely fast relative to the trimerization and the tetramerization reactions. Whereas the oligomerization of 1-butene resulted in significant isomerization of the dimer and trimer, the reverse was true of iso-butene.

In comparing the relative rates of oligomerization of the various olefins it was found that the C_6 alkenes, with the exception of 1-hexene, oligomerized at comparable rates. This is almost certainly due to the rapid isomerization that takes place. At best the 1-hexene will isomerize to 2-hexene or 3-hexene, hence always giving rise to secondary carbonium ions, whereas the methyl-pentenes will always give rise to tertiary carbonium ions and thus the slower rate of 1-hexene oligomerization. The differences that did occur can be attributed to the fact that equilibrium was probably not reached. Taking the entire group of olefins examined, the order of decreasing reactivity was found to be as follows (although the rates of 1-butene and 2-methyl-1-pentene were found to be fairly comparable):

iso-butene
1-butene
2-methyl-1-pentene
1-hexene
propene

From the pure feed results, no conclusions could be reached regarding the relative rates of the following other than to say neither was negligible with respect to each other:

$$C_6 + C_6 \longrightarrow C_{12}$$
$$C_3 + C_9 \longrightarrow C_{12}$$

To sumarize, the reaction pathways for the pure propene and pure 1-butene/iso-butene oligomerization are re-ilustrated here. Accompanying each pathway is a symbol which serves to indicate which of the pathways are believed to be very likely, those that are believed to be unlikely and those about which no conclusions can be reached. The symbols and their designations are as follows:

s = significant
i = insignificant
u = significance unknown

Most of these three symbols are followed by a number. The number refers to the Section number from which the decision was based regarding the significance of that particular pathway, e.g., s(5) indicates that the pathway being considered was considered to be significant and this decision was based mainly on the results and discussion of Section 2.5.5. By implication then, any number ($) refers to Section 2.5.$.

Care should be taken in interpreting these indicators, e.g., the production of C_7 and C_{10} from the cracking of C_9 in the pure propene experiments was considered to be significant which means that of the C_9 cracked it is believed that a significant proportion cracked via this

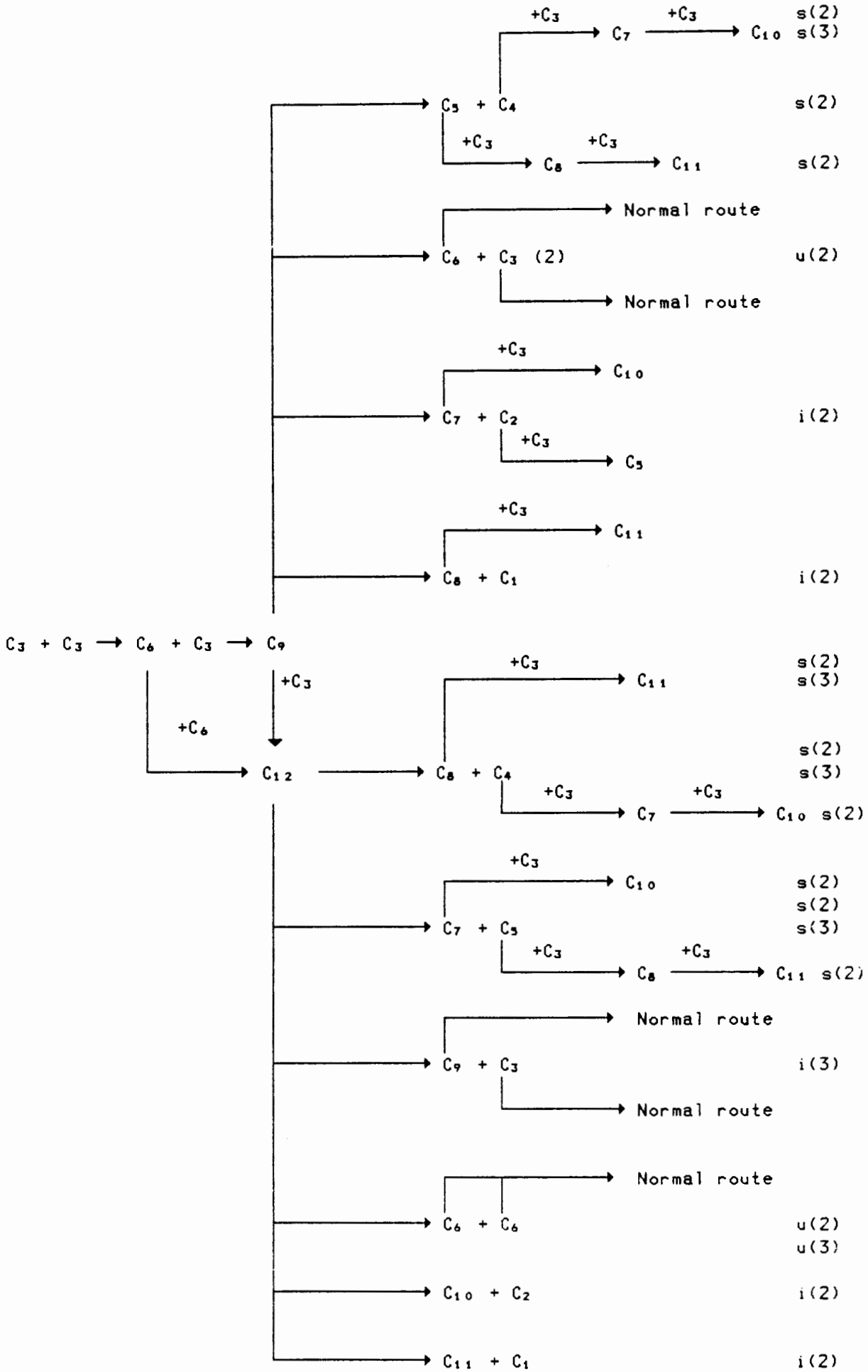
C3 + C3 → C6 + C3 → C9
+C3
+C6
C12 → C8 + C4
+C3
C7
+C3
C10
s(2)
s(3)
C5 + C4
s(2)
+C3
+C3
C8
C11
s(2)
Normal route
C6 + C3 (2)
u(2)
Normal route
+C3
C10
C7 + C2
i(2)
+C3
C5
+C3
C11
C8 + C1
i(2)
+C3
C11
s(2)
s(3)
s(2)
s(3)
+C3
+C3
C7
C10
s(2)
+C3
C10
s(2)
s(2)
C7 + C5
s(3)
+C3
+C3
C8
C11
s(2)
Normal route
C9 + C3
i(3)
Normal route
Normal route
C6 + C6
u(2)
u(3)
C10 + C2
i(2)
C11 + C1
i(2)

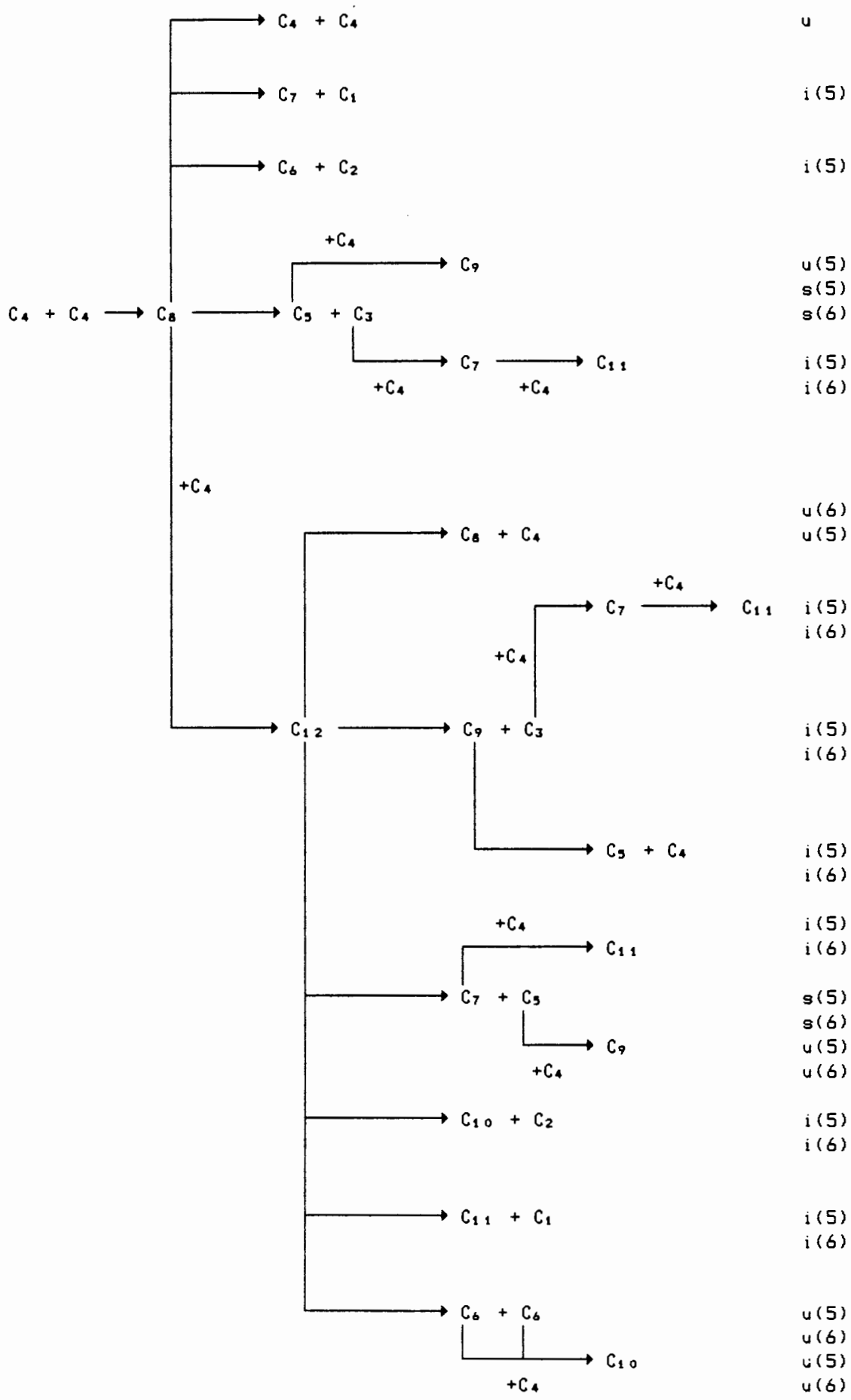
C4 + C4
u
C7 + C1
i(5)
C6 + C2
i(5)
+C4
C9
u(5)
s(5)
C4 + C4
C8
C5 + C3
s(6)
C7
C11
i(5)
+C4
+C4
i(6)
+C4
u(6)
C8 + C4
u(5)
+C4
C7
C11
i(5)
i(6)
+C4
C12
C9 + C3
i(5)
i(6)
C5 + C4
i(5)
i(6)
+C4
i(5)
C11
i(6)
C7 + C5
s(5)
s(6)
C9
u(5)
+C4
u(6)
C10 + C2
i(5)
i(6)
C11 + C1
i(5)
i(6)
C6 + C6
u(5)
u(6)
C10
u(5)
+C4
u(6)

route, the relative amount (relative to the other cracking routes) being subject to the concentrations in of the hydrocarbon in question. The production of C_{12} from both the dimerization of C_6 and the reaction of propene with C_6 was considered to be significant since it is belived (from the results of Sections 2.5.2 and 2.5.3) that the contribution from each route was significantly dependent on the concentrations of C_6, C_3 and C_9. For this reason the production of C_{12} from both routes was considered to be significant. It is quite clear from these examples that care must be taken as to the context in which some of the reactions are considered to be either significant or insignificant.

2.6.2 Mixed feeds oligomerization

Similar conclusions to the above were found using mixed feeds. It was also found that the rate of production of C_9 from propene + 2-methyl-1-pentene was faster than the rate of C_{10} production from 1-butene + 2-methyl-1-pentene. It was found, when using a mixed feed of either of the butenes as the one feed and either propene or 2-methyl-1-pentene as the other and maintaining the butene concentration constant, that as the concentration of C_3 or C_6 was increased the butene conversion fell. This is not only indicative of the slower rate of propene or 2-methyl-1-pentene oligomerization compared to that of the butenes, but also of the slower rate of propene + butene and 2-methyl-1-pentene + butene polymerization.

It was found that the rate of propene dimerization was faster in the presence of iso-butene than it was when propene was reacted alone (pure feed).

In the propene + 2-methyl-1-pentene experiments it was found that at the lower propene concentrations, where the ratio of propene to 2-methyl-1-pentene was approximately 1.5:1 and the propene to C_9 ratio was approximately 10:1, the C_{12} fraction was produced solely from the dimerization of the 2-methyl-1-pentene. At higher propene concentrations, where the respective ratios were approximately 6:1 and 15:1, about 50% of the C_{12} fraction was estmated to be produced from C_6 dimerization and 50% from propene + C_9 polymerization. This might suggest that in an industrial reactor (fixed bed), at the top of the reactor, where the ratio of propene to C_6 and C_9 is high, most of the C_{12} fraction could be formed from propene + C_9 polymerization, whilst as the reaction mix moves further down the bed and the ratio of C_3 to C_6 and C_9 drops the production of the C_{12} fraction could be largely due to the dimerization of the C_6 alkene fraction.

3. KINETIC STUDIES USING AN INTERNAL GAS RECIRCULATION REACTOR

3.1 INTRODUCTION

3.1.1 The Use of Gradientless Reactors to Obtain Intrinsic Kinetic Data

Before kinetic data can be obtained, several performance tests must be carried out to determine the significance of the various transport processes and to determine the degree of mixing. These are necessary to ensure that the reactor behaves as an ideal CSTR and that it is the intrinsic kinetics that is being determined.

Heat and mass transport effects lead to temperature and concentration gradients in the following regimes:

intraparticular - within the catalyst particle
interphase - between the external surface of the catalyst and the adjacent bulk fluid phase
interparticular - between local bulk fluid regimes and from catalyst particle to catalyst particle

Interparticular effects are manifested by radial and axial temperature and concentration gradients. These effects are difficult to analyse. In this work the significance of ~~interphase~~ inter-particle effects was not examined directly but the ratio of catalyst bed height to catalyst particle diameter was greater than 100 in almost all experimental runs. Doraiswamy and Tajbl (1974) have noted that axial dispersion and axial heat conduction can be neglected if this ratio is greater than 30. The large superficial gas velocities encountered in internal recycle reactors significantly reduces radial and axial effects significantly. Temperature measurements in and outside the catalyst bed showed that the reactor as a whole and the catalyst bed were operating isothermally, giving a further indication of the insignificance of interparticular heat and mass transfer effects. Based on these measurements and the catalyst bed height to particle diameter it was assumed that interparticular effects were negligible and therefore were not examined directly.

The measurement of intraparticular temperature gradients is very difficult for very small catalyst particles. For intraparticular effects, however, the concentration gradient within a catalyst particle

is more serious than the temperature gradient. For gas-solid systems if the reaction is fast enough to introduce non-isothermal effects, then the temperature gradient occurs primarily across the gas film, not within the particle (Hutchings & Carberry, 1966; McGreavy & Cresswell, 1969a, b; McGreavy & Thornton, 1970; McGreavy, 1970). We may therefore expect to find a significant film ΔT, before any ΔT within the particle becomes evident. The significance of intraparticular effects can therefore be determined by examining the significance of intraparticular diffusion.

Temperature gradients can occur either across the gas film or within the particle. For gas-solid systems, however, the most likely temperature effect to intrude on the rate will be the temperature gradient across the gas film. Consequently, if experiments show that gas film resistance is absent, then we may expect the particle to be at the temperature of its surrounding fluid and hence isothermal conditions may be assumed to prevail (Levenspiel, 1972).

The following characterization procedures are necessary:

1. Residence time studies to determine the degree of mixing in the reactor (how close the vessel approaches perfect CSTR behavior).

2. Testing for interphase transport effects (with and without reaction).

3. Testing for intraparticular diffusion effects.

4. The estimation of linear gas velocities through the bed and the calculation of the recycle ratio.

3.1.1.1 Residence time distribution studies

One parameter models

The tanks-in-series model is a one parameter model widely used to represent non-ideal flow (Levenspiel, 1972). The fluid is viewed to flow through a series of equalized, perfectly mixed tanks, and the one parameter of this model is the number of tanks in the chain. For N tanks in series, it can be shown (Levenspiel, 1972) that their variance is equal to

$$\sigma^2 = \frac{\bar{t}^2}{N}$$

where $\bar{t}$ = mean residence time in the N tank system.

The most important measure of characterizing a distribution is the location or mean value of the distribution. For a concentration-time curve, the mean residence time is given by

$$\bar{t} = \frac{\int_0^\infty t\ C\ dt}{\int_0^\infty C\ dt}$$

If the distribution curve is known only at a number of discrete time values t_i then

$$\bar{t} = \frac{\sum t_i C_i \Delta t_i}{\sum C_i \Delta t_i}$$

The spread of the distribution is commonly measured by the variance, σ^2, which is defined as

$$\sigma^2 = \frac{\int_0^\infty (t-\bar{t})^2\ C\ dt}{\int_0^\infty C\ dt} = \frac{\int_0^\infty t^2\ C\ dt}{\int_0^\infty C\ dt} - \bar{t}^2$$

$$- \frac{\sum t_i^2\ C_i \Delta t_i}{\sum C_i \Delta t_i} - \bar{t}^2$$

The variance represents the square of the spread of the distribution and has units of $(\text{time})^2$.

where t_i = time elapsed at stage i
C_i = concentration at time t_i
Δt_i = the time difference between the various t_i's along the curve.

Having calculated $\bar{t}$ and $\bar{\sigma}^2$ from the distribution, the number of tanks in series can therefore be calculated. Obviously, N can only be greater than or equal to one. The greater the value of N the less well mixed is the reactor.

The mean residence time, $\bar{t}$, calculated from the residence time distribution, should be equal to V/v

where V = reactor volume
v = volumetric flow rate of fluid.

Discrepancies can arise due to error in flowrate measurements, error in volume available for fluid, tracer not being inert, or leaks.

Multi parameter models

These models have the advantage that, unlike the one parameter models, they should not only give an indication of the degree of non-ideality of the reactor, but should also identify the type of non-ideality. There are many multi-parameter models available (Wen and Fan, 1975). The model used in this study was a five parameter model based on the model proposed by Cholette and Cloutier (1959), developed by Claasens (1983) and is to some extent an extension of the tanks-in-series model.

The model was developed to handle a series of stirred tanks. A schematic diagram of the model is shown in Figure 3.1.

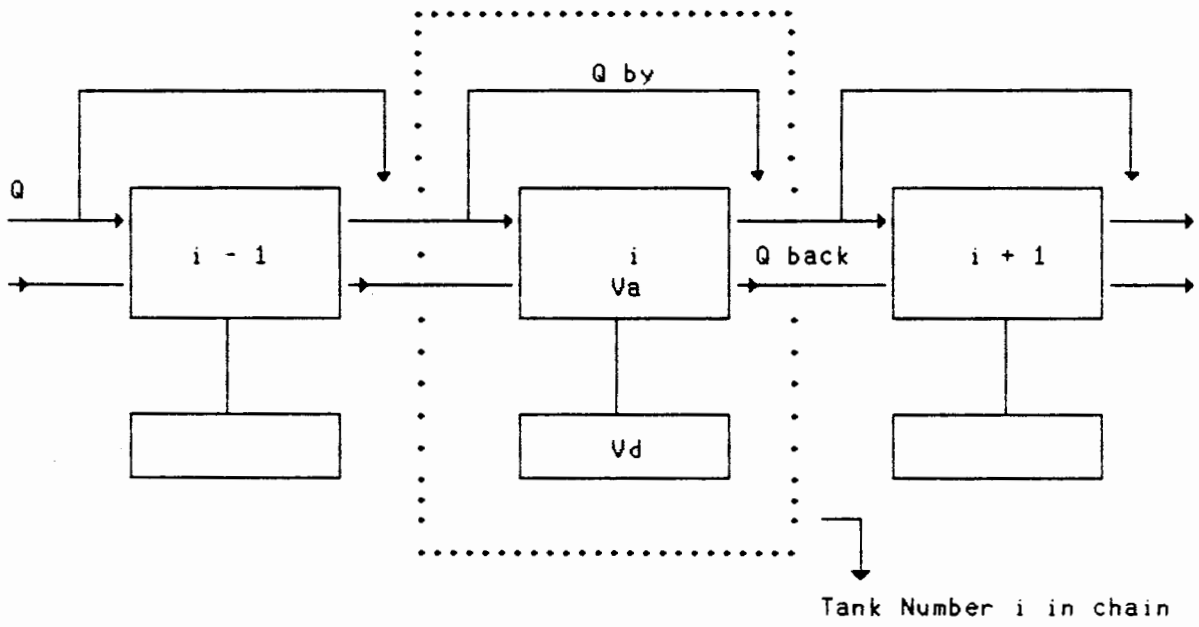

Figure 3.1 Schematic diagram of the extended tanks-in-series model.

The following five parameters are modelled:

1. An 'active', perfectly mixed region (V_a)
2. A completely 'dead' region with no transfer to the other region (V_d)
3. A certain fraction of the feed which bypasses both regions (Q_{by})
4. Backmixing (Q_{back})
5. Time lag at the inlet to each reactor (t)

Bypassing

In a CSTR, bypassing may result from inefficient baffling or mixing. It may decrease the conversion in a reactor considerably. Levenspiel (1972) and Himmelblau & Bischoff (1968) have shown how bypassing may be detected.

Backmixing

This phenomenon usually occurs in packed, liquid-liquid, liquid-gas and fluidized reactors. It can be compared to axial dispersion.

Dead volume

Himmelblau and Bischoff (1968) have shown a number of ways that dead volume may be modelled.

Time lag

The tracer injection point will rarely be situated at the inlet to the reactor and therefore the measured response will be delayed.

A complete mathematical development of the model has been given by Classens (1983). The model parameters are obtained from the given inlet and outlet tracer concentration curves and flowrate. The method is illustrated in the following algorithm:

1. Enter inlet and outlet tracer concentration curves as discrete functions in time.
2. Enter flowrate of fluid through reactor and volume of reactor.
3. Enter an estimated set of parameters.
4. Calculate the outlet tracer concentration curve from the input data parameters by solving a set of differential equations using the Euler method.
5. Compare the calculated output curve with the experimental output curve.

6. Guess a new set of parameters and repeat from step 4. until a preset criterion is satisfied.
7. Output the parameters.
8. End.

A non-linear optimization routine (Nelder & Mead simplex) was used to search for a set of parameters that would minimize the difference between the experimental and the model outlet tracer concentration curves. The sum of the squared errors at equally spaced time steps was used to calculate the difference between the model and experimental curves. Occasionally problems of instability and local minima resulted.

Some of the parameters may lie only between certain limits to ensure meaningful results. The number of tanks in series, for example, may not be less than one. The following constraints were placed on the parameters:

1. The number of tanks, N, $\geq$ 1 and only integers.
2. 0 $\leq$ a(bypassing), b(backmixing) $\leq$ 0.5. These parameters must be less than or equal to one, but in order to obtain stability, they were limited to 0.5.
3. 0 $\leq$ C $\leq$ 1; for the sake of obtaining stability, however, the limits of C (active volume) were set to 0.6 $\leq$ C $\leq$1.
4. Time lag, t, $\geq$ 0 and only integers.

The model which was written in computer language FORTRAN (level 8) was executed on a mainframe SPERRY (UNIVAC 1100).

3.1.1.2 Interphase transport effects

Napthalene sublimation can be used to estimate mass transfer coefficients in an internal recycle reactor. The determination of mass transfer coefficients in this way has been carried out by several researchers (Periera & Calderbank, 1975; Brisk et al., 1968; Caldwell, 1982, 1983a).

Typically the catalyst basket is loaded with napthalene pellets of known surface area. At a given set of conditions and stirrer speed, the overall mass transfer coefficient can be determined. The overall mass transfer coefficient can be defined as (Bird et al., 1963):

$$N_{AGO} = k_G (P_{AC} - P_{AB})$$

where N_{AGO} = moles transferred per unit area per unit time

P_{AC} = equilibrium saturation pressure of A in the bulk phase

P_{AB} = pressure of A in the bulk phase

k_G = overall mass transfer coefficient = $\frac{k_c}{RT}$

$F_{AGO} = N_{AGO} \times a$

where a = surface area (e.g., naphthalene)

$$F_{AGO} = \frac{F \times P_{AB}}{\Pi}$$

where Π = total pressure

F = total molar flow rate

Substituting for k_G, N_{AGO} and F_{AGO} gives:

$$k_c = \frac{P_{AB}}{(P_{AC} - P_{AB})} \times \frac{FRT}{a\Pi}$$

If the concentrations are to be measured by GC which, for a fixed sample size, will give relative concentrations, the mass transfer coefficient, k_c, can be expressed as follows:

$$k_c = \frac{\text{GC response}}{\text{GC response at F=0 - GC response}} \times \frac{FRT}{a\Pi}$$

In this way, the variation of k_c with stirrer speed can be determined.

The significance of film mass transfer (interphase mass transfer) can also be estimated under reaction conditions. For an internal recycle reactor with an internal blower, the maximum theoretical head, ΔH_{gen}, generated by the blower is given by:

$$\Delta H_{gen} = \frac{\Pi^2 (r_2^2 - r_1^2) N^2}{1800g}$$

where N = impeller speed, revs/min

r_1 = inner radius of blades, cm

r_2 = outer radius of blades, cm

g = acceleration of gravity, $cm \cdot s^{-1}$

provided all kinetic energy imparted to the blades is converted to pressure energy,

As ΔH_{gen} increases, the pressure drop across the bed increases and the superficial gas velocity is increased. The film mass transfer coefficient, k_c, will also increase. If the film mass transfer is significant and influences the rate, then as ΔH_{gen} is increased, so the reaction rate will also increase. If the film mass transfer does not influence the rate, then the reaction rate should not increase as ΔH_{gen} is increased. The theoretical head increases or decreases as N is increased or decreased, respectively. In this manner, by increasing N from zero, the limiting value of N can be found (for a given set of conditions and reactions) where the film mass transfer is rapid enough not to have any influence on the reaction rate.

3.1.1.3 Intraparticular diffusion effects

To measure how much the reaction rate is lowered because of the resistance to pore diffusion, the effectiveness factor, ϵ, is defined as (Levenspiel, 1972):

$$\epsilon = \frac{\text{actual reaction rate within pore}}{\text{rate if not slowed by pore diffusion}}$$

The use of the effectiveness factor in establishing a reaction model and energies of activation in experimental work can be a source of error, especially when high gradients occur within the catalyst. Where isothermal conditions prevail throughout the catalyst, the effectiveness factor is always less than unity (Hougen, 1961).

For first order reactions it can be shown that, in the region of strong pore resistance,

$$\epsilon = 1/ML \quad \text{(Levenspiel, 1972)}$$

where L = length of pore

$M = (k/\mathcal{D})^{-2}$

k = first order rate constant (volume/time)

$\mathcal{D}$ = diffusivity

The dimensionless quantity ML is called the Thiele modulus.

Comparing the rates, in this region, of a bed of catalyst particles of size R_1 (radius) to another of size R_2 will yield:

$$\frac{-r_{A'1}}{-r_{A'2}} = \frac{ML_2}{ML_1} = \frac{R_2}{R_1}$$

Therefore the reaction rate varies inversely with the particle size. Comparing the rates in the region where pore resistance is negligible (ϵ=1) would yield:

$$\frac{-r_A'_1}{-r_A'_2} = \frac{\epsilon_1}{\epsilon_2} = 1$$

It can be shown that, in the region of strong pore resistance, an n-th order reaction behaves like a reaction of order (n+1)/2.

Temperature dependency of reactions is also affected by strong pore resistance. The observed activation energy for reactions influenced by strong pore resistance is approximately one half the true activation energy (Levenspiel, 1972; Hougen, 1961).

The effectiveness factor, as a function of ML under isothermal conditions, is shown in Figure 3.2 for various catalyst shapes and for volume change during reaction.

Prater (1958) has shown that, for particles with temperature gradients inside the pore, the change in temperature across the pellet as a whole is given by:

$$\Delta T_{particle} = (T_{centre} - T_s) = \frac{D_e(C_{AS} - C_{A\ centre})\ (-\Delta H_r)}{k_{eff}}$$

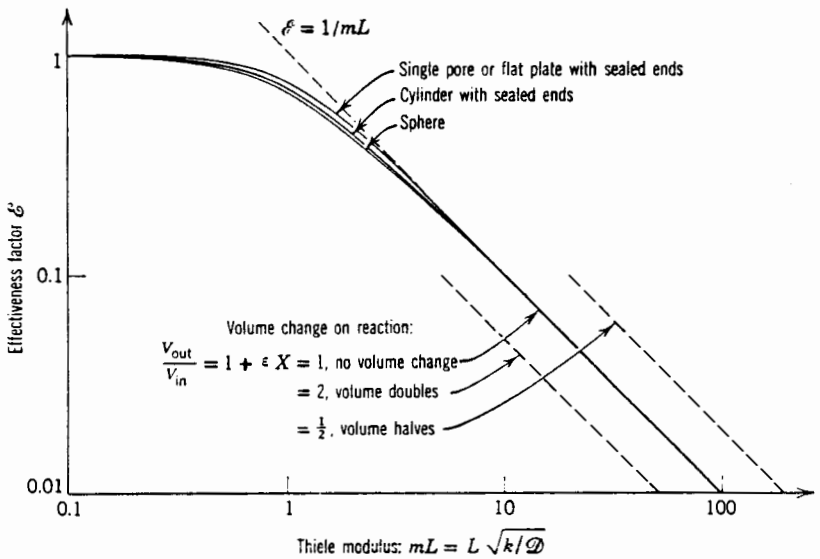

Figure 3.2 The effectiveness factor as a function of the parameter ML for various catalyst shapes and for volume change during reaction (Aris, 1957; Thiele, 1939).

where k_{eff} = the effective thermal conductivity within the particle

D_e = the effective diffusivity.

For temperature gradients within particles alone, the corresponding non-isothermal effectiveness factor curves have been calculated by Carberry (1961), Weisz and Hicks (1962) and others. Figures 3.3 and 3.4 illustrate the sequence of events which occur with exothermic reactions as heat effects become progressively more severe. This sequence can result from raising the reaction rate or raising the temperature of the ambient fluid, Tg. The effectiveness factor refers to the rate for a particle bathed uniformly in reactant fluid at temperature Tg. Thus the effectiveness factor accounts for both reactant depletion within the particle and non-isothermal effects (Levenspiel, 1972) as follows:

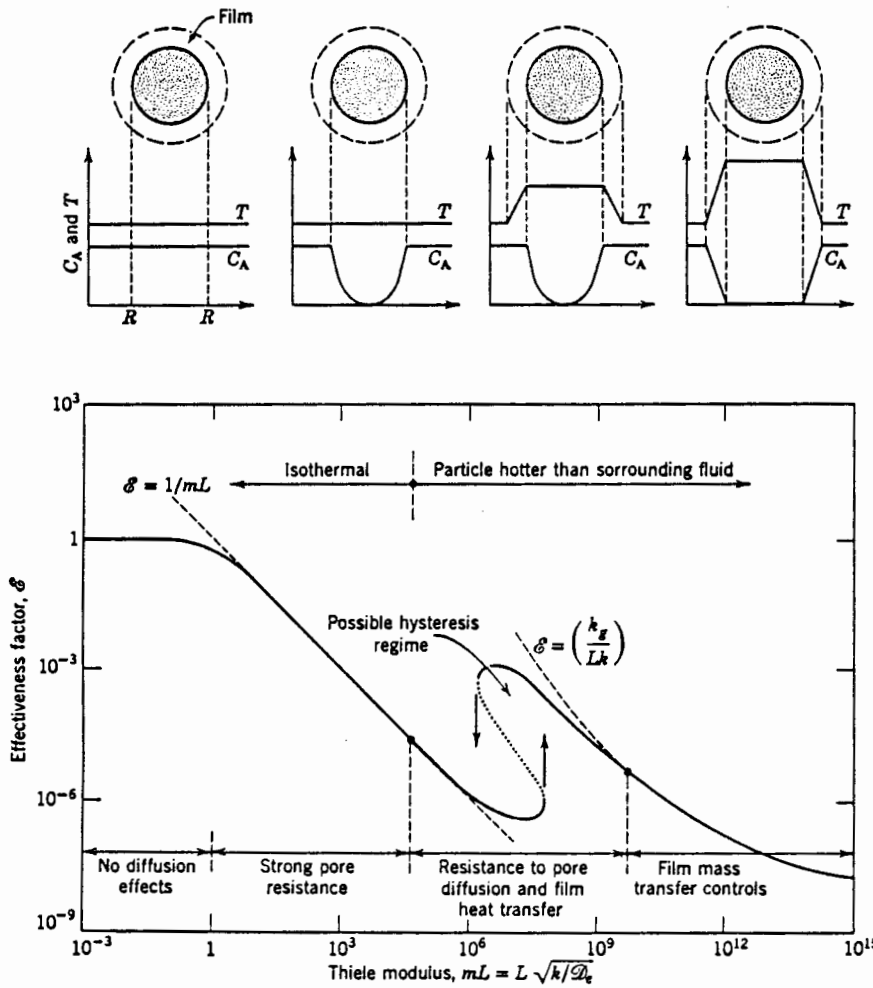

Figures 3.3 and 3.4. Different rate controlling regimes for strongly exothermic reactions in porous catalysts (McGreavy & Cresswell, 1969b).

1. For slow reaction rates relative to intraparticular diffusion the concentration of reactants and products is uniform throughout the

pellet and the heat generated is removed rapidly enough to keep the pellet at the temperature of the gas.

2. For an increased reaction rate, pore resistance becomes the first non-uniformity to intrude. The temperature is almost uniform and hence the use of the isothermal effectiveness factor.

3. For even higher reaction rates, the particle, still uniform in temperature, becomes progressively hotter than the surrounding gas. Pore diffusion effects become more pronounced and most of the reaction occurs in a thin shell close to the catalyst surface. Here the heat generation rate may well outstrip the heat removal rate, yielding autothermal behaviour with an accompanying temperature jump and hysteresis effect.

4. For extremely high rates the particle is hot enough so that all reactants are consumed as they reach its exterior surface. In this region the supply of reactants becomes the slow step and mass transfer through the gas film will control the rate of reaction.

Haynes (1983) has noted that for a batch of catalyst of mixed particle sizes the use of a mean particle size is strictly valid only in the asymptotic limit of strong intraparticular diffusion resistance (or in the case where ϵ is unity, in all particles). Outside this region, calculations that are based on a mean particle size are only approximate.

3.1.1.4 Superficial gas velocities and the recycle ratio

The assumption of a perfectly mixed CSTR is valid only for recycle ratios, R, greater than 20 (Berty, 1974) to 25 (Li et al., 1980; Carberry, 1964). The determination of recycle ratio, R, is therefore very useful in determining the degree of mixing. The minimum R for perfect mixing is not a constant and varies with feed rate (Ke-Chang & Nobile, 1986).

The superficial gas velocity through the bed can be calculated directly from the recycle ratio, R, for a given set of operating conditions. The superficial velocity is not only useful in comparing different internal recycle reactors, but also in comparing the performance of these reactors to industrial reactors. The superficial gas velocity can be calculated theoretically (based on the maximum theoretical head generated by the blower) from various pressure drop equations (depending

on whether the flow is laminar or turbulent), e.g., Blake-Kozeny (Hougen, 1961), Ergun (Leva, 1959) and Leva (Leva, 1959). Superficial velocities can also be estimated from measured mass transfer coefficients using the correlations of Hougen (1961) and Dwivedi & Upadhay (1977). Comparisons between the theoretical and calculated values can give an indication of internal blower efficiency.

The flowrate through the catalyst bed can be calculated by means of devices designed by Berty (1974) or Ke-Chang & Nobile (1986). The flow device, for measuring pressure drop versus flowrate, of Ke-Chang & Nobile, is shown in Figure 3.5.

A catalyst charge with a given particle size to be calibrated can be placed in the device and the relationship between pressure drop, Δp, (measured by an inclined tube differential manometer) and flowrate, G, (measured by flowmeter) determined. The charge can then be moved into

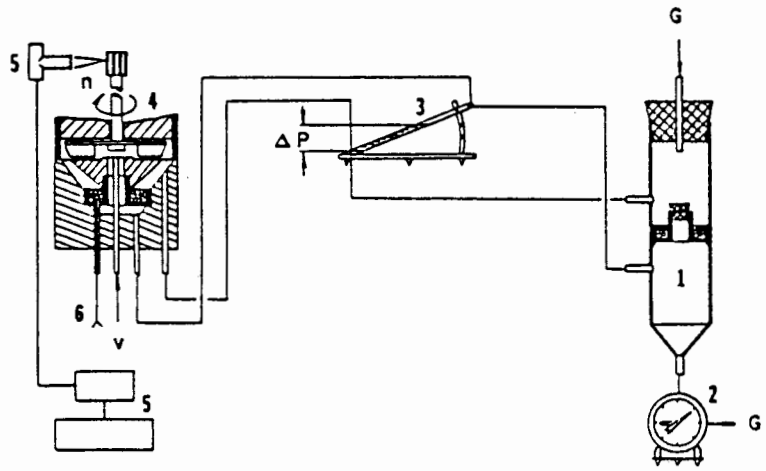

Figure 3.5 Flow device for measuring pressure drop versus flowrate through the bed in an internal recycle reactor (Ke-Chang & Nobile, 1986).

the reactor. Pressure drop across the catalyst bed can then be measured (using pressure taps on either side of the catalyst bed) vs impeller speed. Thus by establishing the relationship between pressure drop and impeller speed, the relationship between flows through the bed and impeller is established. Under a fixed set of conditions, therefore, the recycle ratio can be determined.

Once the above characterization procedures have been completed and the operating region, where both intrinsic kinetics and good CSTR performance can be found, has been determined, the gradientless reactor can be used to obtain (intrinsic) kinetic data.

In the desired operating region (isothermal conditions with uniform concentrations, minimal transport resistances and good CSTR performance) the determination of reaction rates is simple. As already mentioned (Mahoney et al., 1978), the reaction rate can now be calculated, for each steady state experiment (at known reactor concentrations), from the ordinary difference equation:

$$\frac{W}{F} = \frac{X_o - X_i}{r_p}$$

3.1.2 The Modelling of Kinetic Data Obtained from Gradientless Reactors

3.1.2.1 Background to kinetic models

The ultimate goal of kinetics is to develop a fundamental rate equation that fits the observed kinetic data and is consistent with observations of the reaction mechanism (Anderson, 1968). However, the attainment of more limited objectives is valuable in understanding and using the catalytic process.

For any reacting system an entire spectrum of models is possible, each of which fits certain overlapping ranges of the experimental variables. This spectrum includes the purely empirical models, models accurately describing every detail of the reaction mechanism and many models between these extremes (Kittrell, 1970).

The following points should be kept in mind when building and testing kinetic models:

1. The effects of chemical and physical processes should be separated.
2. The results from numerical curve fitting should be examined critically to ensure that an inconsequential correlation has not been obtained.
3. Certain partial pressure terms, especially those of small magnitude compared with experimental uncertainties, may be eliminated from an equation in systematic fashion to determine the simplest equation capable of reproducing the data with moderate accuracy.
4. Does the reaction approach equilibrium?
5. Generally, kinetic data at different operating pressures are very useful in determining the form of reasonable kinetic equations.

6. It would be most useful to put the models through a tough test by examining their extrapolating abilities for variations in conversion, temperature, pressure, concentrations of reactants, etc.
7. The mechanism and rate controlling step may change in the various parts of the operating region.
8. Many authors find that the use of nonlinear regression techniques to solve complex equation sets is rather unreliable and can give spurious results.
9. In internal recycle reactors one can get falsification of kinetic data in operating regions where, at a given recycle ratio, the conversions are high.

There are two major aspects to modelling (Kittrell, 1970):

a) Developing the functional form of the rate equation (models).
b) Solving and testing the models.

3.1.2.2 Building Kinetic Models

When a heterogeneous catalytic reaction occurs, several physical and chemical processes must take place in proper sequence. Hougen & Watson (1947), and others, have broken down the steps that occur on a molecular scale in the following manner:

1. Mass transfer of reactants from the main body of the fluid to the gross exterior surface of the catalyst particle.
2. Molecular diffusion and/or Knudsen flow of reactants from the exterior surface of the catalyst particle into the interior pore structure.
3. Chemisorption of at least one of the reactants on the catalyst surface.
4. Reaction on the surface (This may involve several steps).
5. Desorption of (chemically) adsorbed species from the surface of the catalyst.
6. Transfer of products from the interior catalyst pores to the gross external surface of the catalyst by ordinary molecular diffusion and/or Knudsen diffusion.
7. Mass transfer of products from the exterior surface of the particle into the bulk of the fluid.

There are many common model types, the most common being power function models, for example Hougen-Watson and Langmuir-Hinshelwood. The model

must not be too simple or too complex (Kittrell, 1970). It must include as much theory as possible and confirm any substantial extrapolation by experiments. More than one set of models is quite possible.

The error in the data is generally not the limiting factor in interpretation (Kittrell, 1970). Rather, the locations at which the data are taken most severely hinder progress towards a mechanistic model. Some of the more standard model types are listed below:

1. Purely empirical models.
2. Power laws.
3. Langmuir-Hinshelwood type models.

   Langmuir models:

   a) Single species adsorbing
   b) Two or more species adsorbing
   c) Dissociation of A as it adsorbs

   The Langmuir isotherm ignores the following:

   a) Surface non-uniformity
   b) Interaction between neighbours
   c) Multilayer adsorption

4. The BET approach - takes multilayer adsorption into account.
5. The heuristic approach.
5. Hougen-Watson type models- Chemical reaction controlling. In addition to the assumption implicit in the use of the Langmuir isotherm, the following assumption is applicable to all Hougen-Watson models: The reaction involves at least one species chemisorbed on the catalyst surface. If reaction takes place between two adsorbed species, they must be adsorbed on neighbouring sites in order for reaction to occur. The probability of reaction between adsorbed A and adsorbed B is assumed to be proportional to the product of the fractions of the sites occupied by each species.

   One of two mutually incompatible assumptions is usually chosen as a basis for the analysis. The two limiting cases are as follows:

   1. Those in which adsorption equilibrium is maintained.
   2. Those in which it is not.

   Category 1: Adsorption equilibrium is maintained. Examples are:

   (i) $A \longrightarrow R$ (irreversible)

   (ii) $A + B \longrightarrow R + S$ (A and B on the same type site)

   (iii) $A + B \longrightarrow R + S$ (different site types)

   (iv) $A + B \longrightarrow R + S$ (A adsorbed, B in fluid)

   (v) $A \rightleftharpoons R + S$ (all adsorbed)

   There are many more examples.

Category 2: No adsorption equilibrium (adsorption and desorption are rate controlling).

Example:

1. $A + B \rightleftharpoons R + S$

(A has not reached its adsorption equilibrium. Note, however, that it is very different for the case where desorption of a product is rate controlling.)

6. Yang and Hougen (1950) have presented a classification of a multitude of possible models.

To choose a model using adsorption isotherms the following procedure should be used (Heller, 1975):

1. Choose a particular surface reaction as rate limiting.
2. Assume that a conventional mass action law applies to such surface reactions.
3. Assume that some isotherm equation relates the surface concentration of any species to the observable partial pressures of all species in the bulk phase.
4. Deduce the corresponding rate equation relating the global kinetics to the observable partial pressures.

With respect to the above procedures and assumptions, the following should be noted:

(i) The assumptions used are severe.

(ii) There are many different rate equations that can be used with the above (Hougen & Watson, 1947; Yang & Hougen, 1950).

3.1.2.3 Solving and analysing kinetic models

In general, parameter estimation techniques can be divided into three categories (Watanabe & Himmelblau, 1983):

1. The extended Katman filter
2. Iterative methods in which iterative numerical integration of a set of ordinary differential equations is followed by an iterative optimization algorithm (Himmelblau et al., 1967; Froment, 1975; Seinfeld, 1970; and
3. Non-iterative procedures in which a process model is discretized by a proper integration formula and then the set of resulting algebraic equations is solved simultaneously (Glowinski & Stochi, 1981).

In the analysis of kinetic models, problems can be encountered when one relies too heavily on linear or non-linear methods. There are several methods available with which kinetic models can be solved. A summary of some of the more common methods is given by Himmelblau et al. (1967). These methods will be briefly mentioned.

Taking a proposed kinetic model and some sets of ordinary non-linear differential equations in time, which are linear in the coefficients to be estimated, there are six methods that can be used to estimate the coefficients:

1. Analytical integration (exact or approximate) of the set of differential equations and subsequent application of iterative, non-linear least-squares regression techniques.
2a. Linear regression for fitting the empirical data, differentiation of the empirical regression equation, followed by linear regression to estimate the coefficients.
2b. Differentiation of the empirical data directly and subsequent application of linear least-squares regression techniques.
3a. Numerical integration of the sets of differential equations using empirical data directly, followed by iterative non-linear least squares.
3b. Linear regression to fit the empirical data, followed by numerical integration of the set of differential equations.
4. Trial and error search using analog computers to match the empirical data.
5. Method of differential correctness.
6. Quasi-linearization.

With respect to the above procedures method (1) can handle only small and simple sets of data. Method (2) generally results in too much error. Method (3) is too time consuming and does not lead to clear cut measures of best fit. Method (4) is good and widely used. The best example is that of Wei and Prater (1962) for first order reactions. They showed how the set of linear differential equations can be reduced by matrix transformations to an alternate set, each of which contains only one dependent variable. These can then be integrated to give, one by one, the usual exponential type of solution. To carry out the calculation the rate coefficients must be used and so an iterative calculation is required. Method (4) extends beyond the first order. It is limited to some extent by the number of coefficients it can handle.

3.1.2.4 Tests for model accuracy

The estimated parameters in the model must be reasonable, e.g.:

a) Adsorption and rate constants must be consistent.
b) Log k vs 1/T must be linear with negative slope.
c) The log of the adsorption constant vs 1/T (abs) should be linear with positive slope.
d) The model should adequately fit the data.

The conventional methods of testing the ability of a model to fit a particular set of data are the analysis of variance and the test of residuals (Kittrell, 1970).

Analysis of variance

The analysis is used to compare the amount of variability of the data itself. By such a comparison it can be determined whether:
a) The overall model is adequate
b) Each portion of the model under scrutiny is necessary.

Residual analysis

More subtle model inadequacies can exist, even though the overall goodness of fit is quite acceptable. These inadequacies can often be detected through an analysis of the residuals of the model. A residual is defined as the difference between the observed and predicted values of some response of interest.

3.1.2.5 Use of diagnostic parameters

Diagnostic parameters allow a discrimination among several rival models. These parameters can be grouped into two broad classes - those that are inherently present in the model and those that are introduced solely for the purpose of model discrimination (Kittrell).

There are two primary advantages to the use of diagnostic parameters in reaction rate modelling. First the use of these parameters allows an easy analysis of the adequacy of the model. Second, in some cases, the diagnostic analysis will not only indicate a model's inadequacies but also can suggest the precise nature of the inadequacy.

3.1.2.6 Empirical modelling techniques

Empirical analysis of the data can be very useful (Anderson, 1968) with regard to the following:

1) To delineate the general character of the kinetics.
2) To provide guidelines for choosing fundamental rate equations.
3) To test data consistency.

There are methods to obtain quantitative mathematical representations of the entire reaction rate at the surface. These models can be entirely empirical, bearing no direct relationship to the underlying physical phenomena generating the data. In certain cases empirical models can describe the characteristic shape of the kinetic surface and thus provide information regarding the reaction mechanism. The empirical model may, for example, require a given reaction order or a maximum in the rate surface, each of which can eliminate broad classes of mechanisms (Kittrell).

3.1.2.7 Examples of kinetic studies and modelling

Many kinetic studies have been carried out on heterogeneously catalyzed reactions (Himmelblau et al., 1967; Domnesteanu, 1982; Ramage et al., 1980; Orr et al., 1983; Raghavan & Doraiswamy, 1977; Young & Greene, 1977; Petrus et al., 1984; Skrzypek et al., 1985; Meier & Gut, 1978; Sundaram & Froment, 1977; Outi et al., 1981; Groeneveld et al., 1983; Martin & Hill, 1976; Li, 1985; Maatman, 1976; Temkin, 1979; Froment, 1986).

Box & Hill (1967) developed a sequential procedure in which calculations made after each experiment determined the most discriminatory process conditions for use in the next experiment. The method is used to discriminate amongst a number of possible mathematical models. Glowinski & Stochi (1981) have described a calculation technique for estimating initial parameters for a set of non-linear first order differential equations. The method consists of the minimization of a suitable criterion function. Watanabe & Himmelblau (1983) have described a quick estimation technique for parameters in kinetic models by means of process discretization and evaluating errors engendered by the technique. Froment (1986) has recommended that the Hougen-Watson approach be used for expressing rates of catalytic reactions, since power law equations insufficiently account for the interaction of the reacting species with the catalyst. The application of this approach is

shown by examples drawn from hydrodesulphurization, butene dehydrogenation and methanol synthesis. Ratkowsky (1985) has shown that there is a general form of parameterization for the Hougen-Watson approach that corresponds to a "close to linear" model, i.e., one whose statistical properties approach that of a linear model even for small samples. Spencer (1981) has noted that the kinetics observed in systems far from equilibrium can be very different from equilibrium kinetics. He derived exact constants for first order kinetics and found limits to individual rate constants in two component systems only.

A very good case study comparison using non-linear parameter estimation is given by Biegler et al. (1986). Five models are compared in a parameter estimation problem formulated by the Dow Chemical Company.

Choudhary and Doraiswamy (1975) used a gradientless reactor (Carberry type) to study the isomerization of n-butene to iso-butene over florinated δ-alumina. Two kinetic models were discussed. The modelling of kinetic data obtained from internal recycle reactors has received significant attention (Santacesaria et al., 1981; Gut & Jaeger, 1982; Santacesaria & Carra., 1983).

Paynter & Schutte (1971) examined the kinetics of the polymerization of mixed alkenes over solid phosphoric acid in a fixed bed reactor. The experiments were, however, carried out in the presence of mass transfer limitations and the ortho-phosphoric acid concentration was not measured.

3.1.3 Literature Review of Kinetic Studies on the Catalytic Polymerization over Solid Phosphoric Acid

Control variables of importance in olefin polymerization with phosphoric acid catalysts include catalyst acid strength, reaction temperature, pressure, contact time and feedstock composition. These variables control the extent of conversion, the quality and the composition of the polymer. Reliable quantitative data are limited (McMahon et al., 1963); in most published studies the level of some important variable has either been left uncontrolled or has not been reported (McMahon et al., 1963).

Langlois & Walkey (1951) studied the kinetics of the polymerization of propene and mixed n-butenes as catalyzed by phosphoric acid on quartz chips using a pilot plant sized fixed bed reactor (of which the

dimensions were not given). They correlated their data against an empirical rate equation that is approximately first order with respect to monomer:

$$\int \frac{(1+BC)^2\, dC}{(1-C)^2 + 0.3C(1-C)} = \frac{k}{S}$$

where C = fractional conversion of monomer

S = space rate in gas volumes at reaction conditions per volume of catalyst voids per hour, hrs^{-1} (void volume is assumed to be 42% of the bulk volume).

k = specific reaction rate constant, hrs^{-1}

B = fractional increase in the number of moles per unit mass for complete reaction of the monomer, i.e.,

$$B = N_m \times \frac{M_m}{M_p} - 1$$

where N_m = mole fraction of monomer in the feed

M_m = molecular weight of the monomer

M_p = molecular weight of the polymer

Langlois and Walkey (1951) did not tabulate their data so it is impossible to judge the quality of fit of their rate expression.

Bethea and Karchmer (1956) studied the kinetics of propene polymerization with liquid phosphoric acid as catalyst in a pilot plant sized reactor (3.3m long). They correlated their data in terms of a modified first order rate equation:

$$\left[\frac{Ni}{No} + \frac{1}{n}\right] \ln\left[\frac{1}{1-f}\right] + \left[1 - \frac{1}{n}\right] f = \frac{kVrP}{NoZRT}$$

where k = first order rate constant, volume of olefin per volume of reactor per hour.

Ni = gram moles inerts fed per hour.

No = gram moles olefins fed per hour.

n = gram moles olefins required to produce 1 mole of polymer.

f = fraction of olefins converted.

Vr = reactor volume, litres.

P = absolute reactor pressure, atmospheres.

Z = average compressibility factor of hydrocarbons in reactor.

R = gas constant, $atm \cdot l^{-1} \cdot K^{-1}$.

T = absolute reactor temperature, K.

McMahon et al. (1963) compared graphically, the rate constants of both Langlois & Walkey and Bethea & Karchmer at equivalent acid concentrations (see Figure 3.6). The rate constants of Langlois & Walkey appeared to be about five times greater than those of Bethea & Karchmer.

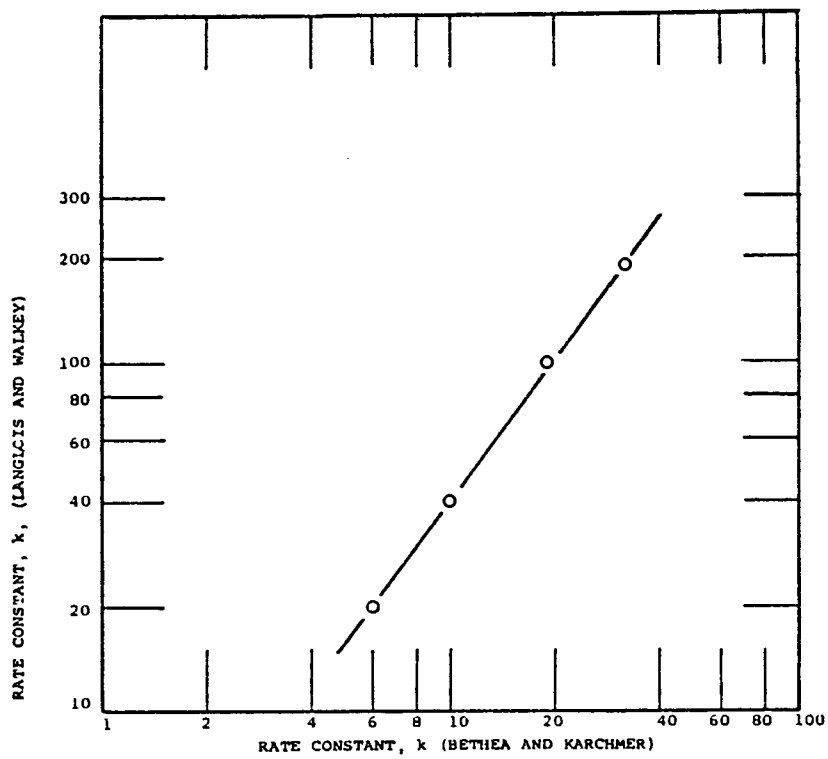

Figure 3.6 Comparison of the rate constants of both Langlois & Walkey and Bethea & Karchmer at equivalent acid concentrations.

Friedman & Pinder (1971) carried out a kinetic study on the polymerization of a mixture of propene and butene isomers to their dimerized products over solid phosphoric acid on kieselguhr. The purpose of their work was to obtain a rate equation which would describe the polymerization of an industrial mixture of olefins on a commercially available solid phosphoric acid catalyst. The mechanism of the reaction was not considered. They found that the following empirical equation gave a reasonably good fit to their data:

$$r = kC_o \frac{(1-x)^2}{(1+x)^2}$$

where r = rate of reaction, mole olefin$\cdot hr^{-1} \cdot cm^3_{cat}$

k = reaction rate constant, cm^3 olefin$\cdot hr^{-1} \cdot cm^3_{cat}$

C_o = initial olefin concentration, moles olefin•cm^3_{feed}

x = fractional conversion of olefins

The phosphoric acid concentration was not controlled.

3.1.3.1 The effect of phosphoric acid concentration

The rate of olefin polymerization is dependent on acid concentration (McMahon et al., 1963). The rate constant of Langlois and Walkey increases by a factor of 4 as the acid concentration ($\%H_3PO_4$) is increased from 100 to 110% where

$$\%H_3PO_4 = \frac{\text{weight of phosphoric acid in sample if all phosphorous was present as } H_3PO_4}{\text{actual weight of sample}} \times 100$$

The rate of olefin polymerization triples, in terms of Bethea & Karchmer's rate constant, as the acid concentration is increased from 100 to 110% (Figure 3.7).

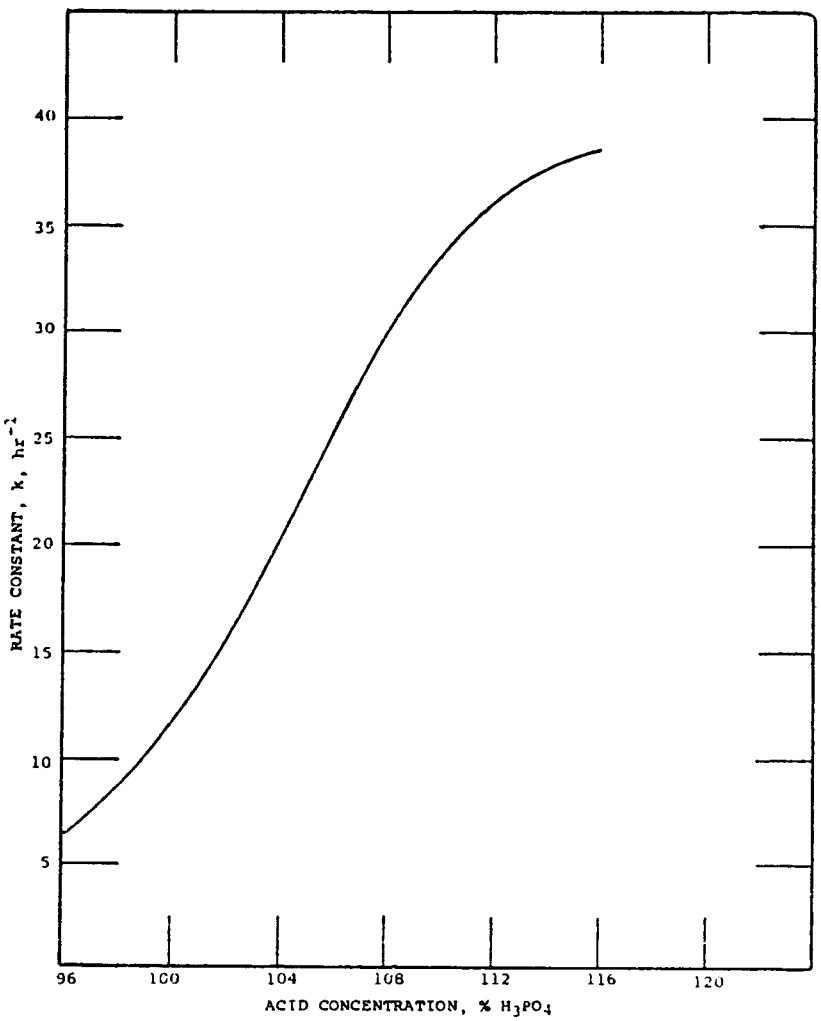

Figure 3.7 Bethea & Karchmers' rate constant as a function of the ortho-phosphoric acid concentration.

3.1.3.2 The effect of space velocity, pressure and olefin concentration.

Both Bethea & Karchmer (1956) and Langlois & Walkey (1951) studied the effect of pressure and space velocity on the rate of polymerization of propene. Both arrived at definitions of specific reaction rate constants that were independent of pressure, residence time and olefin concentration. Their residence times were based on volumes of hydrocarbon in the reactor under reaction conditions. Friedman & Pinder (1971) did not examine the effect of pressure or space velocity.

3.1.3.3 The effect of temperature

In their study of the effect of temperature on the rate of propene polymerization over phosphoric acid on quartz chips, Langlois & Walkey (1951) did not specify the acid concentration employed in their experiments. Bethea & Karchmer (1956) determined the effect of temperature on the rate of propene polymerization at the following liquid phosphoric acid strengths: 98%, 103% and 109% H_3PO_4.

McMahon et al. (1963) adjusted the above sets of data to the same basis and deduced that the data of Langlois & Walkey were obtained at 98% H_3PO_4. The Arrhenius plots are shown in Figure 3.8. The plots indicate an activation energy of about 5000 cal.mole^{-1} (20.93 kJ/mole).

Friedman & Pinder (1971) examined the effect of temperature on the rate of their mixed feed polymerization. Their acid concentration was neither measured nor controlled. From an Arrhenius plot they found an activation energy of about 7500 cal•mole^{-1} (31.4 KJ/mole).

3.1.3.4 The effect of feed composition

The polymerization of ethylene is not only slow but also leads to the formation of conjunct (non-oligomer) polymers (Ipatieff & Pines, 1935). Internationally there is little commercial incentive to polymerize pentenes since they are already valuable for blending into gasoline (McMahon et al., 1963), although there are examples of where this is done, e.g., SASOL.

Of the propene and butene olefins, propene polymerizes the most slowly, n-butenes polymerize at about twice the rate of propene and iso-butene polymerizes very much faster than the n-butenes (McMahon et al, 1963;

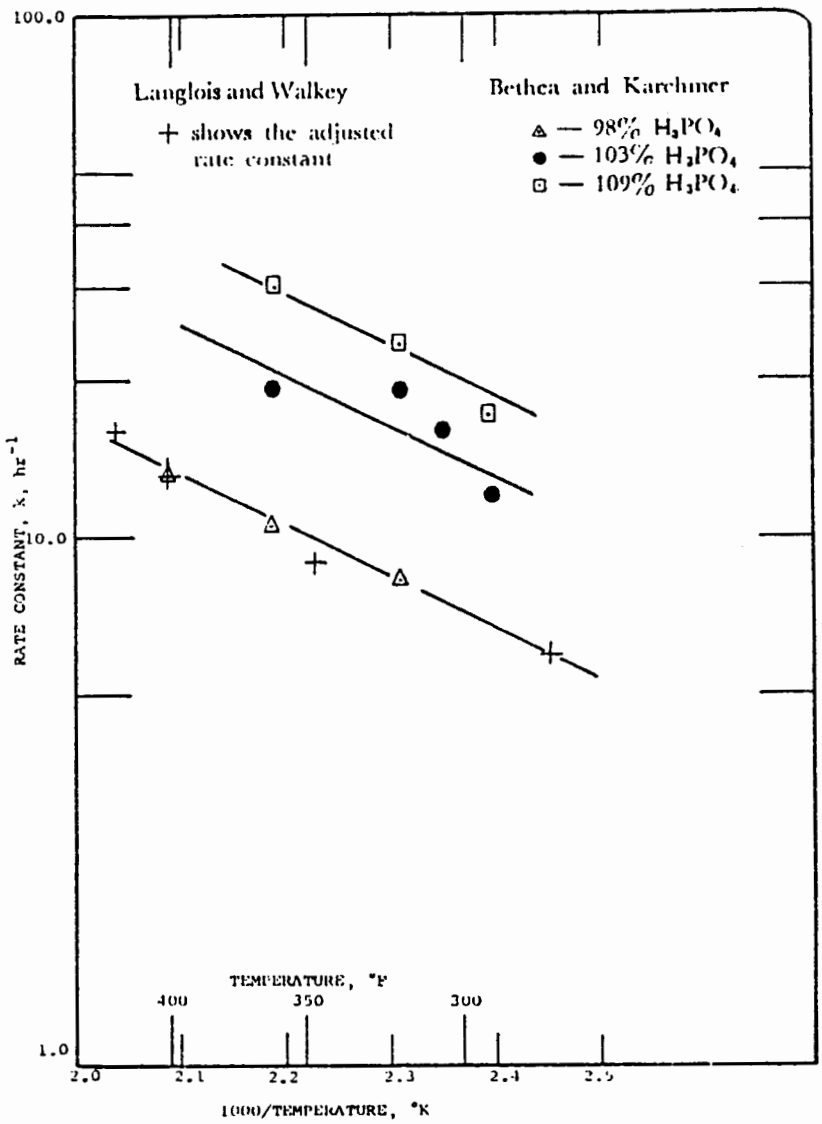

Figure 3.8 Arrhenius plots of both Bethea & Karchmer and Langlois & Walkey.

Langlois & Walkey, 1951). Rates of polymerization for mixed feeds cannot be predicted from the behavior of single components (McMahon et al., 1963). The rate of reaction of mixtures of n-butene and propene is a linear function of the butene content. Langlois & Walkey (1951) found that iso-butene accelerates the rate of the mixed feeds considerably, especially in the low conversion region (conversion levels not given).

Friedman & Pinder found that the order of increasing reactivity was trans-2-butene, cis-2-butene, propene, iso-butene and 1-butene. Their results do not agree with those of previous workers in the field (Ipatieff, 1935; Langlois & Walkey, 1951). Friedman & Pinder suspect that the lack of agreement is possibly due to the isomerization reactions which occur. It appears, however, that these comparisons were

made on the basis of mixed feed experiments. No comparison is valid under these conditions due to the wide difference in concentration between the components. At the very least, an approximate comparison can be made only by comparing each component's activity based on equal feed concentrations. A true comparison, however, can be made only by examining the activity of each component over a wide range of individual concentrations.

McMahon et al. (1963) predicted rate constants for mixed and single component C_3-C_4 feeds, based on the data reported graphically by Langlois & Walkey (1951) for feeds containing propene, n-butenes and iso-butene (Figure 3.9). They obtained a correction factor, F, which is a multiplicative term used to adjust the rate constant k in the Bethea & Karchmer rate expressions for propene; i.e., the rate constant for a mixed feed, according to McMahon et al. is equal to k, read from Figure 3.6, multiplied by F, read from Figure 3.9.

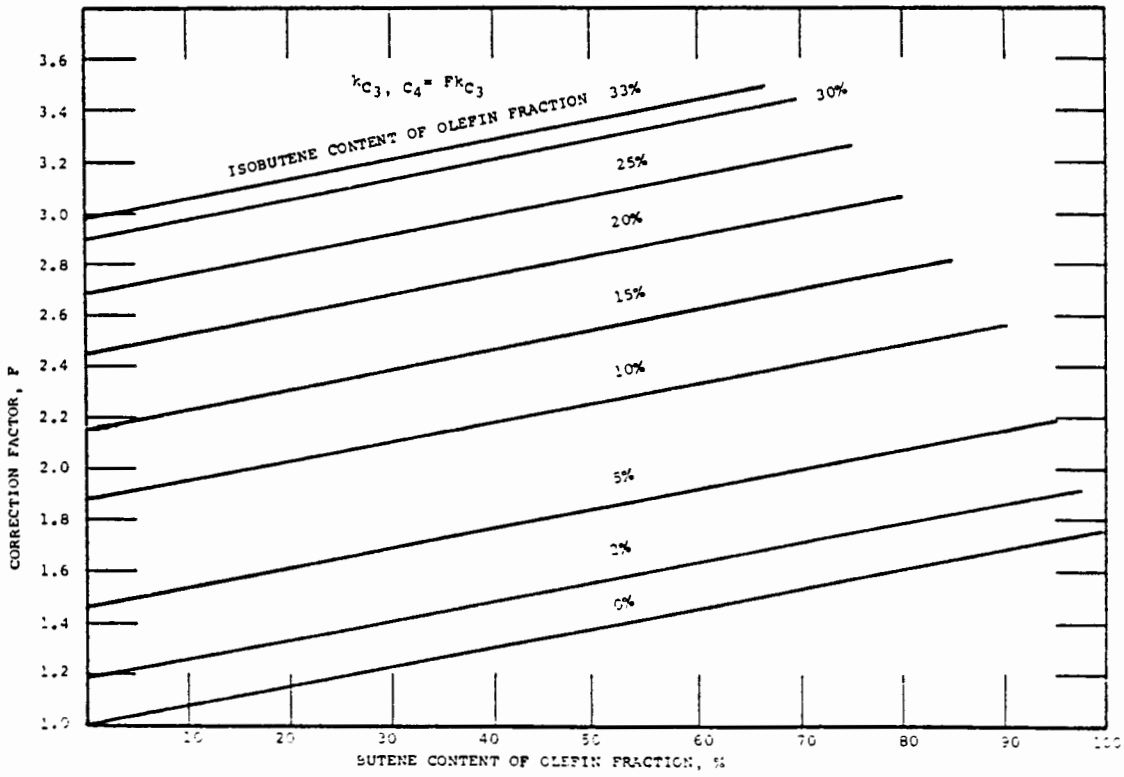

Figure 3.9 Rate constant correction factor of McMahon et al. (1963).

McMahon et al. tested the validity of their calculation method by comparing their rate constants with those for a mixed olefin and also a pure butene polymerization over a copper pyrophosphate catalyst reported by Steffens et al. (1949). Their calculations were made on the basis of a reactor volume equivalent to the total phosphoric acid potentially available in the catalyst.

A comparison of their observed and predicted rate constants is shown in Figure 3.10. The range of uncertainty is indicated. McMahon et al. consider the agreement between the observed and predicted rate constants to be satisfactory due to the uncertainty of the acid strength and also due to the wide range of olefin concentrations, feed compositions and temperatures. The results of Steffens et al. were predicted (copper pyrophosphate catalyst) by combining the propene data of Bethea & Karchmer (liquid phosphoric acid) with the data of Langlois & Walkey (phosphoric acid on quartz). McMahon et al. believe that all phosphoric acid catalysts are essentially the same.

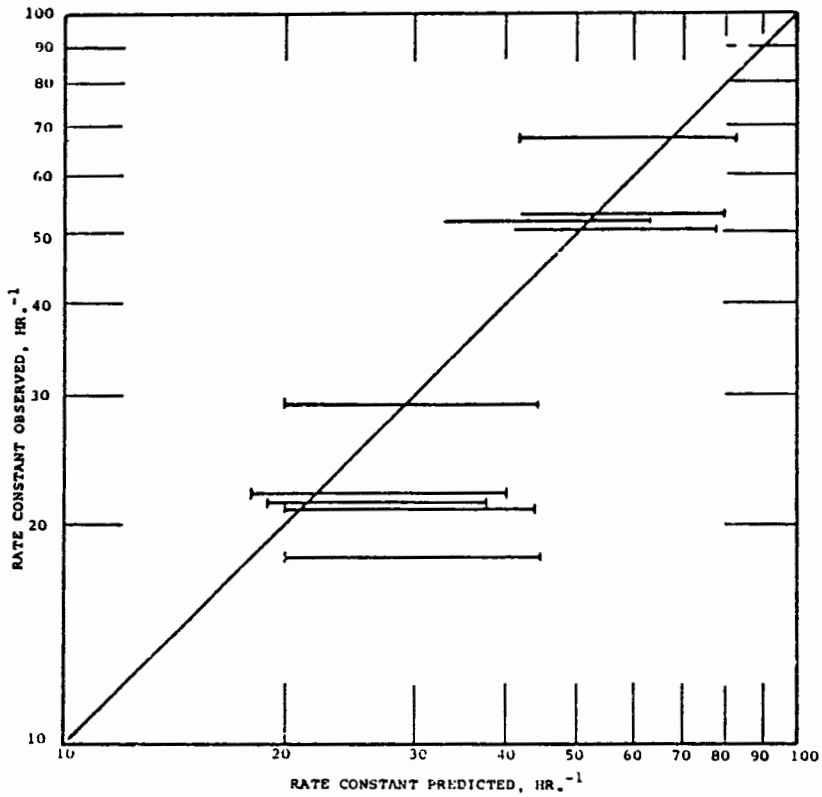

Figure 3.10 A comparison of the observed and predicted rate constants produced by McMahon et al. (1963).

3.1.3.5 The effect of process variables on product yield and quality

There is very little published data on the effect of process variables on product yield and quality and yet it is clear that yield and quality are rather insensitive to operating conditions (McMahon et al., 1963).

Bethea & Karchmer (1956) concluded that the product octane number and gasoline fraction in the total polymer were primarily determined by acid strength - low acid strength being desirable for high octanes. McMahon et al. have pointed out that this conclusion is questionable since in Bethea & karchmer's experiments the extent of conversion also increased

with acid strength. The product quality is certainly dependent on conversion.

Commercially, low temperatures, high pressures and low conversions per pass all favour high yields of gasoline range products and high octane numbers.

3.1.3.6 The effect of transport resistances

Friedman & Pinder (1971) conducted their experiments in a 2" diameter, 12" long fixed bed reactor. By carrying out experiments at different flow rates, but constant V/F (V=volume of catalyst and F=feed flowrate), they found the conversion to be independent of flowrate, indicating that gas film resistance was not important. By performing experiments at different catalyst sizes, they found that pore diffusion was quite appreciable.

Langlois & Walkey (1951) obtained their data from pilot plant experiments using a fixed bed reactor of unspecified dimensions. They did not test for transport resistances.

Bethea & Karchmer (1956) conducted their experiments in a pilot plant sized reactor. The reactor was constructed from an 11 foot length of Hastelloy alloy B pipe. Measurement of transport processes in a liquid phase system (liquid phosphoric acid) is difficult. Bethea & Karchmer noted however that, with a four-fold increase in the acid (H_3PO_4) recirculation rate, the conversion of olefins increased from 87 to 97%. They suggested that it was due to better dispersion of gaseous hydrocarbon in the more viscous catalyst. This is a bulk diffusion transport problem. The conversions were, however, too high to obtain a good indication of the significance of mass transfer, but it was clear that there was some degree of diffusional resistance.

3.2 OBJECTIVES OF THE KINETIC STUDIES

The objectives of the kinetic studies are two-fold.

In the first instance it is of primary interest to obtain intrinsic kinetic data for the oligomerization of propene and butenes over solid phosphoric acid on kieselguhr and from the data to postulate basic

mechanistic pathways. Intrinsic kinetic data, by definition, must be free from mass and heat transport resistances.

Secondly, it is also the objective of this study to model the kinetic data.

The objectives of this study may therefore be listed as follows:

1. To construct a laboratory reactor system that can be used to obtain intrinsic kinetic data for the oligomerization of low chain length olefins.

2. To completely characterize the reactor system and determine an operating region where transport effects are minimal.

3. To obtain intrinsic kinetic data for propene oligomerization at different propene partial pressures, reactor temperatures and H_3PO_4 concentrations.

4. To obtain intrinsic kinetic data for butene oligomerization at different butene partial pressures, reactor temperatures and H_3PO_4 concentrations.

5. To model the kinetic data obtained in respect of (3) and (4) above.

3.3 EXPERIMENTAL APPARATUS AND PROCEDURE

The reactor used for the residence time distribution studies, the mass transfer studies and the kinetic studies was an internal recycle reactor. The reactor was built at the Council for Scientific and Industrial Research, Pretoria, South Africa. The reactor which was designed by Dr. L. Caldwell is a Berty type reactor (internal recycle, fixed catalyst basket). The amendments to the standard Berty type design were made in order to improve the gas side (bulk phase) mass transfer coefficients. The reactor will be discussed in detail in Section 3.3.2.

3.3.1 The Reactor System

3.3.1.1 The reactor system used for the residence time distribution studies

The reactor system used is shown schematically in Figure 3.11, and consists of the reactor and ancillary equipment.

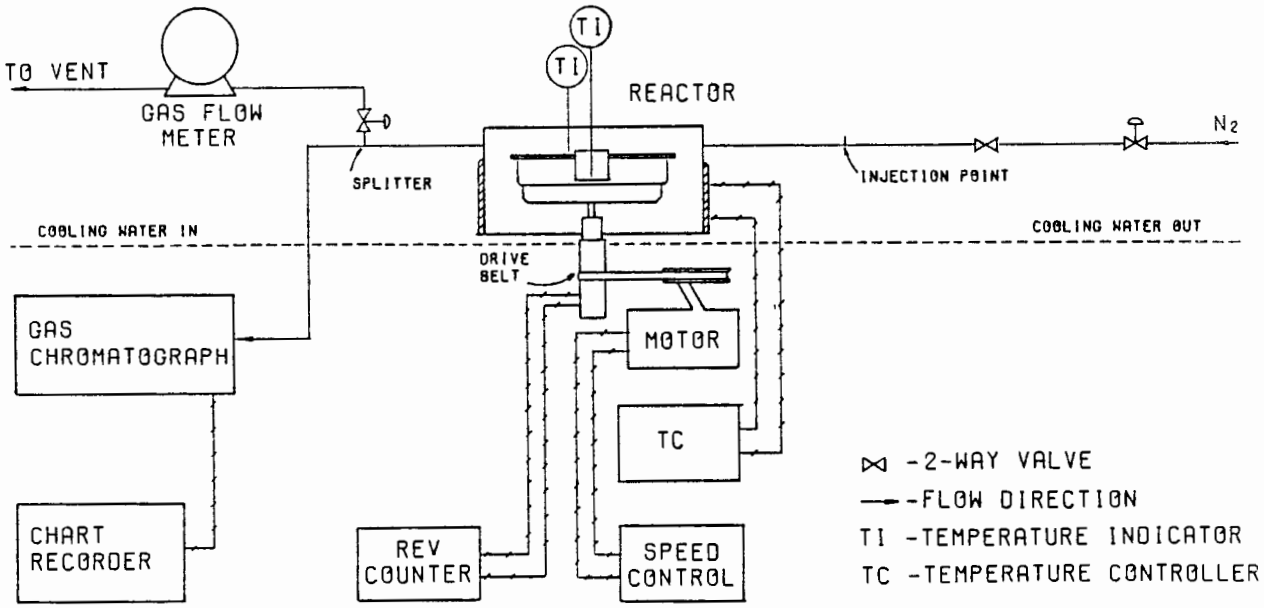

FIGURE 3.11 REACTOR SYSTEM USED FOR RESIDENCE TIME STUDIES

Using classical residence time distribution techniques (Levenspiel, 1972), a pulse of ethylene was introduced by gas syringe into a nitrogen carrier stream immediately upstream of the reactor. The pulse was carried into the reactor, was mixed and left through an 1/8" stainless steel pipe directly to an F.I.D. on a gas chromatograph (VARIAN model 3700). A magnetic drive (A Magnedrive) rotated the internal blower. The F.I.D. analyzed for the mass of ethylene. Mass was found to be proportional to area count within the linear range of the detector. The carrier flowrate was kept constant for each experiment and hence mass was proportional to concentration. A chart recorder (JJ Instruments, CR600) which was attached to the gas chromatograph recorded the decaying concentration-time plot. For experiments with very high flowrates (which would have resulted in the F.I.D. flame being blown out) a flow splitter upstream of the detector controlled the flow to the detector. The splitter flow was controlled by adjusting the size of an orifice in a bleed off line.

3.3.1.2 The reactor system used for the mass transfer studies (no reaction).

The reactor system used for the mass transfer studies, using napthalene sublimation is shown schematically in Figure 3.12.

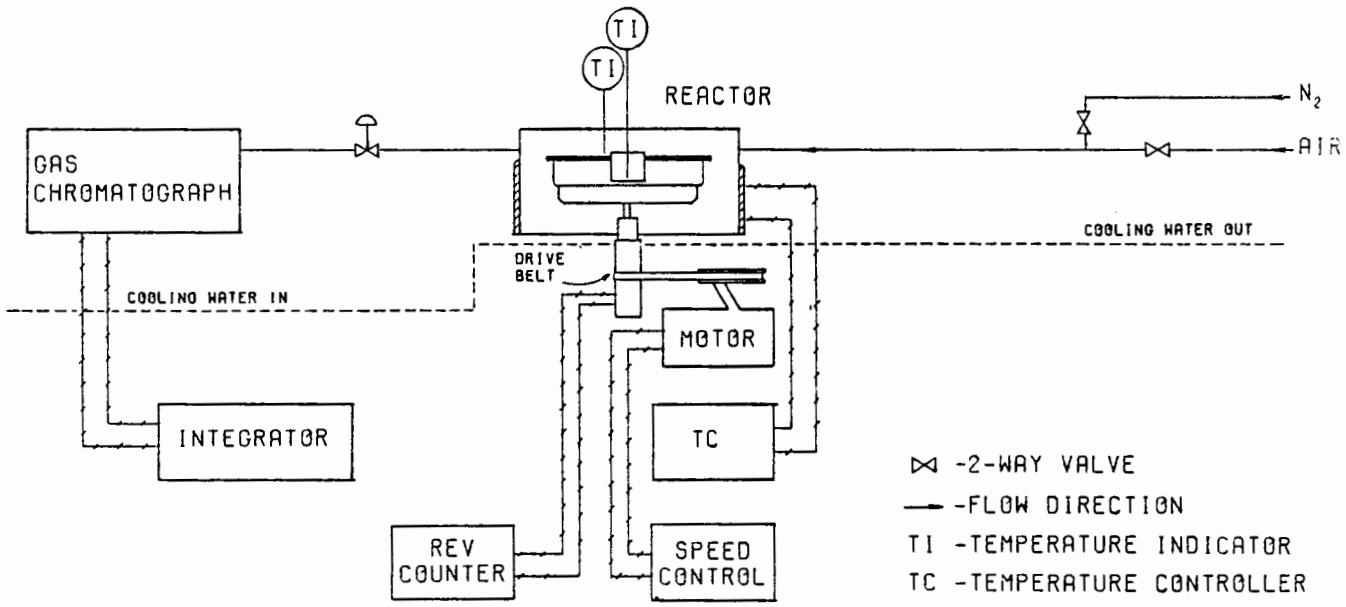

FIGURE 3.12 THE REACTOR SYSTEM USED FOR THE MASS TRANSFER STUDIES

The performance of the reactor in this regard was assessed by measuring mass transfer coefficients (k_c) from the sublimation of napthalene into a stream of flowing air or nitrogen. Under normal operation the nitrogen or air, which was stored in high pressure cylinders, was sent to the reactor in 1/8" stainless steel pipes. The gas entered the reactor, was mixed and left via 1/8" stainless steel tubing. The napthalene was stored in the catalyst basket. The rotational speed of the reactor blower was controlled by an A magnedrive. The system pressure was controlled by regulators on the high pressure cylinders. A metering valve situated immediately after the reactor was used to set the flowrate. The exit gas, after leaving the valve, passed directly to a gas chromatograph (VARIAN model 3700). Samples were captured using a gas sampling valve (similar to the procedure described in Section 2.3.2). Samples were analyzed by F.I.D.. Sample integration was performed on a VARIAN CD101 data system.

3.3.1.3 The reactor system used for the kinetic studies

The reactor system used for the oligomerization experiments is shown schematically in Figure 3.13.

The feed was stored as a liquid under its vapor pressure in an inverted Cadac No.7 domestic gas cylinder (3 kg capacity) which was heated by ISOPAD heating tapes (ITH-33, 115W, 220V) and controlled by a Eurotherm temperature controller (model 101). The output from the controller was passed through a Yokoyama variac (No.3046, 0-250V) which was set at 100V. This restricted the maximum temperature to 328 K and hence prevented overheating of the cylinder.

The vapour pressure of the feed was thus raised by heating and this avoided any cavitation in the pump by maintaining the olefins in the liquid phase. A pressure relief valve was attached to the exit line from the feed cylinder and was set to open at 1.8 MPa. The Cadac cylinder was rated to 3.0 MPa and had been tested to 6.0 MPa. In the unlikely event of temperature runaway and a rise in vapour pressure to 1.8 MPa, the pressure relief valve would have opened and the entire contents of the cylinder would have been vented.

From the cylinder the feed flowed over 3A molecular sieves and a 60 micron filter to a high pressure diaphragm pump (Lewa model FLM-1). An ethylene glycol water solution (at 283 K) was used to chill both the feed prior to reaching the pump as well as the pump head. During normal operation the pump head and the fluid being pumped were maintained at approximately 286 K. The pump raised the system pressure to that set by the back-pressure regulator and controlled the flowrate. From the pump the feed passed to a water bath where the feed was bubbled through a bath of water. The water bath temperature was controlled by a continuous stream of water which was contained in a jacket around the bath. The water stream could either be heated or cooled. The temperature of the water bath controlled the vapour pressure of the water in the bath and hence the water content in the feed. The temperature of the outlet line from the water bath to the reactor was controlled. The line was heated by ISOPAD heating tapes (ITH-150). From the water bath the feed passed via a metering valve to the reactor and on to a dome loaded diaphragm-type back pressure regulator (Grove, Mity Mite model 591 XH), where the system pressure was released to the atmosphere. The exit line from the reactor, up to and including the back pressure regulator, was heated by heating tapes (ISOPAD, ITH-150). The exit line was heated to maintain the reactants and products in the gas phase and the back

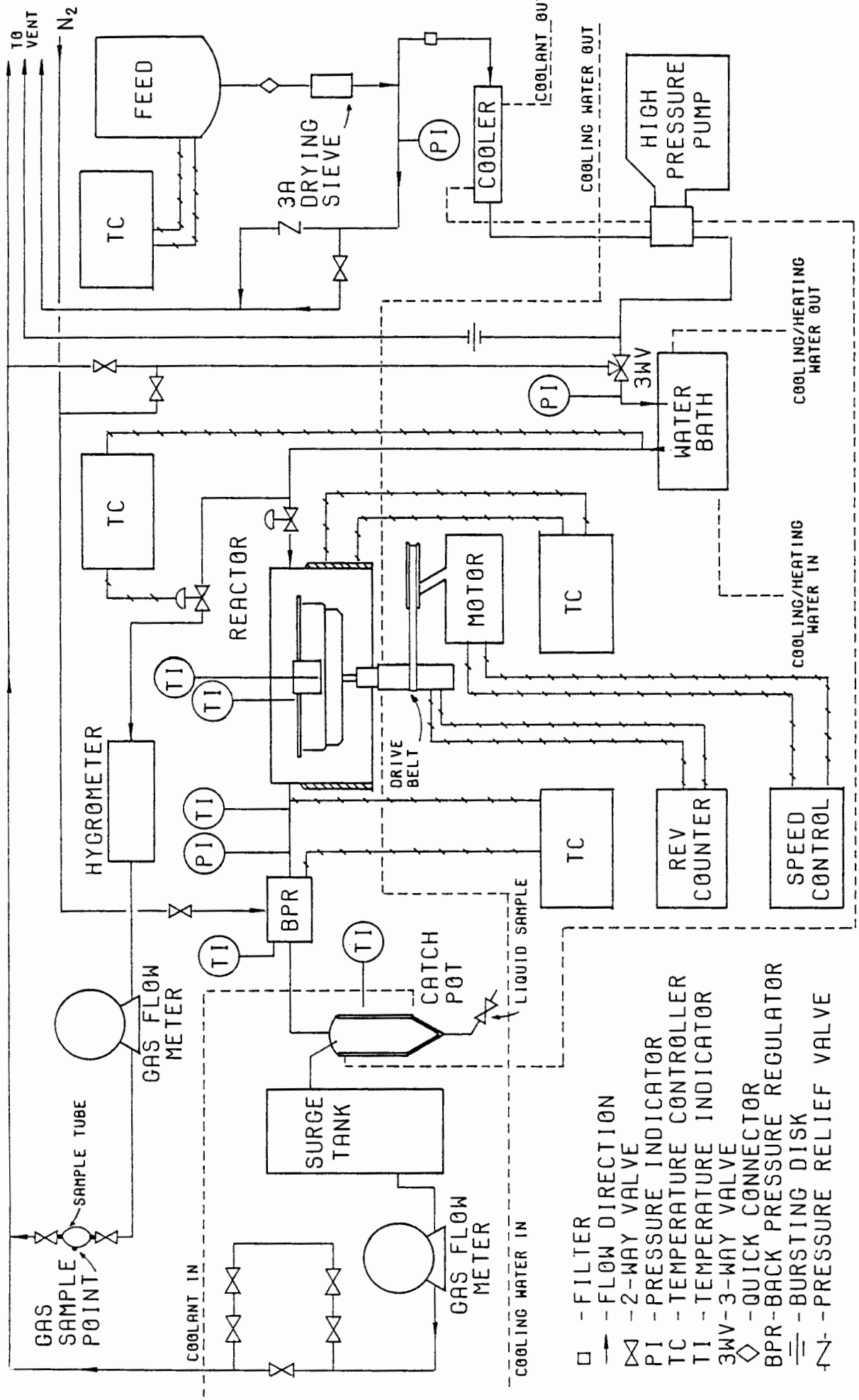

FIG 3.13 SCHEMATIC OF INTERNAL GAS RECIRCULATION REACTOR SYSTEM

pressure regulator was heated to prevent freezing as the pressure was released to the atmosphere (especially at the higher conversions).

The water vapour content of the feed was measured. On the inlet line to the reactor prior to the metering valve a bleed was taken off. The bleed flowrate was controlled by an identical metering valve. Downstream of this valve the pressure was obviously reduced to atmospheric. The stream was passed over an aluminium oxide sensor. The sensor signal was converted to a dew point reading by a Panametrics model 700 hygrometer. The stream then passed through a gas flowmeter, a gas sampling port and was vented. The temperature up to and including the bleed metering valve was controlled at the same temperatures as the feed inlet lines to the reactor by the same set of heating tapes.

A bursting disk on the inlet line, positioned immediately after the pump, was set to burst at 4.0 MPa. The reactor was rated to 5.0 MPa. In the event of 4.0 MPa being reached, the disk would have burst and the entire gaseous contents of the reactor system would have been vented.

The 2-phase reactor effluent was separated in a jacketed catch-pot which was maintained at approximately 283 K by coolant. After separation in the catch-pot, the effluent gas passed through a surge tank to a wet gas flow meter, a gas sampling valve and was finally vented. Liquid product which collected in the catch-pot was drained as desired.

The entire piping system was constructed of 1/8" stainless steel tubing. Temperatures were measured at the back pressure regulator, the catch-pot, the reactor exit line, inside the reactor (2 measurements), the water bath, the inlet line to the reactor, the wet gas flow meters and the feed cylinder. Pressures were measured at the exit of the feed cylinder, the inlet to the reactor, and at the exit from the reactor.

3.3.2 The Reactor

An internal recycle reactor (Berty type) developed by Caldwell (1983a) was used in this study. The reactor blower was driven by a magnedrive (Magnedrive II assembly model 75-2). The reactor and magnedrive are shown in Figures 3.14 and 3.15.

The reactor was a modified version of the standard Berty design. Unlike the Berty design, this reactor had a larger diameter impeller (70mm), longer blade length (12mm) and a close-sided impeller construction (Caldwell, 1983a). The reactor incorporated sixteen blades of length

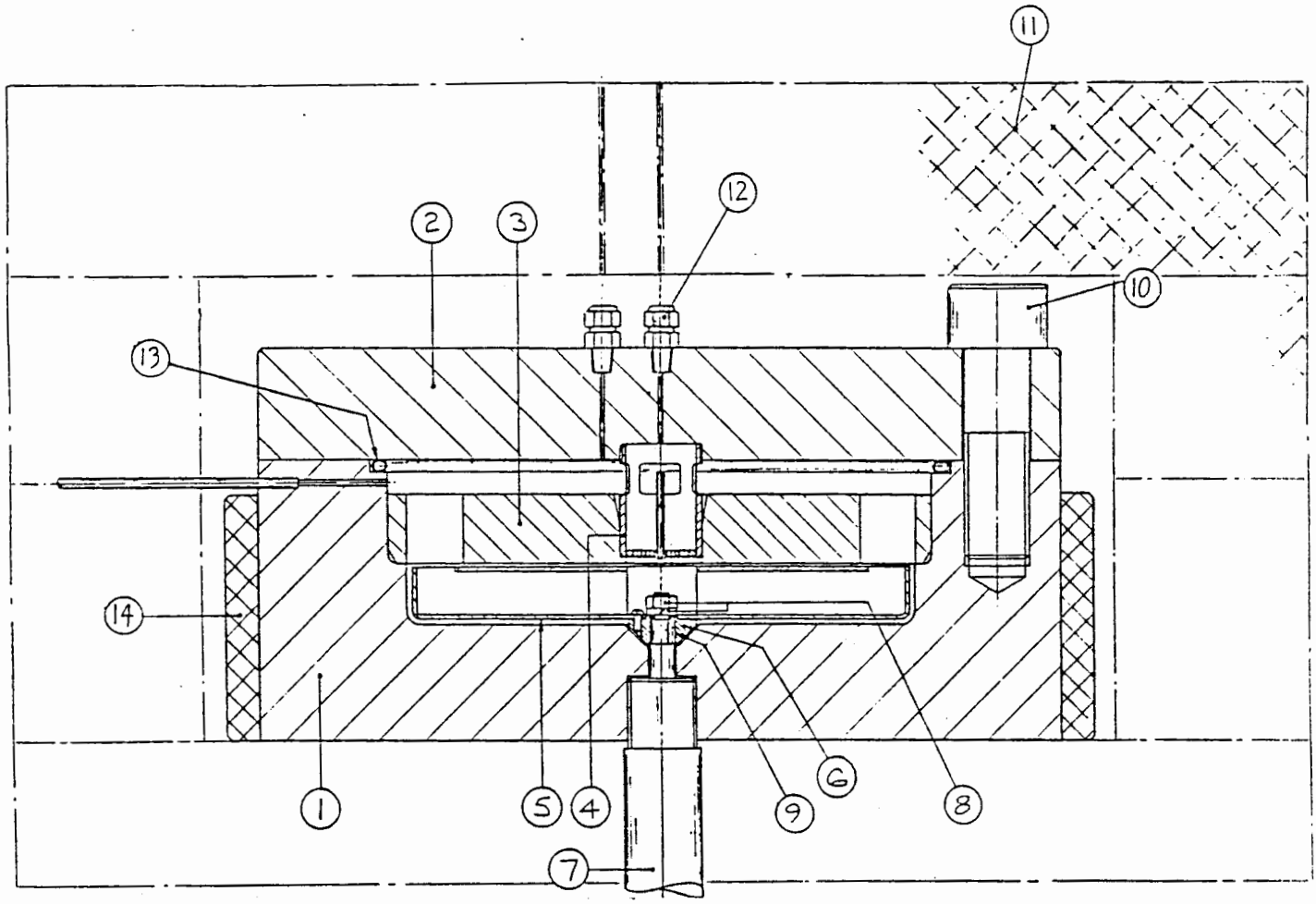

1. REACTOR BODY
2. REACTOR LID
3. BASE PLATE
4. BASKET
5. IMPELLER
6. HUB
7. MAGNEDRIVE
8. NUT
9. KEY
10. CAP SCREW
11. INSULATION
12. 1/16" CONNECTOR
13. HELICOFLEX SEAL
14. CERAMIC BAND HEATER

FIGURE 3.14 THE INTERNAL RECYCLE REACTOR ASSEMBLY

77mm, with the tips of diameter 180mm. The blades were enclosed on both sides and flow was directed upwards at the periphery. The impeller was driven by an A (Autoclave Engineers) magnedrive.

An insert plate was located immediately above the impeller (clearance <1mm). This plate had 12 holes, approximately 26x20 mm, equally spaced around the periphery for the upward flow of gas from the impeller, and a central hole of 30mm diameter in which the catalyst basket sat. The hole

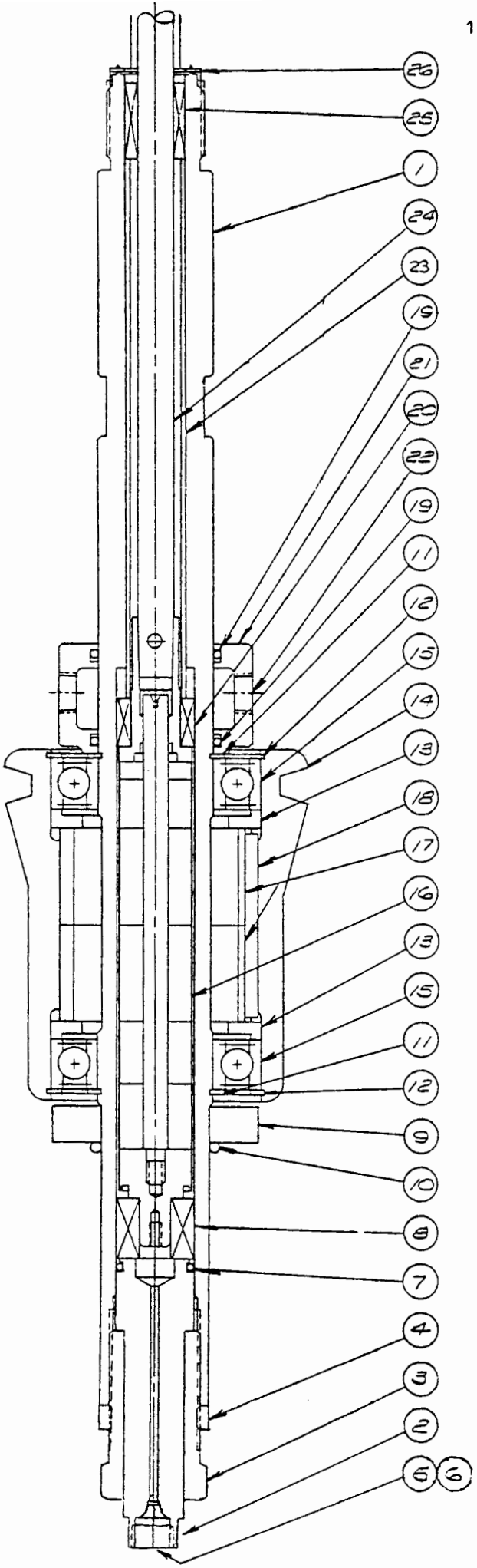

KEY

1. HOUSING
2. COVER
3. GLAND
4. LOCK NUT
5. 1/8" GLAND
6. 1/8" PLUG
7. O-RING
8. BEARING
9. TACHOMETER PICK-UP
10. O-RING
11. RETAINING RING
12. RETAINING RING
13. BEARING SPACER RING
14. HOLDER
15. BALL BEARING
16. ENCAPSULATED MAGNET ASSY
17. STATOR MAGNET
18. KEY - 12"SQ X 1.88"LG
19. O-RINGS
20. BEARING
21. COOLING JACKET
22. QUICK DISCONNECT CPLG
23. SPACER
24. DRIVE SHAFT COMPLETE
25. BEARING
26. GASKET

FIGURE 3.15 DETAILED DIAGRAM OF MAGNEDRIVE ASSEMBLY

was tapered at the top. The catalyst basket had an overall length of 41 mm, an internal diameter of 26 mm and the base was drilled with thirty 3 mm diameter holes. Four ports permitted the entry of gas to the top of the basket. A central tube 3.2 mm o.d. was welded to the base of the basket permitting the passage of a thermocouple to measure exit gas temperature. In assembly the thermocouple was first threaded into this tube, the basket was then screwed into the reactor bed, and finally the basket was located at the insert plate when the reactor lid was bolted down. A second thermocouple port in the reactor lid permitted the measurement of the gas temperature at the inlet to the basket.

The seal between the reactor body and the basket was obtained with a Helicoflex seal, outside diameter 208.8 mm, taurus 5.6 mm and copper lined (double lining) with inconel wire. The vessel was constructed of stainless steel 316 and was rated for 5.0 MPa at 773 K. Gas entered and left by diametrically opposed ports above the insert plate. A three sectioned 4KW ceramic band heater was clamped around the reactor body, and the entire assembly was insulated with 25 mm asbestos plate. A counterweight connected to the lid via pulleys facilitated the lifting of the reactor lid.

The A magnedrive assembly was designed to fulfill additional requirements not obtained in conventional packed drives. Leakage, contamination and packing heat generation problems were eliminated. The high speed rotary agitation was affected by the rotation of external magnets which actuated internal magnets fastened to the shaft. The external drive magnet assembly consisted of an outer aluminium holder containing the stator magnets. This outer holding was placed over a pressure sealed housing containing the encapsulated rotor magnets which were mounted on a center rod. A strong magnetic field made the inner center rod rotate at the same speed as the outer holder. The drive had the following specifications:

maximum allowable working pressure - 6000 psi
maximum RPM - 3000
maximum horsepower capacity - 0.76

It was found that operating the magnedrive above 2000 RPM shortened bearing life considerably which resulted in regular fouling of the impeller on the base plate. The magnedrive was therefore seldom operated at rotational speeds above 2000 RPM. The inner shaft of the drive was lubricated by three carbon graphite bearings which were designed to run dry. Cooling water which flowed through the coolant jacket maintained

the shaft and magnets cool. The seal at the shaft end was provided by a teflon "O" ring.

The controlling thermocouple was placed between the outer reactor body and the ceramic band heater. This was found to be the most reliable position despite the slow heating rates. Oscillation and temperature overshoot were avoided in this way. The temperature was controlled using a Eurotherm temperature programmer-controller system (model 101). The power from the controller was sent to the three sections of the heater. Each section of the heater could be switched on or off at will depending on the heating requirements.

The temperatures in the reactor were measured by both a Digitron digital thermometer, and a Honeywell recorder.

3.3.3 Experimental Procedure and Analysis

3.3.3.1 Residence time distribution studies

Using standard techniques, pulses of ethylene (100 µl at STP) were introduced by syringe into a nitrogen stream entering the reactor. Five sets of tracer experiments were carried out. In each case the pulse size was kept constant. The outlet N_2 and ethylene mixture which was passed directly to the F.I.D. was detected and recorded on the chart recorder (nitrogen is not detected). The following sets of tracer experiments were carried out:

(a) Basket empty
   1. Runs at varying impeller speeds
   2. Runs at different flow rates
   3. Runs at different temperatures

(b) Basket filled with 4 mm spherical glass beads
   1. Runs at different impeller speeds
   2. Runs at different flow rates

Runs at different pressures were not possible due to the use of a hand injected syringe (low pressure) through a rubber septum. Higher pressure injections resulted in the leakages at the septum and poor input pulses.

3.3.3.2 Mass transfer studies

It was concluded by Caldwell (1983) that due to the larger and more effective impeller, performance in this reactor is a considerable

improvement over comparable and commercially available Berty and Carberry type reactors. Due to the controversy surrounding this claim (Caldwell, 1983b; Berty, 1983; Carberry, 1985) and the fact that the reactor used in this study was only the second one produced, it was decided that the results of Caldwell needed to be confirmed. The procedure followed is therefore quite similar to that of Caldwell (1983a) and is described below.

Mass transfer coefficients were determined for the napthalene-hydrogen system. Experiments were carried out for the basket filled with spherical glass beads (diameter, 4 mm) plus two randomly placed napthalene pellets, and also with the empty basket apart from the two pellets. The filled bed depth was 21 mm with a void fraction of 0.41. Only two napthalene pellets were employed per experiment, the external surface area being determined by micrometer measurements. The average loss in surface area per run was 5%. Results obtained for losses above 10% were discarded. The calculation of k_c took into account area changes.

Gas concentrations were measured by F.I.D. The saturation response for napthalene was determined by measurement for each k_c value, instead of being calculated from vapour pressure data. This procedure had the following advantages:

(a) Errors in temperature became relatively unimportant
(b) There was no need for accurate vapour pressure data
(c) Detector calibration was not necessary because the calculation of k_c involved only a ratio of responses.
(d) Problems associated with calibration drift were largely eliminated.

The saturation response was determined by plotting the reciprocal of the response against gas flowrate at constant stirrer speed and taking the intercept value. An example is shown in Figure 3.16. This was performed at the following conditions:

non-diffusing component: hydrogen
RPM: 2400
P_T: 103 kPa
Temp: 294 K
a: 0.861 cm^2

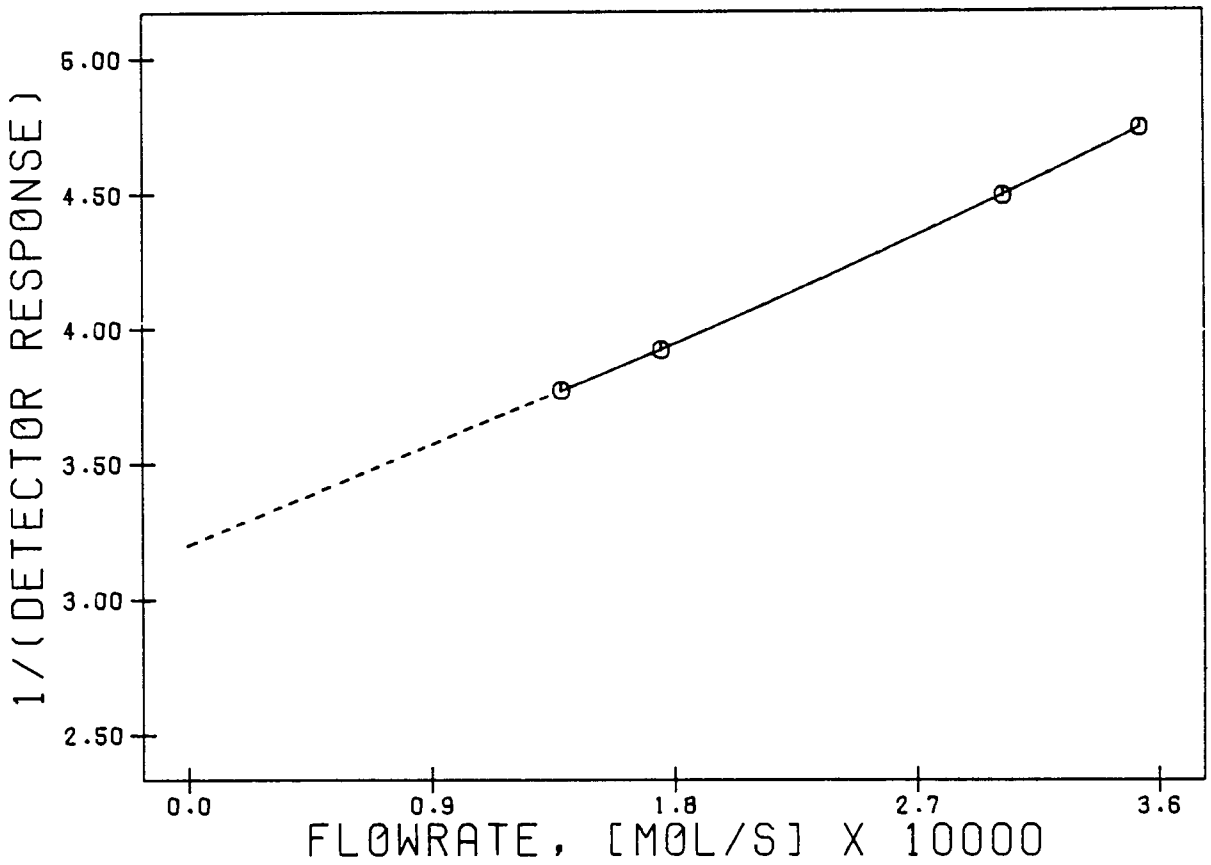

FIG 3.16 CALCULATION OF MASS TRANSFER COEFFICIENTS

from Figure 3.16: response at 3.53×10^{-4} mol•s^{-1} = 0.211

response at zero flow = 0.329

$$Kc = \left[\frac{0.211}{0.329-0.211} \right] \times 3.53 \times 10^{-4} \times \frac{RT}{aP}$$

$$= 17.4 \text{ cm} \cdot \text{s}^{-1}$$

3.3.3.3 Kinetic studies (and mass transfer with reaction)

The general procedure for the oligomerization reactions is presented below. Individual kinetic experiments varied with regard to the moisture content of the feed, feed type, reaction temperature and feed concentration. Reactor characterization experiments varied with respect to the impeller speed, particle size and water content of the feed. The feed flowrate, catalyst mass and reaction pressure were not varied.

Phosphoric acid on a kieselguhr support (solid phosphoric acid) was used for all experiments. The catalyst was supplied as cylindrical pellets ranging from 2 to 12 mm in length and with an approximate diameter of 7

mm. The pellets were crushed and sieved into the appropriate size fractions. For the intra-particular studies various size fractions were used while a size fraction of 0.11 to 0.18 mm was used for the kinetic experiments. Six grams were packed into the catalyst basket for each experiment. The base of the basket was lined with gauze of mesh size 0.11 mm. The bed occupied, on average, a volume of 6.3 cm^3 with a bulk density of 0.95 $g \cdot cm^{-3}$. The reactor was cleaned thoroughly before each run. The magnedrive permitted limited build up of liquid at its base (due to the low temperatures there) and was therefore drained and wiped clean before each run. No water was used in the cleaning process due to the effect that this could have had on the acid strength during operation. Once the catalyst had been loaded into the basket and the basket attached to the reactor lid, the lid was immediately bolted down and sealed. The urgency here was to limit the contact time between the extremely hydrophillic catalyst and the "wet" atmosphere. (Although difficult to quantify, this procedure improved the reproducibility of the experiments.) Following this the reactor was pressurized with high purity nitrogen up to 2.0 MPa and tested for leaks. Once the leak tests were complete the system pressure was dropped to atmospheric. The pressurizing with nitrogen had the added advantage of diluting the air inside the reactor approximately 20 times with dry nitrogen thus reducing the concentration of the water contained in the air.

Each run was started by first heating up the reactor and feed cylinder to the required temperatures. Approximately two hours were required to bring the reactor up to the desired temperature (within 10 K of set point). While the reactor was being heated all coolant flows were switched on. During this period all inlet and outlet lines that required heating were brought up to their required temperatures.

Once the desired reactor temperature had been reached the pressure setting of the back pressure regulator was raised to 1.53 MPa (absolute) and the reactor filled with feed at a controlled rate (by adjustment of the metering valve on the inlet side to the reactor). While filling, the impeller was started and its speed gradually increased up to the desired set point. It was necessary to start the impeller at this point to avoid any temperature runaway in the catalyst bed. Care had to be taken when raising the impeller speed to ensure that no catalyst was blown out of the bed and that no fouling occurred between the impeller and the internals of the reactor. Once the reactor was filled, feed was pumped into the reactor, bringing the reactor up to the set pressure. The bleed line to the hygrometer was then opened and set to approximately 1 $g \cdot hr^{-1}$ after which the pump was set to the desired flowrate. Once the desired

flowrate had been set the water bath temperature was adjusted to the approximate value required. The water bath required approximately fifteen minutes to reach a semi-stable condition at which time the catch-pot was emptied. This time was considered time zero for the reaction. At time zero a gas sample was collected and the feed cylinder was disconnected from the system, weighed and returned. The removal of the cylinder had no noticeable effect on the stability of the system. During the initial few hours the system was fine-tuned to the desired operating conditions. This would sometimes involve small adjustments to the pump flowrate, the bleed flowrate and the water bath setting.

It should be noted that the procedure used here, viz. first heating the reactor up to the desired temperature and only then introducing the feed, was necessary to avoid condensation of the feed which would have occurred were the feed introduced first followed by raising of the pressure and heating of the reactor.

From time zero the following data were recorded at various regular intervals:

1. The gas meter reading and effluent gas temperature.
2. The mass of liquid sample collected.
3. Measurable temperatures, pressures and the dew point of the water in the feed (at atmospheric pressure).
4. Gas chromatographic analysis of gas and liquid samples.

At some point after steady state had been reached the reaction was terminated by isolating the pump from the reactor. The reactor was cooled over approximately 5 hours to below 323 K.

At the chosen end point for each experiment, final samples and readings were taken, all equipment was switched off, except coolant flows, and the feed cylinder was weighed. Once the reactor had cooled to below 323 K the coolant flows were switched off, the system pressure was released and the reactor opened up. All condensables that had accumulated both as a result of condensation during the reaction and the cooling of the reactor after the run had been terminated, were collected. The catalyst was also weighed.

3.3.3.4 Product analyses

The composition of the gaseous and liquid effluents were determined by GC (Gow Mac and Varian 3400 respectively).

The analysis of the effluent gas and feed streams was determined using a 6 mm long SS (stainless steel) column packed with n-octane/poracil C. Details of the method and relative response factors used are given in appendix E. All isomers of the hydrocarbon gases up to and including C_4 were separated and identified. The C_5 fraction was grouped. Identification was achieved using gas standards.

Liquid products were separated on a 2.8 mm long, 6 mm O.D. glass column packed with 3% silicone/OV-101 on Chromosorb W-HP, 100/120 mesh. The products were separated into approximate oligomer fractions. Identification of the chromatographic peaks was achieved by mass spectroscopy. The gas chromatograph detector used was identical to that used in the pulse experiments (section 2.4.1). As a result, all response factors were taken as unity. Dietz (1967) and Froment (1983) have shown that this is reasonable. For similar reasons to those shown in Section 2.3.3.4, peaks were grouped according to chain length. A typical gas chromatograph and mass spectrograph are shown in appendices B and C, respectively.

3.3.3.5 Reaction data workup

Due to the method of feeding and the unavailability of a mass flowmeter the feed flowrate during the oligomerization experiments was estimated by back calculating from the effluent mass flowrate. As will be shown later, mass balances were good (>95%) and hence little error was introduced by using this procedure. In the final analysis of the run data a corrected estimate was used by taking into account condensation inside the reactor and mass loss.

3.4 RESULTS

3.4.1 Reactor Characterization Without Reaction

3.4.1.1 Residence time distribution studies

Three sets of tracer experiments were carried out:

1. Runs with varying impeller speed
2. Runs with varying flowrates
3. Runs with varying temperature

Sets 1. and 2. were carried out under two sets of conditions:

(a) Basket empty

(b) Basket filled with 4 mm spherical glass beads

All runs were carried out at atmospheric pressure.

1. The effect of varying impeller speed

The runs were carried out at the following impeller speeds: 0, 600, 1200, 1800 and 2400 rpm.

The analysis of these curves was made using both standard E curve analysis techniques with the tanks in series one parameter model as well as a five parameter model discussed in Section 3.1.1.1. The results are shown in Tables 3.1, 3.2 and 3.3.

Table 3.1 Equivalent N (number of tanks) for various mixing speeds (one parameter model).

Temperature 290 K	Flowrate 0.97$cm^3 \cdot s^{-1}$
	N (number of tanks in series)
Impeller speed, rpm	Basket full	Basket empty
0	1.3	1.3
600	1.3	1.3
1200	1.2	1.3
1800	1.1	1.0
2400	1.0	1.0

Table 3.2 Five parameter model analysis for varying impeller speeds: basket empty.

Temperature 290 K Flowrate 0.98 $cm^3 \cdot s^{-1}$					
	Mixing rate, rpm				
	0	600	1200	1800	2400
N	1.0	1.0	1.0	1.0	1.0
A	0.00	0.00	0.00	0.00	0.00
B	0.20	0.00	0.00	0.00	0.00
C	0.95	1.00	1.00	1.00	1.00
T	0.00	0.00	0.00	0.00	0.00

where N=number of tanks in the chain
A=the fraction of the feed that bypasses the reactor
B=the fraction that is back-mixed
C=The fraction of the total volume that is the active volume
t=time lag

Table 3.3 Five parameter model analysis for varying impeller speeds: basket full.

Temperature 293 K Flowrate 1.01 $cm^3 \cdot s^{-1}$					
	Mixing rate, rpm				
	0	600	1200	1800	2400
N	1.0	1.0	1.0	1.0	1.0
A	0.06	0.02	0.02	0.00	0.00
B	0.12	0.11	0.10	0.08	0.00
C	0.93	0.95	0.96	0.99	1.00
T	0.00	0.00	0.00	0.00	0.00

The above results were calculated for normalized concentration-time curves where C (normalized concentration) varied between 1 and 0.015, omitting the long tail as recommended by most workers in the field. The value of $\bar{t}$ (mean residence time) calculated from V/v gave:

$$\bar{t} = \frac{1000\ cm^3}{0.98\ cm^3 \cdot s^{-1}}$$

where V = volume of reactor = 1000 cm^3

v = volumetric flowrate of gas through the reactor

The values of $\bar{t}$ calculated from each concentration-time distribution (see Section 3.1.1.1) varied from $\bar{t}$=15.2 mins to $\bar{t}$=17.3 mins. The variation can be the result of several factors such as the long tails, imperfections in the injection technique, or leaks.

The N sets in Table 3.1 indicate that there was little difference between the full and empty basket. It would appear from the values of N that the reactor was becoming well mixed above 1200 rpm and by 1800 rpm could be regarded as being very well mixed.

The results from the five parameter model analysis indicate for an empty basket that the reactor was perfectly mixed above 600 rpm. The one parameter tanks in series model produced an N value of 1.3 at this impeller speed. This model also produced an N value of 1.3 at zero rpm while the five parameter model indicated a significant amount of back-mixing and a small "dead volume" fraction. This tends to indicate that the one parameter model could be insensitive and provide only a rough estimate of the quality of mixing.

For the full basket the five parameter model indicates, similar to the one parameter model, that ideal CSTR conditions were achieved only at about 1800 rpm (under those conditions).

It must be pointed out that in the experiments at the lower impeller speeds (1200 r.p.m. and less) in the full basket experiments, reproducibility of the five parameter model results was not very good. The value of B (backmixing) in particular was rather inconsistent. The results quoted are the arithmetic means of several experiments.

2. The effect of varying flowrates

Runs were carried out at the following flowrates: 6.0, 11.4, 18.0 and 26.7 $cm^3 \cdot s^{-1}$. The temperature and impeller speed were held constant at 291 K and 2400 rpm, respectively. The results are shown in Tables 3.4, 3.5, and 3.6.

Table 3.4 N, the number of tanks in series, for various flowrates (one parameter model).

Temperature: 291 K	Impeller speed: 2400 rpm	
	N, number of tanks	
Flowrate, cm3.s-1	Basket full	Basket empty
6.0	1.3	1.4
11.4	1.3	1.0
18.0	1.1	1.1
26.7	1.0	1.0

Table 3.5 Five parameter model analysis for varying flowrates: basket full.

Temperature: 291 K			Mixing rate: 2400 rpm	
	Flowrate, $cm^3 \cdot s^{-1}$			
	6.0	11.4	18.0	26.7
N	1.0	1.0	1.0	1.0
A	0.00	0.00	0.00	0.00
B	0.00	0.00	0.00	0.00
C	1.00	1.00	1.00	1.00
T	0.00	0.00	0.00	0.00

Table 3.6 Five parameter model analysis of varying flowrates: basket empty.

Temperature: 291 K			Mixing rate: 2400 rpm	
	flowrate, $cm^3 \cdot s^{-1}$			
	6.0	11.0	18.0	26.7
N	1.0	1.0	1.0	1.0
A	0.00	0.00	0.00	0.00
B	0.00	0.00	0.00	0.00
C	1.00	1.00	1.00	1.00
T	0.00	0.00	0.00	0.00

The one parameter tanks in series model indicates an improvement in the quality of mixing as the flowrate was increased (notably for the full

basket) yet as the flowrate was increased the recycle ratio decreased which should have resulted in a poorer degree of mixing. This seems to be another indication of the insensitivity of the one parameter model to changes in the degree of mixing or it could be a measure of the accuracy of this method.

The five parameter model indicates that, for both the full and empty basket, perfect mixing was obtained at all of the flowrates employed.

3. The effect of varying temperatures

Three runs were carried out in an empty basket at the following conditions:

mixing rate:	900 rpm
nitrogen flowrate:	0.73 $cm^3 \cdot s^{-1}$
temperatures:	303 K, 373 K and 418 K

The results are shown in Table 3.7

Table 3.7 N, number of tanks in series, for various temperatures: basket empty.

Temperature (K)	N, number of tanks in series
303	1.1
373	1.1
418	1.0

The results indicate no significant change in the quality of mixing over the temperature range examined. It is quite clear from previous results that a change of 0.1 in the value of N is not significant.

From these results it is clear that at atmospheric pressure and an impeller speed of 2400 rpm the reactor was well mixed at flowrates of up to at least 26.7 $cm^3 \cdot s^{-1}$ irrespective of temperature (over the range examined).

3.4.1.2 Interphase mass transfer studies using napthalene

Mass transfer coefficients were obtained for napthalene-hydrogen and napthalene-air by the following technique used by Caldwell (1983a) (see Section 3.3.3.2).

The results are shown in Figures 3.17 and 3.18 for an empty and full basket (filled with 4 mm spherical glass beads). The results obtained show good agreement with those of Caldwell. Also shown are the results obtained by Caldwell (1982) using a Carberry type reactor (spinning basket). In all cases the particle size was the same but bed depth was not. The experiments were carried out at slightly different temperatures and pressures (100 kPa and 293 K).

The variation of kc with total pressure is shown in Figure 3.19. These results compare favourably with those of Caldwell (1983a).

The original conclusions reached by Caldwell based on his results have been discussed (Berty, 1983; Caldwell, 1983a, b; Carberry et al., 1985). The results presented here illustrate that in this reactor:

1. The mass transfer coefficient varied linearly with stirrer speed.
2. The mass transfer coefficient dropped with increasing pressure (in the range 100 to 500 kPa).

These results are discussed in detail in Section 3.5.2.

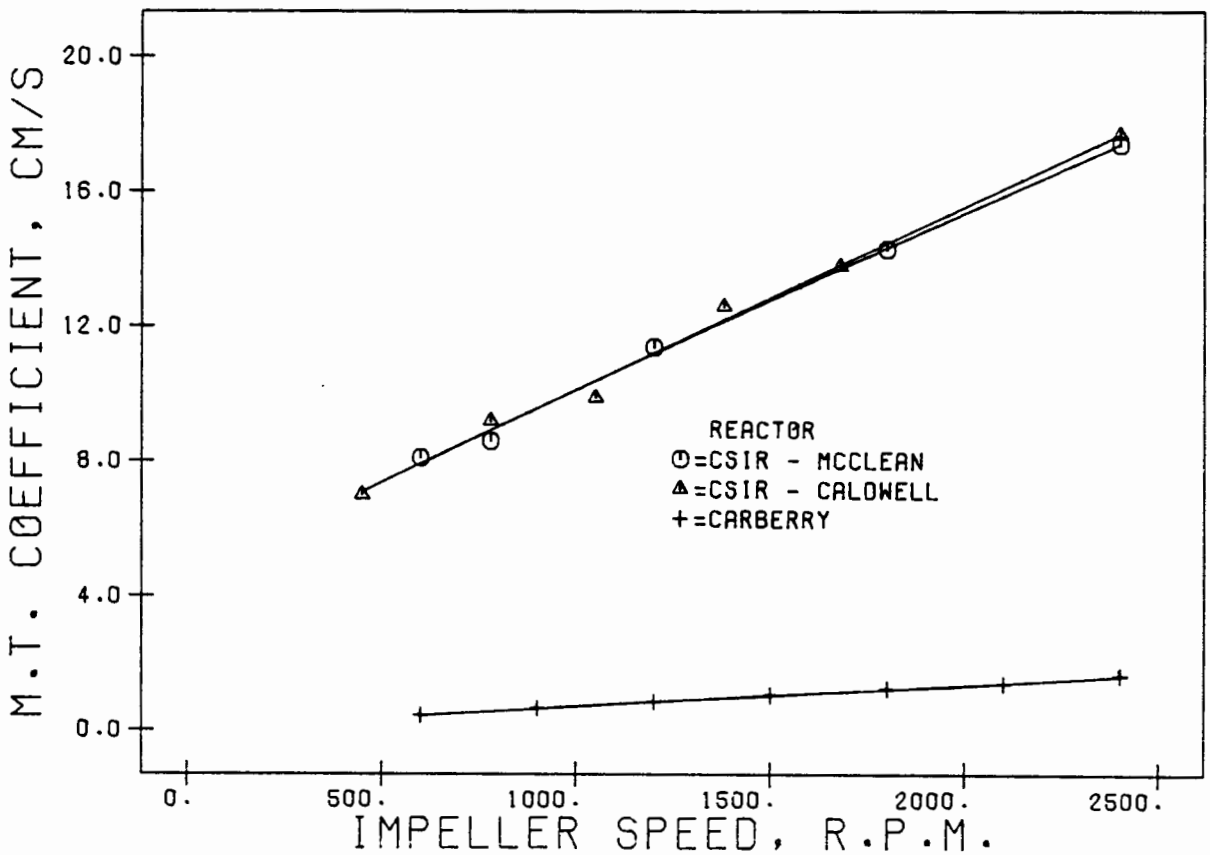

FIG 3.17 MASS TRANSFER COEFFICIENTS FOR NAPTHALENE IN HYDROGEN: BASKET EMPTY

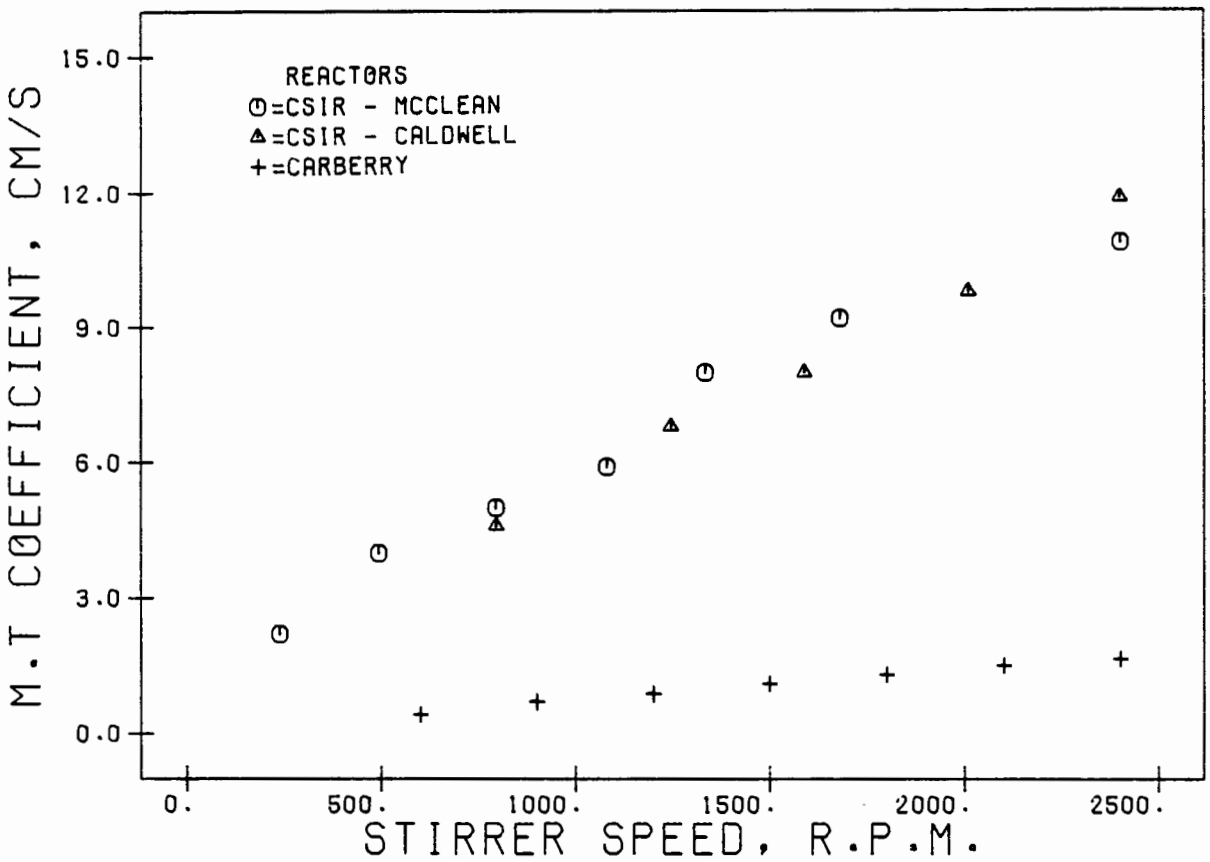

FIG 3.18 MASS TRANSFER COEFFICIENTS FOR NAPTHALENE IN HYDROGEN: BASKET FULL

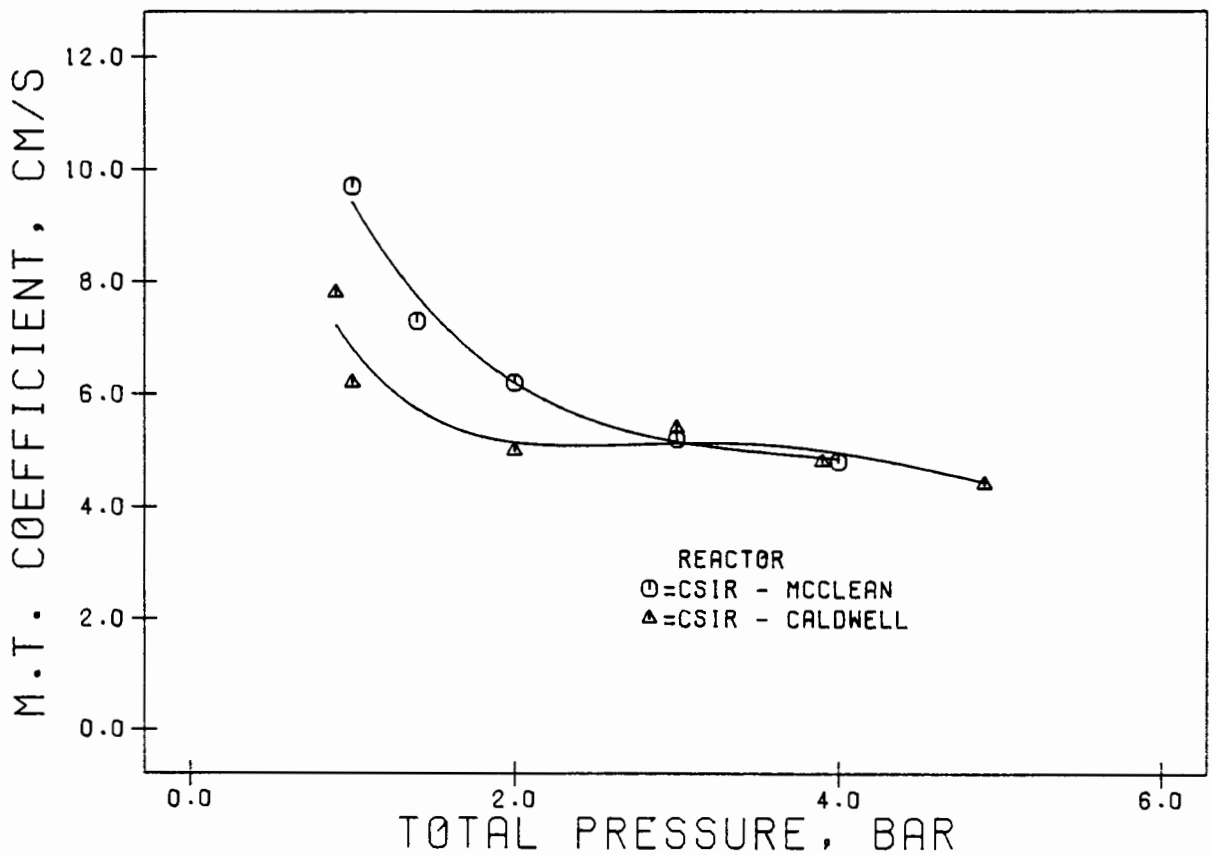

FIG 3.19 MASS TRANSFER COEFFICIENT AS A FUNCTION OF PRESSURE: NON DIFFUSING COMPONENT - AIR

3.4.2 Reactor Characterization with Reaction

3.4.2.1 Detailed analysis of a typical run

In this section a detailed analysis of a typical oligomerization experiment is given in order to indicate some of the features common to all the experiments. Some of the features, although dependent on the other experimental parameters being investigated, can be considered to represent the trends of other runs. Although some of the parameters (e.g., temperature versus time) provide indications of the system's stability, a detailed analysis of system stability and the factors affecting it will not be given in this section, but will be addressed elsewhere. The mass balance is critical and relatively small changes in the mass balance can have significant effects on the calculated reaction rate depending on whether the mass was lost as feed, liquid product, tail gas or a combination of these. For this reason, the procedures followed in determining the mass balances will be discussed separately in the next section.

With the initial reactor characterization experiments, teething problems were experienced in obtaining stability during experiments and reproducibility between different experiments. Some of the more pertinent problems will be discussed later. The experiment examined here is one which has been carried out after these characterization procedures had been completed. Less than 1.6% of the total mass fed was unaccounted for.

The experimental conditions for this run are listed in Table 3.8.

1. Conversion and WHSV versus time

Due to the internal recycle in this reactor WHSV takes on a different meaning to that of a fixed bed reactor. For the purposes of these discussions WHSV will be defined as the total mass hourly flowrate per gram of the catalyst. Initially the WHSV was low, but stabilized quite rapidly. Once stable, the maximum deviation from the mean was $\pm 2\%$. Conversion followed a similar pattern. Figure 3.20 shows the conversion and WHSV as a function of time during the reaction.

Table 3.8 Experimental Conditions for Typical Oligomerization Run of Section 3.4.2.1.

Catalyst	
Type	Phosphoric acid
Mass, g	6.0
Size, microns	106-180
Bed density, g/cm^3	0.95
Bed depth, mm	12
Dew point, K	264
H_3PO_4 concentration, %	103
Reaction	
Feed	98.6 mole % propene
	1.4 mole % propane
Flow, g/hr	38.5
WHSV	6.4
Temperature (set), K	463
Inside bed, K	464
Outside bed, K	464
Pressure, kPa	1.53
Mass balance, %	98%
Impeller speed	2000

2. Catalyst bed temperature versus time

Due to the generally low conversions obtained in the internal recycle reactor, maintaining the catalyst bed temperature constant and at the desired set point was simple. No temperature difference between the bulk gas phase and the bed could be detected. The reactor bed temperature profile and conversion versus time are shown in Figure 3.21.

3. Product spectrum versus time

The product spectrum was quite insensitive to the changing conditions as the system was stabilizing. Within the short space of about 2 hours after start up, the product spectrum had stabilized and from that time remained unchanged throughout the run. The product spectrum is shown in Figure 3.22. Products are grouped according to carbon number and only the most abundant are shown. The liquid products generally contained entrained monomer (2-4%), but this has been removed in the calculation.

The seeming insensitivity of the product quality to the initial change in conversion may be misleading. Initially the rate of condensation in the 'cold' magnedrive shaft was likely to be high, resulting in an

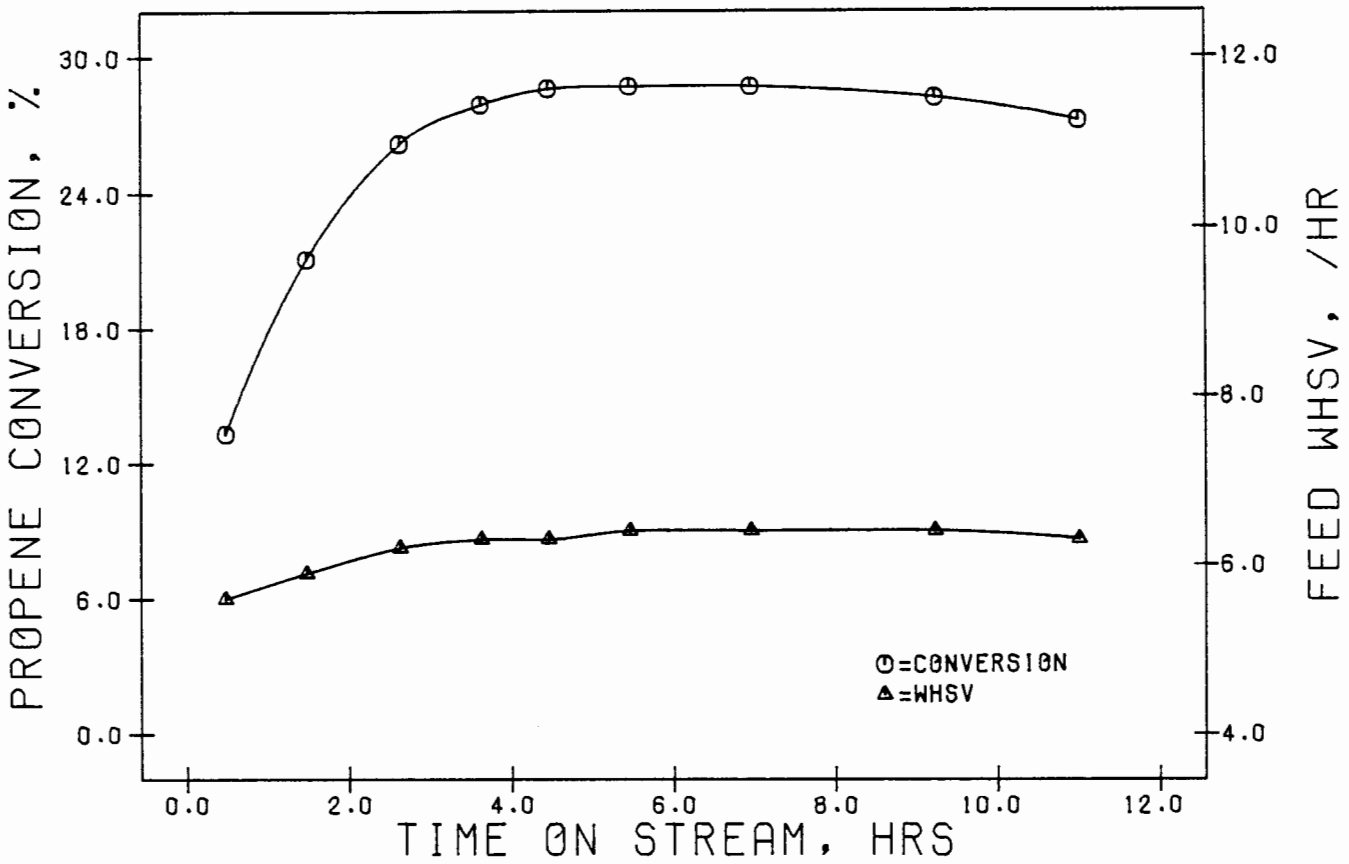

FIG 3.20 TYPICAL OLIGOMERIZATION EXPERIMENT CONVERSION AND WHSV VERSUS TIME

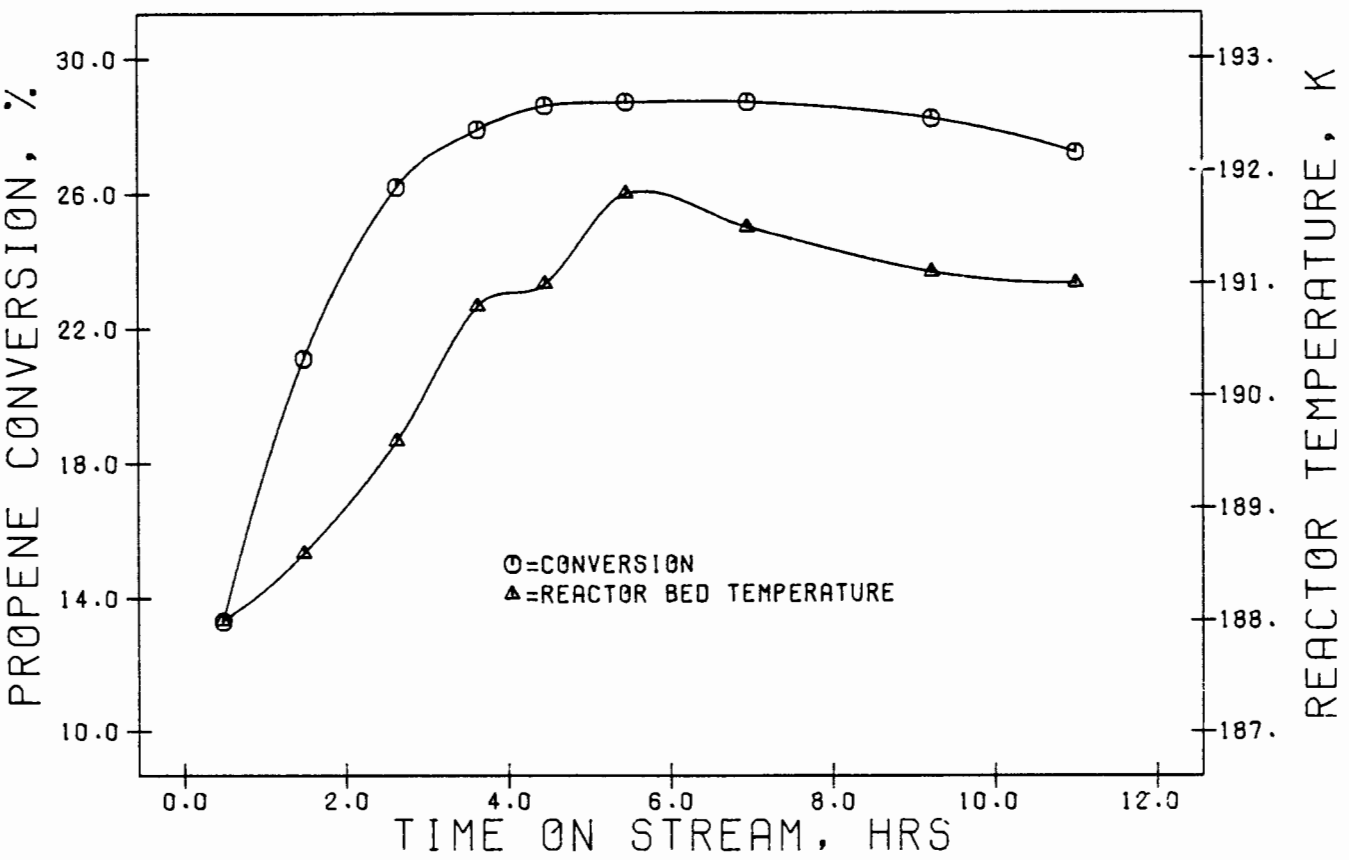

FIG 3.21 TYPICAL OLIGOMERIZATION EXPERIMENT REACTOR TEMPERATURE AND CONVERSION AS FUNCTIONS OF TIME

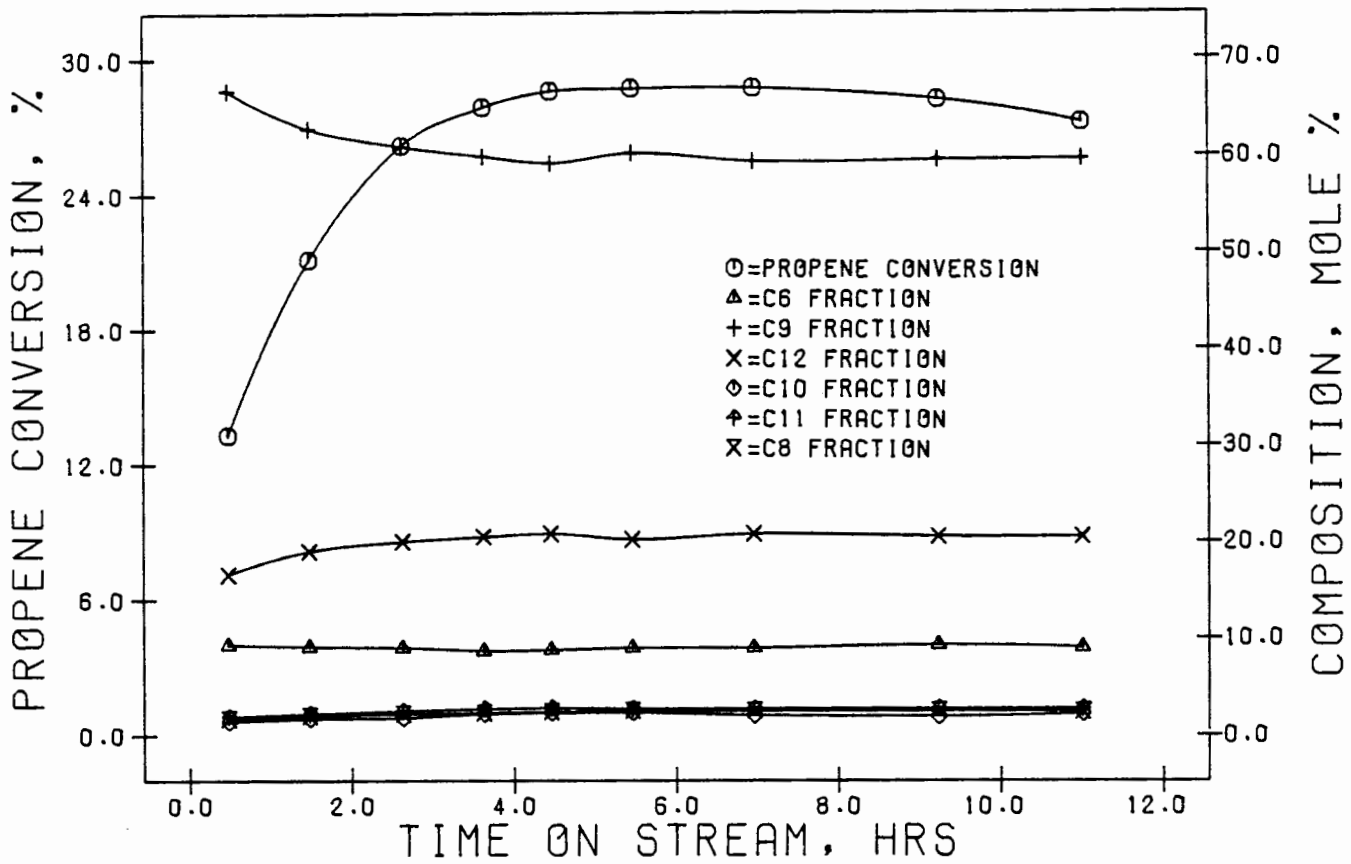

FIG 3.22 TYPICAL OLIGOMERIZATION EXPERIMENT LIQUID PRODUCT COMPOSITION AND PROPENE CONVERSION VERSUS TIME

observed low conversion level. The initial rise in observed conversion may therefore have been a result of a progressively slower rate of condensation as the 'cold' magnedrive shaft filled up. Once filled, the conversion should have stabilized, as was observed.

Due to both the constant steady state conversion levels and product spectra, the production rates of individual oligomers remained constant and hence will not be shown.

4. Reaction rate versus time

The reactor behaved as an ideal CSTR and as such can be analyzed using the classical performance equation for a perfectly mixed reactor.

$$\frac{W}{F_{A0}} = \frac{X_A}{-r_A}$$

where W = mass of catalyst

F_{A0} = molar flowrate of reactant in the feed

X_A = conversion of reactant (fractional)

$-r_A$ = rate of disappearance of reactant

THe calculation of the rate of disappearance of propene is therefore simple and is shown, versus time on stream, in Figure 3.23.

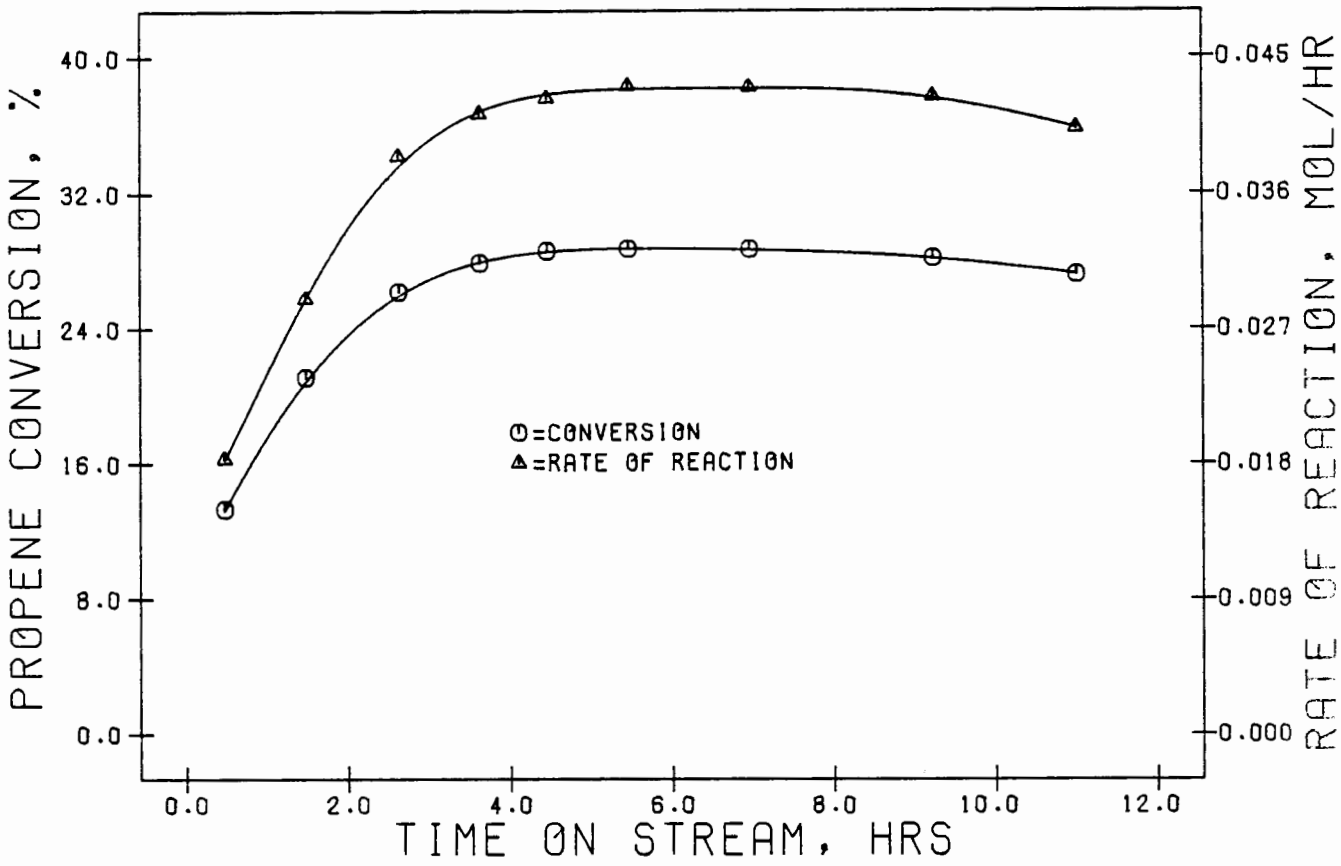

FIG 3.23 TYPICAL OLIGOMERIZATION EXPERIMENT RATE OF PROPENE REACTION AND CONVERSION VERSUS TIME

5. Product quality

Product quality resulting from the oligomerization of alkenes over solid phosphoric acid on kieselguhr and other phosphoric acid catalysts is relatively insensitive to most operating variables (McMahon et al., 1963). Since the introduction of polymerization catalysts, the quality of the products produced from the oligomerization of olefins over phosphoric acid has been widely reported (Ipatieff et al., 1935; Egloff, 1936; Ipatieff & Corson, 1936; Sullivan et al., 1935; Ipatieff, 1935a; Ipatieff & Pines, 1936; Ipatieff and Schaad, 1938; Shanley & Egloff, 1939; Ipatieff & Schaad, 1948; Weinert & Egloff, 1948; Steffens et al., 1949; Langlois, 1953; Bethea & Karchmer, 1956; Langlois & Walkey, 1951; Egloff & Weinert, 1951; M^{c}Mahon et al, 1963; Ebeid et al., 1976). Since the quality of the fuel in terms of ASTM (or SABS) specifications was not a primary objective of this study and due to the wealth of information, the ASTM quality of the fuel will not be examined.

6. Dew point of water in the feed versus time

Control of the water content in the reactor was essential in fixing the H_3PO_4 strength inside the reactor. The monitoring of the dew point of the water contained in the feed was therefore critical. Figure 3.24

shows the change in measured dewpoint with time. The high initial dewpoint was not due to the water in the feed, but was due to moisture that had built up on the probe and tube walls around the probe between experiments. The settled value was equivalent to about 103% H_3PO_4.

7. Feed composition versus time

Feed samples were analyzed as often as product samples in most cases. The propene concentration in the feed was found to vary between 98.6 and 98.8 % (mole %) with an average of 98.6 %.

3.4.2.2 Mass balance over the reactor system

Due to the sensitivity of reaction rate to the mass balance, especially at low conversion, it was essential to ensure that any masses that could be accounted for were done so correctly and accurately. The mass balance equations were written as a computer program on a SPERRY UNIVAC 1100 mainframe computer. The following is a summary of the program functions:

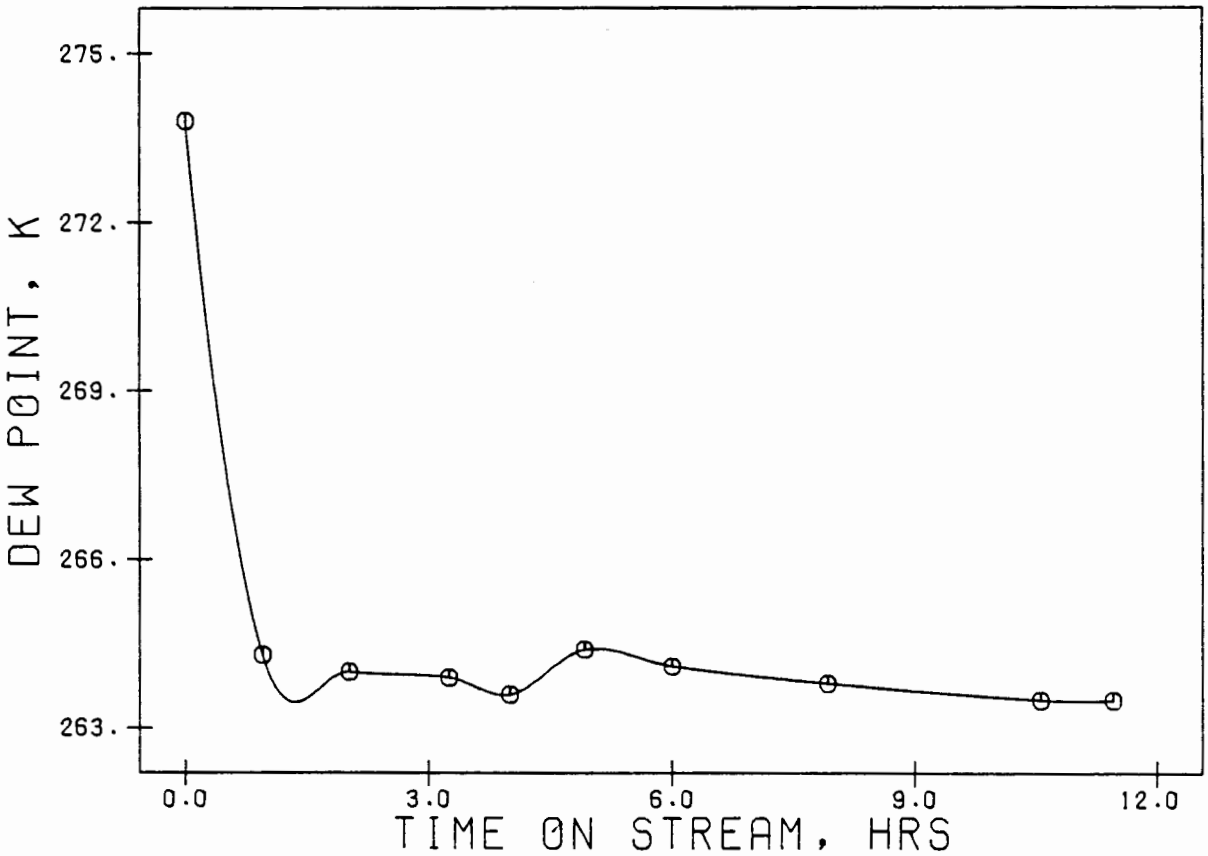

FIG 3.24 TYPICAL OLIGOMERIZATION EXPERIMENT WATER DEW POINT IN FEED VS TIME ON STREAM

1. To read in the necessary data
2. To calculate compressibility factors for the following:
   (1) The gas mixture in the reactor at steady state
   (2) The tail gas

3. To perform a mass balance over the reactor
4. To calculate flowrate versus time data
5. To calculate conversion versus time data
6. To determine the concentrations of the reactants and products inside the reactor at steady state (grouped according to carbon number)
7. To calculate the rate of propene disappearance versus time an stream.
8. To calculate the average reaction rate, propene conversion etc and the deviations from the mean.

(i) To print out the results.

A more detailed description of the procedure followed by the program is given in Appendix K.

3.4.2.3 Catalytic activity of the empty reactor

The reactor body was made of 316 stainless steel and the Helicoflex seal consisted of an inconel x 750 spring which was double lined with copper. The activity of the reactor system was carefully measured under two sets of conditions using propene and one set of conditions using iso-butene. In the first case, for propene, the reactor was maintained at 503 K (maximum temperature used under reaction conditions), 1.53 kPa and 2000 R.P.M. Propene was fed at 40g/hr and water was introduced such that, had there been catalyst in the reactor, the H_3PO_4 concentration would have been maintained at the 108% level. In the second case with propene only the amount of water injected was changed. Here water was injected such that, had there been catalyst in the reactor, the H_3PO_4 concentration would have been maintained at the 102% level. The iso-butene run was carried out under the same conditions as the first propene run described above.

In all three experiments, which were carried out over 6 hours, no detectable activity of the empty reactor was observed.

3.4.2.4 Reproducibility and steady state behaviour of experiments

1. Acid concentration

Initially many problems were experienced with both the steady state behaviour of the reactor system and the reproducibility of experiments. It was as a direct result of the H_3PO_4 concentration that the system behaviour was unstable. With control and measurement of the acid concentration the steady state behaviour of the system improved

dramatically and could have been considered to be excellent. Examples of system stability (measured in the form of reaction rate) versus time on stream for two runs where the acid concentration was controlled and uncontrolled (no water addition and hence gradual dehydration of the catalyst) are shown in Figure 3.25. Different feed concentrations were used for each of these experiments.

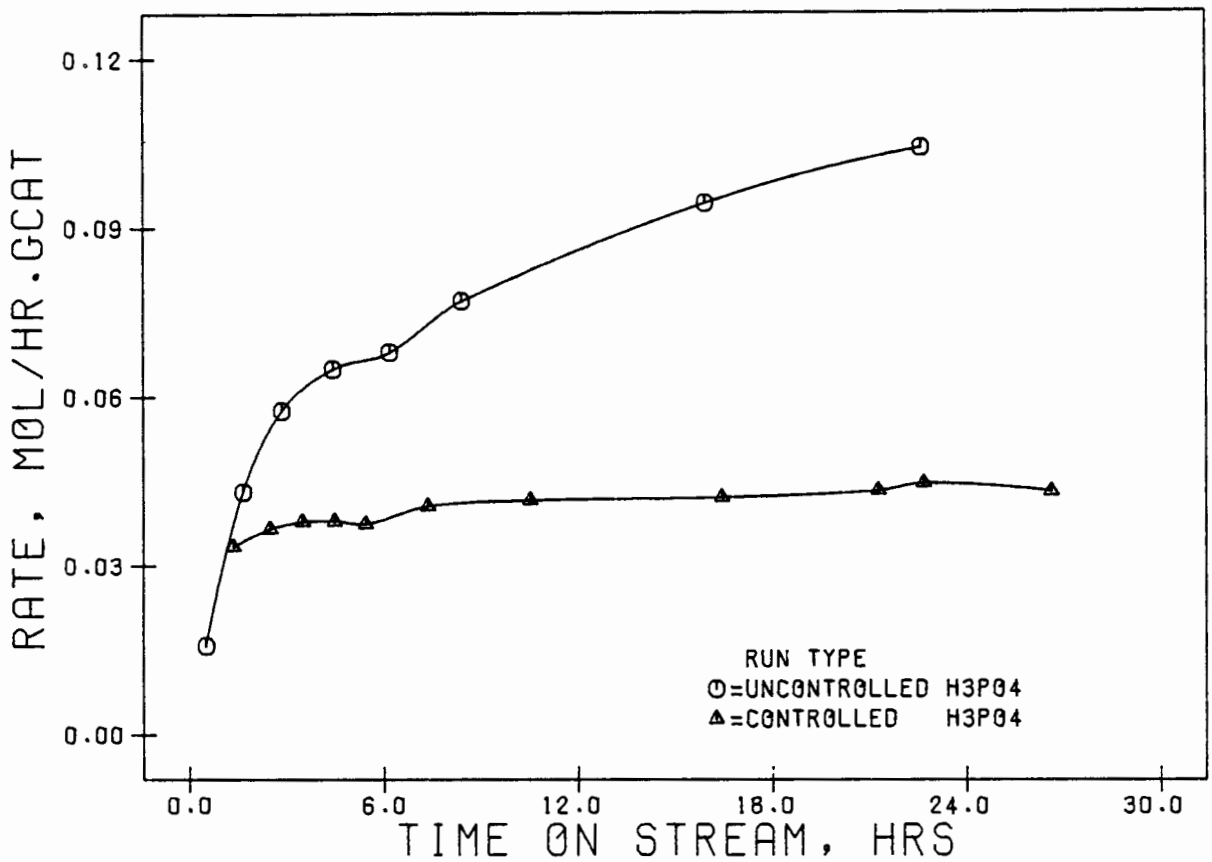

FIG 3.25 STEADY STATE BEHAVIOUR OF THE INTERNAL RECYCLE REACTOR: THE EFFECT OF CONTROLLING ACID CONCENTRATION

The gradual increase in the activity of the uncontrolled H_3PO_4 concentration run was not entirely unexpected. The gradual loss in water resulted in a higher H_3PO_4 concentration and hence an increase in activity. The dehydration would have, however, ultimately resulted in a more rapid deactivation of the catalyst.

2. Water balances

Considering the importance of acid concentration control it was decided to carry out a water balance over the reactor. The determination of the acid concentration and its relation to water content in the reactor is described in detail in Section 2.3.3.3. An example of the dew point response versus time on stream is shown in Figure 3.24 of Section 3.4.2.2.

The water balance was determined by measuring the dew points of the water in the feed and in the exit tail gas during the steady state period of a particular set of runs. The water content of the liquid product was analyzed on a Metrolin semi-automatic analyzer using the Karl-Fischer technique. The balance was performed on two separate runs. The results are listed in Table 3.9. The masses shown are based on what was fed over a 4 hr period during both experiments which were performed at identical conditions.

Table 3.9 Water balance over the internal recirculation reactor.

	Water in feed	Water in tail gas	Water in liquid product	Mass Balance
Run no.	$gx10^3$	$gx10^3$	$gx10^3$	%
1	84.1	73.0	10.8	99.7
2	82.3	71.1	10.4	99.2

The results indicate excellent water balances over the reactor system and also indicate that the bulk of the water in the exit remains as a vapour in the tail gas.

3. Control of operating variables

In obtaining accurate and reproducible data, good and stable control of all operating variables such as catalyst mass, temperatures, pressures, mass losses, impeller speed, flowrates, acid concentrations and feed composition is essential.

With practice and experience the accurate control over reactor temperatures and pressures, feed flowrates, impeller speeds and catalyst mass proved quite straight-forward. Feed mixtures were made up accurately from pure component feeds and regular analysis during experiments enabled accurate determination of the compositions. The mass balance has been determined in detail in Section 3.4.2.2 and both the effect and control of H_3PO_4 concentration has already been discussed in that section. Good control of the above variables not only provided excellent (stable) steady state behavior of the system, but resulted in reasonable reproducibility of experiments.

4. System induction time

Due to the relatively large volume of the reactor and the changing conditions during the first few hours of operation (such as the changing acid concentration, changing reactor temperature and the condensation of products in the magnedrive shaft) the system exhibited an induction period before attaining steady state. The example of reaction rate (propene disappearance) versus time on stream in Figure 3.26 is a very representative example of the time required for the system to reach its steady state. The time required to reach steady state was generally about 6 to 7 hours.

The result in Figure 3.26 also shows that the steady state value obtained after 6 to 7 hours was maintained and was not a temporary steady state period. Several other runs which were operated for up to 30 hours have shown similar results indicating that the system had indeed stabilized completely after the first 6 to 7 hours.

5. Reproducibility of experiments

Figure 3.27 shows the reproducibility of three reactor runs all carried out under the same conditions. These experiments were carried out after the reactor had been completely characterized, i.e., the system was stable, mass balances were all within 3 % and all reactor operating variables were controlled accurately and with good stability. It can be seen from Figure 3.27 that the reproducibility is satisfactory with a maximum steady state deviation between the rates of about 6 %. The feed used was an 80:20 propene-propane mixture.

3.4.2.5 Equilibrium conversions and phase equilibria

The methods used to obtain equilibrium compositions and phase equilibria are described in detail in Sections 2.4.9 and 2.4.10. It was pointed out in Section 2.4.9 that free energy and heat of formation data for the longer chain length branched alkenes is limited. The examination of the straight alkene data (Figures 2.11, 2.12 and 2.13 of Section 2.4.9), however, indicates quite clearly that at the higher pressures used in the kinetic experiments (1.55 to 1.65 MPa) the reaction of propene to completion is thermodynamically favourd. In the kinetic experiments the conversions were kept as low as possible. In some cases significantly higher conversions than desired (>50%) were used, e.g., in the high H_3PO_4 and high temperature experiments. In general, for most of the experiments, conversions of between 20% and 30% were maintained.

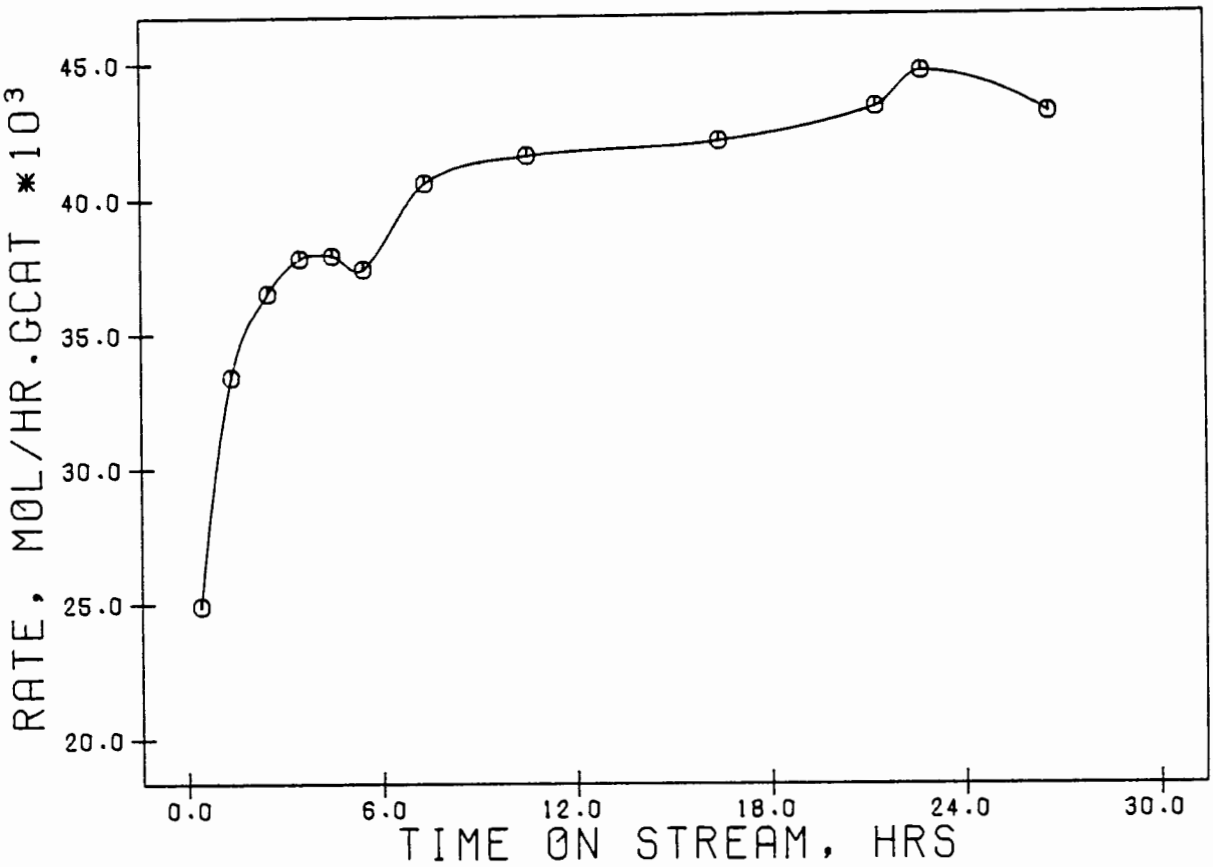

FIG 3.26 INTERNAL RECYCLE REACTOR INDUCTION PERIOD

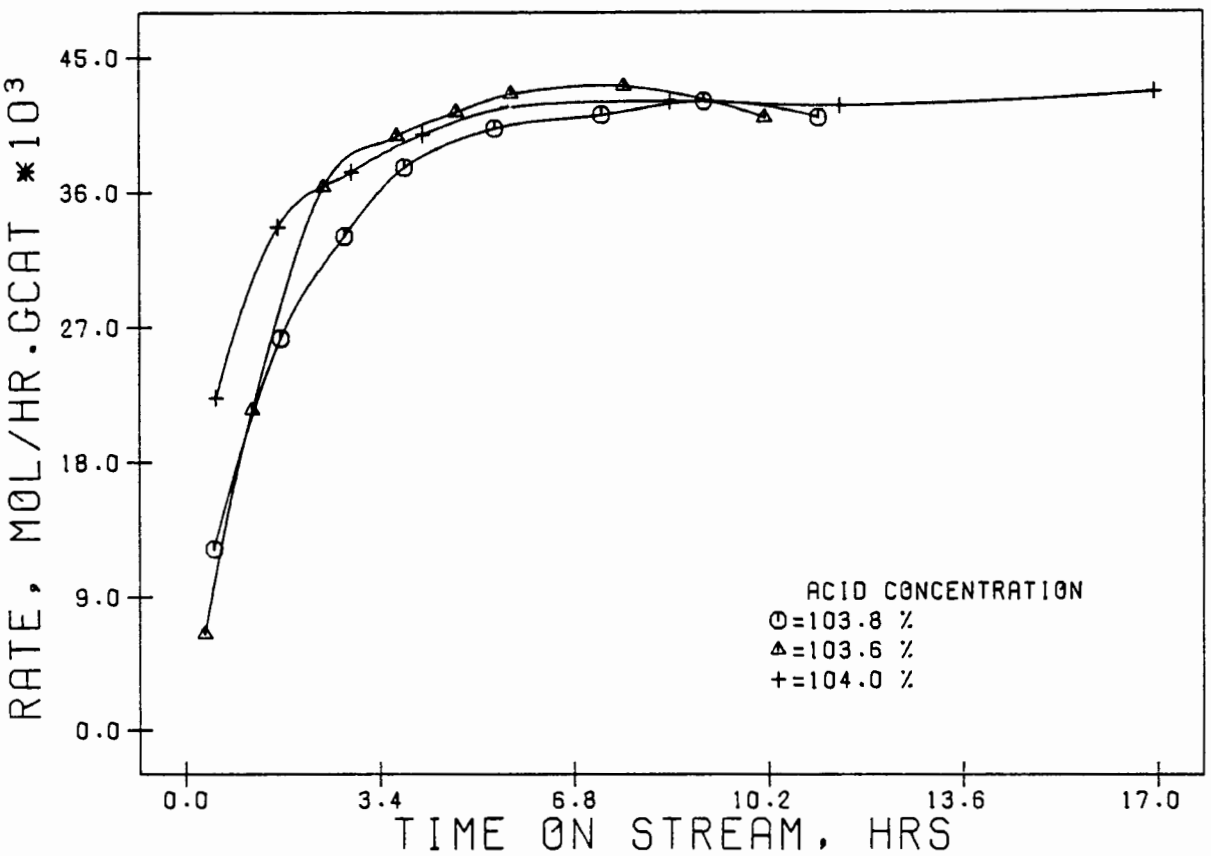

FIG 3.27 INTERNAL RECYCLE REACTOR:REPRODUCIBILITY

The phase diagram in Figure 2.17 of Section 2.4.10 is representative of a propene and iso-butene feed (initial molar ratio of propene: iso-butene was approximately 2:1) and related products mixture. The products are representative of a 41% conversion of iso-butene and a 19% conversion of propene. From Figure 2.17 it can be seen that at approximately 1.6 MPa (pressure of the kinetic experiments) and above 430 K, no liquid phase is present. The bulk of the kinetic experiments were performed at either similar or lower conversions and also at ~~lower~~ higher temperatures, indicating that in these cases no liquid phase was present. In some of the more stringent kinetic experiments where higher conversions were obtained (such as those at the high H_3PO_4 concentrations) it is possible that some liquid phase may have been present.

3.4.2.6 Mass transfer with reaction

It was noted in Section 3.1.1 that if intra-particular transport effects are present then it is likely that the concentration gradient within the catalyst particle will be more serious than the temperature gradient. The significance of intra-particular transport effects can therefore be determined by examining the significance of intra-particular diffusion.

The other significant transport problem is transport across the gas film. It was also pointed out in Section 3.1.1 that if experiment shows that that gas phase resistance is absent then we may expect the temperature to be that of its surrounding fluid, and hence isothermal conditions may be assumed to prevail (Levenspiel, 1972).

If it can be shown therefore that intraparticular mass transfer and bulk gas phase mass transfer (interphase) are absent in a certain operating region then the reaction rates found in this region can be regarded as being the intrinsic reaction rates devoid of any heat and mass transfer influences.

1. Bulk gas phase (interphase) mass transfer

Two sets of experiments were carried out, one at a high H_3PO_4 concentration and the other at a low H_3PO_4 concentration. In both sets of experiments the impeller speed was varied between 800 and 2000. This has the effect of changing the superficial gas velocity without affecting the catalyst to feed ratio. The conditions used for both sets

of experiments are shown in Table 3.10. The results are shown in Figures 3.28 and 3.29.

Table 3.10 Experimental conditions for bulk gas phase mass transfer experiments.

		Set 1	Set 2
Catalyst:	mass, g	6.00	6.00
	size, μm	106-180	106-180
	H_3PO_4 conc, %	101.5 and 101.2	109.5
Feed:	composition	99% propene	99% propene
	flowrate, g•hr-1	38-40	38-40
Reactor:	temperature, K	464	478
	pressure, MPa	1.53	1.53
Impeller speed, rpm		variable	variable

The results in Figure 3.28 show that the reaction rate no longer increases at impeller speeds above approximately 1800 rpm. The data point at 2000 rpm represents the identical value obtained from two independent runs (100% reproducibility). The results in Figure 3.29 indicate that the rate remains approximately constant above an impeller speed of about 1600 rpm. The operating conditions for the set of experiments in Figure 3.29 represent the most extreme conditions encountered in the kinetic study. This implies that the significance of bulk gas phase mass transfer (interphase mass transfer) is negligible above an impeller speed of 1800 rpm.

2. Intraparticular diffusion

Two sets of experiments were carried out to examine the significance of intraparticular transport by varying the catalyst particle sizes. The conditions used are listed in Table 3.11 and the results are shown in Figures 3.30 and 3.31.

The results in Figure 3.30 indicate clearly that the reaction rate does not increase at particle sizes below a range of 0.2 to 0.3 mm at these conditions. The conditions used for these experiments encompass the conditions used in most experiments. There were however some experiments

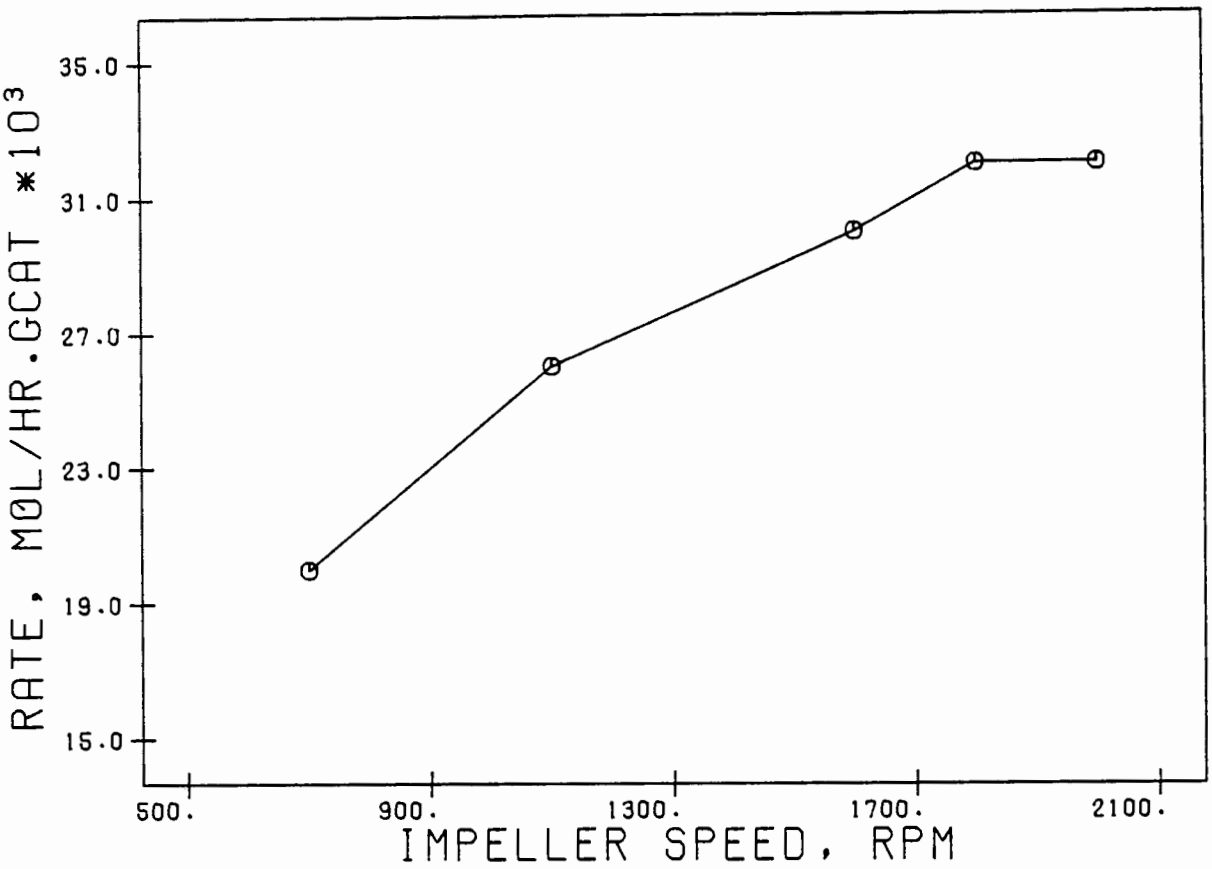

FIG 3.28 INTERNAL RECYCLE REACTOR: REACTION RATE VERSUS IMPELLER SPEED AT 101.5% H3P04 AND 464 K

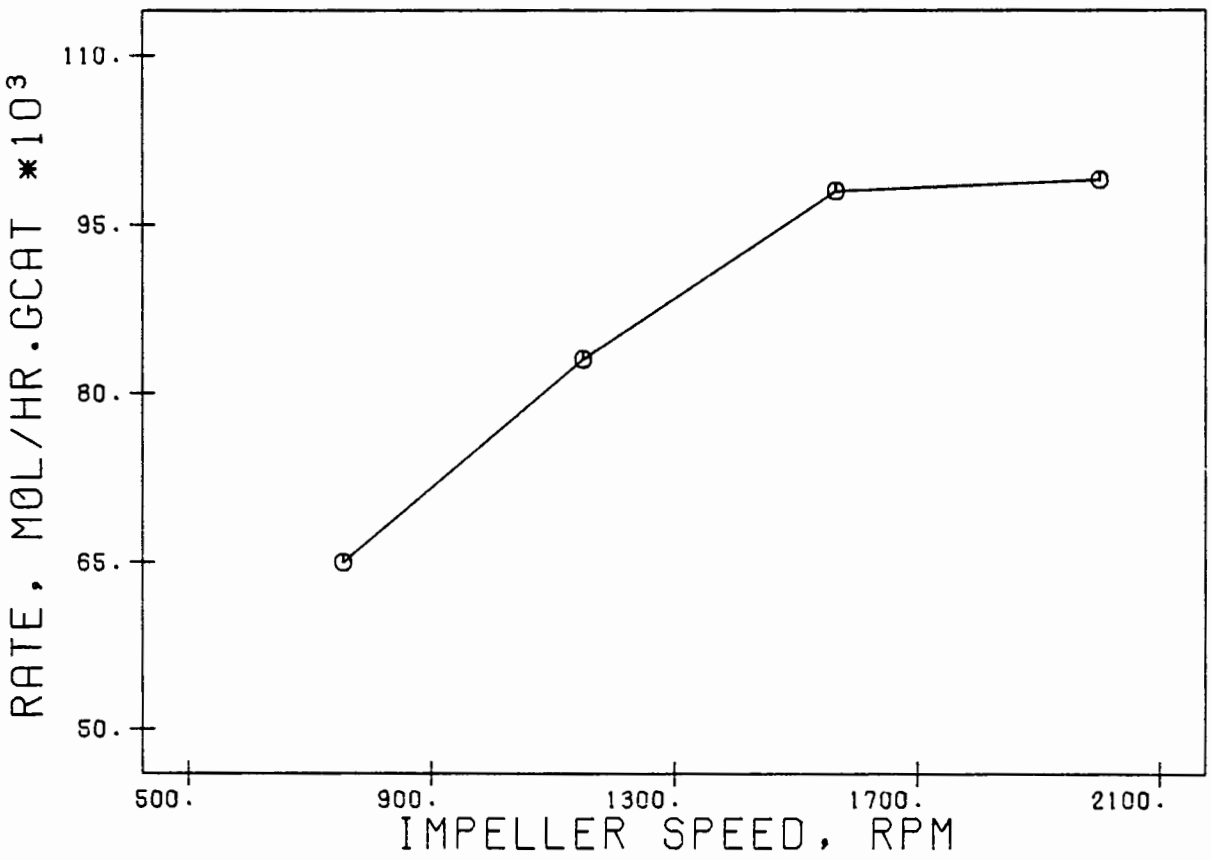

FIG 3.29 INTERNAL RECYCLE REACTOR: REACTION RATE VERSUS IMPELLER SPEED AT 114% H3P04 AND 478 K

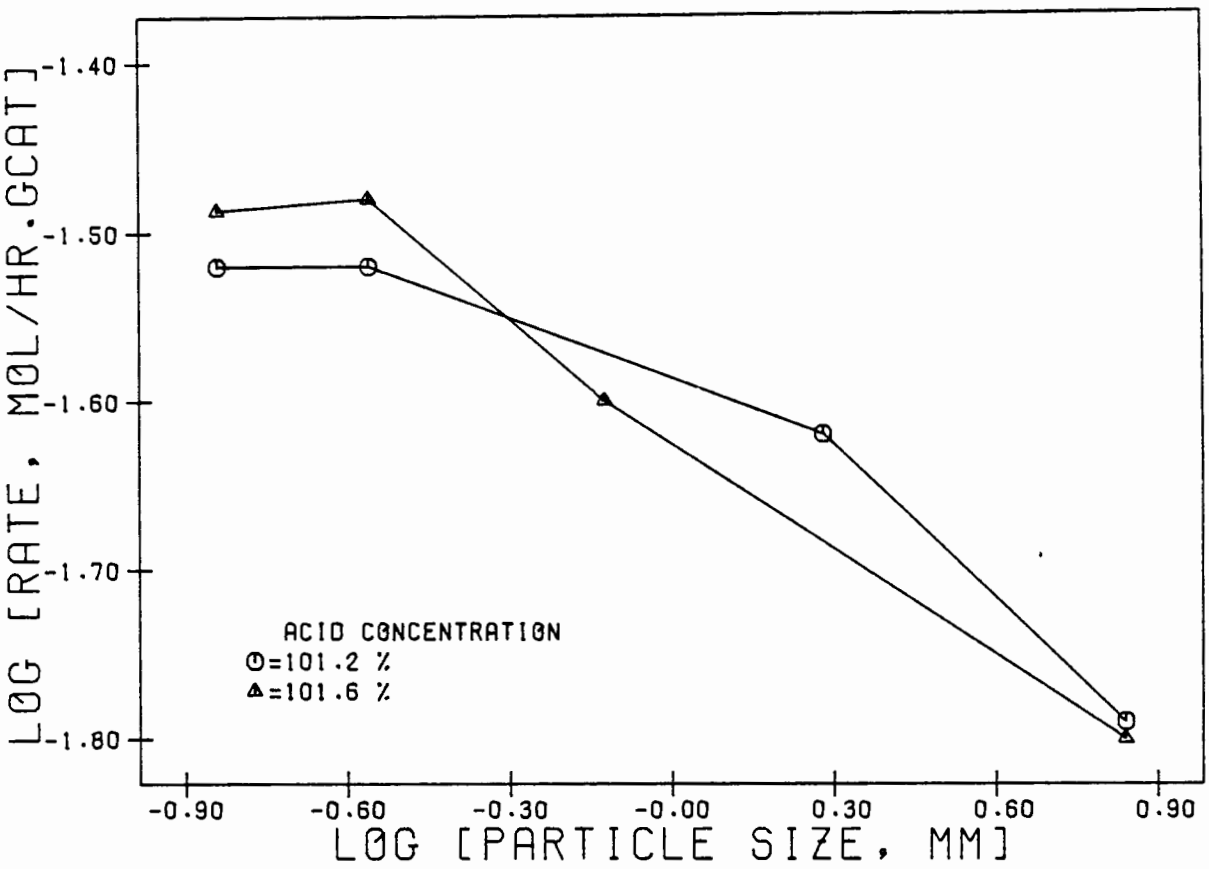

FIG 3.30 INTERNAL RECYCLE REACTOR: REACTION RATE VERSUS PARTICLE SIZE AT 464 K

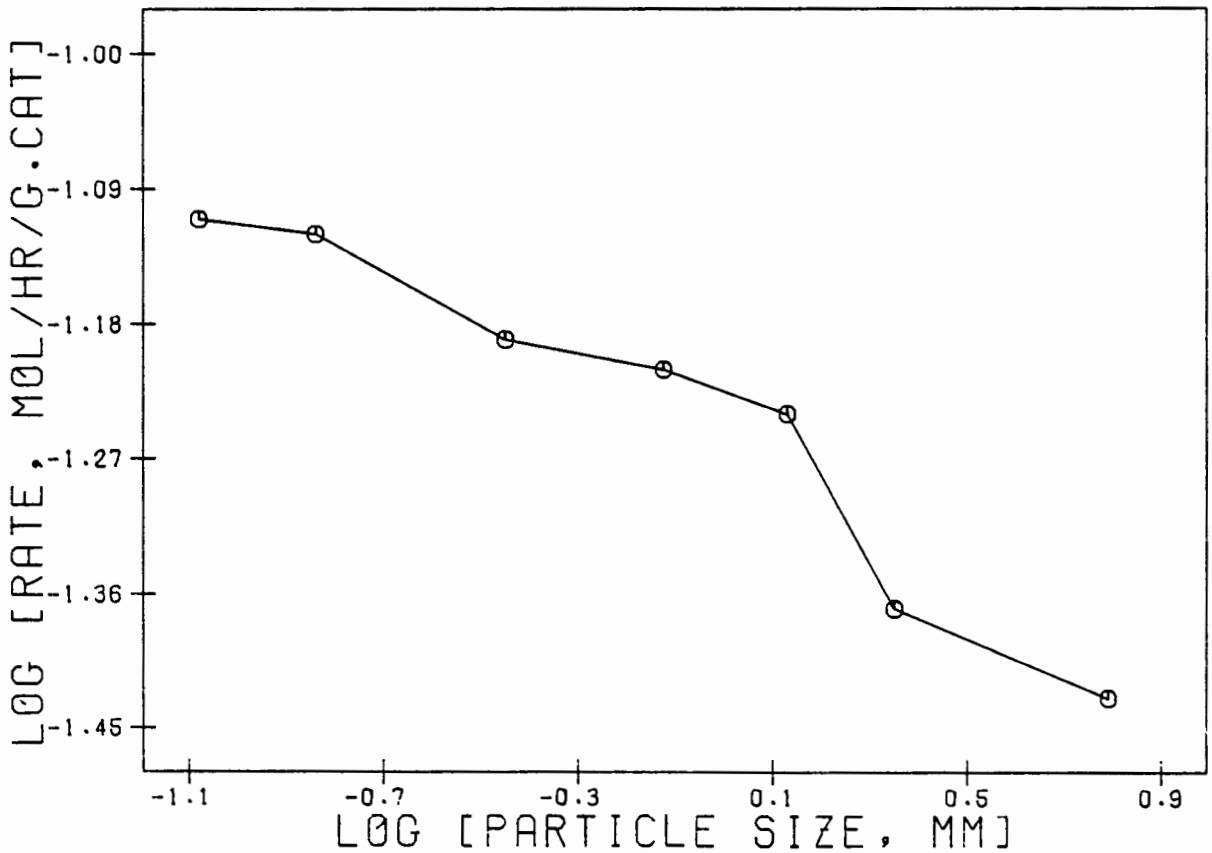

FIG 3.31 INTERNAL RECYCLE REACTOR: REACTION RATE VERSUS PARTICLE SIZE AT 114% H3P04 AND 503 K

Table 3.11 Experimental conditions used for intraparticular diffusion experiments.

		Set 1	Set 2
Catalyst:	mass, g	6.00	6.00
	size, μm	variable	variable
	H_3PO_4 conc, %	101.2 and 101.5	114
Feed:	composition	98.6% propene	98.6% propene
	flowrate, $g \cdot hr^{-1}$	38-40	38-40
Reactor:	temperature, K	464	477
	pressure, MPa	1.53	1.53
Impeller speed, rpm		2000	2000

that used more extreme conditions (higher H_3PO_4 concentrations and temperatures) than those used to generate Figure 3.30. The experiments of Figure 3.31 encompass even the most extreme of cases. The results show that the reaction rate remains approximately constant below a particle size range of 106-180 microns (log=-0.84). This demonstrates that intraparticular transport is insignificant for size ranges equal to or smaller than 106-180 μm.

In summary, if the reactor system is operated at an impeller (internal blower) speed of 1800 rpm or higher and with a catalyst size fraction equal to or greater than 106-180 μm at conditions as extreme as or less extreme than those used here then the effects of interphase transport and intraparticular transport on the reaction rate are insignificant. In these regions the reaction rate can be regarded as the intrinsic reaction rate.

It should be pointed out that to avoid fouling of the impeller inside the reactor the maximum impeller speed that could be used was 2200 rpm. For this reason it was decided not to use an impeller speed of more than 2000 rpm. With respect to the catalyst size fraction it was found that at sizes below 75 to 90 microns catalyst spillage became a problem. The best choice of catalyst size fraction is obviously the largest possible size (lower pressure drop through bed) that is not accompanied by intraparticular effects. The size fraction chosen was the 106-180 μm fraction.

The system pressure chosen for all experiments was approximately 1.5 MPa. This was chosen by determining the highest pressure that could be used without the problem of condensation of liquid products inside the

reactor. In some of the higher conversion experiments this did prove to be a problem.

3. Estimation of recycle ratio

The recycle ratio in the reactor under normal operating conditions is estimated using the Leva pressure drop equation as described in Section 3.5. The reactor conditions used are those described in Table 3.11 with a catalyst size fraction of 0.106-0.180 mm. The maximum theoretical head generated is equal to 1811 cm of propene (assumed pure propene). The voidage fraction is equal to 0.3 and the shape factor is taken as 0.9. From the Leva equation the superficial gas velocity is calculated as:

$$U_g = 15.4 \text{ cm} \cdot \text{s}^{-1}$$

The density of propene in the reactor under these conditions is equal to 1.735×10^{-2} g·cm^3 and hence at a feed flowrate of 40 g·hr^{-1} the recycle ratio (R) is equal to 38.

This is significantly higher than the minimum of 20 (Berty, 1974) or 25 (Li et al., 1980; Carberry, 1964) required for perfect mixing.

3.4.3 Preliminary Results

Due to the initial delay in the delivery of the hygrometer, which was used to determine accurately the dew points of water in the reactor feeds, it was decided to carry out a preliminary investigation into the qualitative effects of the ortho-phosphoric acid concentration, determined by the vapour pressure of the water in the reactor, on the reaction products and reactor system behavior.

It has already been pointed out in Section 3.4.2.4. that control over the acid concentration is essential in obtaining reproducible and stable steady state behavior of experiments. It has also been shown by other workers in the field (McMahon et al., 1963) that the reaction rate increases strongly with an increase in the acid concentration.

Six experiments were carried out at the reaction conditions shown in Table 3.12. The hydration level of the catalyst (H_3PO_4 concentration) in each of the six experiments was varied as indicated below. Estimates of the H_3PO_4 concentration are given in brackets in each case.

Table 3.12 Experimental conditions used to examine the effect of catalyst hydration on reactor behavior.

Catalyst	size, μm	106-180
	mass, g	6.00
Feed:	type	99% propene
	flowrate, $g \cdot hr^{-1}$	38-40
Reactor:	pressure, MPa	1.53 (abs)
	temperature, K	464
Impeller speed, rpm		2000
H_3PO_4 concentration, %		unknown but variable

Run 1. The catalyst was loaded into the reactor "as is" and the experiment carried out. No water was injected during the run (%H_3PO_4 gradually increasing throughout run).

Run 2. Here the catalyst was "dried" in the reactor for 45 hours at 464 K during which time high purity nitrogen was passed through the reactor. The reaction was then carried out with no addition of water to the reactor (%H_3PO_4 $\geqq$ 114%).

Run 3. Here the catalyst was "dried" for 15 hours as in Run 2 and the reaction carried out with no addition of water (%H_3PO_4 $\geqq$ 110%).

Run 4. The catalyst was loaded into the reactor and the run was started without any pretreatment. Throughout the experiment, however, water was introduced with the feed by passing the feed over the water in the water bath which was held at 313 K (%H_3PO_4 = 103-104%).

Run 5. The procedure in Run 4 was repeated but here the water bath was held at 325 K (%H_3PO_4 < 101%).

Run 6. Here the catalyst was dried in the reactor for 64 hours. Following this the run was started, throughout which the water bath was held constant at 313 K (%H_3PO_4 = 103-104%).

For each of these experiments, reaction rates versus time on stream are shown in Figure 3.32 and the major oligomer products are shown in Figure 3.33. Only the trimer and tetramer are shown since, firstly, these are the major oligomer fractions and secondly, to limit congestion on the graphs. Only the product spectra of runs 1, 3 and 6 are shown.

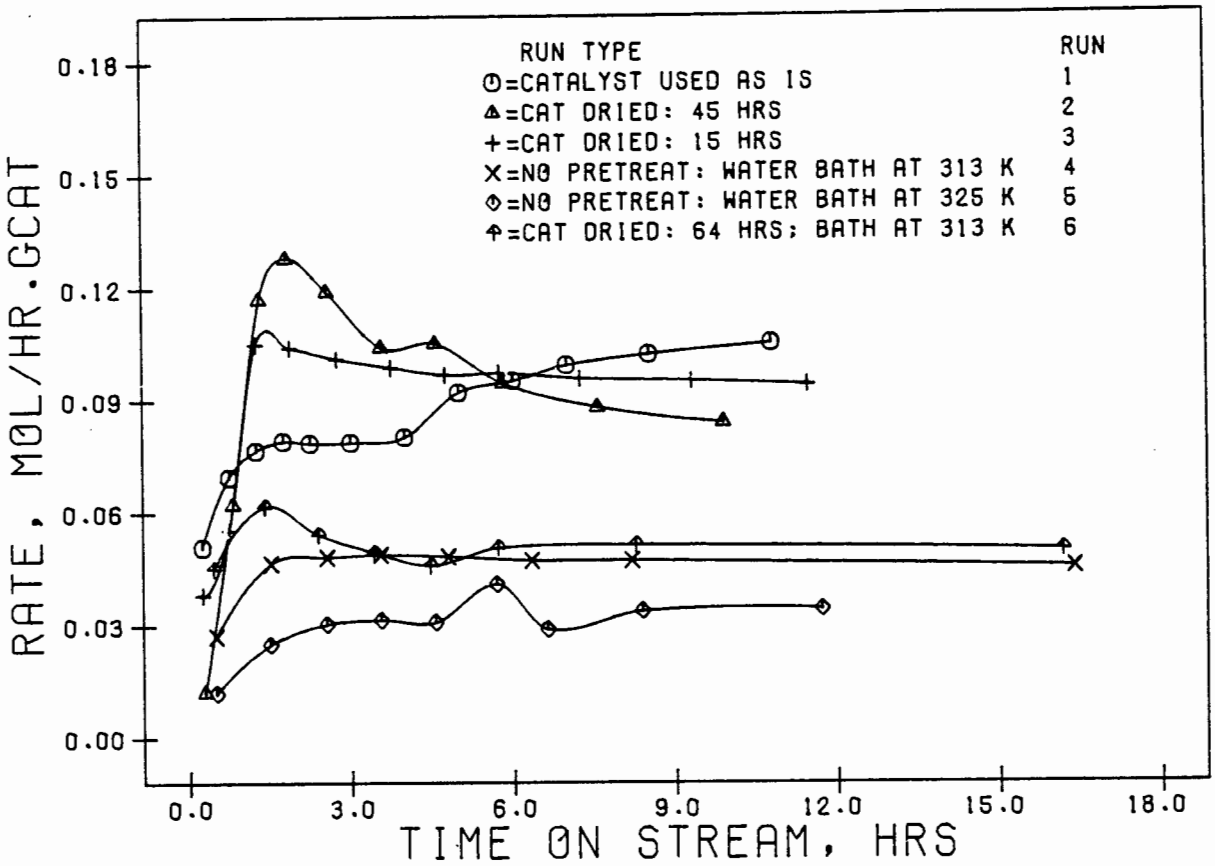

FIG 3.32 THE EFFECT OF HYDRATION ON REACTION RATES

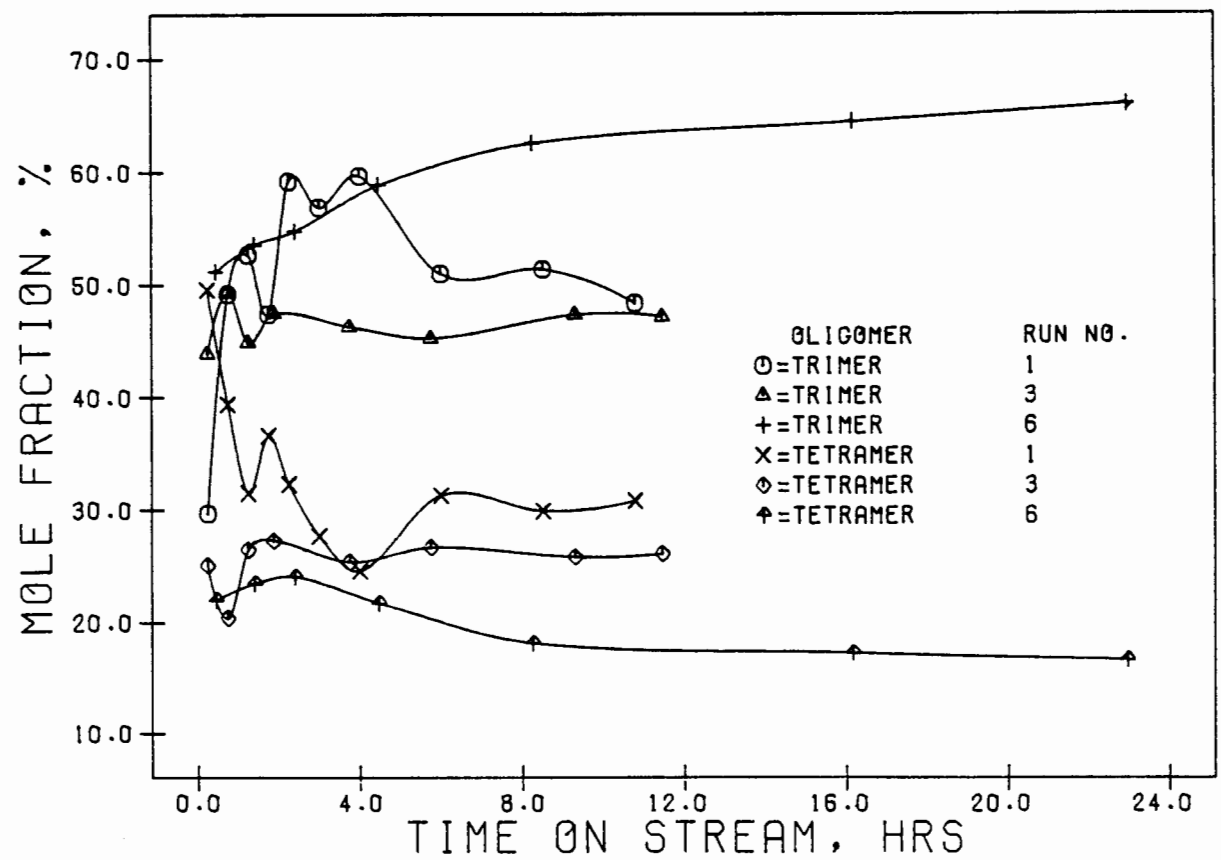

FIG 3.33 THE EFFECT OF HYDRATION ON PRODUCT SPECTRA

From runs 1, 2 and 3 (Figure 3.32) it can be seen that steady state behavior was not been obtained after 10 hours on stream. In run 1 the activity was quite stable for the first few hours but jumped quite dramatically after approximately 4.5 hours on stream. This is possibly due to the loss of water from the system which results in an increase in the H_3PO_4 concentration. In Run 2 where the catalyst was "dried" for 45 hours the initial high activity was to be expected due to the very high H_3PO_4 concentration. The high concentrations, however, resulted in the formation of polyolefinic tars which coated the catalyst and reduced its activity (McMahon et al., 1963). The dehydration of the orthophosphoric acid also yields a series of acids of variable P_2O_5 content (Jameson, 1959). The rapid deactivation is therefore expected. The lower initial activity of Run 3 compared with Run 2 is expected, since, due to the shorter "drying" period, the initial H_3PO_4 concentration is lower.
A comparison between Runs 4 and 6 indicates that despite the 64 hour "drying" period (Run 6), once rehydrated, it appears as though the expected H_3PO_4 concentration was re-established completely.

Run 5 indicates, as expected, that at the higher hydration level (lower H_3PO_4 concentration level) the activity of the catalyst was lowered.

Comparing the product spectra of Run 1 with Run 3 it would be expected that if the differences between the spectra were due solely to the conversion levels then the product spectra would be quite similar from about 8 hours on stream until the end of the Runs. Despite the fact that the product concentrations are still changing during this period it appears that the product spectra are becoming quite similar.

3.4.4 Propene Oligomerization Experiments

The primary function of the propene oligomerization studies was to obtain intrinsic kinetic data that could be used, in the first instance, to develop a rate equation relating the rate of disappearance (by reaction) of propene to its reactor concentration, the reactor temperature and the phosphoric acid (H_3PO_4) concentration and in the second instance to develop a kinetic model which would relate the rate of production of the primary products to the propene reactor concentration, the reactor temperature and the H_3PO_4 concentration.

For these purposes kinetic data were obtained at various:

1. propene reactor concentrations;
2. temperatures; and
3. H_3PO_4 concentrations.

For each set of experiments the following results are reported here either in tabular or graphical form:

1. Rate of propene disappearance versus its reactor concentration and, at each propene concentration, the reactor concentrations of the products (grouped according to carbon chain length).

2. Plots of the rate of propene disappearance versus either its reactor concentration, the reactor temperature or the H_3PO_4 acid strength.

3. A plot of the product reactor concentration versus the propene reactor concentrations.

In this section only the raw data are shown either in tabular or graphical form. The workup and modeling of the data is described in Section 3.5.

3.4.4.1 The effect of propene concentration at 103% H_3PO_4 concentration

Several experiments were carried out by varying the propene feed concentration and maintaining all other conditions constant. The conditions used are listed in Table 3.13

Table 3.13 Experimental conditions used to determine the effect of varying propene concentration.

Phosphoric acid catalyst:		
	mass, g	6.00
	size, microns	106-180
	H_3PO_4 concentration, %	103
Feed:		
	type	propane/propene
	flowrate, g/hr	38-41
	WHSV, h^{-1}	6.3-6.8
Reactor:		
	temperature, K	464
	catalyst bed temperature, K	464
	temperature outside bed, K	464
	pressure, MPa	1.53 (abs)
	impeller speed, rpm	2000

The inlet feed concentration was varied by diluting with propane. The mass balances on propane indicated that under the reaction conditions

used in these experiments there was very little or no alkylation or propene hydrogenation and hence these reactions may be ignored. It is possible that good propane balances were the result of equal amounts of alkylation and propene hydrogenation. However this is extremely unlikely given the wide set of concentration ratios of propene and propane used.

Runs with a 5% mass loss or more were discarded. Of the results used the average mass loss was 3.4% with a minimum of 0.8% and a maximum of 4.8%. Table 3.14 lists the rate of propene disappearance and product concentrations as functions of the propene reactor concentrations.

Table 3.14 Internal recycle reactor: product reactor concentrations and rate of propene reaction as functions of propene reactor concs at 103% H_3PO_4.

	Propene reactor concs, [mole·l^{-1}]x10^3								
	382	354	299	191	251	273	171	369	289
Feed flowrate, g/hr	40.6	39.1	39.9	38.1	41.1	38.7	38.1	38.1	37.7
Fraction of propene in feed, mass%	98.6	93.6	79.4	54.1	68.1	73.7	48.2	99.1	80.8
Propene conversion, mass%	26.4	29.4	24.8	26.9	25.3	26.2	25.7	28.3	29.4
Mean residence time, hrs	.44	.46	.45	.48	.44	.46	.48	.47	.48
Reaction rate [mole/hr/g_{cat}]x10^2	4.2	4.3	3.1	2.2	2.8	3.0	1.9	4.2	3.5
Product concentrations [mole·l^{-1}]x10^3									
Butenes	0.0	0.0	0.0	0.0	0.0	0.0	0.0	0.0	0.0
Pentenes	0.0	0.0	0.0	0.0	0.0	0.0	0.0	0.0	0.0
Hexenes	4.6	4.2	3.1	1.9	2.2	2.9	1.4	4.3	4.1
Heptenes	0.6	0.6	0.5	0.3	0.4	0.5	0.3	0.5	0.4
Octenes	1.2	1.2	0.9	0.5	0.7	0.8	0.4	1.1	1.1
Nonenes	25.0	26.7	17.6	10.8	14.6	18.7	10.3	27.3	21.6
Decenes	0.9	0.9	0.7	0.8	0.8	0.7	0.6	0.9	0.8
Un-decenes	1.1	1.0	0.8	0.5	0.7	0.7	0.5	1.1	0.9
Do-decenes	8.9	10.5	6.8	5.7	6.2	6.0	4.0	9.5	7.7
Tri-decenes	0.0	0.1	0.1	0.2	0.1	0.0	0.1	0.2	0.2
Tetra-decenes	0.1	0.1	0.0	0.2	0.1	0.1	0.1	0.1	0.1
Penta-decenes	0.8	0.9	0.6	0.5	0.5	0.5	0.5	0.8	0.7

The rate of propene disappearance with respect to its reactor concentration is plotted in Figure 3.34. The order will be examined in detail in Section 3.5. The reactor concentration of the products relative to the reactor concentration of propene are shown in Figure 3.35.

3.4.4.2 The effect of propene concentration at 114% H_3PO_4 concentration

To determine the effect of propene concentration at an H_3PO_4 concentration of 114% and a temperature of 464 K, experiments were carried out in a similar manner to those of Section 3.4.4.1. Experiments performed at these extremely high acid concentrations resulted in less stable performance of the reactor system due to the less stable activity of the catalyst.

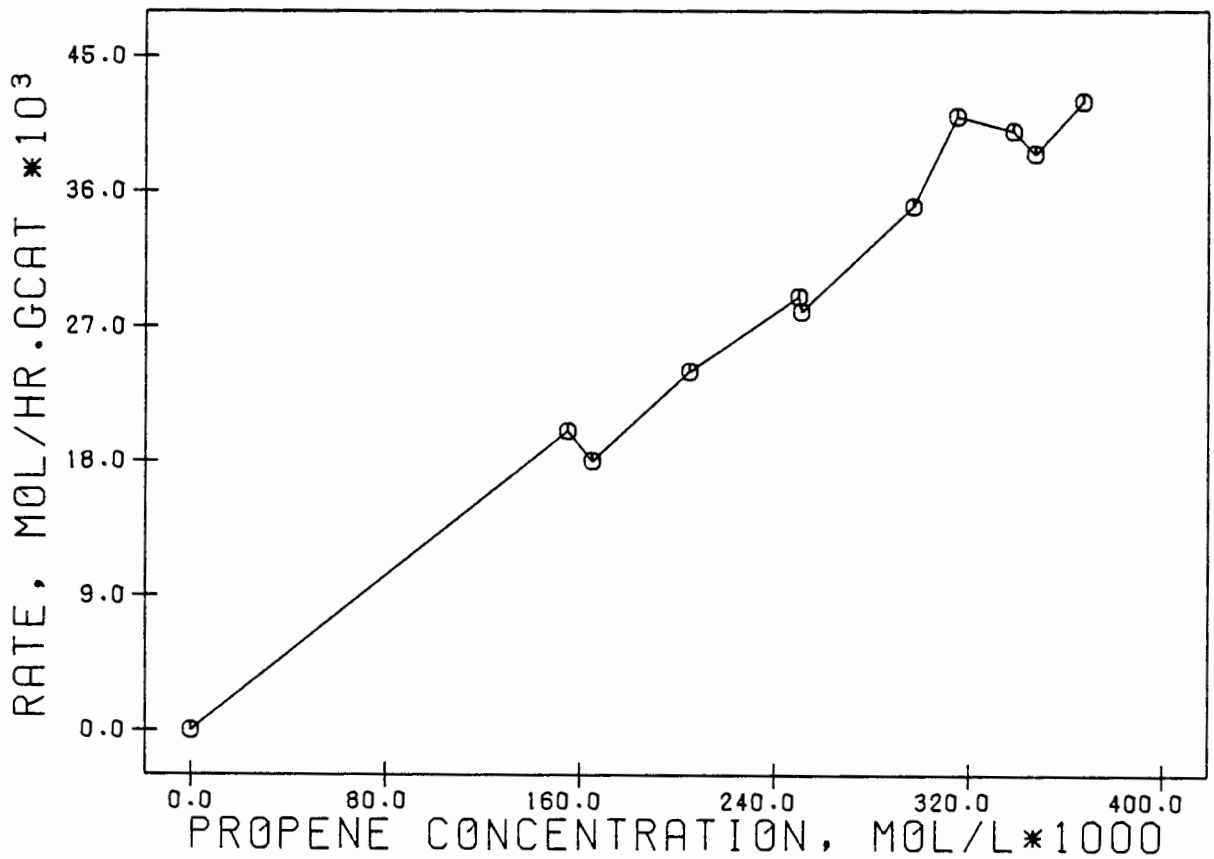

FIG 3.34 RATE OF PROPENE REACTION AS A FUNCTION OF PROPENE REACTOR CONCENTRATION AT 103% H3P04

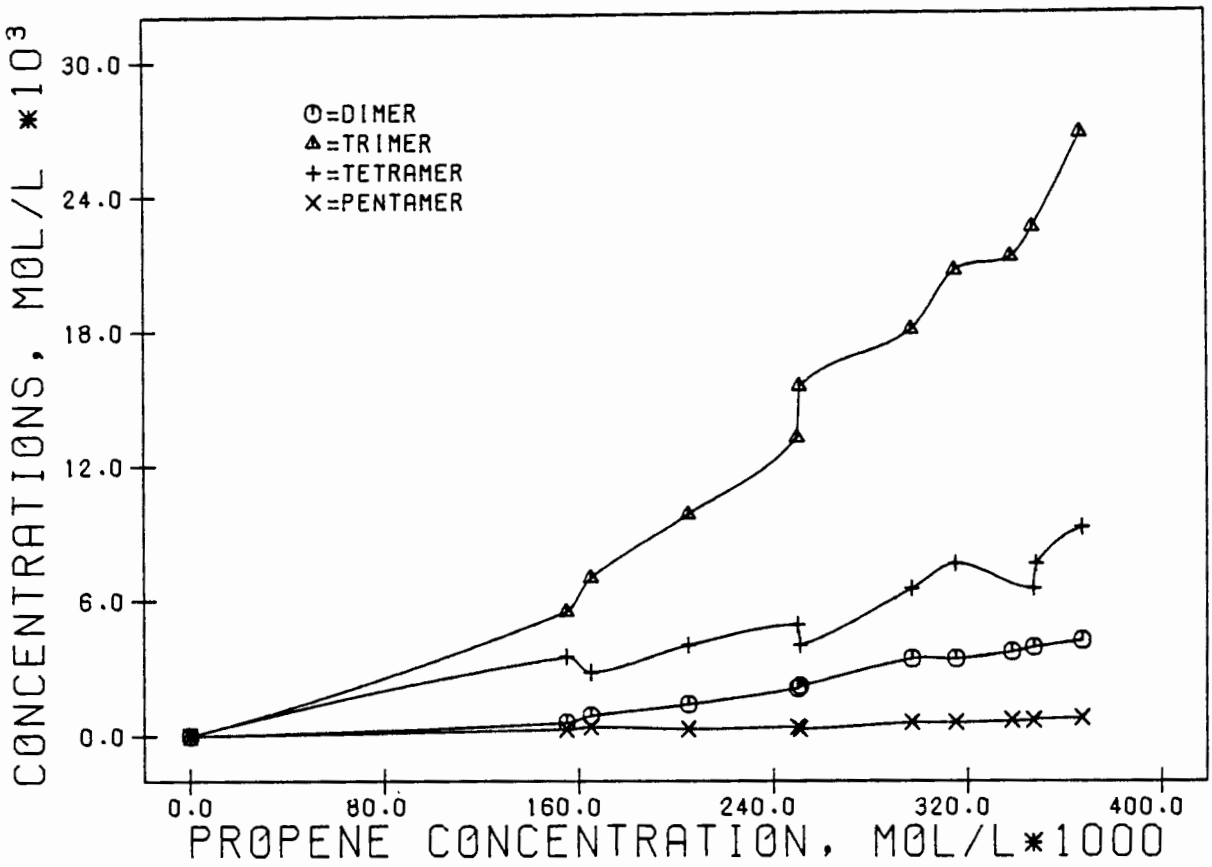

FIG 3.35 PRODUCT CONCENTRATIONS AS FUNCTIONS OF THE PROPENE REACTOR CONCENTRATION AT 103% H_3PO_4

The feed concentration was controlled in a similar manner to that of Section 3.4.4.1. Runs with mass losses of 5.2% or more were discarded. The average mass loss was 3.2% with a maximum of 5.2% and a minimum of 1.2%. The rate of propene reaction and product reactor concentrations are shown as functions of the propene reactor concentration in Table 3.15.

The rate of propene reaction is plotted in Figure 3.36 as a function of the reactor concentration of propene.

The trend in Figure 3.36 is quite similar to that in Figure 3.34. The detailed analysis will be examined in Section 3.5. Figure 3.37 shows the reactor concentrations of the products as functions of the propene reactor concentrations. Note that the rates at these higher H_3PO_4 concentrations are much higher than those at the lower H_3PO_4 concentrations (Figure 3.34).

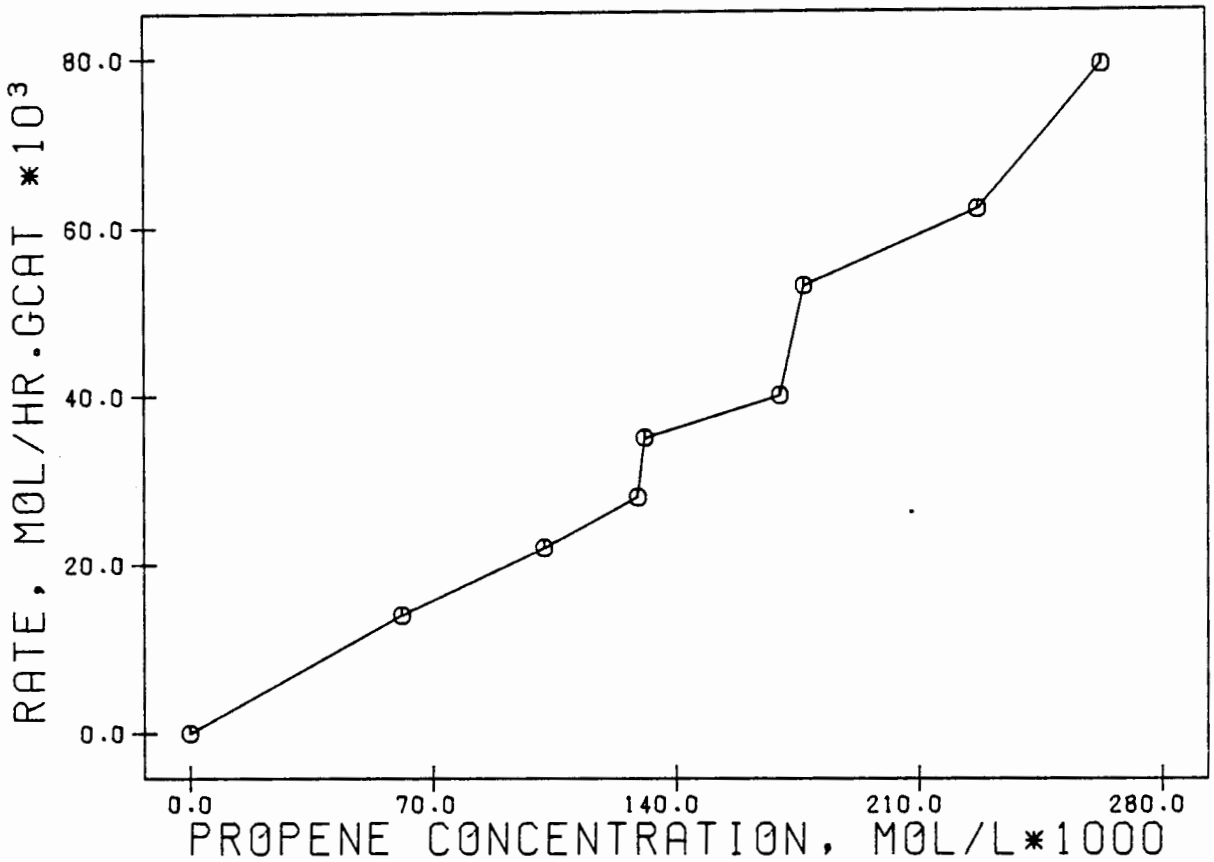

FIG 3.36 RATE OF PROPENE REACTION AS A FUNCTION OF THE PROPENE REACTOR CONCENTRATION AT 114% H3P04

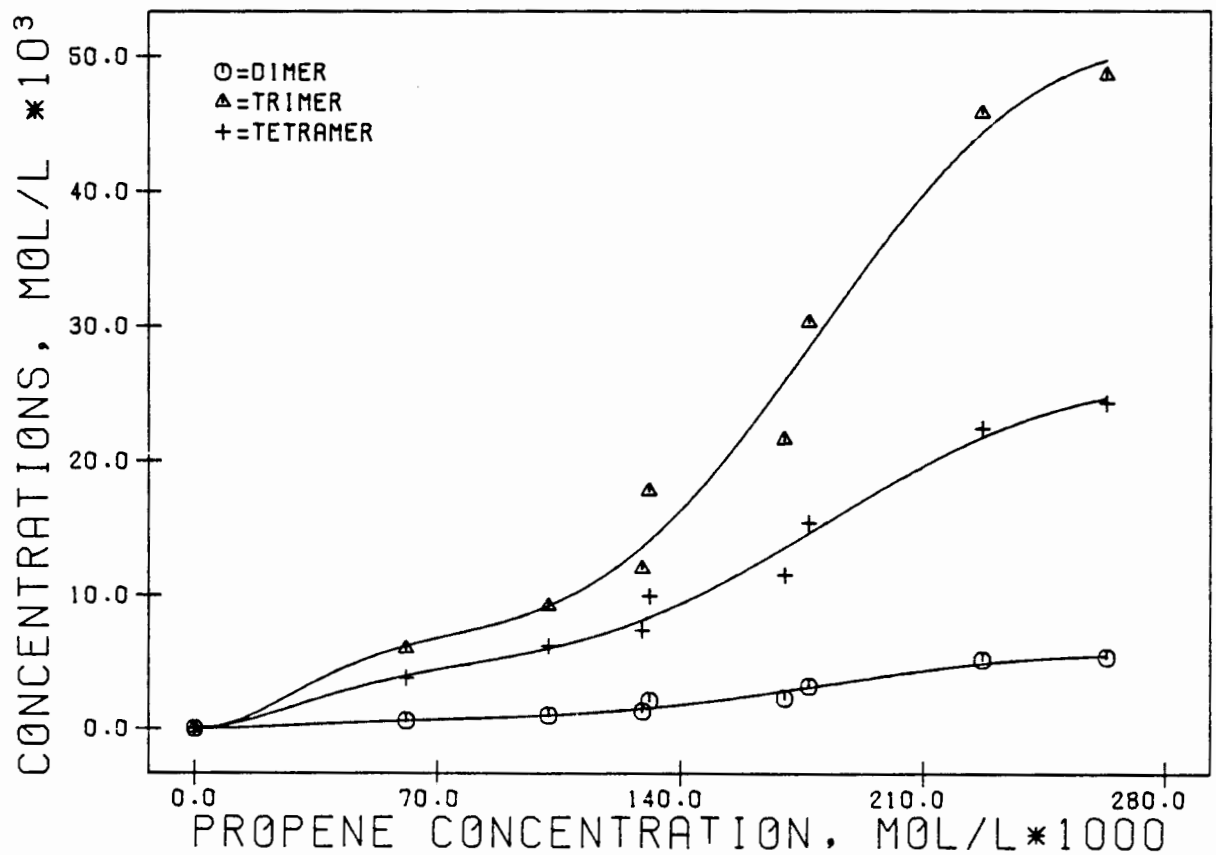

FIG 3.37 PRODUCT CONCENTRATIONS AS FUNCTIONS OF THE PROPENE REACTOR CONCENTRATION AT 114% H3P04

Table 3.15 Internal recycle reactor: product reactor concentrations and rate of propene reaction as functions of the propene reactor concentration at 114% H_3PO_4.

	Propene reactor concs, [mole·l^{-1}]x10^3							
	227	263	177	170	131	129	102	61
Reaction rate, [mole/hr/g_{cat}]x10^2	6.2	7.9	5.3	4.0	3.5	2.8	2.2	1.4
Feed flowrate, g/hr	36.1	44.0	40.6	39.2	39.8	42.4	40.4	40.2
Propene in feed, %	77.8	84.1	63.2	57.1	47.0	42.3	34.4	21.9
Propene conversion, mass%	56	54	52	45	47	39	39	40
Mean residence time, hrs	.50	.41	.44	.46	.46	.43	.45	.46
Product concs, [mole·l^{-1}]x10^3								
Butenes	0.0	0.0	0.0	0.0	0.0	0.0	0.0	0.0
Pentenes	0.0	0.2	0.1	0.1	0.1	0.0	0.0	0.0
Hexenes	5.2	5.4	3.2	2.3	2.1	1.3	1.0	0.6
Heptenes	1.6	1.4	0.8	0.5	0.6	0.4	0.3	0.2
Octenes	3.4	3.5	2.2	1.5	1.3	1.0	0.7	0.4
Nonenes	45.8	48.6	30.3	21.6	17.8	12.0	9.2	6.0
Decenes	3.2	3.5	2.0	1.4	1.2	0.8	0.6	0.4
Un-decenes	3.9	4.0	2.6	1.7	1.4	0.9	0.8	0.5
Do-decenes	22.4	24.3	15.4	11.5	9.9	7.4	6.2	3.8
Tri-decenes	0.6	0.8	0.4	0.4	0.3	0.2	0.2	0.1
Tetra-decenes	0.4	0.5	0.4	0.2	0.2	0.2	0.1	0.1
Penta-decenes	1.9	2.0	1.1	0.9	0.7	0.6	0.4	0.2

3.4.4.3 The effect of temperature at 111% H_3PO_4 concentration

These experiments were conducted at similar conditions to those listed in Table 3.13 but at an ortho-phosphoric acid concentration of 111% and using a pure propene (99%) feed. In a similar manner to Sections 3.4.4.1 and 3.4.4.2, runs with mass losses above 5.2% were discarded. The average mass loss was 3.5% with a maximum of 5.2% and a minimum of 0.7%. The rate of propene disappearance and product reactor concentrations as functions of reactor temperature are shown in Table 3.16.

The rate of propene disappearance is plotted as a function of temperature in Figure 3.38. Examination of the curve indicates that the rate doubles over approximately 50 K. A similar result was found by

Bethea and Karchmer (1956) and Langlois & Walkey (1951) using liquid phosphoric acid and phosphoric acid on quartz respectively.

The reactor concentrations of the products are shown as a function of temperature in Figure 3.39.

Table 3.16 Internal recycle reactor: product reactor concentrations and rate of propene reaction as functions of reactor temperature at 111% H_3PO_4.

	Reactor temperatures, K			
	472	508	486	454
Propene concentration, $[mole \cdot l^{-1}] \times 10^3$	338	281	299	374
Feed flowrate, g/hr	37.1	42.3	40.6	39.8
Propene in feed, %	98.8	98.8	98.8	98.8
Propene conversion, mass%	48.8	65.3	60.4	33.7
Mean residence time, hrs	.48	.42	.44	.45
Reaction rate, $[mole/hr/g_{cat}] \times 10^2$	7.1	10.8	9.6	5.3
Product concentrations, $[mole \cdot l^{-1}] \times 10^3$				
Butenes	0.0	0.0	0.0	0.0
Pentenes	0.0	0.0	0.0	0.0
Hexenes	8.2	17.7	13.7	3.5
Heptenes	2.3	7.5	4.3	0.8
Octenes	3.9	9.1	6.0	1.6
Nonenes	54.7	92.4	78.1	31.4
Decenes	2.9	4.1	4.0	1.9
Un-decenes	3.1	5.9	4.7	1.4
Do-decenes	22.7	30.3	30.1	15.5
Tri-decenes	0.6	1.0	0.6	0.3
Tetra-decenes	0.4	0.8	0.6	0.2
Penta-decenes	1.9	2.0	2.5	1.3

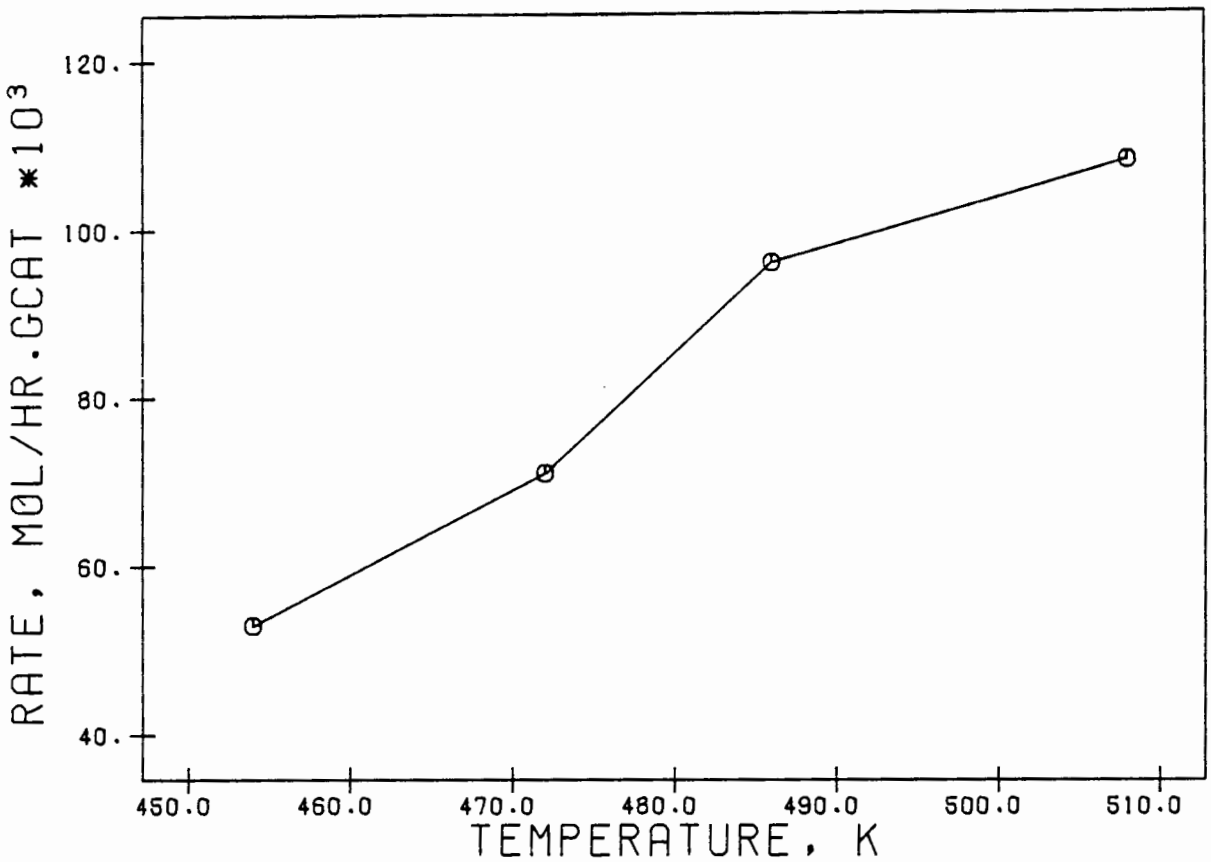

FIG 3.38 RATE OF PROPENE REACTION AS A FUNCTION OF TEMPERATURE AT 111% H3P04

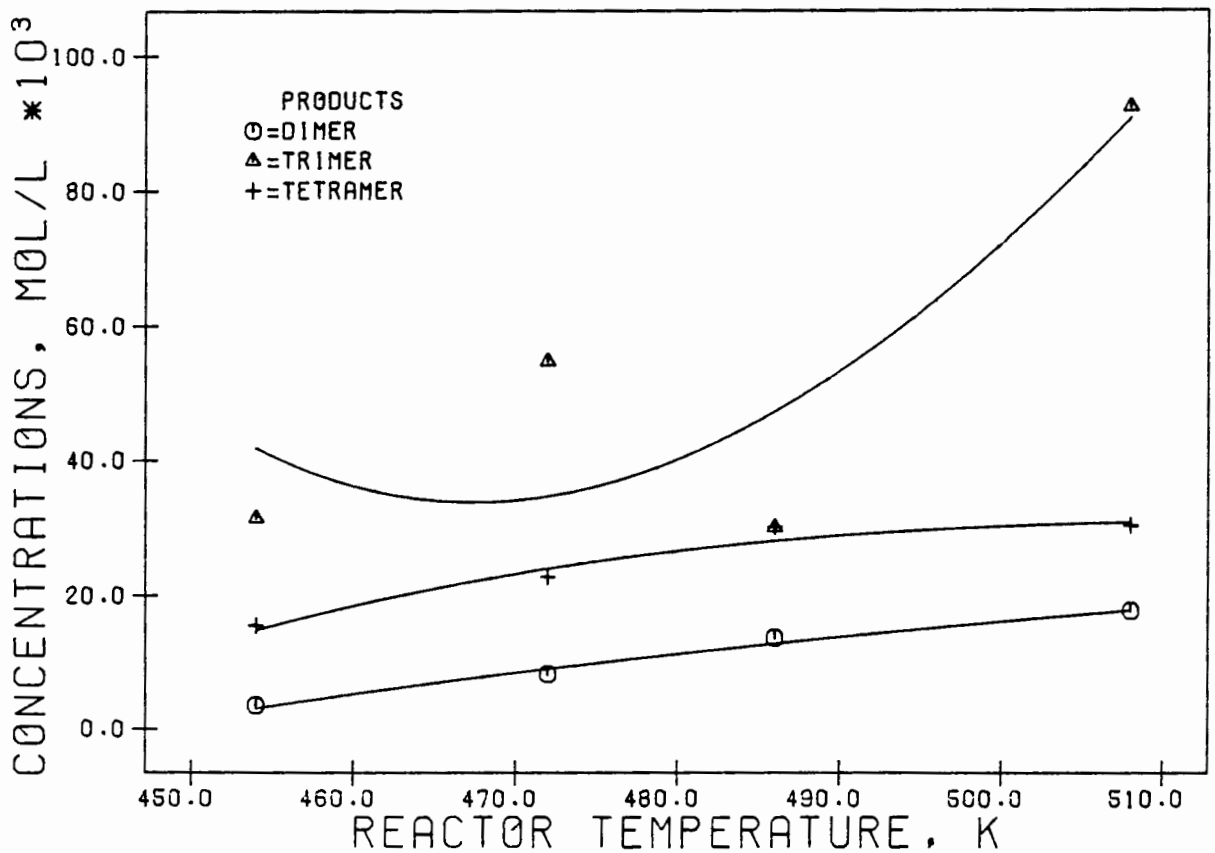

FIG 3.39 PRODUCT CONCENTRATIONS AS FUNCTIONS OF THE REACTOR TEMPERATURE AT 111 % H3P04

3.4.4.4 The effect of temperature at 102% H_3PO_4

A similar set of experiments was conducted to those in Section 3.4.4.3 but at an H_3PO_4 concentration of 102%. A pure propene feed (99%) was used. No run had a mass loss of greater than 3.9%. The average mass loss was 1.2% with a minimum of 0%. The rate of propene disappearance and product reactor concentrations as functions of reactor temperature are listed in Table 3.17.

Table 3.17 Internal recycle reactor: product reactor concentration and rate of propene disappearance as functions of reactor temperature at 102% H_3PO_4.

	Reactor temperature, K			
	464	473	453	443
Propene concs, $[mole \cdot l^{-1}] \times 10^3$	371	371	381	390
Reaction rate, $[mole/hr/g_{cat}] \times 10^2$	3.8	4.2	3.4	2.9
Feed flowrate, g/hr	36.1	36.8	37.6	35.9
Propene in feed, mass%	99.2	99.1	99.1	99.1
Propene conversion, %	27.7	27.2	26.3	23.0
Mean residence time, hrs	.49	.47	.48	.47
Product concs, $[mole \cdot l^{-1}] \times 10^3$				
Butenes	0.0	0.0	0.0	0.0
Pentenes	0.0	0.0	0.0	0.0
Hexenes	4.2	4.9	2.9	1.6
Heptenes	0.5	0.6	0.3	0.2
Octenes	1.0	1.1	0.7	0.4
Nonenes	27.5	26.3	22.0	18.8
Decenes	0.8	0.7	0.7	0.6
Un-decenes	1.1	0.9	0.6	0.7
Do-decenes	9.0	7.6	7.8	7.3
Tri-decenes	0.1	0.1	0.1	0.1
Tetra-decenes	0.1	0.1	0.0	0.1
Penta-decenes	0.7	0.6	0.6	0.6

Similar plots to those in Figures 3.38 and 3.39 are shown in Figures 3.40 and 3.41. The relationship between the rate of propene disappearance and reactor temperature in Figure 3.40 can be seen to be very similar to that in Figure 3.38 with a forecasted doubling in the rate over a temperature rise of 50 K.

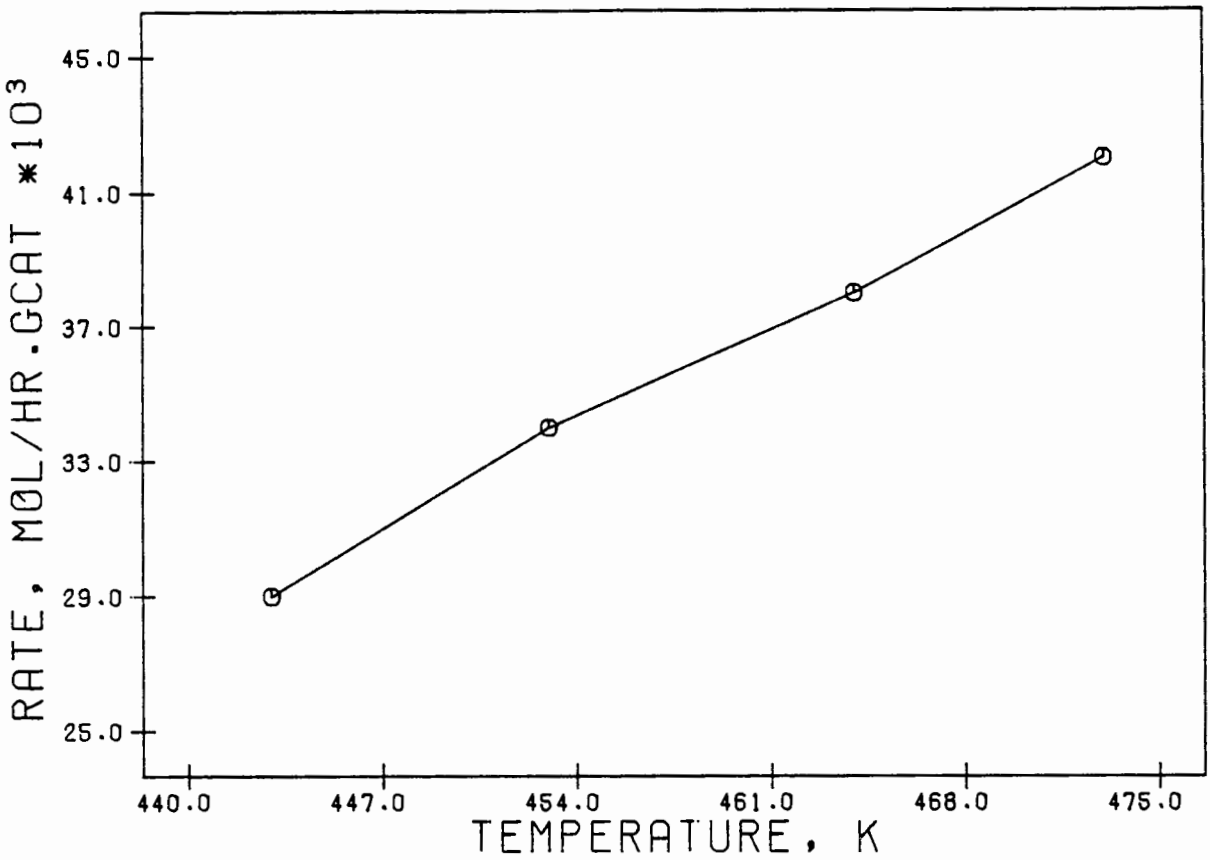

FIG 3.40 RATE OF PROPENE REACTION AS A FUNCTION OF TEMPERATURE AT 102 % H3P04

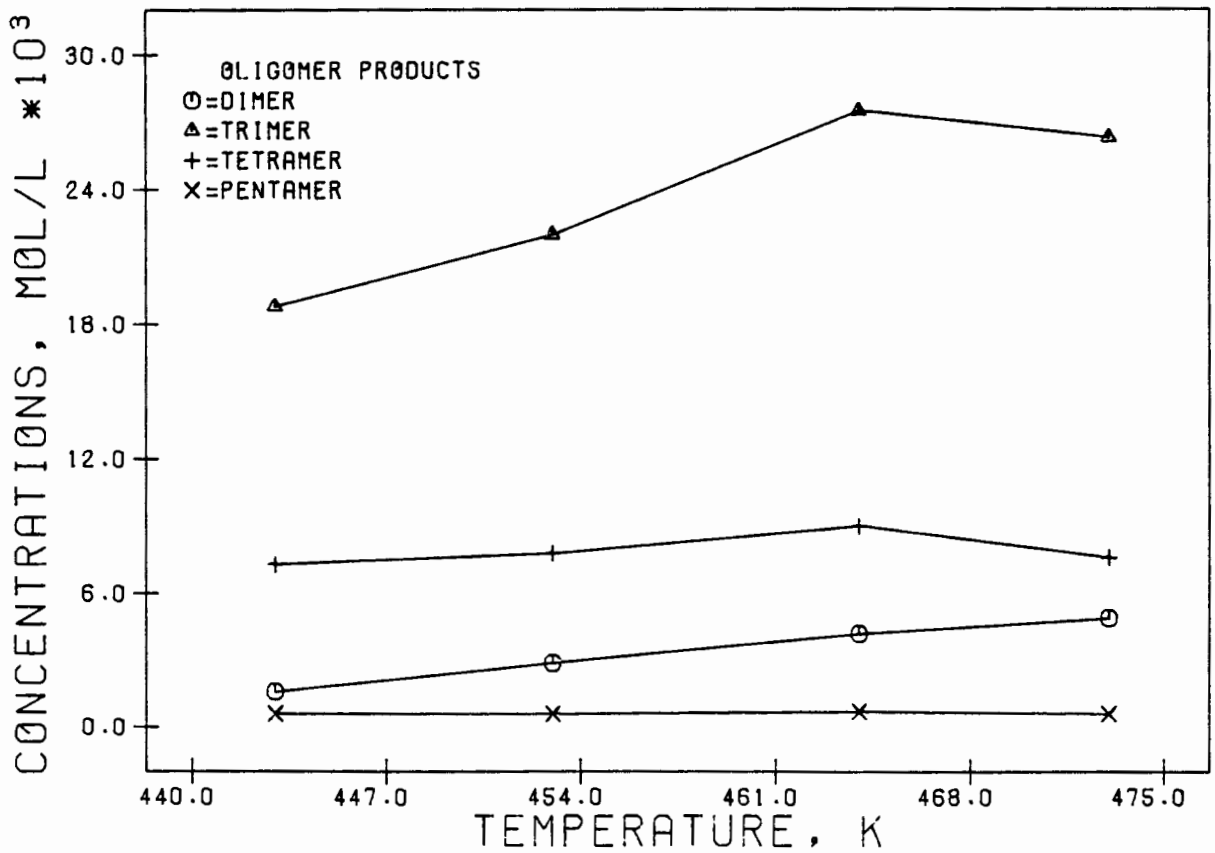

FIG 3.41 PROPENE PRODUCT CONCENTRATIONS AS FUNCTIONS OF REACTOR TEMPERATURE AT 102% H3P04

3.4.4.5 The effect of ortho-phosphoric acid (H_3PO_4) concentration using a pure propene feed.

Similar experiments to those carried out in Section 3.4.4.5 were carried out at 464 K but with a pure propene feed and covering a much wider range of H_3PO_4 concentrations. The average mass loss over a five run series was 1.3% with a minimum of 0.8% and a maximum of 5.0%. The results are tabulated and plotted in an identical manner (Table 3.18 and Figures 3.42 and 3.43) to those of Section 3.4.4.5.

Table 3.18 Internal recycle reactor: product concentrations, propene concentrations and reaction rate as functions of H_3PO_4 concentration for a pure propene feed.

	H_3PO_4 concentration, %				
	104.5	106.4	107	102	103
Propene concentration, [mole·l^{-1}]x10^3	357	355	347	371	368
Reaction rate, [mole/hr/g_{cat}]x10^2	4.9	5.5	5.8	3.5	4.0
Feed flowrate, g/hr	36.0	37.7	36.7	36.1	37.8
Propene in feed, mass%	99.1	99.7	99.7	99.1	99.1
Propene conversion, %	34.0	36.4	39.4	28.2	29.3
Mean residence time, hrs	.49	.47	.48	.49	.47
Product concentrations, [mole·l^{-1}x10^3]					
Butenes	0.0	0.0	0.0	0.0	0.0
Pentenes	0.0	0.0	0.0	0.0	0.0
Hexenes	4.9	5.6	5.4	4.1	4.2
Heptenes	0.8	0.9	1.1	0.5	0.5
Octenes	1.5	1.7	2.0	1.0	1.1
Nonenes	31.3	34.5	38.5	27.4	27.6
Decenes	1.5	1.6	2.0	0.8	1.0
Un-decenes	1.8	2.0	1.8	1.1	1.3
Do-decenes	12.1	13.4	15.6	9.0	9.7
Tri-decenes	0.2	0.3	0.3	0.1	0.2
Tetra-decenes	0.2	0.2	0.2	0.1	0.1
Penta-decenes	1.1	1.2	1.2	0.7	0.9

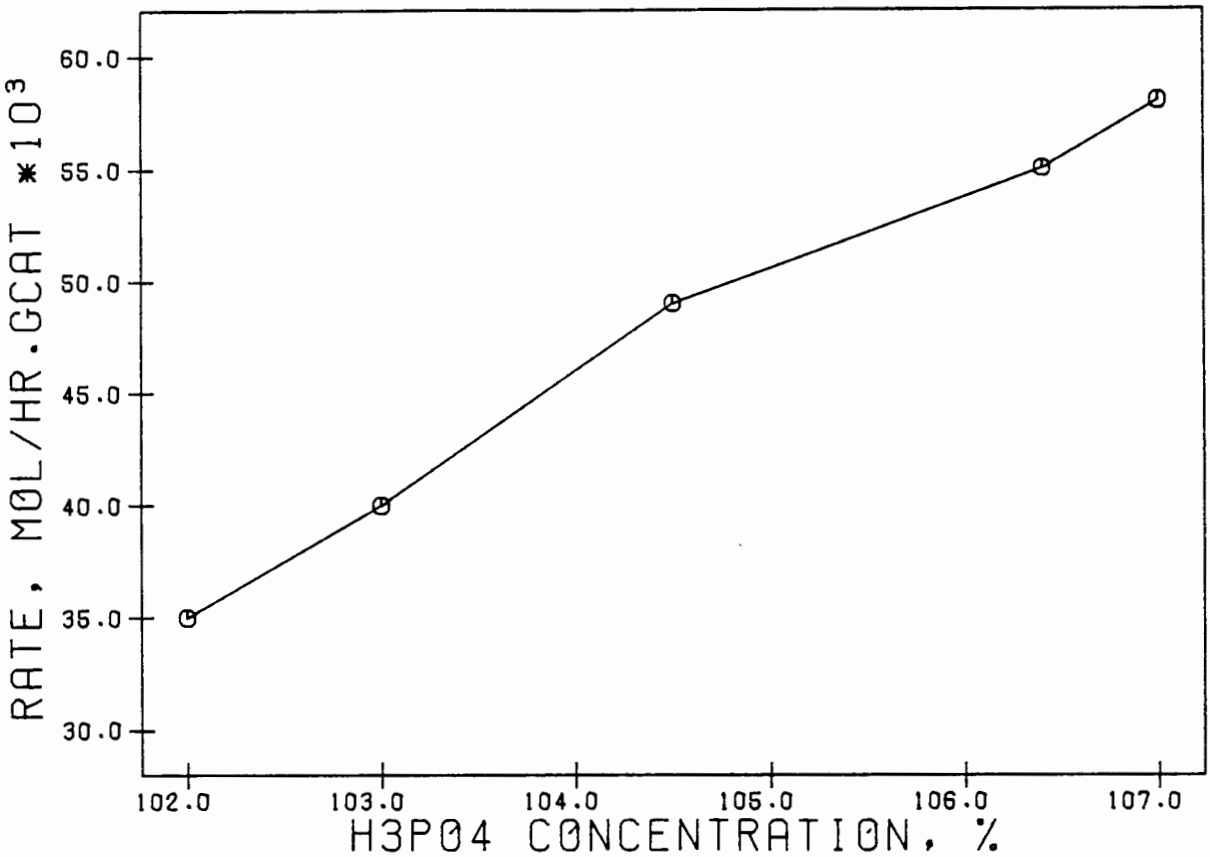

FIG 3.42 RATE OF PROPENE REACTION AS A FUNCTION OF H3P04 CONCENTRATION FOR A PURE PROPENE FEED

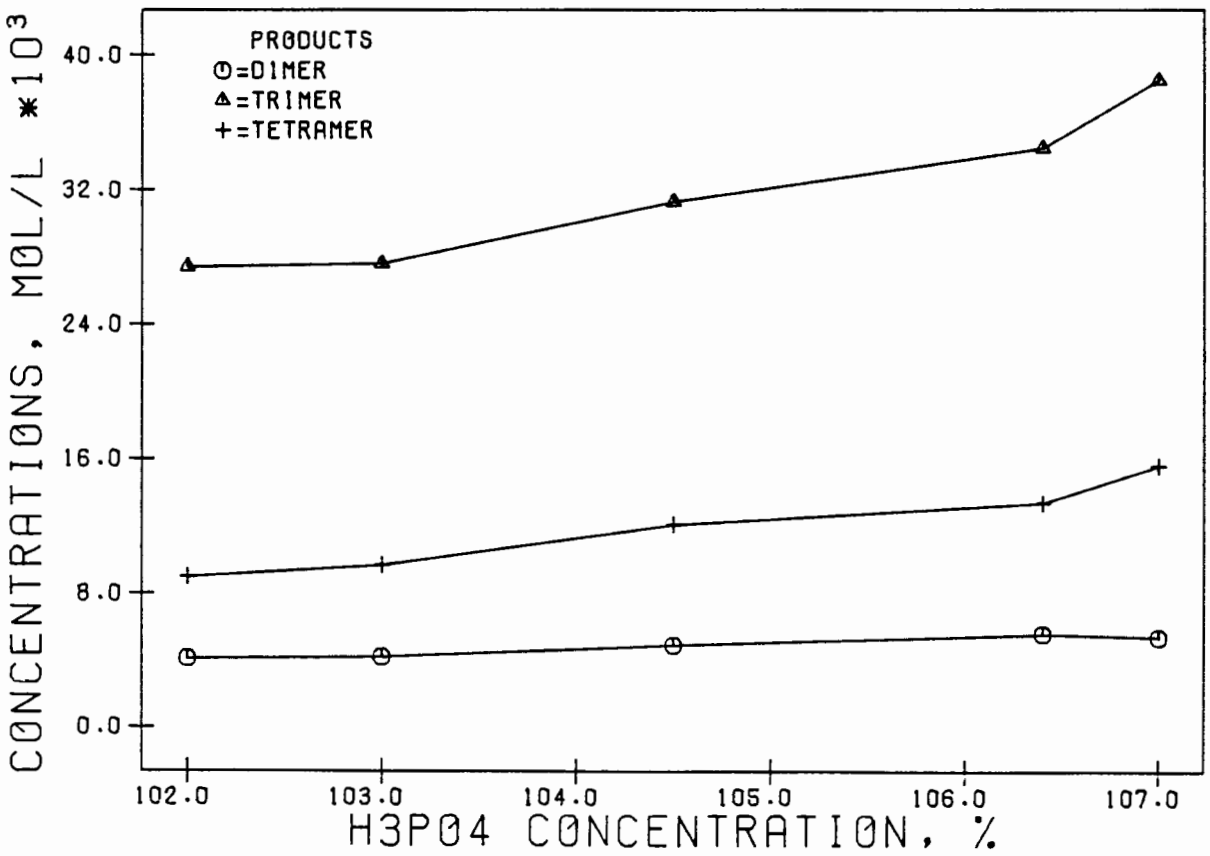

FIG 3.43 PROPENE PRODUCT CONCENTRATIONS AS FUNCTIONS OF H3P04 CONCENTRATION FOR A PURE PROPENE FEED

3.4.4.6 Low conversion experiments

Two experiments were carried out at low conversions primarily to examine the effect of conversion on liquid fuel composition. The experiments were carried out by varying the mass of catalyst. A comparison between the data obtained is listed in Table 3.19. There were some variations in the acid strengths between these experiments with the acid strength varying between 102.5% and 104%. The results depicted in Table 3.22 have been adjusted to the same acid strength equivalent of 104%. Figure 3.44 shows a comparison between the major oligomer fractions of each experiment as functions of the degree of conversion.

Table 3.19 Product spectra, reaction rate and propene concentration as functions of propene conversion.

	Propene conversion, %		
	5.0	13.7	32.0
Catalyst mass, g	1.0	3.0	6.0
Propene conc, $[mole \cdot l^{-1}] \times 10^3$	372	367	360
Reaction rate, $[mole/hr/gcat] \times 10^2$	4.9	4.6	4.7
Product concs, $[mole \cdot l^{-1}] \times 10^3$			
Butenes	0.0	0.0	0.0
Pentenes	0.0	0.0	0.0
Hexenes	0.3	2.0	4.7
Heptenes	0.0	0.2	0.7
Octenes	0.0	0.4	1.3
Nonenes	3.7	12.1	30.2
Decenes	0.1	0.3	1.3
Un-decenes	0.2	0.6	1.6
Do-decenes	1.5	3.6	11.0
Tri-decenes	0.0	0.0	0.2
Tetra-decenes	0.0	0.0	0.2
Penta-decenes	0.1	0.3	0.9

3.4.5 1-Butene Oligomerization Experiments

The primary function of these experiments was similar to that of the propene experiments, namely, to develop a rate equation relating the rate of reaction of 1-butene to process variables and to develop a kinetic model which would relate the rate of reaction of 1-butene and the rate of production of products to process variables.

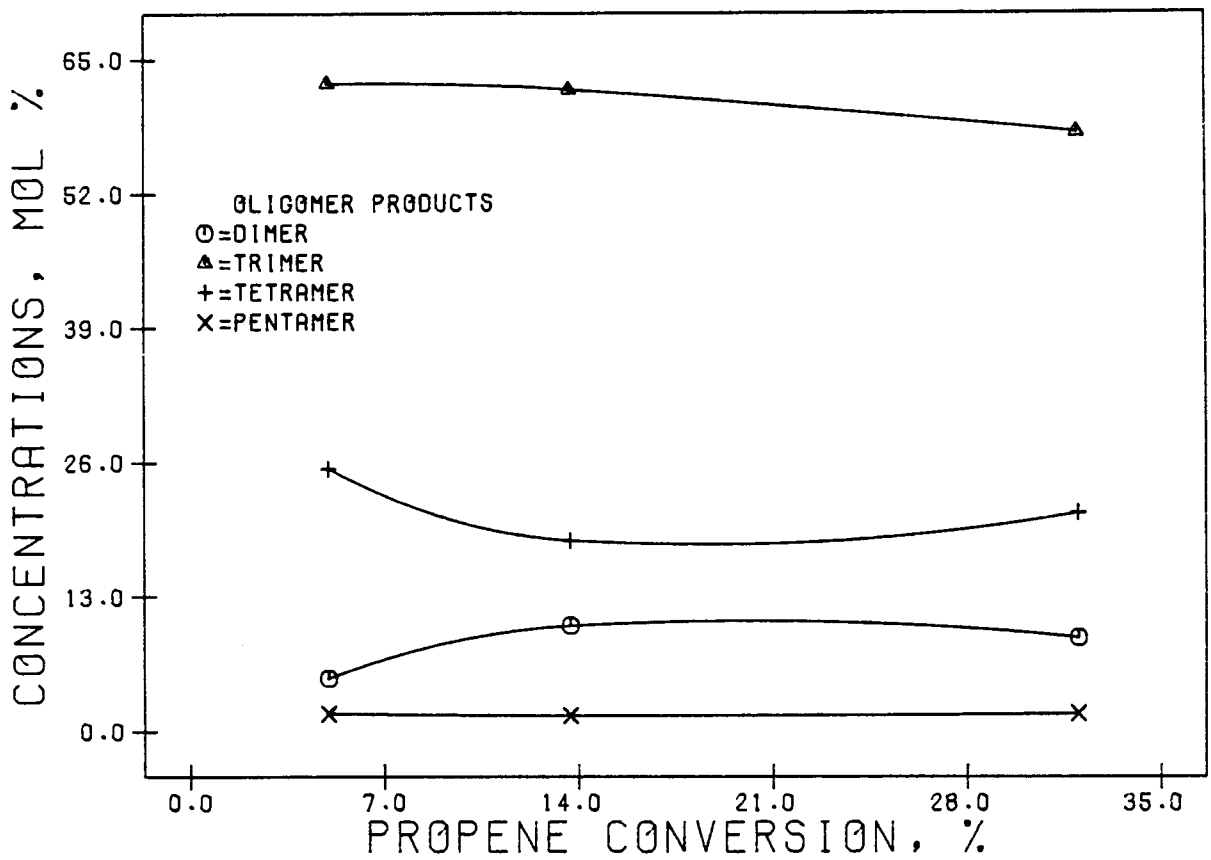

FIG 3.44 THE EFFECT OF CONVERSION ON PRODUCT DISTRIBUTION FOR A PURE PROPENE FEED

The following sets of data were obtained:

1. Rate-concentration data at different 1-butene concentrations.
2. Rate-concentration data at different temperatures.
3. Rate-concentration data at several H_3PO_4 concentrations.

The raw data are reported in the following form:

1. Tables of either 1-butene concentrations, temperatures or acid concentrations as functions of product concentrations and rates of reaction of 1-butene.

2. Plots of the rate of 1-butene reaction as a function of either 1-butene reactor concentrations, reactor temperatures or acid concentrations.

3. Plots of product reactor concentrations versus either 1-butene reactor concentrations, reactor temperatures or acid concentrations.

Only the data in its raw form will be presented in this section. Analysis and modeling of the data will be described in Section 3.5.

The non-variable experimental conditions used throughout these experiments are listed in Table 3.20.

Table 3.20 Conditions used for the oligomerization of 1-butene.

Phosphoric acid catalyst:		
	mass, g	6.00
	size, microns	106-180
Feed:		
	composition	propane/1-butene
	flowrate, $g \cdot hr^{-1}$	38-42
	WHSV, hr^{-1}	6.3-7.0
Reactor:		
	pressure, MPa	1.53
	impeller speed, rpm	2000

In a similar manner to the propene experiments, feed concentration was controlled by diluting with propane. Propane balances were good, indicating little or no alkylation. No 1-butene hydrogenataion was observed from GC analysis.

In general, product chain length was shorter than that of propene and hence there was even less condensation in the magnedrive shaft. The solubility of the monomer was significantly higher than that of propene, and hence greater care had to be taken with the product analysis to ensure accurate determination of the dissolved gas content.

3.4.5.1 The effect of 1-butene concentration

Experiments were carried out by varying the 1-butene concentration (by diluting the feed with propane) and maintaining all other process conditions constant. The temperature was maintained at 464 K and the acid concentration at 103%. The average mass loss was 1.7% with a maximum of 3.3% and a minimum of 0.4%. Table 3.21 lists the rate of 1-butene reaction and the product concentrations as functions of the 1-butene reactor concentration. In the product concentrations of Table 3.21 the concentration of any propane or propene (resulting from

Table 3.21 Internal recycle reactor: product reactor concentrations and rate of 1-butene reaction as functions of 1-butene concentrations.

	1-Butene reactor concs, [mole•l^{-1}]x10^3						
	115	375	225	122	378	229	162
Reaction rate, [mole/hr/g_{cat}]x10^2	1.7	5.6	4.7	1.8	5.9	3.8	2.6
Feed flowrate, g/hr	37.1	38.0	40.8	38.5	38.7	38.0	38.6
1-butene in feed, mass%	41.3	99.1	76.0	43.5	99.8	73.6	56.0
1-butene conversion, %	36.6	49.8	50.9	36.9	51.0	45.2	40.7
Mean residence time, hrs	.60	.70	.60	.58	.69	.64	.60
Product concentrations, [mole•l^{-1}]x10^3							
Pentenes	0.0	0.0	0.0	0.0	0.0	0.0	0.0
Hexenes	0.4	3.0	2.2	0.4	3.2	2.4	0.9
Heptenes	0.3	2.6	2.0	0.4	2.7	1.8	8.6
Octenes	21.0	130	79.4	23.9	134	62.3	36.0
Nonenes	1.4	6.4	3.8	1.3	6.8	3.4	2.1
Decenes	0.9	4.3	3.0	0.9	4.6	2.4	1.5
Un-decenes	0.7	2.6	1.8	0.5	2.7	1.4	0.8
Do-decenes	4.7	21.2	13.4	4.6	24.3	11.3	7.0
Tri-decenes	0.0	0.0	0.0	0.0	0.0	0.0	0.1
Tetra-decenes	0.0	0.0	0.0	0.0	0.4	0.0	0.0
Penta-decenes	0.0	0.4	0.3	0.0	0.0	0.1	0.0
Hexa-decenes	0.4	1.7	1.3	0.5	1.7	1.4	0.9

cracking) is not reported since these peaks on the chromatograph would be swamped by the large propane peaks present in most cases. Figure 3.45 shows the rate of 1-butene reaction as a function of the reactor concentration of 1-butene. The reaction order will be examined in detail in Section 3.5. The reactor concentration of the products relative to the 1-butene concentration are shown in Figure 3.46. A comparison between Figures 3.46 and 3.43 highlights the lower boiling polymer of the 1-butene.

3.4.5.2 The effect of temperature

To examine the effect of temperature, experiments were carried out at similar conditions to those listed in Section 3.4.5.1 but using a pure

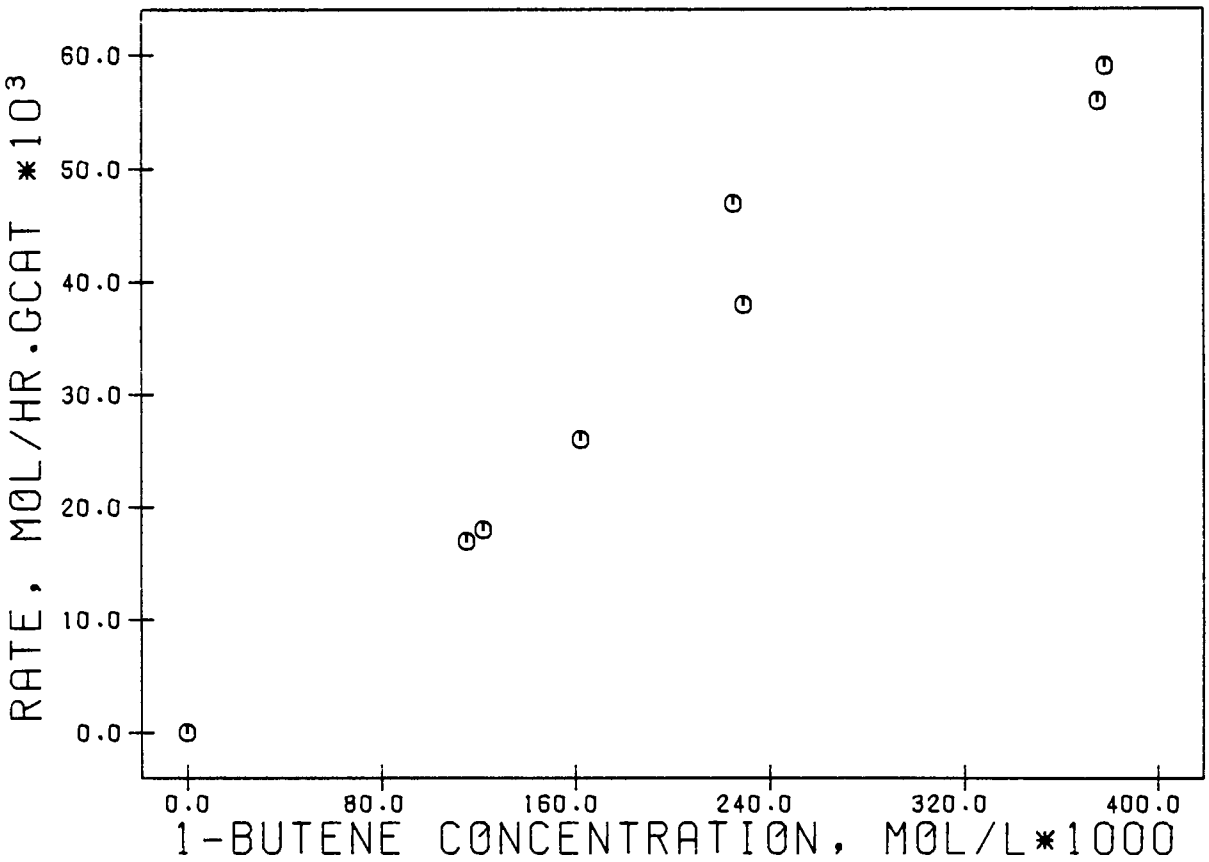

FIG 3.45 RATE OF 1-BUTENE REACTION AS A FUNCTION OF THE 1-BUTENE REACTOR CONCENTRATION

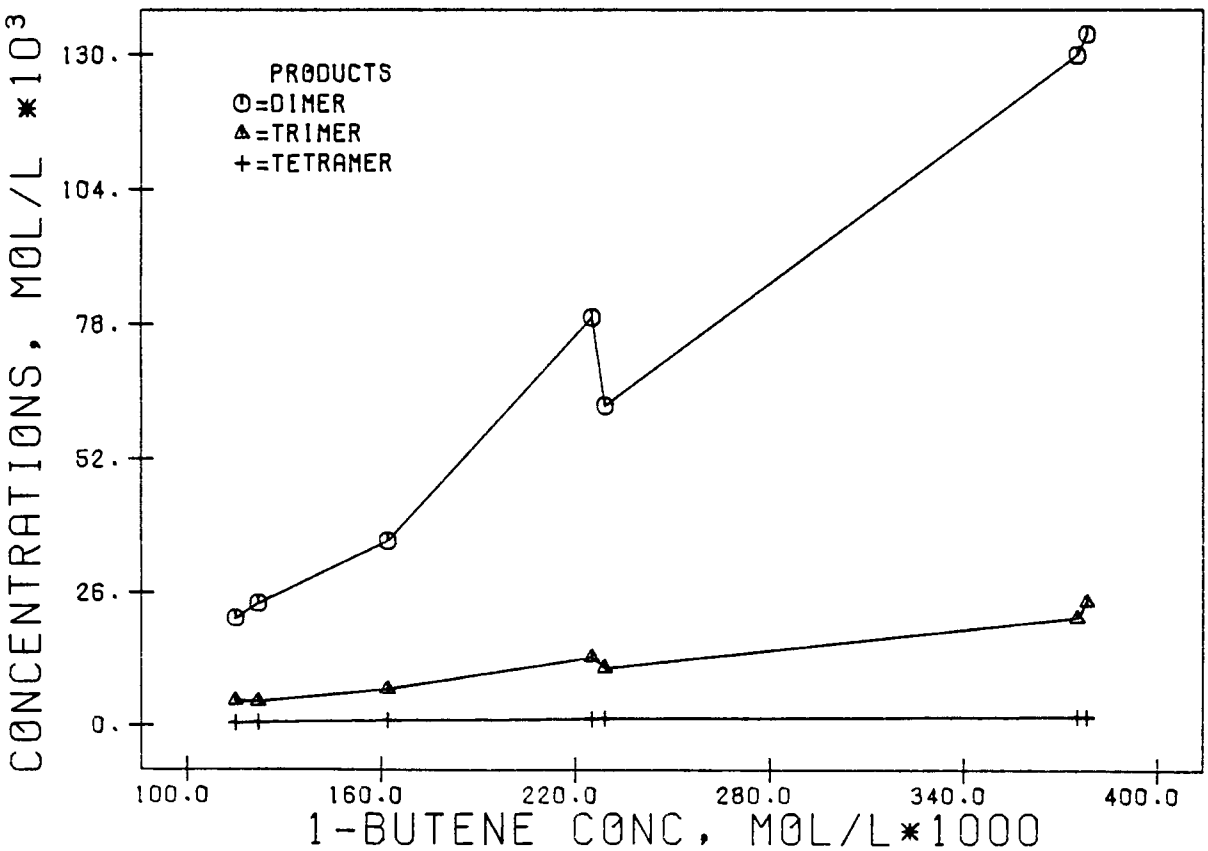

FIG 3.46 PRODUCT CONCENTRATIONS AS FUNCTIONS OF THE 1-BUTENE REACTOR CONCENTRATION

1-butene feed (99%), an acid concentration of 103% and varying the temperature over a 40 K range. The average mass loss was 2.7% with a maximum of 5.1% and a minimum of 0.3%. The rate of 1-butene reaction and product reactor concentrations are shown as functions of reactor temperature in Table 3.22.

Table 3.22 Internal recycle reactor: Product reactor concentrations, 1-butene reactor concentrations and reaction rates as functions of reactor temperature.

	Reactor temperature, K				
	465	424	433	454	447
1-butene concentration, [mole·l^{-1}]x10^{3}	375	455	446	411	423
Feed flowrate, g/hr	38.0	40.7	38.9	40.7	39.8
1-butene in feed, mass%	99.1	99.3	99.3	99.3	99.3
1-butene conversion, %	49.8	13.0	18.8	37.7	29.4
Mean residence time, hrs	.70	.65	.68	.65	.67
Reaction rate, [mole/hr/g_{cat}]x10^{2}	5.6	1.6	2.2	4.4	3.7
Product concentrations, [mole·l^{-1}]x10^{3}					
Pentenes	0.0	0.0	0.0	0.0	0.0
Hexenes	2.9	0.2	0.26	1.2	0.9
Heptenes	2.5	0.3	0.4	1.5	1.1
Octenes	130	21.1	32.7	85.1	76.0
Nonenes	6.4	1.1	2.0	4.3	3.7
Decenes	4.3	0.9	1.5	2.8	2.5
Un-decenes	2.6	0.5	0.8	1.6	1.5
Do-decenes	21.3	5.4	7.7	13.5	12.4
Tri-decenes	0.0	0.0	0.0	0.0	0.0
Tetra-decenes	0.0	0.0	0.0	0.0	0.0
Penta-decenes	0.4	0.1	0.1	0.0	0.0
Hexa-decenes	1.7	0.5	0.7	1.2	1.0

The rate of 1-butene disappearance is plotted as a function of temperature in Figure 3.47. The reactor concentrations of the products are shown as a function of temperature in Figure 3.48.

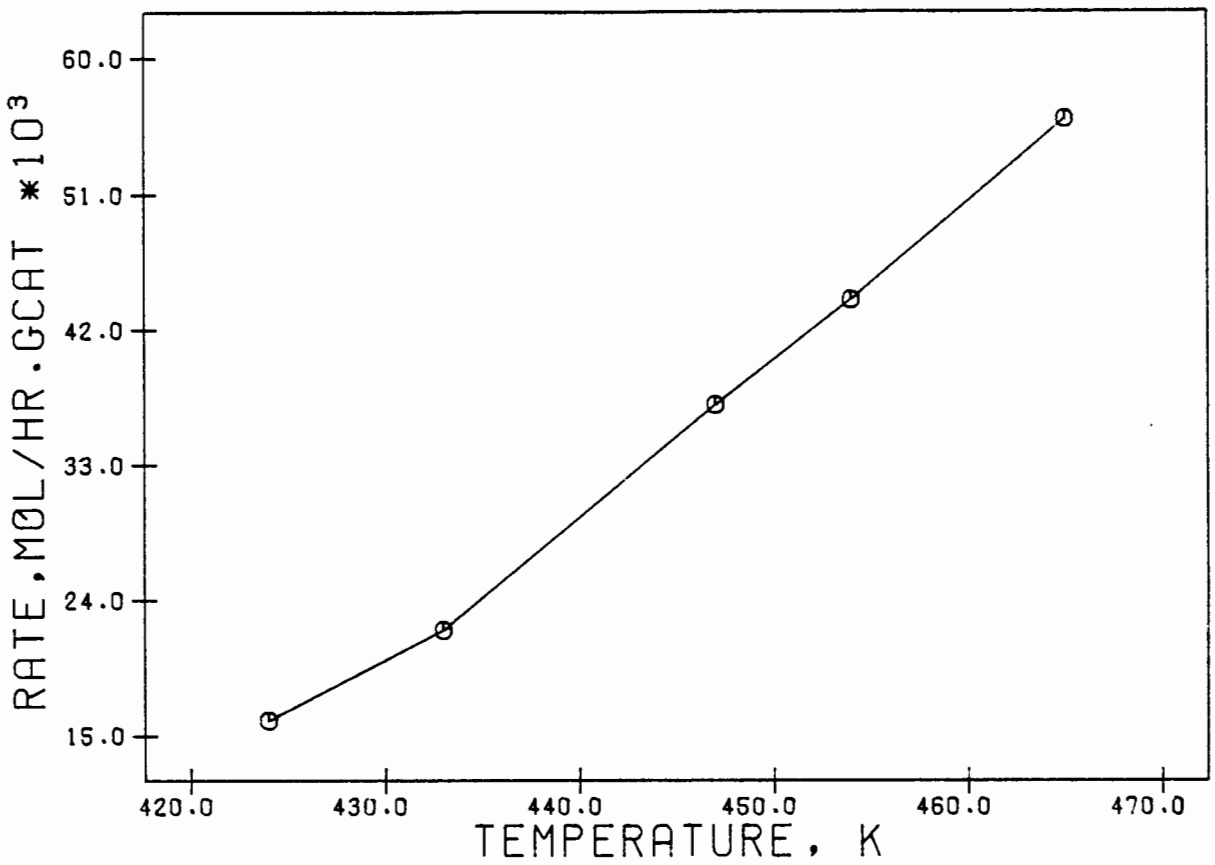

FIG 3.47 RATE OF 1-BUTENE REACTION AS A FUNCTION OF TEMPERATURE AT 103% H3P04

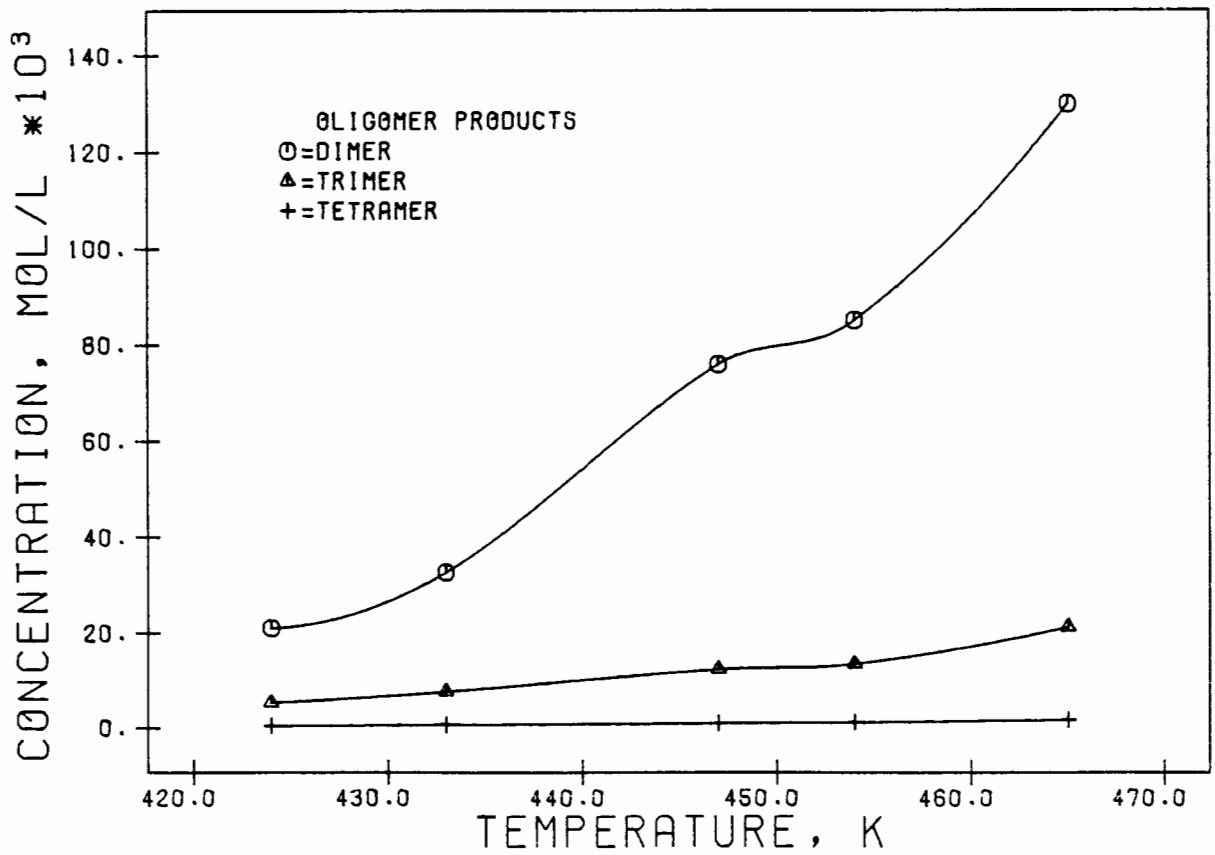

FIG 3.48 PRODUCT CONCENTRATIONS AS FUNCTIONS OF THE REACTOR TEMPERATURE

3.4.5.3 The effect of acid concentration

Several experiments were carried out over a range of H_3PO_4 concentrations using a pure 1-butene feed. The experiments were carried out at the conditions listed in Table 3.20. A temperature of 446.5 K was used. The average mass loss was 3.3% with a maximum of 3.7% and a minimum of 3.0%. The results are shown in Table 3.23.

Table 3.23 Internal recycle reactor: product concentrations, reaction rates and 1-butene concentrations as functions of H_3PO_4 concentration.

	H_3PO_4 concentration, %			
	106	102	103	104
1-Butene concentration, [mole·l^{-1}] x10^3	394	432	423	392
Reaction rate, [mole/hr/g_{cat}] x10^2	5.3	3.4	3.7	4.4
Feed flowrate, g/hr	39.4	40.0	39.8	39.4
1-butene in feed, mass%	99.8	99.8	99.3	99.4
1-butene conversion, %	45.5	28.8	29.4	34.8
Mean residence time, hrs	.67	.67	.67	.67
Product concentrations, [mole·l^{-1}] x10^3				
Pentenes	0.0	0.0	0.0	0.0
Hexenes	2.1	0.6	0.9	1.3
Heptenes	2.1	0.8	1.1	1.5
Octenes	115	61.6	76.0	94.0
Nonenes	6.0	2.7	3.7	4.6
Decenes	3.9	1.7	2.5	2.9
Un-decenes	2.1	1.0	1.5	1.6
Do-decenes	17.0	10.2	12.4	14.6
Tri-decenes	0.2	0.2	0.0	0.0
Tetra-decenes	0.2	0.1	0.0	0.0
Penta-decenes	0.0	0.0	0.0	0.0
Hexa-decenes	2.5	1.2	1.0	1.8

The rate of disappearance of 1-butene as a function of H_3PO_4 acid concentration is shown in Figure 3.49. The product concentrations are shown as functions of the H_3PO_4 concentration in Figure 3.50. A

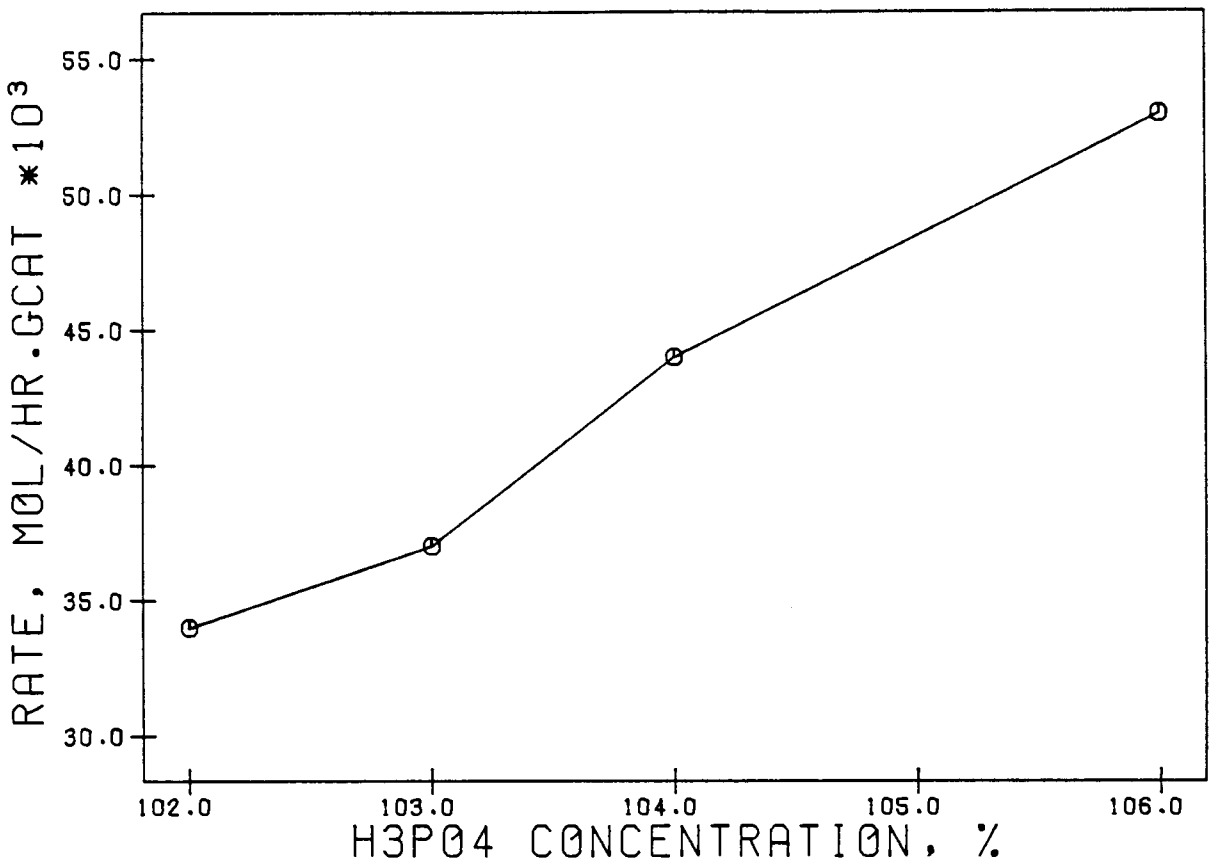

FIG 3.49 RATE OF 1-BUTENE REACTION AS A FUNCTION OF OF H3P04 CONCENTRATION AT 446.5 K

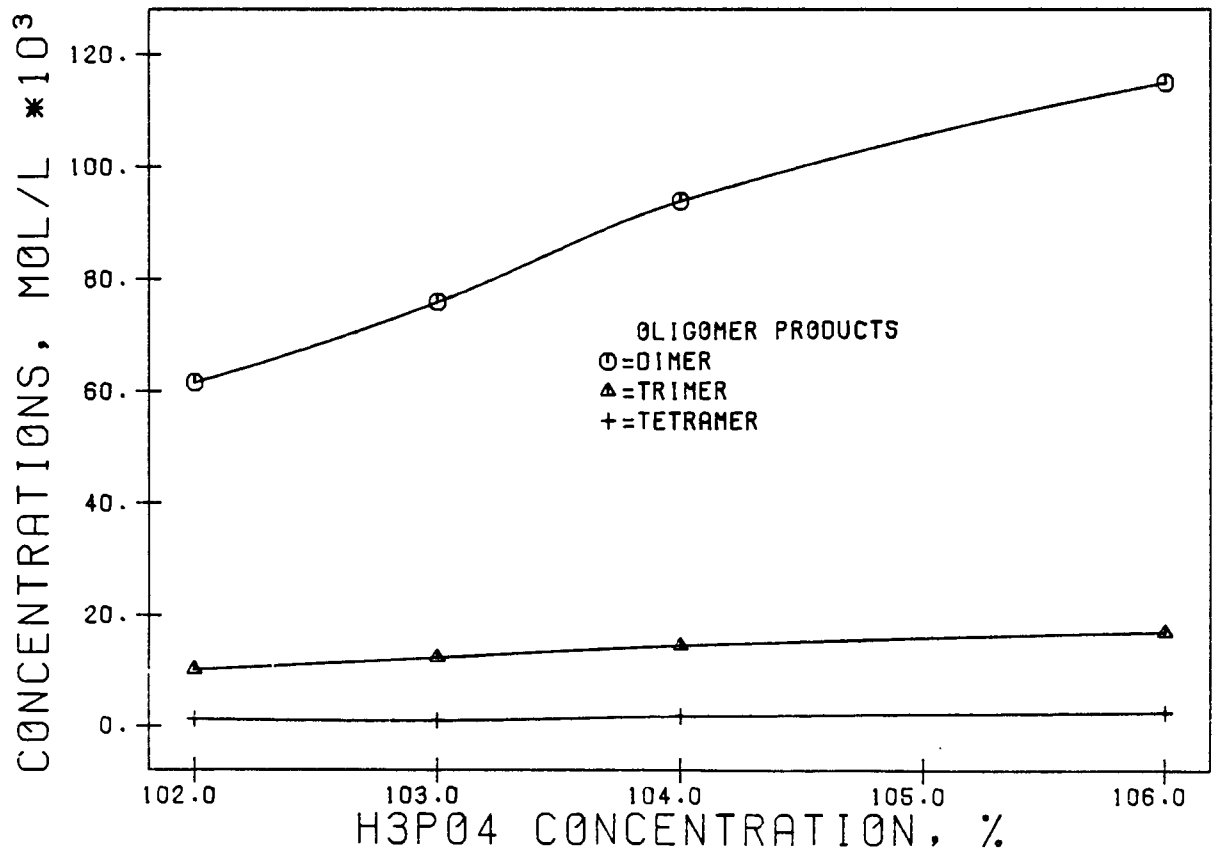

FIG 3.50 PRODUCT CONCENTRATIONS AS FUNCTIONS OF THE H3P04 CONCENTRATION

comparison between Figures 3.42 and 3.50 shows that the rates of reaction of 1-butene and propene have similar dependencies on the ortho-phosphoric acid concentration. Run times were long enough to obtain steady state but not long enough for the catalyst to start deactivating.

3.4.6 The Oligomerization of Iso-Butene

It was originally intended to study the kinetics of the oligomerization of iso-butene in a similar manner to that of propene and 1-butene. However, due to the extremely high reactivity of the iso-butene over phosphoric acid at the experimental conditions of interest, extremely small quantities of catalyst had to be used to provide conversion levels that could be regarded as reasonable for kinetic studies. As a result two additional problems arose. Firstly due to the very small mass of catalyst, reproducibility problems became significant not only due to the problems of some catalyst spillage (despite the fact that the catalyst was dispersed amongst 300 μm glass beads) but also due to the difficulty in obtaining a consistently representative sample. The second problem was the catalyst lifetime, when compared to the other feeds was dramatically reduced. This was not unexpected since the total liquid production per gram of catalyst was of the order expected, viz., it is possible that the high reactivity of the iso-butene could have resulted in the rapid formation of long chain polyolefinic tars which could have coated the catalyst and hence resulted in its deactivation.

It was clear from the results that were obtained that reliable kinetic data for the iso-butene/phosphoric acid system could not be obtained under these conditions. It was therefore decided not to examine the kinetics of the oligomerization of iso-butene. The results of a single experiment are shown below. The reaction rate is estimated at about 2.0 $mole \cdot hr^{-1} \cdot g_{cat}$ (rate of iso-butene reaction) at the conditions listed below. (This is an estimate of the rate during the first few hours of the reaction.) This is approximately 50 to 70 times higher than that of propene and 1-butene at these conditions.

The typical product spectra of an experimental run is listed in Table 3.24. The conditions used for the experiment were similar to those listed in Table 3.20 with the following changes:

feed:	99% iso-butene
catalyst mass:	0.1g
reactor temperature:	413 K
acid concentration:	108%

The run was stopped after seven hours on stream after the conversion of iso-butene had dropped from 31% to 20%. It was found that the product spectra did not change significantly over this period despite the loss of activity. The product spectra are listed in Table 3.24 and are shown graphically in the form of a bar chart in Figure 3.51.

Table 3.24 Internal recycle reactor: iso-butene product spectra.

	Product carbon chain length											
	C_5	C_6	C_7	C_8	C_9	C_{10}	C_{11}	C_{12}	C_{13}	C_{14}	C_{15}	C_{16}
Mass fraction, %	0	0	0	76.9	0	0	0	22.0	0	0	0	1.1

3.4.7 The Oligomerization of 1-Hexene

A single experiment was carried out using pure 1-hexene as the feed. The purpose of the experiment was to obtain an indication of the products obtained and the rate of reaction of the 1-hexene. Due to the high boiling point of the mixture at 15.3 atmospheres control of the water concentration in the feed and hence the H_3PO_4 concentration was difficult. The conditions used are similar to those listed in Table 3.20 but with a reaction temperature of 465 K and an estimated H_3PO_4

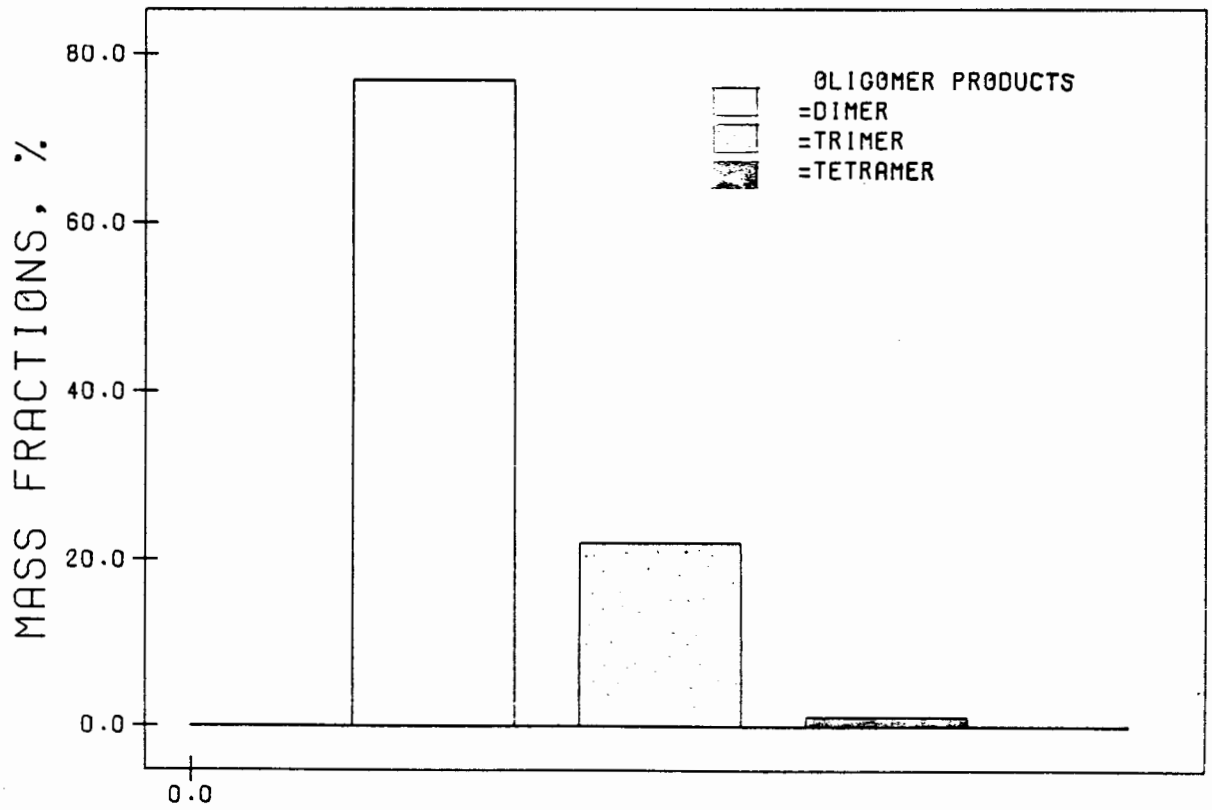

FIG 3.51 TYPICAL PRODUCT SPECTRA FROM ISO-BUTENE OLIGOMERIZATION OVER SOLID PHOSPHORIC ACID

concentration of 108%. The 1-hexene conversion, reaction rate, concentration and product concentrations are listed in Table 3.25.

Table 3.25 Internal recycle reactor: 1-hexene product spectra and reaction rate.

Reaction rate, [mole/hr^{-1}/gcat^{-1}]x10^{2}	1.0
1-Hexene concentration, [mole•l^{-1}]x10^{3}	397
1-Hexene conversion, %	11
Product fractions, mole%	
Propene	8.0
Butenes	4.0
Pentenes	9.6
Heptenes	10.3
Octenes	2.0
Nonenes	2.7
Decenes	4.0
Un-decenes	2.2
Do-decenes	57.3

Due to the onset of catalyst deactivation, the experiment was terminated after 5.4 hours and the variation in product spectra was slight. The product concentrations are shown graphically in Figure 3.52.

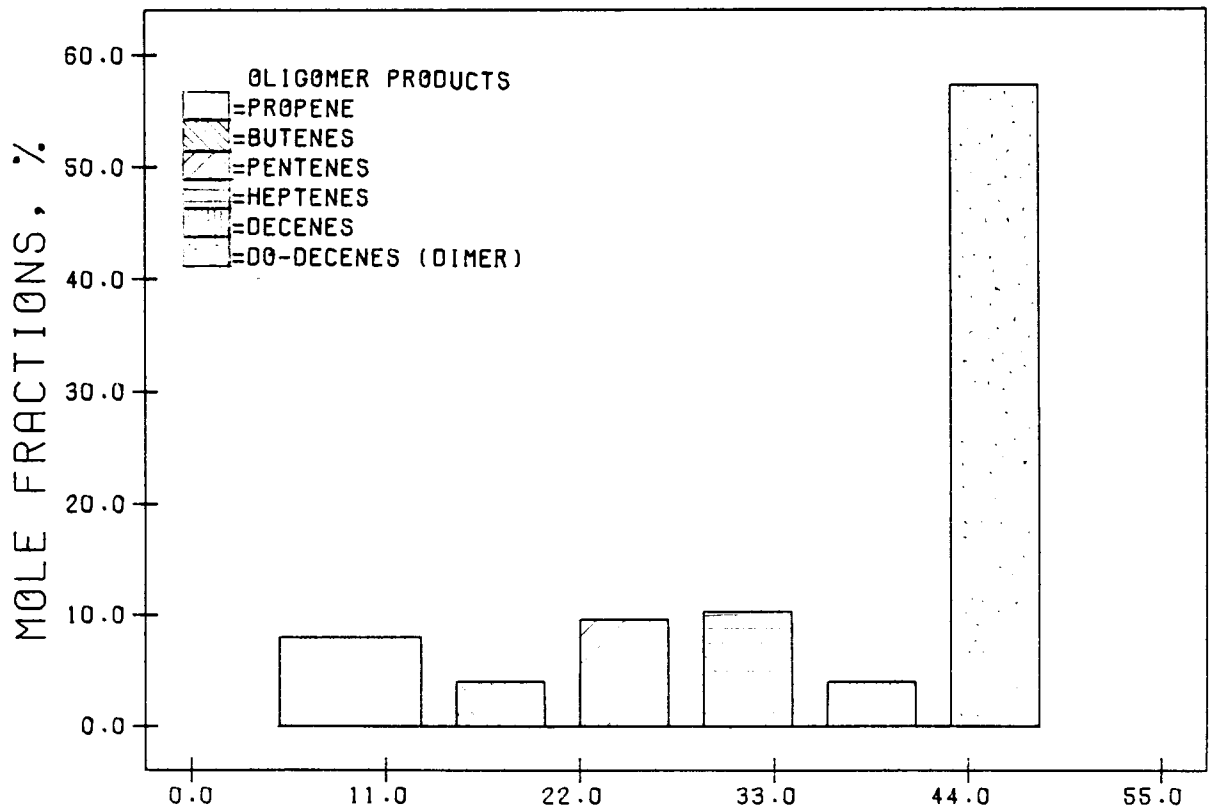

FIG 3.52 TYPICAL PRODUCT SPECTRA FROM 1-HEXENE OLIGOMERIZATION OVER SOLID PHOSPHORIC ACID

3.5 DISCUSSION

The results of the residence time distribution studies together with the mass transfer studies indicate that mass and heat transfer limitations can be significantly reduced using the internal gas recirculation reactor and that good CSTR performance can be obtained in this reactor. The bulk of the kinetic studies were performed in operating regions where good CSTR performance and good mass and heat transfer rates (relative to the rate of reaction) were found to occur.

The modeling of the kinetic data will be carried out in this section from two points of view. The first is the development of a simple rate equation relating rate of monomer reaction to monomer concentration, reaction temperature and H_3PO_4 concentration. The second is the development of more complex rate equations relating, not only the rate of monomer reaction, but also the rate of formation of the oligomeric products to the monomer concentration in the reactor. The results will be discussed in the following order:

1. Residence time distribution studies
2. Mass transfer studies
3. General qualitative findings
4. Simple power law modeling of the rate of monomer reaction
5. Modeling of the rate of monomer reaction and the rate of product formation
6. The choice of the best models and their usefulness.

3.5.1 The Residence Time Distribution Studies

These studies, which were developed to indicate whether the reactor system could achieve ideal CSTR status under relatively ideal conditions, have shown that the reactor is quite capable of behaving as an ideal CSTR under a wide range of conditions. Firstly it was shown that the reactor approaches ideal CSTR behaviour at impeller speeds of between 600-1200 rpm at room temperature, N_2 feed flowrate of $0.98cm^3/s$ and atmospheric pressure. The recycle ratio at 600 rpm is equal to approximately 20. (The flowrate through the catalyst bed is determined by using the Leva pressure drop equation to estimate the superficial gas velocity through the bed, as is done in section 3.4.1.2). It was also shown, however, at room temperature, atmospheric pressure, 2400 rpm and a nitrogen flowrate of $26.7cm^3/s$ that ideal CSTR behavior was obtained. This set of operating conditions corresponds to a recycle ratio of approximately 15. It would

appear, therefore, that the minimum recycle ratio required for perfect mixing would fall within the range of 15 to 25. This is in reasonable agreement with minimum recycle ratios found by Berty (1974), Li et al. (1980) and Carberry (1964).

3.5.2 Mass Transfer Studies

3.5.2.1 Mass Transfer Studies Using Napthalene

It was pointed out in section 3.1.1 that, of the possible temperature and concentration effects that could influence the oligomerization reaction, if intra-particular and interphase mass and heat transport effects could be shown to be minimal, then all other mass and heat transport effects could be assumed to be negligible. It was also noted that, if interphase mass transfer was negligible, then interphase heat transfer would probably be negligible as well. For these reasons it was decided to determine the regions in which intra-particular and interphase mass transport was negligible. The mass transfer experiments using napthalene sublimation were carried out to confirm the results obtained by Caldwell (1983a). The results showed good agreement with those of Caldwell. It was found that the mass transfer coefficient varied linearly with stirrer speed and the mass transfer coefficient dropped with increasing pressure (in the range 1-5 bar).

A likely explanation for the linear variation of kc with impeller speed is that the flow through the bed is largely laminar. Equation (4) used by Caldwell is as follows:

$$k_c \propto S_c^{-2/3} \left[\frac{\phi \epsilon^3}{1-\epsilon} \times \frac{d_p}{L} \right]^{0.5} \times N \times r$$

where k_c = mass transfer coefficient
S_c = Schmidt number
ϕ = shape factor
ϵ = bed voidage fraction
d_p = particle diameter
L = bed depth
N = impeller speed
r = radial distance

This equation is obtained by combining Hougen's equation for low Reynolds number (laminar) with the Blake-Kozeny equation (Hougen, 1961). This

equation is applicable only for laminar flow and shows that $k_c \propto N$ in this region.

The drop in k_c with increasing pressure has two possible explanations. In the laminar region based on the above equation, k_c is independent of pressure (the Schmidt number has little dependence on pressure). However, in the turbulent region the mass transfer coefficient decreases with an increase in pressure. It was suggested above (at atmospheric pressure) that the flow here is laminar (since $k_c \propto$ impeller speed). As the pressure is increased so too does the gas density (while the head generated is not changing) and so the mass flowrate increases. It is possible that the k_c versus impeller speed experiments were carried out at the upper end of the laminar region. If this is so then as the pressure is increased the flow drifts into the more turbulent region. With this shift the resistance to flow would gradually change from linear to quadratic relationships, hence the linear velocity would drop and with it the mass transfer coefficient (Berty, 1983). Caldwell also found that the mass transfer coefficient obtained in the Carberry type reactor did not change with pressure. If these experiments were carried out at the upper limit of the laminar region then it is quite reasonable to expect that the experiments in the Carberry type reactor were carried out well into the laminar region and hence despite the increase in pressure, flow was still laminar.

An alternative explanation for the drop in k_c with increasing pressure is the possibility that the correlating factor could be the diffusivity rather than the Schmidt number as suggested by Caldwell (1983a) to explain the higher mass transfer coefficients found with hydrogen compared to air. Several workers have suggested that this is possible (Mehta & Sharma, 1966; Vidwans & Sharma, 1967; Yadav & Sharma, 1979). Mehta & Sharma (1966) pointed out that when the pressure is increased for a particular system, the Schmidt number remains substantially the same but the diffusivity varies inversely with the pressure and hence the mass transfer coefficient should decrease with an increase in pressure at a given superficial gas velocity. This would also qualitatively explain why Caldwell obtained, as he pointed out, higher mass transfer coefficients for hydrogen than for air under identical conditions.

In a similar manner to that used by Caldwell (1983a) the superficial gas velocities for the napthalene-air system at a stirrer speed of 2000 RPM are calculated. The mass transfer coefficient obtained and the conditions used are shown in Table 3.26.

The velocities are calculated as follows:

(a) From the head generated by the impeller combined with the Leva and Ergun equations respectively, and
(b) From measured mass transfer coefficients inserted in the correlations of Hougen (1961) and Dwivedi & Uphaday (1977).

The maximum theoretical head is developed when all the kinetic energy imparted by the blades to the gas is converted into pressure energy. For an impeller speed of N RPM this is given by (Caldwell, 1983a):

Table 3.26 Conditions used to obtain superficial gas velocities for the napthalene-air system

Parameter	Value
Mass transfer coefficient, kc	8.5 $cm \cdot s^{-1}$
Bed depth	2.1 cm
Temperature	296 K
Pressure	1.0 bar
Air density	1.0×10^{-3} $g \cdot cm^{-3}$
Voidage fraction	0.41
Air viscosity	1.8×10^{-4} $g \cdot cm^{-1} \cdot s^{-1}$
Shape factor, ϕ	1
Schmidt number	1.80

$$\Delta h_{theo} = \frac{\Pi^2 (r_1^2 - r_2^2) N^2}{1800\ g}$$

where r_1=outer radius of impeller blade, cm
r_2=inner radius of impeller blade, cm
g =acceleration of gravity, $cm \cdot s^{-2}$

The Ergun pressure drop equation is given by (Leva, 1959; Hougen, 1961):

$$\frac{\Delta P}{L} \frac{g_c}{} \frac{D_p}{G u_o} \left[\frac{\epsilon^3}{1-\epsilon} \right] = 150 \left[\frac{1-\epsilon}{Re} \right] + 1.75$$

where ΔP=pressure drop, $lb \cdot ft^{-2}$
L=bed depth, ft
g_c=32.2 $lbm \cdot s^2 \cdot lbf^{-1} \cdot ft^{-1}$
D_p=particle diameter, ft
G=ρu_o, $lb \cdot ft^{-2} \cdot s^{-1}$

ρ=density of fluid, $lb \cdot ft^{-3}$

u_o=superficial gas velocity, $ft \cdot s^{-1}$

ϵ=bed voidage fraction

Re=reynolds number

The Leva pressure drop equation is given by (Leva, 1959):

$$\frac{\Delta P}{L} = \frac{3.50 G^{1.9} \mu^{0.1} (1-\epsilon)^{1.1}}{D \rho^{1.1} \phi_s^{1.1} \rho g_c \epsilon^3}$$

where the terms are as described previously and

ϕ_s=shape factor.

The Hougen equations are given as follows (Hougen, 1961):

$$j_D = 0.84 Re^{-0.51} \quad (0.01 < Re < 50)$$

$$j_D = 0.57 Re^{-0.41} \quad (50 < Re < 1000)$$

$$j_D = \frac{k_c Sc^{2/3}}{U_o}$$

$$Re = \frac{\rho u D_p}{6(1-\epsilon)\phi\mu}$$

where the terms are as previously described and

j_D=mass transfer number

Sc=Schmidt number

$$= \left[\frac{\rho D_p}{\mu} \right]^{-1}$$

k_c=gas side mass transfer coefficient, $ft \cdot s^{-1}$

The following equations were proposed by Dwivedi & Uphaday (1977):

$$\epsilon j_D = 1.1068 Re^{-0.7200} \quad (\text{for } Re < 10)$$

$$\epsilon j_D = 0.4548 Re^{-0.4069} \quad (\text{for } Re > 10)$$

$$j_D = \frac{k_c Sc^{2/3}}{U_o}$$

$$Re = \frac{D_p U_o \rho}{\mu}$$

The results are also compared with those obtained by Caldwell (1983a) using Berty and Carberry type reactors. The results are shown in Tables 3.27 and 3.28.

Table 3.27 Superficial velocities estimated from various pressure drop equations

	Radius cm	ΔHgen cm air	Bed depth cm	Ergun	Leva
A Carberry	1.75	68.5	1.8	25.1	30.8
A Berty	3.50	273.9	1.6	65.2	67.4
Caldwell	9.00	1810	2.1	153	146
This study	9.00	1810	2.1	139	145

Table 3.28 Superficial gas velocities estimated from mass transfer coefficients.

	k_c $cm \cdot s^{-1}$	U (Hougen) $cm \cdot s^{-1}$	U (Dwivedi) $cm \cdot s^{-1}$
A Carberry	1.2	3.4	4.9
A Berty	2.0	9.1	11.1
Caldwell	8.8	158	135
This study	8.5	137	104

It should be noted that the expected superficial gas velocities calculated from the pressure drop equations of Ergun and Leva are lower than those of Caldwell due to the smaller bed voidage fraction. The superficial gas velocities calculated from the mass transfer coefficient combined with the Hougen formulation compares very favourably with the maximum superficial gas velocities expected from the Ergun and Leva equations. The correlation of Dwivedi & Uphaday (1977) gives lower values of k_c for both Caldwell's results and the results obtained here. Dwivedi & Uphaday have noted however that their generalized correlations, which are based on the results of many workers, have deviations of 23.15% for $Re < 10$ and 16.83% for $Re > 10$. This could explain the large difference

(25%) between the two calculated superficial velocities. Taking an average calculated superficial velocity of 121 $cm \cdot s^{-1}$ this would imply that at least 85% of the theoretical head generated is converted to pressure (all of which is used in the internal recycle).

The estimated and calculated values of the superficial gas velocities for the Berty (3" impeller) and Carberry type reactors are those calculated by Caldwell (1983a). Both show significantly lower values of U_o than this reactor, but what is rather striking is the difference between the calculated and the theoretical values. Caldwell attributes this to significant bypassing.

Berty (1983) has correctly pointed out that the comparison between his 3" and Caldwell's reactor under these conditions is not quite justified since the 3" design was designed to be operated at higher impeller speeds (10000 rpm) and it is the diameter times the impeller speed that is important. At 10000 rpm using a Berty type reactor with a 3" impeller the mass transfer coefficients (based on the results in Table 3.28) obtained should be quite similar to those obtained in Caldwell's reactor. It has however been noted by Berty that the open sided construction of his impeller is a disadvantage. (Caldwell's reactor has a close sided construction). This certainly contributes to the poorer efficiency of the blower in Berty's reactor.

Regarding pressure, Berty (1974, 1983) has recommended that: "For lower limits of pressure, 45 $lb \cdot in^{-2}$ gauge is recommended, because at lower pressure and corresponding lower gas densities it is difficult to maintain good mass velocities". Caldwell (1983b), however, has pointed out that it is not necessary to operate at high pressure since the mass transfer coefficient is not improved. He noted that if flow is laminar then the mass transfer coefficient is independent of gas pressure while if flow is turbulent then the mass transfer coefficient is expected to decrease with an increase in pressure. Caldwell (1983b) has noted that an advantage of operating at high pressures is the increase in residence time and hence the recycle ratio.

3.5.2.2 Intra-particular and Interphase Mass Transfer with Reaction

It has been shown in section 3.4.2.6, under the most extreme conditions used in these experiments, that interphase mass transfer was negligible at impeller speeds of 1800 rpm or greater. With respect to intra-particular mass transfer it was found, at the more extreme conditions of acid concentration (109.5% H_3PO_4) and temperature (478K), that the

reaction rate still increased, to a small extent, as the particle size was reduced to below a size fraction of 106-180 microns. At an acid concentration of 101.5% and a reactor temperature of 464K it was found that the reaction rate no longer increased with a decrease in particle size to below a size range of 106 - 180 microns. Although this method of monitoring reaction rate as a function of particle size does not necessarily provide conclusive proof of the absence of intra-particular diffusion short of carrying out rigorous and time consuming studies, it does provide a very good indication as to the significance of intra-particular diffusion.

Based on these results, it can be accepted under most of the conditions used in this study (using a catalyst size fraction of 106-180 microns) that intra-particular diffusion was negligible. The areas where intra-particular diffusion starts to intrude are in the experiments where both high acid concentration (109% H_3PO_4) and high temperatures (>473K) were employed.

These results are also assumed to be valid for the 1-butene oligomerization experiments, despite the fact that the 1-butene molecule is longer that the propene, since the 1-butene products have lower chain lengths (on average) than those of propene.

It should be re-emphasized that, at catalyst size fractions below 106-180 microns, catalyst spillage from the basket became a serious problem and hence, taking this into account, together with the mass transfer results, a catalyst size fraction of 106-180 microns was chosen for the kinetic experiments.

3.5.3 General Qualitative Findings

3.5.3.1 Propene Experiments

From the preliminary results of section 3.4.3 it is quite clear that acid concentration has a dramatic effect on both reaction rates and catalyst life, and its control is critical. As is well known, too high or too low an H_3PO_4 concentration has a detrimental effect on the catalyst life. It does appear as though, once underhydrated, the catalyst can be re-hydrated to the desired level (desired H_3PO_4 concentration) without any significant effect on reaction rate. The relationship between acid strength and product spectra cannot be deduced from Figures 3.32 and 3.33 due to the differences in reaction rates.

From the results of sections 3.4.4.1 and 3.4.4.2 it is clear that, as the propene concentration was increased from one experiment to another (all else being equal), there is a modest decrease in the average molecular weight of the liquid product as the conversion increases. The trend appeared to be more marked at the higher acid concentration levels.

A similar trend, although less marked, was found with the increase in reaction temperature, which was accompanied by an increase in reaction rate.

Examination of the rate versus H_3PO_4 concentration experiments (section 3.4.4.6), yields a different trend to the above. Here there was a modest shift to a higher molecular weight product as the acid concentration was increased (which was accompanied by an increase in rate of propene reaction). Closer examination of the results in sections 3.4.4.1 and 3.4.4.2 confirm that the shift is not linked to a change in conversion level. Comparing runs in these two sections of similar rates of propene reaction at similar feed reactor concentrations, yields the same trend as was found above. The results of the "low conversion experiments" in section 3.4.4.7 indicate no clear direction of a shift in product molecular weight as the conversion of propene was increased from 5 to 33%. It seems likely, therefore, that the shift in product spectrum, although modest, was due to the change in H_3PO_4 acid concentration.

3.5.3.2 1-Butene and Iso-Butene Experiments

With the 1-butene experiments, the only detectable shift in the product spectrum was a very slight shift to a lower molecular weight product with an increase in temperature (between the temperature range of 424 to 465K - see section 3.4.5.2). There was no noticeable shift with changes in 1-butene concentration or H_3PO_4 strength (accompanied by the appropriate changes in conversion).

Due to the problems of deactivation with the iso-butene experiments, the qualitative effect of process variables on product spectra could not be examined.

3.5.4 Simple Power Law Modeling of the Rate-Concentration Data

3.5.4.1 Modeling of the propene data

The first approach to the modeling of the propene rate/concentration data was to model the rate of monomer reaction as a function of monomer

concentration, reaction temperature and H_3PO_4 concentration by using a simple power law function of the following form:

$$-rC_3 = k' \cdot [\%H_3PO_4/100]^m \cdot e^{-E/RT} \cdot C_3^n$$

where k' = pre-exponential factor

$\%H_3PO_4$ = concentration of H_3PO_4, %

E = activation energy

R = universal gas constant

T = reaction temperature, K

C_3 = concentration of propene, mo/l

n = reaction order

m = constant

The division of the H_3PO_4% by 100 was only done to simplify the handling of the constant n. The above rate equation at constant temperature and H_3PO_4 concentration simplifies to: $-rC_3 = k \cdot C_3^n$. A straight line plot of $\ln(C_3)$ versus $\ln(-rC_3)$ would have a slope of n and an intercept of ln k.

Using the data of Table 3.14, $\ln(C_3)$ was plotted as a function of $\ln(-rC_3)$ in Figure 3.53. The straight line correlation coefficient was

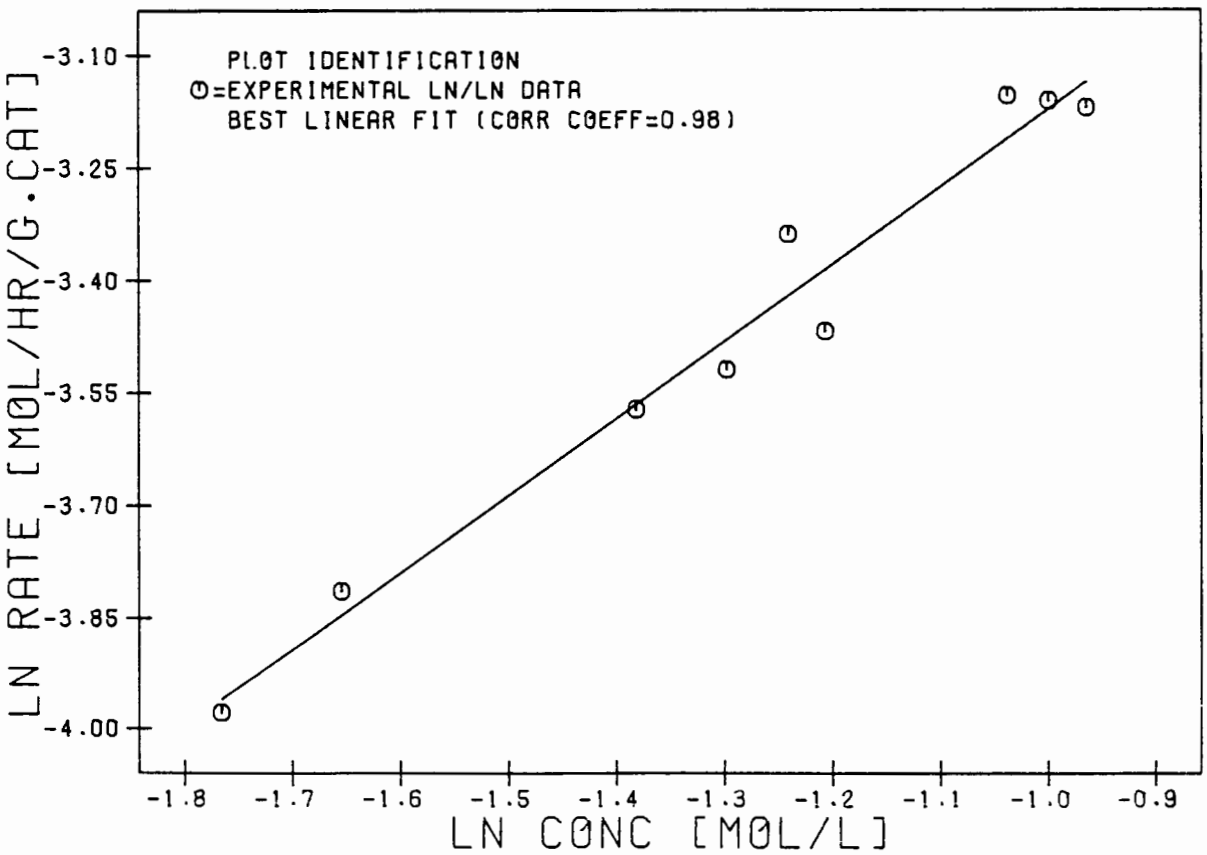

FIG 3.53 SIMPLE POWER LAW FIT TO PROPENE RATE/ CONCENTRATION DATA OBTAINED AT 464 K AND 103% H3P04

equal to 0.984. The reaction order was found to be 1.03 and the rate constant was equal to 0.117 $mol^{-0.03} \cdot l^{1.03} \cdot hr^{-1} \cdot g_{cat}^{-1}$. ~~and the reaction order was found to be 1.03~~.

The dependence of the rate constant, k, as determined above, on H_3PO_4 concentration and reaction temperature will be assumed to be of the following form: $k = k' \cdot [\%H_3PO_4/100]^m \cdot e^{-E/RT}$

A straight line plot of ln $[\%H_3PO_4/100]$ versus ln k (determined at 464 K and based on the data of Table 3.18) will have a slope of m and a y-axis intercept of ln $(k' e^{-E/RT})$. A plot of ln $[\%H_3PO_4/100]$ as a function of k is shown in Figure 3.54. The linear least squares correlation coefficient was found to be 0.998. From the slope and y-axis intercept the values of m and $k' e^{-E/RT}$ were found to be: m = 8.65 and $k' e^{-E/RT} = 9.5 \times 10^{-2}$ $mol^{-0.03} \cdot l^{1.03} \cdot hr^{-1} \cdot g_{cat}^{-1}$.

The rate constant, k, is assumed to have an Arrhenius type dependence on temperature as has already been indicated above. A straight line plot of ln 1/T versus ln k (based on the data of Table 3.17 (102% H3PO4)) will have a slope of -E/R and a y-axis intercept of ln $(k' \cdot [\%H_3PO_4/100]^m)$. A plot of ln 1/T versus ln k is shown in Figure 3.55. The linear least squares correlation coefficient was found to be 0.991. The values of E/R and $k' \cdot [\%H_3PO_4/100]^m$ were found to be 3060 K and 76.4 $mol^{-0.03} \cdot l^{1.03} \cdot hr^{-1} \cdot g_{cat}^{-1}$, respectively

Therefore, from the data in Tables 3.16, 3.19 and 3.21 the values of n, m, k', k_1 and E can be found. The values as indicated above are as follows:

n = 1.03,

m = 8.65,

k' = 66.9, $mol^{-0.03} \cdot l^{1.03} \cdot hr^{-1} \cdot g_{cat}^{-1}$

and E/R = 3060 K.

It must be pointed out that the value of the pre-exponential factor, k', can be calculated from both the rate/temperature data and the rate/$\%H_3PO_4$ data. Two values were found in this way, i.e., k' = 69.5 $mol^{-0.03} \cdot l^{1.03} \cdot hr^{-1} \cdot g_{cat}^{-1}$ and k' = 64.4 $mol^{-0.03} \cdot l^{1.03} \cdot hr^{-1} \cdot g_{cat}^{-1}$. It was decided therefore to take an arithmetic mean of these two values.

The general rate equation therefore, for the rate of reaction of propene at the conditions used in this work can be given as follows:

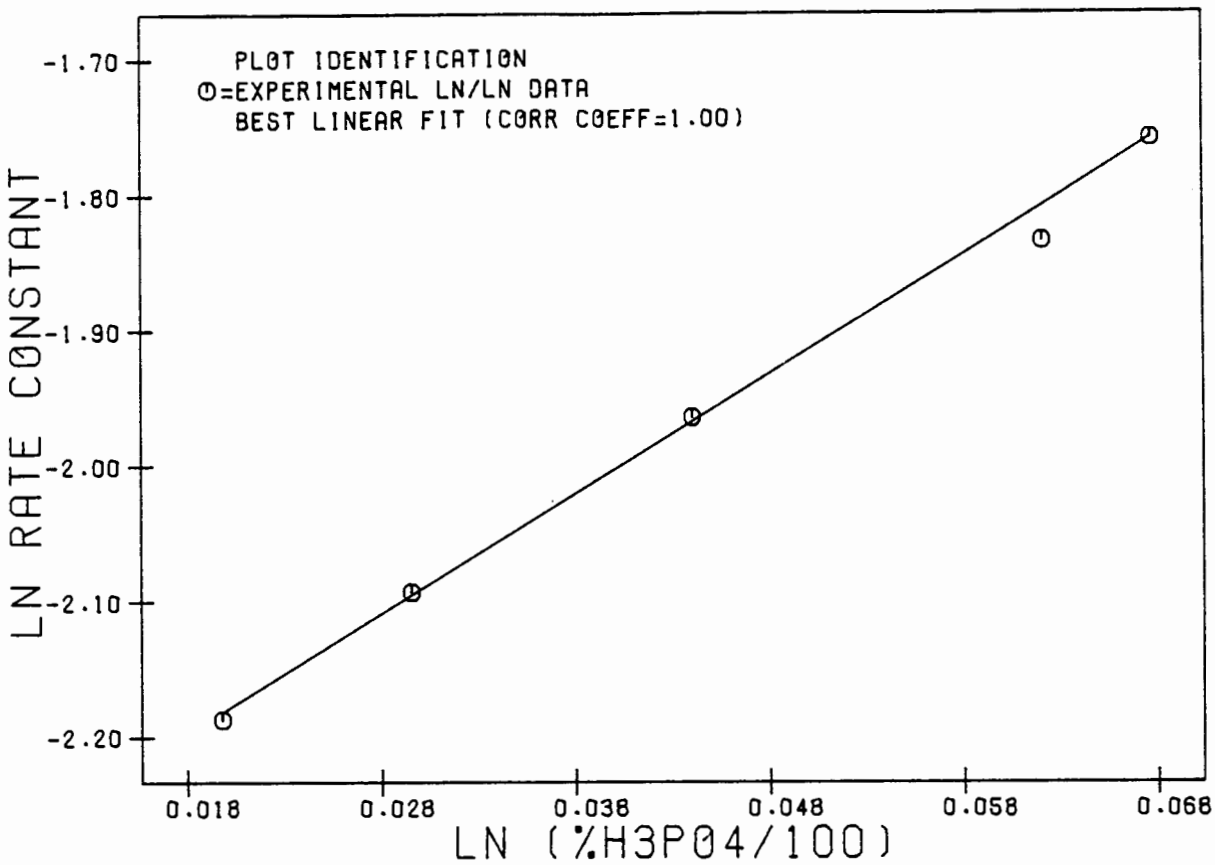

FIG 3.54 POWER LAW FIT TO RATE CONSTANT VS H3P04 CONCENTRATION DATA AT 464 K FOR PROPENE OLIGOMERIZATION

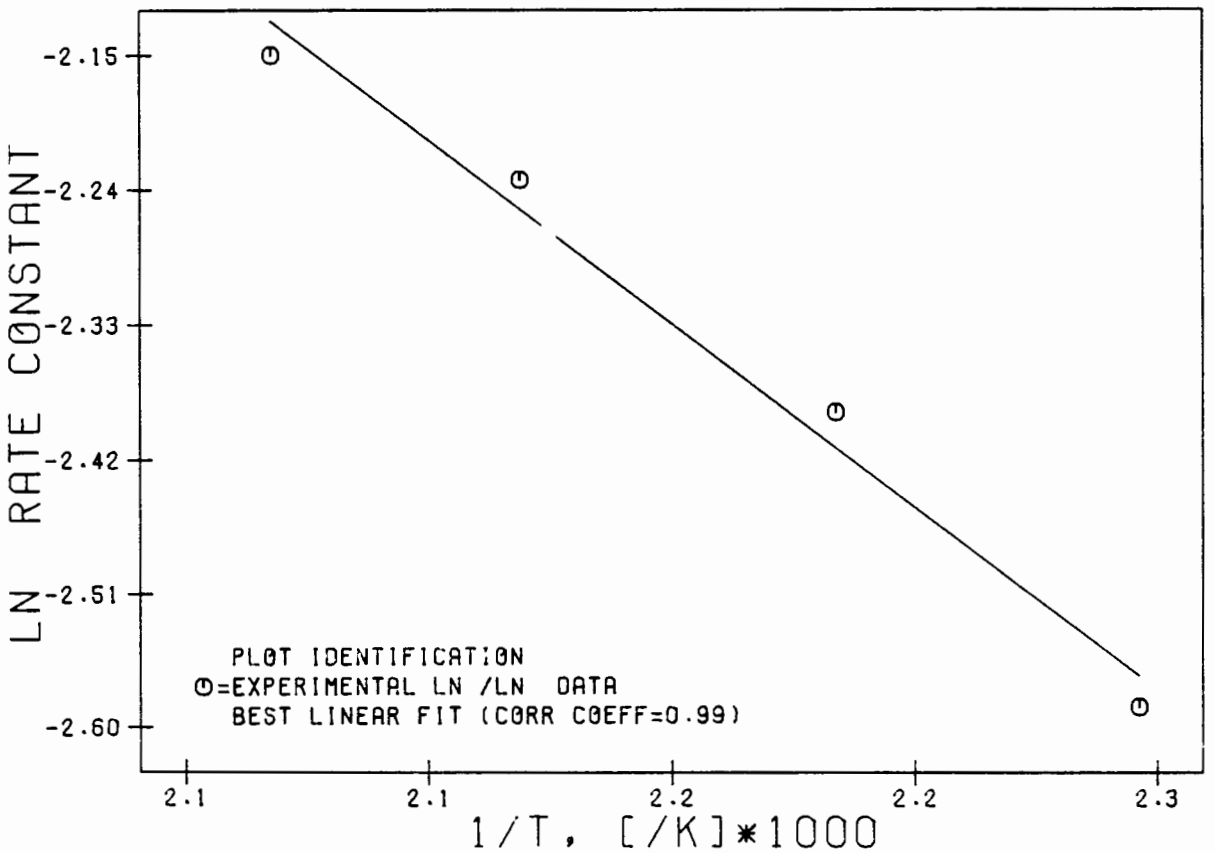

FIG 3.55 ARRHENIUS TYPE PLOT OF RATE CONSTANT AS A FUNCTION OF TEMPERATURE FOR PROPENE OLIGOMERIZATION AT 102% H3P04

$$-rC_3 = k' \cdot [\%H_3PO_4/100]^m \cdot e^{-E/RT} \cdot C_3^n$$

where $k' = 66.9\ mol^{-0.03} \cdot l^{1.03} \cdot hr^{-1} \cdot g_{cat}^{-1}$,

$E/R = 3058\ K$,

$m = 8.65$,

and $n = 1.03$.

Prediction at 464 K and 114% H_3PO_4 over a range of C_3 concentrations

The rate equation developed above was tested on the data of Table 3.15 which was obtained at a constant temperature (464 K) and a constant H_3PO_4 concentration (approximately 114%) but over a range of propene concentrations. The experimental and predicted results are listed in Table 3.29 and are plotted in Figure 3.56 as functions of the propene reactor concentration.

Table 3.29 Predicted and experimental rates of propene reaction at 464 K and 114% H_3PO_4.

	Propene concentration [mol/l], x 10^3							
	227	263	179	170	131	129	102	61
Experimental rates, $mol \cdot hr^{-1} \cdot g_{cat}^{-1}$ x 10^2	6.2	7.9	5.3	4.0	3.5	2.8	2.2	1.4
Predicted rates, $mol \cdot hr^{-1} \cdot g_{cat}^{-1}$ x 10^2	6.3	7.2	4.8	4.6	3.5	3.5	2.7	1.6

It should be noted that the H_3PO_4 concentration used was well outside the range over which the rate equation was determined. For the purposes of determining the deviation of the predicted from the experimental data, the experimental data was smoothed. Maximum and average deviations were then calculated based on the smoothed curve. The maximum deviation of the predicted curve from the experimental (at propene concentrations above 0.06 mol/l) was approximately 20% (i.e., 20% of the experimental value). In order to determine the average deviation of the predicted rate equation from the experimental data a form of error analysis was performed. The result is shown graphically in Figure 3.57. Figure 3.57 is simply a plot of percentage deviation of the predicted rate from the experimental rate as a function of propene concentration. In the determinations of the percentage deviations in this plot the actual experimental results are used (not the smoothed results). The percentage deviation is given by:

$$\text{deviation, \%} = \frac{\text{predicted rate - actual rate}}{\text{actual rate}} \times 100$$

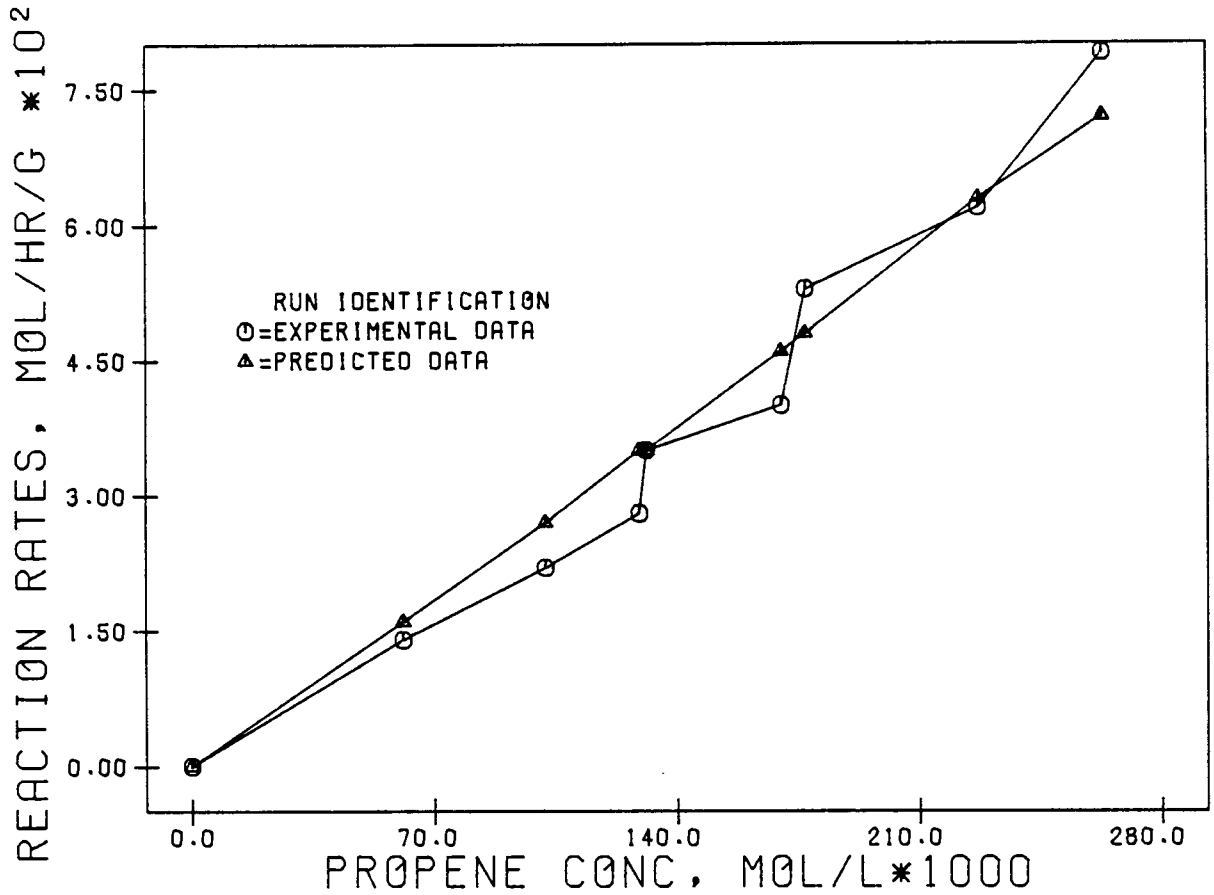

FIG 3.56 PREDICTED AND EXPERIMENTAL PROPENE REACTION RATES AS FUNCTIONS OF PROPENE CONCENTRATION AT 464 K AND 114% H3P04

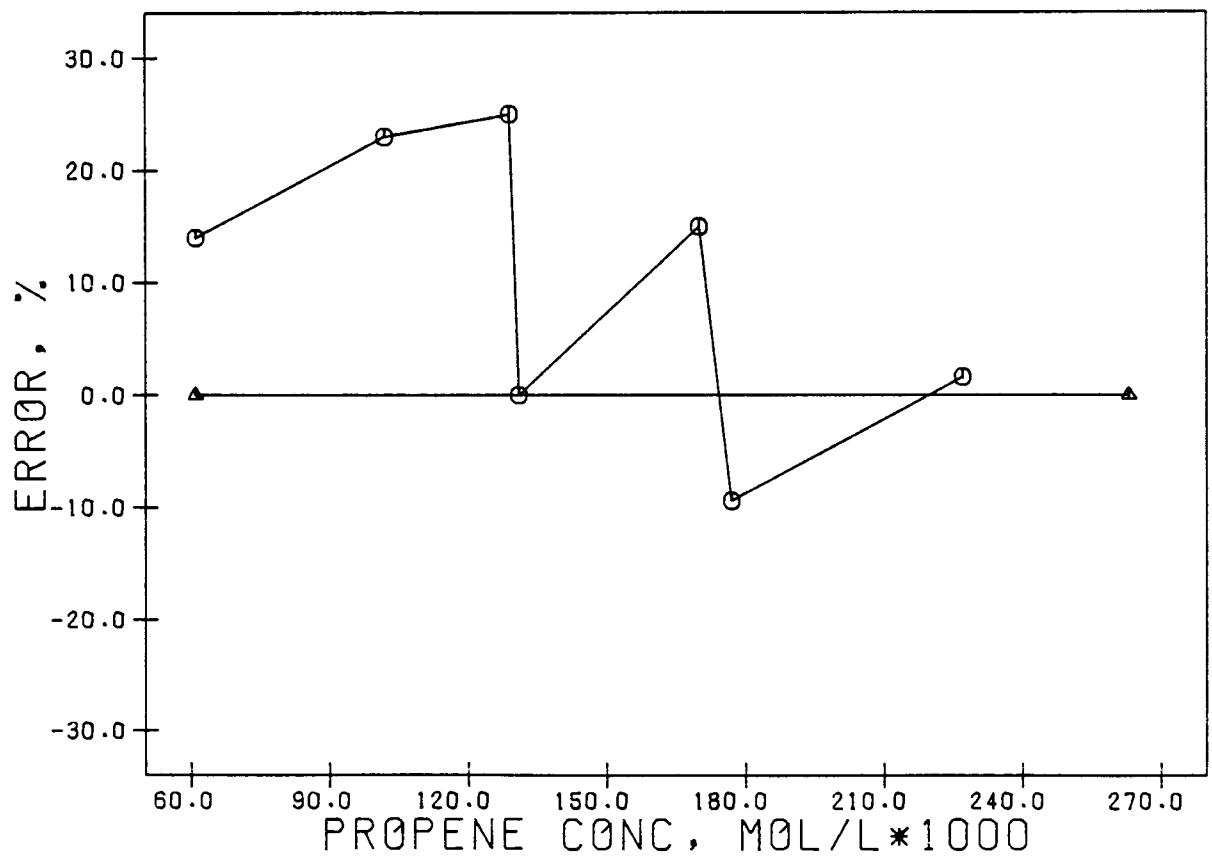

FIG 3.57 PERCENTAGE ERROR ANALYSIS AS DETERMINED FROM PREDICTED AND EXPERIMENTAL PROPENE REACTION RATES AS FUNCTIONS OF PROPENE CONCENTRATION AT 464 K AND 114% H3P04

Ideally the averaged %deviation would be equal to zero, indicating that the deviations were due to experimental data scatter. From Figure 3.57 it can be seen that the data has a scatter generally above the zero %deviation line with an average of +5.6%, indicating that, on average, over this region (at these conditions) the rate equation over-predicts the experimental data by 5.6%.

Prediction at 111% H_3PO_4 and over a range of temperatures

The rate equation was tested in a similar manner to that above, using the data of Table 3.16. The predicted and experimental reaction rates are indicated in Table 3.30 and are plotted in Figure 3.58.

In this instance both the H_3PO_4 concentration and the reactor temperature extended outside the range over which the rate equation was determined. The error analysis plot is shown in Figure 3.59. Although the data is limited it does appear that the slopes of the experimental and the predicted rates versus temperature curves (Figure 3.58) are distinctly different.

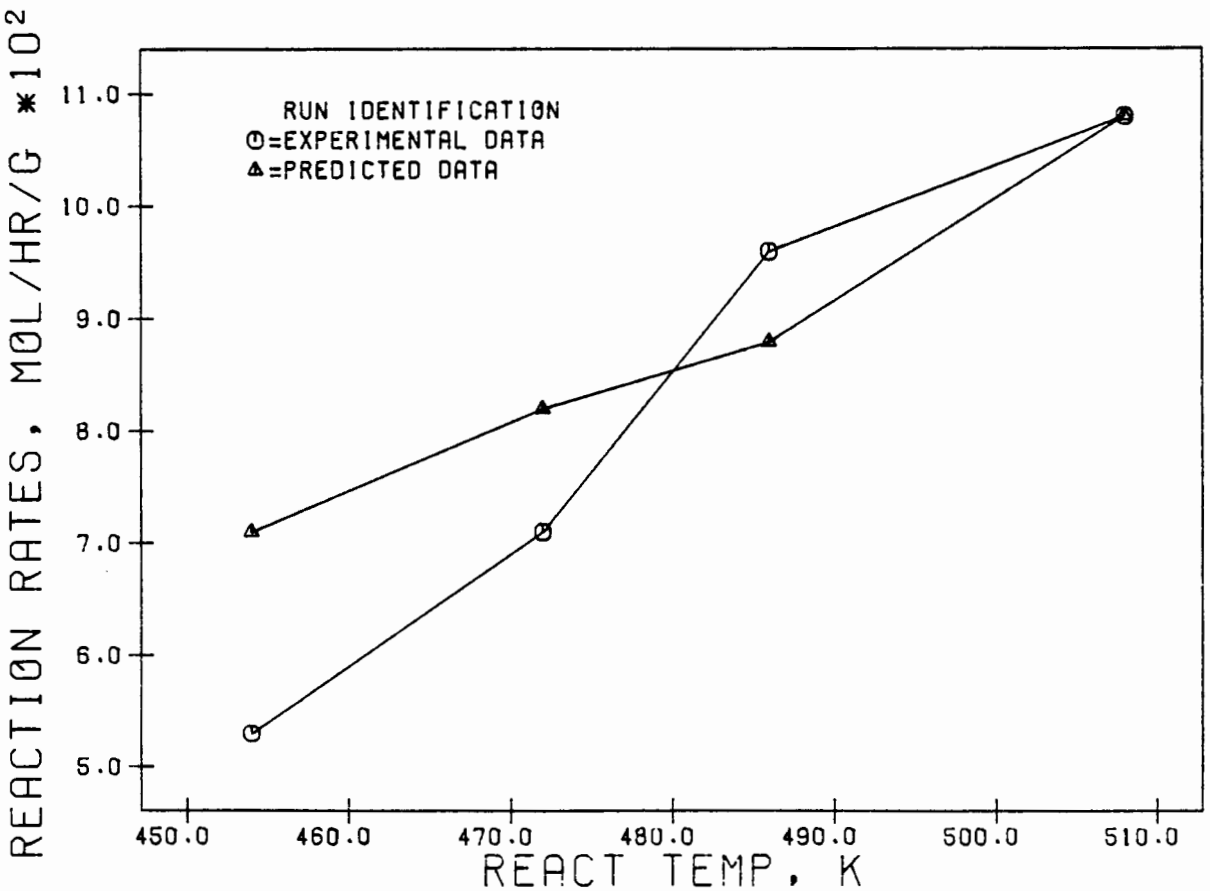

FIG 3.58 PREDICTED AND EXPERIMENTAL PROPENE REACTION RATES AS FUNCTIONS OF REACTOR TEMPERATURE AT 111% H3P04

Table 3.30 Predicted and experimental rates of propene reaction at 111% H_3PO_4.

	Reactor temperature, K			
	472	508	486	454
Experimental rates, $mol \cdot hr^{-1} \cdot g_{cat}^{-1} \times 10^2$	7.1	10.8	9.6	5.3
Predicted rates, $mol \cdot hr^{-1} \cdot g_{cat}^{-1} \times 10^2$	8.2	10.8	8.8	7.1

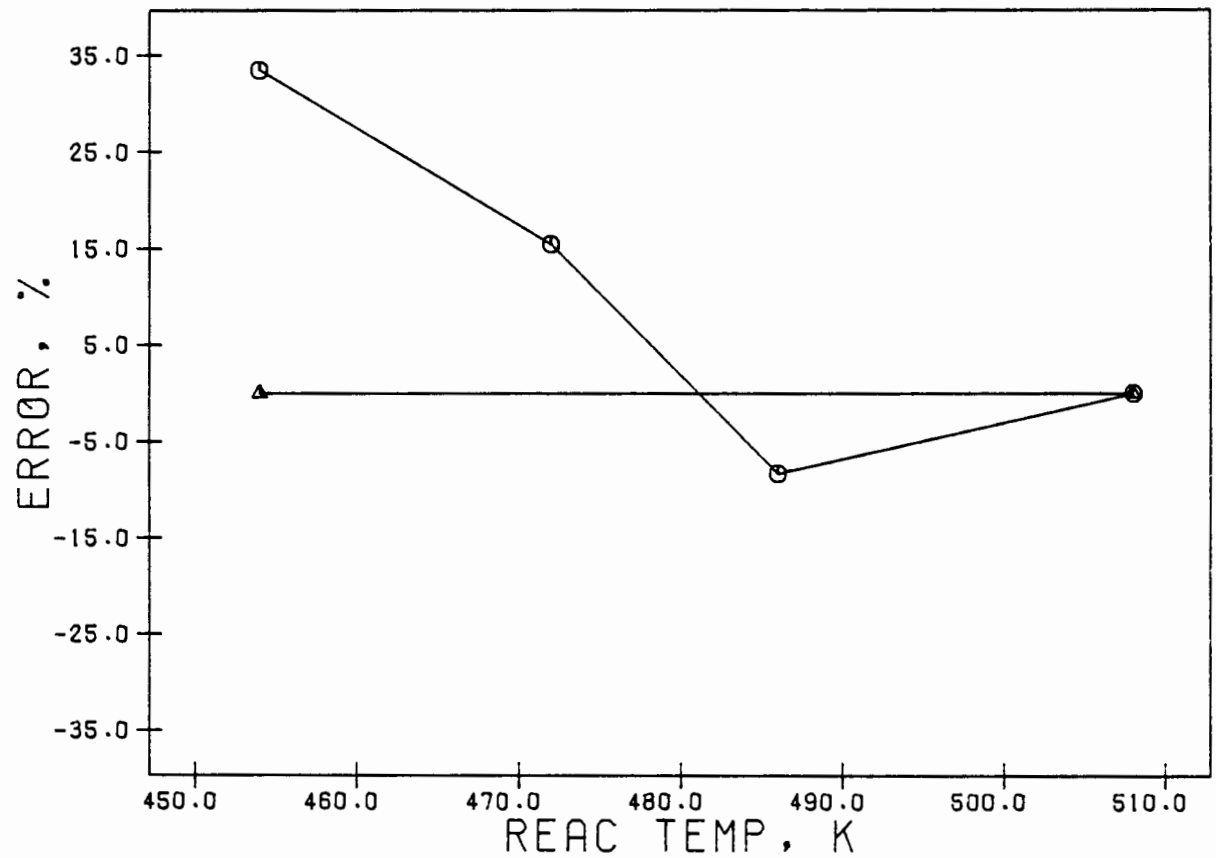

FIG 3.59 PERCENTAGE ERROR ANALYSIS AS DETERMINED FROM PREDICTED AND EXPERIMENTAL PROPENE REACTION RATES AS FUNCTIONS OF REACTOR TEMPERATURE AT 111% H3P04

The average %deviation as indicated in Figure 3.59 is equal to 6.9%. It is extremely likely that the data would have a significant scatter due to the fact that at these extremely high H_3PO_4 concentrations it is difficult to control the H_3PO_4 accurately due to the small quantities of make up water (for the reactor during reaction) required for this purpose. Another difficulty was the accurate measurement of the water concentrations at these levels and also the relatively short times over

which steady state was maintained due to the rapid deactivation of the catalyst at these high acid concentrations.

Despite the difficulty in obtaining accurate data at H_3PO_4 concentrations of 111 and 114%, examination of the Bethea and Karchmer rate constant in Figure 3.7 makes it quite clear that the relationship between H_3PO_4 concentration and the rate constant is expected to change at the higher H_3PO_4 concentrations. The model would therefore be expected to over predict the rate at the higher H_3PO_4 concentrations, which it did as indicated by the average %deviations given above. Although the rate equation would be expected to over-predict to an even greater extent at 114% than at 111%, this was not observed. This is probably due to the even greater errors incurred in the accurate determination of H_3PO_4 concentration at the 114% level and the further complication of even more rapid deactivation.

It must be pointed out that the extreme conditions over which the rate equation was tested are unlikely to be encountered industrially, but the conditions were used to merely test the equation at extremities.

3.5.4.2 Modeling of the 1-butene data

The 1-butene data was modeled in an identical manner to that of the propene using an identical form of rate equation. The data was taken from Tables 3.21, 3.22 and 3.23. The appropriate plots of ln $-r_A$ versus ln C_4, ln k versus ln [$\%H_3PO_4/100$] and ln k versus 1/T, where k is similar to that used for the propene rate equation, are shown in Figures 3.60, 3.61 and 3.62. The rate equation and the appropriate constants are given below:

$$-rC_4 = k' \cdot [\%H_3PO_4/100]^m \cdot e^{-E/RT} \cdot C_4^n$$

where $k' = 2.38 \times 10^7$ $mol^{-0.24} \cdot l^{1.24} \cdot hr^{-1} \cdot g_{cat}^{-1}$

$E/R = 8780$ K,

$m = 18.1$,

and $n = 1.24$.

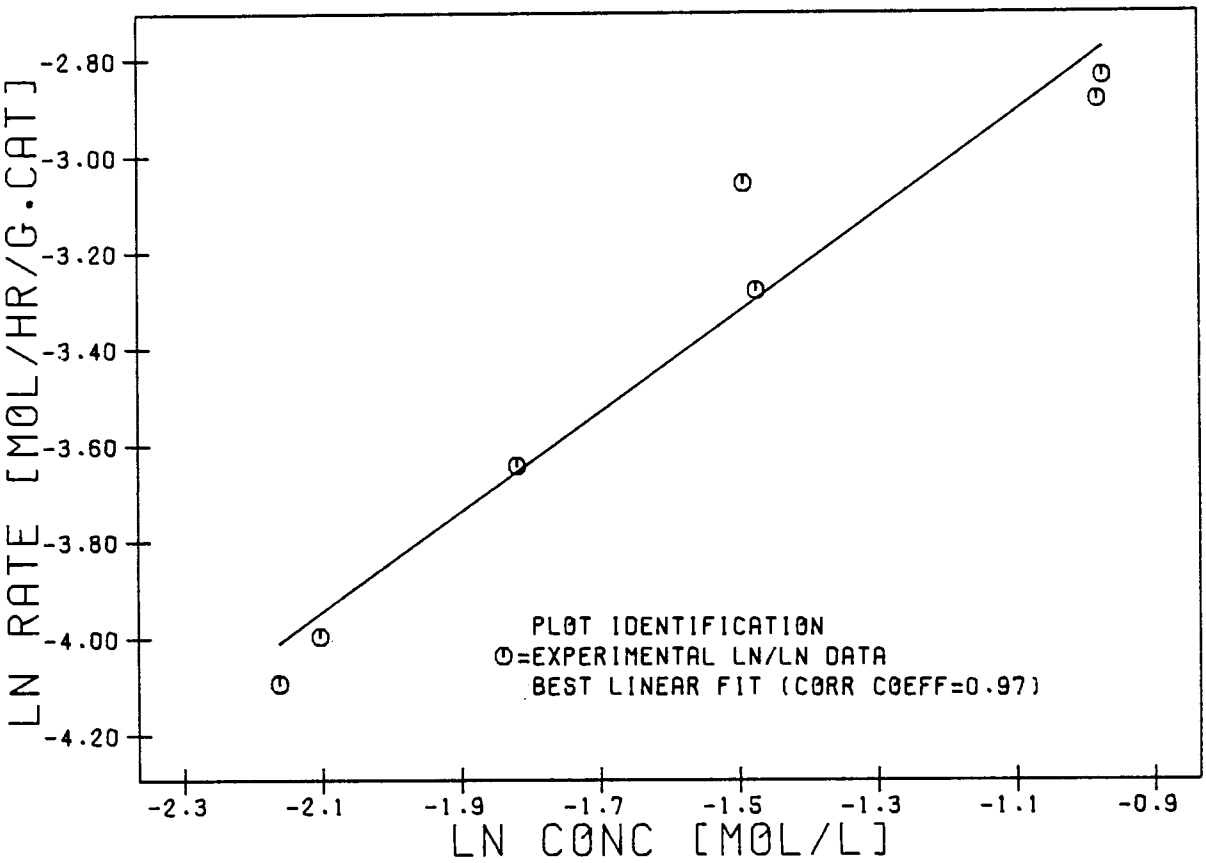

FIG 3.60 SIMPLE POWER LAW FIT TO 1-BUTENE RATE/ CONCENTRATION DATA AT 464 K AND 103% H3P04

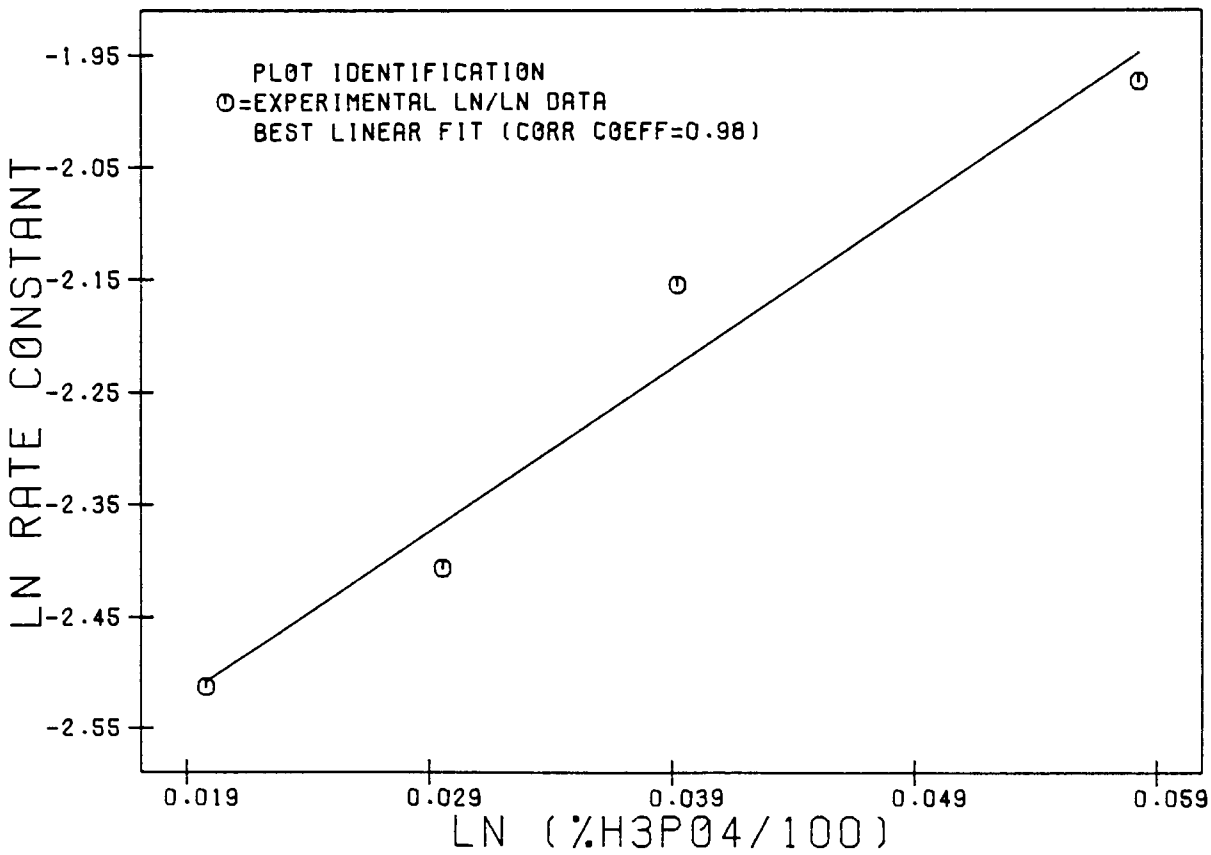

FIG 3.61 POWER LAW FIT TO RATE CONSTANT VS H3P04 CONCENTRATION FOR 1-BUTENE OLIGOMERIZATION AT 446.5 K

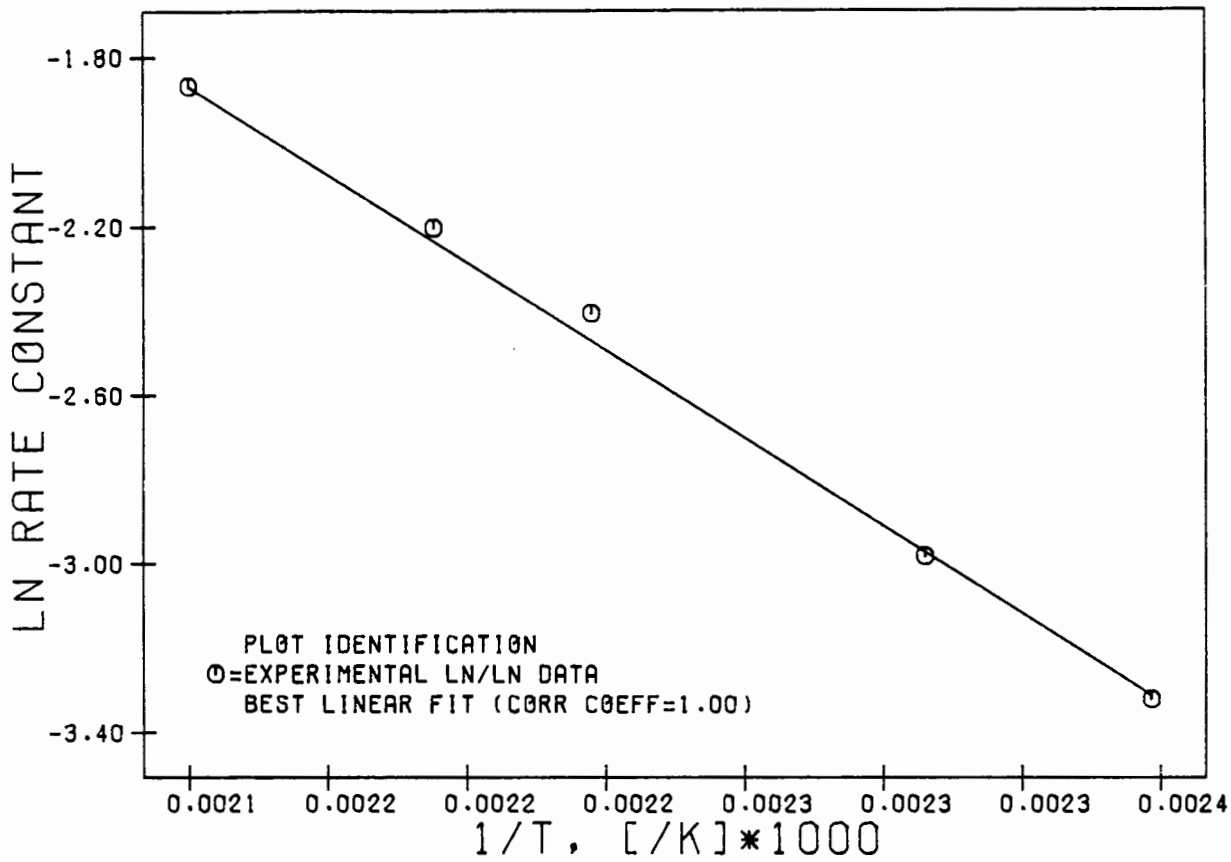

FIG 3.62 ARRHENIUS TYPE PLOT OF RATE CONSTANT VERSUS REACTION TEMPERATURE AT 103% H3P04 FOR 1-BUTENE OLIGOMERIZATION

3.5.5 Modeling of the Rate of Monomer Reaction and Rates of Product Formation

3.5.5.1 Modeling of the propene rate data

Several models were examined and tested for their ability to fit not only the rate of propene reaction but also the rate of production of the major oligomer products. Five models in total were examined, two of which were purely empirical. Although the primary criterion for discrimination between the models was the quality of the fit to the experimental data, it was considered to be of great importance to choose, if at all possible, a model that could be described by mechanistic considerations. In general the following reactions were considered for each of the models:

$$C_3 + C_3 \underset{k_2}{\overset{k_1}{\rightleftharpoons}} C_6$$

$$C_3 + C_6 \underset{k_4}{\overset{k_3}{\rightleftharpoons}} C_9$$

$$C_3 + C_9 \underset{k_6}{\overset{k_5}{\rightleftharpoons}} C_{12}$$

$$C_6 + C_6 \underset{k_8}{\overset{k_7}{\rightleftharpoons}} C_{12}$$

$$C_{12} \xrightarrow{k_9} C_{15} + \text{cracked products}$$

For all of the models tested, the assumption was made that the bulk of the cracked products were produced from the cracking of the C_{12} fraction. Each of the models will now be discussed individually.

MODEL P1 (PROPENE 1)

The basis for this model has two major assumptions besides the assumption regarding the cracking of the C_{12} fraction (an assumption which is inherent in all of the models to be discussed). The assumptions are:

1. Reverse reactions were considered to be negligible.
2. All of the oligomerization reactions (dimerization, trimerization and tetramerization) were considered to be elementary reactions.

The following set of reactions were therefore considered:

$$C_3 + C_3 \xrightarrow{k_1} C_6$$

$$C_3 + C_6 \xrightarrow{k_3} C_9$$

$$C_3 + C_9 \xrightarrow{k_5} C_{12}$$

$$C_6 + C_6 \xrightarrow{k_7} C_{12}$$

$$C_{12} \xrightarrow{k_9} C_{15} + \text{cracked products}$$

The resultant rate equations were as follows:

$$-dC_3/dt = k_1C_3^2 + k_3C_3C_6 + k_5C_9C_3$$

$$dC_6/dt = \tfrac{1}{2}k_1C_3^2 - k_3C_3C_6 - k_7C_6^2$$

$$dC_9/dt = k_3C_3C_6 - k_5C_3C_9$$

$$dC_{12}/dt = k_5C_3C_9 + \tfrac{1}{2}k_7C_6^2 - k_9C_{12}$$

where C_i = concentration of i

$-dC_3/dt$ = rate of propene reaction

dC_i/dt = rate of production, where i = 6, 9 or 12

It was decided to obtain the solution to this model by using the least squares technique and solving the resultant set of non-linear simultaneous equations by using the Nelder and Mead optimization technique (simplex optimization) for the desired constants. A detailed analysis of the above model is given in Appendix L.

From the rate concentration data of Table 3.14 the following constants were obtained for k_1, k_3, k_5, k_7, and k_9, this being the set that gave the best fit to the data:

$$k_1 = 1.28 \text{ mol}^{-1} \cdot \text{hr}^{-1}$$

$$k_3 = 49.4 \text{ mol}^{-1} \cdot \text{hr}^{-1}$$

$$k_5 = 2.74 \text{ mol}^{-1} \cdot \text{hr}^{-1}$$

$$k_7 = 19.3 \text{ mol}^{-1} \cdot \text{hr}^{-1}$$

$$k_9 = 0.55 \text{ hr}^{-1}$$

The quality of fit was observed by reinserting the above constants into the original set of rate equations and using the equations to predict the concentrations of the products, the mean residence time (because it was necessary to express the rates in terms of concentrations and mean residence time in order to solve the set of non-linear simultaneous equations), and hence the rate of reaction of propene and the rates of formation of the products as functions of the propene concentration in the reactor, the propene concentration being an independent variable. For this purpose, the initial concentration of propene in the feed (at reaction conditions) and the conversion, must be known parameters. The details of these calculation are shown in Appendix L. It should be noted that in the determination of the concentrations and rates the change in density of the system must be taken into account (Appendix L). The model can now be used to predict the necessary concentrations and rates at the conditions used in the experiments of Table 3.14. It should be noted, however, that since the model predicts product concentrations as well as mean residence time it is effectively also predicting, by default, reaction rates. For this reason the comparison between predicted and experimental results must include rates as well as concentrations. For this model, and hence for each model examined, two graphs were plotted, one showing a comparison between predicted and experimental product concentrations (as functions of propene reactor concentrations) and the other a comparison between predicted and experimental rates. The comparisons for model P1 are shown in Figures 3.63 and 3.64. The data for each of these figures is listed in Appendix M.

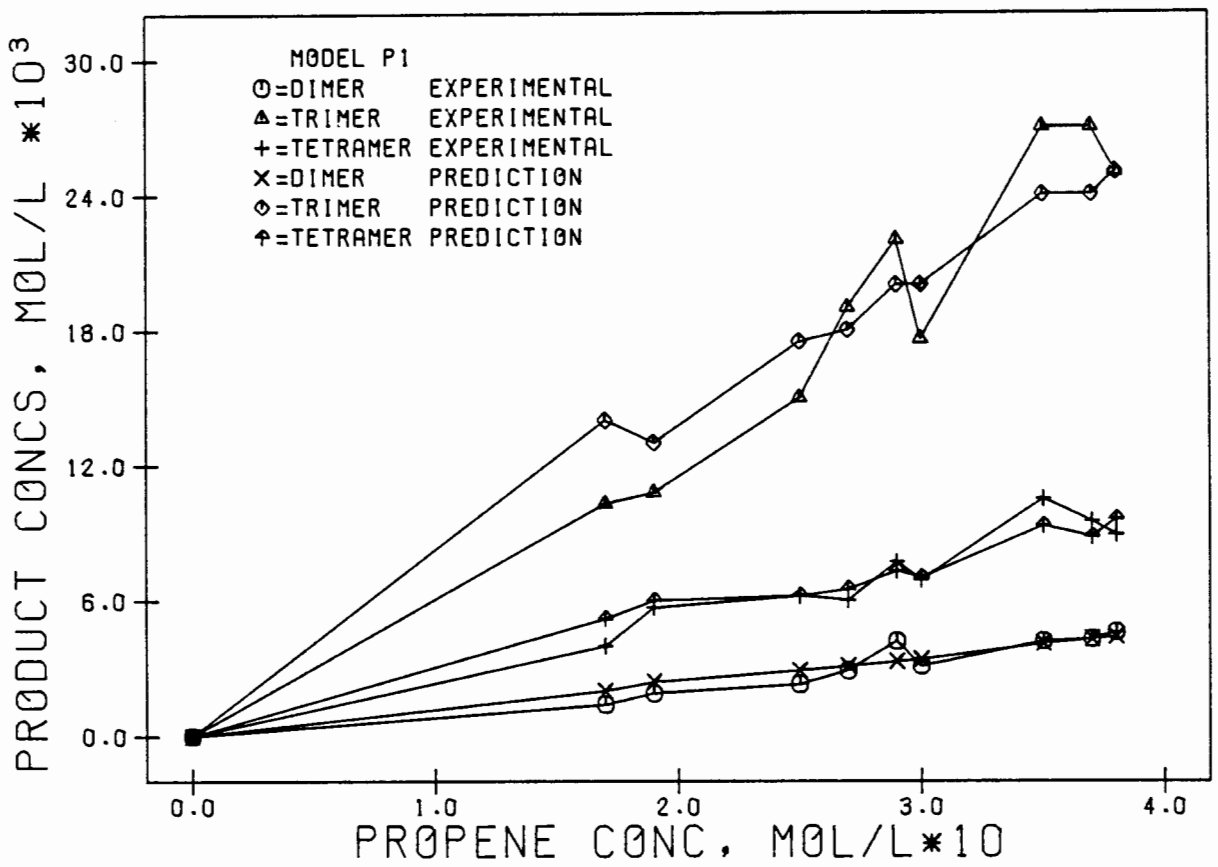

FIG 3.63 MODEL P1: PREDICTED AND EXPERIMENTAL PRODUCT CONCENTRATIONS AS FUNCTIONS OF PROPENE CONCENTRATIONS AT 103% H3P04 AND 464 K

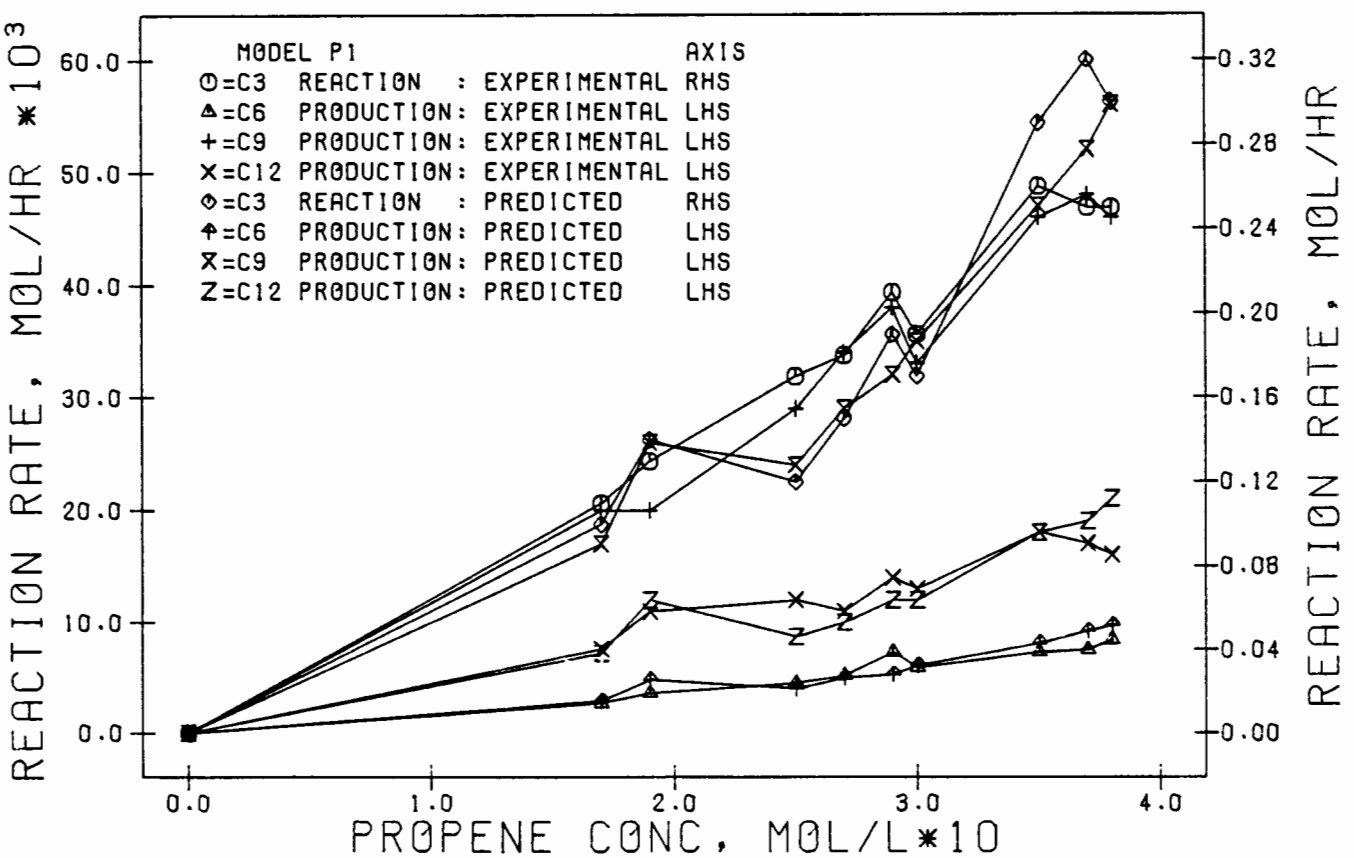

FIG 3.64 MODEL P1: PREDICTED AND EXPERIMENTAL REACTION RATES AS FUNCTIONS OF PROPENE CONCENTRATIONS AT 103% H3P04 AND 464 K

6.0 g of catalyst were used for all of the experiments in question (including the 1-butene experiments) and so it was decided to simply quote the rates as mol/hr as opposed to $mol \cdot hr^{-1} \cdot g_{cat}^{-1}$ for brevity.

MODEL P2

This model is quite similar to that of model P2 but with the reverse reactions included. As before, it was assumed that all reactions were considered to be elementary reactions.

The model is described by the following reaction scheme and rate equations:

$$C_3 + C_3 \underset{k_2}{\overset{k_1}{\rightleftharpoons}} C_6$$

$$C_3 + C_6 \underset{k_4}{\overset{k_3}{\rightleftharpoons}} C_9$$

$$C_3 + C_9 \underset{k_6}{\overset{k_5}{\rightleftharpoons}} C_{12}$$

$$C_6 + C_6 \underset{k_8}{\overset{k_7}{\rightleftharpoons}} C_{12}$$

$$C_{12} \xrightarrow{k_9} C_{15} + \text{cracked products}$$

$$-dC_3/dt = k_1C_3^2 - 2k_2C_6 + k_3C_3C_6 - k_4C_9 + k_5C_9C_3 - k_6C_{12}$$

$$dC_6/dt = \tfrac{1}{2}k_1C_3^2 - k_2C_6 - k_3C_3C_6 + k_4C_9 - k_7C_6^2 + 2k_8C_{12}$$

$$dC_9/dt = k_3C_3C_6 - k_4C_9 - k_5C_3C_9 + k_6C_{12}$$

$$dC_{12}/dt = k_5C_3C_9 - k_6C_{12} + \tfrac{1}{2}k_7C_6^2 - k_8C_{12} - k_9C_{12}$$

The solution procedure is identical to that used for model P1. In the optimization search, however, the routine attempted to assign negative values to some of the rate constants. As a result, a penalty function was introduced into the model in the form of a large objective function value (in the simplex), thus forcing the search away from these regions. The following values were found for the rate constants:

$k_1 = 1.38\ mol^{-1} \cdot hr^{-1}$	$k_4 = 8.6 \times 10^{-10}$	$k_7 = 33.9\ mol^{-1} \cdot hr^{-1}$
$k_2 = 2.05\ hr^{-1}$	$k_5 = 3.21\ mol^{-1} \cdot hr^{-1}$	$k_8 = 6.67 \times 10^{-2}\ hr^{-1}$
$k_3 = 48.3\ mol^{-1} \cdot hr^{-1}$	$k_6 = 0.623\ hr^{-1}$	$k_9 = 0.58\ hr^{-1}$

Based on the optimized constants the model was used to predict rates and concentrations in a similar manner to and at the same conditions as model P1. The relevant rates and concentrations are plotted as functions of

propene concentration in Figures 3.65 and 3.66. The data for these figures is listed in Appendix M.

MODEL P3

Due to the relatively poor fit of model P1 and Model P2 to the experimental data it was decided to examine an empirical model. In order to keep the model as simple as possible it was decided to consider only the forward reactions. The following reaction scheme was considered:

$$C_3 + C_3 \xrightarrow{k_1} C_6$$

$$C_3 + C_6 \xrightarrow{k_3} C_9$$

$$C_3 + C_9 \xrightarrow{k_5} C_{12}$$

$$C_{12} \xrightarrow{k_9} C_{15} + \text{cracked products}$$

The essential difference between this model and model P1 is that this model accepts that the reactions are not elementary although an alternative mechanism is not discussed in this model, i.e., the reaction orders chosen are those that best fit the data. Another major difference between this model and model P1 is that this model assumes that the C_{12} fraction is produced entirely from the reaction of propene with its trimer fraction, i.e., $C_6 + C_6 \longrightarrow C_{12}$ does not occur. The rate equations for this model are as follows:

$$-dC_3/dt = k_1 C_3^1 + k_3(C_3C_6)^{0.43} + k_5(C_9C_3)^{0.3}$$

$$dC_6/dt = \tfrac{1}{2}k_1 C_3^1 - k_3(C_3C_6)^{0.43}$$

$$dC_9/dt = k_3(C_3C_6)^{0.43} - k_5(C_3C_9)^{0.3}$$

$$dC_{12}/dt = k_5(C_3C_9)^{0.3} - k_9(C_{12})^{1.2}$$

The following values were found for the rate constants (optimized solution) using the data of Table 3.17:

$k_1 = 0.401\ hr^{-1}$ $\qquad$ $k_5 = 0.088\ mol^{0.4} \cdot l^{0.6} \cdot hr^{-1}$

$k_3 = 1.05\ mol^{0.14} \cdot l^{0.86} \cdot hr^{-1}$ $\qquad$ $k_9 = 1.52\ mol^{-0.2} \cdot l^{1.2} \cdot hr^{-1}$

Using these constants the model was used to predict rates and concentrations at identical conditions to those used in Models P1 and P2. The results are shown in Figures 3.67 and 3.68. The data for these figures are listed in Appendix M.

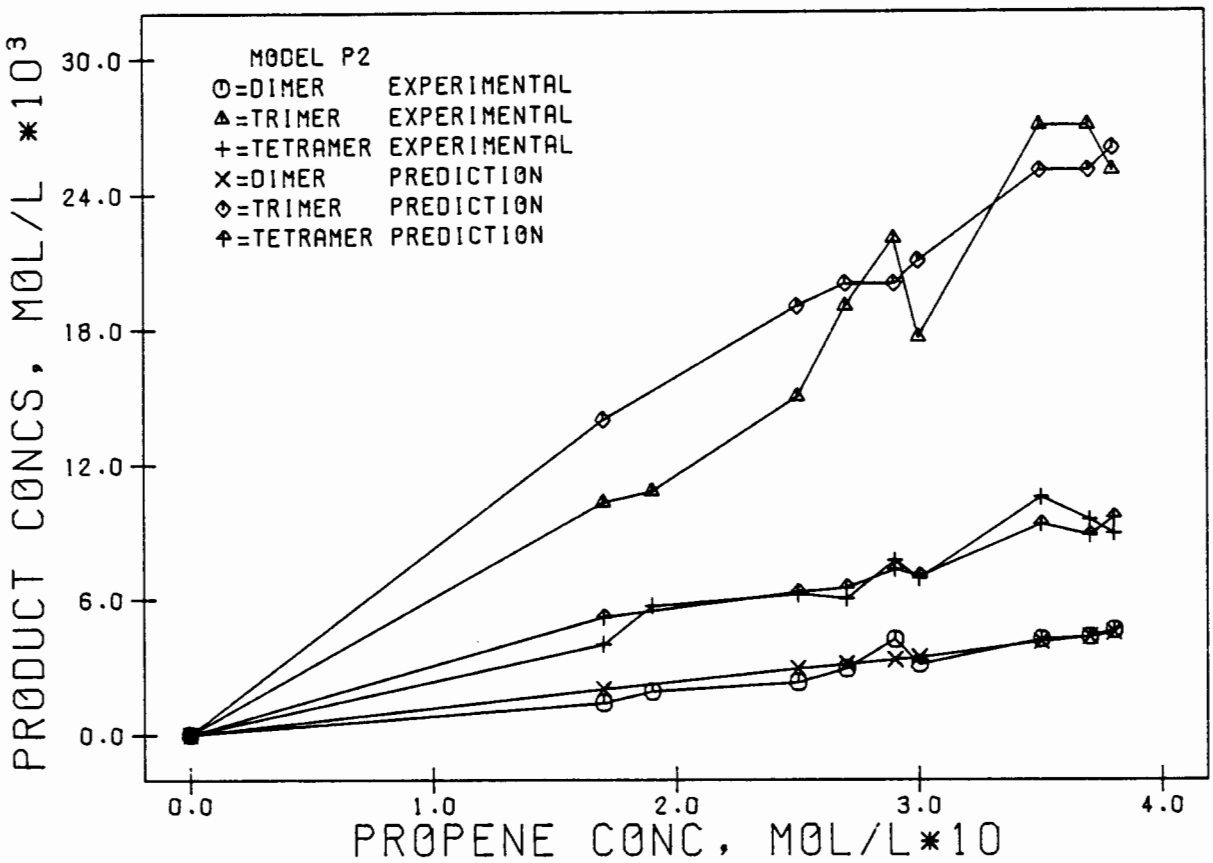

FIG 3.65 MODEL P2: PREDICTED AND EXPERIMENTAL PRODUCT CONCENTRATIONS AS FUNCTIONS OF PROPENE CONCENTRATIONS AT 103% H3P04 AND 464 K

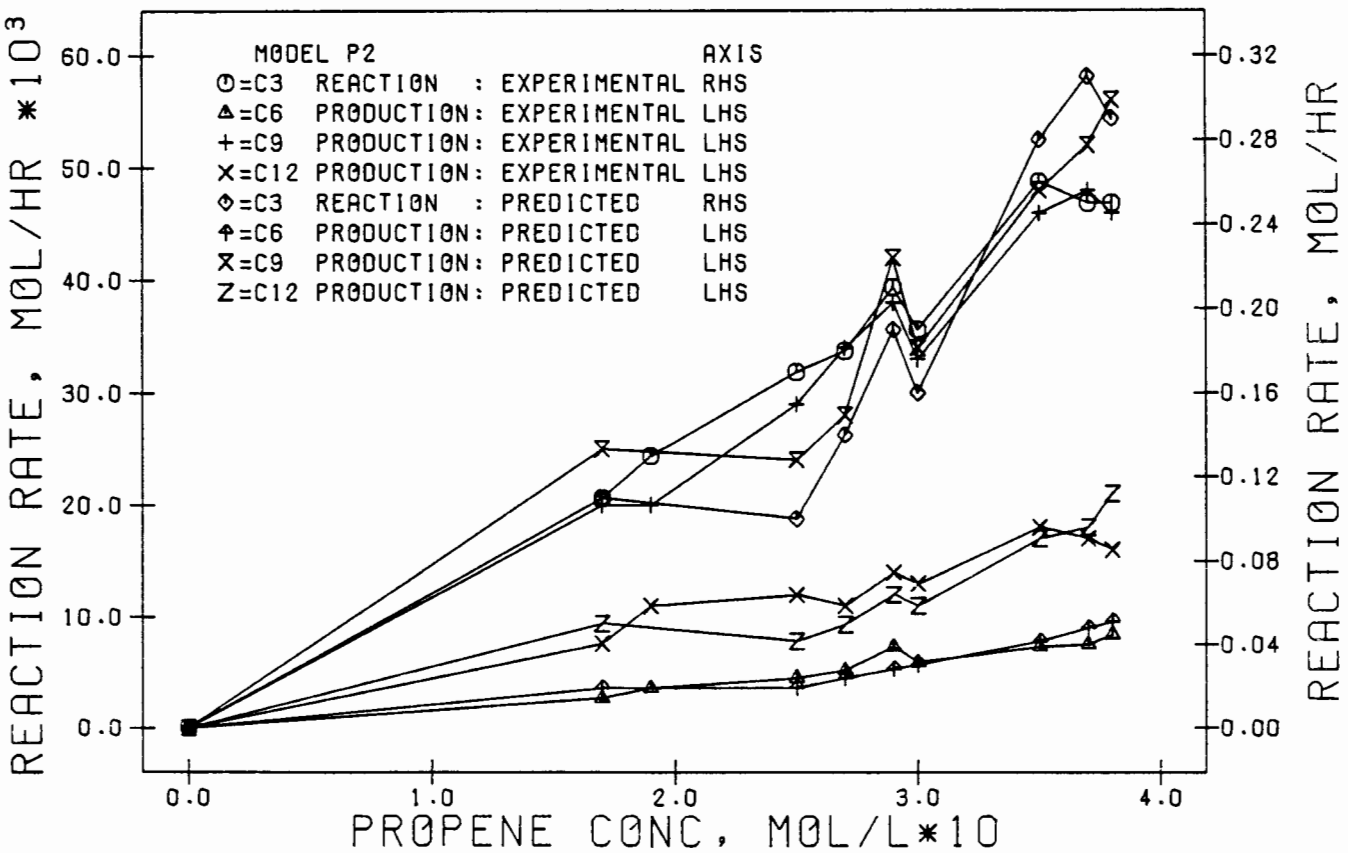

FIG 3.66 MODEL P2: PREDICTED AND EXPERIMENTAL REACTION RATES AS FUNCTIONS OF PROPENE CONCENTRATIONS AT 103% H3P04 AND 464 K

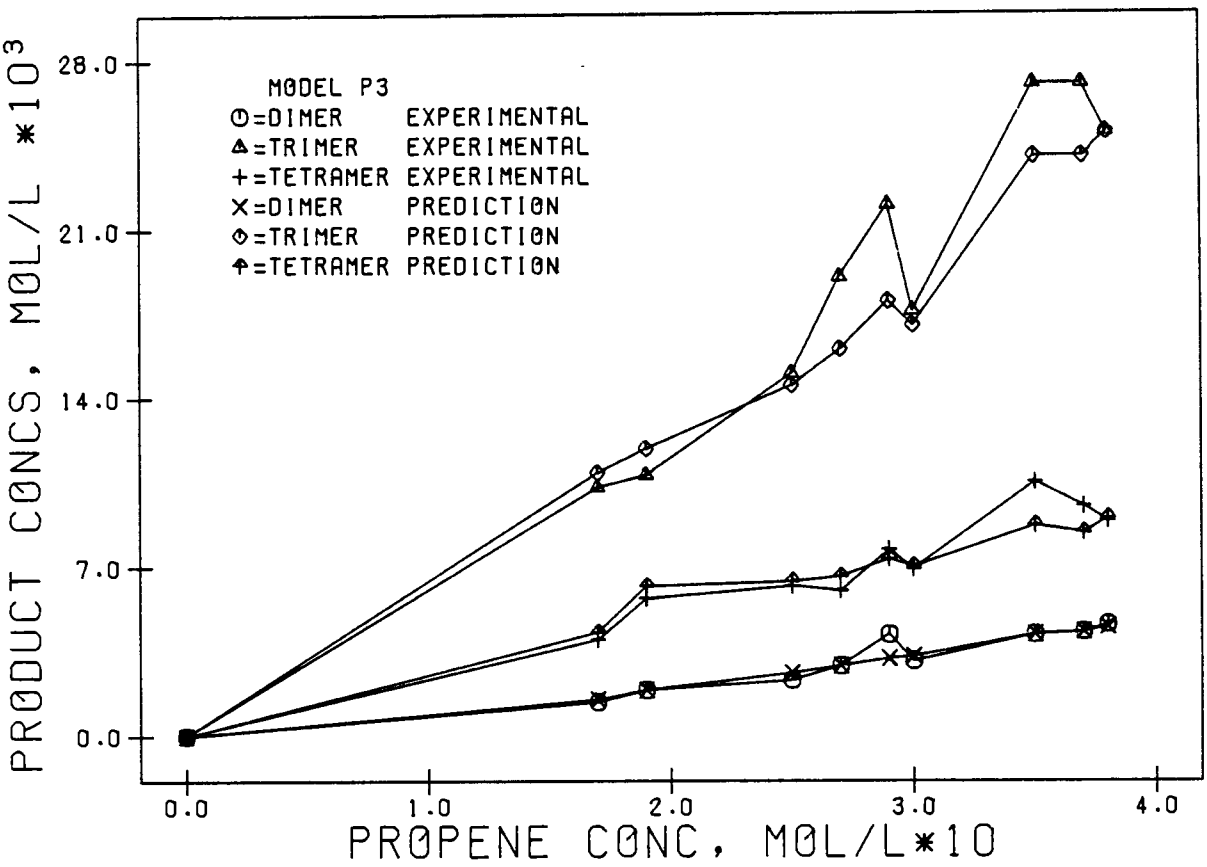

FIG 3.67 MODEL P3: PREDICTED AND EXPERIMENTAL PRODUCT CONCENTRATIONS AS FUNCTIONS OF PROPENE CONCENTRATIONS AT 103% H3P04 AND 464 K

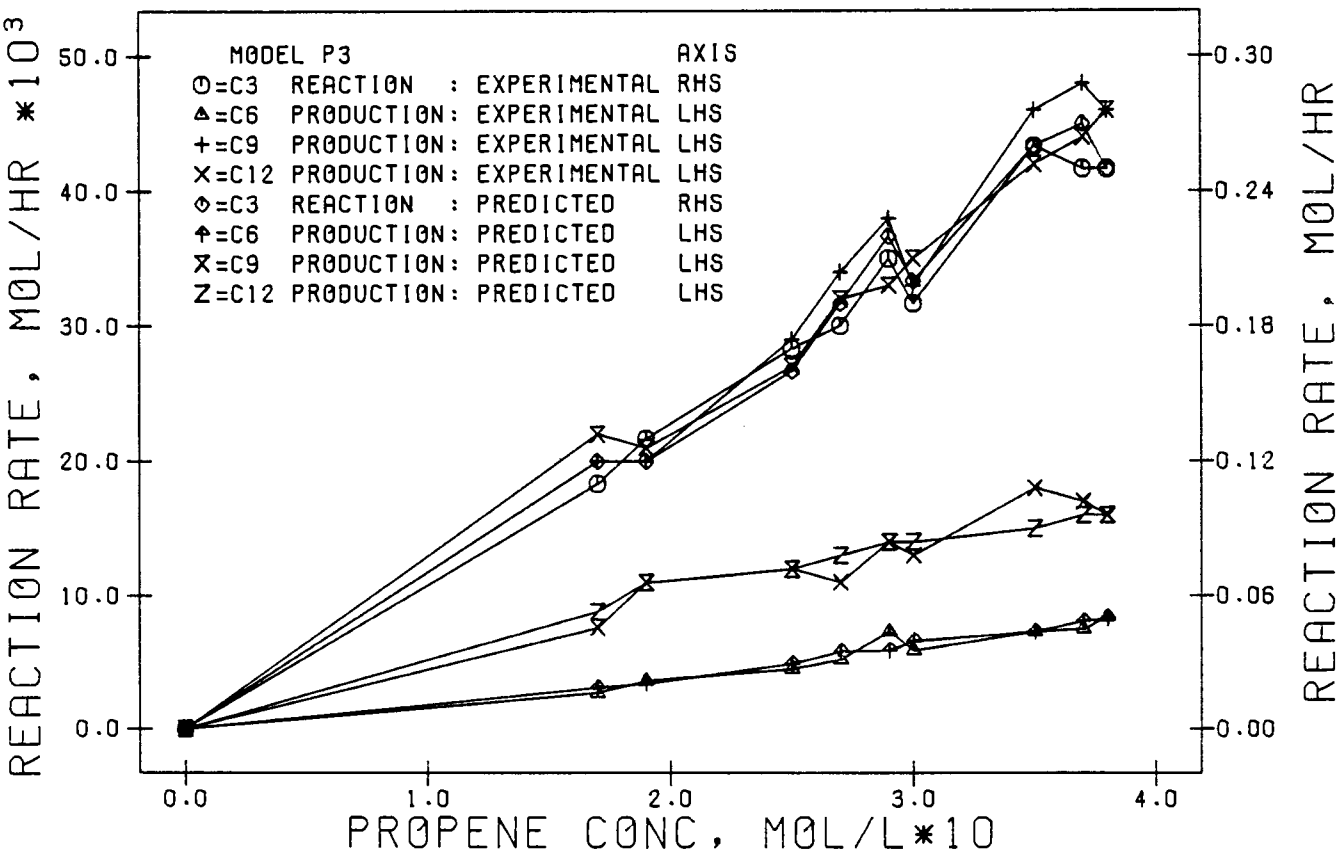

FIG 3.68 MODEL P3: PREDICTED AND EXPERIMENTAL REACTION RATES AS FUNCTIONS OF PROPENE CONCENTRATIONS AT 103% H3P04 AND 464 K

MODEL P4

Model P4 is also an empirical model, similar to model P3 with only one major difference. In this model, unlike model P3, it is assumed that the C_{12} fraction is produced entirely from the dimerization of C_6. The reaction $C_3 + C_9 \longrightarrow C_{12}$ is assumed not to occur. The reaction scheme is as follows:

$$C_3 + C_3 \xrightarrow{k_1} C_6$$

$$C_3 + C_6 \xrightarrow{k_3} C_9$$

$$C_6 + C_6 \xrightarrow{k_7} C_{12}$$

$$C_{12} \xrightarrow{k_9} C_{15} + \text{cracked products}$$

The rate equations are as follows:

$$-dC_3/dt = k_1 C_3^{0.9} + k_3 (C_3 C_6)^{0.5}$$

$$dC_6/dt = \tfrac{1}{2} k_1 C_3^{0.9} - k_3 (C_3 C_6)^{0.5} - k_7 C_6^{0.5}$$

$$dC_9/dt = k_3 (C_3 C_6)^{0.5}$$

$$dC_{12}/dt = \tfrac{1}{2} k_7 C_6^{0.5} - k_9 C_{12}$$

Using the data of Table 3.17 the following optimized values for the constants were found:

$$k_1 = 0.459 \ \text{mol}^{0.1} \cdot \text{hr}^{-1}$$

$$k_3 = 1.08 \ \text{l} \cdot \text{hr}^{-1}$$

$$k_7 = 0.63 \ \text{mol}^{0.5} \cdot \text{hr}^{-1}$$

$$k_9 = 0.55 \ \text{hr}^{-1}$$

Predicted and experimental rates and concentrations are plotted as functions of the propene reactor concentration in Figures 3.69 and 3.70. The data is listed in Appendix M.

It is quite clear from the graphical presentations that models P3 and P4 provide better fits to the experimental data. An error analysis was performed on each of the predicted and experimental data sets for both the rates and concentrations. The analysis was based on the data of Table 3.17. The results are shown for all four models for each of the following cases:

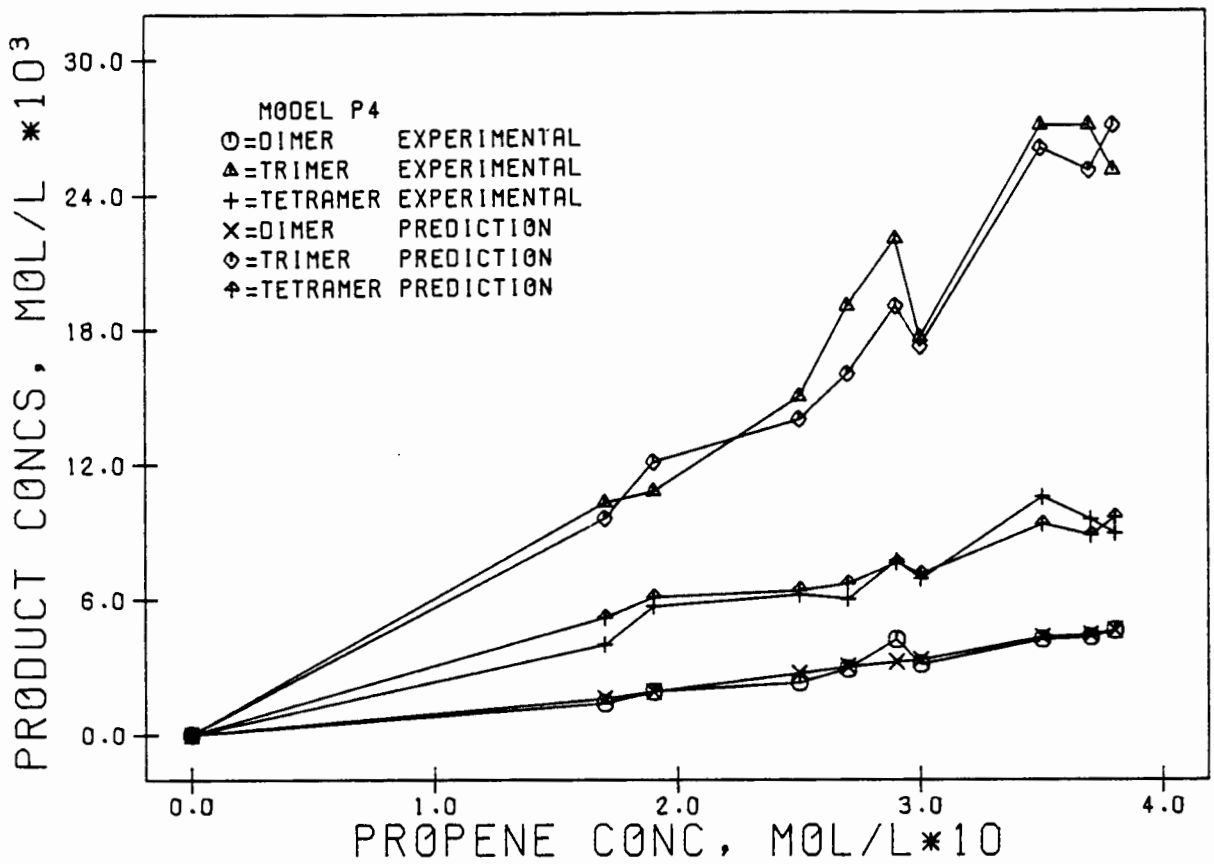

FIG 3.69 MODEL P4: PREDICTED AND EXPERIMENTAL PRODUCT CONCENTRATIONS AS FUNCTIONS OF PROPENE CONCENTRATIONS AT 103% H3P04 AND 464 K

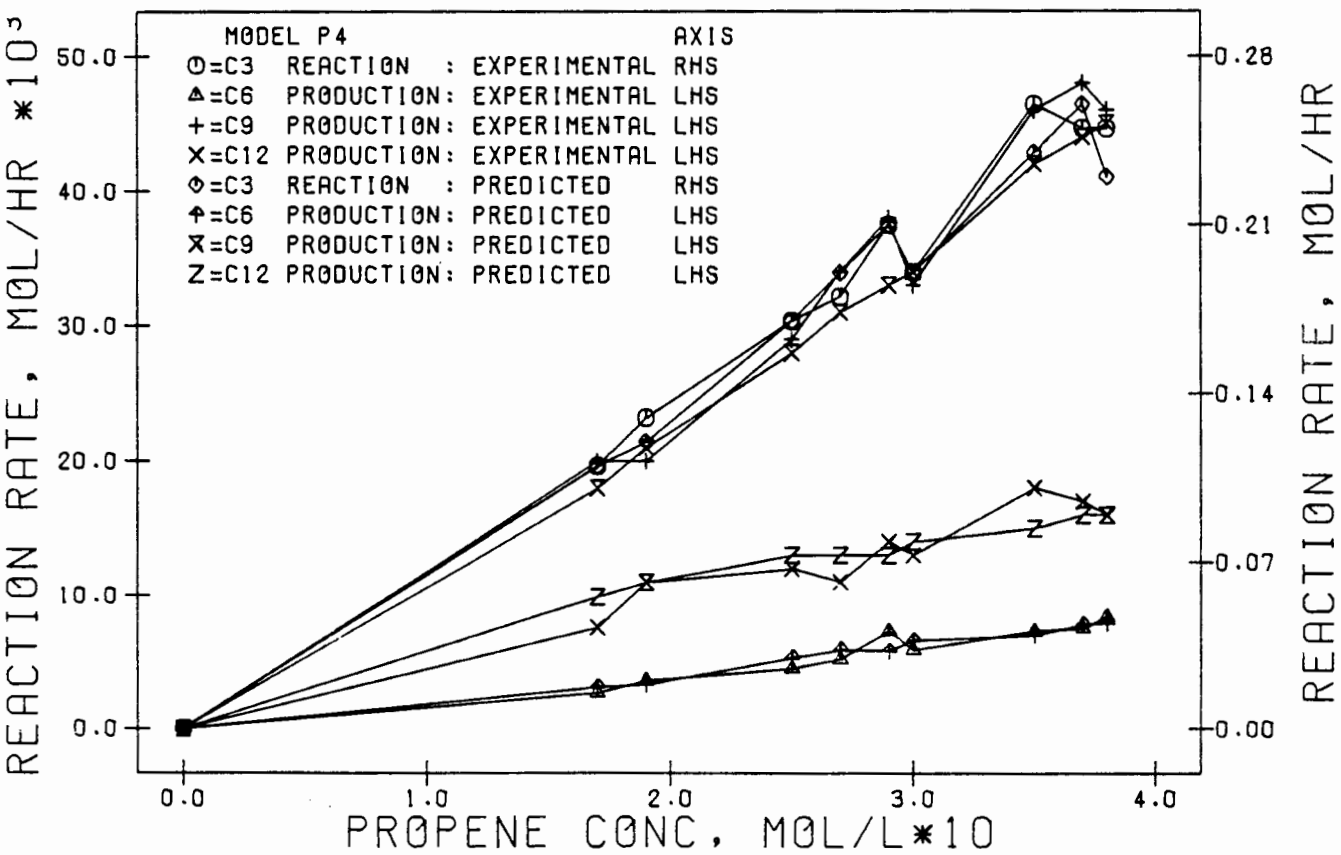

FIG 3.70 MODEL P4: PREDICTED AND EXPERIMENTAL REACTION RATES AS FUNCTIONS OF PROPENE CONCENTRATIONS AT 103% H3P04 AND 464 K

1. Predicted versus experimental concentrations for the dimer
2. Predicted versus experimental concentrations for the trimer
3. Predicted versus experimental concentrations for the tetramer
4. Predicted versus experimental rates for the rate of propene reaction
5. Predicted versus experimental rates for the rate of dimer production
6. Predicted versus experimental rates for the rate of trimer production
7. Predicted versus experimental rates for the rate of tetramer production

The results are shown in Figures 3.71 to 3.77. The average percentage deviation lines are not shown in these figures but are given in Table 3.31.

From the model predictions and the error analysis presentations it is quite clear that the empirical models P3 and P4 have significantly better fits to the data than models P1 and P2. The ability of models to predict

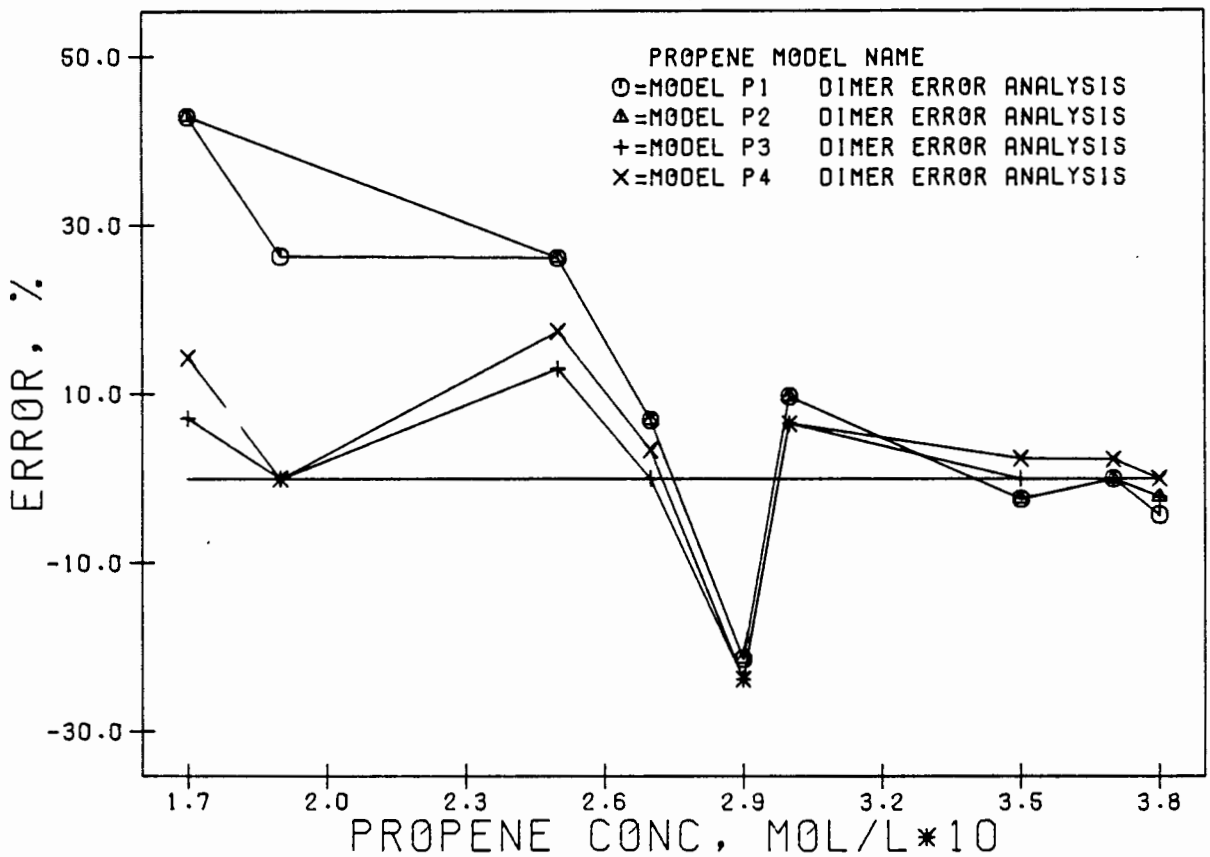

FIG 3.71 PERCENTAGE ERROR ANALYSIS, AS DETERMINED FROM THE PREDICTED AND EXPERIMENTAL DIMER CONCENTRATION, AS FUNCTIONS OF PROPENE CONCENTRATION AT 464 K AND 103% H3PO4 FOR MODELS P1, P2, P3 AND P4

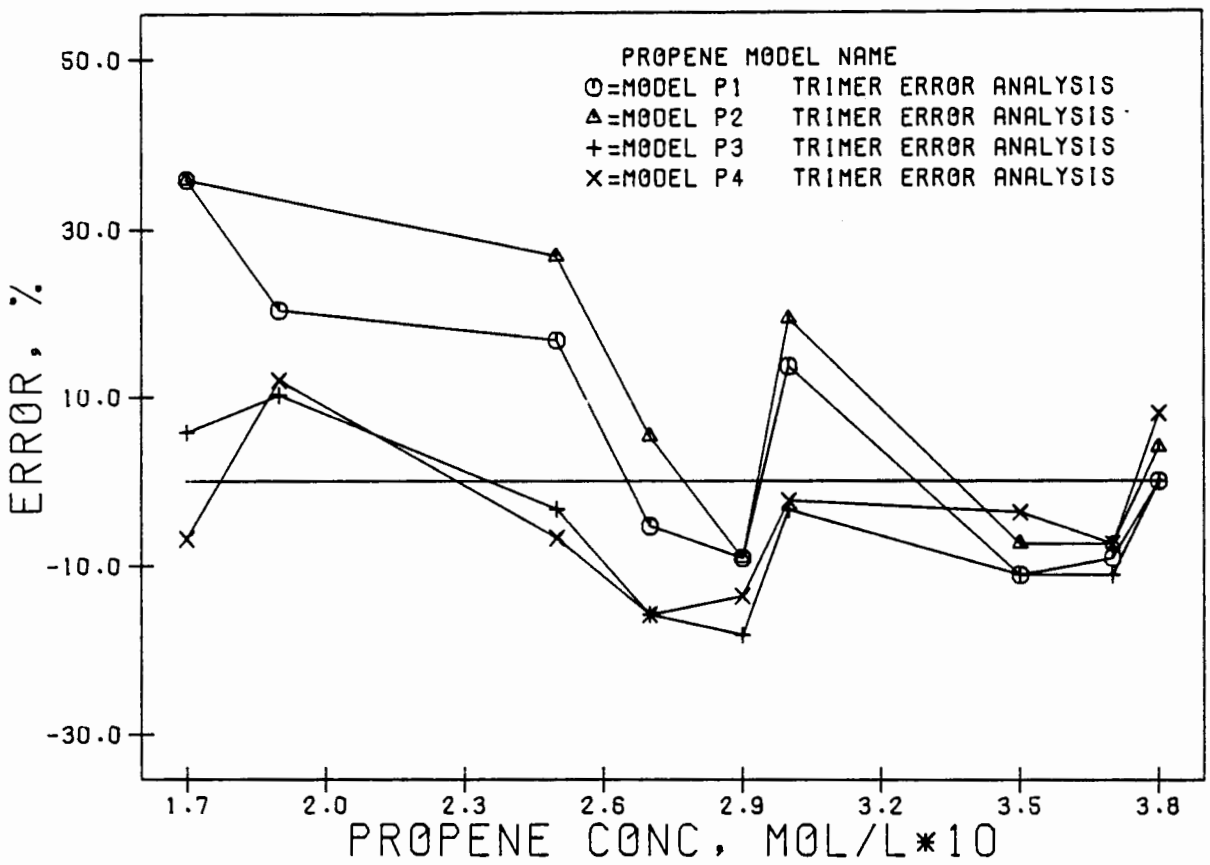

FIG 3.72 PERCENTAGE ERROR ANALYSIS, AS DETERMINED FROM THE PREDICTED AND EXPERIMENTAL TRIMER CONCENTRATION, AS FUNCTIONS OF PROPENE CONCENTRATION AT 464 K AND 103% H3P04 FOR MODELS P1, P2, P3 AND P4

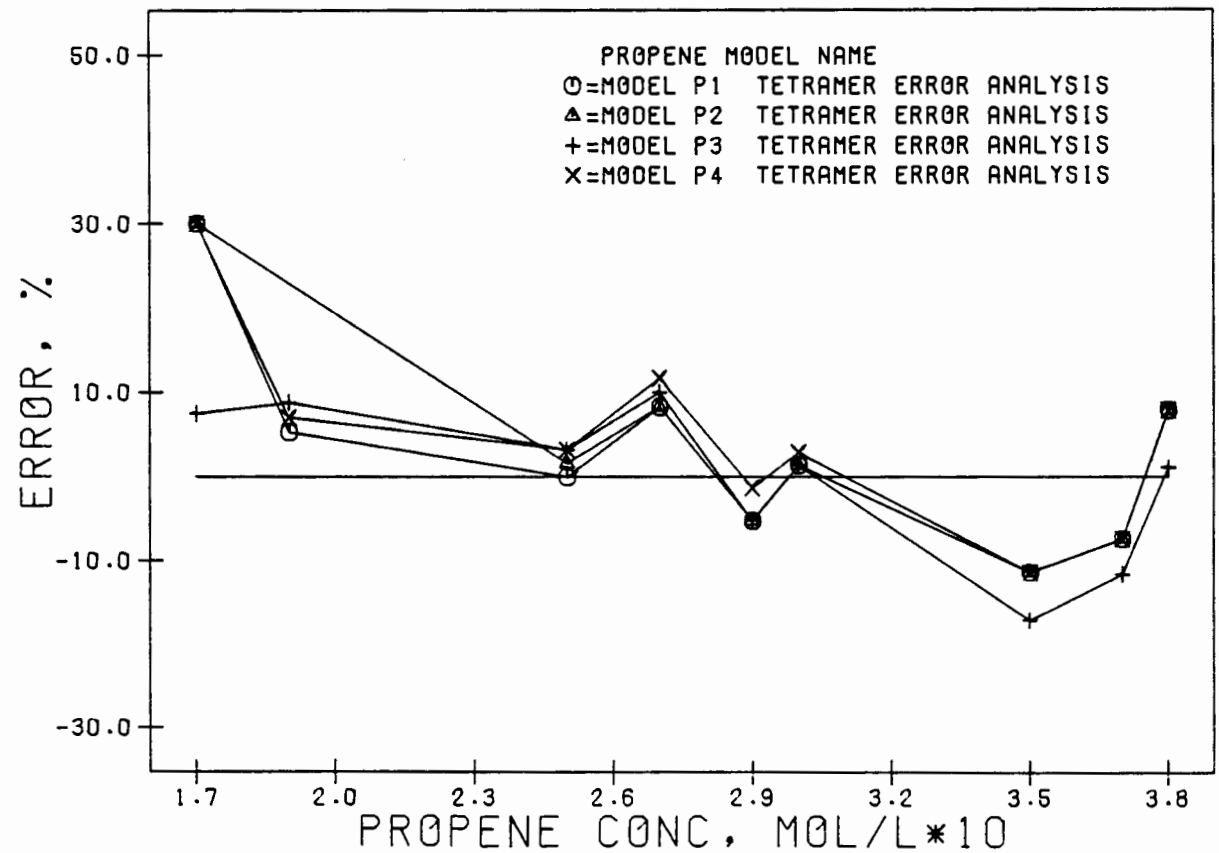

FIG 3.73 PERCENTAGE ERROR ANALYSIS, AS DETERMINED FROM THE PREDICTED AND EXPERIMENTAL TETRAMER CONCENTRATION, AS FUNCTIONS OF PROPENE CONCENTRATION AT 464 K AND 103% H3P04 FOR MODELS P1, P2, P3 AND P4

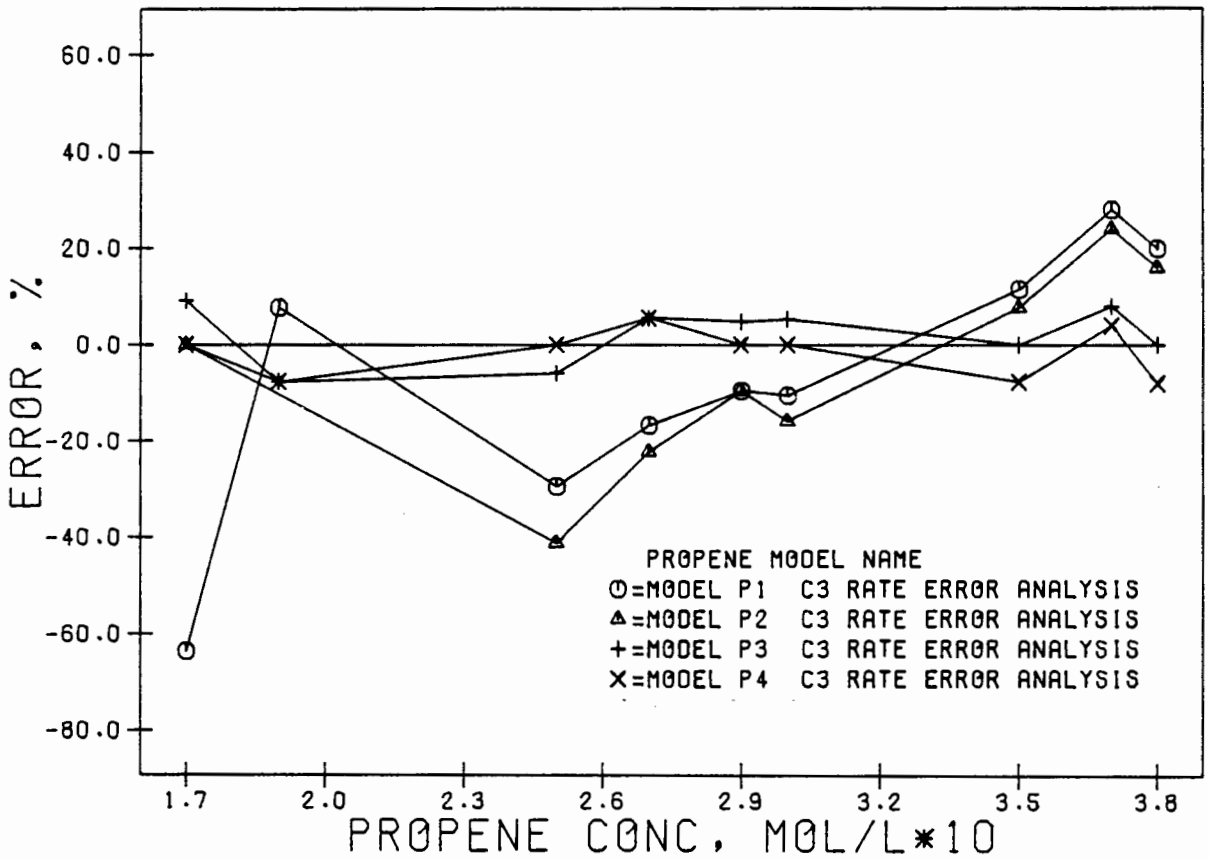

FIG 3.74 PERCENTAGE ERROR ANALYSIS, AS DETERMINED FROM THE PREDICTED AND EXPERIMENTAL PROPENE RATE, AS FUNCTIONS OF PROPENE CONCENTRATION AT 464 K AND 103% H3P04 FOR MODELS P1, P2, P3 AND P4

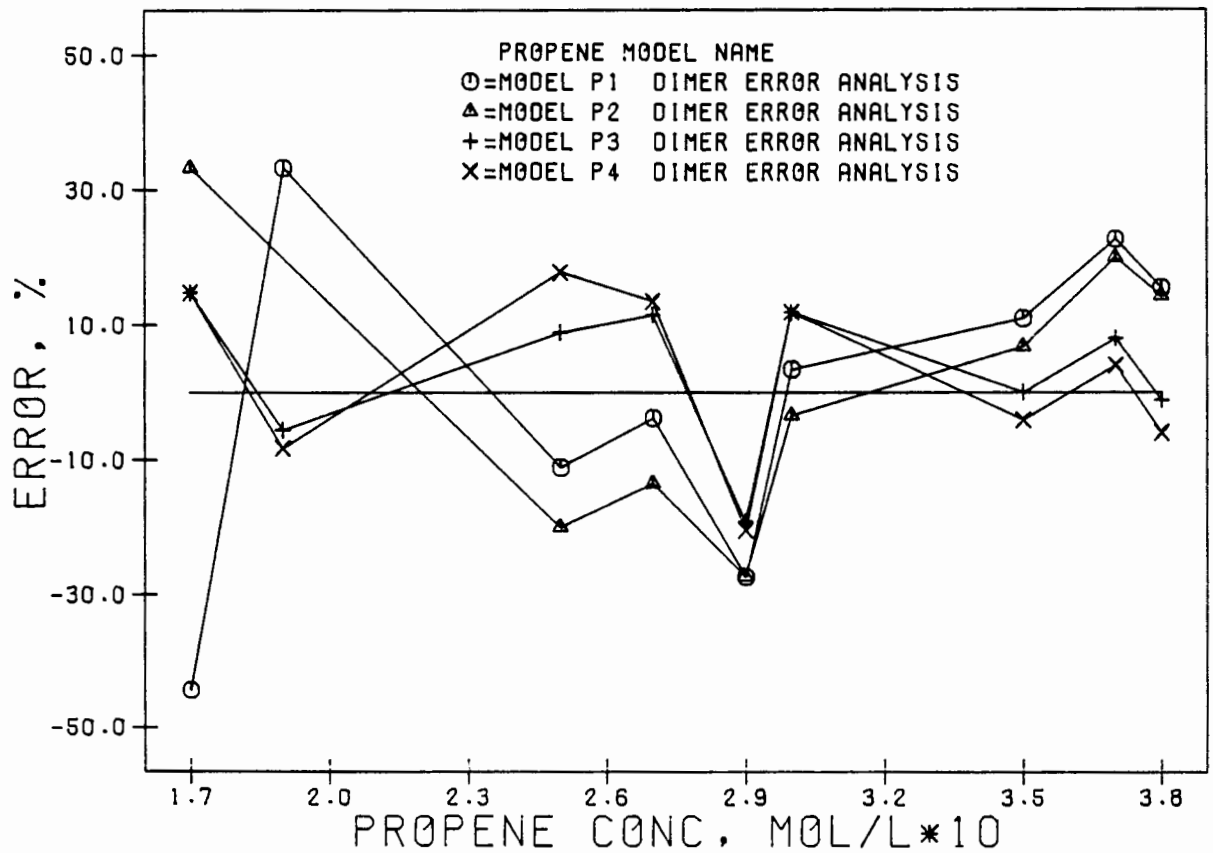

FIG 3.75 PERCENTAGE ERROR ANALYSIS, AS DETERMINED FROM THE PREDICTED AND EXPERIMENTAL DIMER RATE, AS FUNCTIONS OF PROPENE CONCENTRATION AT 464 K AND 103% H3P04 FOR MODELS P1, P2, P3 AND P4

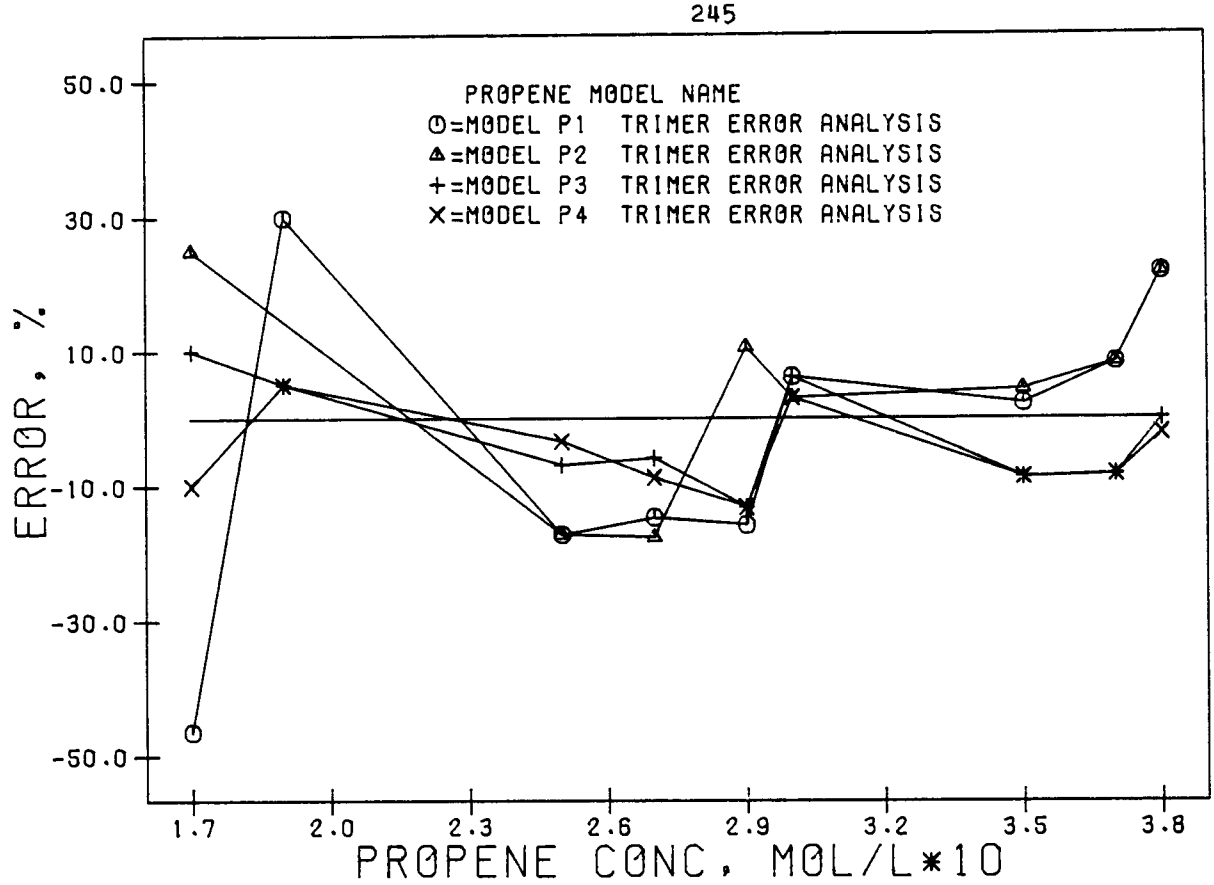

FIG 3.76 PERCENTAGE ERROR ANALYSIS, AS DETERMINED FROM THE PREDICTED AND EXPERIMENTAL TRIMER RATE, AS FUNCTIONS OF PROPENE CONCENTRATION AT 464 K AND 103% H3PO4 FOR MODELS P1, P2, P3 AND P4

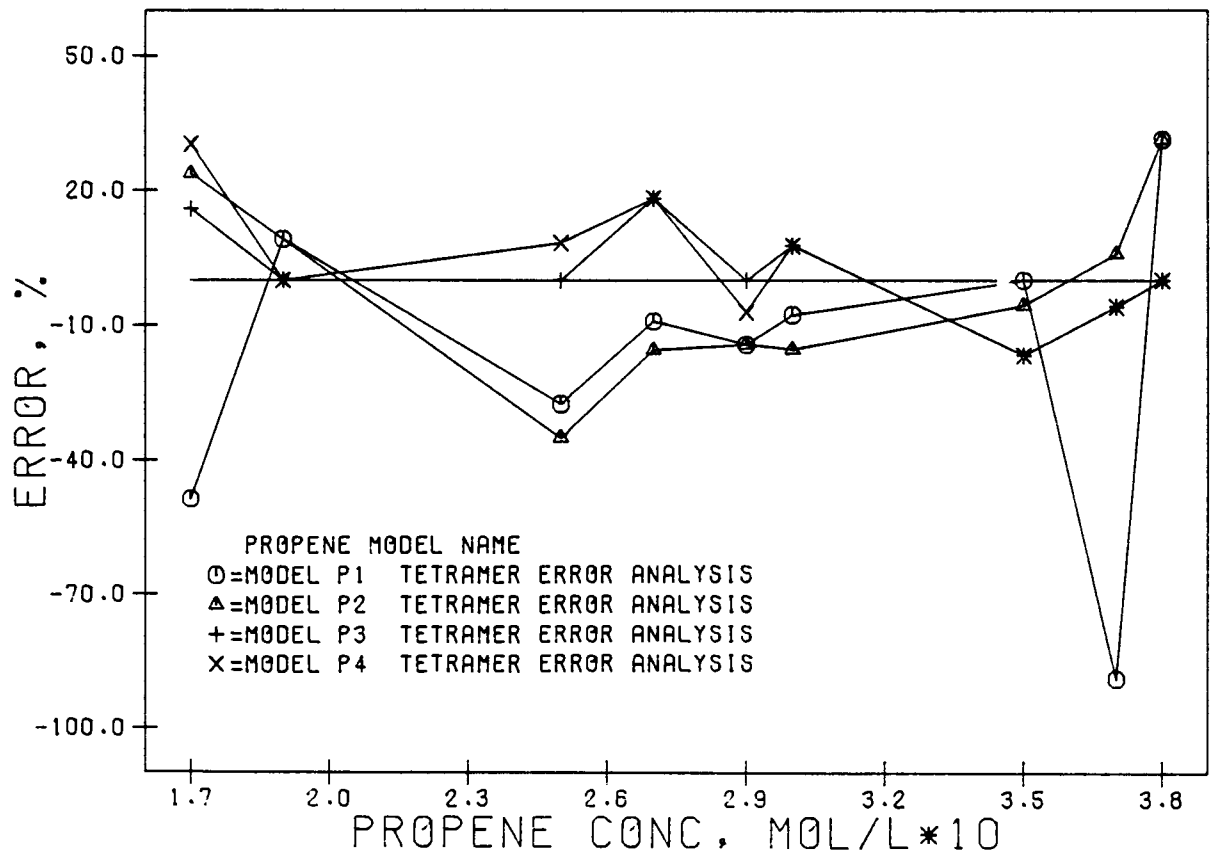

FIG 3.77 PERCENTAGE ERROR ANALYSIS, AS DETERMINED FROM THE PREDICTED AND EXPERIMENTAL TETRAMER RATE, AS FUNCTIONS OF PROPENE CONCENTRATION AT 464 K AND 103% H3PO4 FOR MODELS P1, P2, P3 AND P4

Table 3.31 The average percentage deviation lines for the error analysis plots of both the oligomer concentrations and rates of reaction/production for the models P1 to P4.

	Concentration deviations, %				Rate deviations, %		
	C_6	C_9	C_{12}	C_3	C_6	C_9	C_{12}
MODEL NO.							
P1	9.3	5.6	3.2	-6.9	-0.1	-2.9	-17.3
P2	7.5	8.4	3.2	-5.2	1.2	4.7	-3.1
P3	0.1	-5.2	-0.2	2.1	3.2	-2.4	2.1
P4	2.5	-4.0	4.7	-1.5	2.6	-5.2	3.9

can be misinterpreted if based solely on the deviation data listed in Table 3.31, since this table does not take into account the degree of spread around the zero deviation line. This can only be detected accurately from Figures 3.71 to 3.77. It is still quite clear from Table 3.31 that models P3 and P4 have a better fit to the data. The error analysis plots in combination with the deviation data of Table 3.31 show that models P1 and P2 do not give satisfactory fits to the experimental data. Deviations which regularly exceeded 20% were considered to be unacceptable.

At this point models P1 and P2 were discarded and model P5 was formulated. It was hoped from the empirical models that some mechanistic pointers could could have been obtained, which would have helped in the formulation of model P5 which is a model based on a fundamental acid site type approach. The model is based on the two step catalytic approach used by Boudard (1972). In each of the oligomerization reactions it is assumed that there are only two kinetically important steps. Here it is assumed that the rate determining step in each of these reactions is the reaction of the adsorbed molecule with the alkene and it is also assumed that the reactant is in adsorption equilibrium with the surface. For the dimerization of propene, for example, the following two steps would be considered to be important:

$$C_3 + * \overset{K_1}{\rightleftharpoons} \bar{C}_3$$

$$C_3 + \bar{C}_3 \overset{k_1}{\rightleftharpoons} \bar{C}_6$$

where the equilibrium constant K1 is given by

$$K_1 = \frac{\bar{C}_3}{C_3 \cdot *}$$

* = total number of free acid sites

and $\bar{C}i$ = adsorbed species i

Following this procedure for the formation of each each of the oligomers yields the following set of rate equations:

$-dC_3/dt = k_1\bar{C}_3C_3 + k_3\bar{C}_6C_3 + k_5\bar{C}_9C_3$

$dC_6/dt = \frac{1}{2}k_1\bar{C}_3C_3 - k_3\bar{C}_6C_3 - k_7\bar{C}_6C_6$

$dC_9/dt = k_3C_3\bar{C}_6 - k_5C_3\bar{C}_9$

$dc_{12}/dt = k_5C_3\bar{C}_9 + \frac{1}{2}k_7\bar{C}_6C_6 - k_9\bar{C}_{12}$

The total number of acid sites can be set equal to unity as follows:

$\bar{C}_3 + \bar{C}_6 + \bar{C}_9 + \bar{C}_{12} + * = 1$ and therefore by substituting for each of the adsorbed species terms using the expressions for each of the equilibrium constants gives the following relationship for total number of acid sites:

$(K_1C_3 + K_2C_6 + K_3C_9 + K_4C_{12} + 1)\cdot * = 1$

If $\propto$ is defined as $1/(K_1C_3 + K_2C_6 + K_3C_9 + K_4C_{12} + 1)$ then the rate equations can be expressed as follows, in terms of measurable parameters:

$-dC_3/dt = K_1k_1\propto C_3^2 + k_3K_2\propto C_6C_3 + k_5K_3\propto C_9C_3$

$dC_6/dt = \frac{1}{2}k_1K_1\propto C_3^2 - k_3K_2\propto C_6C_3 - k_7K_2\propto C_6^2$

$dC_9/dt = k_3K_2\propto C_3C_6 - k_5K_3\propto C_3C_9$

$dc_{12}/dt = k_5K_3\propto C_3C_9 + \frac{1}{2}k_7K_2\propto C_6^2 - k_9K_4\propto C_{12}$

This model can now be solved for the rate constants k_1, k_3, k_5, k_7, and k_9 and the equilibrium constants K_1, K_2, K_3, and K_4 using the optimization procedures used for models P1, P2, P3 and P4. This solution procedure was attempted but it was found that due to the complexity of the model it was not able to reach a global minimum in the minimum error functions due to the large number (9) of constants that required optimization. Two solutions to this problem were considered, viz., redicing the number of independent variables that required optimization and secondly by using a manual trial and error search. With respect to reducing the number of independent variables it was found that no reasonable basis for either the removal or the fixation of any of the variables could be made. Therefore, for the sake of avoiding unreasonable assumptions it was decided to try fixing the values of the equilibrium constants and thus by using a wide range of equilibrium constants obtain an optimized set of rate constants, k1, k3, k5, k7, and k9 at each of the equilibrium constants.

Twenty sets of equilibrium constants were used and it was found that these results did not improve on the fit of models P1 and P2 to the data, although the best results obtained, using this procedure, were approaching similar goodness of fits to the data as models P1 and P2.

Based on the findings for model P5 it was not possible to determine conclusively whether this model was satisfactory or not. It could only be concluded that the severe complexity of the model had to be reduced before a satisfactory optimized solution could be found, such as by reducing the number of constants.

The rate constants of models P3 and P4 only (since these two models gave the best fits to the data) were then examined for their temperature and H_3PO_4 concentration dependency. With respect to the temperature dependency of the rate constants, an Arrhenius type dependency was assumed to exist. The dependence of the rate constants on H_3PO_4 concentration was assumed to be of the form used in Section 3.5.4, i.e., $k = k' \cdot (\%H_3PO_4/100)^n$ at constant temperature. The following relationship was therefore assumed to exist for each constant:
$k = k' \cdot (\%H_3PO_4/100)^n \cdot e^{-E/RT}$.

The solution to this type of equation, for the constants k', n and E, has been described in Section 3.5.4. To determine the temperature dependence of these constants, the data of Table 3.17 was used (102% H_3PO_4). And to determine the dependence on H_3PO_4 concentration the data of Table 3.18 were used (464 K).

Dependence of the constants k_1, k_3, k_5 and k_9 of model P3 on temperature and H_3PO_4 concentration.

Each of the rate constants, k_1, k_3, k_5 and k_9, were determined at each temperature. The rate constants are shown in Table 3.32.

A straight line plot of ln k versus 1/T will have a slope of -E/R and a y-axis intercept of $\ln[k' \cdot (\%H_3PO_4/100)^n]$. From the Arrhenius plot the following results were obtained:

$k_1 = 535 \cdot e^{-E/RT}$ hr^{-1} where E/R = 3354 K
$r^2 = 0.99$

$k_3 = 0.269e^{-E/RT}$ $mol^{0.14} \cdot l^{0.86} \cdot hr^{-1}$ where E/R = -643 K
$r^2 = 0.88$

Table 3.32 The calculated rate constants k_1, k_3, k_5, and k_9 of model P3 at various temperatures calculated from the data of Table 3.17.

	Temperature, K			
	464	473	453	443
Rate constants				
k_1, hr^{-1}	0.39	0.49	0.33	0.27
k_3, $mol^{0.14} \cdot l^{0.86} \cdot hr^{-1}$	1.07	1.06	1.08	1.17
k_5, $mol^{0.4} \cdot l^{0.6} \cdot hr^{-1}$	0.081	0.085	0.078	0.073
k_9, $mol^{0.2} \cdot l^{1.2} \cdot hr^{-1}$	1.57	1.60	1.53	1.50

$k_5 = 0.743e^{-E/RT}\ mol^{0.4} \cdot l^{0.6} \cdot hr^{-1}$ where E/R = 1026 K

$r^2 = 0.99$

$k_9 = 4.22e^{-E/RT}\ mol^{0.2} \cdot l^{1.2} \cdot hr^{-1}$ where E/R = 459 K

$r^2 = 1.00$

The units of the rate constants are not indicated above but are as indicated previously. It must be remembered that the constants preceding the activation energy terms are dependent on the concentration of H_3PO_4, e.g., from the Arrhenius relationship for k_1 it must be remembered that $k_1' \cdot (\%H_3PO_4/100)^a = 535.\ hr^{-1}$

The activation energy for the production of the trimer was found to be negative. This surprising result must be considered in the light of the data in Table 3.32. Close examination of the rate constant/temperature data in the temperature range of 453 to 473 indicates quite clearly that this reaction is very insensitive to changes in temperature, and that the rate constant, k_3, found at 443 K is not consistent with the values of k3 found at the other temperatures. This is verified by the poor linear least squares correlation coefficient (r2 = 0.88) obtained from the arrhenius plot for this reaction.

The solution procedure to determine the dependency of rate constants on $\%H_3PO_4$ has been described in detail in Section 3.5.4. The rate constants as determined at each acid concentration (of Table 3.18) are listed in Table 3.33.

Table 3.33 The calculated rate constants k_1, k_3, k_5, and k_9 of model P3 at various H_3PO_4 concentrations calculated from the data of Table 3.18.

	H_3PO_4 concentration, %				
	104.5	106.4	107	102	103
Rate constants					
k_1, hr^{-1}	0.47	0.53	0.58	0.39	0.42
k_3, $mol^{0.14} \cdot l^{0.86} \cdot hr^{-1}$	1.17	1.26	1.37	1.07	1.14
k_5, $mol^{0.4} \cdot l^{0.6} \cdot hr^{-1}$	0.10	0.11	0.12	0.08	0.09
k_9, $mol^{0.2} \cdot l^{1.2} \cdot hr^{-1}$	1.45	1.54	1.46	1.56	1.60

The following power law relationships were found for each of the rate constants as functions of H_3PO_4 concentration. The Linear least squares correlation coefficient, r^2, is given for each constant.

$$k_1 = k_1' e^{-E/RT} \cdot [\%H_3PO_4/100]^{7.9} \quad hr^{-1} \qquad \text{where } r^2 = 0.99, \; k_1' e^{-E/RT} = 0.33$$

$$k_3 = k_3' e^{-E/RT} \cdot [\%H_3PO_4/100]^{4.49} \quad mol^{0.14} \cdot l^{0.86} \cdot hr^{-1} \qquad \text{where } r^2 = 0.96, \; k_3' e^{-E/RT} = 1.02$$

$$k_5 = k_5' e^{-E/RT} \cdot [\%H_3PO_4/100]^{7.75} \quad mol^{0.4} \cdot l^{0.6} \cdot hr^{-1} \qquad \text{where } r^2 = 0.99, \; k_5' e^{-E/RT} = 0.07$$

$$k_9 = k_9' e^{-E/RT} \cdot [\%H_3PO_4/100]^{-1.2} \quad mol^{0.2} \cdot l^{1.2} \cdot hr^{-1} \qquad \text{where } r^2 = 0.59, \; k_9' e^{-E/RT} = 1.60$$

The dependency of the rate constant k_9 on the H_3PO_4 concentration gave a very poor fit to the power law relationship assumed. This result must be taken in the context of the results as indicated in Table 3.33. It would appear from the k_9 values in this table that the rate constant, k_9, despite the large fluctuations, is quite insensitive to changes in the H_3PO_4 concentration and hence the possibility of a poor fit to the power law relationship was not entirely surprising.

The linear least squares correlation coefficient, r^2, for the k_9 case above is extremely poor. Examination of the k_9 data in Table 3.33 seems to indicate that the rate constant k_9 has little dependence on the H_3PO_4 concentration. The various k' values can now be determined from the

results given above. Taking k_1 for example, the value of k_1' can be found from each of the following equations separately:

$$k_1' \cdot (\%H_3PO_4/100)^a = 535 \text{ hr}^{-1}$$
$$k_1' \cdot e^{-E/RT} = 0.33 \text{ hr}^{-1}$$

The values of k' found in this way are:

$$k_1' = 456 \text{ hr}^{-1}$$
$$k_3' = 0.251 \text{ mol}^{0.14} \cdot l^{0.86} \cdot \text{hr}^{-1}$$
$$k_5' = 0.637 \text{ mol}^{0.4} \cdot l^{0.6} \cdot \text{hr}^{-1}$$
$$k_9' = 4.31 \text{ mol}^{0.2} \cdot l^{1.2} \cdot \text{hr}^{-1}$$

This now completes the description of model P3. A similar treatment regarding temperature and H_3PO_4 concentration dependency of the constants of model P4 was carried out.

Dependence of the constants k_1, k_3, k_7 and k_9 of model P4 on temperature and H_3PO_4 concentration.

Each of the rate constants, k_1, k_3, k_7 and k_9, were determined at each temperature. The rate constants are shown in Table 3.34.

Table 3.34 The calculated rate constants k_1, k_3, k_5, and k_9 of model P4 at various temperatures calculated from the data of Table 3.17.

	Temperature, K			
	464	473	453	443
Rate constants				
k_1, $\text{mol}^{0.1} \cdot \text{hr}^{-1}$	0.45	0529	0.38	0.31
k_3 $l \cdot \text{hr}^{-1}$	1.16	1.07	1.18	1.29
k_7 $\text{mol}^{0.5} \cdot \text{hr}^{-1}$	0.61	0.53	0.66	0.76
k_9 hr^{-1}	0.54	0.68	0.48	0.38

From the Arrhenius plot the following results were obtained:

$$k_1 = k_1' \cdot (\%H_3PO_4/100)^a \cdot e^{-E/RT} \text{ mol}^{0.1} \cdot \text{hr}^{-1}$$

where $E/R = 3580$ K

$r^2 = 1.00$

$$k_1' \cdot (\%H_3PO_4/100)^a = 1007 \text{ mol}^{0.1} \cdot \text{hr}^{-1}$$

$$k_3 = k_3' \cdot (\%H_3PO_4/100)^n \cdot e^{-E/RT} \quad l \cdot hr^{-1}$$

where $E/R = -7778$ K

$r^2 = 0.83$

$k_3' \cdot (\%H_3PO_4/100)^n = 6.4 \times 10^{-8}$ $l \cdot hr^{-1}$

$$k_7 = k_7' \cdot (\%H_3PO_4/100)^n \cdot e^{-E/RT} \quad mol^{0.5} \cdot hr^{-1}$$

where $E/R = -2400$ K

$r^2 = 0.99$

$k_7' \cdot (\%H_3PO_4/100)^n = 3.36 \times 10^{-3}$ $mol^{0.5} \cdot hr^{-1}$

$$k_9 = k_9' \cdot (\%H_3PO_4/100)^n \cdot e^{-E/RT} \quad mol^{0.5} \cdot hr^{-1}$$

where $E/R = 2360$ K

$r^2 = 0.91$

$k_9' \cdot (\%H_3PO_4/100)^n = 83.4$ $mol^{0.5} \cdot hr^{-1}$

It can be seen from the above activation energy data that the activation energies of the rate constants k_3 and k_7 were decisively negative. Unlike the rate constant k_3 of model P3 (where the temperature dependency of the rate constant k_3 was found to be very small) the rate constants k_3 and k_4 show a significant drop with increasing temperature. This could be an indication that model P4, although empirical, does not describe the set of reactions adeqately as a result of this inconsistency.

The rate constants as determined at each acid concentration (of Table 3.18) are listed in Table 3.35.

Table 3.35 The calculated rate constants k_1, k_3, k_7, and k_9 of model P3 at various H_3PO_4 concentrations calculated from the data of Table 3.18.

	H_3PO_4 concentration, %				
	104.5	106.4	107	102	103
Rate constants					
k_1, $mol^{0.1} \cdot hr^{-1}$	0.55	0.62	0.68	0.44	0.49
k_3, $l \cdot hr^{-1}$	1.22	1.26	1.37	1.16	1.21
k_7, $mol^{0.5} \cdot hr^{-1}$	0.75	0.83	0.87	0.61	0.69
k_9, hr^{-1}	0.57	0.49	0.49	0.53	0.57

The following power law relationships were found for each of the rate constants as functions of H_3PO_4 concentration. The linear least squares correlation coefficient, r^2, is given for each constant.

$$k_1 = k_1' e^{-E/RT} \cdot [\%H_3PO_4/100]^{8.48} \quad mol^{0.1} \cdot hr^{-1}$$

where $r^2 = 0.99$

$k_1' e^{-E/RT} = 0.38 \quad mol^{0.1} \cdot hr^{-1}$

$$k_3 = k_3' e^{-E/RT} \cdot [\%H_3PO_4/100]^{2.82} \quad l \cdot hr^{-1}$$

where $r^2 = 0.91$

$k_3' e^{-E/RT} = 1.09 \quad l \cdot hr^{-1}$

$$k_7 = k_5' e^{-E/RT} \cdot [\%H_3PO_4/100]^{6.89} \quad mol^{0.5} \cdot hr^{-1}$$

where $r^2 = 0.99$

$k_7' e^{-E/RT} = 0.55 \quad mol^{0.5} \cdot hr^{-1}$

$$k_9 = k_9' e^{-E/RT} \cdot [\%H_3PO_4/100]^{-2.57} \quad hr^{-1}$$

where $r^2 = 0.70$

$k_9' e^{-E/RT} = 0.60 \quad hr^{-1}$

The power law relationship between k_9 (and to a much lesser degree k_3) and the H_3PO_4 concentration as indicated above, resulted in a rather poor fit to the experimental data ($r2 = 0.70$). This suggests that some degree of error will be introduced when using this relationship. The values of k' were determined as follows:

$k_1' = 850 \quad mol^{0.1} \cdot hr^{-1}$

$k_3' = 5.9 \times 10^{-8} \quad l \cdot hr^{-1}$

$k_7' = 3.0 \times 10^{-3} \quad mol^{0.5} \cdot hr^{-1}$

$k_9' = 92.3 \quad hr^{-1}$

Prediction of model P3 and P4 at 464 K and 114% H_3PO_4 over a range of C_3 concentrations

Using the above relationships between rate constants and H_3PO_4 concentration and reaction temperature, models P3 and P4 were used to predict oligomer product concentrations, rates of formation of the oligomeric products and the rate of reaction of the monomer at the same conditions as were used to find the data of Table 3.15. This data was obtained at approximately 114% H_3PO_4 and 464 K. The experimental and predicted data are shown in Appendix M. This data is plotted for model P3 in Figures 3.78 (product concentrations versus propene concentration) and 3.79 (rates as functions of propene concentration), and for model P4 in Figure 3.80 and 3.81. The jump in the product concentrations and the rates at a propene concentration of 0.13 mol/l is a result of two experiments having been performed at identical concentrations but having

had different mean residence times. It should be noted that the predicted curves are based on predictions at the conditions of each experimental point and as a result the predicted curves are not smooth.

Examination of the results in Figures 3.78 to 3.81 shows that both models P3 and P4 give similar predictions of the experimental data at these conditions, both models tending to overpredict the experimental concentrations and rates, as would be expected at these high H_3PO_4 concentrations.

Prediction of model P3 and P4 at 111% H_3PO_4 and over a range of temperatures

In a similar manner to that above, both models P3 and P4 were used to predict product spectra and rates at identical conditions to the experiments of Table 3.16. The data is listed in Appendix M. The predicted and experimental data are shown in Figure 3.82 to 3.85. As has been previously pointed out it was not expected that the models would predict the experimental data accurately at these extremely high acid concentrations, not only due to the changing relationship between $\%H_3PO_4$ and the rate constants but also due to the rapid deactivation of the catalyst at these conditions, making the measurement of the reaction rates difficult. Model P3 prdicted the experimental concentrations of dimer, trimer and tetramer as well as the rates of production of dimer, trimer and tetramer with reasonable accuracy. The model P3 prediction of the rate of propene reaction, however, had significant scatter when compared to the experimental data, but in general tended to overpredict the rates as would be expected at these high H_3PO_4 concentrations. The prdiction of model P4 at these conditions can be seen to be significantly poorer than that of model P3 with respect to both rates and concentrations of reactant and products.

3.5.5.2 Modeling of the 1-butene rate data

The 1-butene data was modeled in a similar manner to the propene data. Four models were tested, one of them being an empirical model. The first model tested, B1, was similar to the propene model P1. Models B2 and B3 were variations of model B1 whereas the empirical model, B4, was simply a model that fitted the data as best as was possible, but had no mechanistic background as its basis. The rate/concentration data was taken from 3.21 of Section 3.4.5.1 (determined at 464 K and 103% H_3PO_4).

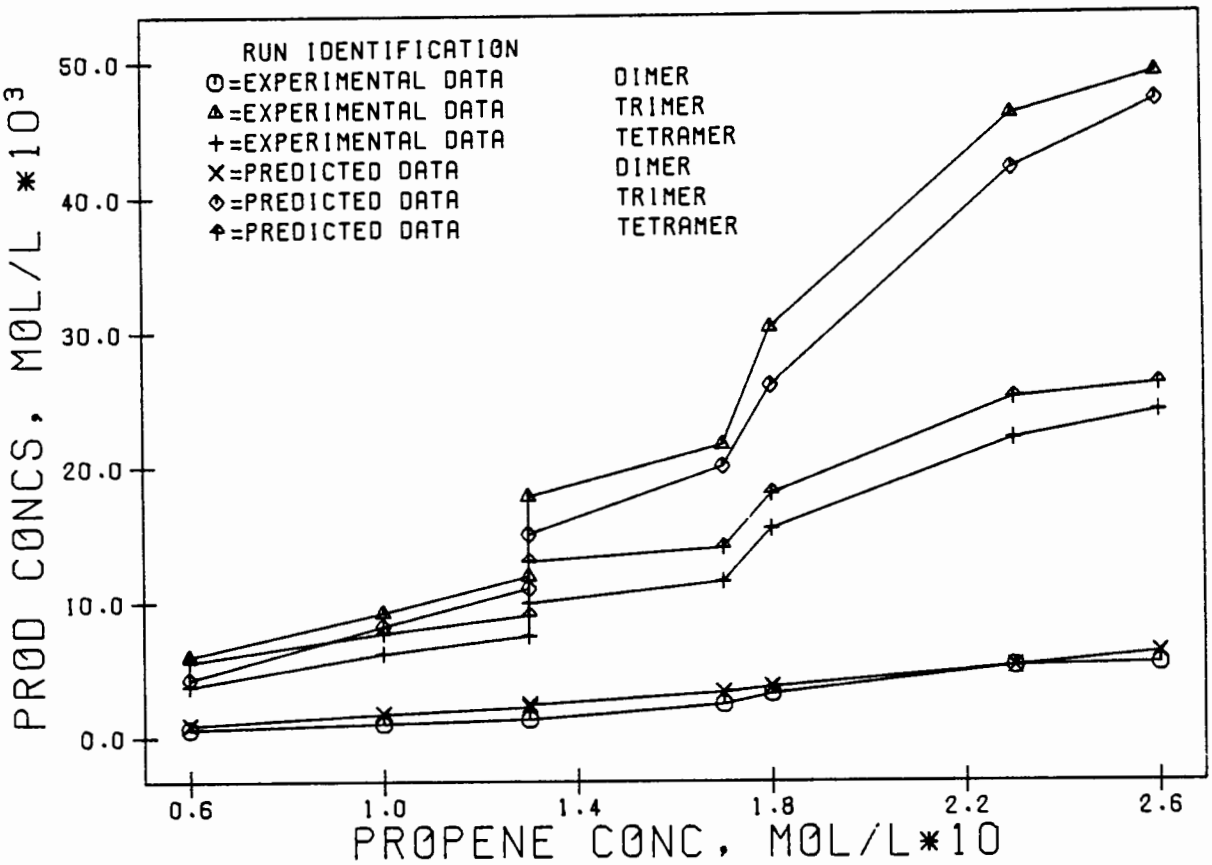

FIG 3.78 PREDICTED AND EXPERIMENTAL PRODUCT CONCENTRATIONS AS FUNCTIONS OF PROPENE CONCENTRATION AT 464 K AND 114% H3P04 USING MODEL P3

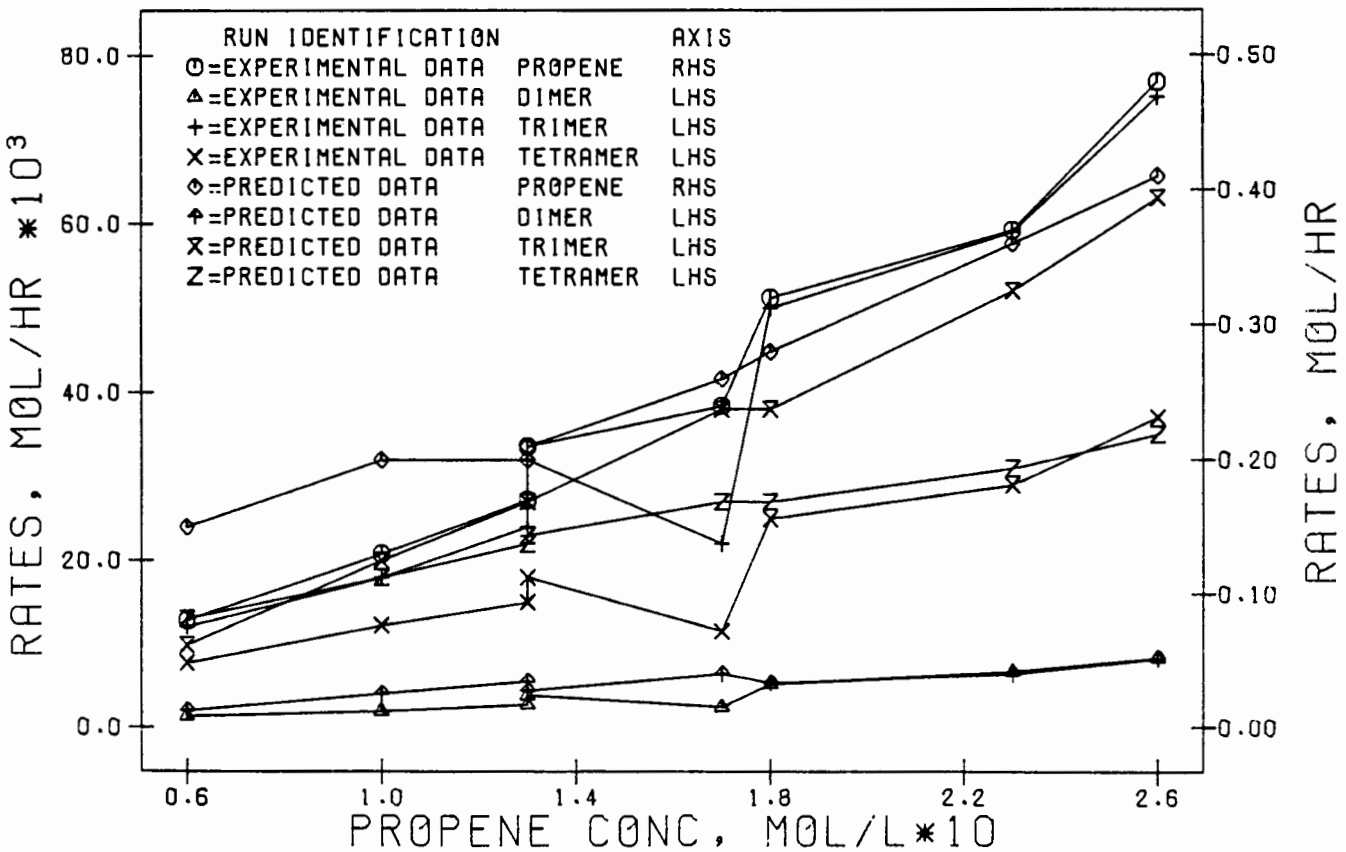

FIG 3.79 PREDICTED AND EXPERIMENTAL RATES AS FUNCTIONS OF PROPENE CONCENTRATION AT 464 K AND 114% H3P04 USING MODEL P3

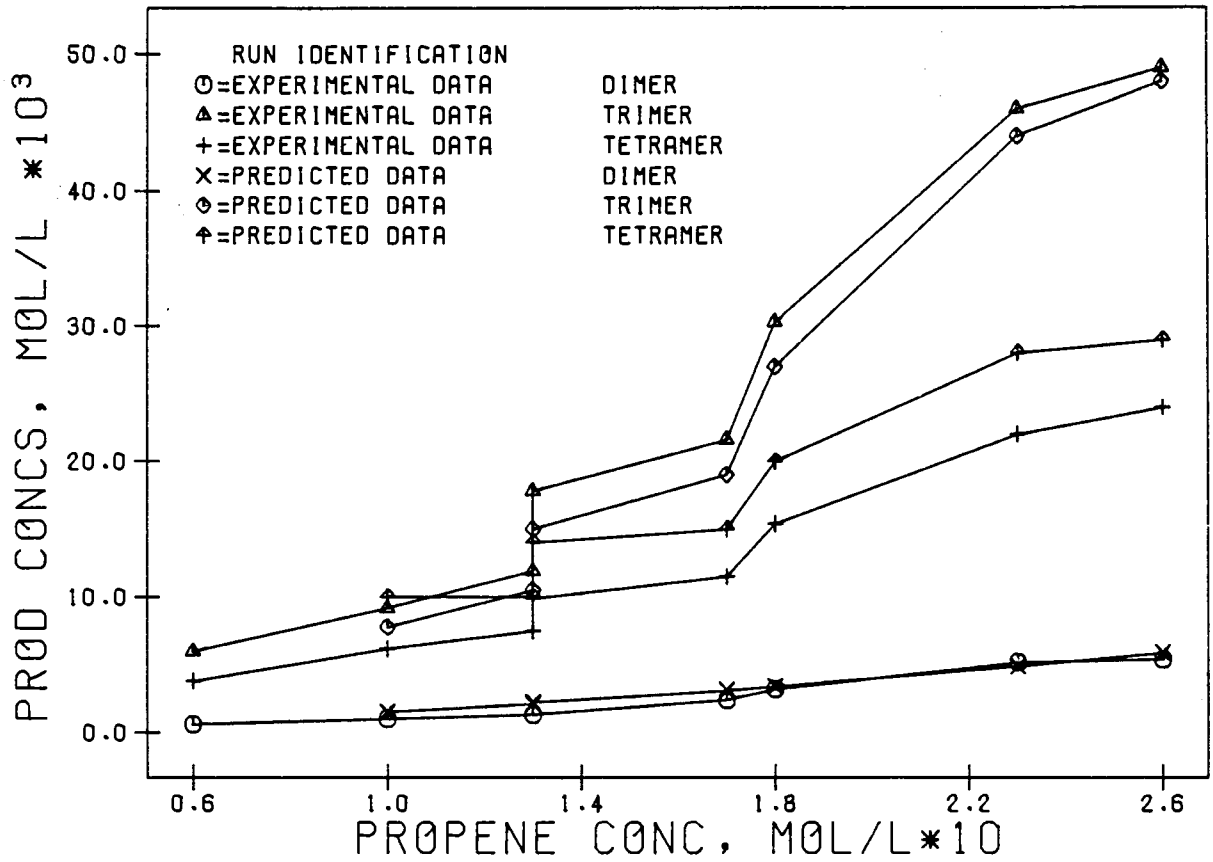

FIG 3.80 PREDICTED AND EXPERIMENTAL PRODUCT CONCENTRATIONS AS FUNCTIONS OF PROPENE CONCENTRATION AT 464 K AND 114% H3P04 USING MODEL P4

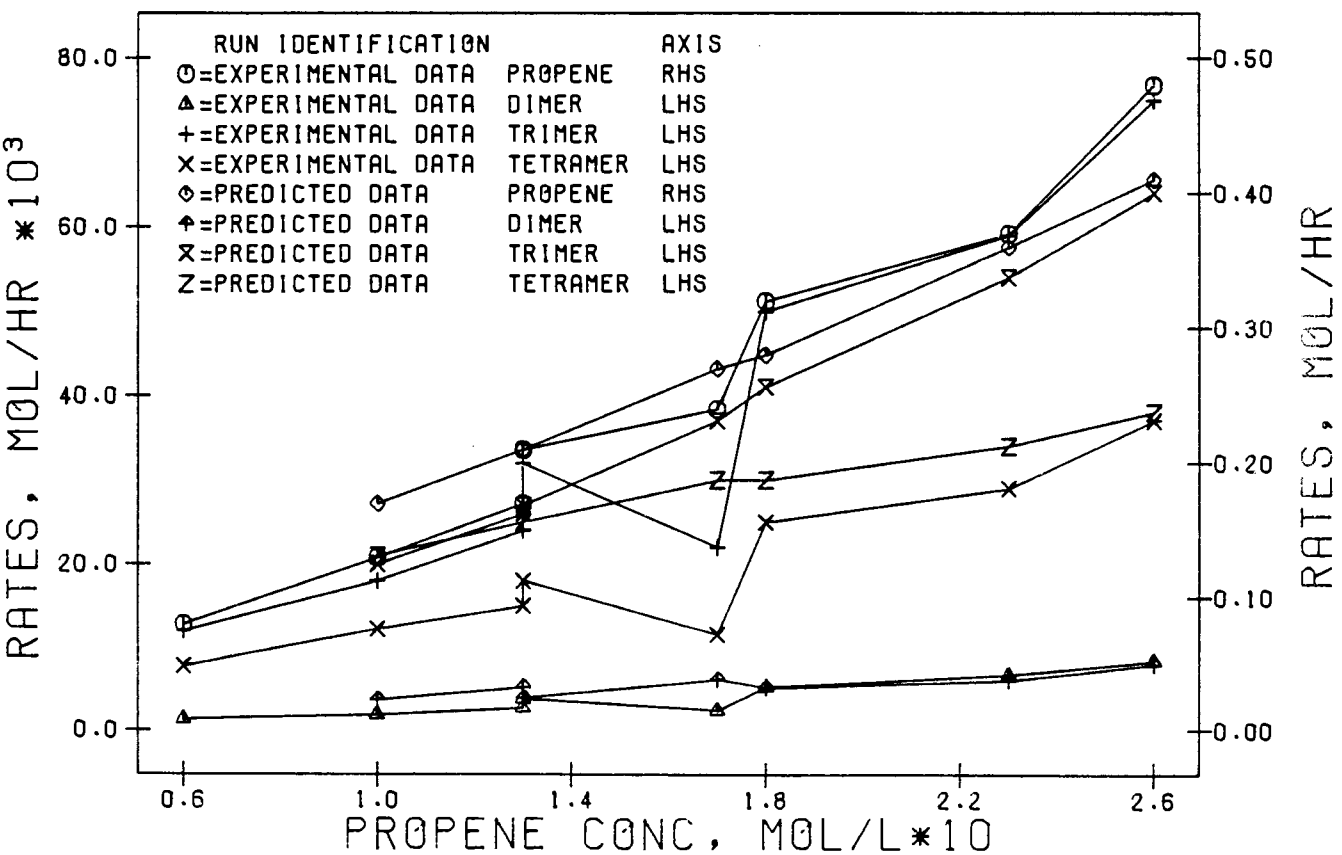

FIG 3.81 PREDICTED AND EXPERIMENTAL RATES AS FUNCTIONS OF PROPENE CONCENTRATION AT 464 K AND 114% H3P04 USING MODEL P4

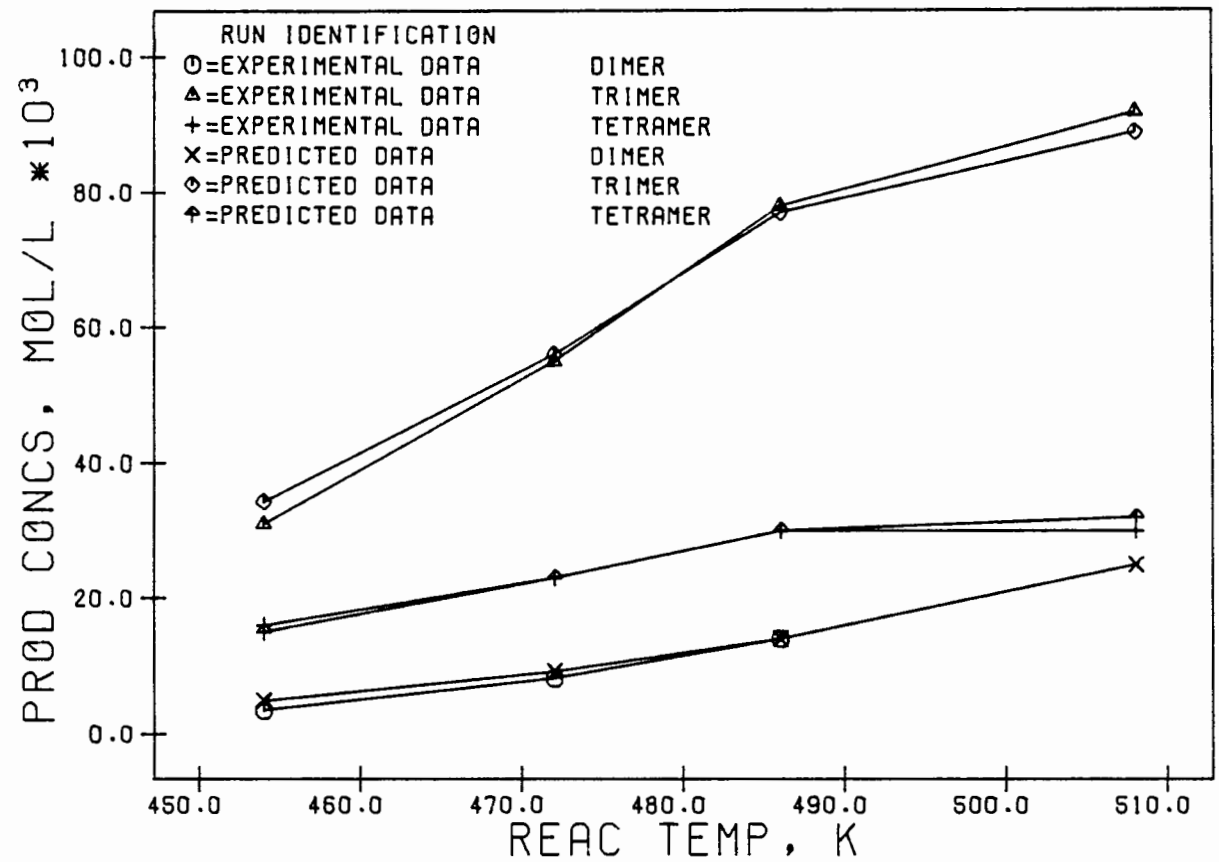

FIG 3.82 PREDICTED AND EXPERIMENTAL PRODUCT CONCENTRATIONS AS FUNCTIONS OF REACTOR TEMPERATURE AT 111% H3P04 USING MODEL P3

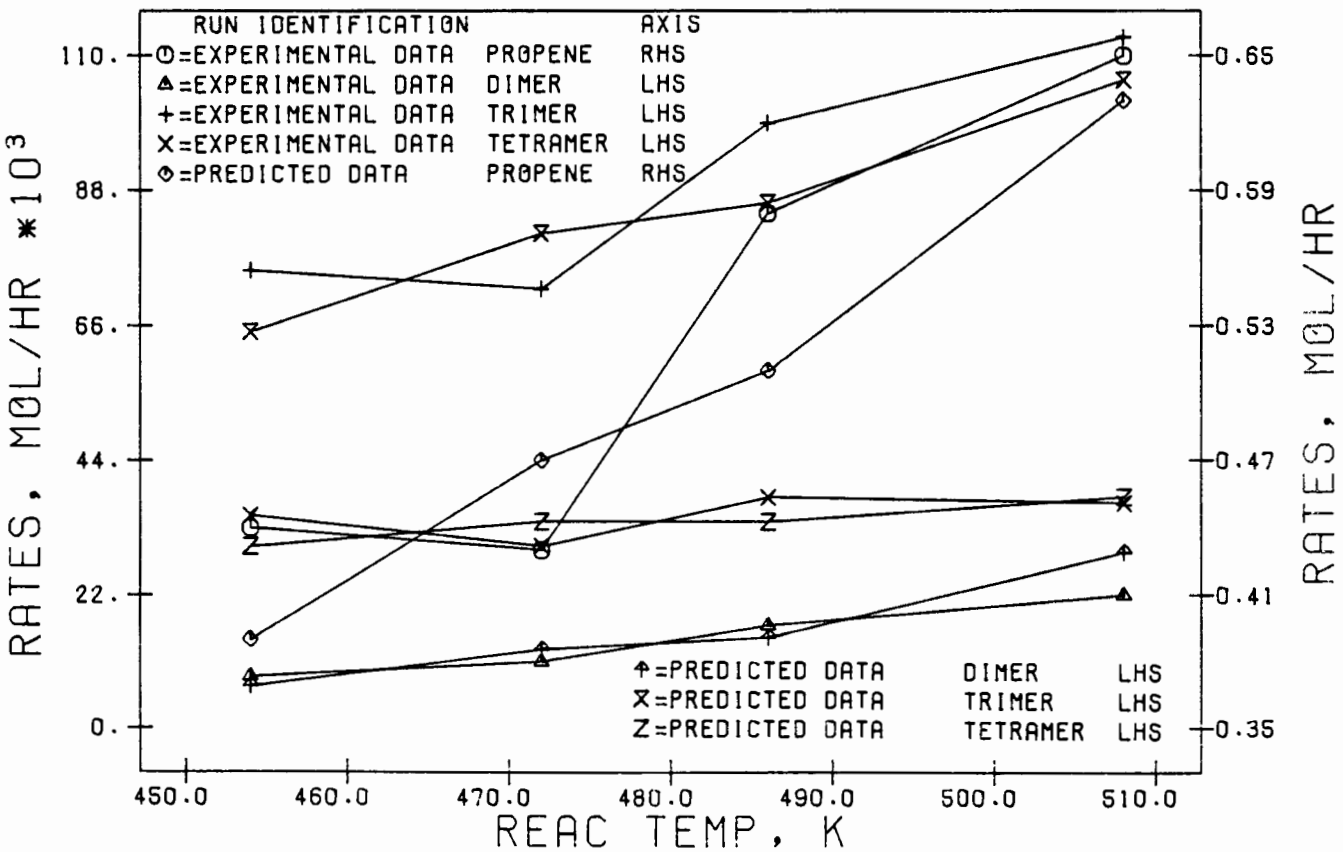

FIG 3.83 PREDICTED AND EXPERIMENTAL RATES AS FUNCTIONS OF REACTOR TEMPERATURE AT 111% H3P04 USING MODEL P3

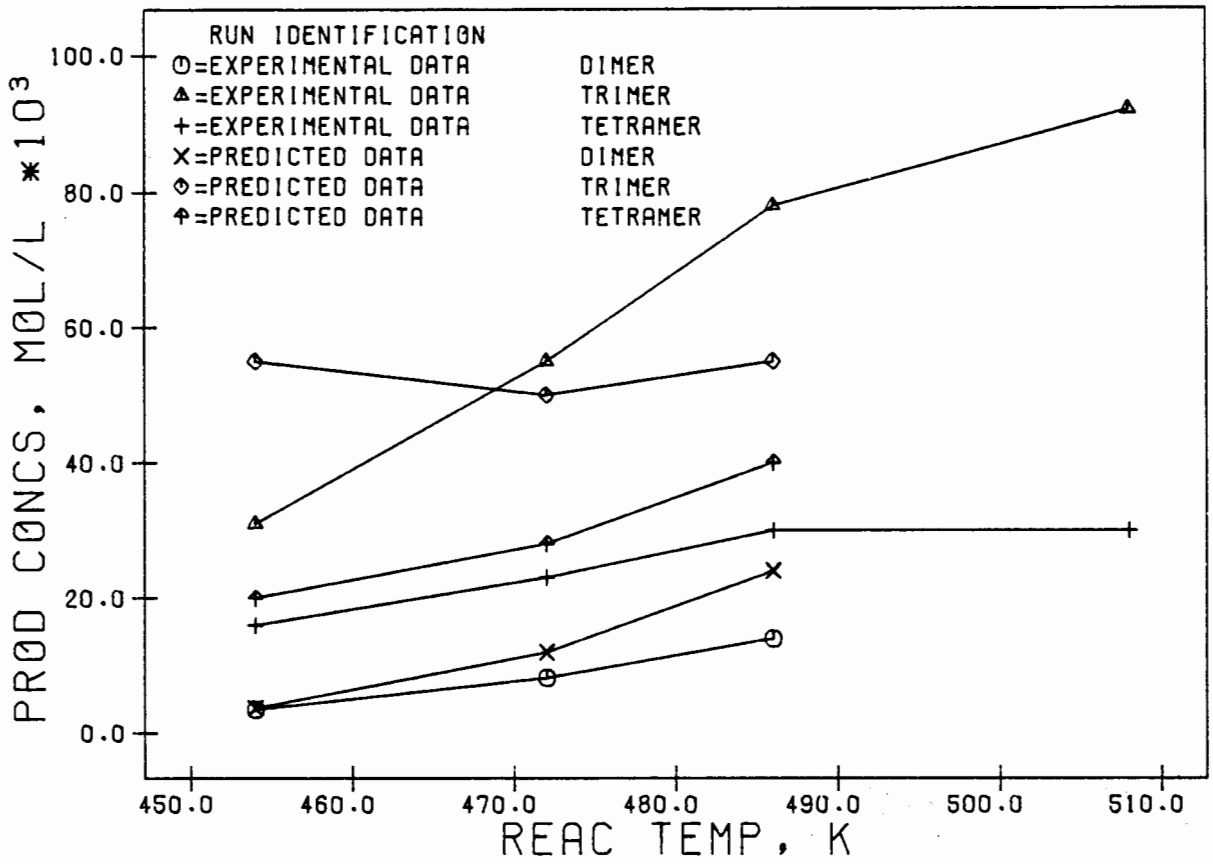

FIG 3.84 PREDICTED AND EXPERIMENTAL PRODUCT CONCENTRATIONS AS FUNCTIONS OF REACTOR TEMPERATURE AT 111% H3P04 USING MODEL P4

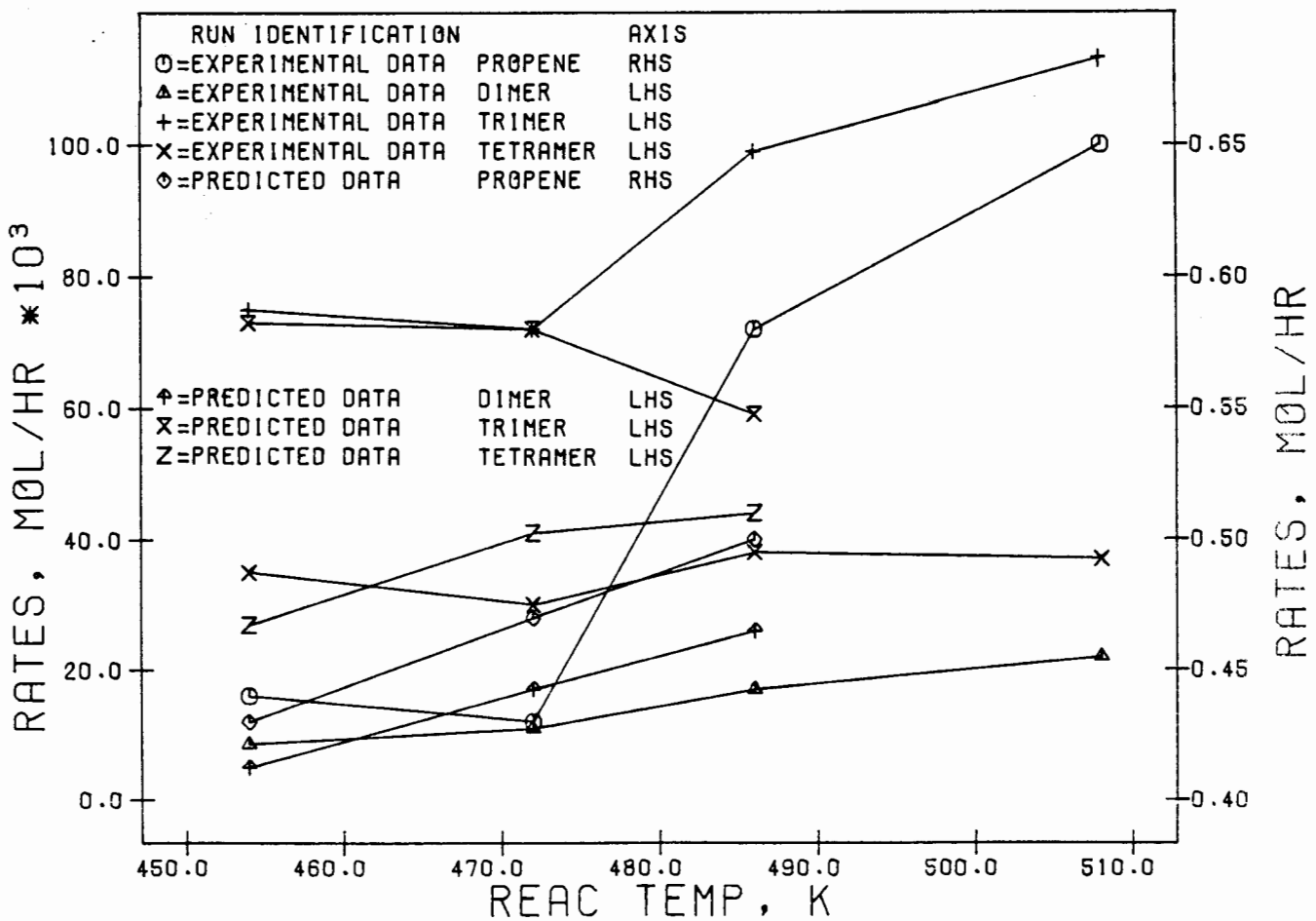

FIG 3.85 PREDICTED AND EXPERIMENTAL RATES AS FUNCTIONS OF REACTOR TEMPERATURE AT 111% H3P04 USING MODEL P4

MODEL B1 (1-BUTENE MODEL 1)

This model was based on three major assumptions which are as follows:

1. Reverse reactions were considered to be negligible.
2. All of the oligomerization reactions were considered to be elementary reactions.
3. All of the cracked products were assumed to be formed from the cracking of the C_{12} fraction alone.

The following set of reactions was therefore considered:

$$C_4 + C_4 \xrightarrow{k_1} C_8$$

$$C_4 + C_8 \xrightarrow{k_3} C_{12}$$

$$C_{12} \xrightarrow{k_5} \text{cracked products}$$

The resultant rate equations were as follows:

$$-dC_4/dt = k_1 C_4^2 + k_3 C_4 C_8$$

$$dC_8/dt = \tfrac{1}{2}k_1 C_4^2 - k_3 C_4 C_8$$

$$dC_{12}/dt = k_3 C_4 C_8 - k_5 C_{12}^1$$

where C_i = concentration of i

$-dC_4/dt$ = rate of 1-butene reaction

dC_i/dt = rate of production of oligomer; i = 8 or 12

The solution procedure was identical to that of the propene models P1 to P4. The set of rate constants that gave the best solution to the model are as follows:

$$k_1 = 2.53\ l^2 \cdot mol^{-1} \cdot hr^{-1}$$

$$k_3 = 0.68\ l^2 \cdot mol^{-1} \cdot hr^{-1}$$

$$k_5 = 0.84\ hr^{-1}$$

MODELS B2 AND B3

Model B_2 was very similar to model B_1, the only difference being that the rate of production of C_8 from C_4 was taken to be of the form $\frac{1}{2}k_1 C_4^1$ as opposed to $\frac{1}{2}k_1 C_4^2$ as in model B_1. Model B_3 was equivalent to model B_1 but with the reverse reaction of $C_{12} \xrightarrow{k_5} C_8 + C_4$ included.

The rate equations with the optimized constants are as follows:

Model B2

$$-dC_4/dt = k_1C_4^1 + k_3C_4C_8$$
$$dC_8/dt = \tfrac{1}{2}k_1C_4^1 - k_3C_4C_8$$
$$dC_{12}/dt = k_3C_4C_8 - k_5C_{12}^1$$

$k_1 = 0.87\ hr^{-1}$

$k_3 = 0.68\ l^2 \cdot mol^{-1} \cdot hr^{-1}$

$k_5 = 0.84\ hr^{-1}$

Model B3

$$-dC_4/dt = k_1C_4^2 + k_3C_4C_8$$
$$dC_8/dt = \tfrac{1}{2}k_1C_4^2 + k_4C_{12} - k_3C_4C_8$$
$$dC_{12}/dt = k_3C_4C_8 - K_4C_{12} - k_5C_{12}^1$$

$k_1 = 2.53\ l^2 \cdot mol^{-1} \cdot hr^{-1}$

$k_3 = 0.72\ l^2 \cdot mol^{-1} \cdot hr^{-1}$

$k_4 = 3.2 \times 10^{-8}\ hr^{-1}$

$k_5 = 0.84\ hr^{-1}$

MODEL B4

Model B4 was purely an empirical model consisting of the following set of equations:

$$C_4 + C_4 \xrightarrow{k_1} C_8$$

$$C_4 + C_8 \xrightarrow{k_3} C_{12}$$

$$C_{12} \xrightarrow{k_5} \text{cracked products}$$

The resultant rate equations were as follows:

$$-dC_4/dt = k_1C_4^n + k_3(C_4C_8)^m$$
$$dC_8/dt = \tfrac{1}{2}k_1C_4^n - k_3(C_4C_8)^m$$
$$dC_{12}/dt = k_3(C_4C_8)^m - k_5C_{12}^p$$

where $m = 0.415$

$n = 1.26$

$p = 0.77$

The following set of optimized constants were obtained:

$k_1 = 0.94 \quad mol^{-0.26} \cdot hr^{-1} \cdot l^{1.26}$

$k_3 = 0.096 \quad mol^{0.17} \cdot hr^{-1} \cdot l^{0.83}$

$k_5 = 0.139 \quad mol^{0.23} \cdot hr^{-1} \cdot l^{0.77}$

The quality of fit of the models to the data

Models B1, B2 and B3 gave very poor fits to the experimental data. Model B4 gave quite a reasonable fit to the data. Of models B1, B2 and B3 only the predictive concentrations from model B2 will be shown (since this model gave the best fit of these three). The experimental data (Table 3.21) and the predicted data from models B2 and B4 are shown in Tables 3.36 and 3.37.

Table 3.36 Experimental and predicted concentration data for 1-butene models B2 and B4.

	1-butene concentrations mol/l x 10						
Product concs mol/l x 10^3	1.15	3.75	2.25	1.22	3.78	2.29	1.62
Experimental							
C_8	20	130	79	24	134	62	36
C_{12}	4.7	21	13.4	4.6	24	11.3	7.0
Predicted Model B2							
C_8	32	160	106	35	168	87	53
C_{12}	0.5	12	4.9	0.6	13	3.5	1.3
Predicted Model B4							
C_8	21	128	74	23	134	62	36
C_{12}	4.6	22	16	4.8	24	12.6	7.7

It can be seen from the above data that the fit of model B2 (and hence B1 and B3, as was mentioned previously) to the data is extremely poor. For this reason a residual analysis was performed only on model B4. The predicted versus experimental rates and concentrations for model B4 are plotted as functions of the 1-butene concentration in Figures 3.86 and 3.87. The residual analysis plots for the concentrations of C_8 and C_{12} and for the rate of reaction of C_4 as well as the rates of production of C_8 and C_{12} are shown in Figure 3.88 for model B4 only. The average percentage deviations for this analysis are shown in Table 3.40. Two sets of deviation data are shown in Table 3.38. The first set comprises all of the data whereas the second set has one of the experiments removed as it is quite clear from Figure 3.88 that the worst deviation point is due to a poor experimental run and therefore the removal of this experiment from the analysis is quite justified.

Table 3.37 Experimental and predicted rate data for 1-butene models P2 and P4

Reaction rates	1-butene concentrations mol/l x 10						
	1.15	3.75	2.25	1.22	3.78	2.29	1.62
Experimental							
$-dC_4/dt$, mol/hrx10^3	100	335	280	110	350	225	160
dC_8/dt, mol/hrx10^3	32	116	96	37	120	74	51
dC_{12}/dt, mol/hrx10^3	7.2	19	16	7.1	22	13.6	9.9
Predicted Model B2							
dC_4/dt, mol/hrx10^3	299	990	586	310	1000	590	410
dC_8/dt, mol/hrx10^3	145	426	265	150	420	270	200
dC_{12}/dt, mol/hrx10^3	2.1	31	12	2.4	32	10.7	4.8
Predicted Model B4							
$-dC_4/dt$, mol/hr•10^3	99	346	203	106	350	206	142
dC_8/dt, mol/hr•10^3	31	118	64	34	119	70	46
dC_{12}/dt, mol/hr•10^3	6.8	21	13	7.2	21	14.1	9.9

Table 3.38 The average percentage deviations for the residual analysis plots for the rates and concentrations of model B4

Concentration deviations, %		Rate deviations, %		
C_8	C_{12}	C_4	C_8	C_{12}
-1.0	6.8	-6.9	-8.4	-1.9
-0.1	4.8	-3.5	-4.2	0.9

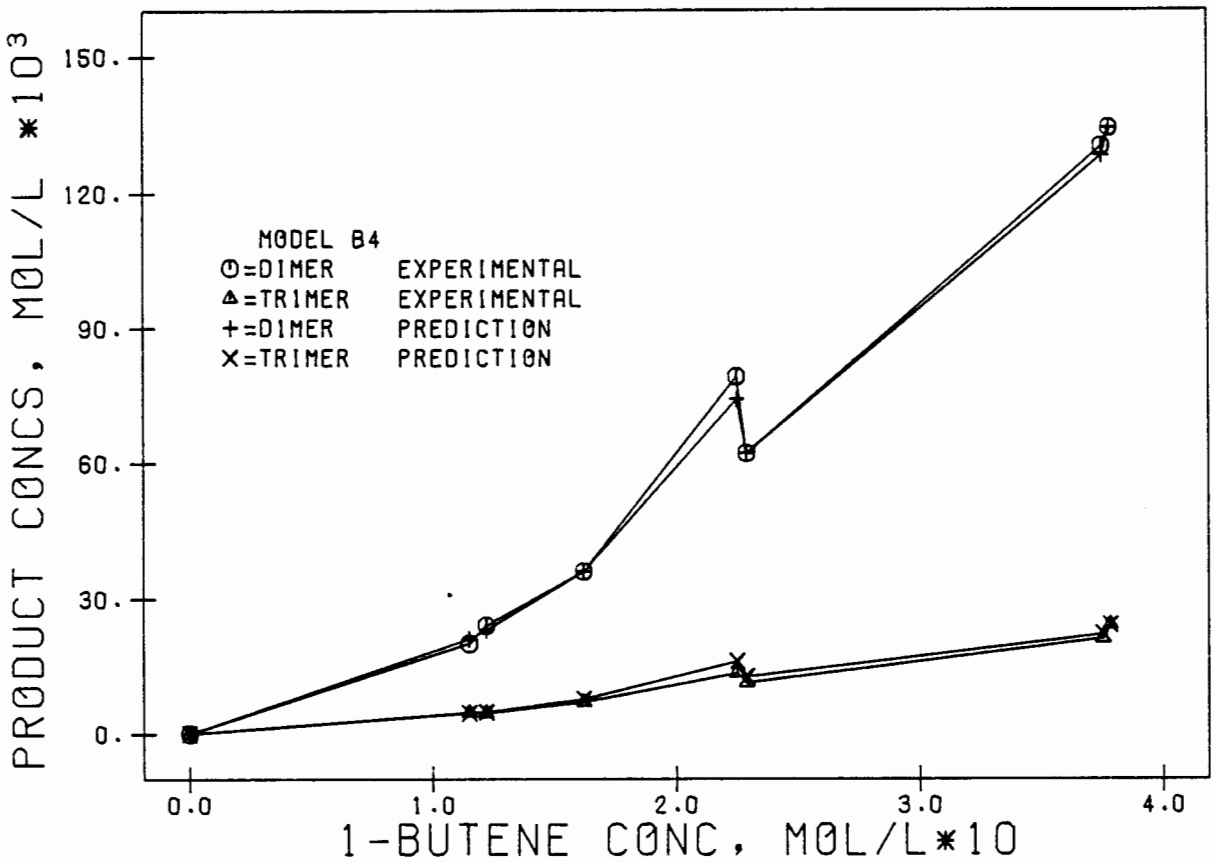

FIG 3.86 MODEL B4: PREDICTED AND EXPERIMENTAL PRODUCT CONCENTRATIONS AS FUNCTIONS OF 1-BUTENE CONCENTRATION AT 103% H3P04 AND 464 K

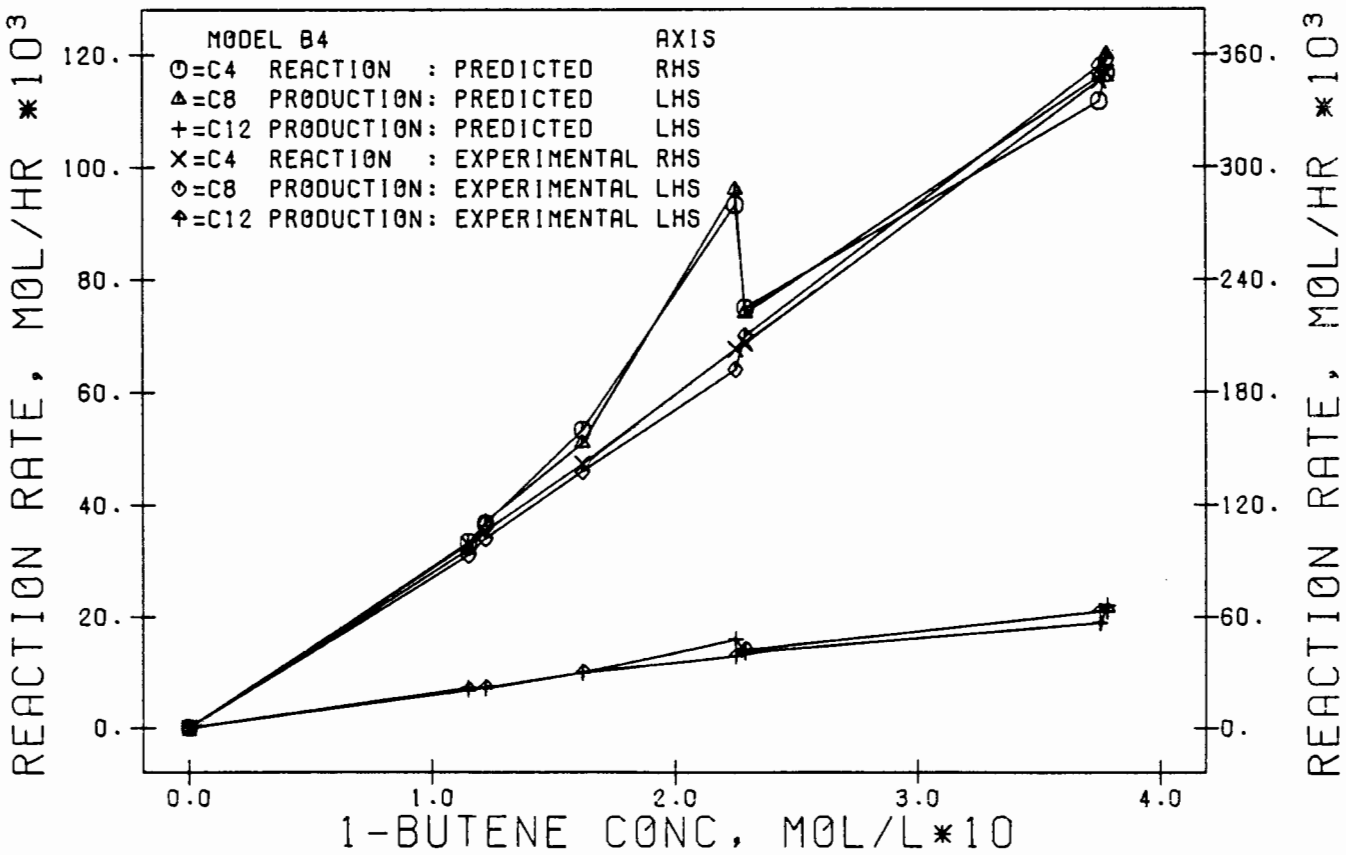

FIG 3.87 MODEL B4: PREDICTED AND EXPERIMENTAL REACTION RATES AS FUNCTIONS OF 1-BUTENE CONCENTRATIONS AT 103% H3P04 AND 464 K

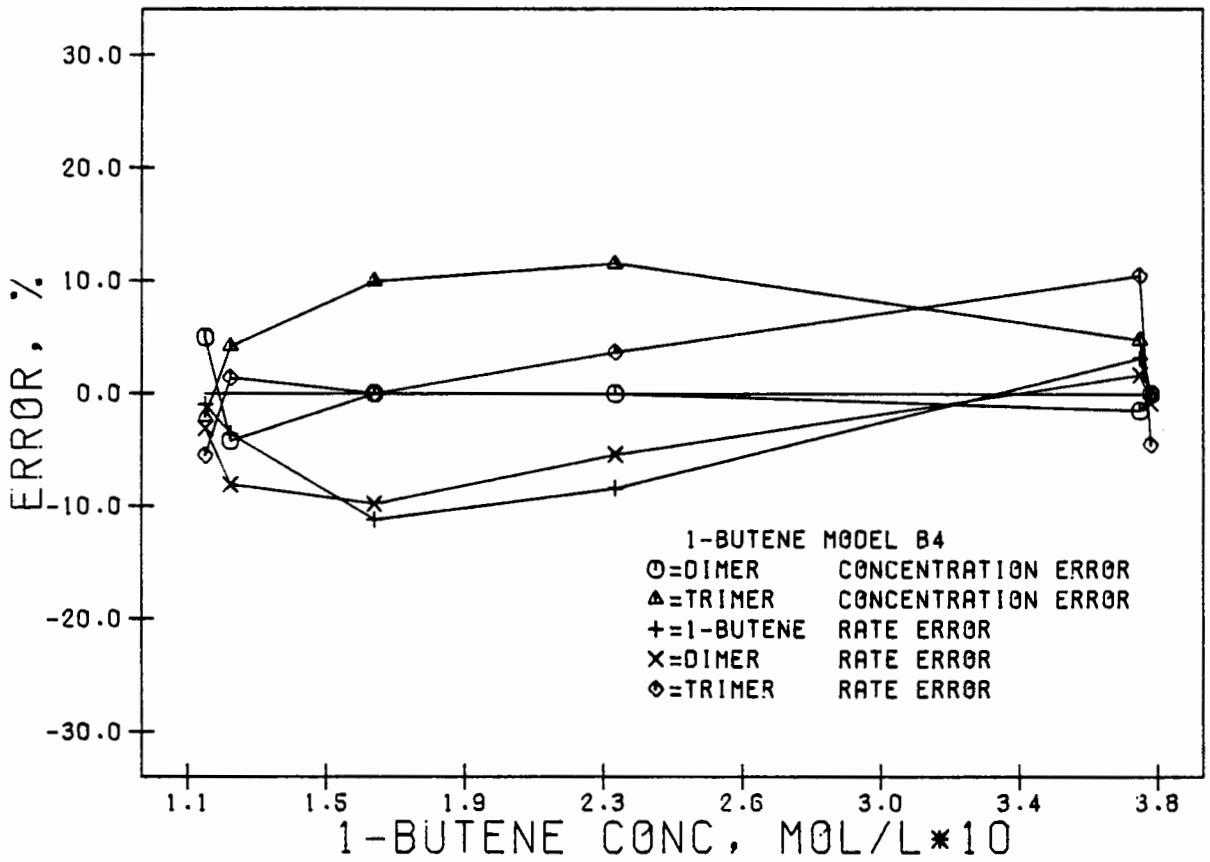

FIG 3.88 PERCENTAGE ERROR ANALYSIS, AS DETERMINED FROM THE PREDICTED AND EXPERIMENTAL CONCENTRATION, AS FUNCTIONS OF 1-BUTENE CONCENTRATION AT 464 K AND 103% H_3PO_4 FOR MODEL B4

Examination of Figures 3.88 and the results in Table 3.38 indicates clearly that this model predicts the data adequately with deviations that are not severe. The dependence of the model constants on temperature and H_3PO_4 concentration will now be examined.

Dependence of the constants k_1, k_3 and k_5 of model B_4 on temperature and H_3PO_4 concentration.

In a similar manner to models P3 and P4 the rate constants k_1, k_3 and k_5 were determined at each of the temperatures of Table 3.22. The rate constants are shown in Table 3.39. From the Arrhenius plot the following results were obtained:

$$k_1 = k_1' \cdot (\%H_3PO_4/100)^a \cdot e^{-E/RT} \quad mol^{-0.26} \cdot hr^{-1} \cdot l^{1.26}$$

where $E/R = 7440$ K

$r^2 = 1.00$

$$k_1' \cdot (\%H_3PO_4/100)^a = 8.07 \times 10^6 \quad mol^{-0.26} \cdot hr^{-1} \cdot l^{1.26}$$

Table 3.39 The calculated rate constants k_1, k_3 and k_5 of model B4 as calculated at the conditions of the experiments in Table 3.22.

	Temperature, K				
	465	424	433	454	447
Rate constants					
k_1 $mol^{-0.26} \cdot hr^{-1} \cdot l^{1.26}$	0.875	0.192	0.275	0.634	0.500
k_3 $mol^{0.17} \cdot hr^{-1} \cdot l^{0.83}$	0.0867	0.056	0.064	0.075	0.073
k_5 $mol^{0.23} \cdot hr^{-1} \cdot l^{0.77}$	0.132	0.100	0.112	0.137	0.123

$$k_3 = k_3' \cdot (\%H_3PO_4/100)^a \cdot e^{-E/RT} \ mol^{0.17} \cdot hr^{-1} \cdot l^{0.83}$$

where $E/R = 1984$ K

$r^2 = 0.99$

$$k_3' \cdot (\%H_3PO_4/100)^a = 6.1 \ mol^{0.17} \cdot hr^{-1} \cdot l^{0.83}$$

$$k_5 = k_5' \cdot (\%H_3PO_4/100)^a \cdot e^{-E/RT} \ mol^{0.23} \cdot hr^{-1} \cdot l^{0.77}$$

where $E/R = 1445$ K

$r^2 = 0.94$

$$5' \cdot (\%H_3PO_4/100)^a = 3.1 \ mol^{0.23} \cdot hr^{-1} \cdot l^{0.77}$$

In a similar manner, using model B4, the rate constants were determined at each H_3PO_4 concentration of Table 3.23. The rate constants are listed in Table 3.40.

The following power law relationships were found for each of the rate constants as functions of H_3PO_4 concentration. Linear least squares correlation coefficients, r^2, are given for each constant.

Table 3.40 The rate constants k_1, k_3, and k_5 of model B4 at various H_3PO_4 concentrations calculated from the data of Table 3.23.

	H_3PO_4 concentration, %			
	102	103	104	106
Rate constants				
k_1 $mol^{-0.26} \cdot hr^{-1} \cdot l^{1.26}$	0.461	0.500	0.579	0.794
k_3 $mol^{0.17} \cdot hr^{-1} \cdot l^{0.83}$	0.065	0.073	0.075	0.082
k_5 $mol^{0.23} \cdot hr^{-1} \cdot l^{0.77}$	0.119	0.123	0.130	0.159

$$k_1 = k_1' e^{-E/RT} \cdot [\%H_3PO_4/100]^{14.5} \quad mol^{-0.26} \cdot hr^{-1} \cdot l^{1.26}$$

where $r^2 = 0.99$

$k_1' e^{-E/RT} = 0.335 \; mol^{-0.26} \cdot hr^{-1} \cdot l^{1.26}$

$$k_3 = k_3' e^{-E/RT} \cdot [\%H_3PO_4/100]^{5.60} \quad mol^{0.17} \cdot hr^{-1} \cdot l^{0.83}$$

where $r^2 = 0.96$

$k_3' e^{-E/RT} = 0.060 \; mol^{0.17} \cdot hr^{-1} \cdot l^{0.83}$

$$k_5 = k_5' e^{-E/RT} \cdot [\%H_3PO_4/100]^{7.71} \quad mol^{0.23} \cdot hr^{-1} \cdot l^{0.77}$$

where $r^2 = 0.97$

$k_5' e^{-E/RT} = 0.10 \; mol^{0.23} \cdot hr^{-1} \cdot l^{0.77}$

The values of k' were found to be as follows:

$k_1' = 5.52 \times 10^6 \; mol^{-0.26} \cdot hr^{-1} \cdot l^{1.26}$

$k_3' = 5.13 \; mol^{0.17} \cdot hr^{-1} \cdot l^{0.83}$

$k_5' = 2.51 \; mol^{0.23} \cdot hr^{-1} \cdot l^{0.77}$

A comparison between the dimerization, trimerization and C_{12} cracking reactions rate constants of the 1-butene model B4 and the propene model P3 indicates that the activation energies of each of the 1-butene rate constants are significantly higher than those of propene.

Attempts were made to relate the orders of the reactions in the empirical model B4 to possible orders of reactions arising from mechanistic models but no relationships could be found.

3.6 CONCLUSIONS

It has been found from the residence time distribution studies and the mass transfer studies that, over a wide range of operating conditions, mass and heat transfer limitations can be significantly reduced and that the reactor performed as a perfect continuous stirred tank reactor.

Residence time distribution studies have shown that, at atmospheric pressure and ambient temperature, using a spiked nitrogen feed flowrate of 0.98 $cm^3 \cdot s^{-1}$ (τ = 0.28 hrs.), the reactor approaches ideal CSTR behaviour at impeller speeds between 600 (recycle ratio of approximately 20) and 1200 rpm. It has also been found that at a recycle ratio of approximately 15 (2400 rpm, 26.7 cm3•s-1, atmospheric pressure and ambient temperature) that ideal CSTR behaviour was obtained thus

confirming the results found by other workers (Carberry, 1964; Berty, 1974; Li et al., 1980).

The mass transfer results using napthalene confirmed the results published by Caldwell (1983a). Iit was found that the mass transfer coefficient varied linearly with stirrer speed up to 2400 rpm and dropped with increasing pressure up to 5 MPa. It is believed from these results that at atmospheric pressure the flow through the bed may have been at the upper end of the laminar range (approaching turbulent conditions) and hence the linear variation of K_c with impeller speed. With the increase in pressure the flow becomes turbulent and a decrease in K_c with increasing pressure is expected.

An alternative explanation for the drop in K_c with pressure as has been postulated by other workers in the field (Mehta & Sharma, 1966; Vidwans & Sharma, 1967; Yadav & Sharma, 1979) is that the correlating factor could be the diffusivity rather than the Schmidt number. Caldwell also suggested this possibility when, under identical conditions, he found higher mass transfer coefficients in hydrogen than in air. Comparisons between superficial gas velocities estimated from Ergun and Leva pressure drop equations and those estimated from mass transfer coefficients using the Hougen equations showed very good agreement as was found by Caldwell. Hence good CSTR conditions and high mass transfer coefficients can be obtained using this reactor.

Intraparticular diffusion and interphase mass transfer studies at 1.5 MPa, 2000 rpm, 464 K and 101.5% H_3PO_4 showed that both of these transport effects were insignificant. At the severe oligomerization conditions of 1.5 MPa, 2000 rpm, 114% H_3PO_4 and temperatures of up to 503 K interphase mass transfer was insignificant and intraparticular diffusion was largely eliminated.

The ortho-phosphoric acid concentration of the catalyst was found to have a dramatic effect on both reaction rates and catalyst life. Control of the ortho-phosphoric acid concentration was therefore extremely critical in obtaining reproducibility. From the preliminary studies it was found that if the catalyst was under-hydrated it was possible to rehydrate to the desired ortho-phosphoric acid concentration level without affecting the performance of the catalyst. It has also been shown that there is a small but measurable increase in the in the molecular weight of the product as the ortho-phosphoric acid concentration is increased.

The average molecular weight of the product decreased as the conversion of the propene feed increased. This trend was more marked at the higher temperatures. It is postulated that the reason for this trend lies in the fact that at the higher conversions the fraction of the reactor contents which is in the liquid phase is increasing. Although it has been shown that mass transfer limitations are insignificant at these conditions, it is possible that the longer chain products begin experiencing diffusional problems as the liquid phase fraction in the reactor increases as the conversion is increased sufficiently. It will be shown Chapter 4 that in the fixed bed reactor experiments when the system pressure was raised from 1.6 MPa to 4.4 MPa the average molecular weight of the product dropped significantly thus supporting this postulate. As a result of the above discussion in order to raise the average molecular weight of the products it would be necessary, contrary to thermodynamic expectations, to shift the reaction mixture towards the gas phase, either by lowering the conversion, lowering the pressure or decreasing the reaction temperature.

The average molecular weight of the product spectra from the 1-butene and iso-butene oligomerization reactions was lower than that from the polymerization of propene. Dimer was found to be the major oligomer product in the butene oligomerization whereas the trimer followed by the tetramer were found to be the major oligomers from the polymerization of propene. The reasons for this trend could possibly be due to steric hindrance experienced by monomer molecules obtaining access to the adsorbed species or could also be due to the heats of adsorption of the C_8 and C_9 fractions which may be similar and result in the preferential desorption of these molecules.

The butene products were found to be less sensitive to changes in reaction conditions than the propene products. The only detectable shift was a slight decrease in molecular weight of the product as the reaction temperature was increased. This trend is consistent with the behaviour observed the propene products.

A power law model of the propene rate concentration data yielded the following rate equation, which is first order in the concentration of propene. This equation described the rate of propene reaction adequately:

$$-rC_3 = k' \cdot [\%H_3PO_4/100]^m \cdot e^{-E/RT} \cdot C_3^n$$

where $k' = 66.9\ l^{1.03} \cdot mol^{-0.03} \cdot hr^{-1} \cdot g_{cat}^{-1}$

$m = 8.65$

$E/R = 3060\ K$

$n = 1.03$

Due to the nonuniformity of catalyst surfaces and lack of accurate knowledge of the structure of chemisorbed species and their concentrations it is debatable how much detail should be postulated in formulating equations for rates of reaction. The most simple approach, wholly empirical, would be to use the power-law form of the rate equation. Frequently, but not always, such an equation can correlate experimental rates just as accurately, and with fewer adjustable parameters than more elaborate methods (Smith, 1981).

At the other extreme the adsorption and surface reaction steps could be separated. The resultant equations are not only extremely complex but dependent on so many assumptions that the results may be no more meaningful than the power-law approach (Smith, 1981).

have In using this model to predict reaction rates at 464 K, 1.6 MPa and 114% H_3PO_4 it was found that the model over-predicted, by an average of 5.6% in the propene concentration range of .06 to 0.28 mol/l. This over-prediction was considered to be very reasonable since these conditions of temperature and H_3PO_4 concentration are severe and based on the findings of Bethea and Karchmer (1956) with the use of liquid phosphoric acid the relationship that was found between rate constant and H_3PO_4 was not expected to hold at these conditions. Using 111% ortho-phosphoric acid in a range of reactor temperatures of 454 to 508 K, the model over-predicted the experimental data by 6.9%. at the lower temperatures in this range. At the high acid concentrations employed here it was expected that the model would over-predict.

Using a similar power law fit the following rate equation was found to fit the butene oligomerization data adequately:

$$-rC_4 = k' \cdot [\%H_3PO_4/100]^m \cdot e^{-E/RT} \cdot C_4^n$$

where $k' = 2.38 \times 10^7\ l^{1.24} \cdot mol^{-0.24} \cdot hr^{-1} \cdot g_{cat}^{-1}$

$m = 18.1$

$E/R = 8780\ K$

$n = 1.24$

Five kinetic models were examined for their ability to fit and predict the propene feed and product concentrations and rates. In each of the models, only the oligomerization reactions were considered with the addition of one other reaction, which was the cracking of the C_{12} fraction to cracked products. The production of C_{15} from C_{12} was also incorporated in the line describing the rate of C_{12} disappearance. Although the quantities of cracked products and C_{15} were small it was necessary to include these terms for mass balance purposes. The five models tested are described briefly below:

1. Model P1 was formulated on the basis of the forward reactions only with the assumption that each of the reactions are elementary reactions.

2. Model P2 was based on model P1 but in this model the reverse reactions were considered.

3. In the formulation of model P3 the production of C_{12} was based only on the reaction of propene with the C_9 fraction. The model did not consider the production of C_{12} from the dimerization of C_6. This constraint was imposed not because it was believed that this would be representative of the mechanism but was imposed merely to serve as a guide, when compared to model P4, as to which of the two possible major reaction pathways for the production of C_{12} might be dominant under these conditions.

4. Model P4 was formulated on the same basis as model P3 but here the C_{12} fraction was considered to be solely produced by the dimerization of C_6.

5. Model P5 was based on a more fundamental approach of taking into account the formation of the carbonium ions in the model formulation. Again, only the forward reactions were considered.

Based on error analysis data and the deviations about the zero error line, models P3 and P4 gave the best fits to the data. The error analysis has shown that the weakness in models P1 and P2 lay particularly in their inability to fit the data at the lower propene concentrations used (below 0.24 mol/l). Although the ability of models P1 and P2 to fit the data at higher propene concentrations was considered to be acceptable, models P1 and P2 were discarded on the basis of their relatively poorer overall fit to the data.

Model P5 proved to be an extremely difficult model to solve due to the inclusion of four equilibrium constants in addition to the five rate constants considered. Therefore the attempts to solve for nine unknowns was found to be too complex to handle and although solutions were obtained from the optimization routines, it is found that the solutions were always close to the initial estimates (as required by the optimization routine) of each of the parameters to be optimized. This indicated that only local minima (based on the least error squared) were being found and that a global minimum was not. Due to the lack of published information on equilibrium constants of these complex reactions no basis could be found to simplify the model by reducing the number of independent parameters. The second alternative which was to fix the equilibrium constants in the optimization and to use many different sets of these constants was attempted. In the use of 20 sets of equilibrium constants it was found that the best fit to the data had errors of slightly larger magnitude than those of models P1 and P2.

In the discrimination between models P3 and P4 it was found on the basis of the error analyses that discrimination between these two models was subtle due to their similarities. Based purely on error analysis, neither of the two models could be rejected. It has been found, however, on the basis of rather limited data that in the comparison of the predictive capabilities of these two models at the extreme conditions (H_3PO_4 concentrations) of 464 K and 114% H_3PO_4 and also at 111% H_3PO_4 (over a range of temperatures) that at the former set of conditions both models P3 and P4 had quite similar predictive capabilities. At the latter set of conditions it was found that model P3 gave a significantly better fit to the data than model P4. With respect to the fit of both model P3 and P4 to the data at these conditions it was expected that neither of these models would predict well due to the high H_3PO_4 concentrations and the high temperature in the 111% H_3PO_4 runs. The quality of the fit was considered to be better than expected except the fit of model P4 in the 111% H_3PO_4 experiments and the rates of propene reaction of both models at these conditions.

It was shown in the pulse studies, that at propene to C_6 and C_9 ratios of 1.5:1 and 10:1 respectively, the C_{12} fraction was produced predominantly from the dimerization of C_6 whereas at ratios of 6:1 and 15:1 respectively, it was estimated that approximately 50% of the C_{12} fraction was produced from C_6 dimerization. The molar ratios of propene to C_6 and C_9 used in this study for the determination of the model solutions varied from approximately 83:1 and 15:1 to 122:1 and 17:1. On the basis of the findings of the pulse experiments it would be expected

that the bulk of the C_{12} fraction in this reactor would be produced from the reaction of propene with the C_9 fraction and hence model P3 would be the better model to use on this basis.

It was found from examination of the empirical models P3, P4 and the mechanistic model P5 that no relationship could be found between the fundamental rate equations of model P5 and the orders of the empirical model rate equations.

From the activation energy data of models P3 and P4 it has been shown that the highest activation energy occurs in the dimerization of the propene. This together with the low value of the dimerization rate constant suggests that this reaction is possibly a rate limiting step in the rate of propene disappearance. In support of this it will be shown in Chapter 5 that in the one dimensional modelling of the fixed bed reactor it was found that the first order rate equation gave reasonable results. Several inconsistencies were found in the activation energy data of models P3 and P4 in that the activation energy of the trimerization reaction of model P3 and that of the trimerization and tetramerization reaction of model P4 were negative. Close examination of the k3 rate constant/temperature data of model P3 (unlike model P4) indicate that this rate constant is extremely insensitive to temperature and hence very small errors could result in negative values being found. This provides further support for the choice of model P3 rather than P4 at over the conditions used in this experiment.

In all of the models it was found that the rate constant for the production of trimer was larger than for the production of dimer, possibly indicating that the dimerization of propene, as is expected, was the more difficult step of the two.

From the 1-butene data, which was modelled in a similar manner to the propene data, it was also found after examination of several models that the empirical model, B4 which modelled the dimerization, trimerization and the cracking of the C_{12} fraction, gave a good fit to the data. No relation could be found between the orders found in this empirical model and those resulting from a mechanistic model.

It is thus concluded that the intrinsic rate of disappearance of propene and butene in this study is first order. No definite conclusions can be drawn with respect to the detailed mechanism but suitable empirical models have been proposed. Purely mechanistic models were not found to fit the data as accurately.

4. ALKENE OLIGOMERIZATION REACTIONS OVER SOLID PHOSPHORIC ACID, USING A FIXED BED REACTOR

4.1 INTRODUCTION

In a fixed bed integral reactor (as opposed to a fixed bed differential or micro-reactor) the variations in reaction rate within the reactor are so large that they must be accounted for in the method of analysis. Unlike the internal gas recirculation reactor under reasonable operating conditions, the integral reactor can have large temperature variations from point to point. This is particularly true of gas-solid systems. This reactor is very useful for modelling the operations of larger packed beds with their heat and mass transfer limitations.

A detailed review of alkene oligomerization reactions over solid phosphoric acid, using fixed bed reactors, will not be given here, but the reader is referred to the general review given in Section 1.5. A brief summary will now be given of the important control variables in olefin polymerization with phosphoric acid catalysts, as well as their effect on the product quality and feed conversion. A brief outline of the findings of the more relevant workers in this field will also be given, but a more detailed discussion can be found in Section 3.1.5.

The following variables are of importance in olefin polymerization with phosphoric acid catalysts:

- catalyst and strength (H_3PO_4 concentration)
- reaction temperature
- reaction pressure
- weight hourly space velocity
- feed composition

As pointed out by McMahon et al. (1963), it is these variables that control the degree of feed conversion, and the quality and composition of the polymer. They noted, however, that reliable quantitative data are limited.

Using liquid phosphoric acid in a downflow packed reactor, Bethea & Karchmer (1956) concluded that the research octane number increased with a decrease in H_3PO_4 strength. This conclusion is questionable (McMahon et al., 1963). In general, low temperatures, high pressures and low

conversion per pass all favour high yield of gasoline range products and high octane numbers.

In studying the kinetics of the polymerization of propene and mixed n-butene over phosphoric acid on quartz chips, in a pilot plant sized reactor, Langlois & Walkey (1951) correlated their data against an empirical rate equation that is approximately first order with respect to the monomer. The rate equation is given in Section 3.1.5. They found that the reaction conditions (within the typical operating region) had little effect on the octane number of the polymer. They also found that increased temperature and pressure resulted in a lower boiling polymer and that the character of the polymer did not change significantly in the acid concentration range of 100 to 108%. They also found that propene polymer was usually higher boiling than was butene polymer.

In their study on the polymerization of propene with liquid phosphoric acid in a downflow packed reactor, Bethea & Karchmer (1956) correlated their data in terms of a modified first order rate equation (which is shown in Section 3.1.5).

Friedman & Pinder (1971) studied the polymerization of a mixture of propene and butene isomers over solid phosphoric on kiesulguhr, using a fixed bed reactor of 2" in diameter and 12" long. They correlated their data with an empirical equation (given in Section 3.1.5). They found that the effect of pore diffusion in their work was quite appreciable using pellets of screen size between 4.76 and 6.73mm.

With regard to the industrial catalytic polymerization of propene and butenes, Weinert & Egloff (1948) have presented a summary of the UOP (Universal Oil Products) catalytic polymerization units, these being:

1. The low pressure regenerative type
2. Small high pressure units (non-regenerative)
3. Tubular or reactor unit type

Weinert & Egloff (1948) have also given a summary of the process factors affecting the polymerization of propene and butenes over phosphoric acid.

Steffens et al. (1949) examined the polymerization of propene & butenes over a copper pyrophosphate catalyst on a commercial scale plant. They correlated their operating variables graphically, by presenting a chart for predicting the weight percent conversion of the olefins in the total

feed, for a wide range of operating conditions. They found that the conversion of the olefins increased with:

1. increase in catalyst ~~activity~~ acidity
2. increase in reactor temp
3. decrease in olefin space velocity
4. decrease in total space velocity
5. decrease in weight ratio of propene and normal butenes to isobutene.

They found no relationship between the operating variables and the octane number of the polymer produced.

Langlois (1953) has reviewed the polymerization of olefin hydrocarbons, using acidic catalysts. He also presented a reaction mechanism embracing both Friedel-Crafts and acid-type catalysts. The reaction conditions which favour true polymerization, copolymerization and conjunct polymerization, are also discussed.

McMahon et al. (1963), besides reviewing the mechanism of propene polymerization, the properties of phosphoric acid, polymerization process variables and the kinetics of olefin polymerization over phosphoric acid (Section 3.1.5), also investigated the effect of process variables on product yield and quality and on catalyst life. They noted that yield and quality are quite insensitive to operating conditions.

4.1.1 Modelling the Behavior of Fixed Bed Catalytic Reactors

The degree of complexity of reactor models can range from the simplest pseudo-homogeneous, one-dimensional models to complex heterogeneous, two-dimensional models. Although the purpose of a model is to give the best description of the physical and chemical processes occurring in the reactor, simplifications are important to keep the complexity to a reasonable limit.

Baiker & Epple (1986) have pointed out that, although the behaviour of fixed bed reactors, with strongly exothermic reactions, have usually been described by heterogeneous models (Gros & Bugarel, 1977; Karanth & Hughes, 1974), both Sharma & Hughes (1979) and Smith & Carberry (1976) have shown that the temperature gradient between the fluid phase and the catalyst has often only a limited influence on the mean reactor temperature, and can thus be ignored.

The choice of whether a one-dimensional or a two-dimensional model should be used to model a non-adiabatic, non-isothermal reactor has been discussed by several authors (Gros & Bugarel, 1977; Finlayson, 1971; Baiker & Bergougnan, 1985; Lee & Agnew, 1977). According to Finlayson, if the Biot number, $h_w \cdot R/k_e$,

where h_w = heat transfer coefficient through reactor wall, $J \cdot m^{-2} \cdot s^{-1} \cdot K^{-1}$,

R = radius of reactor tube, m

and k_e = radial heat conductivity, J•m-1•s-1•K-1

is smaller than 1, 75% of the heat resistance lies in the reactor wall, and hence the reactor behavior can be described quite accurately using a one-dimensional model. Baiker & Epple have noted, however, that with larger Biot numbers, a one-dimensional model can be used with reasonable accuracy, if a mean cross-section temperature can be defined (Baiker & Bergougnan, 1985).

4.2 OBJECTIVES OF THE FIXED BED REACTOR STUDIES

The objectives of the fixed bed reactor studies are essentially three-fold.

The first objective is to briefly examine the typical product spectrum obtained in this type of reactor, and to do so at a few H_3PO_4 concentrations and reactor pressures, for each of the pure propene and 1-butene feeds. It is also intended to examine briefly the activity of iso-butene in this reactor. It has been found by other workers in the field (Kriel, 1986) that changes in the H_3PO_4 concentration, when using commercial sized pellets of solid phosphoric acid in pilot sized equipment, had no effect on the catalyst activity. Two experiments were carried out here to examine this finding.

The second objective is to compare the products obtained in this reactor with those obtained in the internal gas recirculation reactor, noting that mass and heat transfer effects will be intruding in the fixed bed reactor.

The third objective is to model the behaviour of the fixed bed reactor using both a one-dimensional model and the rate equation obtained from the internal gas recirculation reactor data.

The objectives of this study may therefore be listed as follows:

1. To examine the product spectra obtained in this reactor at a few reactor pressures and H_3PO_4 concentrations, using a pure propene feed.

2. To repeat the investigation in 1., using pure 1-butene feed and a pure iso-butene feed.

3. To investigate the influence that catalyst particle size has on the response of the system to changes in H_3PO_4 acid concentration.

4. To investigate and compare the product spectra obtained in this reactor, with those of the internal gas recirculation reactor.

5. To model the behaviour of the fixed bed reactor using a one-dimensional model.

4.3 EXPERIMENTAL APPARATUS AND PROCEDURE

4.3.1 The Reactor System

The Reactor system used for these oligomerization experiments is shown schematically in Figure 4.1, and consists of the reactor (which will be discussed in detail in Section 4.3.2) and ancilliary equipment.

In a similar manner to the kinetic studies using an internal gas recirculation reactor (Section 3.3.1.3), the feed is stored as a liquid under its vapour pressure in an inverted Cadac No. 7 domestic gas cylinder (3kg capacity) which is heated by heating tapes (ISOPAD ITH-33, 115H, 220V) and controlled by a Eurotherm temperature controller (model 101). The maximum cylinder temperature is restricted, as described in Section 3.3.1.3. By heating the feed cylinder, the feed vapour pressure is raised, hence avoiding any cavitation in the pump. The pump head is cooled to approximately 283 K. A pressure relief valve on the exit line is set to open at 1.75 MPa. This is a precautionary measure to protect the feed cylinder, which is rated to 3 MPa and tested (nondestructively) to 6 MPa.

From the cylinder, the feed passes over 3A molecular sieves and a 30 micron filter to a high pressure diaphragm pump (Lewa model FLM-1). An ethylene glycol-water solution (ca. 10 K) is used to chill the feed prior to reaching the pump and the pump head. Similar to the gas recirculation

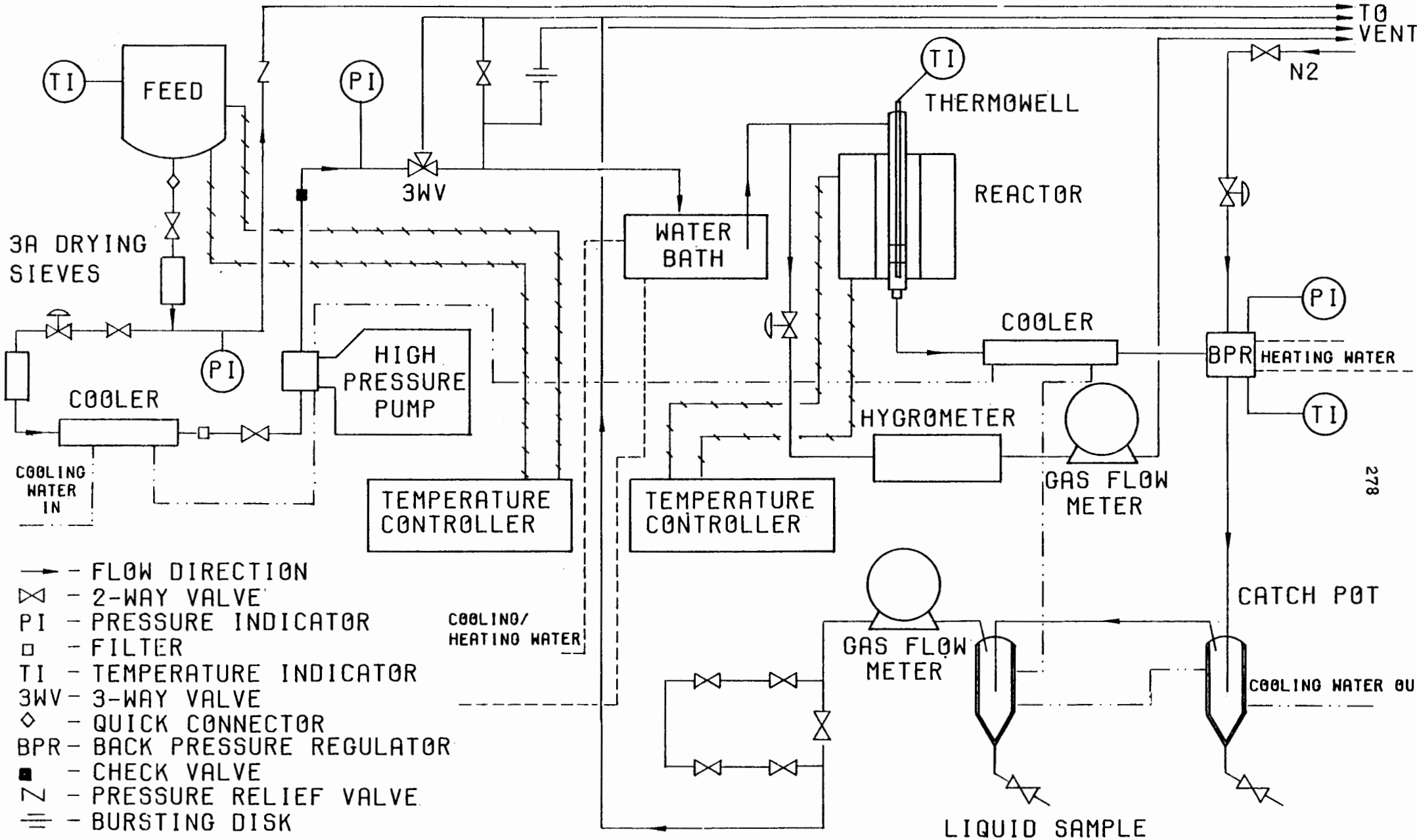

FIG 4.1 SCHEMATIC OF FIXED BED REACTOR SYSTEM

reactor system, the pump raises the system pressure to that set by the back pressure regulator and controls the flowrate. From the pump, the feed passes to a water bath, where the feed is passed over a bath of water, the temperature of which is controlled (as explained in detail in Section 3.3.1.3).

From the water bath the feed passes, via a metering valve, to the reactor. Reactants and products then move on to a dome loaded diaphragm-type back pressure regulator (Grove, Mity Mite model 591 XH), where the system pressure is released to atmospheric. The pipes and valve from the water bath to the reactor are heated to reactor temperature. The exit line from the reactor is not heated, but the back pressure regulator is heated to about 323 K (to prevent freezing as the pressure is released to atmosphere) with warm water carried in rubber tubing which is coiled around the regulator.

The water vapour content of the feed is measured in a similar manner to that described in Section 3.3.1.3, by taking a bleed from the inlet line and passing this over the aluminium oxide sensor (see Section 3.3.1.3 for details). The bleed gas flowrate and temperature is monitored by means of a wet gas flow meter.

In this system, the bursting disk on the inlet line is set to burst at 7 $\pm$ .7 MPa. The 2-phase reactor effluent is also separated in a jacketed catch-pot which is maintained at approximately 283 K by coolant. After separation, the flue gas passes directly to a wet gas flow meter, a gas sampling tube and is finally vented. Liquid product can be drained from the catch-pot as desired.

This piping system is also constructed of 1/8" stainless steel tubing. Temperatures are recorded at the feed cylinder, inside the reactor (by means of a thermowell), the water bath, the inlet line to the reactor and the wet gas flow meters. Pressures are recorded at the exit of the feed cylinder, between the pump and the reactor entrance and at the back pressure regulator.

4.3.2 The Reactor

A micro-reactor (Figure 4.2) developed by Snel (1982) has been modified for use in this study. The catalyst basket has been extended to a depth of 6cm, at the expense of shortening the preheat section. A further modification has been the removal of the tube bundle used by Snel (1982)

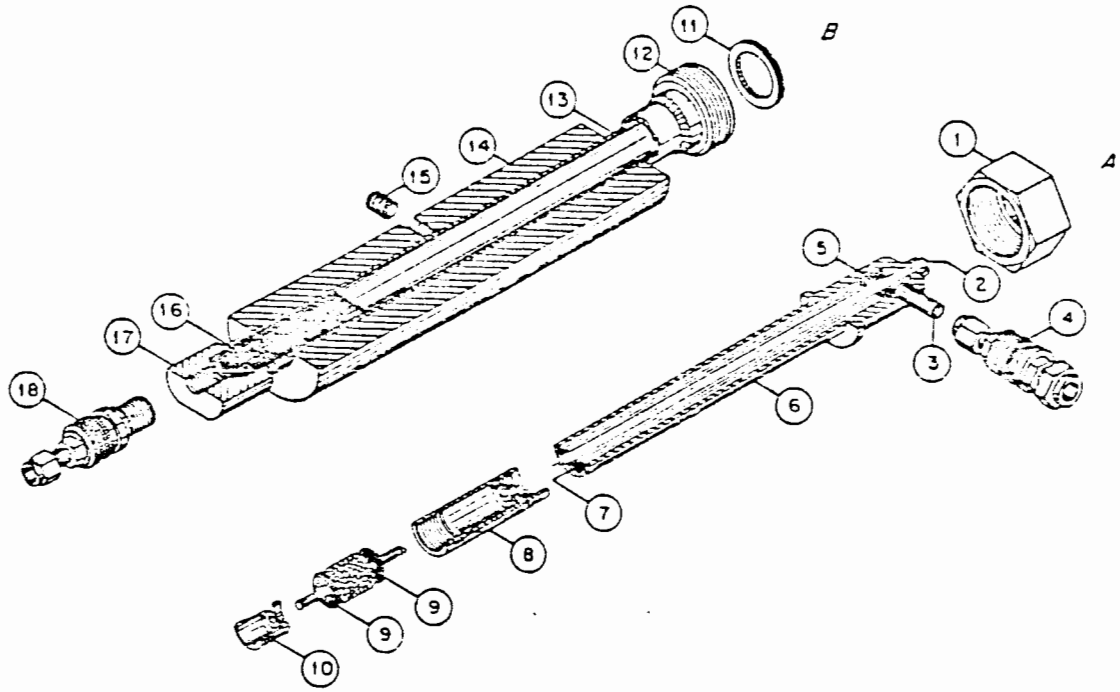

Inner tube A

1. Nut, M42 x 2, SS316
2. Thermocouple well, 240 x 2.2 mm id, SS EN58E
3. Inlet tube, 25 x 4.2 mm id, SS EN58E
4. Quick connector, Swagelock-pat'd QF4-B/S, SS316
5. Wire basket, SS316
6. Inner tube body, 227 x 18 mm id, SS316
7. Heat exchanger tubes, 190 x 1 mm id, SS EN58E
8. Catalyst chamber, 30 x 18 mm id, SS316
9. Screen, 100 mesh, SS316
10. Adjustable support plate, 17 x 16 mm id, SS316

Outer tube B

11. Helico flex seal, HN 220, 24.9 mm id, 3.3 torus inconel/ nimonic, Joints fargère industrie
12. Outer tube head, 22 x 22.5 mm id, top recess 31.5 x 2.5 mm deep, M42 x 2 thread outside SS316
13. Outer tube body, 230 x 22.5 mm id, SS316
14. Heatsink, 203 mm x 68 mm od x 26.8 mm id, copper
15. Grub screw, M8 x 1.25
16. Wire mesh, Düren-RL, MW = 0.20 mm, DR = 0.13 mm, SS316
17. Reactor bottom, 53 x 16 mm id, SS316
18. Quick connector, Swagelok-pat'd QF-B/S, SS316

Figure 4.2 Micro-reactor developed by Snel (1982)

to achieve liquid distribution and heat transfer in the preheat section. Instead, 2 and 4mm diameter glass beads are packed in this region to achieve the same effect. The overall length of the preheat section is 18cm.

The reactor was identically packed for every experiment performed in this study (although the quantity of catalyst was changed, depending on the feed), thus ensuring identical feed distribution. In all experiments, only one catalyst bed section was used. Two 750 W cartridge heaters and a controlling thermocouple were inserted into the copper blocks surrounding the reactor body. The cartridge heaters (0.96cm diameter) extend the full length of the copper heat sink and provide a stable and uniform reactor.

Temperatures in the preheat and catalyst bed sections of the reactor are measured by inserting a thermocouple down the central thermowell to the

desired position. These temperatures are measured with a Digitron digital thermometer.

4.3.3 Experimental Procedure and Analysis

4.3.3.1 Run procedure

The general procedure for the oligomerization reactions is presented below. Individual experiments varied in regard to the H_3PO_4 acid concentration, mass of catalyst, feed type, reaction temperature, catalyst size and reaction pressure. Some variation in feed flowrate was observed, although this was not an intended variable, as such.

The catalyst was sieved, and the appropriate mass of the 106-180 micron fraction was packed in one section of the reactor. Glass beads fill the void above the catalyst bed. The complete packed reactor is schematically indicated in Figure 4.3. The catalyst bed had a bulk density of $0.95 g \cdot cm^{-3}$. Once packed, the reactor was assembled, sealed and installed in the cylindrical furnace. It was connected to the reactor line via Swagelok quick-connectors.

Each run was started by first heating up the reactor and feed cylinder to the required temperatures. Approximately 1hr was required to bring the reactor up to the desired temperature (within 283 K of the set point). While the reactor was being heated, all coolant flows were switched on. During this period, all inlet and outlet lines that required heating were brought up to their required temperatures.

Once the desired reactor temperature had been reached, the pressure setting of the back pressure regulator was raised to 1.53 MPa (absolute) and the reactor filled with feed at a controlled rate (by adjustment of the metering valve on the inlet side of the reactor).

Once the reactor was filled, feed was pumped into the reactor, bringing the reactor up to the set pressure. The bleed line to the hygrometer was then opened and set to approximately $1 g \cdot hr^{-1}$, after which the pump was set to the desired flowrate. Once the desired flowrate had been set, the water bath temperature was adjusted to the approximate value required. The water bath required approximately fifteen minutes to reach a semi-stable condition, at which time the catch pot was emptied. This time was considered to be time zero for the reaction. At time zero, a gas sample was also collected.

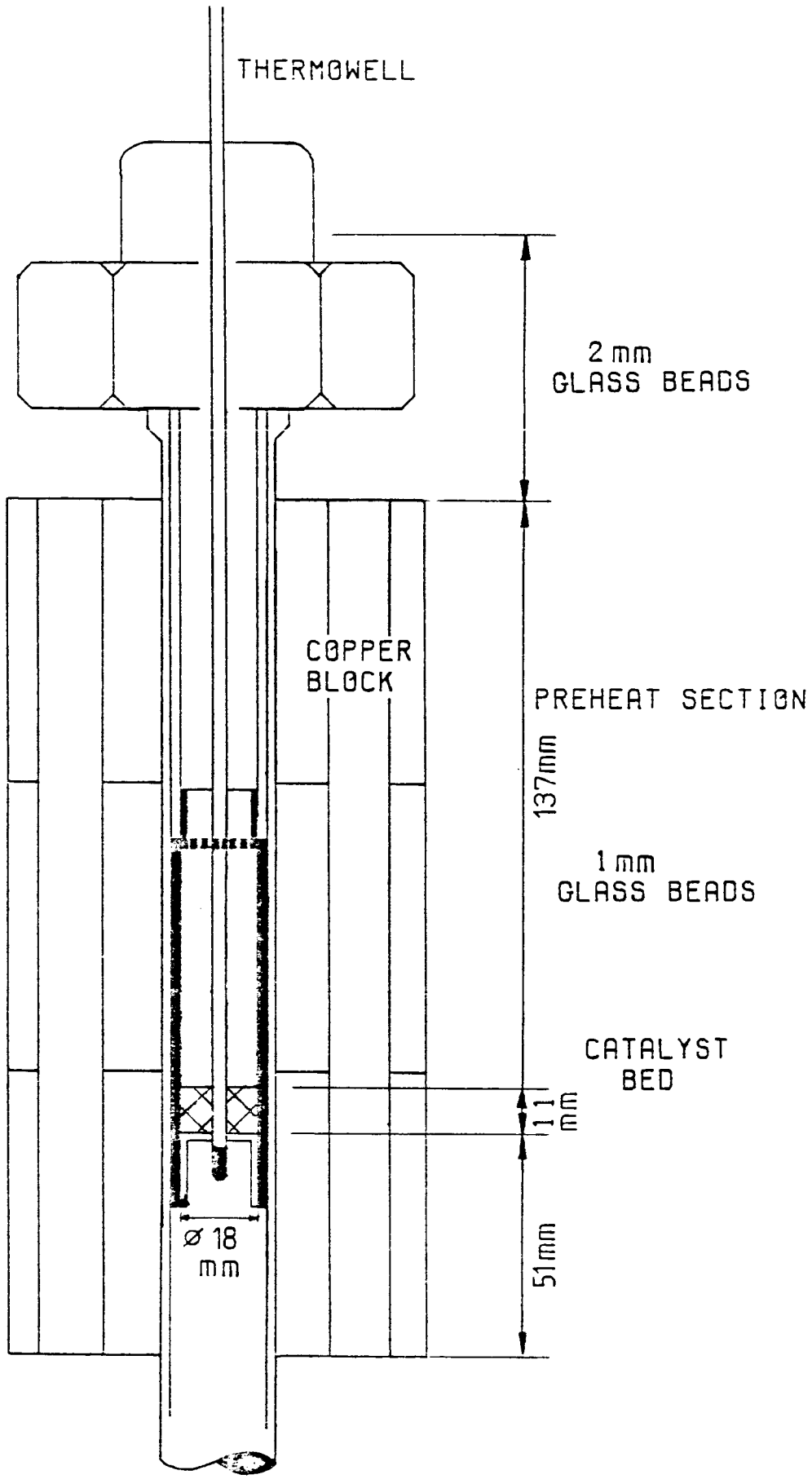

FIG 4.3 SCHEMATIC LAYOUT OF THE PACKED SMALL REACTOR VOLUME

Hereafter the following data were recorded at various intervals:

1. The gas meter readings and effluent gas temperatures.
2. The mass of liquid product collected.
3. The temperature at various points above, in and below the catalyst bed.
4. A gas and liquid sample were collected and analysed by gas chromatography.
5. Dewpoint of water in feed.
6. All relevant temperatures and pressures.

The reaction is terminated, when desired, by isolating the pump from the reactor and releasing the back-pressure. The reactor cooled, over approximately 2 hours, to below 323 K.

4.3.3.2 Product analyses

The compositions of the gaseous and liquid effluents were determined by GC (Gow Mac and Varian 3400, respectively).

The analysis of the effluent gas and feed streams was performed using a 6mm long SS (stainless steel) column, packed with n-octane/poracil C. Details of the method and relative response factors used, are given in Appendix I. The analysis is identical to that described in Section 3.3.3.4.

Liquid products were separated on a 2.8mm long, 6mm O.D. glass column packed with 3% silicone/OV-101 on Chromasorb W-HP, 100/120 mesh, as described previously. A typical gas chromatograph and mass spectrograph are shown in appendices E and F, respectively.

4.3.3.3 Reaction data workup

The average feed flowrate, over an entire run, was calculated by dividing the total mass fed (measured by weighing cylinder, before and after each run) by the total run time. During the oligomerization experiments, the feed flowrate was estimated by back-calculating from the effluent mass flowrate. As will be shown later, mass balances were good (97.5 ± 2.5) and hence little error was introduced by using this procedure. In the final analysis of the run data, a corrected estimate was used, by taking into account condensation inside the reactor and mass loss.

4.4 RESULTS

4.4.1 Preliminary Results

4.4.1.1 Reproducibility of experiments

Although the feed flowrate was intentionally varied in some of the experiments, in many of the experiments it was intended to keep the flowrate constant. Some degree of flowrate variation was, however, experienced (up to 10% maximum, i.e., ±5%, deviation from the derived flowrate). This variation was found to have little effect relative to the effects of acid concentration, reactor pressure and feed type used.

Two reproducibility runs were carried out, using a pure 1-butene feed, at the following conditions:

mass of catalyst	3g
catalyst size	106-180 microns
reactor temperature	462-473 K (spread over bed)
reactor pressure	15.5 to 16.5 atm (abs)
H_3PO_4 concentration	108%
feed flow rate	27g/hr

1-Butene conversion is shown, as a function of time on stream, for these two experiments in Figure 4.4. The initial differences in conversion levels were due to different initial hydration levels on the catalyst, different initial reaction temperatures and feed flowrates. The rapid drop in the conversion at 2.5 hrs. on stream was due only to a manual adjustment of the pump speed (see Figure 4.6) thus giving rise to an increase in the WHSV and hence a decrease in the conversion. The subsequent correction to the pump speed can be seen in Figure 4.6. Once the systems had been stabilized at the desired operating conditions, the reproducibility, as can be seen in Figure 4.4, was considered to be satisfactory. This was despite the somewhat different temperature profiles in each catalyst bed, measured at steady state. These temperature profiles are shown in Figure 4.5 as functions of the catalyst bed depth (moving down the bed).

4.4.1.2 Complete analysis of a typical oligomerization run

A detailed analysis of a typical oligomerization experiment is given here in order to indicate features common to all the experiments. The analysis provides an indication of the stability of various parameters in all the runs (e.g., flowrate stability).

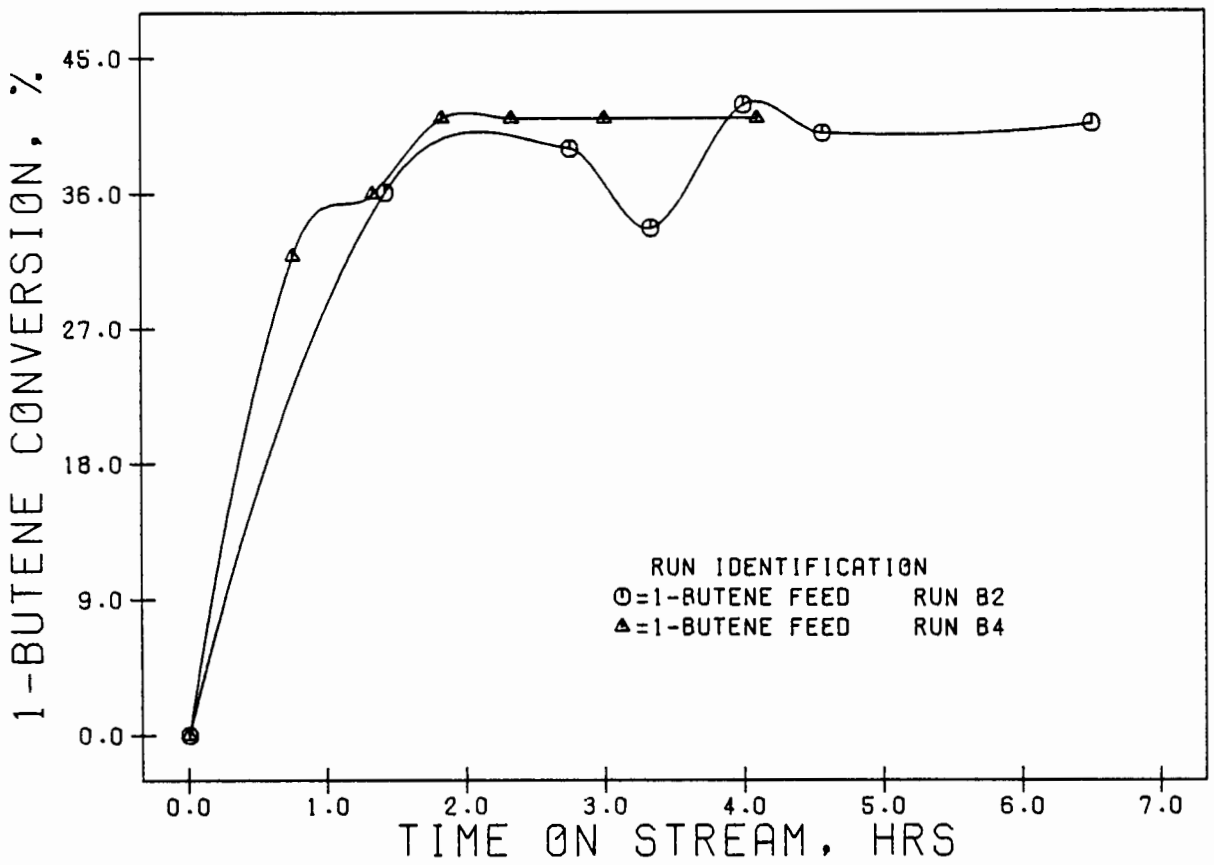

FIG 4.4 INTEGRAL REACTOR REPRODUCIBILITY RUNS: 1-BUTENE CONVERSION AS A FUNCTION OF TIME ON STREAM

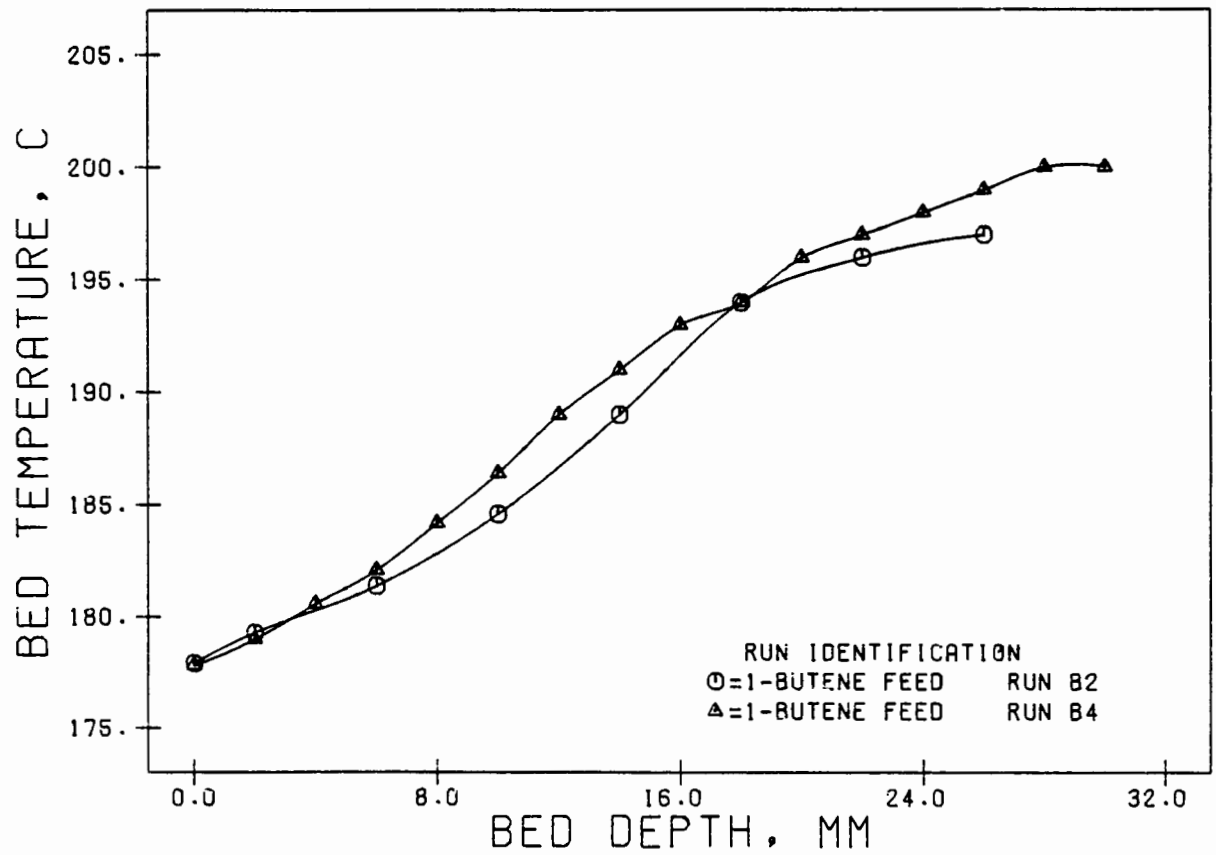

FIG 4.5 INTEGRAL REACTOR REPRODUCIBILITY RUNS: CATALYST BED TEMPERATURE DURING THE RUN AS A FUNCTION OF CATALYST BED DEPTH

The experiment to be considered is Run B2, presented in Figures 4.4 and 4.5. The experimental conditions used are listed in Table 4.1.

Table 4.1 Experimental conditions for typical oligomerization run of Section 4.4.1.2.

Catalyst	
Type	Solid phosphoric acid (on kiesulguhr)
Mass, g	3.0
Size, microns	106-180
Bed density, g/cm^3	0.95
Bed depth, mm	12.5 to 13
Reaction	
Feed	>99% 1-butene
Flow, WHSV	9.0 - 9.3
Temperature (set), K	464
Temperature (mean), K	466
Pressure, MPa	1.65
Mass balance, %	97

WHSV and conversion versus time

Despite the variation in the WHSV during the first few hours (due to manual alterations to the pump setting), the set WHSV of 9 was easily maintained during steady state. It should be noted that the rapid increase in WHSV at 2.5 hrs. on stream, as can be seen in Figure 4.6, was due to a manual adjustment of the pump speed. The accompanying increase in the conversion of 1-butene can also be seen in Figure 4.6. The WHSV was readjusted back to 9 at approximately 3.4 hrs. on stream as can be seen. The variation over the steady state period (which is indicated in the latter portion of Figure 4.6) was slight (±2%) despite the large fluctuations between 2.5 and 4.5 hrs.

Catalyst bed temperature versus time

It was found that there was very little change in the catalyst bed temperature profile during the course of the run. The change in bed temperature with bed depth was found to be significant, and has been shown in Figure 4.5 (Run B2).

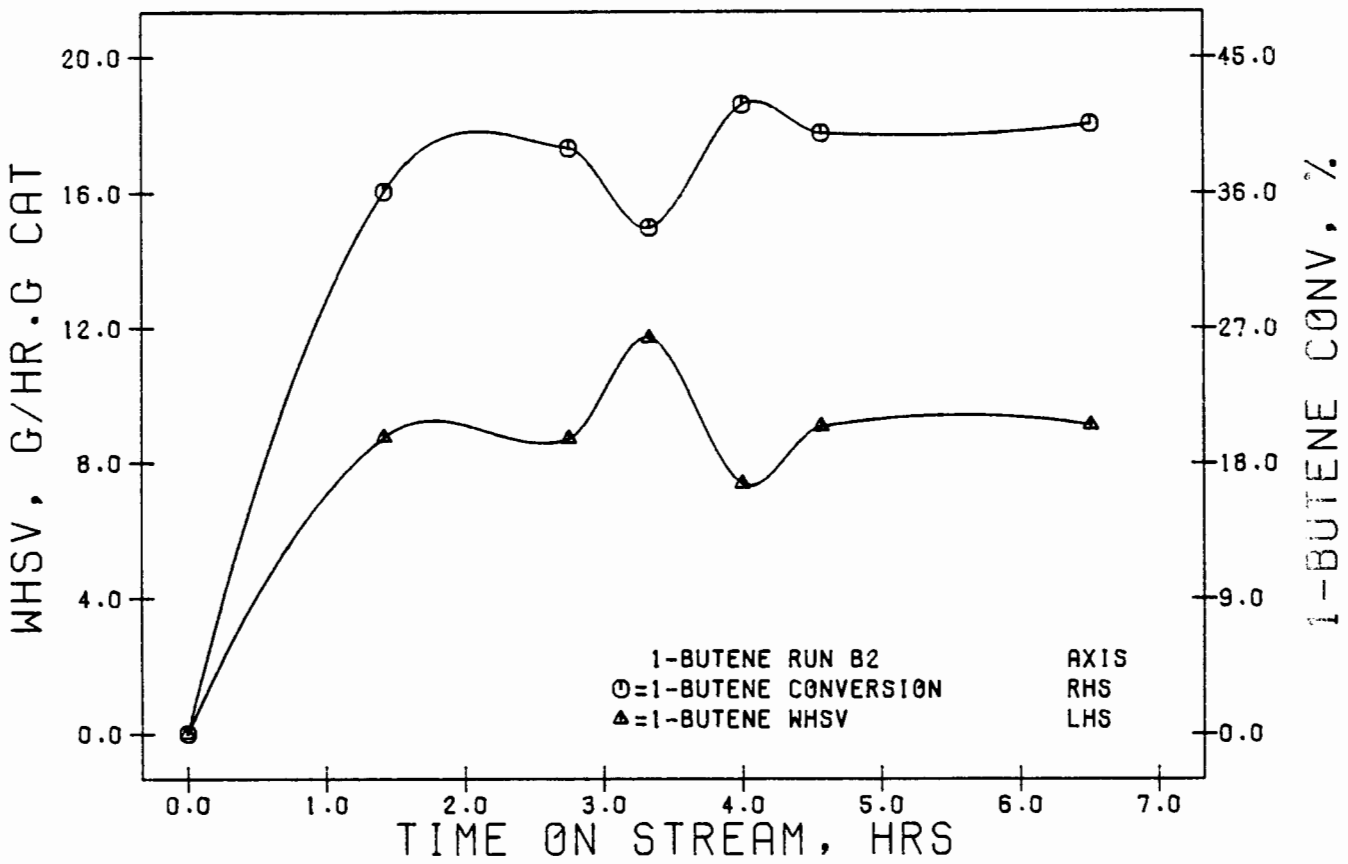

FIG 4.6 1-BUTENE CONVERSION AND WHSV AS FUNCTIONS OF TIME ON STREAM

Product spectrum versus time

It was found that, during the entire length of the run, the product spectrum remained approximately constant, indicating that the reaction remains quantitatively unchanged during this period. This is shown in Figure 4.7.

Given the results in Figure 4.7 and the WHSV in Figure 4.6, it is clear that the rate of production of the various oligomers remained approximately constant, once steady state was reached.

4.4.2 Propene Oligomerization

Four experiments were carried out using pure (>99%) propene as a feed. Three of these experiments were carried out at conditions similar to those used in the internal recycle reactor, with the variables being acid concentration (102% and 108% H_3PO_4) and reactor pressure. The experimental conditions used are listed in Table 4.2.

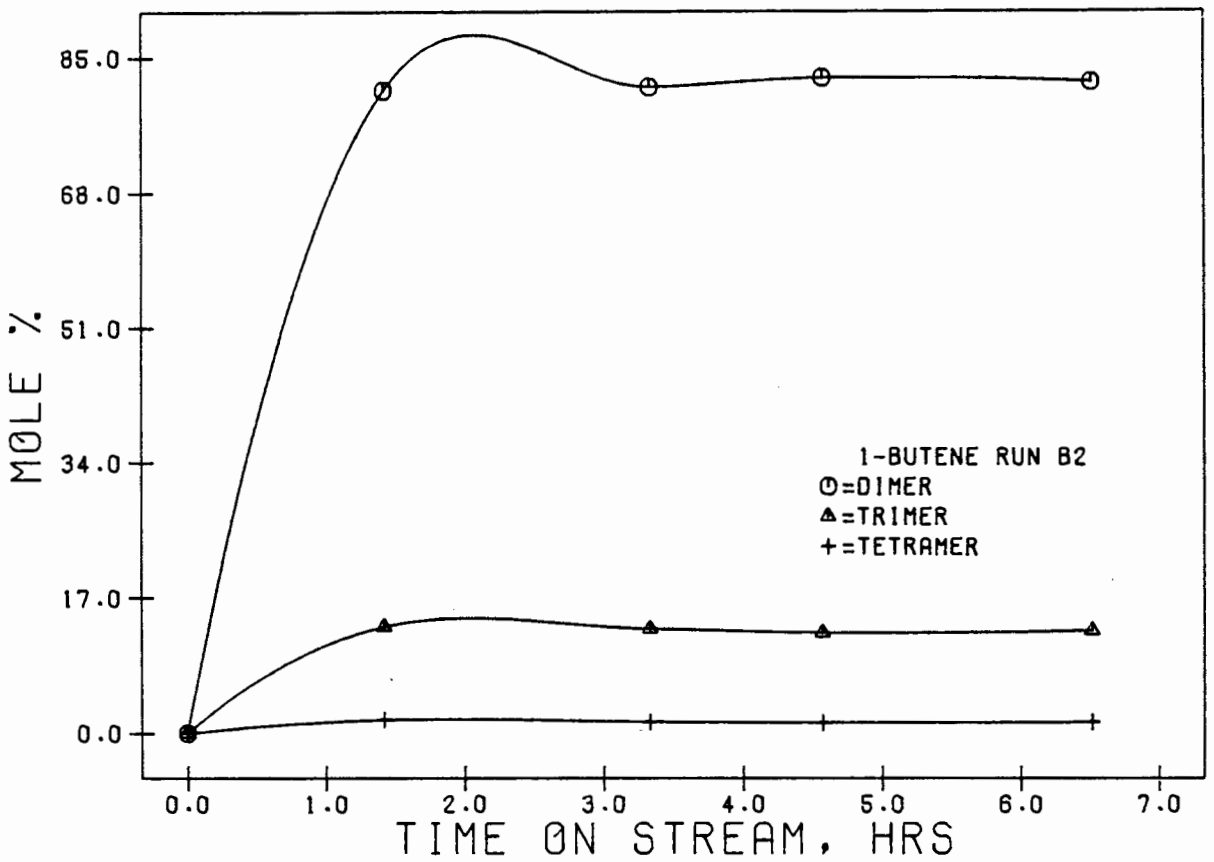

FIG 4.7 PRODUCT SPECTRUM AS A FUNCTION OF TIME ON STREAM FOR A TYPICAL OLIGOMERIZATION EXPERIMENT USING A 1-BUTENE FEED

Table 4.2 Experimental conditions used for propene oligomerization experiments.

	Run P1	Run P2	Run P3	Run P4
Catalyst				
Type	← Solid phosphoric acid →			
Mass, g	3	1	3	3
Size, μm	← 106 - 180 →			
Bed density, g/cm^3	0.95	---	---	---
Bed depth, mm	12-13	25-27	31	31
Reaction				
Feed	← 95% propene →			
Flow, WHSV	9	11-13	9	9
Temperature (set), K	464	464	464	464
Temperature (mean), K	465	463	460	464
Pressure, MPa	1.63	4.4	1.68	1.68
H_3PO_4 conc., %	103.5	102	108	101

The following should be noted when examining Table 4.2.

1. It was decided in Runs P2, P3 and P4 to disperse the catalyst amongst 300 μm (diameter) glass beads (thus resulting in a larger bed depth) to enable easier control of the catalyst bed temperature (due to the highly exothermic nature of the reaction).

2. In Run P2 the feed flowrate was controlled in such a way as to provide the same propene conversion level as Run P1, and hence the higher WHSV due to the higher operating pressure (since conversion increases with pressure).

4.4.2.1 The effect of H_3PO_4 concentration

Although it was not the direct intention of this work to study the effect of H_3PO_4 concentration, three H_3PO_4 concentration runs were carried out to provide an indication of the effect of H_3PO_4 concentration in this reactor and also to indicate whether the influence of mass and heat transfer effects have any significant effect on the expected activity level of the catalyst. The steady state conversion level of propene, as well as the steady state compositions of the liquid product, are listed in Table 4.3 for Runs P1, P3 and P4. The product compositions, in terms of dimer, trimer, tetramer and pentamer, are plotted as functions of reaction time (on stream) for Runs 3 and 4, in Figure 4.8.

Table 4.3 Propene conversion and liquid product oligomer concentrations of Runs 1, 3 and 4 of Section 4.4.2.

		Run P1	Run P3	Run P4
Propene conversion, %		22.0	20.2	11.2
H_3PO_4 conc., %		103.5	108	101
Liquid compositions, mole%				
	C_6	14.5	9.0	10.8
	C_9	54.6	57.5	58.5
	C_{12}	18.1	22.7	19.2
	C_{16}	1.8	2.6	1.8

4.4.2.2 The effect of reaction pressure

Two runs were carried out, at 1.68 MPa and 4.4 MPa. It was attempted to maintain the conversion level in the 44 bar experiment (Run P2) at a

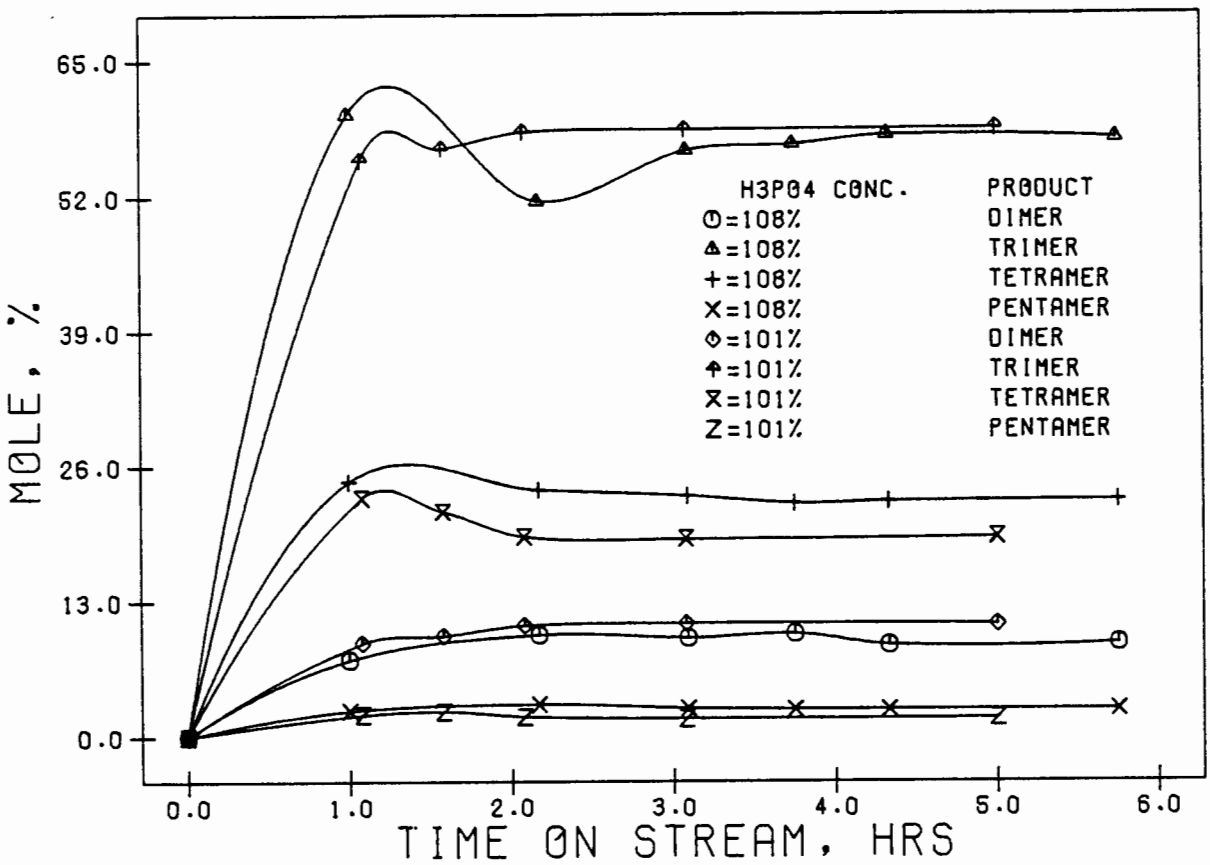

FIG 4.8 INTEGRAL REACTOR: PROPENE OLIGOMERIZATION PRODUCT SPECTRUM VERSUS TIME ON STREAM FOR DIFFERENT ACID CONCENTRATIONS

similar level to that of Run P4 (1.68 MPa). The conversion level at 4.4 MPa, however, was somewhat higher than at 1.68 MPa. Steady state propene conversion levels and liquid product compositions are listed in Table 4.4. Product compositions of Runs 2 and 4 are plotted as functions of reaction time in Figure 4.9.

Table 4.4 Propene conversion and liquid product oligomer compositions of Runs P1, P2 and P4 of Section 4.4.2.

	Run P2	Run P4
Propene conversion, %	26.5	11.2
Liquid compositions, mole%		
C_6	18.1	10.8
C_9	71.2	58.5
C_{12}	7.5	19.2
C_{16}	0.2	1.8

4.4.3 1-Butene Oligomerization

In total, seven experiments were carried out using a pure 1-butene feed.

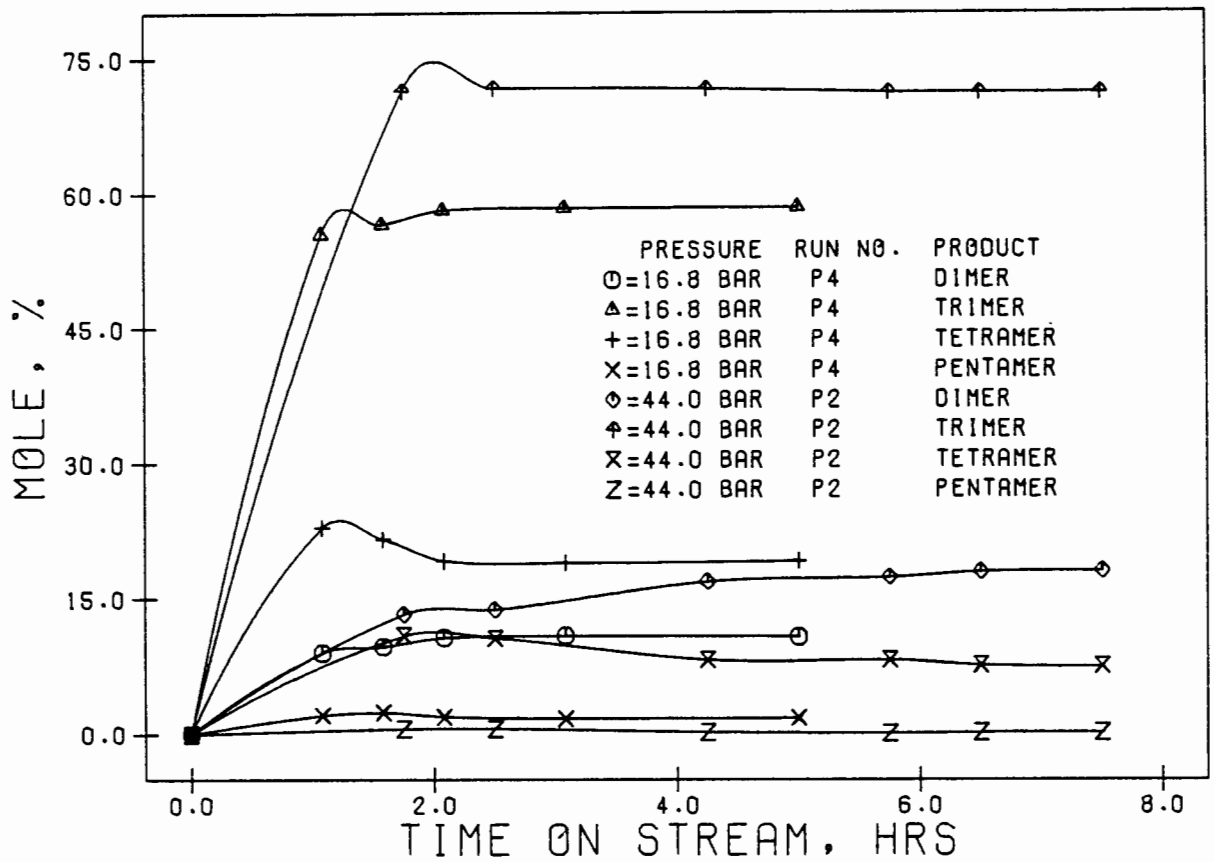

FIG 4.9 INTEGRAL REACTOR: PROPENE OLIGOMERIZATION PRODUCT SPECTRUM VERSUS TIME ON STREAM AT DIFFERENT REACTOR PRESSURES

Runs were carried out to examine the effect of the following:

1. H_3PO_4 concentration with runs at 102% and 108% H_3PO_4, each of which was reproduced.
2. Reaction pressure with runs at 1.55 and 4.55 MPa.
3. Catalyst particle size with runs using crushed catalyst of 106-180 μm and also industrial sized catalyst pellets (6x6.4 mm).

The experimental conditions used for each of these runs are listed in Table 4.5. The catalyst bed depth and bed density are not given in Table 4.5 since, in each experiment, the catalyst was mixed with glass beads (300μm).

4.4.3.1 The effect of H_3PO_4 concentration

Four experiments were carried out (Runs B1, B2, B3 and B4) at two H_3PO_4 concentrations. Two of these runs were reproducibility runs. Reproducibility has been discussed in detail in Section 4.4.1.1. Steady state 1-butene conversion and product concentrations are listed in Table 4.6.

Table 4.5 Experimental conditions used for 1-butene oligomerization experiments.

	Run numbers						
	B1	B2	B3	B4	B5	B6	B7
Catalyst							
Mass, g	3.0	3.0	3.0	3.0	1.0	3.0	3.0
Size, μm	←		106-180		→	6000-6400	
H_3PO_4 conc., %	102	108	102	108	102/103	102	108
Reaction							
Feed	←			1-butene			→
Flow, WHSV	8.7	9.0	9.2	9.2	10.7	9.2	9.4
Temp (set), K	464	464	464	464	464	464	464
Temp (mean), K	463	463	462	462	460	461	461
Pressure, MPa	1.65	1.65	1.55	1.55	4.55	1.52	1.52

Table 4.6 1-Butene conversion and liquid product oligomer concentrations of Runs B1 and B2 of Section 4.4.3.

		Run B1	Run B2
1-Butene conversion, %		22	40
Liquid product composition, mole%			
	C_8	82.4	81.3
	C_{12}	12.6	12.5
	$C_{16}+$	1.3	0.5

4.4.3.2 The effect of pressure

Two experiments were carried out, one at 1.65 MPa and the other at 4.55 MPa. 1-Butene conversions and liquid product compositions (all at steady state) are listed in Table 4.7.

Table 4.7 1-Butene conversion and liquid product oligomer concentrations of Runs B1 and B5 of Section 4.4.3.

		Run B1	Run B5
1-Butene conversion, %		22	21
Liquid product composition, mole%			
	C_8	82.4	84.5
	C_{12}	12.6	11.1
	$C_{16}+$	1.3	1.5

4.4.3.3 The effect of particle size on activity (intra-particular diffusion) and H_3PO_4 concentration.

A total of four experiments were carried out, two experiments using catalyst pellets (6x6.4 mm), one experiment at an H_3PO_4 concentration of 102% and the other at 108% and the other two experiments using 106-180 µm phosphoric acid particles also at 102% and 108% H_3PO_4. The results are shown in Table 4.8. The experimental conditions at which these experiments were carried out are listed in Table 4.5.

Table 4.8 1-Butene conversion and liquid oligomer concentrations of Runs B6 and B7 of Section 4.4.3.

		Run B1	Run B2	Run B6	Run B7
1-Butene conversion, %		22	40	8.5	10.1
Liquid product composition, mole%					
	C_8	82.4	81.3	64.2	64.7
	C_{12}	12.6	12.5	24.6	23.7
	$C_{16}+$	1.3	0.5	3.2	4.5

4.4.4 Iso-Butene Oligomerization

In total, four experiments were carried out, using pure iso-butene and mixed iso-butene/propane feeds. Due to the extremely high reactivity of the iso-butene over phosphoric acid, extremely small amounts of catalyst (0.1 g) had to be used, rendering good reproducibility potentially difficult. The experiments were carried out at the conditions listed in Table 4.9.

Table 4.9 Experimental conditions used for iso-butene oligomerization experiments.

	Run C1	Run C2	Run C3	Run C4
Catalyst				
Mass, g	0.1	0.1	0.1	0.1
Size, μm	← 106-180 →			
H_3PO_4 conc., %	106	105	107/108	102
Reaction				
Feed	← iso-butene →			
Flow, WHSV	410	280	300	55
Temp (set), K	413	464	464	464
Temp (mean), K	415	464	472	462
Pressure, MPa	1.52	1.60	4.65	1.55

It can be seen from Table 4.9 that the WHSV is dramatically high. It was necessary to maintain these high levels in order to keep the conversion levels reasonably low. In Runs B1, B2 and B3, where a pure iso-butene feed was used (>99%, w/w), it was found to be very difficult to control the acid concentration, due to the rapid deactivation of the catalyst. An example of the rapid deactivation can be seen in Figure 4.10 where the iso-butene conversion of Run C1 is plotted as a function of time on stream.

The rapid catalyst deactivation is not entirely unexpected, since it appears as though the total amount of fuel produced in these experiments, per gram of catalyst, would eventually approach that expected in a commercial reactor (1000-1700 g per gram of catalyst (McMahon et al., 1963)) despite the low pressures in many of the experiments. Figure 4.11 shows the cumulative total mass of fuel produced in Run C1 as a function of reaction time.

The product spectra (C_8, C_{12} and C_{16} fractions) of Runs C_1, C_2, C_3 and C4 are shown in Figure 4.12. These three fractions constitute more than 97% (w/w) of the products in each of the four cases. A striking feature of the iso-butene product spectrum is the noticeably small number of C_8 and C_{12} isomers that are produced, unlike the propene or 1-butene product spectra.

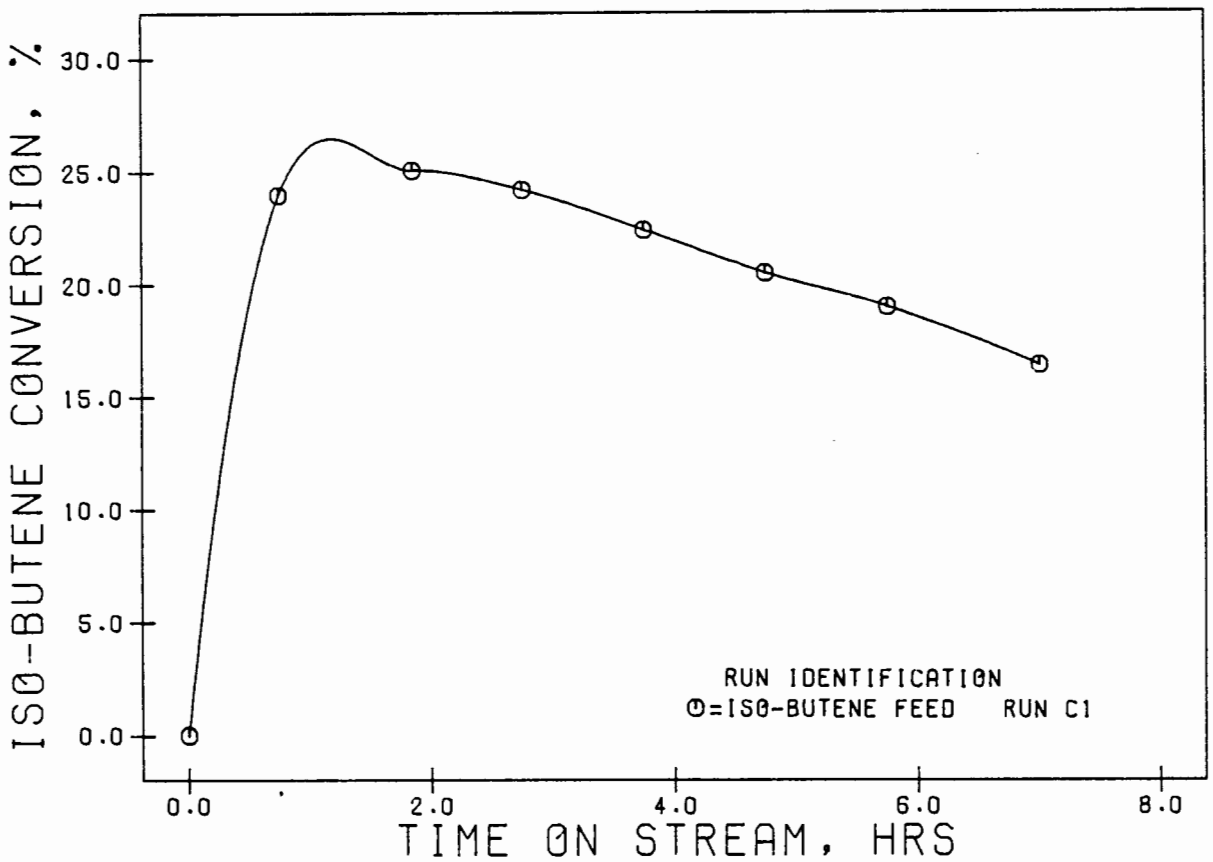

FIG 4.10 INTEGRAL REACTOR RUNS: ISO-BUTENE CONVERSION AS A FUNCTION OF TIME ON STREAM

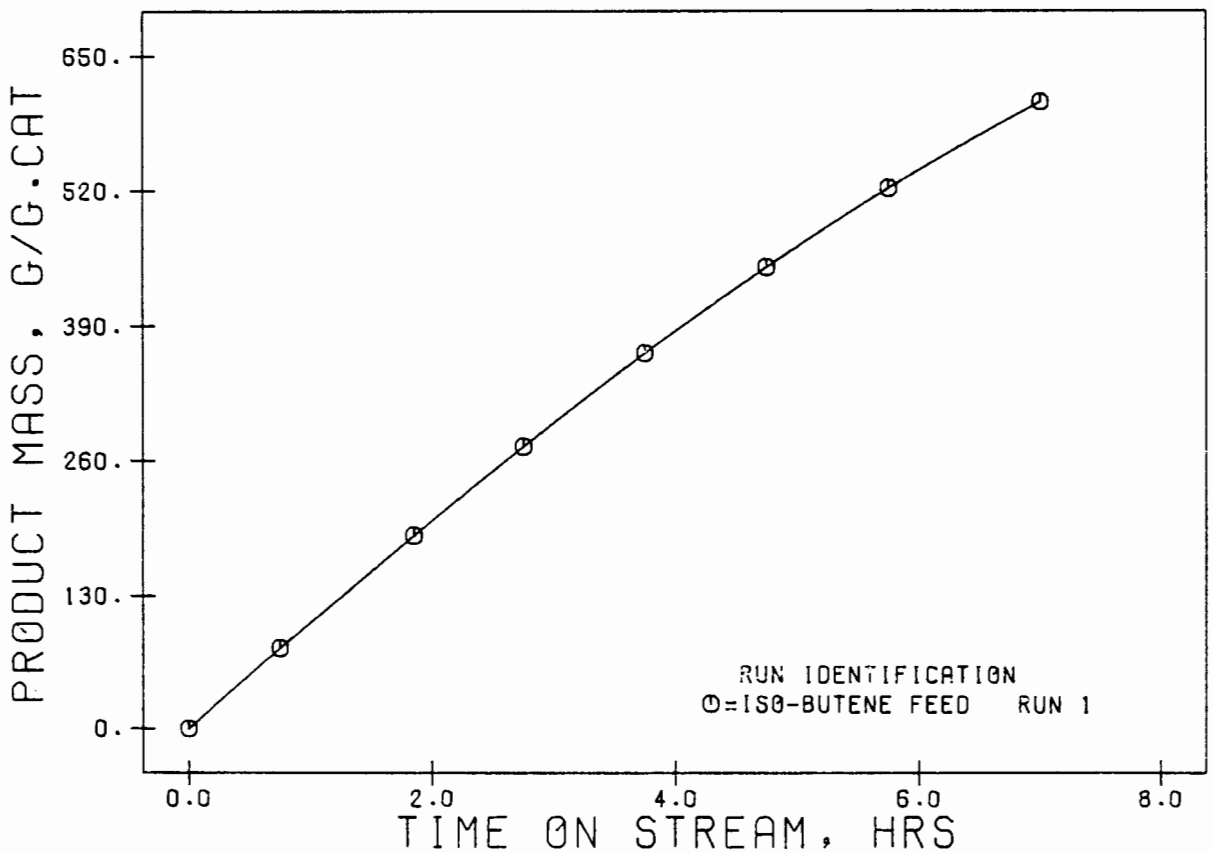

FIG 4.11 INTEGRAL REACTOR RUNS: ISO-BUTENE RUN C1 ACCUMULATIVE PRODUCT MASS VS TIME ON STREAM

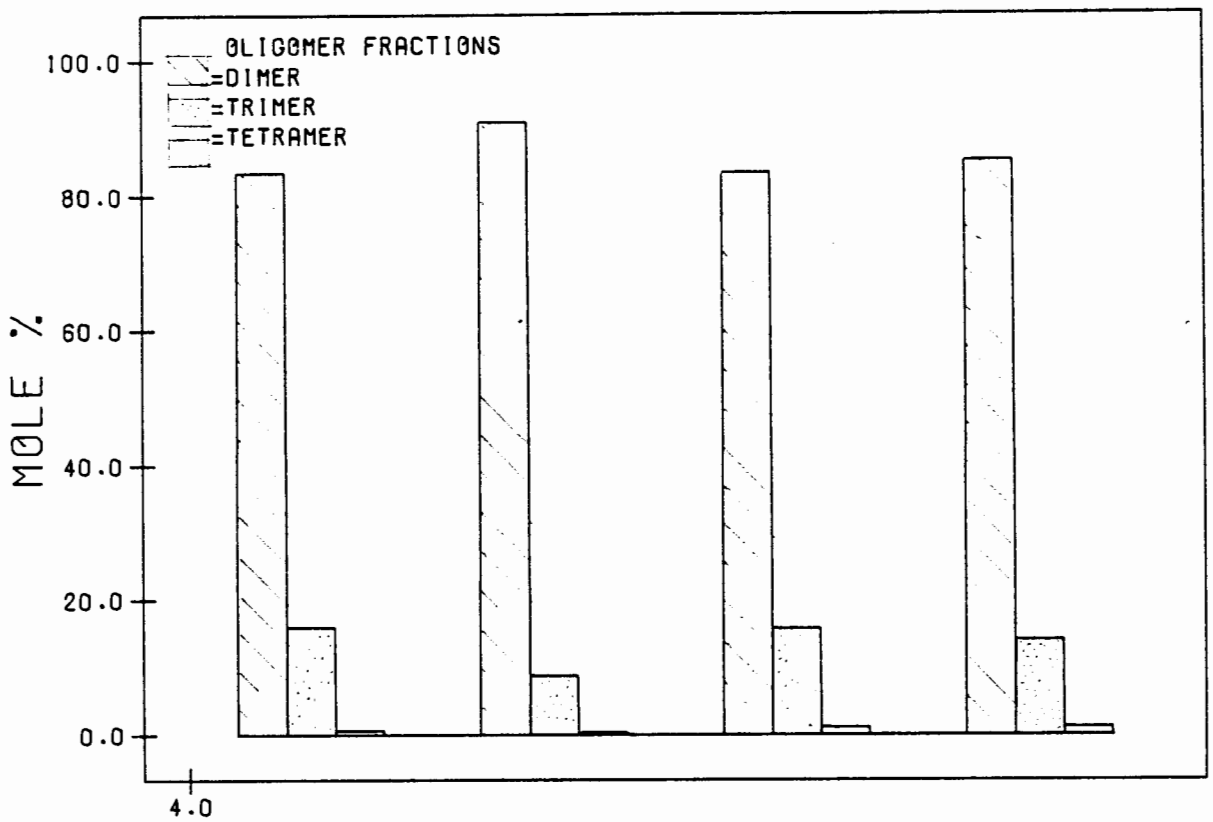

FIG 4.12 INTEGRAL REACTOR RUNS: ISO-BUTENE RUNS C1 TO C4 MOLE FRACTIONS OF DIMER, TRIMER AND TETRAMER

4.5 DISCUSSION

It must be emphasized that the integral reactor studies were not intended to be exhaustive either qualitatively or quantitatively. The results were intended to provide some indication of the differences in behaviour between the internal gas recirculation reactor and the fixed bed reactor with respect to both conversion levels observed and product quality (in terms of carbon chain length). A simple one dimensional analysis was performed on the fixed bed reactor, providing, amongst other things, evidence of the significance of mass transfer at the operating conditions used.

4.5.1 The Effects of Process Variables

From the propene oligomerization runs it was found that changes in the H_3PO_4 concentration had minimal effect on the product spectrum observed, despite the increase in propene conversion as the acid concentration was increased. An interesting feature of the results in Table 4.3 is that, although the conversion in Run 1 was expected to be higher than that of

Run 4 (due to the higher acid concentration), the differences in conversion were greater than expected. It was is also expected that the conversion in Run 3 should be significantly higher than that in Run 1 despite the fact that the temperature in Run 3 was 5 K lower. Although the WHSV, reaction temperature and pressure were essentially the same, Run 1, in spite of its low acid concentration, gave the highest conversion. It is believed that this arose from the fact that in Runs 3 and 4 glass beads were used to disperse the catalyst, hence providing an ~~heat sink~~ inert surface. In this fixed bed reactor it is quite likely that a temperature gradient existed from the bulk phase to the catalyst particles. The glass beads, providing an ~~heat sink~~ inert mass, could then serve to lessen this gradient and therefore at similar bulk temperature levels the catalyst particles which were dispersed amongst glass beads would have lower surface temperatures, resulting in lower reaction rates and conversion levels.

The results in Table 4.4 indicate quite clearly that as the pressure was increased from 16.8 bar to 44 bar, the average molecular weight of the liquid product decreased quite significantly as the product spectrum shifted from the tetramer to the trimer. This result has been observed by several researchers (Jacobs, 1987; Harms, 1987) using other acid catalysts. It is believed that the shift occurs due to the shift in the products from the gas phase to liquid phase, thus resulting in more severe mass transfer limitations. It should be noted from Table 4.4 that the conversions were not maintained constant. However the differences in conversion levels in Table 4.4 are not unlike those in Table 4.3, where it can be seen that the product spectra are quite similar.

The 1-butene experiments showed a similar trend to the propene experiments (bearing in mind the 4 K temperature difference between Runs P3 and P4) with regard to H_3PO_4 concentrations, indicating an approximate doubling of the 1-butene conversion with an increase in the H_3PO_4 concentration from 102 to 108%. Unlike the propene experiments, the effect of pressure was examined by maintaining the conversion levels constant. Very little change in the product spectrum was observed with a change in the pressure from 16.5 to 45.5 bar.

The 1-butene particle size experiments (Table 4.8) indicated clearly that for particles sizes of 6x6.4 mm, there were significant intra-particular mass transfer limitations, ~~although~~ Lower ~~temperatures~~ conversions were expected to a small degree since the WHSV was higher and the temperatures and pressures were lower, in Runs 6 and 7 than in 1 and 2 (compare the results of Table 4.8 to 4.6). Using the larger industrial sized pellets, it was found that

changes in acid concentration provided rather surprising results. The results here revealed that the increase in conversion as the acid concentration was raised from 102% to 108% was unexpectedly minimal. One distinct possibility is that due to the larger particle sizes used, the catalyst particles could take longer to attain the set acid concentrations, i.e., the time taken for the catalyst particles to dehydrate to the required level may be longer due to the slow rate of mass transfer through the larger catalyst. The run times used in these experiments were based on the times taken for the 106-180 micron catalyst fraction to reach equilibrium. The run times may therefore have been too short for the 6.0-6.4 mm catalyst particles to reach equilibrium. Although this possibility seems quite likely, a similar result was found by Kriel (1986), in oligomerizing propene over solid phosphoric acid using a pilot plant sized reactor. Kriel found, up to 24 hrs after the reactor hydration level had been changed (such that the H_3PO_4 concentration should have increased from 102% to 108%), that the conversion level had not changed significantly.

In the examination of particle size effects using a 1-butene feed, it was found that as the particle size was ~~decreased~~ increased from 106-180 µm to 6000-6400 µm the decrease in conversion was accompanied by an increase in the average molecular weight of the product as the trimer yield increased at the expense of the dimer. This is consistent with the results of the internal gas recirculation reactor experiments in Chapter 3.

As expected, the iso-butene experiments showed the iso-butene to be dramatically more reactive than either the propene or the 1-butene. The extremely high activity resulted in rapid deactivation of the catalyst, so much so that a steady state period was not obtained before the catalyst started deactivating (see Figure 4.11). It can be seen from Figure 4.13 that there was very little change in the product spectrum despite the variation in operating conditions.

Similar to the results of the kinetic experiments in Chapter 3, the average molecular weight of the product spectra from the 1-butene and iso-butene oligomerization reactions was lower than that from the polymerization of propene. In this reactor dimer was also found to be the major oligomer product in the butene oligomerization whereas the trimer followed by the tetramer were found to be the major oligomers from the polymerization of propene. The reasons for this trend as suggested in Chapter 3 could possibly be due to steric hindrance experienced by monomer molecules obtaining access to the adsorbed species or could also

be due to the heats of adsorption of the C_8 and C_9 fractions which may be similar and result in the preferential desorption of these molecules.

4.5.2 Comparison of the integral reactor results with those of the internal gas recirculation reactor

With respect to changing H_3PO_4 concentration for propene oligomerization, the results obtained with the two reactors were found to be quite similar with respect to both product quality and conversion. Pressure effects were not examined in the internal gas recirculation reactor because it was necessary to maintain everything in the gas phase, or as much of it as possible; hence the pressure was not raised above 1.6 MPa. No noticeable differences between the two reactors were observed.

For 1-butene conversion, both reactors gave similar results for different H_3PO_4 concentrations. (The internal gas recirculation reactor results had to be extrapolated up to the 108% H_3PO_4 level.) Both reactor studies confirmed that intraparticular diffusion was significant when using pellets of 6000-6400 μm. In both reactors it was found that as the particle size was decreased from 6000-6400 μm the average molecular weight of the product decreased with the accompanying increase in conversion.

The iso-butene results, which have been described, were quite similar in both reactors.

4.5.3 One dimensional analysis of the integral reactor

A simple one dimensional model was used to predict the conversion and temperature profile down the catalyst bed. This was done to test the simple power law rate equation obtained from the kinetic experiments of the previous chapter and to obtain an indication of the severity of mass and heat transport effects, if any. It must be emphasized that it was not intended to perform a rigorous analysis. It was from this point of view that some of the assumptions were made.

Being a one dimensional model, radial temperature and concentration gradients were not examined. The model is based on the simultaneous solution of the following three equations at various depth increments moving down the catalyst bed:

1. Rate equation describing the rate of propene reaction as a function of propene concentration and reaction temperature.

2. Mass balance.
3. Energy balance.

The three equations are given as follows

Rate equation: $-rC_3 = f(X_A, T) = k_0 e^{-E/RT} [C_3]^n$

Mass balance: $-rC_3 dW = FC_3 dX_A$

Energy balance: $F_t C_p dT = (-rC_3) dW(-\Delta H)$

where $-rC_3$ = rate of propene reaction

$[C_3]$ = propene concentration

$n = 1.03$

$k_0 = 29.49\ mol^{-0.03} \cdot l^{1.03} \cdot hr^{-1}$

$E/R = 2568\ K$

A complete description of the model and the solution procedure is given in Appendix J. The model was used to predict the conversions and bed temperatures for propene oligomerization at conditions identical to those of Run 1 in Table 4.2. The following assumptions were made in the model:

1. The heats of formation for the C_9 and C_{12} fractions were assumed to be those of the normal straight alkenes due to the lack of heat of formation data on any other alkene isomers.
2. The product composition was assumed to be constant throughout the reactor. This assumption had to be made due to the lack of information on the changing product composition as the reaction front moved down the bed.
3. The fractions of C_{12} formed from $C_6 + C_6$ and $C_9 + C_3$ were assumed to be constant irrespective of position in the catalyst bed. For the result shown below the entire C_{12} fraction was assumed to be formed from $C_9 + C_3$. Using the assumption of the C_{12} fraction being formed solely from the dimerization of C_6 would result in a catalyst bed temperature of 471 K and a predicted bed depth of 13.5 mm at the 22.5% propene conversion level.
4. The reactor was assumed to behave adiabatically.

The results of the model prediction are shown in Table 4.10.

The actual experimental results are as follows:

total catalyst bed depth:	12.6 mm
propene conversion at exit from reactor:	22.0%
reactor temperature at exit from catalyst bed:	472 K

The modelled results show very good agreement with the experimental results. This could be an indication that firstly, the effects of mass

Table 4.10 Results of the one dimensional model analysis for propene oligomerization at the conditions described for Run 1 in Table 4.2.

Conversion, %	Bed depth, mm	Temperature, K
1.5	1.978	454.1
3.0	1.981	454.3
4.5	2.97	454.7
6.0	3.97	455.2
7.5	4.96	455.8
9.0	5.93	456.7
10.5	6.9	457.7
12.0	7.8	468.9
13.5	8.7	460.2
15.0	9.6	461.8
16.5	10.5	463.5
18.0	11.3	465.3
19.5	12.1	467.4
21.0	12.8	469.6
22.5	13.5	472.0

and heat transfer are not severe and secondly that the rate equation adequately describes the rate of propene reaction. For comparative purposes the model was also tested by using a second order and also a first order rate equation in propene concentration. Using the second order rate equation and taking the propene conversion to be the independent variable, the second order rate equation predicted a bed depth of 37.7 mm and an exit reactor temperature of 467.5 at the 22.5% propene conversion level. The zero order rate equation predicted a bed depth of 13.9 mm and an exit reactor temperature of 468 at the 22.5% propene conversion level. These predicted results which do not compare favourably with the first order results and hence the experimental results.

It has been pointed out that the effect of heat of reaction in the production of C_{12} depending on whether the C_{12} fraction was assumed to have been formed from the dimerization of C_6 or the reaction of propene with C_9 had no significant effect on the model prediction.

The assumption of the average composition of the reaction products was found to be significant. The results presented in Table 4.10 are based on the constant molar compositions in the liquid product of 50% dimer, 40% trimer and 10% tetramer. Using the constant molar compositions of 30% dimer, 60% trimer and 10% tetramer results in a predicted bed depth of 13.9 mm and an exit reactor temperature of 468 K at the 22.5% propene conversion level. The predicted bed depth in this case is 3% higher and the exit reactor temperature is 1.5% lower than the predictions of Table 4.10.

The rate equation developed by Bethea and Karchmer using liquid phosphoric acid predicted that the expected fractional conversion of propene in this fixed bed reactor would be approximately 40% at these conditions. This is significantly higher than that predicted using the solid phosphoric acid catalyst in the internal gas recirculation reactor and is therefore not comparable in the one dimensional modelling.

It must be emphasized that the good agreement between the modelled and the experimental results does not necessarily imply that the assumptions made above were good (despite the fact that they were necessary). Only a thorough test of the model over a range of experimental conditions would confirm or refute this.

4.6 CONCLUSIONS

The fixed bed reactor studies have shown over the range of conditions used in this work, that the quality of the oligomerization products from both propene and 1-butene oligomerization is quite insensitive to changes in reaction conditions.

For identical masses of catalyst the conversion decreased with the introduction of glass beads in the catalyst bed. It is believed that the glass beads may have provided a heat sink thus lessening the temperature gradient between the bulk gas phase and the catalyst particles and by doing so may have resulted in lower catalyst surface temperatures, resulting in lower reaction rates and conversion levels.

Although product quality was found to be quite insensitive to change in reaction conditions the fixed bed results confirmed the findings of the kinetic experiments in Chapter 3 in that the average molecular weight of the product was found to decrease with an increase in conversion,

particularly when conversion was increased as a result of operating at higher reactor pressures. It was postulated in Chapter 3, at the conditions used in these studies, that the increase in conversion which was accompanied by an increase in the fraction of liquid phase in the reactor was therefore accompanied by poorer mass transfer coefficients particularly for the longer chain products. Therefore although mass transfer may have been shown to be negligible at the conditions used in the kinetic experiments it is possible that at the higher conversion levels, such as at the very high temperatures and H_3PO_4 concentrations, the longer chain products, particularly C_{12}, may have started experiencing diffusional resistances. The 1-butene product spectra did not change with an increase in the system pressure from 16.5 to 45.5 while the conversion was maintained constant. From the above postulate it was expected that the average molecular weight of the product should have decreased by some extent since the increase in the pressure the liquid phase in the reactor would have increased.

The industrial sized H_3PO_4 pellets were accompanied by significant mass transfer limitations as was found in the internal gas recirculation reactor experiments of Chapter 3. These sized particles were also very insensitive to changes in H_3PO_4 concentration at the conditions used in this work. This has also been found by Kriel (1986) using solid phosphoric acid catalyst at similar temperatures but at higher pressures and over longer experimental periods. It is possible, due to the poorer mass transfer coefficients, that these industrial sized particles would have required significantly longer times than were used to attain the set H_3PO_4 concentration levels. The testing of smaller sized catalyst particles on pilot plant scale, although costly, could prove to be advantageous.

From a one dimensional analysis it was found that the exit reactor bed temperature, the propene feed conversion and the catalyst bed depth could be predicted to within 0-10% of the experimental results. The model was particularly limited by the lack of heat of formation data for branched alkenes. Inherent in the model were the assumptions that the reactor behaved adiabatically, that the liquid product (C_6+) composition was constant throughout the reactor. The assumption of how much of the C_{12} fraction was produced solely from the dimerization of C_6 and how much was produced from the reaction of propene with trimer was found to have very little effect on the predicted results.

The good fit of the predicted data to the experimental data may be an indication that mass transfer limitations at the conditions used were not very significant. It was expected that intraparticular effects were negligible since a 106-180 μm catalyst size fraction was used for the

model prediction comparisons and secondly, a weight hourly space velocity of 9 was used.

The rate equation of Bethea and Karchmer (1956), at the conditions used for the model prediction, which was obtained by using liquid phosphoric acid, predicted a propene conversion of approximately 40%. This was significantly higher than that obtained in the fixed bed reactor. ~~It would appear therefore that the rate equation of Bethea & Karchmer (1956) may not applicable to the fixed bed reactor at these conditions~~.

5. CONCLUDING REMARKS

This section summarizes some of the salient points of this work. Detailed and complete conclusions can be found at the end of each discussion section viz., Sections 2.6, 3.6 and 4.6 for the pulse, internal gas recirculation and fixed bed reactors respectively.

This work examined, inter alia, the oligomerization of C_3, C_4 and C_6 alkenes over solid phosphoric acid, the primary objective being to examine the intrinsic kinetics of propene and butene oligomerization using an internal recycle reactor in which mass and heat transfer effects have been minimized. The oligomerization of propene, butene (1-butene and iso-butene), and various C_6 alkene isomers was also studied using a pulse reactor with a view to examining the relative reactivities of the reaction intermediates with a view to determining the mechanistic pathways followed. The empirical rate equations developed for propene oligomerization in the internal gas recirculation reactor were used to predict the propene conversions and reactor temperatures at given bed depths in a fixed bed reactor using a one-dimensional model. The predicted results were compared to the experimental results obtained.

The internal gas recirculation reactor which was designed by Caldwell (1983a), was based on the Berty design with several modifications aimed at improving the performance of the blower. This reactor was characterized by performing residence time studies and and mass transfer studies with and without reactions.

The residence time distribution studies and the mass transfer studies in the internal recycle reactor confirmed that this reactor is easily capable of operating as a perfect stirred tank reactor. The reactor approaches ideal CSTR behaviour at recycle ratios between 15 and 20. Superficial gas velocities for the napthalene-air system estimated at atmospheric pressure and 2000 rpm from various pressure drop equations and also from mass transfer coefficients, confirmed the results of Caldwell (1983a). High superficial gas velocities and mass transfer coefficients can be obtained such that mass and heat transfer limitations can be rendered insignificant. Good comparisons between the superficial gas velocities estimated from pressure drop equations and those estimated

from mass transfer coefficients served to indicate that the blower (impeller) in this reactor was at least 85% efficient at these conditions where efficiency is defined as the percentage of the theoretical head generated that is converted to pressure.

As a result of the linear variation of the mass transfer coefficient with impeller speed and the drop in mass transfer coefficient with increasing pressure (up to 5 MPa) it is possible that the flow through the bed was at the upper end of the laminar range (hence the linear variation of Kc with impeller speed) and as the pressure was increased so the flow became turbulent, accompanied by a decrease in Kc. It is possible that the diffusivity rather than the Schmidt number is the correlating factor as suggested by Caldwell (1983a).

Intraparticular diffusion and interphase mass transfer effects are insignificant when propene is oligomerized over solid phosphoric acid at 1.5 MPa, 2000 rpm, 464 K, 101.5% H_3PO_4 and using a catalyst size fraction of 106-180 μm. At the extreme conditions of 114% H_3PO_4, 503 K and at 1.5MPa, 2000 rpm with a catalyst size fraction of 106-180μm, interphase mass transfer was insignificant and intraparticular diffusion was largely eliminated.

The pulse experiments were carried out at low alkene partial pressures. As a result cracking, which was thermodynamically favoured at these conditions, was fairly extensive. At a pressure of 1.65 MPa (total system pressure which was due to the nitrogen carrier), reaction temperature of 473 K, constant C_{12}/C_9 mole ratios and C_{12} concentrations above 1x10-4 mol/l, the bulk of the cracked products were a result of C_{12} cracking. With respect to the cracking of the C_9 and C_{12} fractions it was found that at these conditions the following initial routes were the most likely:

$$C_{12} \longrightarrow C_7 + C_5,$$
$$C_{12} \longrightarrow C_8 + C_4$$

and for C_9 cracking $\quad C_9 \longrightarrow C_5 + C_4$

In the pulse reactor isomerization of the C_6 alkenes over phosphoric acid catalyst was extremely rapid. The relative lack of change in reactivity

between 2-methyl-2-pentene, 3-methyl-1-pentene, 3-methyl-2-pentene, 4-methyl-1-pentene and cis-4-methyl-2-pentene is attributed to the very rapid rate of isomerization of each of these hexenes. Slight changes in reactivities are attributed to the possibility that the isomerization reactions have not reached equilibrium. The slower rate of 1-hexene oligomerization relative to the rates oligomerization of the methyl-pentenes can be attributed to the formation of the secondary carbonium ion.

Taking the 2-methyl-1-pentene as being representative of the rates of reaction of the methyl-pentenes, the alkenes were found to oligomerize in the following order of decreasing reactivity in the pulse reactor: iso-butene, 1-butene, 2-methyl-1-pentene (although the 1-butene and 2-methyl-1-pentene were found to oligomerize at similar rates), 1-hexene and propene.

In the presence of iso-butene, propene was found to oligomerize at a faster rate than when only a pure propene feed was used.

In the pulse reactor it was found that the percentage of C_{12} formed from the dimerization of C_6 as opposed to the reaction of propene with C_9 depended on the molar ratios of both propene to C_9 and propene to C_{12}. At 473 K, 1.63 MPa and propene and 2-methyl-1-pentene reactor concentrations (averaged reactor concentrations) of $1.23x^{10-2}$ mol/l and $0.83x^{10-2}$ mol/l (viz. propene: 2 Me1P ratio of 1.5) in addition to propene: C_9 molar ratios of 10:1, the C_{12} fraction was produced solely from the dimerization of 2-methyl-1-pentene. At the higher propene concentration of 4.97x10-2 mol/l and a 2-methyl-1-pentene concentration of 0.86x10-2 mol/l, (molar ratios of 6:1) and C_3:C_9 molar ratios of 15:1, it was estimated that approximately 50% of the C_{12} fraction was produced from C_6 dimerization.

The C_{12} fraction is therefore unlikely to be produced from only one of the above two routes in an industrial fixed bed reactor. The industrial reactors are operated at high conversions and, as a result, the ratio of propene to C_6 and C_{12} would change dramatically as the reaction front moves down the catalyst bed. It is probable that at the top of these reactors, the bulk of the C_{12} is produced by the reaction of propene with C_9. At the bottom of the reactor, the majority of the C_{12} is produced by

the dimerization of the C_6 fraction. This shift in mechanism occurs as the reaction front moves down the bed and is due to the corresponding drop in the concentration of propene.

In Section 2.6 suggested routes of the basic reaction pathways believed to be most likely for the oligomerization of propene and butene (and also for the resultant cracking reactions) at these conditions were presented in the form of two reaction pathway networks.

The activity and lifetime of the catalyst is extremely dependent on H_3PO_4 concentration, high acid concentrations resulting in rapid deactivation of the catalyst. Control of the H_3PO_4 concentration is therefore critical.

The average molecular weight of the liquid product in the internal recycle and the fixed bed reactor decreased moderately with significant increases in the conversion of the propene feed. It is suggested that this could be due to a shift in the phase of the reactor contents towards the liquid phase accompanied by the possible onset of diffusional hindrances for the longer chain length products. The mass transfer results, however, have confirmed that, with respect to the rate of propene reaction, mass transfer was insignificant at these conditions. The possibility of a shift in the mechanism for the production of the C_{12} as the propene concentration decreases (to the dimerization of C_6) cannot be ignored.

The butenes oligomerize mainly to dimers whereas propene oligomerizes predominantly to trimers and also tetramers. It is suggested that this could be due to steric hindrances experienced by monomer molecules in obtaining access to the adsorbed intermediate, or could also be due to the heats of adsorption of the C_8 and C_9 fractions which would be similar and result in the preferential desorption of these molecules.

The results obtained from the kinetic studies in the recirculation reactor were used to develop rate expressions. Simple power law modelling of the rate of propene reaction over the temperature range 443 to 473K, H_3PO_4 range of 102 to 107% and at a pressure of 1.53MPa yielded a rate equation which was close to first order with respect to propene concentration. At extreme conditions of temperature and H_3PO_4

concentration (up to 114% H_3PO_4 and 508 K) the rate equation, although fitting the data reasonably well, tended to over-predict. The rate of 1-butene reaction fitted a similar power law rate equation which had an order of 1.24 with respect to 1-butene concentration.

Five models were examined in the modelling of the rates of formation of products and the rate of propene disappearance. Two of the models (referred to as P1 and P2) were based on each of the reactions being elementary, the one model taking the reverse reactions into account. Two more of the models (P3 and P4) were purely empirical, model P3 having been based on the production of the C_{12} fraction from C_6 dimerization only and the other based on the production of C_{12} from the reaction of propene with C_9. The fifth model(P5) was based on a more fundamental approach, taking, for each reaction, the adsorption equilibrium into account and assuming the rate of reaction of carbonium ion with alkene to be rate limiting.

The empirical models (P3 and P4) fitted the rate data significantly better than did models P1, P2 and P5. Model P3 predicted the rate and concentration data more accurately than model P4 at the extreme conditions of temperature and H_3PO_4 concentration. Based on this result (% error analysis) and the finding of the pulse experiments - that at the high ratios of propene : C_9, the C_{12} formed from $C_3 + C_9$ becomes substantial - it is concluded that model P3 is probably the better of the two models. It is suggested that in the reaction sequence it is the dimerization of the propene that is possibly rate limiting due to the relatively high activation energy of this reaction and the relatively small value of the rate constant (which was found in all cases).

Attempts were made to fit a proposed mechanistic model with the empirical models obtained but no adequate correlations were found.

The 1-butene models were formulated in a similar manner to those of propene. Similar conclusions can be drawn from the 1-butene modelling since the empirical model B4 gave the best fit to the data. Activation energies in each of the 1-butene oligomerization reactions were found to be consistently greater than those found from the propene reaction network.

The fixed bed reactor results have confirmed the internal recycle reactor results in that products of oligomerization from propene and butene oligomerization were found to be the same. In a similar manner to the results obtained in the internal recycle reactor, it was found in the fixed bed reactor that as the conversion of propene increased, the average molecular weight of the product decreased. This was found to be particularly true of the increase in conversion accompanying the increase in pressure from 1.63 to 4.4 MPa. Mass transfer limitations were significant when industrial sized catalyst pellets were used. These large (6.0 to 6.4 mm) cylindrical shaped pellets were found to be very insensitive to changes in H_3PO_4 concentration as opposed to the fine particles used in the internal recirculation reactor.

Preliminary studies were carried out using a one dimensional analysis of the fixed bed reactor based on the power rate law developed for propene oligomerization obtained from the internal recycle reactor data. The model predicted the catalyst bed depth and the exit reactor temperature as functions of propene conversion. The model incorporated the following assumptions:

1. The heats of formation data for the C_9 and C_{12} fractions were based on straight chain heat of formation data due to the difficulty of obtaining heat of formation data on branched alkenes.
2. The liquid product composition (C_6+) was assumed to be constant throughout the reactor.
3. The fractions of C_{12} formed from the dimerization of C_6 and the fractions formed from the reaction of propene with C_9 were assumed to be constant throughout the reactor.
4. The reactor was assumed to behave adiabatically.

Notwithstanding these rather over-simplifying assumptions, the model, which was by no means intended to be exhaustive, predicted the experimental results to within 10%.

REFERENCES

Adrian J.P. & Smith J.M. (1970) J. Catal. 18, 57.

American Process Industries (API) (1953) Project 44 - Selected Values of Physical & Thermodynamic Properties of Hydrocarbons & Related Compounds. Carnegie Press, Pittsburgh, Pennsylvania.

Anderson J.R., Mole T. & Christov V. (1980) J. Catal. 61, 477-484.

Anderson R.B. (1956) in: Catalysis 4 (P.H. Emmett, editor). Reinhold, New York.

Anderson R.B. (1968) Chapter 1 in: Experimental Methods in Catalysis Research. Academic Press, New York & London.

A.O.A.C. (1950) pp9-10 in: Methods of Analysis. 7th ed, Washington, D.C.

Aris R. (1957) Chem. Eng. Sci. 6, 262.

Baiker A. & Bergougnan M. (1985) Can. J. Chem. Eng. 63, 146.

Baiker A. & Epple D. (1986) Applied Catalysis 22, 55-69.

Ballivet-Tkatchenko D., Duc Chali N. & Tkatchenko I. (1982) Metals Entrapped in Zeolites as Fischer-Tropsch Catalysts. International Coal Conversion Conference, CSIR, South Africa.

Banks R.L. (August 1979) CHEMTECH, 494-500.

Barcicki J., Nazimek D., Grzegorczyk M., Borowiercki T. & Krizywania B. (1981) Ann. Univ. Mariae Curie - Sklodowska Sect. AA 36, 13, 169-174.

Basset D.W. & Habgood H.W. (1960) J. Phys. Chem. 64, 769-773.

Bell R.N. (1948) Ind. Eng. Chem. 40, 1464.

Bennett C.O., Cullip B. & Yang C.C. (1972) Chem. Eng. Sci. 27, 2255-2264.

Bercik P.G. (1978) U.S. Patent 1031282.

Bercik P.G. (1979) U.S. Patent 4153638.

Bercik P.G., Metzger K.J. & Swift H.E. (1978) Ind. Eng. Chem. Prod. Res. Dev. 17, 3, 214-219.

Berman A.D., Yanovskii M.I. & Roginskii S.Z. (1970) Dokl. Akad. Nauk SSSR, 190.

Berty J.M. (1974) Chem. Eng. Prog. 70, 5, 78-84.

Berty J.M. (1977) ACS Annual Meeting, August 29, pp1-11.

Berty J.M. (1979) Catal. Rev. Sci. Eng. 20, 1, 75-96.

Berty J.M. (1983) Applied Catalysis 8, 289-291.

Berty J.M. (1984) Plant/Operations Progress 30, 163-168.

Berty J.M., Hambrick J.O., Malone T.R. & Ullock D.S. (1969) Reactor for Vapour-Phase Catalytic Studies - Paper no. 42, Sixty-fourth National Meeting of the A.I.Ch.E, New Orleans, March 16-20.

Bethea S.R. & Karchmer J.H. (1956) Ind. Eng. Chem., Eng. Process Des. Dev. 48, 3, 370-377.

Bett J.A.S. & Hall W.K. (1968) J. Catal. 10, 105-113.

Biegler L.T., Damiano J.J. & Blau G.E. (1986) Am. Inst. Chem. Eng. J. 32, 1, 29-43.

Bird R.B., Stewart W.E. & Lightfoot E.N. (1963) Chapter 21 in: Transport Phenomena. John Wiley & Sons, Inc., New York.

Blanton W.A. Jr., Byers C.H. & Merrill R.P. (1968) Ind. Eng Chem. Fundam. 7, 4, 611-617.

Box G.E.P & Hill W.J. (1967) Technometrics 9, 1, 57-71.

Brink A. & Swart J.S. de K (1982) The Fischer-Tropsch Synthesis as Applied at Secunda with Special Reference to Product Work Up and Product Quality. International Coal Conversion Conference, CSIR, South Africa.

Brisk M.L. et al. (1968) Catal. Rev. Sci. Eng. 20, 1, 75-96.

Brown C.E. & Bennet C.O. (1970) Am. Inst. Chem. Eng. J. 16, 817.

Brown E.H. & Whitt C.D. (1952) Ind. Eng. Chem. 44, 615.

Butt J.B., Walker C.A. & Bliss R.H. (1962) Am. Inst. Chem. Eng J. 8, 42.

Caldwell L. (1982) Applied Catalysis 4, 13.

Caldwell L. (1983a) Applied Catalysis 8, 199-213.

Caldwell L. (1983b) Applied Catalysis 8, 293-294.

Carberry J.J. (1961) Am. Inst. Chem. Eng. J. 7, 350.

Carberry J.J. (1964) Ind. Eng. Chem. 56, 39-45.

Carberry J.J., Tipnis P. & Schmitz R. (1985) CHEMTECH 15, 316-319.

Chao K.C. & Seader J.D. (1961) Am. Inst. Chem. Eng. J. 7, 4, 598-605.

Cholette A. & Cloutier L. (1959) Can. J. Chem. Eng. 37, 105.

Choudhary V.R. & Doraiswamy L.K. (1972) Ind. Eng. Chem. Process Des. Dev. 11, 420.

Choudhary V.R. & Doraiswamy L.K. (1975) Ind. Eng. Chem. Process Des. Dev. 14, 3, 227-235.

Christoffel E.G. (1982) Catal. Rev. Sci. Eng. 24, 2, 159-232.

Claasens T. (1983) Final year undergraduate project, University of Cape Town, South Africa.

Cooke C.G. (November 1979) ChemSA, 175-176.

Deeter M.G. (1950) Oil & Gas Journal 48, 252.

Deitz M.A. (February 1967) J. Gas Chromatogr., 68-71.

Denisova T.A. & Rozental A.L. (1967) Kinet. Katal. 8, 441.

Doi Y., Murata M., Yano K. & Keii T. (1982) Ind. Eng. Chem. Prod. Res. Dev. 21, 580-585.

Domnesteanu R.G. (1982) Chem. Eng. Sci. 37, 3, 480-482.

Doraiswamy L.K. & Tajbl D.G. (1974) Catal. Rev. Sci. Eng. 10, 2, 177-219.

Dry M.E. (1981) p159 in: Catalysis: Science and Technology 1 (J.R. Anderson & M. Boudart, editors). Springer-Verlag, New York.

Dry M.E. (August 1982a) High Yield High Quality Diesel from Fischer-Tropsch Processing. International Coal Conversion Conference, CSIR, South Africa.

Dry M.E. (December 1982b) CHEMTECH, 744-750

Dunstan A.E. & Howes D.A. (1936) J. Inst. Pet. Technol. 22, 347-413.

Durgin C.B., Lum J.H. & Malowan J.E. (1937) Trans. Am. Chem. Inst. Chem. Eng. 33, 643.

Dwivedi P.N. & Upadhyay S.N. (1977) Ind. Eng. Chem. Process Des. Dev. 16, 2, 157-165.

Ebeid F.M., Habib R.M., Rihan T.I. & El-Khatib S.A.M. (1976) Egypt. J. Chem. 19, 5, 853-863.

Egloff G. (March 1936) Oil & Gas Journal, 140-142.

Egloff G. & Weinert P.C. (1951) pp201-214 in: Proceedings of the Third World Petroleum Congress - Sec iv. The Hague, Netherlands.

Evans A.G. & Polanyi M. (1947) J. Chem. Soc., 252.

Fajula F. & Gault F.G. (1981) J. Catal. 68, 291-311.

Fasol R.E. (1983) The Catalytic Conversion of Low Chain Length Hydrocarbons to Liquid Fuels using Zeolite Y. MSc Thesis, University of Cape Town, South Africa.

Falbe J., Frohning C.D., Cornils B. & Moraw K. (1982) Catalyst Development for Selective Syntheses via the Fischer-Tropsch Process. International Coal Conversion Conference, CSIR, South Africa.

Finlayson B.A. (1971) Chem. Eng. Sci. 26, 1081.

Fletcher J.C.Q. (1984) The Acidity of Synthetic Mica - Montmorillonite and its Activity for Propene Oligomerization. PhD Thesis. University of Cape Town, South Africa.

Flory P.J. (1969) pp 217-224 in: Principles of Polymer Chemistry. Cornell University Press, Menasha.

Ford F.E. & Perlmutter D.D. (1964) Chem. Eng. Sci. 19, 371.

Friedman P. & Pinder K.L. (1971) Ind. Eng. Chem. Process. Des. Dev. 10, 4, 548-551.

Fraenkel D. & Gates B.C. (1980) J. Am. Chem. Soc. 102, 2478.

Frohning C.D., Ko"lbel H., Ralek M., Rottig W., Schnur F. & Schulz H. (1982) in: Chemical Feedstocks from Coal (J. Falbe, editor). Wiley, New York.

Froment G.F. (1975) Am. Inst. Chem. Eng. J. 21, 1401.

Froment G.F. (1983) Rijks University, Gent, Belgium. Private Communication.

Froment G.F. (1986) Applied Catalysis 22, 3-20.

Frye C.G. & Mosby J.F. (1967) Chem. Eng. Prog. 63, 9, 66.

Furusawa T., Susuki M. & Smith J.M. (1976) Catal. Rev. Sci. Eng. 13, 1, 43-76.

Galeski J.B. & Hightower J.W. (1970) Can. J. Chem. Eng. 48.

Gangwal S.K. (February, 1982) Research Triangle Institute, Project No. 47N2182, NCEI Contract No. 54, pp1-17.

Garanin V.I., Kurkchi U.M. & Minachev Kh.M. (1967) Kinet. Katal. 8, 701.

Garkisch O.L. & Gaensslen H. (1982) Coal to Synfuels via Methanol. International Coal Conversion Conference, CSIR, South Africa.

Gati Gy. & Kno"zinger H. (1972) The Reactivity of Substituted Olefins and the Mechanism of the Double Bond Isomerization on Alumina. Catal., Proc. Int. Congr., 5th (J.W. Hightower, editor). 1, 819-831.

Gaube J. (1983) University of Darmstadt, W Germany. Private Communication.

Gaziev G.A., Filinovskii V.Y. & Yanovskii M.I. (1963) Kinet. Katal. 4, 599.

Germain J.E. (1969) Catalytic Conversion of Hydrocarbons. Academic Press, London & New York.

Glowinski J. & Stochi J. (1981) Am. Inst. Chem. Eng. J. 27, 6, 1041-1043.

Groenewald C., Wittgen P., Lavrijsen J.P. & Schuit G.C. (1983) J. Catal. 82, 77-91.

Gros J.B. & Bugarel R. (1977) Chem. Eng. J. (Lausanne) 13, 165.

Gut G. & Jaeger R. (1982) Chem. Eng. Sci. 37, 2, 319-326.

Haag W.O. (1967) Chem. Eng. Prog. Symp. Ser. 63, 73, 140-146.

Habeshaw J. (1973) Oligomers and Co-oligomers of Propylene. Pp115-154 in: Propene and its Industrial Derivatives (E.G. Hancock, editor). Wiley.

Hall W.K. & Emmett P.H. (1959) J. Phys. Chem. 63, 1102-1110.

Hall W.K., MacIver D.S. & Weber H.P. (1960) Ind. Eng. Chem. 52, 5, 421-426.

Hammer H., Biendarra G., Bittner D., Friedricks G., Jorisch W., Koppenhagen H. & MU"ller S. (1982) Non-conventional Heterogenous Catalysts for the Selective Fischer-Tropsch Synthesis. International Coal Conmversion Conference, CSIR, South Africa.

Harms S. (1987) Unpublished Results. Dept. of Chem. Eng., University of Cape Town, South Africa.

Hart H. (1964) pp394-400 in: Kirk-Othmer Encyclopedia of Chemical Technology 4, 2nd Ed.

Hattori H., Miliron D.L., & Hightower J.W. (1973) Mechanistic Studies of Hydrocarbon Reactions over Synthetic Mica-Montmorrillonite Catalysts. Pp 33-51 in: American Chemical Society, Division of Petroleum Chemistry, Dallas, 8-13 June.

Hattori T. & Murakami Y. (1968) J. Catal. 12, 166.

Hattori T. & Murakami Y. (1973) J. Catal. 31, 127-135.

Hattori T. & Murakami Y. (1974) J. Catal. 33, 365-375.

Haynes H.W. Jr. (1983) J. Catal. 79, 470-474.

Heinemann H. (1981) p1 in: Catalysis: Science and Technology 1 (J.R. Anderson & M. Boudart, editors). Springer-Verlag, New York.

Heinemann J.J.L., Freriks I.L.C., Gaaf J., Pott G.T. & Coolegem J.G.F. (1983) J. Catal. 80, 145-153.

Hilderbrand J.H., Prausnitz J.M. & Scott R.L. (1970) Regular and Related Solutions. Van Nostrand Reinhold, New York.

Himmelblau D.M. & Bischoff K.B. (1968) Process Analysis & Simulation - Deterministic Systems. Wiley & Sons.

Himmelblau D.M., Jones C.R. & Bischoff K.B. (1967) Ind. Eng. Chem. Fundam. 6, 4, 539-543.

Hoogendoorn J.C. (May 1982) Hydrocarbon Processing, 34E-34Q.

Hougan O.A. (1961) Ind. Eng. Chem. 53, 7, 509-527.

Hougan O.A. & Watson K.M. (1947) Chemical Process Principles - Part 3. John Wiley & Sons, New York.

Hutchings J. & Carberry J.J. (1966) Am. Inst. Chem. Eng. J. 12, 20.

Igarashi A. & Ogino Y. (1982) Applied Catalysis 2, 339-345.

I.G. Farbenindustrie Report, U.S. Government Technical Oil Mission Reel No 54, Item 10, pp486-525 (Consultants' Bureau Translation FL-74)

Inui T., Ishimara T., Morinaga N., Takeuchi G., Matsuda H. & Takegami Y. (1982) Ind. Eng. Chem. Process Des. Dev. 22, 26-30.

Inui T. & Takegami Y. (November 1982) Hydrocarbon Processing, 147-150.

Ipatieff V.N. (1934) U.S. Patent 1960631, 29 May.

Ipatieff V.N. (1935a) Ind. Eng. Chem. 27, 9, 1067-1069.

Ipatieff V.N. (1935b) U.S. Patent 2018065, 22 October.

Ipatieff V.N. (1935c) U.S. Patent 2018066, 22 October.

Ipatieff V.N. & Corson B.B. (1935a) Ind. Eng. Chem. 27, 9, 1069-1071.

Ipatieff V.N. & Corson B.B. (1935b) Ind. Eng. Chem. 27, 9, 1077-1081.

Ipatieff V.N. & Corson B.B. (1936) Ind. Eng. Chem. 28, 7, 860-863.

Ipatieff V.N. & Corson B.B. (September 1938) Ind. Eng. Chem., 1316-1317.

Ipatieff V.N., Corson B.B. & Egloff G. (1935) Ind. Eng. Chem. 27, 9, 1077-1081.

Ipatieff V.N. & Grosse A.V. (1936) J. Am. Chem. Soc. 58, 915.

Ipatieff V.N. & Komarewsky V.I. (1937) Ind. Eng. Chem. 29, 8, 958.

Ipatieff V.N. & Pines H. (1935) Ind. Eng. Chem. 27, 11, 1364-1369.

Ipatieff V.N. & Pines H. (1936) Ind. Eng. Chem. 28, 6, 684-686.

Ipatieff V.N. & Schaad R.E. (1938) Ind. Eng. Chem. 30, 5, 596-599.

Ipatieff V.N. & Schaad R.E. (1948) Ind. Eng. Chem. 40, 1, 78-80.

Jacobs L. (1987) Unpublished results, Dept. of Chemical Engineering, University of Cape Town, South Africa

Jager B. (1978) Fischer-Tropsch Synthesis. Spring School in Coal Conversion, Rand Afrikaans University, South Africa.

Jager B., Holtkamp H. & Gaensslen H. (1982) Opportunities for Low Temperature Fischer-Tropsch Processing. International Coal Conversion Conference, CSIR, South Africa.

Jameson R.F. (1959) J. Chem. Soc, 752.

Janardanarao M. (1980) Chem. Eng. World 15, 12, 37-43.

Jankowski H., Nelles J., Adler R., Kubias B. & Salzer C. (1978) Chem. Technol. Berlin 30, 9, 441-446.

Jones E.K. (1956) pp219-238 in: Adv. Catal. 8. Academic Press Inc., New York.

Karanth N.G. & Hughes R. (1974) Adv. Chem. Ser. 133, 449.

Ke-Chang X.I.E. & Nobile A. Jr. (1986) Applied Catalysis 20, 53-77

Keulemans A.I.M. & Vogue H.H. (1959) J. Phys. Chem. 63, 476-480.

Kirk R.E. & Othmer D.F. (1951) pp621-626 in: Encyclopedia of Chemical Technology 7. Interscience Encyclopedia Inc., New York.

Kittrell J.R. (1970) Mathematical Modeling of Chemical Reactions, in: Adv. Chem. Eng. 8 (T.B. Drew, J.W. Hoopes, G.R. Cokelet & T. Vermeulen, editors). Academic Press.

Klein R.A. (October 1980) Hydrocarbon Processing, 113-115.

Kocirik M. (1967) J. Chromatogr. 30, 459.

Kohll E.A. & Leonard J.P. (1982) Coal Based Liquid Fuels (for transportation): Economic Comparison of Liquefaction and Gassification Routes. International Coal Conversion Conference, CSIR, South Africa.

Kokes R.T., Tobin H. & Emmett P.H. (1955) J. Am. Chem. Soc. 77, 5860.

Kriel K. (1986) Sasol Research, South Africa. Private Communication.

Kubin M. (1965) Collect. Czech. Chem. Commun. 30, 1104.

Kucera E. (1965) J. Chromatogr. 19, 237.

Kuchanski G. R. & Squires R. G. (1976) J. Catal. 41, 486-488.

Lachance P. & Eastham A. M. (1976) J. Polym. Sci. Symp. 56, 203-210.

Langer S. H., Yurchak J. Y. & Patton J. E. (1969) Ind. Eng. Chem. 61, 4, 11.

Langlois G. E. (1953) Ind. Eng. Chem. 45, 7, 1470-1476.

Langlois G. E. & Walkey J. E. (1951) An Improved Process for Polymerization of Olefins with Phosphoric Acid on Quartz Catalyst. P 191 in: Proceedings of the Third World Petroleum Congress. Sec iv, The Hague, Netherlands.

Lapidus A. L., Isakov Y. A. I., Rudakova L. N., Minachev K. H. M. & Eidus Y. A. T. (1973) Catalytic Oligomerization of 1-Butene on Zeolites. Symposium on Mechanisms of Hydrocarbon Reactions, Siofok, Hungary, 5-7 June.

Lee B. I., Erbar J. H. & Edmister W. C. (1973) Am. Inst. Chem. Eng. J. 19, 349.

Lee R. H. S. & Agnew J. B. (1977) Ind. Eng. Chem. Process Des. Dev. 16, 490.

Leinroth J. P. & Sherwood T. K. (1964) Am. Inst. Chem. Eng. J. 10, 524.

Leva M. (1959) p48 in: Fluidization. McGraw-Hill.

Levenspiel O. (1972) Chapter 9 in: Chemical Reaction Engineering, 2nd edition. J Wiley & Sons, New York.

Li G. (1985) Chem. Eng. Sci. 40, 6, 939-949.

Li S. F. et al., (1980) Huagongxuebao 1, 65.

Livbjerg H. & Villadsen J. (1971) Chem. Eng. Sci. 26, 1945.

Lloyd L. (1972) Modern Developments in the Use of Catalyst in Industry. Imperial Chemical Industries Ltd, Catalyst and Licencing Department.

Maatman R. W. (1976) J. Catal. 43, 1-17.

Mahoney J. A. (1974) J. Catal. 32, 247-253.

Mahoney J.A., Robinson K.K. & Myers E.C. (1978) CHEMTECH 8, 758-763.

Makar K. & Merrill R.P. (1972) J. Catal. 24, 546.

Manor Y. & Schmitz R.A. (1984) Ind. Eng. Chem. 23, 243.

Manudhane A.R., Czajkowski G.J., Otto C.K. & Sikonia J.C. (1982) Maximum Diesel Fuel and Petro-Chemical Feedstock Production from H-Coal Syncrudes. International Coal Conversion Conference, CSIR, South Africa.

Marsh S.K., Owen H. & Wright B.S. (1984) U.S. Patent 4456781, 26 June.

Martin G.E. & Hill L.W. (1976) J. Catal. 42, 344-349.

Masamune S. & Smith J.M. (1964) Ind. Eng. Chem. Fundam. 3, 179.

McCubbin R.J. (1931) J. Am. Chem. Soc. 53, 356.

McGreavy C. (1970) Chem. Eng. Sci. 25, 303.

McCubbin R.J. & Adkins H. (1930) J. Am. Chem. Soc. 52, 2547

McGreavy C. & Cresswell D.L. (1969a) Can. J. Chem. Eng. 47, 583.

McGreavy C. & Cresswell D.L. (1969b) Chem. Eng. Sci. 24, 608.

McGreavy C. & Thornton J.M. (1970) Can. J. Chem. Eng. 48, 187.

McMahon J.F., Bednars C. & Solomon E. (1963) Polymerization of Olefins as a Refinery Process. Chapter 5 in: Adv. Pet. Chem. Refin. 1 (J.J. McKetta, Jr, editor). Interscience Publishers.

Mehta V.D. & Sharma M.M. (1966) Chem. Eng. Sci. 21, 361.

Meier H. & Gut G. (1978) Chem. Eng. Sci. 33, 123-131.

Monroe L.A. & Gilliland E.R. (1938) Ind. Eng. Chem. 30, 1, 58-63.

Monsanto Chemical Co. (1946) Phosphoric Acid. Technical Bulletin No. P-26, St. Louis, Mo.

Murakami Y., Hattori Tatsuhiko & Hattori Tadashi (1968) J. Catal. 10, 123-127.

Murchison C.B. (1981) Synthesis Gas to Hydrocarbon Feedstocks. National Meeting American Chemical Society, New York, August 23-28.

Myers J.N. (1970) Chem. Eng. Prog. Symp. Ser. 66, 103, 94-98.

Myers E.C. & Robinson K.K. (1978) Multiphase Kinetic Studies with a Spinning Basket. Am. Chem. Soc. Symp. Ser., No. 65.

Naccache C. & Ben Taarit Y. (1980) Pure Appl. Chem. 52, 2175-2189.

Norton C.J. (1964) Ind. Eng. Chem. Prod. Res. Dev. 3, 3, 230-236.

Occeli M.L., Hsu J.T. & Galya L.G. (1985) J. Mol. Catal. 32, 377-390.

Oblad A.G., Mills G.A. & Heinemann H. (1958) Chapter 4 in: Catalysis 6 (P.H. Emmett, editor). Reinhold Publishing Corp., Waverly Press Inc, Baltimore.

Orr N.H., Cresswell D.L. & Edwards D.E. (1983) Ind. Eng. Chem. Process Des. Dev. 22, 135-143.

Outi A., Rautavuoma I. & van der Baan H.S. (1981) Applied Catalysis 1, 247-272.

Padberg G. & Smith J.M. (1968) J. Catal. 12, 172.

Paynter J.D. & Schutte N. (1971) Ind. Eng. Chem. Process Des. Dev. 10, 2, 250-257.

Penick J.E., Meisel S.L., Lee N. & Silvestri A.J. (1978) Mobil Process for Conversion of Coal and Natural Gas to Gasoline. Alcohol Fuels, Sydney, 9-11 August, 5.12-5.16.

Periera J.R. & Calderbank P.M. (1975) Chem. Eng. Sci. 30, 167-175.

Perkins T.K. & Rase H.F. (1958) Am. Inst. Chem. Eng. J. 4, 351.

Petrus L., de Roo R.N., Stamhuis E.J. & Joosten G.E. (1984) Chem. Eng. Sci. 39, 3, 433-446.

Pines H. (1981) The Chemistry of Catalytic Hydrocarbon Conversions. Academic Press, New York.

Prater C.D. (1958) Chem. Eng. Sci. 8, 284.

Prausnitz J.M. (1969) pp269-279 in: Molecular Thermodynamics of Fluid Phase Equilibria. Prentice-Hall, Englewood Cliffs, N.J.

Public Relations Department, Sasol (June 1980). Sasol in a Nutshell.

Quang D.V., Raimbault C. & Hellin M. (September 1981) Hydrocarbon Processing, 134-138.

Raghaven N.S. & Doraiswamy L.K. (1972) J. Catal. 48, 21-34.

Ramage M.P., Graziani K.R. & Krambeck F.J. (1980) Chem. Eng. Sci. 35, 41-48.

Ratkowsky D.A. (1985) Chem. Eng. Sci. 40, 9, 1623-1628.

Rautenbach M. (1986) The Acidity of Sodium-Ammonium-Mordenite and its Activity for Butene Oligomerization. PhD Thesis. University of Cape Town, South Africa.

Reichle H.T. (November 1981) CHEMTECH, 698-702.

Relyea D.L. & Perlmutter D.D. (1968) Ind. Eng. Chem. Process Des. Dev. 7, 261.

Robinson K.K. & Mahoney J.A. (1977) Symposium on Laboratory and Bench Scale Reactor Design. Am. Chem. Soc., Chicago Meeting, Aug 28-Sept 2.

Robinson R.L. & Chao K.C. (1971) Ind. Eng. Chem. Process Des. Dev. 10, 221.

Roginskii S.Z. & Rozental A.L. (1964) Kinet. Katal. 5, 104.

Roginskii S.Z., Yanovskii M.I. & Gazier G.A. (1961) Dokl. Akad. Nauk SSSR, 140.

Ryland L.B., Tamele M.V. & Wilson J.N. (1958) pp1-91 in: Catalysis 7 (P.H. Emmett, editor). Reinhold Publishing Corp., Waverly Press Inc, Baltimore.

Sachanen A.N. (1940) Conversion of Petroleum (Production of Motor Fuels by Thermal and Catalytic Processes). Reinhold, New York.

Santacesaria E. & Carra S. (1983) Applied Catalysis 5, 345-358.

Santacesaria E., Morbidelli M. & Carra S. (1981) Chem. Eng. Sci. 36, 909-918.

Satterfield C.N. & Roberts G.W. (1968) Am. Inst. Chem. Eng. J. 14, 159.

Schmerling L. & Ipatieff V.N. (1950) Adv. Catal. 2, 21-80.

Schneider P. & Smith J.M. (1968) Am. Inst. Chem. Eng. J. 14, 886.

Schumann W. (1983) The Catalytic Conversion of Low Chain Length Hydrocarbons to Liquid Fuels Using Ion Exchange Resin. MSc Thesis. University of Cape Town, South Africa.

Schwab G.M. & Watson A.M. (1965) J. Catal. 4, 570.

Scott K.F. & Phillips C.S. (1980) J. Chem. Soc. Faraday Trans. 1 76, 683-700.

Seinfeld J.H. (1970) Ind. Eng. Chem. 62, 32.

Shanley W.B. & Egloff G. (18 May 1939) Oil & Gas Journal, 116-130.

Sharma C.S. & Hughes R. (1979) Chem. Eng. Sci. 34, 613.

Sherwood P.W. (May 1957) Polymerization of Light Hydrocarbons. Petroleum, 183-186.

Sica A.M., Valles E.M. & Gigola C.E. (1978) J. Catal. 51, 115-125.

Simon A. & Schultz G.Z. (1939) Z. Anorg. Allg. Chem. 242, 325.

Simulation Sciences Inc. (1983) Process Simulation Program, Houston, Texas.

Skrzypek J., Grzesik M., Galantowicz M. & Solinski J. (1985) Chem. Eng. Sci. 40, 4, 611-620.

Smith J.M. (1981) Chemical Engineering Kinetics, 3rd ed. (J.V. Brown, editor). McGraw-Hill.

Smith J.M. & Van Ness H.C. (1975) Introduction to Chemical Engineering Thermodynamics. McGraw-Hill, Tokyo.

Smith T.G. & Carberry J.J. (1976) Chem. Eng. Sci. 31, 613.

Snel R. (1982) Chemica Scripta 20, 99-101.

Spencer M.S. (1981) J. Catal. 67, 259-265.

Steffens J.H., Zimmerman M.U. & Laituri M.J. (1949) Chem. Eng. Prog. 45, 4, 269-277.

Steingaszner P. & Pines H. (1966) J. Catal. 5, 356-360.

Stowe R.A. & Murchison C.B. (January 1982) Hydrocarbon Processing, 147-150.

Striplin M.M. (1948) Development of Processes and Equipment for Production of Phosphoric Acid. T.V.A., Chemical Engineering Report No. 2, Wilson Dam, Alabama.

Stul M.S., van Leemput L. & Uytterhoeven J.B. (1983) Clays and Clay Minerals 31, 2, 158-159.

Sullivan F.W. Jr., Ruthruff R.F. & Kuentzel W.E. (1935) Ind. Eng. Chem. 27, 9, 1072-1076.

Sundaram K.M. & Froment G.F. (1977) Chem. Eng. Sci. 32, 601-608.

Suzuki M. & Smith J.M. (1971) Chem. Eng. Sci. 26, 221-235.

Swift H.E. & Black E.R. (1974) Ind. Eng. Chem. Prod. Res. Dev. 13, 2, 106-110.

Tabak S.A. (1984a) Mobil Olefins to Gasoline and Distillate Process (MOGD). Thailand-United States Natural Gas Utilization Symposium, Bangkok, Thailand.

Tabak S.A. (1984b) Production of Synthetic Diesel Fuel from Light Olefins. Paper no. 42a, A.I.Ch.E. National Meeting. Philadelphia, PA.

Tabak S.A., Wright B.S. & Owen H. (1985) U.S. Patent 4504693, 12 March.

Tajbl D.G. (1969a) Can. J. Chem. Eng. 47, 154-156.

Tajbl D.G. (1969b) Ind. Eng. Chem. Process Des. Dev. 8, 364.

Tajbl D.G., Feldkirchner H.L. & Lee A.L. (1967) Adv. Chem. Ser. 69, 166.

Tajbl D.G., Simons J.B. & Carberry J.J. (1966) Ind. Eng. Chem. Fundam. 5, 2, 171-175.

Tarbutton G. & Deming M.E. (1950) J. Am. Chem. Soc. 74, 2086.

Temkin M.I. (1979) Kinetics of some Industrial Heterogeneous Catalytic Reactions. Pp173-291 in: Adv. Catal. 28 (D.D. Eley, H. Pines & P.B. Weisz, editors). Academic Press, New York.

Thiele E.W. (1939) Ind. Eng. Chem. 31, 916.

Toyota K. & Echigoya E. (1968) Kagaku Kogaku 32, 1005.

United Catalyst Incorporated. Phosphoric Acid Polymerization Operating Instructions.

Van Wazer J.R. (1953) Phosphoric Acids and Phosphates. Pp403-441 in: Encyclopedia of Chemical Technology (R.E. Kirk & D.F. Othmer, editors) 10, Interscience, New York.

Verma A. & Kaliaguine S. (1973) J. Catal. 30, 430-437.

Vidwans A.D. & Sharma M.M. (1967) Chem. Eng. Sci. 22, 673.

Waddams A.L. (1963) Chemicals from Petroleum. John Murray Publishers, London.

Watanabe K. & Himmelblau D.M. (1983) Am. Inst. Chem. Eng. J. 29, 5, 789-795.

Weekman V.W., Jr. (1974) Am. Inst. Chem. Eng. J. 20, 5, 833-840..

Wei J. & Prater C.D. (1962) The Structure and Analysis of Complex Reaction Systems. Pp203-391 in: Adv. Catal. 13. Academic Press, New York.

Weinert P.C. & Egloff G. (June, 1948) Petroleum Processing, 585-593.

Weisz P.B. (1973) CHEMTECH 3, 498-505.

Weisz P.B. (1980) Pure Appl. Chem. 52, 2091-2103.

Weisz P.B. & Hicks J.S. (1962) Chem. Eng. Sci. 17, 265.

Weller S.W. (1975) Adv. Chem. Ser. 148, 26-49.

Wen C.Y. & Fan L.T. (1975) Models for Flow Systems and Chemical Reactors. Chem. Process. Eng. Ser. 3, Marcel Dekker Inc., New York.

Whitmore F.C. (1934a) Ind. Eng. Chem. 26, 94-95.

Whitmore F.C. (1934b) Science 79, 2038, 45-47.

Whitmore F.C & Church J.M. (1932) J. Am. Chem. Soc. 54, 3710.

Whitmore F.C., Rowland C.S., Wrenn S.N. & Kilmer G.W. (1942) J. Am. Chem. Soc. 64, 2970.

Whitmore F.C., Wilson C.D., Capinjola J.V., Tongberg C.O., Fleming G.H., McGrew R.V. & Cosby J.N. (1941) J. Am. Chem. Soc. 63, 2035.

Wolthuizen J.P., van den Berg J.P. & van Hoof J.H.C. (1980) in: Catalysis by Zeolites 5 (Imelik et al., editors). Elsivier, Amsterdam.

Yadov G.D. & Sharma M.M. (1979) Chem. Eng. Sci. 34, 1423.

Yang K.H. & Hougan O.A. (1950) Chem. Eng. Prog. 46, 146.

Yanovskii M.I. & Berman A.D. (1972) J. Chromatogr. 69, 3-15.

Yen L.C. & Woods S.S. (1966) Am. Inst. Chem. Eng. J. 12, 1, 95-99

Young G.W. & Greene H.L. (1977) J. Catal. 50, 258-267.

APPENDICES

APPENDIX A GC METHOD FOR MICROCATALYTIC PULSE ANALYSIS

Instrument : Varian 3700 Gas Chromatograph

Column

- Length : 5.6m (glass)
- Diameter : 6mm (O.D.)
- Packing : 3% silicone/OV-101 on chromasorb W-HP 100/120 mesh

Temperature

- Injector (GSV) : 448 K (maximum value temperature)
- Detector : 573 K
- Column : 313 K (5 min), 10 $K \cdot min^{-1}$, 473 K (0 min)

Gas Flows

- Hydrogen : 30 $ml \cdot min^{-1}$
- Air : 300 $ml \cdot min^{-1}$
- Nitrogen : 30 $ml \cdot min^{-1}$

Range : 10^{-10} amps. mv^{-1}

Attenuation : 1

APPENDIX B EQUILIBRIUM CONVERSION DATA FOR STRAIGHT CHAIN ALKENES

Table B.1 Equilibrium conversion data for straight alkenes at 433 K

Temperature = 433 K					
	Pressure, KPa/100				
	0.001	0.01	0.1	1	10
Propene	0.991	0.978	0.939	0.423	0.009
Cis-2-butene	0.009	0.019	0.040	0.045	0.000
1-Pentene	0.000	0.002	0.008	0.010	0.000
1-Hexene	0.000	0.001	0.005	0.018	0.000
1-Heptene	0.000	0.000	0.003	0.023	0.000
1-Octene	0.000	0.000	0.002	0.025	0.004
1-Nonene	0.000	0.000	0.001	0.028	0.009
1-Decene	0.000	0.000	0.001	0.030	0.018
1-Undecene	0.000	0.000	0.000	0.033	0.044
1-Dodecene	0.000	0.000	0.001	0.234	0.295
1-Tridecene	0.000	0.000	0.000	0.040	0.128
1-Tetradecene	0.000	0.000	0.000	0.043	0.198
1-Pentadecene	0.000	0.000	0.000	0.050	0.295

Table B.2 Equilibrium conversion data for straight alkenes at 458 K

Temperature = 458 K					
	Pressure, KPa/100				
	0.001	0.01	0.1	1	10
Propene	0.995	0.988	0.972	0.868	0.026
Cis-2-butene	0.005	0.011	0.022	0.042	0.004
1-Pentene	0.000	0.001	0.003	0.013	0.000
1-Hexene	0.000	0.000	0.001	0.011	0.004
1-Heptene	0.000	0.000	0.001	0.010	0.004
1-Octene	0.000	0.000	0.000	0.008	0.004
1-Nonene	0.000	0.000	0.000	0.006	0.013
1-Decene	0.000	0.000	0.000	0.006	0.026
1-Undecene	0.000	0.000	0.000	0.005	0.047
1-Dodecene	0.000	0.000	0.000	0.024	0.316
1-Tridecene	0.000	0.000	0.000	0.004	0.124
1-Tetradecene	0.000	0.000	0.000	0.002	0.179
1-Pentadecene	0.000	0.000	0.000	0.002	0.261

Table B.3 Equilibrium conversion data for straight alkenes at 483 K

Temperature = 483 K					
	Pressure, KPa/100				
	0.001	0.01	0.1	1	15
Propene	0.997	0.993	0.985	0.956	0.057
Cis-2-butene	0.003	0.006	0.013	0.029	0.004
1-Pentene	0.000	0.000	0.002	0.007	0.004
1-Hexene	0.000	0.000	0.000	0.004	0.004
1-Heptene	0.000	0.000	0.000	0.002	0.004
1-Octene	0.000	0.000	0.000	0.001	0.008
1-Nonene	0.000	0.000	0.000	0.001	0.016
1-Decene	0.000	0.000	0.000	0.000	0.028
1-Undecene	0.000	0.000	0.000	0.000	0.049
1-Dodecene	0.000	0.000	0.000	0.001	0.326
1-Tridecene	0.000	0.000	0.000	0.000	0.114
1-Tetradecene	0.000	0.000	0.000	0.000	0.159
1-Pentadecene	0.000	0.000	0.000	0.000	0.224

APPENDIX C EQUILIBRIUM CONVERSION OF C_5 AND C_6 ALKENES

Table C.1 Equilibrium conversion of a group of C_5 alkenes

	TEMPERATURE		
C_5 ISOMER	443 K	463 K	483 K
2-methyl-1-butene	0.104	0.105	0.106
3-methyl-1-butene	0.488	0.508	0.527
2-methyl-2-butene	0.363	0.338	0.314
cis-2-pentene	0.018	0.019	0.021
trans-2-pentene	0.025	0.026	0.028
1-pentene	0.002	0.003	0.004

Table C.2 Equilibrium conversion of a group of C_6 alkenes

	TEMPERATURE				
C_6 ISOMER	433 K	443 K	453 K	473 K	493 K
2,3-methyl-1-butene	0.019	0.020	0.020	0.020	0.021
3,3-methyl-1-butene	0.000	0.000	0.000	0.000	0.000
2,3-methyl-2-butene	0.040	0.039	0.038	0.037	0.035
2-ethyl-1-butene	0.041	0.042	0.043	0.044	0.045
cis-2-hexene	0.081	0.083	0.084	0.087	0.089
cis-3-hexene	0.009	0.010	0.010	0.011	0.012
trans-2-hexene	0.063	0.064	0.065	0.067	0.068
trans-3-hexene	0.038	0.038	0.039	0.039	0.040
1-hexene	0.004	0.004	0.004	0.005	0.006
4-methyl-1-pentene	0.003	0.003	0.004	0.004	0.004
4-methyl-cis-2-pentene	0.043	0.043	0.044	0.044	0.045
4-methyl-trans-2-pentene	0.080	0.079	0.078	0.076	0.074
2-methyl-2-pentene	0.244	0.239	0.233	0.222	0.211
3-methyl-cis-2-pentene	0.140	0.138	0.137	0.133	0.130
2-methyl-1-pentene	0.180	0.180	0.180	0.180	0.180
3-methyl-1-pentene	0.015	0.017	0.021	0.029	0.040

APPENDIX D VAPOUR LIQUID EQUILIBRIA DETERMINATION

The procedures developed by Chao & Seader (1961) to determine liquid fugacity coefficients, ϕ_i^L, vapour phase fugacity coefficients, $\hat{\phi}_i$, and liquid phase activity coefficients, γ_i.

1. Determination of liquid fugacity coefficients, ϕ_i^L

The following correlation is used:

$$\log\phi_i^L = \log\phi_i^{(0)} + \omega_i \log\phi_i^{(1)}$$

where the quantities are dependent only on reduced temperatures and pressures and are approximated as follows:

$$\log\phi_i^{(0)} = A_0 + A_1/T_r + A_2T_r + A_3T_r^2 + A_4T_r^3 + (A_5 + A_6T_r + A_7T_r^2)P_r + (A_8 + A_9T_r)P_r^2 - \log P_r$$

$$\log\phi_i^{(1)} = -4.23893 + 8.65808T_r - 1.22060/T_r - 3.15224Tr^3 - 0.025(P_r - 0.6)$$

Where $A_0 = 5.75478$, $A_1 = -3.01761$, $A_2 = -4.98500$, $A_3 = 2.02299$, $A_4 = 0$, $A_5 = 0.08427$, $A_6 = 0.26667$, $A_7 = -0.31138$, $A_8 = -0.02655$, $A_9 = 0.02883$

Special coefficients are required for methane and hydrogen.

2. The vapour phase fugacity coefficients, $\hat{\phi}_i$

These are based on the Redlich-Kwong equation of state and are calculated as follows (Smith & Van Ness, 1975):

$$\ln\hat{\phi}_i = \frac{b_i}{b}(z-1) - \ln(z - zh) + \frac{a}{bRT^{3/2}}\left[\frac{b_i}{b} - \frac{2\sum_k(y_k a_{ik})}{a}\right]\ln(1+h)$$

where a and b are the empirical mixing rules:

$$b = \sum_i(y_i b_i)$$

$$a = \sum_i\sum_j(y_i y_j a_{ij})$$

The b_i's are the constants for the pure components and the a_{ij}'s involve both a's for the pure components (like subscripts) and cross coefficients. (There are no b cross coefficients.) These are given by:

$$b_i = \frac{0.0867RT_{ci}}{P_{ci}} \quad , \quad a_{ij} = \frac{0.4278R^2T_{cij}^{2.5}}{P_{cij}}$$

T_{cij} and P_{cij} are as calculated in Section 3.4.1.1. The compressibility factor z is given by:

$$z = \left[\frac{1}{1-h}\right] - \left[\frac{a}{bRT^{3/2}}\right] x \left[\frac{h}{1+h}\right] \qquad \text{where } h = \frac{bP}{zRT}$$

3. Liquid phase activity coefficients, γ_i

The liquid phase activity coefficients are derived from the Scatchard-Hildebrand theory (Prausnitz, 1969) which is based on the concept of a regular solution (Hilderbrand et al., 1970). The activity coefficient is given by

$$\ln\gamma_i = \frac{V_i}{RT} x (\delta_i - \bar{\delta})^2 \qquad \text{where } \bar{\delta} = \frac{\sum_i (x_i V_i \delta_i)}{\sum_i (x_i V_i)}$$

V_i = molar volume

δ_i = solubility parameter of pure liquid i

$$\delta_i = \left[\frac{\Delta U_i^{vap}}{V_i}\right]^{0.5}$$

ΔU^{vap} is the internal energy change of vapourization of pure component i. Values can be determined from heats of vapourization.

$\delta_i - \bar{\delta}$ is only weakly dependent on temperature so δ_i and V_i are evaluated at 25°C and treated as constants (independent of both temperature and pressure). The parameters δ_i's are determined from pure component data. For non-polar, non-dissociating components these methods usually provide acceptable approximations. Applications are generally limited to hydrocarbons.

The molar volume is given by M/ρ where M = molecular weight

ρ = density

The liquid density can be estimated by an approximation given by Yen & Woods (1966) with a 0.3% error. The equation is valid up to the critical point.

$$\rho = 1 + A(1-T_r)^{1/3} + B(1-T_r)^{2/3} + D(1-T_r)^{4/3}$$

where $A = 17.4425 - 214.578z_c + 989.625z_c^2 - 1522.06z_c^3$

$B = -3.28257 + 13.6377z_c + 107.4844z_c^2 - 334.211z_c^3$ for $z_c \leq 0.26$

$B = 60.2091 - 402.063z_c + 501.0z_c^2 + 641.0z_c^3$ for $z_c \geq 0.26$

$D = 0.93 - B$

APPENDIX E GC CHROMATOGRAM OF TYPICAL PROPENE OLIGOMER PRODUCT

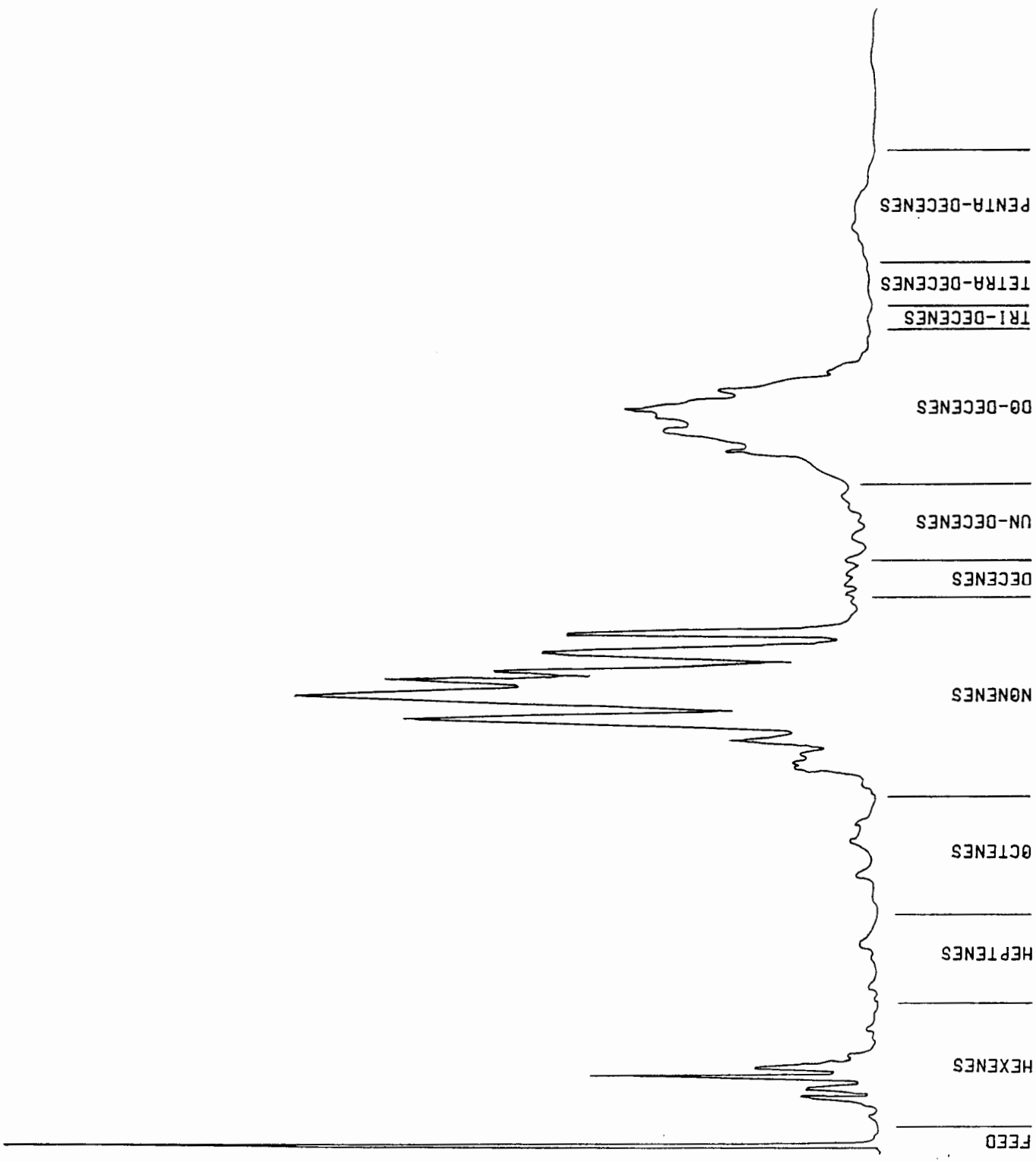

FIGURE E.1 GC CHROMATOGRAM OF TYPICAL PROPENE OLIGOMER PRODUCT

APPENDIX F MASS SPECTROMETER TRACE OF TYPICAL OLIGOMER PRODUCT

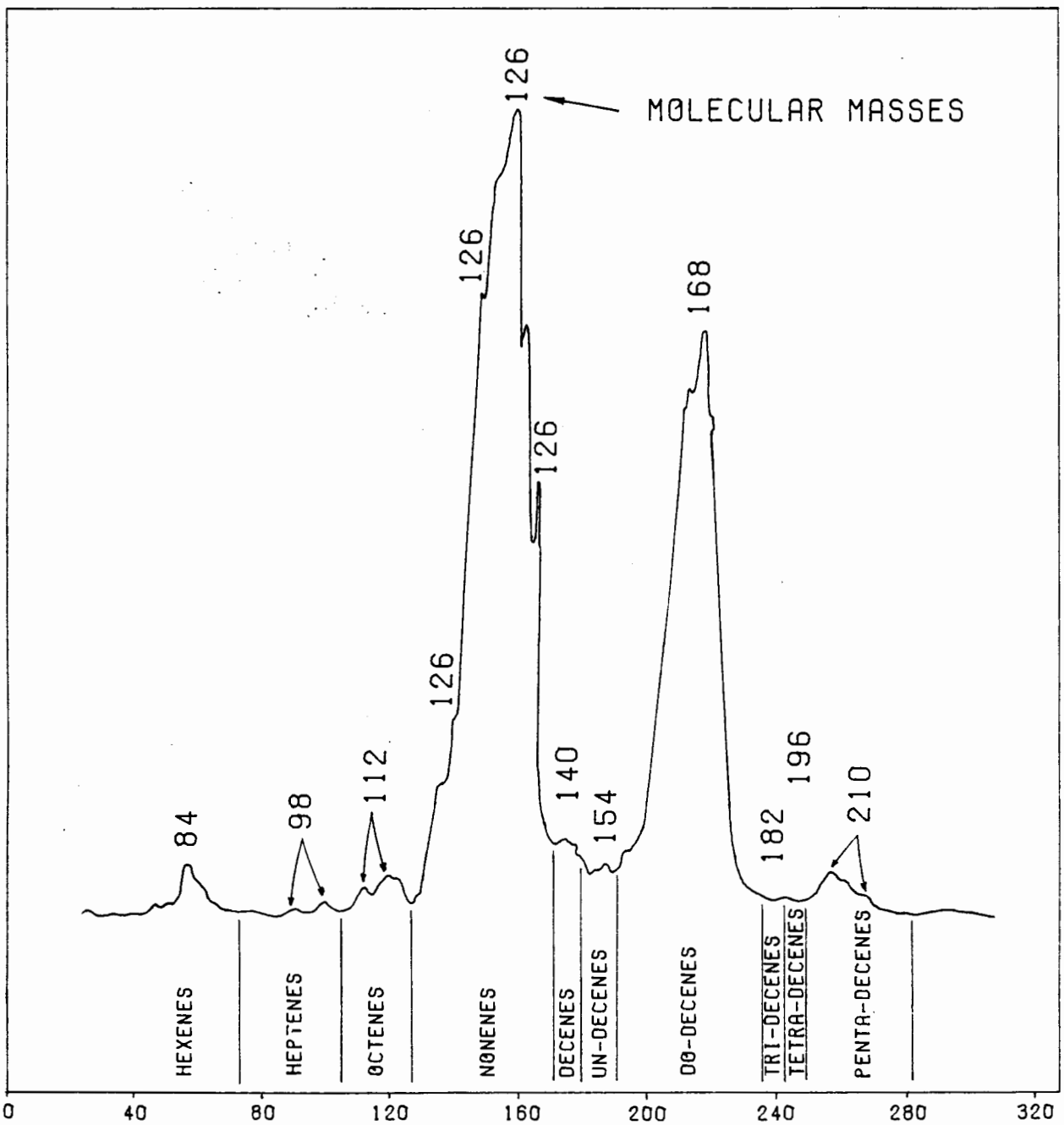

FIGURE F.1 MASS SPECTROMETER TRACE OF TYPICAL OLIGOMER PRODUCT

APPENDIX G DETERMINATION OF THE COMPRESSIBILITY FACTOR, Z

The following method is used to calculate the compressibility factor for a 4:1 (mole ratio) nitrogen:propene mixture at the conditions described in Section 3.2.3.1. The procedure used has been described in detail by Smith & Van Ness (1975). The following critical data for propene and nitrogen are taken from Smith and Van Ness (1975).

Parameter	Propene	Nitrogen
T_c	365.0 K	126.2 K
P_c	45.6 atm	33.5 atm
V_c	181 $cm^3 \cdot gmol^{-1}$	89.5 $cm^3 \cdot gmol^{-1}$
Z_c	0.275	0.290
ω	0.148	0.040

The second virial coefficient of a gaseous mixture is related to composition by

$$B = \sum_i \sum_j (y_i y_j B_{ij})$$

where y is used to represent mole fraction in a gas mixture. The indices i and j identify components in the mixture. The virial coefficient B_{ij} characterizes a bimolecular interaction between a molecule i and a molecule j, and therefore $B_{ij} = B_{ji}$. For a binary mixture the expansion is given by:

$$B = y_1^2 B_{11} + 2y_1 y_2 B_{12} + y_2^2 B_{22}$$

where B_{11} and B_{22} represent the virial coefficients of pure compounds.

The simplest correlation proposed by Pitzer for pure components is for second virial coefficients. It is based on the simplest form of the virial equation which may be written:

$$Z = 1 + \frac{BP_c}{RT_c} \times \frac{P_r}{T_r}$$

The use of this correlation is limited to a range of reduced temperatures and pressures (see Smith & Van Ness, 1975). Pitzer proposed a correlation of the form

$$\frac{BPc}{RT_c} = B_0 + \omega B_1$$

where B_0 and B_1 are well represented by the equations

$$B^0 = 0.083 - \frac{0.422}{T_r^{1.6}}$$

$$B^1 = 0.139 - \frac{0.172}{T_r^{4.2}}$$

Prausnitz (1969) extended Pitzer's correlation for the second virial coefficient to mixtures as follows

$$Bij = \frac{RTc_{ij}}{Pc_{ij}} (B_0 + \omega_{ij} B_1)$$

where B_0 and B_1 are the same functions of T_r as given above. The mixing rules proposed by Prausnitz for the calculation of ω_{ij}, Tc_{ij} and Pc_{ij} are:

$$\omega_{ij} = \frac{\omega_i + \omega_j}{2}$$

$$Tc_{ij} = (Tc_i Tc_j)^{0.5}$$

$$Pc_{ij} = \frac{Zc_{ij}\, RTc_{ij}}{Vc_{ij}}$$

$$Zc_{ij} = \frac{Zc_i + Zc_j}{2}$$

$$Vc_{ij} = \left[\frac{Vc_i^{0.3} + Vc_j^{0.3}}{2} \right]^3$$

The second virial coefficients can now be calculated. The results are shown below.

Table G.1 Second virial coefficients and compressibility factor for propene-nitrogen mixture.

Parameter	Value	Parameter	Value
B_{11}	11.63	B_{12}	-10.89
B_{22}	-120.8	Z	0.999

The value of Z can therefore be assumed to be equal to unity.

APPENDIX H PRODUCT SPECTRA AND RATE/CONCENTRATION DATA FOR VARIOUS ALKENE ISOMERS

1. Pulse Data for 2-Methyl-2-Pentene

Table H.1 Product spectra for 2-methyl-2-pentene.

	Exit concentrations [mol·l^{-1}]x10^{5}			Moles in exit [mol%]		
	Run 1	Run 2	Run 3	Run 1	Run 2	Run 3
C_3	0.4	0.7	1.1	4.7	2.6	2.0
C_4	3.5	6.9	13.0	41.9	26.5	24.2
C_5	1.6	6.9	13.6	19.6	0.1	25.4
C_7	1.2	5.1	14.1	14.1	19.3	26.3
C_8	0.0	1.8	3.0	0.0	7.0	5.6
C_9	0.0	0.1	0.1	0.0	0.5	0.3
C_{10}	0.0	0.2	0.4	0.0	0.6	0.7
C_{11}	0.0	0.0	0.1	0.0	0.0	0.1
C_{12}	1.6	4.5	8.2	19.7	17.1	15.3

Table H.2 2-Methyl-2-Pentene rate/concentration data.

	Reaction rate [mol·hr^{-1}·g_{cat}^{-1}]	2M2P concentration [mol·l^{-1}]	Conversion [%]
Run1	$1.2x10^{-5}$	$1.6x01^{-3}$	4.9
Run2	$3.9x10^{-5}$	$3.8x10^{-3}$	7.1
Run3	$8.0x10^{-5}$	$5.6x10^{-3}$	9.8

2. Pulse Data for 3-Methyl-1-Pentene

Table H.3 Product spectra for 3-methyl-1-pentene.

	Exit concentrations [mol·l^{-1}]x10^{5}			Moles in exit [mol%]		
	Run 1	Run 2	Run 3	Run 1	Run 2	Run 3
C_3	0.3	0.7	2.0	3.3	2.3	2.0
C_4	3.3	7.9	24.1	35.9	26.2	24.3
C_5	1.7	7.7	25.3	18.5	25.6	25.7
C_7	1.6	7.7	25.5	17.4	25.6	25.9
C_8	0.7	2.1	5.2	7.6	7.0	5.3
C_9	0.0	0.0	0.3	0.0	0.0	0.3
C_{10}	0.0	0.2	0.5	0.0	0.7	0.5
C_{11}	0.0	0.0	0.2	0.0	0.0	0.2
C_{12}	1.6	3.8	14.3	17.4	12.6	14.5

Table H.4 3-Methyl-1-Pentene rate/concentration data.

	Reaction rate [mol·hr^{-1}·g_{cat}^{-1}]	3M1P concentration [mol·l^{-1}]	Conversion [%]
Run1	$1.3x10^{-5}$	$1.9x10^{-3}$	5.0
Run2	$4.2x10^{-5}$	$4.4x10^{-3}$	6.9
Run3	$13.9x10^{-5}$	$9.0x10^{-3}$	11.0

3. Pulse Data for 3-Methyl-2-Pentene

Table H.5 Product spectra for 3-methyl-2-pentene.

	Exit concentrations [mol·l^{-1}]x10^{5}			Moles in exit [mol%]		
	Run 1	Run 2	Run 3	Run 1	Run 2	Run 3
C_3	0.2	0.5	1.5	3.4	3.1	1.8
C_4	3.0	5.4	19.6	42.9	33.5	24.0
C_5	1.6	3.6	20.5	22.9	22.4	25.4
C_7	0.8	3.2	21.7	12.9	19.9	26.9
C_8	0.0	0.9	5.3	0.0	5.6	6.6
C_9	0.0	0.1	0.3	0.0	0.6	0.4
C_{10}	0.0	0.0	0.6	0.0	0.0	0.7
C_{11}	0.0	0.0	0.2	0.0	0.0	0.2
C_{12}	1.3	2.4	11.0	18.6	14.9	13.6

Table H.6 3-Methyl-2-Pentene rate/concentration data.

	Reaction rate [mol·hr^{-1}·g_{cat}^{-1}]	3M2P concentration [mol·l^{-1}]	Conversion [%]
Run1	9.1×10^{-6}	1.8×10^{-3}	3.8
Run2	2.3×10^{-5}	2.9×10^{-3}	5.7
Run3	1.2×10^{-4}	7.5×10^{-3}	10.9

4. Pulse Data for 4-Methyl-1-Pentene

Table H.7 Product spectra for 4-methyl-1-pentene.

	Exit concentrations [mol·l^{-1}]x10^{5}			Moles in exit [mol%]		
	Run 1	Run 2	Run 3	Run 1	Run 2	Run 3
C_3	0.4	0.9	1.1	5.1	3.1	3.0
C_4	3.1	8.4	10.0	43.9	30.0	27.6
C_5	1.5	6.3	8.7	21.2	22.5	24.0
C_7	1.0	7.0	8.9	14.2	24.9	24.6
C_8	0.0	1.7	2.4	0.0	6.1	6.6
C_9	0.0	0.1	0.1	0.0	0.3	0.3
C_{10}	0.0	0.0	0.1	0.0	0.2	0.3
C_{11}	0.0	0.0	0.0	0.0	0.0	0.0
C_{12}	1.1	3.4	4.7	15.6	12.8	13.5

Table H.8 4-Methyl-1-Pentene rate/concentration data.

	Reaction rate [mol·hr^{-1}·g_{cat}^{-1}]	4M1P concentration [mol·l^{-1}]	Conversion [%]
Run1	9.3×10^{-6}	2.0×10^{-3}	3.5
Run2	3.8×10^{-5}	4.5×10^{-3}	6.2
Run3	5.0×10^{-5}	5.3×10^{-3}	6.9

5. Pulse Data for Cis-4-Methyl-2-Pentene

Table H.9 Product spectra for cis-4-methyl-2-pentene.

	Exit concentrations [mol.l^{-1}]x10^5			Moles in exit [mol%]		
	Run 1	Run 2	Run 3	Run 1	Run 2	Run 3
C_3	0.3	0.9	1.1	5.3	2.5	2.0
C_4	2.4	10.3	13.1	42.8	28.8	23.7
C_5	1.1	8.5	13.5	19.6	23.8	24.4
C_7	0.7	9.0	14.5	12.5	25.2	26.3
C_8	0.0	2.4	3.2	0.0	6.7	5.8
C_9	0.0	0.0	0.0	0.0	0.6	0.0
C_{10}	0.0	0.2	0.3	0.0	0.6	0.5
C_{11}	0.0	0.0	0.1	0.0	0.0	0.2
C_{12}	1.1	4.4	9.7	19.6	12.3	17.6

Table H.10 Cis-4-Methyl-2-Pentene rate/concentration data.

	Reaction rate [mol•hr^{-1}•g_{cat}^{-1}]	Cis-4M2P concentration [mol•l^{-1}]	Conversion [%]
Run1	$7.6x10^{-6}$	$1.4x10^{-3}$	4.0
Run2	$5.2x10^{-5}$	$4.7x10^{-3}$	7.9
Run3	$8.3x10^{-5}$	$6.0x10^{-3}$	9.9

6. Pulse Data for 1-Hexene

Table H.11 Product spectra for 1-hexene.

	Exit concentrations [mol•l^{-1}] x10^{5}		Moles in exit [mol%]	
	Run 1	Run 2	Run 1	Run 2
C_3	0.6	2.2	4.7	3.8
C_4	4.9	19.8	38.3	34.2
C_5	2.5	13.3	19.5	23.0
C_7	2.7	14.0	21.1	24.2
C_8	1.3	4.1	10.1	7.1
C_9	0.1	0.2	0.8	0.4
C_{10}	0.1	0.5	0.8	0.9
C_{11}	0.0	0.0	0.0	0.0
C_{12}	0.6	3.7	4.7	2.6

Table H.12 1-hexene rate/concentration data.

	Reaction rate [mol•hr^{-1}•g$_{cat}$$^{-1}$]	1-hexene concentration [mol•l^{-1}]	Conversion [%]
Run1	1.6x10-5	3.6x10-3	3.3
Run2	7.5x10-5	9.8x10-3	5.6

APPENDIX I GC METHOD FOR GAS ANALYSIS

Two gas chromatographs were used for the gas analysis, at different periods in time. The operating conditions used and response factors determined with each of the instruments are described below.

Gas chromatograph A

Instrument	: Varian 3700 gas chromatograph
Column	: 6 mm O.D. 5.7 m glass
Packing	: n-Octane/Poracil C

Temperatures

Injector	: 423 K
Detector	: 523 K
Column	: 323 K (5 min), 10 $K \cdot min^{-1}$, 400 K (4 min)

Gas flows

Hydrogen	: 30 $ml \cdot min^{-1}$
Air	: 300 $ml \cdot min^{-1}$
Nitrogen	: 30 $ml \cdot min^{-1}$ (345 KPa guage)

Relative response factors (mass):

Methane	: 1.13
Ethane	: 1.09
Propane	: 1.00
Propene	: 0.77
Iso-butane	: 0.71
n-Butane	: 0.78
1-Butene	: 0.80
Iso-butene	: 0.98
Trans-2-butene	: 0.82
Cis-2-butene	: 0.89
C_5+	: 1.0

Gas chromatograph B

Instrument	:	Gow Mac series 750 P Flame Ionization Detector
Column	:	3.5 m 1/4" stainless steel
Packing	:	n-Octane/Poracil C

Temperatures

Injector	:	423 K
Detector	:	523 K
Column	:	323 K (10 min), 10 $K \cdot min^{-1}$, 398 K (4 min)

Gas flows

Hydrogen	:	30 $ml \cdot min^{-1}$
Air	:	300 $ml \cdot min^{-1}$
Nitrogen	:	40 $ml \cdot min^{-1}$ (345 KPa guage)

Relative response factors (mass):

Methane	:	1.16
Ethane	:	1.09
Propane	:	1.00
Propene	:	0.78
Iso-butane	:	0.65
n-Butane	:	0.76
1-Butene	:	0.82
Iso-butene	:	0.98
Trans-2-butene	:	0.83
Cis-2-butene	:	0.86
C_5+	:	1.0

APPENDIX J ONE DIMENSIONAL ANALYSIS OF FIXED BED REACTOR

Here, a method is described for the one dimensional analysis of the fixed bed reactor in Chapter 4. The solution is specific to the oligomerization of propene over solid phosphoric acid at the conditions used in Run 1 of Table 4.2.

Consider the reactor flowsheet given below.

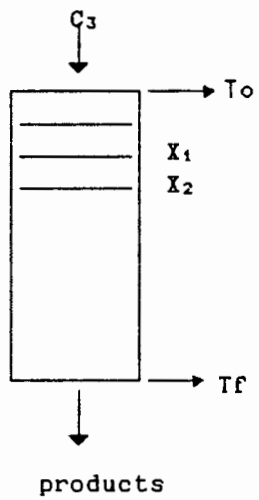

where To = feed inlet temperature, K
Tf = reaction mixture outlet temperature, K

The solution to the model consists of the simultaneous solution of the rate equation, the mass balance and the energy balance at incremental bed depths moving down the catalyst bed. The three equations are as follows:

Rate equation: $-rC_3 = f(X,T) = k_o e^{-E/RT} C_3^n$

Mass balance: $-rC_3 dW = F_{C3} dX_A$

Energy balance: $F_t C_p dT = -rC_3 dW(-\Delta H)$

where $-rC_3$ = rate of propene reaction, $mole \cdot hr^{-1} \cdot g_{cat}^{-1}$
k_o = rate constant
T = reaction temperature, K
W = mass of catalyst, g
F_{C3} = molar flowrate of propene into reactor, $molehr^{-1}$
X_A = conversion of propene, fraction
F_t = total molar flowrate, $mole \cdot hr^{-1}$
Cp = heat capacity of component, $cal \cdot mole^{-1} \cdot {}^{\circ}C^{-1}$
$-\Delta H$ = heat of reaction, $cal \cdot mole^{-1}$
C_3 = propene

APPENDIX E GC CHROMATOGRAM OF TYPICAL PROPENE OLIGOMER PRODUCT

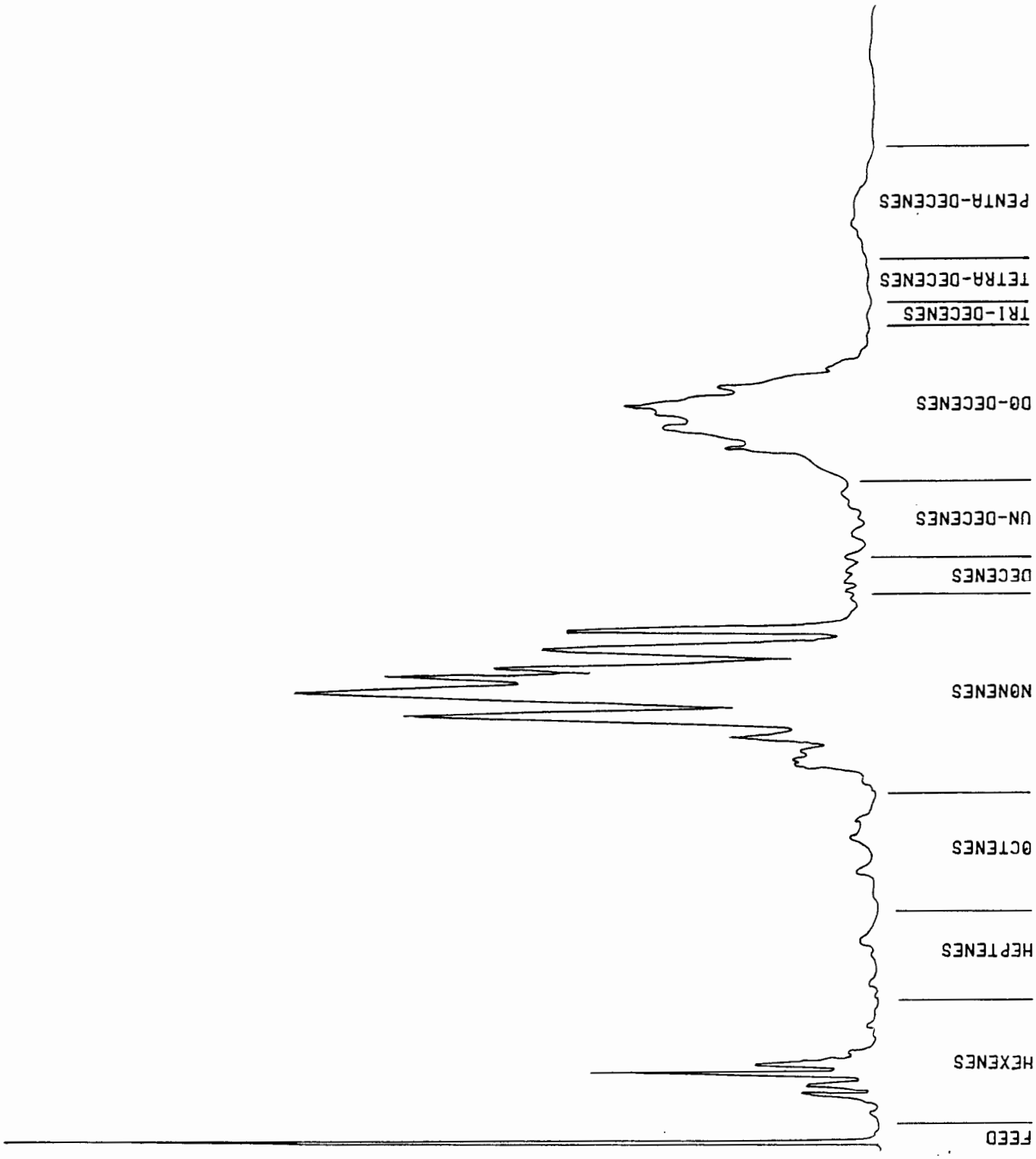

FIGURE E.1 GC CHROMATOGRAM OF TYPICAL PROPENE OLIGOMER PRODUCT

E = activation energy, cal/mole

R = universal gas constant, $cal \cdot mole^{-1} \cdot K^{-1}$

The concentration of propene inside the reactor must be expressed in terms of propene conversion. The expansion factor, ε_A (which takes into account the change in volume of the system between no conversion and complete conversion of reactant), needs to be calculated for this purpose. Assuming linear expansion/contraction with propene conversion, the expansion factor, ε_A, can be expressed as:

$$\varepsilon_A = \frac{V_{X_A=1} - V_{X_A=0}}{V_{X_A=0}}$$

C_3 can now be expressed in terms of X_A by means of the following equation:

$$C_A = C_{A0} \frac{1 - X_A}{1 + \varepsilon_A X_A}$$

where C_{A0} is the feed concentration at the reaction temperature and pressure. The compressibility factor, Z, for the propene feed at these conditions, which is needed to determine the feed concentration, is equal to 0.95.

The calculation of ε_A is based on the following reaction network:

$C_3 + C_3 \longrightarrow C_6$

$C_3 + C_6 \longrightarrow C_9$

$C_6 + C_6 \longrightarrow C_{12}$

$C_3 + C_9 \longrightarrow C_{12}$

The value of ε_A calculated in this way is equal to -0.675.

By rearrangement and combination, the following equations can be obtained:

$$dT = \frac{(-\Delta H)\, F_{C3}}{F_t\, Cp}\, dX \qquad \text{--------(A)}$$

$$dZ = \frac{F_{C3}}{-rC_3\, \rho_B\, A_c}\, dX \qquad \text{--------(B)}$$

where ρ_B = bulk density of the catalyst bed, $g \cdot cm^{-3}$

A_c = cross sectional area of catalyst bed, cm^2

The solution to the model can be performed as follows:

1. Choose a fractional conversion of propene, e.g., 0.1.
2. Using equation (A) (conversion = that chosen in 1. above), calculate ΔT and hence T_1 ($\Delta T = T_1 - To$), which is the temperature at the end of the slice at which point the fractional conversion of propene is equal to that chosen in (1).
3. Using the rate equation, calculate the average rate over the slice.
4. Using equation (B) calculate the bed depth at this point.
5. Continue to the next conversion increment, i.e., repeat the process with the new fractional conversion (chosen) e.g., 0.2.

Data required for the model solution

The reaction rate constant, activation energy and the reaction order, n are those obtained using the internal gas recirculation reactor. The bulk density and catalyst cross sectional area are measured. The data used are given below:

k_0 = 29.49

E/R = 2568

n = 1.03

ρ_B = 0.95

A_c = 2.51

F_{C3} = 0.681

Ft_o = 0.681

To = 454

Tf = 472

Determination of heat capacities and heats of formation

Heat capacities and heats of reactions must be calculated from correlations. The correlation used for each of the oligomers is as follows (API Project 44, 1952):

$Cp = \alpha + \beta T + \gamma T^2$ where T is in K

Cp is in $cal \cdot mole^{-1} \cdot {}^{\circ}C^{-1}$

The values of α, β and γ used for each of the oligomers are those for propene, a weighted average for the hexene isomers, 1-nonene and 1-dodecene. Unfortunately, for the C_9 and C_{12} the data for branched alkenes could not be obtained and therefore the values for the straight 1-alkenes had to be used. The values of α, β and γ used are given below:

	α	β	γ
propene	3.253	45.12×10^{-3}	-13.74×10^{-6}
hexenes	6.399	95.75×10^{-3}	-30.12×10^{-6}
1-nonene	9.689	145.74×10^{-3}	-46.11×10^{-6}
1-dodecene	12.98	195.74×10^{-3}	-62.13×10^{-6}

Heats of reactions are calculated from standard heats of formation ($\Delta H°_{f298}$) at 25°C, and the change in heat capacities of the reactants and products between 25°C and reaction temperature. The heat capacities are calculated as indicated above. Standard heats of formation (at 25°C) are taken from the American Process Industries, Project 44 (1953). The heat of formations are as follows:

	$\Delta H°_{f298}$ kcal·mole^{-1}
propene	4.879
hexenes	-14.33
1-nonene	-24.7
1-dodecene	-39.5

The heat capacities and the heats of reaction are temperature dependent, and therefore must be recalculated at each bed depth increment moving down the catalyst bed. Like the reaction rate, and total molar flowrate, it is the mean value of the heat capacities and the heats of reaction that should be used for each slice.

Note that the mean heat capacity of a mixture is generally given by the equation:

$Cp = \Sigma m_i Cp_i$ where m_i is the number of moles of component i

It is therefore necessary to know the composition of the reaction mixture as it moves through the catalyst bed. For the purposes of this calculation the product composition is assumed to be constant throughout the reactor. The composition used is as follows:

	Mass fraction, %
dimer	50
trimer	40
tetramer	10

APPENDIX K DESCRIPTION OF PROCEDURES FOLLOWED BY MASS BALANCE PROGRAM

The general procedures followed by the mass balance program are described. For the purposes of the description it will be assumed that the feed is a propane/propene mixture. In general the procedure remains approximately the same for other feeds.

1. Data required for the program

The following data is required:

-The number of samples taken including the sample taken at start up (t=0)

-The sample number, time on stream (hrs), %propane and propene in tail gas. This is done for every sample taken, starting from t=0 hrs.

-The liquid product composition for every sample taken, i.e., mass % of C_3, C_4, C_5 ... C_{18}.

-The name of the catalyst
The day, month and year
The catalyst mass in grams (initial)
The reactor temperature (K)
The reactor pressure (bar)
Impeller speed (R.P.M)
Total mass fed to the system
The total volume of tail gas recorded leaving the system
The mass of liquid product collected
The number of the run being analyzed (for record purposes)
The reactor volume

-The mass of liquid collected and the wet gas flow meter readings (tail gas volumes) recorded at each sampling time, starting at t=0.

-The mass (total) of liquid knockout measured after the reaction run has been completed (grams)
The initial mass of catalyst (grams)
The final mass of catalyst (grams)
The steady state temperature inside the catalyst bed (°C)
The steady state temperature inside the reactor (°C)

The steady state temperature on the surface of the reactor (°C)

The steady state temperature on the feed cylinder surface (°C)

The pressure in the feed cylinder (bar)

The steady state tail gas temperature and pressure.

-The title of the run, run group, feed type and catalyst size (mm)

-The sample number which designates the start of steady state

2. Calculation of the compressibility factors

The procedure followed is that described in Section 3.4.1.1 for a two component system. The extension to a three or more component system is quite straight-forward.

The tail gas is regarded as a two component mixture. For a propane/propene feed these are the two components considered. These two components will generally account for more than 96% of the tail gas. The procedure here is identical to that used in Section 3.4.1.1. The fractions of the two components are determined by GC analysis.

For the calculation of the compressibility factor inside the reactor under steady state conditions the hydrocarbons inside the reactor are assumed to represent a three component mixture. For a propene/propane feed the three components are propane/propene, C_9 and C_{12}. The C_9 fraction is taken as $C_8 + C_9 + C_{10}$ and the C_{12} fraction is taken as $C_{11} + C_{12} + C_{13}$.

Although there is some C_6 and C_{15}, the amounts are small and thus are ignored. For the C_4 feeds the three components are taken as propane/C_4 (averaged critical data), C_8 and C_{12}. The composition of the mixture in the reactor is based on the steady state analysis of the exit stream (since for a CSTR the exit concentration is equal to the concentration inside the reactor). From the exit analysis, the mole fractions of the three components can be calculated. The molecular weights used for this calculation are based on the assumption that all of the products are unsaturated. (Mass spectrometry results indicate that this is correct). Once the mole fractions have been calculated the compressibility factor

can be calculated for the three component system based on the procedure in Section 3.4.1.1.

3. Mass balance procedure

The following mass of materials can be accounted for over the entire length of a run

1. The total mass change in the feed cylinder.
2. The mass of feed lost when disconnecting the feed cylinder from the system in order to weigh the contents at the start of the run.
3. The total mass of tail gas in the exit.
4. The total mass of the liquid products collected.
5. The mass of material that accumulated in the reactor over the length of the run due to density change.
6. The total mass of liquid that remained in the reactor after the reactor had been sealed and cooled.
7. The gain in catalyst mass over the length of the run.

The difference between 1 and 2 gives the mass of feed that entered the reactor over the entire length of the run. Experience and persistent checking has shown that no mass is lost between the feed cylinder and the reactor entrance.

The total mass of materials that left the reactor or were accumulated in the reactor which can be accounted for can be calculated from 3, 4, 5 and 6. Knowing the composition of the material at the reactor exit, both at the start and at the steady state period of a run, enables the calculation of the accumulation in the reactor (excluding condensation) due to the density change arising from changes in conversion and product composition.

Knowing the total mass of liquid that remained in the reactor after it had been sealed and cooled, enables the determination of the mass of liquid condensation in the magnedrive shaft during the run. This is calculated by simply determining the mass of product in the reactor at steady state (which would be in the gas phase at reaction conditions, but in the liquid phase after cooling). This mass is subtracted from the total mass of liquid collected in 6. to give the mass of liquid that condensed during the run.

The mass loss is therefore given by:

$$\frac{(1-2) - (3+4+5+\text{liquid in shaft}+7)}{(1-2)} \times 100\ \%$$

4. Feed flowrate versus time

The average feed flowrate into the reactor is determined by dividing the total mass fed by the total time of the run. From the mass balance calculations and the outlet flowrate the feed flowrate is calculated for each time interval over which a sample is taken.

Experience and extensive checking has shown that the mass, when lost, is not lost between the feed cylinder and the reactor or between the reactor exit and the flare, but generally from the reactor, usually at the flange seal between the lid and the body. This loss is therefore assumed to be material of the same composition as in the reactor. The mass loss is assumed to occur at a fixed rate.

It should be noted that the importance of knowing the flowrate is to determine the reaction rate (rate of propene disappearance) at steady state conditions. It is therefore important that the calculated flowrate will represent the correct flowrate at steady state conditions. At steady state, condensation of product in the 'cold' magnedrive shaft has been shown to be negligible. (This has been found time and time again by noting that the total exit flowrate is constant at steady state and is equal to the feed flowrate less the mass loss flowrate) The accumulation of gaseous material in the reactor is also zero at steady state since conversion or product spectrum is no longer changing. Finally, the accumulation of mass on the catalyst, which is extremely small relative to the total mass fed (never exceeding 0.4 mass%), is assumed to be complete by the time steady state has been reached.

For these purposes, therefore, the flowrate is calculated (for each time interval) as follows:

$$\frac{\text{Mass of liquid out} + \text{Mass of gas out} + \text{Mass lost over this time period}}{\text{time period}}$$

Initially, when there is accumulation and condensation taking place this flowrate will be less than the true flowrate (see Figure 3.19). When, however, the reactor does reach steady state conditions, the calculated value will be extremely close to the true value. Two experiments were

conducted to test this by weighing the feed cylinder, not only at the start and end of the run, but also as steady state was reached. The difference between the calculated and actual flowrates over the steady state period was less than 1.5 % in both cases. The reason why this was not done for all the experiments was to avoid any disturbance to the system.

5. Conversion versus time

It was observed for almost all runs , as mentioned in (d) above, that when leaks did occur, they occurred around the Helicoflex seal between the flanges of the reactor lid and its body. Although mass losses were small (any run showing a mass loss above 5 % was discarded) it was decided to account for them in calculating the feed conversions. By doing so, the accuracy of the conversion data was improved marginally. Since the losses were qualitatively found to be issuing from around the reactor seal, at reaction temperatures they were regarded as having the same composition as the gases in the reactor. The conversion of propene, for example, over a sample period was calculated as follows:

Mass of propene feed (Based on input flowrate and feed composition) = P_{IN}

Mass of propene out in tail gas = P_1

Mass of propene out in liquid (contained in entrained gas) = P_2

Mass of Propene contained in mass loss = P_3

$$\text{Conversion} = \frac{P_{IN} - (P_1 + P_2 + P_3)}{P_{IN}} \times 100\ \%$$

The above calculation is cross checked by performing a second calculation based on the same observations, but here using the mass of products formed.

6. Reactant and product concentrations

Not knowing the volume increase coefficients, E_a, for the reactions taking place, standard reaction kinetics methods cannot be used to calculate the reactor concentrations of the components. As a result, the following procedure is used to calculate the reactor concentrations of the reactants and each product component (grouped according to carbon number and known to be unsaturated) for each discrete time interval.

1. Using the compressibility factor determined in (b), the total number of moles in the reactor at steady state can be calculated.
2. From the total mass out over the particular time interval, from the GC analysis and from the carbon number groupings, the mole fractions of each component in the exit, and hence inside the reactor, can be calculated.
3. Knowing the reactor volume, the mole fractions and the total number of moles inside the reactor, the concentrations can be calculated.

Since it has been qualitatively observed that mass losses occur from the reactor, and since these are not only regarded as having the same composition as the reaction mixture, but are very small, they have no influence on the calculation of the reactor concentrations.

7. The rate of disappearance of reactants

Based on the performance equation for a CSTR, as discussed in Section 3.4.2.1, the rate of propene disappearance, for example, over a discrete time interval, is given as follows:

$$-r_A = \frac{X_A F_{A0}}{W}$$

where X_A = fractional conversion of propene as discussed in (e)

F_{A0} = molar feed rate of propene (ml/hr) based on the flowrates as discussed in (d)

W = mass of catalyst (g)

The rate is calculated over each time interval (sample period).

8. Average reaction rates and concentrations

Over the steady state period of the run several discrete samples were taken and hence several reaction rate and concentration values were obtained. Arithmetic means were determined for each of the component concentrations and the rate of reactant disappearance. The following three statistical analyses were performed: the variance, the standard deviation and the expected deviation from the mean.

The variance indicates the degree to which a value (x) varies about the group mean ($\bar{x}$). It is the mean of the squared deviations from the group mean. It is calculated as follows:

$$s^2 = \sum \frac{(x-\bar{x})^2}{N-1}$$

The standard deviation is simply the square root of the variance and the deviation from the mean is, in practical terms, the expected deviation that a specific point will have from the mean and is calculated as follows:

$$\text{estimated deviation from the mean} = \frac{\text{standard deviation}}{(\text{number of points})^{0.5}}$$

The expected deviations from the mean were calculated as percentages of the mean. The number of readings averaged is also calculated.

9. Print out of results

The following results are printed out by the computer program:

- Tail gas compositions and liquid product compositions versus time on stream (mole %)
- The run number and date
- Catalyst information: type of catalyst
  form of catalyst
  size fraction used
  mass (initial) (g)
  final mass (g)
- Reactor conditions : Temperature in the catalyst bed (°C)
  Temperature outside the catalyst bed (°C)
  Temperature of the reactor body (°C)
  Reactor pressure (atm)
- Cylinder conditions: Feed cylinder temperature (°C) and pressure (atm)
- System conditions : The impeller speed (R.P.M) and the overall weight hourly space velocity (hr^{-1})

- General information: Mass of gases (knockout) in the reactor at steady state (g)
  Compressibility factor of the tail gas and the reactor gases
- Reactant data : Mass of reactant fed (g)
  Mass of reactant in exit (g)
- Mass balance data : Total mass fed (g)
  Mass of tail gas out (g)
  Mass of liquid out (g)
  Mass of knockout (g)
  Mass of catalyst gain (g)
  Accumulation (g)
  Total mass out (g)
  % mass lost
- Flowrate data : Calculated feed flowrate (g/hr) versus time on stream (hrs)
- Conversion and reaction rates : Two sets of conversion and reaction rate versus time on stream. The one conversion set is based on reactant disappearance and the other on product formation.
- Concentrations : Concentrations versus time on stream for each component in the reactor
- Averaged rates and concentrations : The averaged (arithmetic mean) steady state values of the component concentrations and reaction rate - for each of these the variance, standard deviation and estimated deviations from the mean (%) are also printed out.

  The starting time and end time (end of run) of the steady state period as well as the number of readings averaged is also printed out.

APPENDIX L OPTIMISED SOLUTION OF KINETIC MODEL "A" OF SECTION 3.4.5.1

The model consists of the following set of equations:

$$C_3 + C_3 \xrightarrow{k_1} C_6$$

$$C_3 + C_6 \xrightarrow{k_3} C_9$$

$$C_3 + C_9 \xrightarrow{k_5} C_{12}$$

$$C_6 + C_6 \xrightarrow{k_7} C_{12}$$

$$C_{12} \xrightarrow{k_9} C_{15} + \text{cracked product}$$

with the following set of rate equations:

$$-dC_3/dt = k_1C_3^2 + k_3C_3C_6 + k_5C_9C_3 \quad \ldots\ldots\ldots (1)$$

$$dC_6/dt = \tfrac{1}{2}k_1C_3^2 - k_3C_3C_6 - k_7C_6^2 \quad \ldots\ldots\ldots (2)$$

$$dC_9/dt = k_3C_3C_6 - k_5C_3C_9 \quad \ldots\ldots\ldots (3)$$

$$dC_{12}/dt = k_5C_3C_9 + \tfrac{1}{2}k_7C_6^2 - k_9C_{12} \quad \ldots\ldots\ldots (4)$$

where C_i = concentration of i

$-dC_3/dt$ = rate of propene reaction

dC_i/dt = rate of production, where i = 6, 9 or 12

Model Solution

As previously mentioned, the optimum set of constants is obtained by using the least squares technique and using a Nelder and Mead routine to optimise the resultant set of non-linear simultaneous equations. The data used to fit the model is listed in table 3.17.

The above rate equations can be expressed in a more general form as follows:

$$y_i = k_1q_i + k_3p_i + k_5x_i + k_4z_i \quad \ldots\ldots\ldots (5)$$

where $q_i = C_3^2$ in equation (1)

$q_i = \tfrac{1}{2}C_3^2$ in equation (2)

$q_i = 0$ in equation (3) and (4) etc

Equation (5) can be rearranged to give:

$$y_i - k_1 q_i - k_3 p_i - k_5 x_i - k_9 z_i = 0 \quad \ldots\ldots\ldots (6)$$

Using a set of constants, the error in equation (6) will be given by:

$$e_i = y_i - (k_1 q_i + k_3 p_i + k_5 x_i + k_9 z_i) \quad \ldots\ldots\ldots (7)$$

Using a set of data, the sum of the error squared will be:

$$\Sigma e_i = \Sigma(y_i - (k_1 q_i + k_3 p_i + k_5 x_i + k_9 z_i)) \quad \ldots\ldots\ldots (8)$$

To provide an optimised solution, this error squared must be minimised. The minimum is obtained by differentiating equation (8) with respect to each constant, and thus equating to zero (best solution). After differentiating and equating to zero the following four equations are obtained:

$$\Sigma y_i q_i - k_1 \Sigma q_i^2 - k_2 \Sigma q_i p_i - k_3 \Sigma q_i x_i - k_4 \Sigma q_i z_i = 0 \quad \ldots\ldots\ldots (9)$$

$$\Sigma y_i p_i - k_1 \Sigma q_i p_i - k_2 \Sigma p_i^2 - k_3 \Sigma x_i p_i - k_4 \Sigma p_i z_i = 0 \quad \ldots\ldots\ldots (10)$$

$$\Sigma y_i x_i - k_1 \Sigma q_i x_i - k_2 \Sigma p_i x_i - k_3 \Sigma x_i^2 - k_4 \Sigma x_i z_i = 0 \quad \ldots\ldots\ldots (11)$$

$$\Sigma y_i z_i - k_1 \Sigma q_i z_i - k_2 \Sigma p_i z_i - k_3 \Sigma x_i z_i - k_4 \Sigma z_i^2 = 0 \quad \ldots\ldots\ldots (12)$$

The above set of equations can be solved using the Nelder and Mead optimization technique. The technique uses an objective function as its criterion for goodness of fit and thus tries to minimize this objective function. The objective function in this case would be a minimization of the LHS (left hand side) of equations (9), (10), (11) and (12). The left hand sides of these equations must be squared to ensure that each is of the same sign, hence avoiding the determination of a false minimum (when positive and negative errors cancel each other out). The terms can also be weighted, for example, equation (1) could be divided by 100 (LHS and RHS) in order to provide comparable values for optimization purposes.

For each experiment the following set of data is required:

$-dC_3/dt$	C_3
dC_6/dt	C_6
dC_9/dt	C_9
dC_{12}/dt	C_{12}

The values of C_3, C_6, C_9, C_{12} and $-dC_3/dt$ (as mol/hr.g cat) appear directly in Table 3.17. The rate of production of products can be calculated as follows:

Rate of production of product i, e.g., $C_6 = \frac{F \times f_{30} \times X_3 \times f_6}{MW_{C6}}$

where F = Total flowrate (g/hr)

f_{30} = Mass fraction of propene in feed

X_3 = Fractional Conversion of propene

f_6 = Mass fraction of C_6 in product

MW_{C6} = Molecular weight of C_6

With respect to the production of C_{15} and the non-oligomeric products, although individually they do not warrant consideration, collectively they form a reasonably significant "product" and therefore it was decided to account for them by assuming that they were all produced from C_{12}. From the experimental data the maximum possible rate of reaction of C_{12} along the route could be determined (knowing the total mass of cracked and C_{15} products). This calculated limit was therefore added as a constraint to the oligomerization routine.

Model prediction

Once a set of constants have been found, the model can be used to predict the product concentrations and reaction rates as functions of the propene reactor concentration (within the limits of the conditions under which these constants were found, i.e., at 103% H_3PO_4 and 464 K). For the purposes of using the model to predict, the rates in equations (1), (2), (3) and (4) must be expressed in terms of concentrations. In order to do this, the change in density of the system must be taken into account. It will be assumed that the change in density varies linearly with the propene conversion. Therefore, in a variable volume reactor, the fractional change in volume, ε_A, is given by:

$$\varepsilon_A = \frac{V_{X3=1} - V_{X3=0}}{V_{X3=0}} \qquad \text{.....(14)}$$

where X_3 = propene conversion

From this it can be shown that:

$$\varepsilon = \frac{\left[\frac{C_{30}(1-X_3)}{C_3} - 1 \right]}{X_3} \qquad \text{.....(15)}$$

The rates in equations (1), (2), (3) and (4) can therefore be expressed as follows:

Rate of propene reaction = $-dC_3/dt = -r_A = \frac{C_{A0} \cdot V \cdot X_3}{\tau}$

where C_{A0} = concentration of propene in the feed at reaction conditions

V = reactor volume

X_A = fractional conversion of propene

τ = mean residence time

$$\text{Rate of production of } C_6 = dC_6/dt = \frac{(C_6 - C_{60}) \times V(1+\varepsilon_A \cdot X_A)}{\tau}$$

where C_6 = concentration of C_6 in the reactor

C_{60} = concentration of C_6 in the feed (which in these experiments is always equal to zero)

The calculations for the C_9 and C_{12} fractions are similar to that of the C_6 fraction.

C_{30} can be calculated from the known reactor temperature, pressure and feed composition. Non-ideality must be taken into account at these conditions.

For the purposes of the model prediction at identical conditions to the experiments listed in Table 3.17, the conversions can be taken from those already quoted. For the purposes of predicting into unknown regions, the conversions can be calculated from the general rate equation given in Section 3.4.4. All other parameters are known except C_6, C_9, C_{12} and τ which must be solved for in the prediction calculation.

APPENDIX M EXPERIMENTAL AND PREDICTED RATES AND CONCENTRATION DATA FOR EACH OF THE MODELS OF SECTION 3.5.5

Listed here, are the experimental and predicted rates and concentration data for each of the models used in Section 3.5.5. The experimental and predicted data for each of the propene models are based on the experimental conditions and the experimental data of Table 3.14. The 1-butene results are based on the data of Table 3.21 and the associated experimental conditions. The experimental data for the propene models is therefore the same for all of the model and likewise for the 1-butene models.

Table M.1 Experimental and predicted concentration data for propene model P1.

	Propene concentrations mol/l x 10								
Product concs mol/l x 10^3	3.8	3.5	3.0	1.9	2.5	2.7	1.7	3.7	2.9
Experimental									
C_6	4.6	4.2	3.1	1.9	2.3	2.9	1.4	4.3	4.2
C_9	25	27	17.6	10.8	15	19	10.3	27	22
C_{12}	8.9	10.5	6.9	5.7	6.2	6.0	4.0	9.5	7.7
Predicted									
C_6	4.4	4.1	3.4	2.4	2.9	3.1	2.0	4.3	3.3
C_9	25	24	20	13	17.5	18	14	24	20
C_{12}	9.6	9.3	7.0	6.0	6.2	6.5	5.2	8.8	7.3

Table M.2 Experimental and predicted rate data for propene model P1.

	Propene concentrations mol/l x 10								
	3.8	3.5	3.0	1.9	2.5	2.7	1.7	3.7	2.9
Reaction rates									
Experimental									
$-dC_3/dt$,	.25	.26	.19	.13	.17	.18	.11	.25	.21
dC_6/dt, mol/hrx10^3	8.4	7.3	5.9	3.6	4.5	5.2	2.7	7.5	7.3
dc_9/dt, mol/hrx10^3	46	46	33	20	29	34	20	48	38
dC_{12}/dt, mol/hrx10^3	16	18	13	11	12	11	7.6	17	14
Predicted									
$-dC_3/dt$,	.30	.29	.17	.14	.12	.15	.10	.32	.19
dC_6/dt, mol/hrx10^3	9.7	8.1	6.1	4.8	4.0	5.0	2.9	9.2	5.3
dc_9/dt, mol/hrx10^3	56	47	35	26	24	29	17	52	32
dC_{12}/dt, mol/hrx10^3	21	18	12	12	8.7	10	7.2	19	12

Table M.3 Experimental and predicted concentration data for propene model P2.

	Propene concentrations mol/l x 10								
Product concs mol/l x 10^3	3.8	3.5	3.0	1.9	2.5	2.7	1.7	3.7	2.9
Experimental									
C_6	4.6	4.2	3.1	1.9	2.3	2.9	1.4	4.3	4.2
C_9	25	27	17.6	10.8	15	19	10.3	27	22
C_{12}	8.9	10.5	6.9	5.7	6.2	6.0	4.0	9.5	7.7
Predicted									
C_6	4.5	4.1	3.4	——	2.9	3.1	2.0	4.3	3.3
C_9	26	25	21	——	19	20	14	25	20
C_{12}	9.6	9.3	7.0	——	6.3	6.5	5.2	8.8	7.3

Table M.4 Experimental and predicted rate data for propene model P2.

	Propene concentrations mol/l x 10								
Reaction rates	3.8	3.5	3.0	1.9	2.5	2.7	1.7	3.7	2.9
Experimental									
$-dC_3/dt$,	.25	.26	.19	.13	.17	.18	.11	.25	.21
dC_6/dt, mol/hrx10^3	8.4	7.3	5.9	3.6	4.5	5.2	2.7	7.5	7.3
dc_9/dt, mol/hrx10^3	46	46	33	20	29	34	20	48	38
dC_{12}/dt, mol/hrx10^3	16	18	13	11	12	11	7.6	17	14
Predicted									
$-dC_3/dt$,	.29	.28	.16	—	.10	.14	.11	.31	.19
dC_6/dt, mol/hrx10^3	9.6	7.8	5.7	—	3.6	4.5	3.6	9.0	5.3
dc_9/dt, mol/hrx10^3	56	48	34	—	24	28	25	52	42
dC_{12}/dt, mol/hrx10^3	21	17	11	—	7.8	9.3	9.4	18	12

Table M.5 Experimental and predicted concentration data for propene model P3.

	Propene concentrations mol/l x 10								
Product concs mol/l x 10^3	3.8	3.5	3.0	1.9	2.5	2.7	1.7	3.7	2.9
Experimental									
C_6	4.6	4.2	3.1	1.9	2.3	2.9	1.4	4.3	4.2
C_9	25	27	17.6	10.8	15	19	10.3	27	22
C_{12}	8.9	10.5	6.9	5.7	6.2	6.0	4.0	9.5	7.7
Predicted									
C_6	4.5	4.2	3.3	1.9	2.6	2.9	1.5	4.3	3.2
C_9	25	24	17	11.9	14.5	16	10.9	24	18
C_{12}	9.0	8.7	7.0	6.2	6.4	6.6	4.3	8.4	7.3

Table M.6 Experimental and predicted rate data for propene model P3.

	Propene concentrations mol/l x 10								
	3.8	3.5	3.0	1.9	2.5	2.7	1.7	3.7	2.9
Reaction rates									
Experimental									
$-dC_3/dt$,	.25	.26	.19	.13	.17	.18	.11	.25	.21
dC_6/dt, mol/hrx10^3	8.4	7.3	5.9	3.6	4.5	5.2	2.7	7.5	7.3
dc_9/dt, mol/hrx10^3	46	46	33	20	29	34	20	48	38
dC_{12}/dt, mol/hrx10^3	16	18	13	11	12	11	7.6	17	14
Predicted									
$-dC_3/dt$,	.25	.26	.20	.12	.16	.19	.12	.27	.22
dC_6/dt, mol/hrx10^3	8.3	7.3	6.6	3.4	4.9	5.8	3.1	8.1	5.9
dc_9/dt, mol/hrx10^3	46	42	35	21	27	32	22	44	33
dC_{12}/dt, mol/hrx10^3	16	15	14	11	12	13	8.8	16	14

Table M.7 Experimental and predicted concentration data for propene model P4.

	Propene concentrations mol/l x 10								
Product concs mol/l x 10^3	3.8	3.5	3.0	1.9	2.5	2.7	1.7	3.7	2.9
Experimental									
C_6	4.6	4.2	3.1	1.9	2.3	2.9	1.4	4.3	4.2
C_9	25	27	17.6	10.8	15	19	10.3	27	22
C_{12}	8.9	10.5	6.9	5.7	6.2	6.0	4.0	9.5	7.7
Predicted									
C_6	4.6	4.3	3.3	1.9	2.7	3.0	1.6	4.4	3.2
C_9	27	26	17.2	12.1	14	16	9.6	25	19
C_{12}	9.6	9.3	7.1	6.1	6.4	6.7	5.2	8.8	7.6

Table M.8 Experimental and predicted rate data for propene model P4.

	Propene concentrations mol/l x 10								
	3.8	3.5	3.0	1.9	2.5	2.7	1.7	3.7	2.9
Reaction rates									
Experimental									
$-dC_3/dt$,	.25	.26	.19	.13	.17	.18	.11	.25	.21
dC_6/dt, mol/hrx10^3	8.4	7.3	5.9	3.6	4.5	5.2	2.7	7.5	7.3
dc_9/dt, mol/hrx10^3	46	46	33	20	29	34	10	48	38
dC_{12}/dt, mol/hrx10^3	16	18	13	11	12	11	7.6	17	14
Predicted									
$-dC_3/dt$,	.23	.24	.19	.12	.17	.19	.11	.26	.21
dC_6/dt, mol/hrx10^3	7.9	7.0	6.6	3.3	5.3	5.9	3.1	7.8	5.8
dc_9/dt, mol/hrx10^3	45	42	34	21	28	31	18	44	33
dC_{12}/dt, mol/hrx10^3	16	15	14	11	13	13	9.9	16	13

Table M.9 Experimental and predicted concentration data for propene model B1.

	1-butene concentrations mol/l x 10						
Product concs mol/l x 10^3	1.15	3.75	2.25	1.22	3.78	2.29	1.62
Experimental							
C_8	20	130	79	24	134	62	36
C_{12}	4.7	2.1	13.4	4.6	24	11.3	7.0
Predicted							
C_8	32	160	106	35	168	87	53
C_{12}	0.5	12	4.9	0.6	13	3.5	1.3

Table M.10 Experimental and predicted rate data for propene model B1.

	1-butene concentrations mol/l x 10						
	1.15	3.75	2.25	1.22	3.78	2.29	1.62
Reaction rates							
Experimental							
$-dC_4/dt$,	100	335	280	110	350	225	160
dC_8/dt, mol/hrx10^3	32	116	96	37	120	74	51
dc_{12}/dt, mol/hrx10^3	7.2	19	16	7.1	22	13.6	9.9
Predicted							
$-dC_4/dt$,	299	990	586	310	1000	590	416
dC_8/dt, mol/hrx10^3	145	426	265	150	420	270	200
dc_{12}/dt, mol/hrx10^3	2.1	31	12	2.4	32	10.7	4.8

Table M.11 Experimental and predicted concentration data for propene model B2.

	1-butene concentrations mol/l x 10						
Product concs mol/l x 10^3	1.15	3.75	2.25	1.22	3.78	2.29	1.62
Experimental							
C_8	20	130	79	24	134	62	36
C_{12}	4.7	2.1	13.4	4.6	24	11.3	7.0
Predicted							
C_8	21	128	74	23	134	62	36
C_{12}	4.6	22	16	4.8	24	12.6	7.7

Table M.12 Experimental and predicted rate data for propene model B2.

	1-butene concentrations mol/l x 10						
	1.15	3.75	2.25	1.22	3.78	2.29	1.62
Reaction rates							
Experimental							
$-dC_4/dt$,	100	335	280	110	350	225	160
dC_8/dt, mol/hrx10^3	32	116	96	37	120	74	51
dc_{12}/dt, mol/hrx10^3	7.2	19	16	7.1	22	13.6	9.9
Predicted							
$-dC_4/dt$,	99	346	203	106	350	206	142
dC_8/dt, mol/hrx10^3	31	118	64	34	119	70	46
dc_{12}/dt, mol/hrx10^3	6.8	21	13	7.2	21	14.1	9.9

Table M13 Experimental and predicted concentration data at 464 K and 114% H_3PO_4 for model P3 and the data of Table 3.15.

	Propene concentrations mol/l x 10							
Product concs mol/l x 10^3	2.3	2.6	1.8	1.7	1.3	1.3	1.0	0.6
Experimental								
C_6	5.2	5.4	3.2	2.4	2.1	1.3	1.0	0.6
C_9	46	49	30.3	21.6	17.8	11.9	9.2	6.0
C_{12}	22	24	15.4	11.5	9.9	7.5	6.2	3.8
Predicted								
C_6	5.2	6.2	3.7	3.3	2.4	2.2	1.7	0.9
C_9	42	47	26	20	15	11	8.2	4.3
C_{12}	25	26	18	14	13	9.0	7.7	5.6

Table M14 Experimental and predicted rate data at 464 K and 114% H_3PO_4 for model P3 and the data of Table 3.15.

	Propene concentrations mol/l x 10							
	2.3	2.6	1.8	1.7	1.3	1.3	1.0	0.6
Reaction rates								
Experimental								
$-dC_3/dt$, mol/hr	.37	.48	.32	.24	.21	.17	.13	.08
dC_6/dt, mol/hrx10^3	6.7	8.3	5.2	2.4	3.8	2.7	1.9	1.3
dc_9/dt, mol/hrx10^3	59	75	50	22	32	24	18	12
dC_{12}/dt, mol/hrx10^3	29	37	25	11.5	18	15	12.2	7.7
Predicted								
$-dC_3/dt$, mol/hr	.36	.41	.28	.26	.21	.20	.20	.15
dC_6/dt, mol/hrx10^3	6.4	8.2	5.3	6.4	4.4	5.5	4.0	2.0
dc_9/dt, mol/hrx10^3	52	63	38	38	27	27	20	9.8
dC_{12}/dt, mol/hrx10^3	31	35	27	27	23	22	18	13

Table M15 Experimental and predicted concentration data at 464 K and 114% H_3PO_4 for model P4 and the data of Table 3.15.

	Propene concentrations mol/l x 10							
Product concs mol/l x 10^3	2.3	2.6	1.8	1.7	1.3	1.3	1.0	0.6
Experimental								
C_6	5.2	5.4	3.2	2.4	2.1	1.3	1.0	0.6
C_9	46	49	30.3	21.6	17.8	11.9	9.2	6.0
C_{12}	22	24	15.4	11.5	9.9	7.5	6.2	3.8
Predicted								
C_6	4.9	5.9	3.4	3.1	2.2	2.1	1.5	—
C_9	44	48	27	19	15	10.5	7.8	—
C_{12}	28	29	20	15	14	10	8.4	—

Table M16 Experimental and predicted rate data at 464 K and 114% H_3PO_4 for model P4 and the data of Table 3.15.

	Propene concentrations mol/l x 10							
	2.3	2.6	1.8	1.7	1.3	1.3	1.0	0.6
Reaction rates								
Experimental								
$-dC_3/dt$, mol/hr	.37	.48	.32	.24	.21	.17	.13	.08
dC_6/dt, mol/hrx10^3	6.7	8.3	5.2	2.4	3.8	2.7	1.9	1.3
dc_9/dt, mol/hrx10^3	59	75	50	22	32	24	18	12
dC_{12}/dt, mol/hrx10^3	29	37	25	11.5	18	15	12.2	7.7
Predicted								
$-dC_3/dt$, mol/hr	.36	.41	.28	.27	.21	.21	.17	—
dC_6/dt, mol/hrx10^3	6.0	7.9	5.1	6.1	3.9	5.2	3.7	—
dc_9/dt, mol/hrx10^3	54	64	41	37	27	26	20	—
dC_{12}/dt, mol/hrx10^3	34	38	30	30	25	25	21	—

Table M17 Experimental and predicted concentration data at 111% H_3PO_4 for model P3 and the data of Table 3.16.

	Reactor temperature, K			
Product concs mol/l x 10^3	472	508	486	454
Experimental				
C_6	8.2	18	14	3.5
C_9	55	92	78	31
C_{12}	23	30	30	16
Predicted				
C_6	9.2	25	14	4.9
C_9	56	89	77	343
C_{12}	23	32	30	15

Table M18 Experimental and predicted rate data at 111% H_3PO_4 for model P3 and the data of Table 3.16.

	Reactor temperature, K			
Reaction rates	472	508	486	454
Experimental				
$-dC_3/dt$, mol/hr	.43	.65	.58	.44
dC_6/dt, mol/hrx10^3	11	22	17	8.6
dc_9/dt, mol/hrx10^3	72	113	99	75
dC_{12}/dt, mol/hrx10^3	30	37	38	35
Predicted				
$-dC_3/dt$, mol/hr	.47	.63	.51	.39
dC_6/dt, mol/hrx10^3	13	29	15	7.0
dc_9/dt, mol/hrx10^3	81	106	86	65
dC_{12}/dt, mol/hrx10^3	34	38	34	30

Table M19 Experimental and predicted concentration data at 111% H_3PO_4 for model P4 and the data of Table 3.16.

	Reactor temperature, K			
Product concs mol/l x 10^3	472	508	486	454
Experimental				
C_6	8.2	18	14	3.5
C_9	55	92	78	31
C_{12}	23	30	30	16
Predicted				
C_6	12	-	24	3.7
C_9	50	-	55	55
C_{12}	28	-	40	20

Table M20 Experimental and predicted rate data at 111% H_3PO_4 for model P4 and the data of Table 3.16.

	Reactor temperature, K			
Reaction rates	472	508	486	454
Experimental				
$-dC_3/dt$, mol/hr	.43	.65	.58	.44
dC_6/dt, mol/hrx10^3	11	22	17	8.6
dc_9/dt, mol/hrx10^3	72	113	99	75
dC_{12}/dt, mol/hrx10^3	30	37	38	35
Predicted				
$-dC_3/dt$, mol/hr	.47	-	.50	.43
dC_6/dt, mol/hrx10^3	17	-	26	5.0
dc_9/dt, mol/hrx10^3	72	-	59	73
dC_{12}/dt, mol/hrx10^3	41	-	44	27